UNIVERSITAT DE BARCELONA

Preparation of CBs immobilized on different types of magnetic nanoparticles for application in selective complexation and catalysis

Lluís Llorens Palomo

PREPARATION OF CBs IMMOBILIZED ON DIFFERENT TYPES OF MAGNETIC NANOPARTICLES FOR APPLICATION IN SELECTIVE COMPLEXATION AND CATALYSIS

LLUIS LLORENS PALOMO

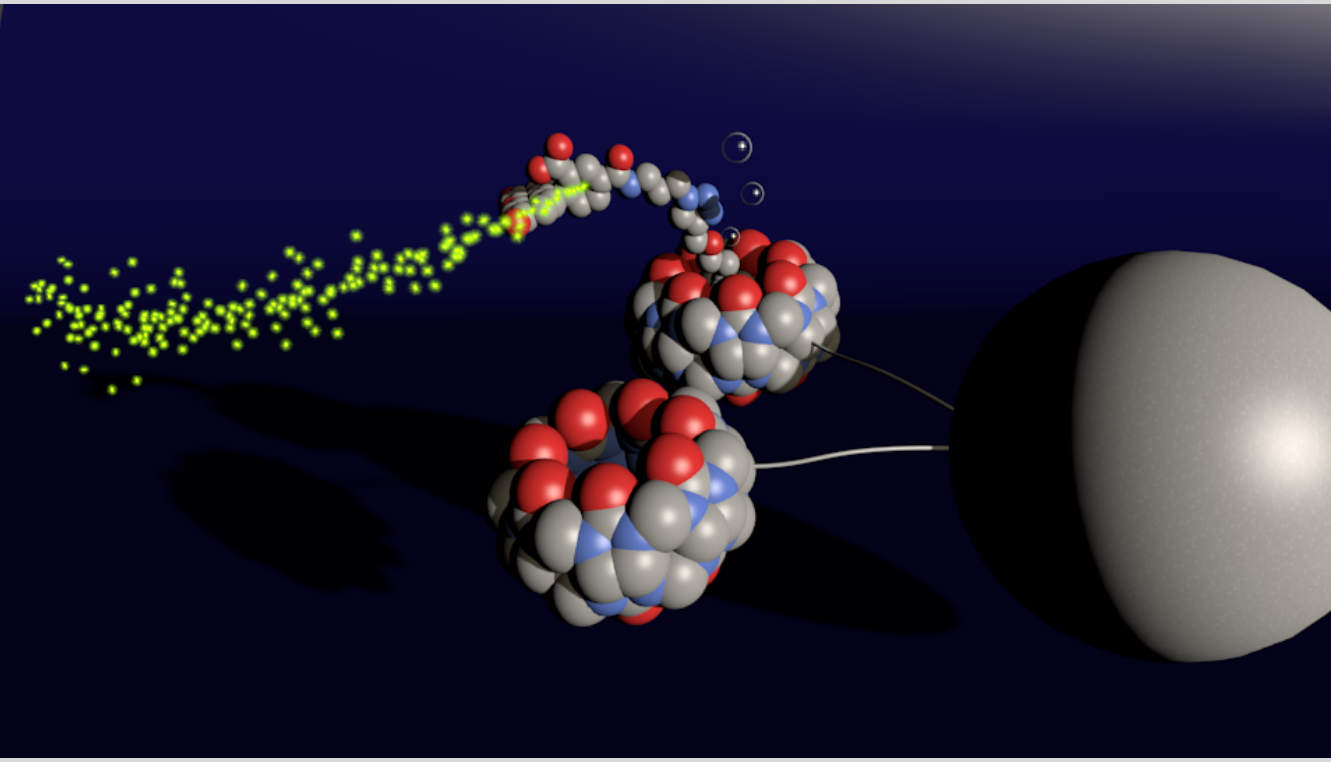

UNIVERSITAT DE BARCELONA

Doctorat en química orgànica: HDK16

101308 catàlisi i química sostenible

PREPARATION OF CBs IMMOBILIZED ON DIFFERENT TYPES OF MAGNETIC NANOPARTICLES FOR APPLICATION IN SELECTIVE COMPLEXATION AND CATALYSIS

Doctoral Thesis by

Lluís Llorens Palomo

Developed under the supervision of:

Prof. Miquel A. Pericàs

Departament de Química Inorganica i Orgànica (UB)

Institut Català d'Investigació Química (ICIQ)

Tarragona

2019

Prof. Miquel A. Pericàs Brondo, Group Leader and Director of the Institute of Chemical Research of Catalonia (ICIQ),

STATE, that the present Doctoral Thesis entitled: “PREPARATION OF CBs IMMOBILIZED ON DIFFERENT TYPES OF MAGNETIC NANOPARTICLES FOR APPLICATION IN SELECTIVE COMPLEXATION AND CATALYSIS”, presented by Lluís Llorens Palomo to receive the degree of Doctor, has been carried out under our supervision at the Institute of Chemical Research of Catalonia (ICIQ).

Tarragona, 6th of September 2019

Ph.D. Thesis Supervisor

Miquel A. Pericàs Brondo

Acknowledgments

I express my appreciation to Professor Miquel A. Pericàs for giving me the chance to perform the research presented in this dissertation. During the last years, I had the opportunity to attend many courses, conferences, and workshops where I met fascinating researchers with whom I learned and engaged in enlightening conversations. I show my gratitude to them, to my lab mates, to Mauro Fianchini and to Alonso Argüelles, a visiting student from the University of Michigan, I had the opportunity to host. He eagerly engaged in my projects and provided me with sage advice.

During my thesis, I had the chance to perform two marvelous stays abroad. First, I went to the JACOBS University in Bremen, under the supervision of Prof. Werner Nau. I received a huge welcome, and they attentively showcased me the lab, their work, and the beautiful German city. I am deeply indebted to their group, with particular emphasis on the help I received from Shuai Zhang and Khaleel I. Assaf. Secondly, I went back to Germany: this time, I departed to the south. I want to thank Prof. Thomas Carell for giving me the chance to work in his laboratories for one year. I learned many things from the group, both professionally and personally. I joined an outstanding group of researchers, and I had the opportunity to integrate into their culture of work. Special thanks to Nobuhiro Tago, Sarah Schiffers and René Rahimoff for their help and guidance.

Most importantly, I express my gratitude to my parents, family, and friends for their support and encouragement when things went smooth, but especially in troublesome times. Finally, the last and most meaningful thanks go to Julia: the most important pillar, she who stabilizes everything and maintains the balance to keep us fighting for our goals.

Financial sources

The present doctoral thesis has been possible thanks to the funding received from the Institute of Chemical Research of Catalonia (ICIQ) Foundation (CERCA Programme/Generalitat de Catalunya).

The works have been developed within the following projects funded by AEI/MINECO (Severo Ochoa Excellence Accreditation 2014−2018 (SEV-2013-0319) and CTQ2015-69136-R) and AGAUR (Grant 2014SGR827).

Unión Europea

Fondo Europeo
de Desarrollo Regional
"Una manera de hacer Europa"

Generalitat de Catalunya
Departament d'Economia i Coneixement

Abbreviations

In this document, the abbreviations and acronyms most commonly used in organic chemistry have been used, according to the recommendations of the ACS "*Guidelines for authors*":

http://pubs.acs.org/paragonplus/submission/joceah/joceah_authguide.

“I can’t change the direction of the wind, but I can adjust my sails to always reach my destination.”

–Jimmy Dean

“Don’t judge each day by the harvest you reap but by the seeds that you plant.”

–Robert Louis Stevenson

Table of Contents

Overall Goals

The main goal of the present thesis is the development of novel magnetically powered nanodevices for the efficient and selective extraction of chemical cargos. Supramolecular chemistry—especial emphasis on cucurbiturils—will play a central lead in this manuscript due to the endogenous chemical properties of the supramolecules, and the robust and modulable nature of their guests. Moreover, we will cover the entire manufacture of the nanodevices or chemical shuttles, their potential use in asymmetric catalysis, and their applicability in molecular recognition and enrichment.

Following these guidelines, the goals of each chapter are:

- **Chapter I** provides the background and fundamental concepts for the following sections. The importance of supramolecular chemistry and the role of cucurbiturils. Additionally, the importance of asymmetric catalysis and the immobilization of catalytically active species will be disclosed herein.
- **Chapter II** showcases the preparation of the novel chemical shuttles instrumental to our work, with special focus on the single components and their overall chemical and physical properties.
- **Chapter III.** Based on previous studies performed in our laboratories for the preparation of immobilized catalyst for their recovery and recyclability, this chapter describes the preparation of recoverable, highly-active, and selectively assembled aminocatalyst for the enantioselective aldol reaction and the Robinson annulation.
- **Chapter IV.** The main purpose of this chapter consists of the selective extraction of testosterone derivatives, from complex mixtures and blood samples, making use of the nanodevices presented in chapter II.
- **Chapter V** targets some computational studies on host–guest binding between cucurbit[7]uril and adamantyl-based guests.
- **Chapter VI** summarizes the essential conclusions unveiled in the present dissertation.

Summary

Cucurbiturils are known to present potential applications in molecular recognition, self-assembly, and nanotechnology. The discovery of ultra-high affinity CB–guest complexes with binding constant values similar than those found in natural complexes beckoned the attention of many groups, that focused their research in the functionalization of cucurbiturils in order to modify their structure and properties, to enhance their solubility, and to provide different functional groups for further transformations. In fact, cucurbiturils have been supported onto different solid surfaces such as gold surface, polymer beads, or nanoparticles. Iron is a bioactive metal with magnetic properties and low toxicity to mammalian cells. The formation of 10 nm magnetic nanoparticles (MNPs) of iron oxide (Fe_3O_4) can be achieved in an affordable and easily reproducible manner by thermal decomposition. This small size of nanoparticles provides a double advantage: first, biodegradability, because particles up to 100 nm can be phagocytosed through liver cells; second, superparamagnetic behavior, so that they become magnetized upon exposure to a magnetic field but have no permanent magnetization once the field is turned off. Prompted by the breadth of possible applications provided by cucurbiturils and our previous experience immobilizing organic molecules on MNPs of Fe_3O_4 and polystyrene resin (PR) (generally, to covalently immobilize catalysts for the preparation of easily recoverable and recyclable catalysts), we speculated that covalently attached cucurbiturils onto MNPs could open up new routes concerning drug delivery and biocatalysis, enable applications in many areas including sensor, transport, separation, and nanomaterials. Hence, the first research project included in this dissertation (chapter II), unveils the development of polystyrene and magnetic nanoparticles coated with a cucurbituril layer. The intrinsic properties of these compounds have been tested on the extraction of selected molecules (guests that bind to cucurbiturils). Also, in this chapter, the preparation and characterization of a library of these novel compounds—that exhibit a potential use in molecular recognition, transport, and separation—is described.

The second project, described in chapter III, illustrates the synthesis of catalysts tagged with an adamantyl moiety to enhance their affinity towards cucurbiturils—for their selective extraction from the reaction media. This is achieved by covalent linking of the cucurbituril receptor to the superparamagnetic Fe_3O_4 nanoparticles to allow magnetic decantation. These compounds were prepared, and their catalytic activity and reusability were tested: first, on the model aldol reaction between ketones and benzaldehydes; secondly, on the enantioselective Robinson annulation with the well-established Wieland-Miescher ketone. Chapter IV showcases the preparation of a quaternary amino

derivatizing reagent decorated with an adamantyl moiety. This reagent reacts with ketone-containing steroids such as testosterone. Upon reaction, the resulting derivative can be selectively extracted from the solution mixture and driven away by the magnetically powered nanoparticles. Finally, chapter V provides some computational insights on the nature and the strength of the cucurbit[7]uril interactions with some adamantyl-based guests. The studies are built on novel and unprecedented computational models able to reproduce experimental procedures on the determination of enthalpic and entropic changes.

Resum

El primer projecte de recerca, inclòs al capítol II, revela el desenvolupament de poliestirè i nanopartícules magnètiques recobertes amb una capa de cucurbituril. Durant aquesta secció, s'han provat les propietats intrínseques d'aquests compostos per a l'extracció de molècules seleccionades (hostes) que s'uneixen als cucurbiturils. A més, en aquest capítol, s'ha fet un esforç per caracteritzar amb precisió una varietat d'aquests nous compostos que presenten un potencial ús en el reconeixement molecular, el transport i la separació.

El segon projecte, descrit al capítol III, il·lustra la síntesi de catalitzadors etiquetats amb un fragment adamantil per millorar la seva afinitat cap als cucurbiturils, i promoure la seva extracció selectiva. Això s'aconsegueix per mitjà de l'enllaç covalent entre el receptor de cucurbituril i les nanopartícules superparamagnètiques (Fe_3O_4), que permetent la decantació magnètica del sistema format. Una varietat d'aquests compostos s'ha preparat, i la seva activitat catalítica així com la reutilitzabilitat s'han posat també a prova: primer, en la reacció aldòlica entre cetones i benzaldehids; després, en la reacció enantioselectiva de Robinson, amb la ben consolidada cetona de Wieland i Miescher.

Al capítol IV es mostra la preparació d'un reactiu derivatitzant que inclou una amina quaternària i un grup adamantil. Aquesta molècula presenta reactivitat amb esteroides que contenen cetones com la testosterona. Després de reaccionar, el derivat resultant es pot extreure selectivament de la barreja de solució i desplaçar-lo a parer, fent ús de les propietats magnètiques de les nanopartícules.

Finalment, el capítol V aporta unes idees sobre la naturalesa i força de les interaccions entre els cucurbiturils i uns determinats hostes, basant-nos en uns models computacionals innovadors i sense precedents que són capaços de reproduir resultats experimentals per a la determinació de canvis entàlpics i entròpics.

1

CHAPTER I

General Introduction

CHAPTER I

General Introduction

I.1. Supramolecular chemistry

Supramolecular chemistry is a relatively young discipline and one of the fastest-growing areas of experimental chemistry. Part of the reason dwells on the fact that supramolecular science is highly interdisciplinary and attracts a wide range of researchers, from chemists and biologists to theoreticians, mathematicians and a host of other areas. Supramolecular chemistry was already recognized by the Nobel Prize to Cram, Lehn, and Pedersen in 1987;[1] and, quite recently, Sauvage, Stoddart, and Feringa received the same prize in 2016 for the application of supramolecular chemistry to the development of molecular machines.[2,3,4] Supramolecular chemistry is deemed to be the chemistry of the intermolecular bond, covering the structure and functions of the entities formed by the association of two or more chemical species.[5] Other definitions refer to supramolecular chemistry as the chemistry of the non-covalent bond, because it is mainly concerned with non-covalent interactions such as hydrogen bonding, hydrophobic and electrostatic interactions, and van der Waals forces, among others. In this sense, we can consider a molecule (a host) binding to another molecule (a guest) to produce a host–guest complex or supramolecule. Therefore, understanding and controling the formation of host–guest complexes through molecular recognition between the host and the guest is the central pillar of supramolecular chemistry.

I.1.1. Classification of supramolecular host–guest assemblies

Host compounds can be divided into two major classes: Cavitands, that are hosts with intramolecular cavities available for guest binding; and clathrands, that are hosts with extramolecular cavities. Cavitands can form complexes when the host–guest aggregate is welded by primarily electrostatic forces such

[1] J.-M. Lehn. *Supramolecular Chemistry.* VCH: Weinheim, **1995**, 1–9.
[2] J.-P. Sauvage, *Angew. Chem. Int. Ed.* **2017**, *56*, 11080–11093.
[3] J. F. Stoddart, *Angew. Chem. Int. Ed.* **2017**, *56*, 11094–11125.
[4] B. L. Feringa, *Angew. Chem. Int. Ed.* **2017**, *56*, 11060–11078.
[5] J.-M. Lehn, *Angew. Chem. Int. Ed.* **1988**, *27*, 89–112.

as ion–dipole, dipole–dipole, hydrogen bonding, etc. or, cavitates when the species are held together by less specific and weaker interactions such as hydrophobic ones or van der Waals forces. Some of the best-known host molecules, cavitands, include crown ethers, cyclodextrins, calixarenes, and cucurbiturils (Figure I-1). Despite some of them generate complexes and others make cavitates, there is a common trend in the literature to use the word complex to cover all types. Some examples of clathrate include water and some organic molecules.

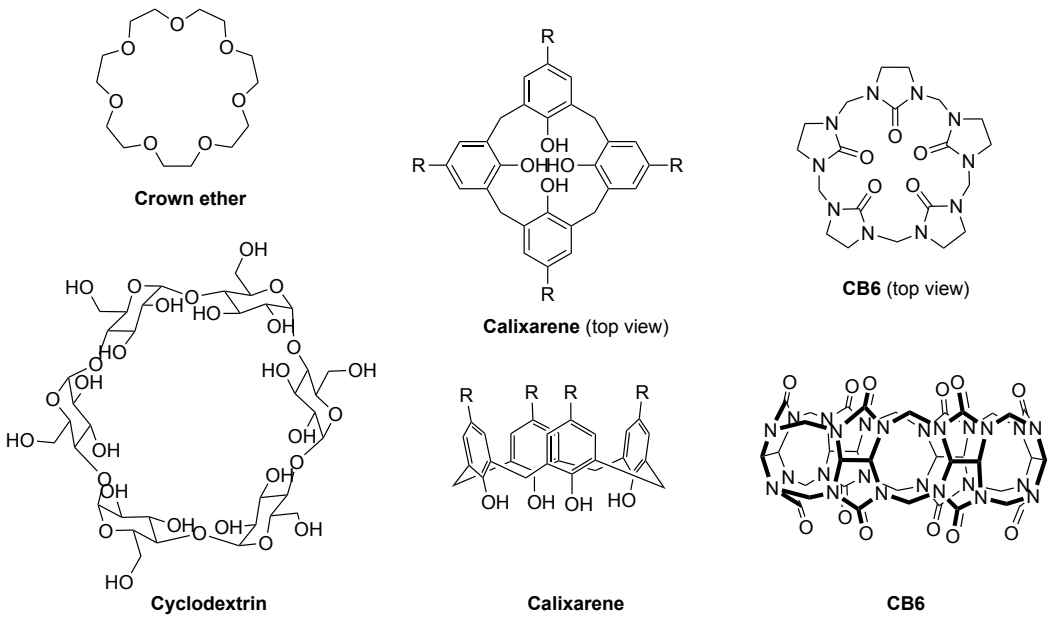

Figure I-1. Representative structures of some cavitands.

I.1.2. Selection of supramolecular host molecules

The building up or selection of supramolecular host molecules has to be focused on bringing summative or multiplicative interactions to generate stable host–guest complexes using as many non-covalent interactions as possible. Each new interaction adds to all the other small stabilizations (summative), and sometimes the interactions of the whole system are synergically greater than the sum of the parts (multiplicative). This extra stabilization is due to the chelate and macrocyclic effects (Figure I-2).[6] These effects, as well as the concept of complementarity and host preorganization, are key to design or select hosts that will selectively bind a particular guest and vice versa.

[6] R. D. Hancock, *J. Chem. Educ.* **1992**, *69*, 615.

Chelate effect: relates to the observation that metal complexes of bidentate ligands are more stable than closely related unidentate ligands due to thermodynamic and kinetic effects.

Macrocyclic effect: cyclic hosts are generally more stable than acyclic compounds with the same type of binding sites since the binding energy is not wasted by the host wrapping the guest. Also, a favorable enthalpic contribution is attributed to less solvated macrocyclic hosts.

Complementarity: a host that perfectly matches with the guest—both sterically (the host must be able to fit physically around the guest) and electronically (the host must present binding sites complementary to those of the guest).[7]

Host preorganization: host–guest interactions occur through binding sites that must be arranged on an organic framework of suitable size to accommodate the guest. Binding sites should be spaced from one another to minimize repulsions between them but arranged so that they can interact simultaneously with the guest.

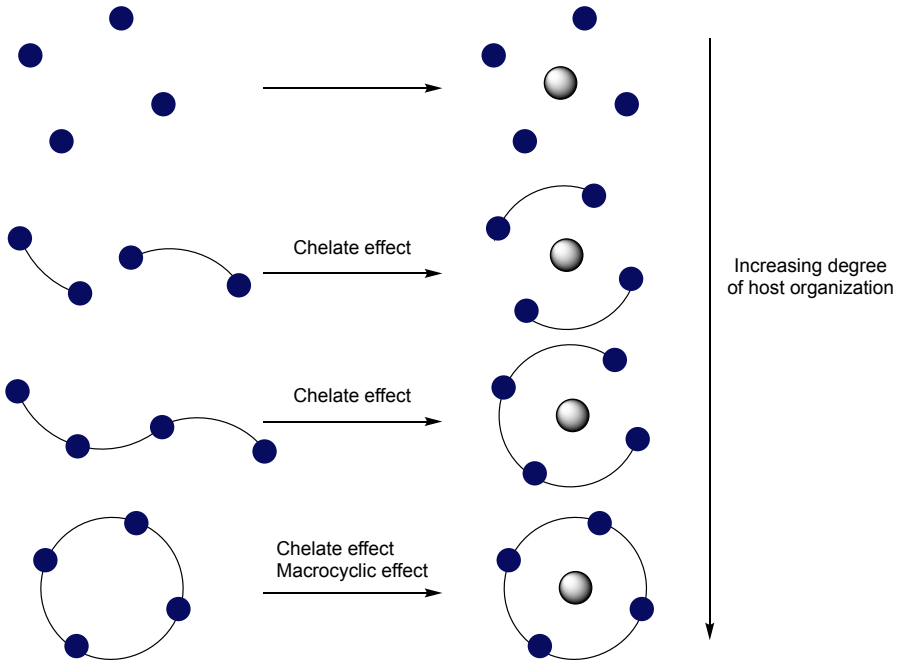

Figure I-2. The chelate and macrocyclic effects.

[7] D. J. Cram, *Angew. Chem. Int. Ed.* **1986**, *25*, 1039–1057.

I.1.3. Supramolecular interactions

We previously referred to supramolecular chemistry as the branch of chemistry that deals with non-covalent interactions. This term encompasses an enormous range of attractive and repulsive forces that need to be considered for each supramolecular system and surroundings. Among the most critical interactions, we can find ion–ion interactions, ion–dipole interactions, dipole–dipole interactions, hydrogen bonding, cation–π interactions, π–π stacking, van der Waals forces, anion–π interactions, close packing (in the solid state), and hydrophobic effects. The most representative interactions for this thesis, along with an indication of their approximate energies, are briefly explained below (Figure I-3).

Ion–ion interactions (bond energy = 100–350 kJ/mol): ionic bonding is comparable in strength to covalent bonding. An example is sodium chloride, that possesses a cubic lattice in the solid state, where six chloride ions surround each sodium cation.

Ion–dipole interactions (bond energy = 50–200 kJ/mol): the bonding of an ion (Na^+) with a polar molecule such as water. The oxygen lone pairs are attracted to the cation positive charge. A supramolecular analog would be crown ethers.

Dipole–dipole interactions (bond energy = 5–50 kJ/mol): one dipole is aligned with another resulting in attractive interactions by matching a single pair of poles on adjacent molecules or opposing alignment of one dipole with the other. These interactions are mostly seen with organic carbonyl compounds.

Hydrogen bonding (bond energy = 4–120 kJ/mol): a sort of dipole–dipole interaction in which a hydrogen atom attached to an electronegative atom (e.g., water) is attracted to a neighboring dipole on an adjacent molecule or functional group. Hydrogen bonding is responsible for the formation of carboxylic acid dimers and, most importantly, the nature of the double helix structure of DNA. It is a directional interaction that comes in a wide range of lengths, strengths, and geometries.

Van der Waals forces (bond energy < 5 kJ/mol): the polarization of an electron cloud by the proximity of an adjacent nucleus results in a weak electrostatic attraction. They are not directional and provide attractive interactions for most

polarizable species. In supramolecular chemistry, they are most important in the formation of inclusion compounds in which small organic molecules are loosely incorporated within crystalline molecular cavities (e.g., the inclusion of toluene within the molecular cavity of calix[4]arene).

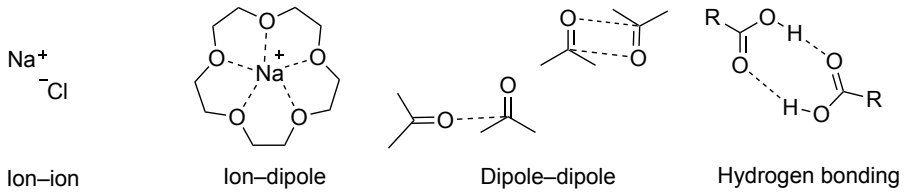

Figure I-3. Examples of non-covalent interactions: ion–ion, ion–dipole, dipole–dipole, and hydrogen bonding.

Hydrophobic effects: relate to the exclusion of weakly solvated particles from polar solvents like water (e.g., via hydrogen bonds or dipolar interactions). At the macroscopic level, the immiscibility between mineral oil and water is an example of such an effect. They are crucial in the binding of organic guests by cavitands such as cyclodextrins, cyclophane hosts, and cucurbiturils in water. The hydrophobic effects may be divided into enthalpic and entropic components. *The enthalpic hydrophobic effect* involves the stabilization of water molecules that are driven from a host cavity upon guest binding. Because host cavities are often hydrophobic, intracavity water does not interact actively with the host walls and is on that account of high energy. Upon release into the bulk solvent, it is stabilized by interaction with other water molecules. *The entropic hydrophobic effect* is related to the fact that the presence of two molecules in solution (host and guest), to form a complex, provokes less disruption in the solvent structure and, hence, fosters an entropic gain that lowers the overall free energy.[8]

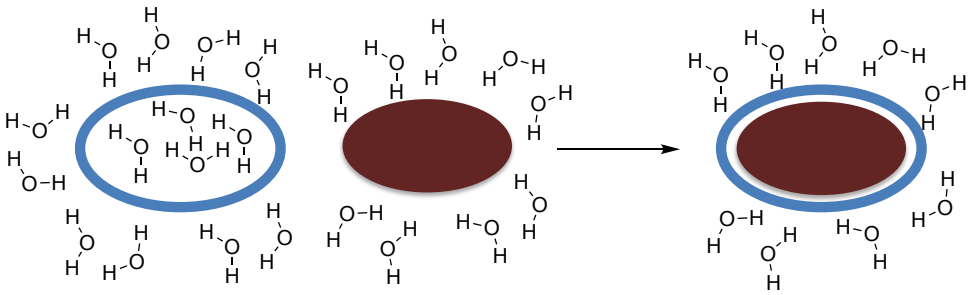

Figure I-4. Hydrophobic binding of organic guests in aqueous solution.

[8] D. B. Smithrud, E. M. Sanford, I. Chao, S. B. Ferguson, D. R. Carcanague, J. D. Evanseck, K. N. Houk, F. Diederich, *Pure Appl. Chem.* **1990**, *62*, 2227.

I.1.4. Selectivity of complexation

Selective and robust binding is the basis of efficient molecular recognition. A successful host exhibits a strong affinity for one particular guest and a much lower affinity for other molecules. The selectivity, though, is governed by a wide variety of factors depending on the nature of the guest. Some crucial factors predominate for cationic species or metal cations: size match between the guest and the host cavity, the preorganization, and complementarity of the host, the electrostatic charge, the solvent, the enthalpic and entropic contributions of the host–guest interactions, the free energies of solvation, and some others. For anion complexation, other factors such as charge and hydrogen bond donor characteristics come as well into play. Organic cations and anions are best suited for hosts with both hydrophilic and hydrophobic regions. Alternatively, neutral molecule guests may lack specific handles such as polar groups that can actively interact with the host. Therefore, the binding may occur via its physical imprisonment due to weak interactions, including van der Waals forces or hydrogen bonds. Unlike charged species, neutral molecules are not bound by strong permanent electrostatic forces, nor do they undergo well-defined coordination interactions, and hence their binding may be weaker.

I.2. Cucurbiturils: history and evolution

Cucurbiturils are a family of macrocyclic host molecules that possess remarkable properties that have beckoned much attention during recent years. The synthesis of cucurbiturils was first heralded in 1905 by Behrend, Meyer, and Rusche when they reported the formation of a crystalline precipitate after the condensation between an excess of formaldehyde and glycoluril.[9] This precipitate was very stable towards several reagents, even in the presence of aggressive reagents such as $KMnO_4$. Despite this, they did not possess the appropriate methods at that time to accurately characterize the substance that we now call cucurbituril. It was not until 1981, that Freeman, Mock, and Shih repeated the synthesis, and thanks to contemporary structural characterization

[9] R. Behrend, E. Meyer, F. Rusche, *Liebigs Ann. Chem.* **1905**, *339*, 1–40.

methods such as X-ray crystallography and NMR,[10] they could describe the product as the hexameric cyclic structure of composition $C_{36}H_{36}N_{24}O_{12}$.

The name was given by Mock, because of its resemblance to a pumpkin, since pumpkins belong to the *Cucurbitaceae* family (Figure I-5). Today, we know that cucurbit[6]uril is a slightly water-soluble molecular container, that accommodates 6 glycoluril units bound together through methylene bridges, giving rise to a macropolycyclic molecule with a hydrophilic rim on each side and comprised of ureido carbonyls and a hydrophobic interior—that offers unique molecular recognition properties.[11] It can accept nonpolar organic residues through the release of "high-energy water" and van der Waals forces. The carbonyl rims or "portals," from which the guest access the cavity, possess partial negative charge densities and, therefore, can hold positively charged compounds that may present ion–dipole interactions.

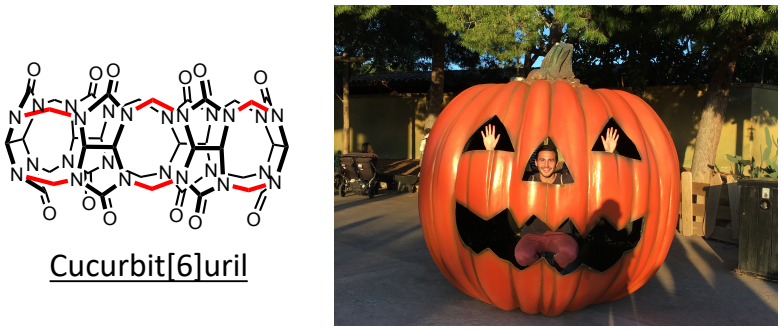

Figure I-5. Chemical structure of the pumpkin-shaped CB6.

I.2.1. Historical landmarks

The early works previous to 2000 gave some insights to the potential of cucurbiturils. However, they were under the shadow of other, more promising macrocycles such as cyclodextrins (CDs) which were the state-of-the-art molecular containers because of their solubility in water, their accessibility to a range of different sizes, from six to eight sugar moieties, and a more extensive range of host–guest chemistry compared to cucurbit[6]uril (CB6), which was the only homolog known and it was just slightly soluble in water. Almost 80 years elapsed from the first synthesis of cucurbiturils in 1905,[9] and the structural characterization of CB6 in 1981.[10] Then, several milestones were attained

[10] W. A. Freeman, W. L. Mock, N. Y. Shih, *J. Am. Chem. Soc.* **1981**, *103*, 7367–7368.
[11] Cucurbiturils present the strongest interactions reported for synthetic host–guest systems.

before entering the 21st century. Some investigations of host–guest chemistry,[12] the first reaction inside CB6,[13] some kinetic and binding studies,[14,15] and the synthesis and isolation of new members of the cucurbituril family containing 5, 7 and 8 glycoluril units, CB5, CB7, and CB8, respectively (CBn, n = 5, 6, 7, 8, Figure I-6).[16] Although CB6 is the major product in the standard preparation, careful control of the reaction temperature allowed access to different homologs.[17] Ensuing investigations on these new molecules revealed that CB7 and CB5 are substantially more soluble in water than CB6 and CB8. The interest in finding new and innovative properties and applications provided by the different structural motif led to an ever-increasing number of publications concerning the synthesis of cucurbituril homologs. For this reason, during the last 20 years, the interest in cucurbituril chemistry has grown, year by year, almost exponentially.[18] Some other milestones achieved during this relatively short period include the functionalization of CBs, that opened up a new range of possibilities and applications to this highly symmetric macrocycles, and the discovery of ultra-high affinity complexes.[19,20,21]

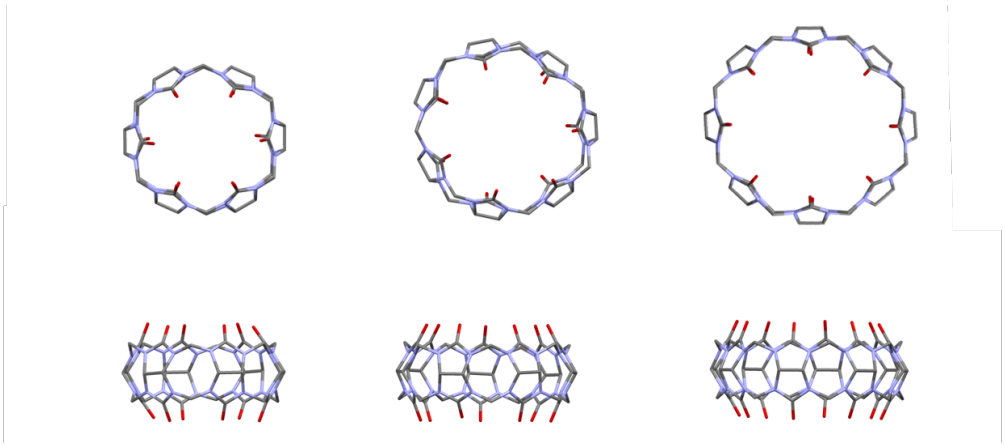

Figure I-6. X-ray crystal structure of CB6, CB7, and CB8, respectively, from left to right.

[12] W. L. Mock, N. Y. Shih, *J. Org. Chem.* **1983**, *48*, 3618–3619.
[13] W. L. Mock, T. A. Irra, J. P. Wepsiec, T. L. Manimaran, *J. Org. Chem.* **1983**, *48*, 3619–3620.
[14] R. Hoffmann, W. Knoche, C. Fenn, H.-J. Buschmann, *J. Chem. Soc. Faraday Trans.* **1994**, *90*, 1507–1511.
[15] W. L. Mock, N. Y. Shih, *J. Org. Chem.* **1986**, *51*, 4440–4446.
[16] J. Kim, I. S. Jung, S. Y. Kim, E. Lee, J. K. Kang, S. Sakamoto, K. Yamaguchi, K. Kim, *J. Am. Chem. Soc.* **2000**, *122*, 540–541.
[17] A. Day, A. P. Arnold, R. J. Blanch, B. Snushall, *J. Org. Chem.* **2001**, *66*, 8094–8100.
[18] Considering the number of publications related to this family of molecules.
[19] S. Liu, C. Ruspic, P. Mukhopadhyay, S. Chakrabarti, P. Y. Zavalij, L. Isaacs, *J. Am. Chem. Soc.* **2005**, *127*, 15959–15967.
[20] W. S. Jeon, K. Moon, S. H. Park, H. Chun, Y. H. Ko, J. Y. Lee, E. S. Lee, S. Samal, N. Selvapalam, M. V Rekharsky, et al., *J. Am. Chem. Soc.* **2005**, *127*, 12984–12989.
[21] M. V Rekharsky, Y. H. Ko, N. Selvapalam, K. Kim, Y. Inoue, *Supramol. Chem.* **2007**, *19*, 39–46.

I.2.2. Functionalization

Although the discovery of new homologs broadened the scope of the CBn chemistry, the invention of distinguished applications was still limited by the low solubility in common organic solvents and the difficulty in introducing new functional groups. The first modified CBn was reported by Stoddart in 1992, who synthesized the equatorially methylated CB5 (Me_{10}CB5) by condensation of dimethylglycoluril with formaldehyde.[22] Unfortunately, the introduction of Me groups at the periphery of CBs did not improve their solubility. Since then, many partially and entirely substituted CBn were prepared in an attempt to overcome this remaining limitation.[23,24,25,26] The condensation of cyclohexanolgycoluril with formaldehyde produced a CB5 derivative with fused cyclohexyl rings decorating the periphery, which was, interestingly, soluble in water (*ca.* 2 x 10^{-1} M) and DMF (*ca.* 3 x 10^{-2} M).[24] A different strategy consisted of the reaction of a blend of glycoluril and substituted glycoluril with formaldehyde to give a mixture of partially substituted CBn. The first partially substituted cucurbituril, diphenylcucurbit[6]uril (Ph_2CB6), was reported by Nakamura.[25] However, the reaction of glycoluril derivatives favored the formation of the smaller CBn homologs: CB5 and CB6, and considering that simple alkylation did not enable further functionalization,[27] different strategies were needed. For many years it was a general belief that the direct introduction of functional groups on the CBs surface was impossible, mainly because of their high chemical stability. However, in 2003, a direct method to prepare perhydroxylated CBn by oxidation of cucurbiturils with persulfates was reported (Scheme I-1).[28a] The product obtained by this procedure allowed further functionalization, leading to enhanced solubility in organic solvents. Unfortunately, while the yield for the smaller members CB5 and CB6 was over 40%, the higher homologs CB7 and CB8 gave yields below 5% due to the instability of the perhydroxylated counterparts. Further improvements and optimization on the reaction conditions

[22] A. Flinn, G. C. Hough, J. F. Stoddart, D. J. Williams, *Angew. Chem. Int. Ed.,* **1992**, *31*, 1475.
[23] A. Day, A. P. Arnold, R. J. Blanch, B. Snushall, *J. Org. Chem.,* **2001**, *66*, 8094.
[24] J. Z. Zhao, H.-J. Kim, J. Oh, S.-Y. Kim, J. W. Lee, S. Sakamoto, K. Yamaguchi, K. Kim, *Angew. Chem., Int. Ed.*, **2001**, *40*, 4233.
[25] H. Isobe, S. Sato, E. Nakamura, *Org. Lett*., **2002**, *4*, 1287.
[26] J. Lagona, J. C. Fettinger, L. Isaacs, *Org. Lett.,* **2003**, *5*, 3745.
[27] So far, there are no reports suggesting the opposite.

afforded better yields on the monofunctionalization of CB7.[28b] Another direct oxidative functionalization approach consisting of the perhydroxylation of CB6 with potassium persulfate (KPS) was introduced by Scherman and co-workers in 2003.[29] These authors also reported the first fully-characterized monofunctional CB6 derivatives, with ammonium persulfate (APS) and solubilizing agents such as bisimidazolium compounds to increase the concentration of the reaction mixture;[30] and in 2017, the monohydroxylation of CB7.[31] On the same line, Ouari and co-workers reported the direct oxidation with hydrogen peroxide, initiated by light for the formation of monofunctionalized CBn (n = 5–8).[32] This last method, the photochemical oxidation of CBs, appears to be one of the best ways to access monohydroxylation of CB derivatives, although the products need to be separated and provide roughly 30% of monofunctionalized CB7 upon purification by silica gel chromatography. More recently, in 2018, Kaifer reported a direct and straightforward method to prepare pure monohydroxylated CB7-OH through the direct oxidation of its precursor, CB7. The reaction mixture allowed straightforward isolation of both the product and the unreacted starting material; however, the conversion is still shallow (14%).[33]

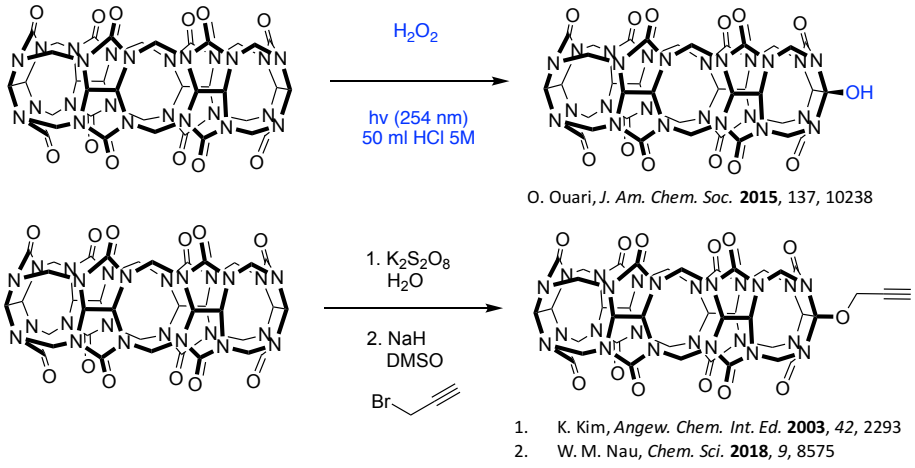

Scheme I-1. Examples of direct functionalization.

[28] A) S. Y. Jon, N. Selvapalam, D. H. Oh, J.-K. Kang, S.-Y. Kim, Y. J. Jeon, J. W. Lee, K. Kim, *J. Am. Chem. Soc.* **2003**, *125*, 10186. B) Y. Ahn, Y. Jang, N. Selvapalam, G. Yun, K. Kim, *Angew. Chem. Int. Ed.* **2013**, *52*, 3140–3144.
[29] S. Y. Jon, N. Selvapalam, D. H. Oh, J.-K. Kang, S.-Y. Kim, Y. J. Jeon, J. W. Lee, K. Kim, *J. Am. Chem. Soc.*, **2003**, *125*, 10186–10187.
[30] N. Zhao, G. O. Lloyd, O. A. Scherman, *Chem. Commun.*, **2012**, *48*, 3070–3072.
[31] J. A. McCune, E. Rosta, O. A. Scherman, *Org. Biomol. Chem.* **2017**, *15*, 998–1005.
[32] M. M. Ayhan, H. Karoui, M. Hardy, A. Rockenbauer, L. Charles, R. Rosas, K. Udachin, P. Tordo, D. Bardelang, O. Ouari, *J. Am. Chem. Soc.* **2015**, *137*, *32*, 10238–10245.
[33] N. Dong, J. He, T. Li, A. Peralta, M. R. Avei, M. Ma, A. E. Kaifer, *J. Org. Chem.* **2018**, *83*, 5467–5473.

Using a building-block approach, Isaacs synthesized monofunctionalized CB7 derivatives through reaction of the acyclic glycoluril hexamer with a glycoluril surrogate delivering a monofunctionalized CB7 with a chloroalkyl tether that could be transformed into the azide functional group for later conjugation after the alkyne azide cycloaddition reaction (click reaction).[34] Alternatively, monofunctional CB6 was obtained by the condensation of the same glycoluril hexamer with modified aldehydes or aldehyde surrogates (Scheme I-2).[35]

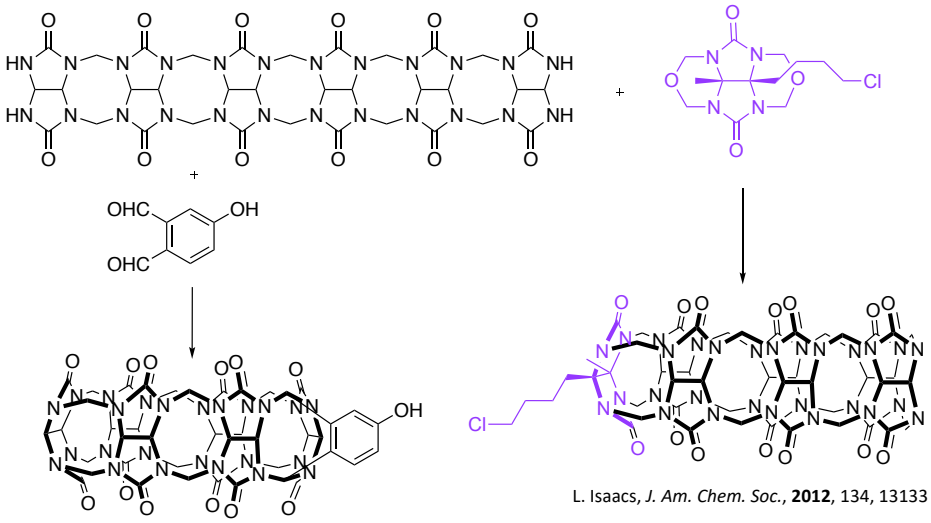

Scheme I-2. Examples of building block approach.

In summary, although there is a wide range of possibilities for CBn functionalization, they all have in common their difficulty to either obtain high-ratios of monofunctionalized CBn or acceptable yields and experimentally affordable synthetic procedures. To date, it is a general agreement that the introduction of any functionality on the periphery of CBn constitutes a formidable task,[36] in part because of the rigid CBn structure, the poor solubility, and the limitation of only C–H reactive sites available for activation. Since CBn has a robust chemical structure that is resistant to strong acids and bases, only a limited range of chemical modifications can be applied. Nevertheless, the development of methods allowing the easy introduction of a single functionality

[34] A) L. Cao, G. Hettiarachchi, V. Briken, L. Isaacs, *Angew. Chemie Int. Ed.* **2013**, *52*, 12033–12037. B) B. Vinciguerra, L. P. Cao, J. R. Cannon, P. Y. Zavalij, C. Fenselau, L. Isaacs, *J. Am. Chem. Soc.*, **2012**, *134*, 13133.
[35] A) D. Lucas, T. Minami, G. Iannuzzi, L. Cao, J. B. Wittenberg, P. Anzenbacher, L. Isaacs, *J. Am. Chem. Soc.* **2011**, *133*, 17966–17976. B) L. Cao, L. Isaacs, *Org. Lett.* **2012**, *14*, 3072–3075.
[36] K. Kim, N. Selvapalam, Y. H. Ko, K. M. Park, D. Kim, J. Kim, *Chem. Soc. Rev*. **2007**, *36*, 267–279.

to form monofunctionalized derivatives is of particular interest, and still represents a synthetic challenge.

Prominent applications arise from the functionalization of CBs. For example, the possibility to immobilize them onto solid surfaces. The preparation of a synthetic underwater adhesive or "supramolecular Velcro" was reported in 2013.[28b] Two polymer solid surfaces were coated with CB7 (the host or "loop") and a cationic ferrocenyl derivative (the guest or "hook"), respectively. When they were pressed together under wet conditions, they adhered to each other with adhesion forces (1.12 MPa) stronger than those shown by industrial Velcro (0.08 MPa). Moreover, the surfaces could be separated by mechanical force or by oxidation of the guest molecule, whose oxidized form does not present such strong binding affinity with the host. Other applications aim to achieve orthogonal paths for the immobilization of biomolecules. The biotin–streptavidin system for the immobilization and purification of tagged biomolecules has been, for many years, the method of choice in this field despite its limitations: difficult dissociation, irreversibility, and denaturation by organic solvents or high temperatures among others. The interest in finding compatible and orthogonal alternatives led researchers to strive to develop host–guest systems, with binding affinities similar to or higher than those reached by biological systems. Since the discovery of ultra-high affinity host–guest pairs, several studies demonstrated the applicability of these novel synthetic macrocycles and provided alternative routes to the immobilization of biomolecules. Moreover, the immobilization of receptors on a solid surface is essential for developing a sensor. To this end, CB7 was anchored onto different surfaces that could selectively immobilize ferrocenyl-substituted biomolecules, giving rise to the preparation of complex systems that could be used for the enrichment of proteins or as biosensors.[37,38] Another example in molecular recognition consisted of anchoring CB6 on a modified glass surface to recognize small molecules and ions.[39]

[37] I. Hwang, K. Baek, M. Jung, Y. Kim, K. M. Park, D.-W. Lee, N. Selvapalam, K. Kim, *J. Am. Chem. Soc.* **2007**, *129*, 4170–4171.
[38] W. Li, A. T. Bockus, B. Vinciguerra, L. Isaacs, A. R. Urbach, *Chem. Commun.* **2016**, *52*, 8537–8540.
[39] S. Y. Jon, N. Selvapalam, D. H. Oh, J.-K. Kang, S.-Y. Kim, Y. J. Jeon, J. W. Lee, K. Kim, *J. Am. Chem. Soc.* **2003**, *125*, 10186.

I.2.3. Host–guest complexes

To comprehend the ability of CBs to form strong host–guest complexes, we first have to understand the structure and properties of the different CBn homologs (Table I-1). The cucurbituril family harbors highly symmetric, cyclic methylene-bridged glycoluril oligomers with a hydrophilic rim or "portal" on each side comprised of urea carbonyls and a hydrophobic interior or cavity. The portals, which are the entrance to the cavity, are roughly 2 Å narrower than the pit itself. That provides a steric barrier to guest association and dissociation. The distortion of hosts by guest inclusion or packing is directly proportional to the size of the host because of its gain in flexibility. Since the volume of the cavity increases through CB5 to CB8, it is expected that each family member will interact with different guests (Table I-2).

Table I-1. Structural parameters and physical properties of CBn.

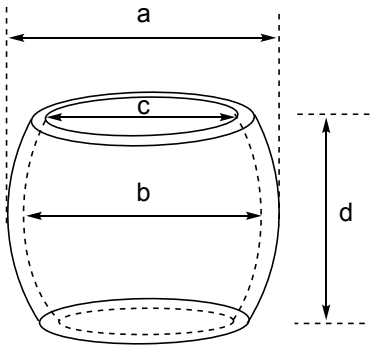

Entry		CB5	CB6	CB7	CB8
1	Outer diameter (a)	13.1	14.4	16.0	17.5
2	Inner cavity (b)	4.4	5.8	7.3	8.8
3	Portal diameter (c)	2.4	3.9	5.4	6.9
4	Height (d)	9.1	9.1	9.1	9.1
5	Volume [Å^3]	82	164	279	479
6	Water solubility [mM]	20–30	0.018	20–30	<0.01
7	Stability [ºC]	>420	425	370	>420

For example, CB5 only encapsulates small gas molecules and makes exclusion complexes with metal cations;[40] CB6 accommodates alkyl ammoniums and small cyclic molecules,[12,15] it makes stable complexes with alkyl diammonium that can bind both portals and thread their alkyl chain through the hole (e.g., 1,5-pentanediammonium);[21] CB7 encapsulates larger and bulkier molecules

[40] H. -J. Buschmann, E. Cleve, K. Jansen, A. Wego, E. Schollmeyer, *J. Incl. Phenom. Macrocycl. Chem.* **2001**, *40,* 117.

such as adamantane derivatives, it exhibits the highest binding constant reported for a synthetic host–guest system with an attomolar dissociation constant;[41] finally, CB8 can even handle two guests in the cavity.[42] Thus, the features and the properties of the CBn are key for molecular recognition.

The principal features that allow CBs to form highly stable host–guest complexes can be divided into two: the properties of the portal, and the attributes of the cavity. The highly polarized and strongly-negative electrostatic potential of the portal facilitates ion–dipole interactions with metal and organic cations.[43,44] On the other hand, the hydrophobic cavity is remarkably non-polar and unpolarizable. It offers no bonds, functional groups, nor lone pairs of electrons pointing into the interior of the CBn and, hence, facilitates hydrophobic interactions.[45] Another consideration is the size and shape complementarity between host and guest to maximize van der Waals forces between the cavity wall and the guest. Finally, desolvation of the guest and the cavity also represents a major driving force of complexation, and the rigidity of the host molecule also helps stabilize the complex. Consequently, ion-dipole interactions, hydrophobic effects, and size complementarity need to be considered when examining CB host–guest complexes. The molecules with the highest affinities tend to be appropriately sized amphiphilic molecules with a cationic group and are preorganized to concurrently make as many interactions with the CBn as possible.

There are several ways to measure binding affinities, the two most common are NMR competition experiments with other guests, which will be further discussed in chapter IV, and multistep ITC experiments with increasing affinity guests. An important consideration is the media that the binding studies are measured in because it has a significant influence on the binding constants. Furthermore, when performing binding studies, it is crucial to bear in mind that experiments done in different media are not directly comparable.

[41] L. Cao, M. Šekutor, P. Y. Zavalij, K. Mlinarić-Majerski, R. Glaser, L. Isaacs, *Angew. Chem. Int. Ed.* **2014**, *53*, 988–993.
[42] D. Sigwalt, M. Šekutor, L. Cao, P. Y. Zavalij, J. Hostaš, H. Ajani, P. Hobza, K. Mlinarić-Majerski, R. Glaser, L. Isaacs, *J. Am. Chem. Soc.* **2017**, *139*, 3249–3258.
[43] S. Senler, W. Li, M. H. Tootoonchi, S. Yi, A. E. Kaifer, *Supramol. Chem.* **2014**, *26*, 677–683.
[44] J. W. Lee, S. Samal, N. Selvapalam, H.-J. Kim, K. Kim, *Acc. Chem. Res.* **2003**, *36*, 621–630.
[45] C. Marquez, W. M. Nau, *Angew. Chem. Int. Ed.* **2001**, *40*, 4387–4390.

Table I-2. Representative guests of CBn.

CB5	CB6	CB7	CB8
N_2, O_2, Ar	Benzene	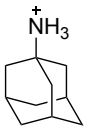	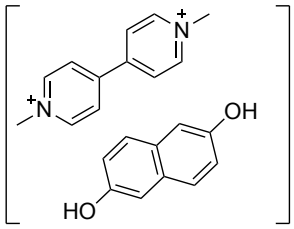
NH_4^+	CO_2	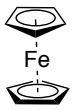	
Pd^{2+}	$H_3N^+(CH_2)_nNH_3^+$	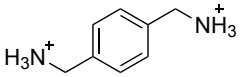	

As early mentioned, the properties of the CBn portal and cavity play a crucial role in molecular recognition, and considering the appreciable solubility of CB7 in water, the exploration of host–guest chemistry with biomolecules has been extensively investigated. Some examples include the recognition by CB7 of phenylalanine,[46] peptides and small proteins such as insulin,[47] and amino saccharides.[48]

I.2.4. Thermodynamics and kinetics

Thermodynamics

CB7 stands out amongst the other members of the cucurbituril family because, in addition to its appreciable solubility in water, it exhibits some of the highest binding constants reported for synthetic host–guest pairs.[41] There are three main reasons why CBs can make such high-affinity interactions. First, they can offset the entropy-enthalpy compensation principle, which describes how molecular recognition enthalpically drives the formation of most host–guest complexes,[49] but an entropic penalty is usually paid because of reduced conformational flexibility. However, this can be neutralized by solvation entropy that tends to be positive due to desolvation of the cavity, the guest and the

[46] J. W. Lee, H. H. L. Lee, Y. H. Ko, K. Kim, H. I. Kim, *J. Phys. Chem. B.* **2015**, *119*, 4628–4636.
[47] J. M. Chinai, A. B. Taylor, L. M. Ryno, N. D. Hargreaves, C. A. Morris, P. J. Hart, A. R. Urbach, *J. Am. Chem. Soc.* **2011**, *133*, 8810–8813.
[48] Y. Jang, R. Natarajan, Y. H. Ko, K. Kim, *Angew. Chem. Int. Ed.* **2014**, *53*, 1003–1007.
[49] S. Moghaddam, C. Yang, M. Rekharsky, Y. H. Ko, K. Kim, Y. Inoue, M. K. Gilson, *J. Am. Chem. Soc.* **2011**, *133*, 3570–3581.

portal,[50,51] the entropy of formation is often net favorable, whereas in other systems it is usually a penalty. Second, hydrophobic interactions are strongly exothermic because of “high energy water”[52] molecules in the cavity. The water molecules inside the cavity cannot form many H-bonds in the hydrophobic cavity. Thus, guest binding releases these water molecules and relieves their energetic frustration. Third, the rigid host molecules discriminate among the size and the shape of the guests, maximizing the selectivity for some tailor-made compounds, unlike more flexible hosts such as CDs.

The ion–dipole interactions are enthalpically neutral because the ion–dipole formed between the guest and CB7 is enthalpically favorable but, at the same time, counterbalanced by the loss of solvation interactions between water molecules and the cationic guest and the CB portal. The net result is that the formation of these ion–dipole interactions is driven entirely by entropy.[49] Experimental evidence supports this hypothesis.[53]

Hydrophobic effects are enthalpically dominated because the water molecules inside CBs are very restricted in the number of H-bonds they can establish, and entropically favored by the displacement of water molecules to the bulk.[54] For narrow containers such as CB5, there are few water molecules inside, and in larger containers such as CB8, there is little difference between the bulk solvent and the encapsulated solvent. Thereby, CB7 complexes have higher exothermic driving forces followed by CB6.

Kinetics

The cavity of CBn has a larger diameter than that of its portal, which means that the portal is a kinetic barrier to guest ingress and egress. This translates into a slow association and even *slower dissociation rate*, due to the constrictive binding mode. Thus, the wider the guest, the slower the complex formation. Moreover, it is also suggested that CBn can form both exclusion and inclusion complexes.[14]

[50] M. V Rekharsky, T. Mori, C. Yang, Y. H. Ko, N. Selvapalam, H. Kim, D. Sobransingh, A. E. Kaifer, S. Liu, L. Isaacs, et al. *Proc. Natl. Acad. Sci.* **2007**, *104*, 20737.
[51] J. D. Chodera, D. L. Mobley, *Annu. Rev. Biophys.* **2013**, *42*, 121–142.
[52] High energy water is a term used by some authors to describe the situation of water molecules inside the cavity of cucurbituril, where compression should lead to a high energy level.
[53] X. Ling, S. Saretz, L. Xiao, J. Francescon, E. Masson, *Chem. Sci.* **2016**, *7*, 3569–3573.
[54] F. Biedermann, V. D. Uzunova, O. A. Scherman, W. M. Nau, A. De Simone, *J. Am. Chem. Soc.* **2012**, *134*, 15318–15323.

Further investigation into the binding mechanism suggested that the rate of ingress is higher when the guest is protonated (i.e., alkylammonium species ingress faster than their unprotonated counterparts, due to the involvement of free amines in the binding mechanism). Two different mechanisms for the formation of a protonated host–guest complex has been suggested (Figure I-7).[55] On the one hand, the free amine guest can enter the CB6 cavity and then be protonated. On the other hand, the alkyl ammonium forms an exclusion complex with the portal due to the formation of ion–dipole interactions, and then, a "flip-flop" mechanism occurs allowing the alkyl chain to move into the cavity. Additionally, the rates of ingression are slower in the presence of metal or other cationic species.

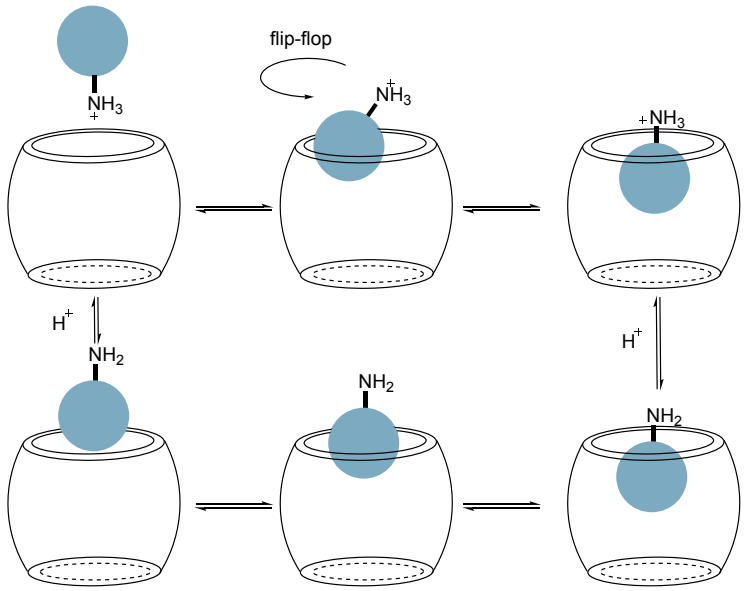

Figure I-7. Binding mechanism of bulky alkyl ammoniums to CB6.

CB7 seems to form host–guest complexes in a single step, and the complex dissociation rate tends to be slow for small guests.[56] For many other adamantyl and ferrocenyl derivatives, the mechanism is not yet well understood. In any case, the complexes are strong enough to persist in biological media, where there are many interfering molecules, allowing supramolecular chemistry to be applied in biological settings.[57,58]

[55] C. Márquez, R. R. Hudgins, W. M. Nau, *J. Am. Chem. Soc.* **2004**, *126*, 5806–5816.
[56] H. Tang, D. Fuentealba, Y. H. Ko, N. Selvapalam, K. Kim, C. Bohne, *J. Am. Chem. Soc.* **2011**, *133*, 20623–20633.
[57] E. A. Appel, F. Biedermann, U. Rauwald, S. T. Jones, J. M. Zayed, O. A. Scherman, *J. Am. Chem. Soc.* **2010**, *132*, 14251–14260.

I.3. Magnetic nanoparticles and polystyrene resins as immobilization supports

Magnetic nanoparticles are a type of nanoparticles (generally, organic or inorganic materials with diameters ranging from 1 to 100 nm)[59] that can be formed from a variety of magnetic materials such as iron, cobalt, nickel, metal oxides such as Fe_3O_4, ferrites, and others. They can be prepared as monodisperse magnetic nanoparticles through a variety of physical and chemical procedures.[60] The reaction parameters: time, temperature, concentration, nature of present additives, etc. are essential to control the size and the shape of the particles.

Nanoparticles of metal oxides such as iron oxides present multiple crystal structures. The most frequently encountered iron oxides are FeO, Fe_3O_4, and γ-Fe_2O_3. Interestingly, they present different magnetic properties. For example, FeO is paramagnetic at room temperature and antiferromagnetic at 183 K while maghemite, γ-Fe_2O_3, and magnetite, Fe_3O_4, are ferromagnetic. Some magnetic nanoparticles also exhibit superparamagnetic properties. They become magnetized upon exposure to a magnetic field but have no permanent magnetization (remanence) once the field is turned off. In other words, when an external magnetic field is applied, the superparamagnetic iron oxide nanoparticles (SPIONS) tend to align along the magnetic field, leading to a net magnetization. In the absence of this external magnetic field, the dipoles are randomly oriented, and there is no net magnetization. Additionally, they have a large surface area to volume ratio and possess high surface energies. For this reason, they tend to agglomerate in order to reduce their surface energy by strong dipole–dipole attractions between particles. The colloidal suspension of magnetic particles, however, can be stabilized by long-chain surfactant or a proper surface coating agent, which additionally provides a surface area that can be further functionalized to widen up the range of applications.

---

[58] K. M. Park, J.-A. Yang, H. Jung, J. Yeom, J. S. Park, K.-H. Park, A. S. Hoffman, S. K. Hahn, K. Kim, *ACS Nano* **2012**, *6*, 2960–2968.
[59] G. Schmid, Ed. *Nanoparticles: from theory to application*. Wiley-VCH: Weinheim, **2004**.
[60] Standard procedures are sputtering, metal evaporation, grinding, electrodeposition, solution-phase metal salt reduction, and decomposition of neutral organometallic precursors.

Synthetic routes towards magnetic nanoparticles have been developed to deliver efficient syntheses that provide shape-controlled, highly stable, and monodisperse magnetic nanoparticles. The most popular methods are the co-precipitation and the thermal decomposition or reduction. The preparation of iron oxide nanoparticles through co-precipitation method is straightforward for magnetite.[61,62,63] Basically, Fe_3O_4 can be prepared in basic conditions by adding Fe^{2+} and Fe^{3+} (1:2) species in an aqueous solution under an inert atmosphere, either at room or high temperature. The resulting black precipitate is magnetite. The size, shape, and composition of the nanoparticles obtained, strongly depend on the type of salts used, the ratio between Fe^{2+} and Fe^{3+}, the pH or the ionic strength of the media, and the temperature. Fortunately, when all these parameters are established, the reaction is highly reproducible. One of the first examples for the preparation of magnetite nanoparticles was reported in 1981 by Massart.[64] The reaction was carried out in alkaline and acidic media where 1 M ferric chloride and 2 M ferrous chloride were added to an ammonia solution. The obtained precipitate had an average size of 12 nm, determined by X-ray diffraction. In order to forestall oxidation by air and agglomeration, magnetite nanoparticles are usually coated with inorganic or organic molecules during the precipitation process under oxygen-free conditions, by bubbling an inert gas. It has been shown that bubbling inert gas confers stability to smaller size nanoparticles in comparison with other methods not involving the removal of oxygen.[65]

On the other hand, the preparation of nanoparticles through thermal decomposition methods allow the synthesis of magnetite nanoparticles with a high degree of monodispersity and reasonable control on the size. This method consists of the decomposition of iron precursors dissolved in high boiling point solvents in the presence of surfactants or coating agents. The most common sources of iron are $[Fe(CO)_5]$, $[Fe(acac)_3]$, etc. For instance, the reaction of $[Fe(acac)_3]$ in the presence of oleic acid, oleylamine, and 1,2-hexadecanediol at

[61] S. Laurent, D. Forge, M. Port, A. Roch, C. Robic, L.-V. Elst, R.-N. Muller, *Chem. Rev.* **2008**, *108*, 2064.
[62] A. –K. Gupta, M. Gupta, *Biomaterials* **2005**, *26*, 3995.
[63] W. Wu, Q. He, C. Jiang, *Nanoscale Res. Lett.* **2008**, *3*, 397.
[64] Massart, R., *IEEE Trans. Magn.* **1981**, *17*, 1247.
[65] Kim, D. K.; Zhang, Y.; Voit, W.; Rao, K. V.; Muhammed, M., *J. Magn. Magn. Mater.* **2001**, *225*, 30.

high temperature was reported by Sun.[66] This procedure delivered spherical nanoparticles with a tunable diameter from 4 to 20 nm. The hydrophobicity could also be controlled by the addition of bipolar surfactants.

The surfactant used as a stabilizing agent plays a vital role in the nucleation and growth of the nanoparticles in solution. It is responsible for the nature of the final aggregates, and hence, careful use of the surfactant allows control over the size, the shape and the magnetic and chemical properties. Common coating agents are amphiphilic capping molecules like carboxylates (e.g., fatty acids) diols and alkyl amines. Oleic acid is widely used for its ability to make very uniform and monodisperse nanocrystals.[67] Other common carboxylates include citric acid or even smaller propanoic or butanoic acids.

Coating the iron oxide nanoparticles ensures stability, prevents them from aggregation, and also provides a convenient way to functionalize the particle surface. For example, silica-coated particles facilitate the dispersion in a wide range of solvents and allow better control on the shape of the final particle while keeping them from aggregation in liquid. It also improves its chemical stability and protects them. The main drawback, though, is a loss of the magnetization, which is directly proportional to the thickness of the coating layer. In order to coat the magnetic nanoparticles surface with a silica layer, Lu described the direct coating of tetraethyl orthosilicate (TEOS) to water-dispersed surfactant stabilized iron oxide magnetic nanoparticles under basic conditions. Careful control over the amount of TEOS enabled control of the thickness of the silica shell.[68] Although polymers or silica coating of nanoparticles are the most common, gold protected magnetic nanoparticles, and carbon coatings have also been studied.[69] Some advantages of the later include higher chemical and thermal stability and better biocompatibility. However, better synthetic procedures still need to be developed. Silanes can easily be grafted onto the nanoparticle and are the most common modifiers for the metal surface. A wide

[66] S. Sun, H. Zeng, D. –B. Robinson, S. Raoux, P. –M. Rice, S. –X. Wang, G. Li, *J. Am. Chem. Soc.* **2004**, *126*, 273.
[67] Y. Sahoo, H. Pizem, T. Fried, D. Golodnitsky, L. Burstein, C. –N. Sukenik, G. Markovich, *Langmuir* **2001**, *17*, 7907.
[68] Y. Lu, Y. –D. Yin, B. –T. Mayers, Y. –N. Xia, *Nano Lett.* **2002**, *2*, 183.
[69] L. –Y. Wang, J. Luo, Q. Fan, M. Suzuki, I. –S. Suzuki, M. –H. Engelhard, Y. –H. Lin, N. Kim, J. –Q. Wang, C. -J. Zhong, *J. Phys. Chem. B* **2005**, *109*, 21593.

variety of them are available, including alkoxysilanes (≡SiOR), hydrogensilane (SiH), chlorosilane (SiCl), etc., that allow the introduction of numerous functionalities and help to modify the intrinsic properties of these nanomaterials. For example, the presence of silanol groups allows derivatization on the surface with a variety of functional groups.[70]

The functionalization of iron oxide magnetic nanoparticles by click chemistry has been intensely investigated, and particularly by the copper-catalyzed alkyne azide cycloaddition (CuAAC) reaction. That requires the preparation of nanoparticles bearing either a terminal alkyne or an azide group. The reaction is robust, proceeds in high yields, without the formation of byproducts and allows a wide range of different experimental conditions.[71,72] Moreover, the functionalization of magnetic nanoparticles opens up a range of applications that have been exploited in the fields of catalysis,[73] MRI,[74] ion and molecular recognition, sensing,[75] and extraction. The notorious advantages that immobilized catalysts bring to the field of catalysis are their straightforward removal from reaction mixtures, the possibility to recycle and reuse them, and attractive routes to scalability for industrial processes. Those are the reasons why our group has devoted myriad efforts to investigate thoroughly, along with the use of polystyrene resins, alternative paths to homogeneous catalysis (Figure I-8).[76]

[70] A. Ulman, *Chem. Rev.* **1996**, *96*, 1533.
[71] G. Chouhan, D. Wang, H. Alper, *Chem. Commun.* **2007**, 4809.
[72] L. Polito, D. Monti, E. Caneva, E. Delnevo, G. Russo, D. Prosperi, *Chem. Commun.* **2008**, 621.
[73] S. Shylesh, V. Schünemann, W. –R. Thiel, *Angew. Chem. Int. Ed.* **2010**, *49*, 3428.
[74] J. Kim, H. –S. Kim, N. Lee, T. Kim, H. Kim, T. Yu, I. –C. Song, W. –K. Moon, T. Hyeon, *Angew. Chem. Int. Ed.* **2008**, *47*, 8438
[75] I. S. Lee, N. Lee, J. Park, B. –H. Kim, Yong-Weon; T. Kim, T. –K. Kim, I. –H. Lee, S. –R. Paik, T. Hyeon, *J. Am. Chem. Soc.* **2006**, *128*, 10658.
[76] Among other: (a) P. Riente, C. Mendoza, M. A. Pericàs, *J. Mater. Chem.* **2011**, *21*, 7350–7355. (b) P. Riente, J. Yadav, M. A. Pericàs, *Org. Lett.* **2012**, *14*, 3668–3671. (c) C. A. Mak, S. Ranjbar, P. Riente, C. Rodríguez-Escrich, M. A. Pericàs, *Tetrahedron* **2014**, *70*, 6169–6173. (d) S. Ranjbar, P. Riente, C. Rodríguez-Escrich, J. Yadav, K. Ramineni, M. A. Pericàs, *Org. Lett.* **2016**, *18*, 1602–1605.

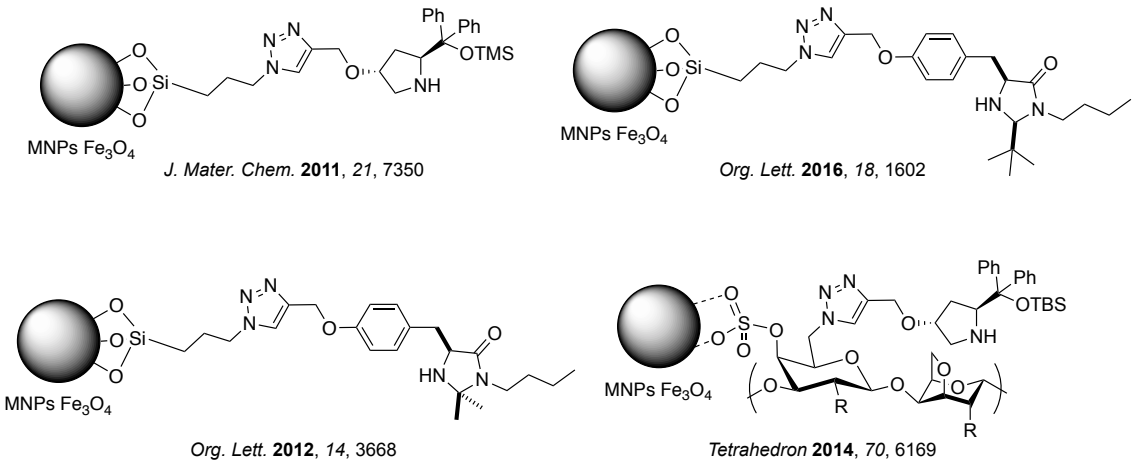

Figure I-8. Immobilization of chiral catalysts on iron oxide magnetic nanoparticles.

Polystyrene resins

The use of insoluble polymers for the immobilization of reagents and catalysts became popular after the pioneering work of Merrifield, who developed the solid-phase peptide synthesis, back in the 1960s,[77] and earned him the Nobel prize in 1984. Since then, the use of insoluble resins has been growing because they surmise a simple way to isolate the reaction products from the crude mixture and provide an easy way to recover and reuse the usually expensive catalysts by simple filtration. Because of this, they have attracted much attention to chemical industries—that harness their usability in continuous flow processes, where the reagents are continuously streamed through a reactor containing the immobilized catalyst.

There are two main groups of polystyrene-based polymers. The macroporous polymers, with a high cross-linking degree (>10% of divinylbenzene, DVB) and permanent pore structure. They tend to be chemically more stable and swell in organic solvents. On the other hand, the microporous polymers, with a cross-linking degree of 1–2% of DVB, which tend to swell in non-protic solvents. The swelling property is a parameter that must be considered because it grants the reagent accessibility through the pores, and hence, reaching the catalytic site of the polymeric catalyst. The so-called Merrifield resin, functionalized with chloromethyl groups, is a well-known example of this type (Figure I-9).

[77] Merrifield, R. B. *J. Am. Chem. Soc.* **1963**, *85*, 2149-2154.

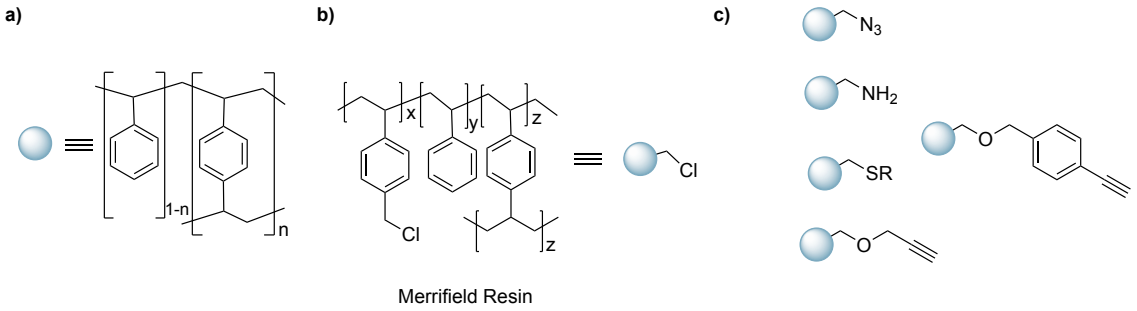

Figure I-9. a) Representation of a polystyrene-DVB polymer. b) Representation of the Merrifield resin, functionalized with chloromethyl groups. c) Representation of common derivatives of the Merrifield resin.

Due to its chemical stability, the appropriate swelling in organic solvents and the easy recovery by simple filtration, the Merrifield resin has been the support of choice in the Pericàs group for the immobilization of many chiral organocatalysts and ligands (Figure I-10 and Figure I-11).[78]

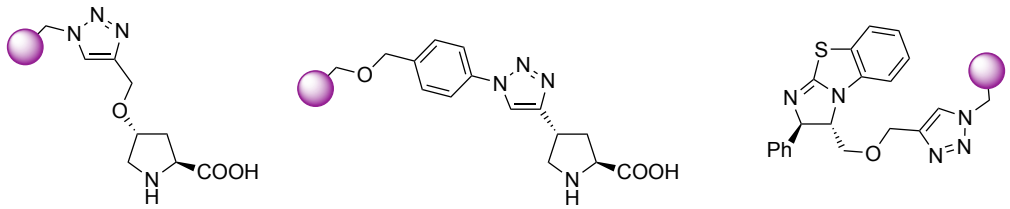

Org. Lett. **2006**, *8*, 4653
Org. Lett. **2007**, *9*, 1943

ChemSusChem **2012**, *5*, 320
Green Chem. **2016**, *18*, 3507

ACS catal **2016**, *6*, 348

Figure I-10. Chiral catalysts immobilized onto polystyrene resins.

[78] Among other: (a) P. Llanes; S. Sayalero; C. Rodríguez-Escrich; M. A. Pericàs, *Green Chem.* **2016**, *18*, 3507-3512. (b) J. Izquierdo-Ferrer; M. A. Pericàs, *ACS Catal.* **2016**, *6*, 348-356. (c) C. Ayats, C; A. H. Henseler; M. A. Pericàs, *ChemSusChem* **2012**, *5*, 320-325.

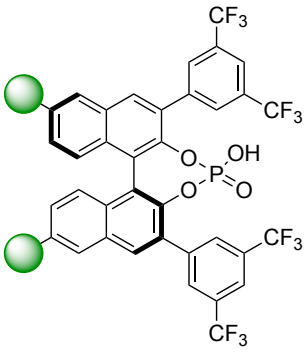

ACS Catal. **2016**, *6*, 7647

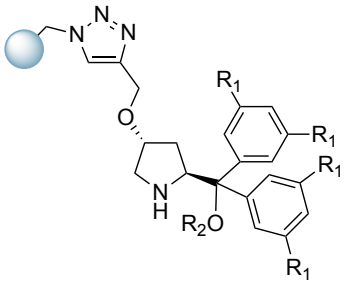

Adv. Synth. Catal. **2012**, *354*, 2971 (R_1= H, R_2 = TBS)
Chem. Eur. J. **2013**, *19*, 10814 (R_1= H, R_2 = TIPS)
Chem. Eur. J. **2014**, *20*, 13089 (R_1= CF_3, R_2 = OH)

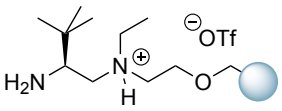

ACS Catal. **2017**, *7*, 1383

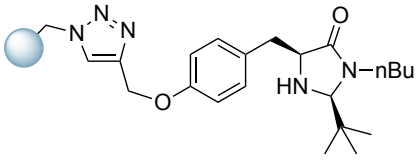

Org. Lett. **2016**, *18*, 1602

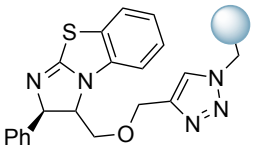

Angew. Chem. Int. Ed. **2017**, *56*, 15068

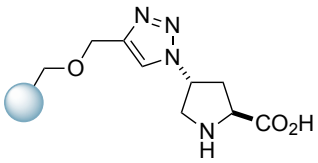

Org. Lett. **2008**, *10*, 337

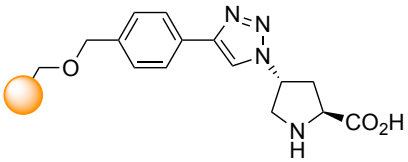

ChemSusChem **2012**, *5*, 320

Polystyrene (1% DVB) Polystyrene (2% DVB) Polystyrene (8% DVB)

Figure I-11. Immobilization of chiral catalysts on polystyrene resins.

2

CHAPTER II

Crafting nanodevices for molecular recognition and catalysis

CHAPTER II

Crafting nanodevices for molecular recognition and catalysis

II.1. Introduction

II.1.1. General considerations

When we started the project in the fall of 2015, cucurbiturils (CBs) were already consolidated as one of the most promising macrocycles for supramolecular chemistry. In financial terms, if you were to compare the rate at which the number of publications related to cucurbiturils was growing over the years with some other charts from the stock market, you would notice that it resembled a lot like an imminent "stock market bubble" (Figure II-1).[1] Is this popularity due to some milestones being reached fast enough as to push the research on cucurbiturils up to the next level before it has time to settle down? Are we in front of the "bitcoins of supramolecular chemistry"? In any case, the research on CBs will keep attracting scientists, and growing along with the imagination of researchers that come up with fresh ideas that open up new possibilities that are usually best fits for cucurbiturils over any other macrocycle and, probably, the *status quo* will prevail until a new macrocycle capable of outperforming the incredible properties of cucurbiturils is born. Bambusurils, pillararenes or inverted CBs were born after CBs but, it does not seem that they came to replace them but to coexist. With all this, and maintaining this financial simile, we could say that we entered a very competitive market and we were just a small fish in the ocean, a "red ocean" as prof. Chan Kim would state.[2,3]

[1] A type of economic bubble (a situation in which asset prices appear to be based on implausible views about the future) that drives stock prices above their value concerning some system of stock valuation. It is sometimes attributed to cognitive biases that lead to groupthink and herd behavior.
[2] W. -C. Kim, R. Mauborgne. (2015) *Blue ocean strategy* Boston, Mass.: Harvard Business Review Press; Expanded edition.
[3] The red ocean or red ocean strategy is all about competition. As the market space gets more crowded (more people working on cucurbiturils), companies (researchers) compete fiercely for a greater share of limited demand (compete to come up with new studies that have not been presented in the literature in order to publish them).

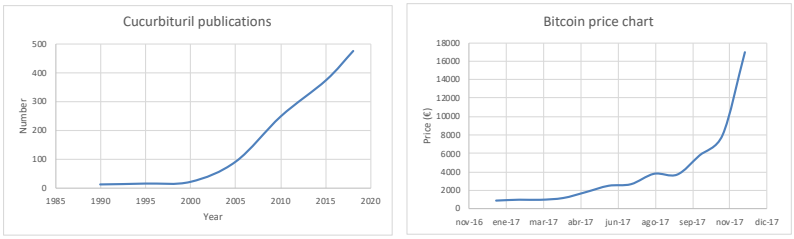

Figure II-1. Publications in the literature involving cucurbiturils (left). Bitcoin price on the stock market exchange (right).

Despite this, the reason why we decided to work on this challenging ever-growing topic was not for the sake of finding a breakthrough or disruptive innovation to pay off the initial investment covered by grants, scholarships, etc. but to do what research in academia is aimed to, fundamental research. It is sometimes referred to as the white innovation,[4] which seems irrational because it demands high amounts of funds and resources (high risk) while bringing low or non-returns at all. However, it is necessary, and it covers an essential need that governments are interested in investing in, even when the projects funded present no apparent economic return. It is the area of fundamental research, that of holistic laboratory innovation. The area that explores the borders of science for the altruistic good of humanity, without expecting economic benefit, but pursuing scientific leadership and the creation of new knowledge that will one day, conceivably, be converted in new blue oceans,[5] that will pay off governments and societies by bringing together the creation of new businesses, employability and quality of life.

It would be naïve, however, to believe in pure science, in the sense that governments, private donors, foundations or businesses altruistically give scientist the money they require to pursue whatever research projects they fancy. Most scientific studies are funded because somebody believes they could help attain some economic, political or even religious goal. This has been in governments agenda for, at least, the past 500 years of modern science. They and not scientist have been responsible to dictate the scientific agenda. For instance, if Darwin had followed a different path, we would probably attribute the theory of evolution to Alfred Russel Wallace, who came up with the idea of natural selection independently of Darwin but just a few years later. However, if the

[4] Prof. Xavier Ferràs uses this term to describe risky investments that require large amounts of capital for projects that apparently may not bring profit.
[5] Blue oceans, in contrast (see reference 2), are unexplored and untainted by competition. They create new demand driven by the creation of new technologies and science yet unknown by the market.

European funds had not financed geographical, botanical and zoological research around the world, neither Darwin nor Wallace would have had the chance to attempt such ambitious studies. For the same reason, in the 1940s striking results of the utmost importance were obtained in the field of nuclear physics due to the interests of the governments of America and the Soviet Union. In recent years, the interests in medicine and efficiency in drug delivery systems have steered the vanguard research in the creation of potential biotechnological tools as a benchmark for the creation of nanodevices for drug delivery, transport, and molecular recognition. However, this is just the tip of the iceberg.

II.1.2. Cucurbituril immobilization

The discovery of CB–guest complexes with the highest binding constant values reported for synthetic host–guest pairs, and affinities similar or superior to those found in natural complexes, beckoned the attention of many research groups, that focused their research in the functionalization of cucurbiturils in order to modify their structure and properties, to enhance their solubility, and to provide different functional groups for further transformations. For example, the immobilization of cucurbiturils onto surfaces has been achieved using three different strategies: direct immobilization onto a metal surface through self-assembled monolayer (SAM);[6] guest-mediated immobilization;[7] and *covalent immobilization*. This final strategy requires the functionalization or modification of the equatorial position of the cucurbituril previous to immobilization onto the desired surface. The functionalization, and especially the monofunctionalization, can be achieved following different methodologies including, the direct functionalization to produce hydroxylated products upon oxidation in water,[8] or through a building-block approach, to obtain monofunctionalized CB6 after condensation of an acyclic glycoluril hexamer with phthalaldehydes,[9] or

[6] Q. An, G. Li, C. Tao, Y. Li, Y. Wu, W. Zhang, *Chem. Commun.* **2008**, 1989–1991.
[7] K. Kim, W. S. Jeon, J.-K. Kang, J. W. Lee, S. Y. Jon, T. Kim, K. Kim, *Angew. Chem. Int. Ed.* **2003**, *42*, 2293–2296.
[8] a) Y. Ahn, Y. Jang, N. Selvapalam, G. Yun, K. Kim, *Angew. Chemie Int. Ed.* **2013**, *52*, 3140–3144. b) J. A. McCune, E. Rosta, O. A. Scherman, *Org. Biomol. Chem.* **2017**, *15*, 998–1005. c) M. M. Ayhan, H. Karoui, M. Hardy, A. Rockenbauer, L. Charles, R. Rosas, K. Udachin, P. Tordo, D. Bardelang, O. Ouari, *J. Am. Chem. Soc.* **2015**, *137*, *32*, 10238–10245.
[9] a) D. Lucas, T. Minami, G. Iannuzzi, L. Cao, J. B. Wittenberg, P. Anzenbacher, L. Isaacs, *J. Am. Chem. Soc.* **2011**, *133*, 17966–17976. b) L. Cao, L. Isaacs, *Org. Lett.* **2012**, *14*, 3072–3075.

monofunctionalized CB7 by condensation with glycoluril surrogates.[10] Albeit, there is a wide range of options, as we have previously seen, they all have in common their difficulty to either obtain high-ratios of monofunctionalized cucurbituril, or acceptable yields of product through affordable synthetic procedures. This approach can lead to many exciting applications, since the covalent tethering of cucurbiturils maintains, in the best expedient way, the fundamental properties of a CBn (e.g., the affinity between CBn–guest). However, the challenges on the synthesis of functionalized CBn makes this last strategy less attractive, and fewer examples have been reported so far. Among others, some studies suggested the use of allyloxy-functionalized CBn immobilized by thiol-ene reaction onto a thiolated surface,[11] a thiol-functionalized polymer,[8a] or by metathesis reaction onto an alkene functionalized gold surface.[12] Other studies reported the immobilization of perhydroxylated CB8 onto magnetic microspheres.[13] They made use of cucurbituril functionalized iron oxide particles for the selective enrichment of ultra-trace cytokinins in plant samples. Furthermore, perhydroxylated CB7 was also immobilized onto *N*-hydroxysuccinimide-functionalized sepharose beads for the enrichment of labeled plasma membrane proteins,[14a] or cytosolic proteins.[14b] Finally, monoazide functionalized CB7 has been attached to an alkyne-functionalized bead via Cu(I) catalyzed alkyne-azide [2 + 3] cycloaddition reaction (CuAAC).[15] This last report cached our attention because our group has been working with MNPs of Fe_3O_4 and polystyrene resin to covalently immobilize catalysts for the preparation of easily recoverable and recyclable catalysts. Prompted by the breadth of possible applications provided by cucurbiturils and our previous experience immobilizing organic molecules, we speculated that covalently attached cucurbiturils onto MNPs could, open up orthogonal routes concerning the use of nanodevices for molecular recognition, transport, separation,

[10] a) L. Cao, G. Hettiarachchi, V. Briken, L. Isaacs, *Angew. Chemie Int. Ed.* **2013**, *52*, 12033–12037. b) B. Vinciguerra, L. Cao, J. R. Cannon, P. Y. Zavalij, C. Fenselau, L. Isaacs *J. Am. Chem. Soc.*, **2012**, *134*, 13133.
[11] S. Y. Jon, N. Selvapalam, D. H. Oh, J.-K. Kang, S.-Y. Kim, Y. J. Jeon, J. W. Lee, K. Kim, *J. Am. Chem. Soc.* **2003**, *125*, 10186–10187.
[12] I. Hwang, K. Baek, M. Jung, Y. Kim, K. M. Park, D.-W. Lee, N. Selvapalam, K. Kim, *J. Am. Chem. Soc.* **2007**, *129*, 4170–4171.
[13] Q. Zhang, G. Li, X. Xiao, S. Zhan, Y. Cao, *Anal. Chem.* **2016**, *88*, 4055–4062.
[14] a) D.-W. Lee, K. M. Park, M. Banerjee, S. H. Ha, T. Lee, K. Suh, S. Paul, H. Jung, J. Kim, N. Selvapalam, et al., *Nat. Chem.* **2010**, *3*, 154. b) J. Murray, J. Sim, K. Oh, G. Sung, A. Lee, A. Shrinidhi, A. Thirunarayanan, D. Shetty, K. Kim, *Angew. Chemie Int. Ed.* **2017**, *56*, 2395–2398.
[15] W. Li, A. T. Bockus, B. Vinciguerra, L. Isaacs, A. R. Urbach, *Chem. Commun.* **2016**, *52*, 8537–8540.

nanomaterials (nanocarriers or chemical shuttles) and biosensors (Figure II-2). Therefore, we embarked on this project to explore new areas and, perhaps, if given the chance, find a new blue ocean. In addition to this, we also studied the immobilization of CBs onto Merrifield resin.

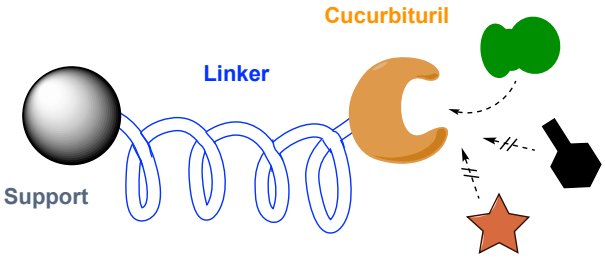

Figure II-2. Schematic representation of covalently immobilized CBs and their applicability in molecular recognition.

II.2. Objectives

In the present work, we strived to develop a method for the preparation of supported CBs onto MNPs and Merrifield resin. To this end, we anchored a pre-functionalized CBn bearing a terminal alkyne moiety to an azide-functionalized surface through the CuAAC reaction. Different types of functional beads were prepared in order to obtain a library of compounds with varying features. The core, made of Merrifield resin or iron oxide MNPs of different size, the linkers of different length, and several members of the cucurbituril family were employed. Additionally, we aimed to test and find a proof of concept to test the applicability of these novel compounds for molecular recognition, transport, and separation.

II.3. Discussion of results

II.3.1. Preparation of nanodevices

Preparation of the cucurbituril counterpart:

Several cucurbiturils are commercially available from well-known suppliers. However, they are still much more expensive than the respective cyclodextrins. Since the synthesis of the higher family members is still rendering low yields, to purchase **CB7** or **CB8** requires an even more significant investment (e.g., 100 mg of **CB8** can be purchased, at the time of writing this manuscript, on Sigma-Aldrich for €500, while 25 g of ß-cyclodextrin costs €87). Since our main goal was to produce larger amounts of **CB7**, we aimed to synthesize it. Considering that I

was the first, in our group, to explore the chemistry behind these macrocycles and that we had no previous experience on the synthesis and preparation of cucurbiturils. I had to start my research from scratch by reviewing the best procedures reported in the literature to optimize the production of **CB7**. At first, I came across with a procedure that reported the preparation, separation, and purification of four CBn homologs (n = 5, 6, 7 or 8).[16] The typical procedure required 100 g of starting material, glycoluril, to afford, after long and tedious steps, each homolog. Attempts on the synthesis at a much lower scale allowed us to obtain crystals of **CB6** and **CB8**. However, in any case, could we isolate **CB7**. Further investigation, and taking advantage of the networking at the ICIQ, I got the chance to spend a couple of weeks at the research lab of prof. Nau, in Bremen, Germany. There, I learned one of the best procedures to prepare the highest amounts of **CB7**. The straightforward stepwise procedure, concocted by them,[17] consisted in the condensation of glycoluril with formaldehyde under acidic conditions at a specific range of temperatures (95–100 ºC) for 72 h (Scheme II-1).

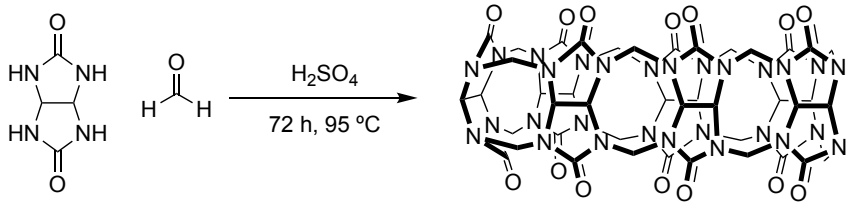

Scheme II-1. Representative synthesis of CB7.

This allowed us to produce, after some purification steps, highly pure **CB7** in relatively good yield (up to 14%) when compared to other procedures. With **CB7** in hand and some time left to spare in their lab, we teamed up to work together at the same line were our interests merged. To this end, we set to study the monofunctionalization by a direct oxidative functionalization approach recently reported at that time (Scheme II-2).[8c]

[16]D. Bardelang, K. A. Udachin, D. M. Leek, J. C. Margeson, G. Chan, C. I. Ratcliffe, J. A. Ripmeester, *Cryst. Growth Des.* **2011**, *11*, 5598–5614.
[17] C. Marquez, F. Huang, W. M. Nau, *IEEE Trans. Nanobioscience* **2004**, *3*, 39–45.

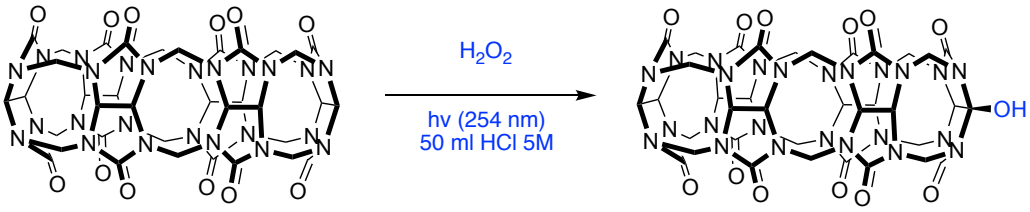

Scheme II-2. Representative synthesis of **CB6-OH** (with peroxides).

The monofunctionalization of cucurbiturils through straightforward free-radical oxidation was a real breakthrough that claimed over 95% yields of monohydroxylated CBn by the reaction of CBn with hydrogen peroxide in water and the presence of UV light (254 nm) as a source of hydroxyl radicals upon photolysis of hydrogen peroxide. However, none of our efforts provided us with not even closer ratios of monofunctionalized **CB7**. It was actually not possible, and soon afterward, a correction to the original paper was published. The product of the reaction was a mixture of CB7-(OH)m (m = 0–3) and the actual conversion of **CB7-OH** was roughly 30% after purification by silica gel chromatography. The error was attributed to a misconception on the NMR measurements, which concealed the true nature of the product. It turns out that the mixture of CB7-(OH)m displayed the same NMR spectrum than that of pure **CB7-OH**, although the MS showed the presence of the other compounds, debunking those disingenuous results. Ensuing studies, to comprehend, and to gain further insights on the mechanism of hydroxylation, demonstrated that the oxidation of CBn through a free-radical approach resulting in stoichiometric monohydroxylation was unattainable.[8b] They provided some improvements to the reaction for how to optimize the production of **CB7-OH** and demonstrated through DFT calculations that the second hydroxyl unit has a thermodynamic preference to bind on the same glycoluril unit as the first one. Despite this, and regarding this procedure, we aimed to prepare CB6-(OH)m and CB7-(OH)m where m < 3 to avoid the purification steps, since having a mixture of CBn, CBn-OH and CBn-$(OH)_2$, resembles, somehow, at having pure CBn-OH in the sense that, further functionalization will probably involve one of the hydroxyl groups, and later immobilization of those will allow us to expel the undesired CBs remaining in solution. The hydroxylation of **CB6** and **CB7** was additionally carried out following an earlier procedure reported by Kim (see ES, the general procedure for the synthesis of **CBn-OH**).[8a] In this procedure, the reaction conditions were optimized

to allow the synthesis of monofunctionalized **CB7** (27% yield) after purification by column chromatography on G-15 Sephadex (Scheme II-3). However, close control over the formation of the perhydroxylated counterparts allowed us, in some cases, to avoid the purification steps. Furthermore, monitoring the oxidation of CBs is not straightforward, and techniques such as NMR are not suitable to understand the substitution pattern nor quantify the distribution of hydroxylation. Since the signals of the OH substituents are not observed due to fast exchange in D_2O and the chemical shifts of the adjacent protons are overlapping with increasing levels of hydroxylation, it is not possible to quantify the ratio of functionalization. On the other hand, the use of electrospray ionization mass spectrometry (ESI-MS) is commonly used as the analytical tool of choice in the characterization of supramolecular systems.[18] For this reason, we decided to employ this technique to quantify the distribution of the CBn oxidation. In order to overcome the difficult ionization of cucurbiturils due to their bulky structure and chemical nature, we employed organic salts or guests that increased the propensity of the complexes to fly. Moreover, we aimed to obtain representative spectra of the bulk solution mixtures. To this end, the use of *p*-xylylenediamine dihydrochloride or cystamine dihydrochloride, that present good affinities to CBs, allowed the detection of the complexes which ionized on account of the guest moiety. Furthermore, both guests are doubly charged species, delivering doubly-charged host–guest complexes that are easily detected by ESI-MS (see ES, section II.4.8.).

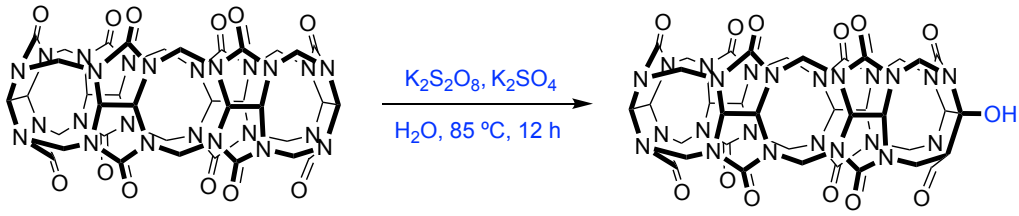

Scheme II-3. Representative synthesis of **CB6-OH** (with persulfates).

Even though myriad efforts, delving into the synthesis of scalable methods to synthesis functionalized CBn, have been undertaken over the years. It is still an unsolved hurdle, and new ideas and procedures are required. Endowed with our knowledge in flow chemistry processes, we made use of this well-established

[18] Z. Qi, T. Heinrich, S. Moorthy and C. A. Schalley, Chem. Soc. Rev., 2015, 44, 515–531.

technique to attempt to deliver higher amounts of functional CBn in less time (Figure II-3).

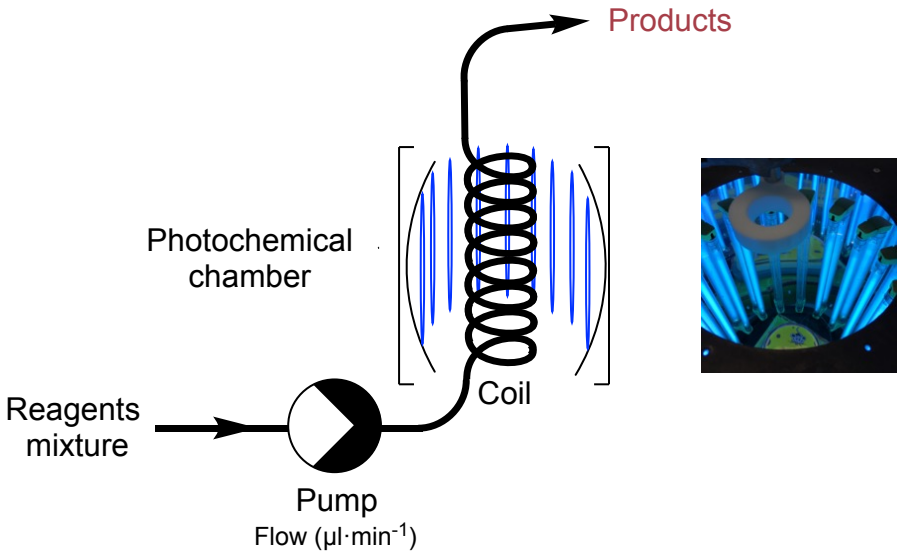

Figure II-3. Setup for the continuous flow hydroxylation.

We combined and edited the settings reported for the hydroxylation of CBn in UV light,[8c] and tried to find optimal conditions to circulate the reagents through a tubular reactor that would be continuously providing the product. First, in order to make the system simple, we tested the possibility to circulate both products from the same solution mixture, rather than separately and joining them just before entering the reaction chamber. A mixture of **CB6** and >10 eq of hydrogen peroxide was stirred overnight. After more than 12 h of reaction, there was no conversion, meaning that the use of the UV light is indispensable and that it was possible to prepare the reaction mixture beforehand. Secondly, the amount of hydrogen peroxide and the flow rate or residence time were evaluated (Table II-1, entries 1–4). The conversion, determined by ESI-MS, was more or less regular despite the concentration of peroxide. Increasing the flow rate (decreasing the residence time) did not seem to lower the number of hydroxylated products significantly. Afterwards, increasing the concentration of reagents (reaching almost the limit of solubilization) in order to produce faster, using different amounts of hydrogen peroxide, and speeding up the flow did not seem to deliver remarkable differences, except for concentrations higher than 2 eq of hydrogen peroxide or residence times lower than 30 min that delivered higher ratios of the perhydroxylated products, and lower ratios of hydroxylation, respectively (Table II-1, entries 5–12). When comparing the outcome of the reaction in flow with the

reaction in batch (see ES, Figure S1 and S2), we found some optimal conditions to produce higher amounts of **CB6-OH** in the presence of starting material while maintaining the formation of perhydroxylated products low (Table II-1, entries 8 and 13). With these optimized conditions, and with "unlimited" **CB6** produced as a byproduct from the preparation of **CB7**. We strived to scale up the production of "monohydroxylated **CB6**". Finally, we were able to produce up to 7 grams of the product mixture in approximately 36 h, at a production rate of 400 mg every two hours.

Table II-1. Reaction conditions for the hydroxylation in flow.[a]

Entry	**CB6** M	H_2O_2 eq	Flow rate $ml \cdot min^{-1}$
1	0.0034	0.5	0.0833
2	0.0034	1	0.0417
3	0.0034	1	0.0833
4	0.0034	1	0.1666
5	0.02	1	0.0417
6	0.02	1	0.0833
7	0.02	0.5	0.1666
8	**0.02**	**1**	**0.1666**
9	0.02	1	0.2500
10	0.02	2	0.1666
11	0.02	4	0.1666
12	0.02	6	0.1666
13	**0.002**	**0.5**	**-**

[a]Conditions: 5M HCl, tubular reactor (10 m, 5 ml, PFA 16''), Rayonet photochemical chamber reactor, HPLC pump, backpressure regulator (40 psi), 30-120 min residence time, 40–50 ºC.

The hydroxylated products were in some cases purified by column chromatography, but in most of the cases, the reaction mixtures were directly used without purification. Then, the corresponding hydroxylated products were reacted with propargyl bromide to add the propargyl moiety on the CBn (Scheme II-4). The reaction proceeded well, but full conversion was not achieved. The purity of the starting material did not interfere much on the outcome. Hence, **CB7-OH** delivered a mixture of starting material and **CB7-OPr**, while, starting with the crude mixture of **CB7-OH** provided an even more complex mixture of **CB7**

derivatives. In order to move the reaction forward, it was necessary to retake the reaction with the crude mixture. This fact was independently confirmed by others.[19]

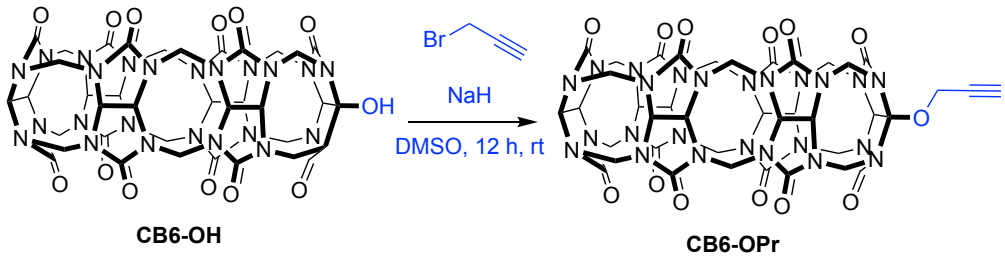

Scheme II-4. Representative synthesis of **CB6-OPr**.

On the other hand, the isolation of large amounts of pure open-chain oligomers requires an extensive synthetic skill. However, the successful synthesis of an open chain hexamer has shown to undergo cyclization with phthalaldehydes to produce highly pure monofunctionalized cucurbiturils (Scheme II-5).[20]

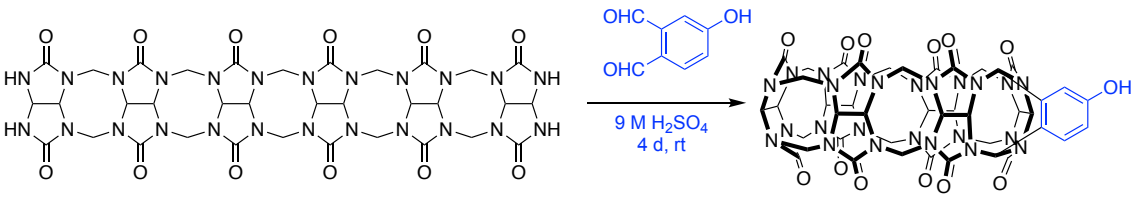

Scheme II-5. Representative synthesis of **CB6-PhOH**.

According to the authors of this work, the procedure is not easily reproducible. Three reactions were prepared at a time to increase the chances to obtain the desired hexamer, (Figure II-4). Usually, one or two out of three reactions were successful and delivered the desired hexamer as a white powder.

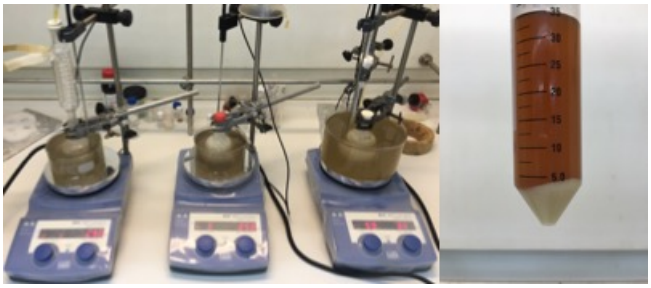

Figure II-4. Synthesis of the hexamer. Formation of the white solid is indicative that the reaction proceeded expectedly.

[19] S. Zhang, Z. Dominguez, K. Assaf, M. Nilam, T. Thiele, U. Pischel, U. Schedler, W. Nau, A. Hennig, *Chem. Sci.* **2018**, *9*, 8575–8581.
[20] L. Cao, L. Isaacs, *Org. Lett.* **2012**, *14*, 3072–3075.

With the hexamer freshly prepared, we synthesized the corresponding phthalaldehydes to deliver the monofunctionalized **CB6** upon reaction (Scheme II-6). The synthetic steps were adapted from previously reported procedures with slight modifications to optimize and enhance the yield of the final products (see the procedures on the ES).

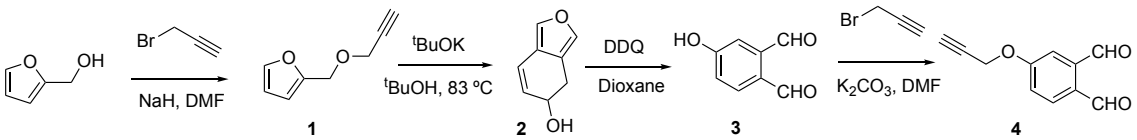

Scheme II-6. Synthesis of phthalaldehydes

Phthalaldehdyes **3** and **4** were used to prepare **CB6-PhOH** and **CB6-PhOPr**, respectively (Scheme II-7). **CB6-PhOH** was propargylated with propargyl bromide, but considering the overall yield of the latest steps [cyclization and propargylation (36%) *vs.* propargylation and cyclization (52%)], it seems clear that performing the propargylation first affords slightly better yields of **CB6-PhOPr**.

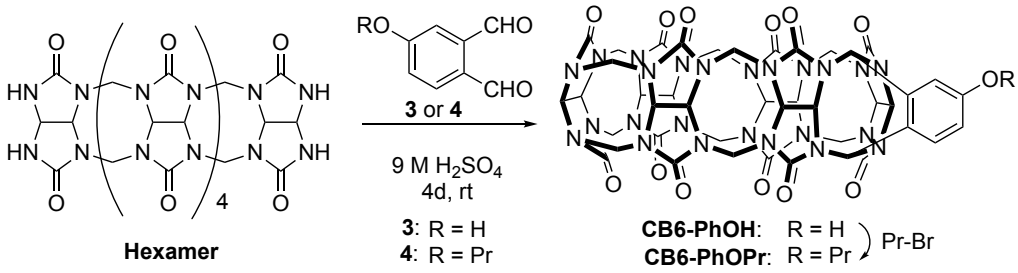

Scheme II-7. Synthesis of **CB6-PhOPr**.

With the three propargylated cucurbiturils, **CB7-OPr**, **CB6-OPr** and **CB6-PhOPr**, in hand. We proceeded with the preparation of the corresponding functional beads.

Preparation of **MNPs** and Merrifield resin:

The preparation of iron oxide nanoparticles was pursued so that the surface of the iron core could be modified through a ligand exchange reaction. This could be accomplished by preparing surfactant stabilized nanoparticles. Bifunctional alkyltrialkoxysilanes were then used to provide a flexible and tunable spacer of variable length (the alkyl moiety), and a moiety that could be anchored to the surface of the MNPs (the trialkoxysilane counterpart). Moreover, the head of the alkyl group could carry a functional group (e.g., azide group) that would allow further functionalization of the nanoparticles. We employed this approach to

prepare tailor-made MNPs coated with the previously propargyl functionalized cucurbiturils (**CB7-OPr**, **CB6-OPr**, and **CB6-PhOPr)**. (Figure II-5).

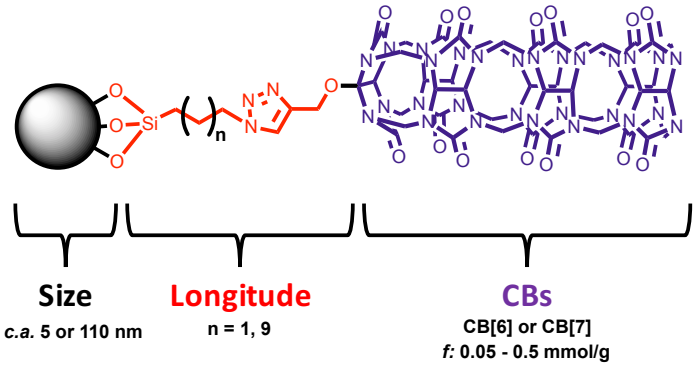

*Figure II-5.*Cucurbituril coated magnetic nanoparticles

In the first step, oleic acid or potassium acetate was used to generate the nanoparticles by the thermal decomposition method. The small nanoparticles, containing oleic acid, were prepared with the method reported by Sun.[21] While the bigger ones, carrying potassium acetate, were prepared following the method described by Cheng (Scheme II-8).[22]

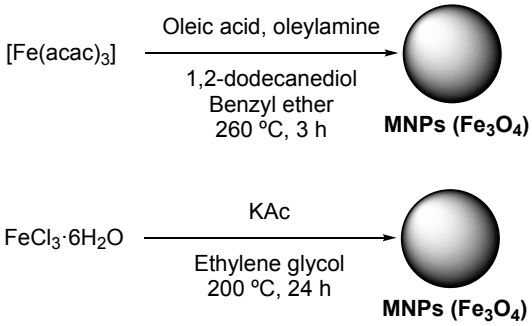

Scheme II-8. Preparation of **MNPs**.

Adequately dispersed spherical nanoparticles of around 5 or 90 nm mean diameter were obtained (Figure II-6, and Table S8), respectively, and further characterized by EA, and TGA.

[21] S. Sun, H. Zeng, D. -B. Robinson, S. Raoux, P. -M. Rice, S. X. Wang, G. Li, *J. Am. Chem. Soc.* **2004**, *126*, 273.
[22] D. Cheng, X. Li, G. Zhang, H. Shi, *Nanoscale Res. Lett.* **2014**, *9*, 195.

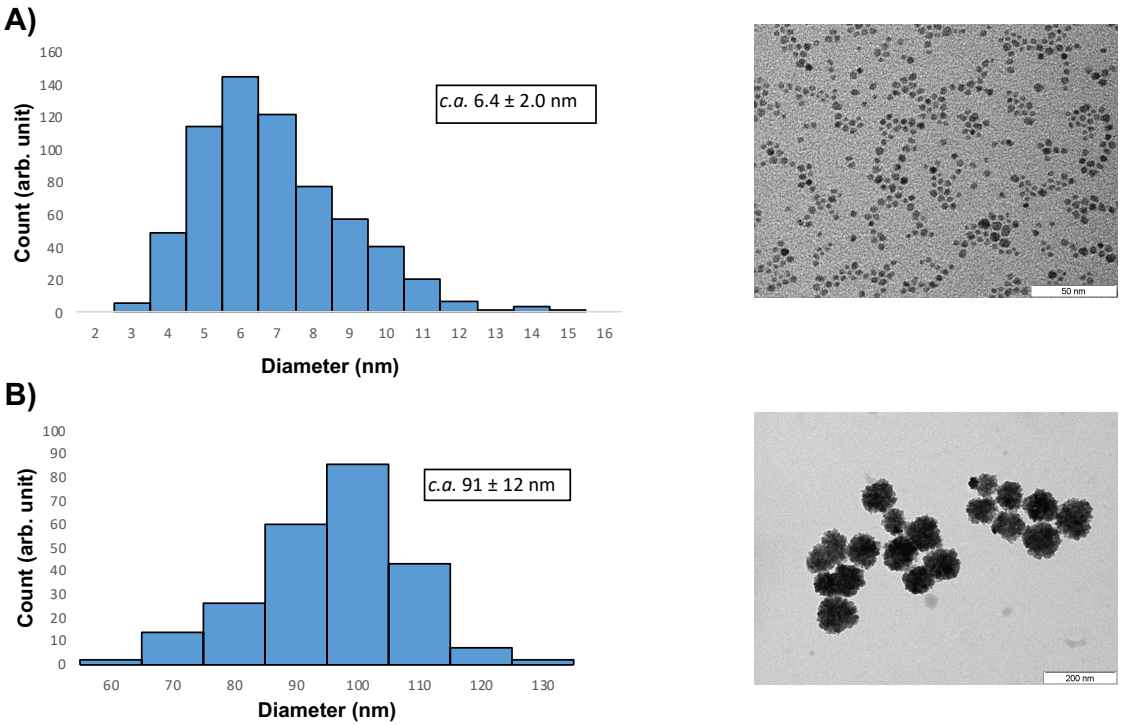

Figure II-6. TEM images and size distribution of **MNPs**.

TGA data shows that the mass loss occurs in two distinct steps. This behavior has been previously described for nanoparticles containing fatty acids.[23] This occurs because there are weakly bound surfactant molecules in a second layer further from the magnetite core. In the second layer, the molecules are bound by a combination of interchain van der Waals interactions and hydrogen bonds between the headgroups.

[23] a) L. Shen, P. E. Laibinis, T. A. Hatton, *Langmuir* **1999**, *15*, 447. b) L. Zhang, R. He, H. -C. Gu, *Appl. Surf. Sci.* **2006**, *253*, 2611. c) R. Massart, E. Dubois, V. Cabuil, E. Hasmonay, *J. Magn. Magn. Mater.* **1995**, *149*, 1.

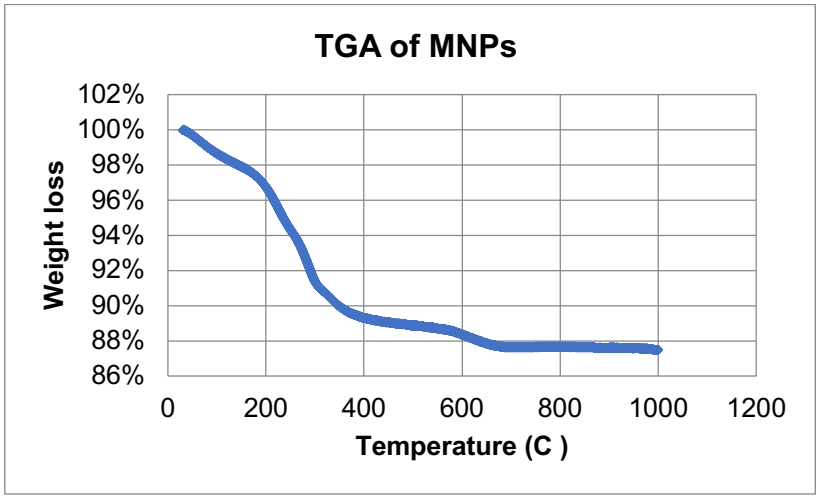

Figure II-7. TGA curve of the oleic acid stabilized **MNPs**.

The next step was to prepare the silane surrogates to be placed on the surface of the nanoparticles.

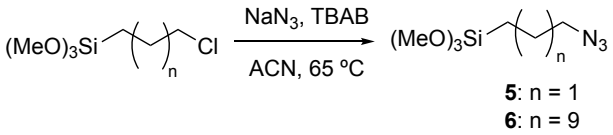

Scheme II-9. Preparation of silanes

3-azidopropyltrimethoxysilane, **5**, and 11-azidoundecyltrimethoxysilane, **6**, were prepared from commercially available chloro-substituted counterparts following a previously reported synthesis.[24] The silanes were used to further functionalize the magnetic core surface by providing two different lengths that would allow us to explore whether a variation on the spacer between the nanoparticles and the macrocycle would have an impact on the performance of the nanodevices (e.g., the capacity of cucurbiturils to make complexes, morphology of the nanoparticles, dispersibility in organic or aqueous solvents, etc.). To this end, we prepared nanoparticles with a short spacer, **7a** (5 nm MNPs), and with a long linker, **8a** (5 nm MNPs) and **8b** (90 nm MNPs).

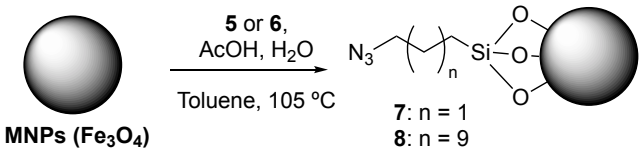

Scheme II-10. Preparation of azido functionalized MNPs.

[24] C. -A. Bradley, B. -D. Yuhas, M. -J. McMurdo, T. -D. Tilley, *Chem. Mater.* **2009**, *21*, 174.

The coated nanoparticles were characterized by IR (presence of the asymmetric stretching band of N_3 at around 2095 cm^{-1}) and EA to confirm the presence of nitrogen-containing compounds, and to determine their functionalization. Interestingly, the morphology of the 5 nm nanoparticles coated with the longer linker, **8a**, was not uniformly maintained and the spherical nanoparticles were poorly dispersed and seemed to agglomerate (see ES, II.4.7.17.). Moreover, the shorter linker was seamlessly integrated onto the surface of the 5 nm particles, and it was abundant (f > 1.0 mmol g^{-1}), while both linkers presented less activity when reacted to the 90 nm particles (f < 0.25 mmol g^{-1}) due to their lower area to volume ratio.

On the other hand, the preparation of the azido functionalized insoluble polymers (Scheme II-11) was accomplished by the reaction of the commercially available chloromethylated resin (Merrifield resin) with sodium azide.

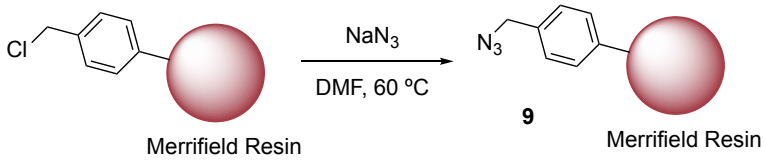

Scheme II-11. Preparation of azido functionalized Merrifield resin.

With the azido functionalized solid supports. The next step was to join both the azide and the propargyl units to produce the desired functional beads upon CuAAC reaction (Scheme II-12).

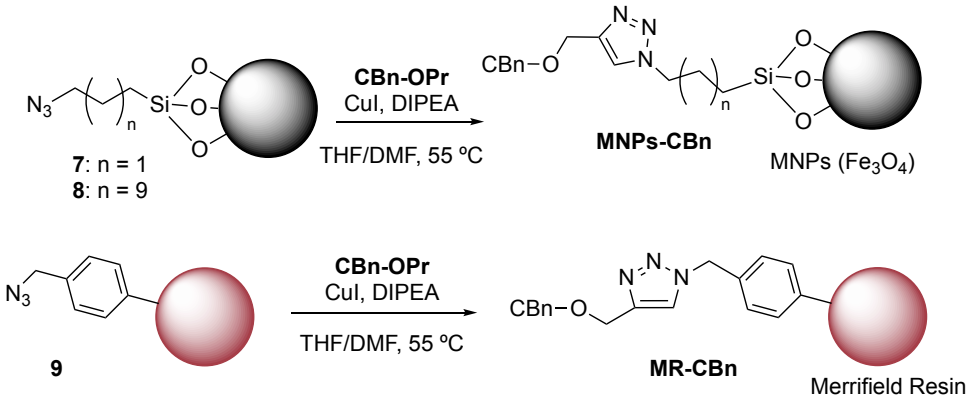

*Scheme II-12.*Preparation of functional beads.

The resulting products were characterized by IR (disappearance of the azide band upon the formation of the triazole ring), EA to measure the functionalization (Table S1 and S4), and TGA to alternatively measure the functionalization (Table S2, S3, and S5). The functionalization by TGA was calculated determining the

difference between the weight loss of the product, **MNPs-CBn**, and that of the starting material, **MNPs-N_3** (Figure II-8). The difference corresponds to the amount of propargylated CBn linked upon reaction, and hence, to the mmol of CBn incorporated per gram of MNPs. The determination of the functionalization by TGA and EA allowed the use of two different methods that provided similar values of functionality. The functionalization of CBn in the small nanoparticles was significantly higher due to higher amounts of free azide groups on the surface layer of the starting material (f > 0.20 mmol g^{-1}). The 90 nm particles, though, presented lower functionalization (f < 0.08 mmol g^{-1}) mainly because they present a lower area to volume ratio. Interestingly, the morphology of the 5 nm particles upon linkage of CBn with the longer linker was not maintained, and they behaved like a ferrofluid (see ES, section II.4.7.21.). This behavior was probably due to the potential difference between the surrounding liquid medium (water or MeOH) and the layer around the particle. The so-called zeta potential relates that particles with higher potential than 30 mV will repel each other and result in a stable ferrofluid.[25]

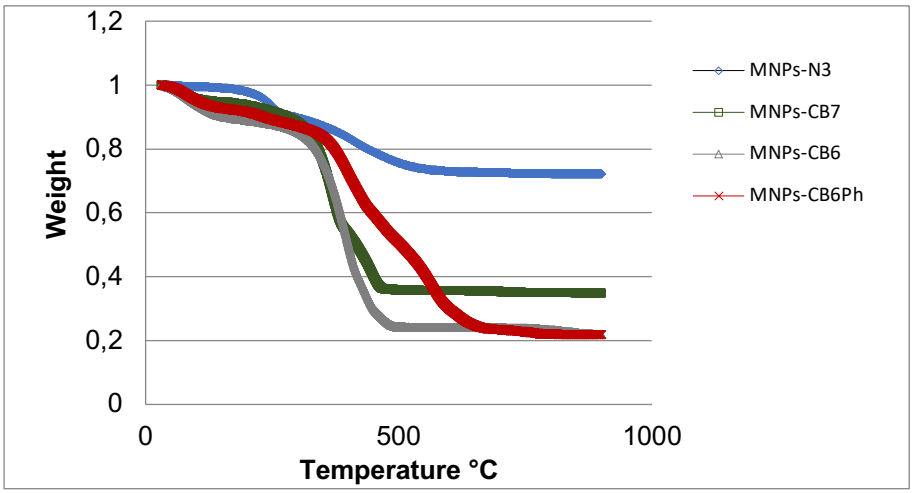

Figure II-8. TGA curves showing the weight loss of several functionalized **MNPs**.

To avoid harsh, tedious and time consuming purification steps after hydroxylation, we studied the possibility to propargylate the crude mixture containing CBn-(OH)m (where m < 3), and to anchor those cucurbiturils bearing a propargyl moiety and separate them from the rest (see ES, section II.4.8.3 and II.4.8.6). The remaining cucurbiturils were then extracted by water washings, dried under vacuum, and reused for another cycle of hydroxylation,

[25]S. Prijic, G. Sersa, *Radiol. Oncol.* **2011**, *45*, 1–16.

propargylation, anchoring of the propargylated ones to the solid surface and recovery of the rest (Scheme II-13). This provided a "0-waste" mechanism beneficial for the more expensive counterparts such as **CB7**. Additionally, this green approach saved us time, and the use of silica gel, acids, and other chemicals involved. Even though new and better methods to produce monofunctional cucurbiturils are still desirable, we believe that our technique is an excellent alternative to produce high amounts of "monofunctionalized mixtures" through continuous flow processes that allow the recovery and recyclability of the starting material after their immobilization onto solid surfaces.

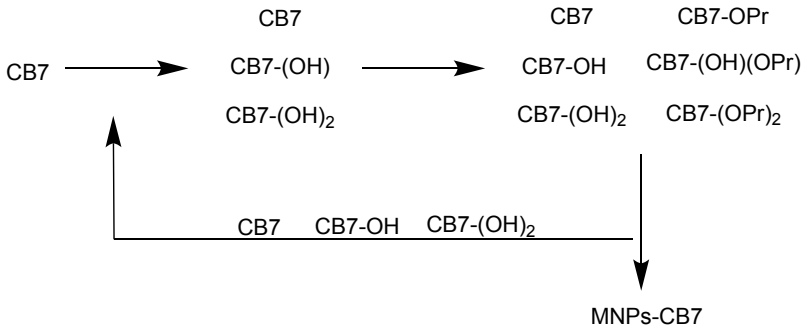

Scheme II-13. CB7 recovery cycle.

Finally, it is important to note that the flow processes have been optimized for the preparation of **CB6-OH**. Additional studies should be considered to optimize the production of the more hindered **CB7-OH**. This could be particularly advantageous for two reasons. First, because the bond dissociation energy of the C–H equatorial bond increases in the larger CBn homologs,[8c] and therefore, they require more energy for the abstraction of the hydrogen in order to form the tertiary radical species (Scheme II-14). Second, because larger CBs also show a narrower range of substitutions (less perhydroxylated derivatives), and hence, better control over perhydroxylation.

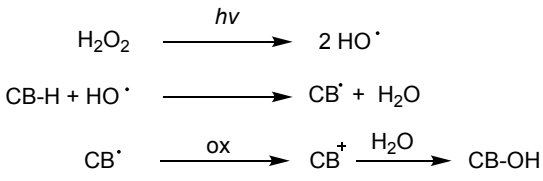

Scheme II-14. Proposed ionic mechanisms for the hydroxylation of CBn.

II.3.2. Characterization

To fully characterize the features of the coated beads, we devised two experiments. One of them would allow us to determine the effective functionalization, which was intended to measure the amount of guest extracted per gram of functional compound, and the second would determine the efficiency of extraction, in order to determine the percentage of guest that could be selectively extracted from a given solution.

II.3.2.1. Effective functionalization

To determine the effective functionalization of each set of functional compounds, we needed to come up with an experiment that would allow us to measure the concentration of a given molecule before and after extraction with the anchored CBs. To this end, we had to find a suitable guest that would display high affinity to CBn. A quick look in the literature allowed us to select the commercially available *p*-xylylenediamine. In order to be able to determine the concentration of this guest at any time, we decided to use an internal standard (IS) that would display very low or non-affinity towards CBn. An adequate IS was dimethyl sulfone because it is readily available from commercial suppliers as a standard for quantitative NMR and displays a chemical shift in a region that does not interfere with the peaks corresponding to the other chemical species involved in these studies. Moreover, even though it shows some affinity to **CB7**, the affinity of *p*-xylylenediamine is several orders of magnitude higher, making the affinity of the IS irrelevant. ^{1}H NMR spectra backed up our conjecture that this IS would not bind to **CB7** in the presence of similar concentrations of the guest and **CB7** as the limiting reagent. Therefore, while ^{1}H NMR spectrum of an equimolar mixture of **CB7** and IS showed complete complexation of the sulfone, the addition of *p*-xylylenediamine to the mixture displaced all the IS from within the **CB7** cavity to the bulk (Figure II-9).

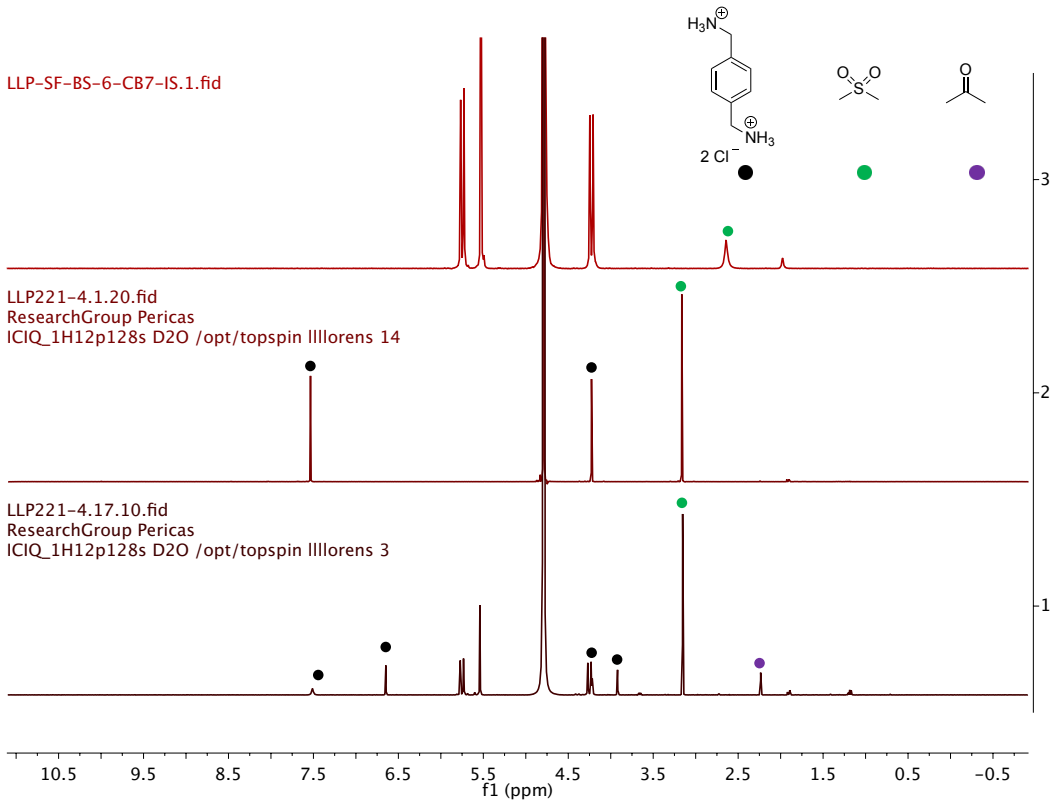

Figure II-9. Top: **CB7** and 2 eq of **IS** (IS = dimethyl sulfone, green dot). Middle: *p*-xylylendediamine (black dot) and 1 eq of **IS**. Bottom: **CB7** and more than 1 eq of *p*-xylylenediamine and **IS**.

Interestingly the interior of cucurbituril comprises a proton-shielding region relative to the aqueous medium inducing a shift on the protons present within the cavity. Moreover, perturbation of NMR peak positions of cucurbituril may also be observed for some other reasons. For guests bearing a cation coordinated to the urea carbonyls of the portal create a different magnetic environment for the close methylene residues.[26]

With these molecules on the play, we aimed to prepare stock solutions of different concentrations of *p*-xylylenediamine and dimethyl sulfone with the intention to use our nanodevices to extract the guest from each solution while determining the concentration previous and upon extraction. The extraction proceeded very fast, just 5 minutes of shaking after addition of the cucurbituril or cucurbituril coated beads was required. In the first experiments, we prepared 4 mM solutions of guest and IS and, then, increasing amounts of **MNPs-CB7** were added. The concentration of the guest was decreasing against the concentration of the IS. After extraction, the remaining concentration of the guest was slightly lower (3

[26] Mock, W. L.; Shih, N. Y. *J. Org. Chem.* **1986**, *51*, 4440-4446.

mM) than the concentration of dimethyl sulfone (4 mM). When we started the extraction experiments with stock solutions of 0.5 mM of guest and IS, the addition of **MNPs-CB7** was enough to pull out most of the guest from the solution (Figure II-10). Using 1.33 mM solutions allowed the extraction of roughly half of the guest, with the amounts of **MNPs-CB7** that were being used each time (up to two grams). On the other hand, the use of **MR-CB7** showed similar behavior than **MNPs-CB7** allowing the extraction of 1.5 mM solutions of the guest. Finally, the addition of **MNPs** or Merrifield resin to stock solutions did not succeed in the extraction of the guest (Table II-2).

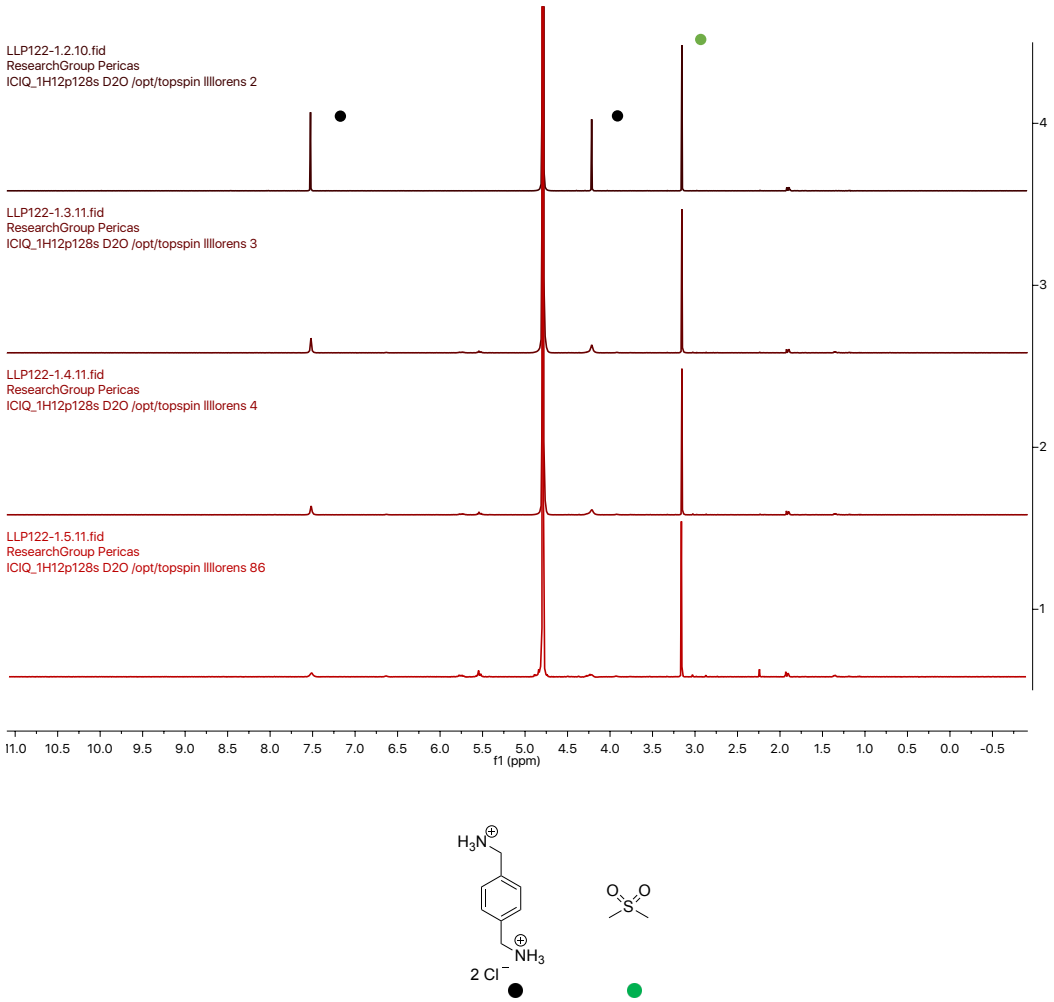

Figure II-10. Extraction of *p*-xylylenediamine with CB coated surfaces.

These experiments allowed the quantification of guest extraction by the integration of the NMR peaks. Then, knowing the amount of guest extracted against the number of immobilized **CB7** used, it was possible to determine the effective functionalization. The functionalization of **MR-CB7** and **MNPs-CB7** were

determined (see: Table II-2, Table II-S6 and Table II-S7), and the results obtained were similar to the functionalization determined with the other techniques (EA and TGA).

Table II-2. Extraction of *p*-xylylenediamine.[a]

Conc. (mM)	MNPs (mg)	MR (mg)	MNPs-CB7 (mg)	MR-CB7 (mg)	Integration of guest[b]	Adsorbed guest (μmol)	*f* (mmol/mg)[c]
3	-	-	-	-	4	-	-
4	-	-	0	-	4	0	-
4	-	-	0.430	-	3.81	0.152	0.35
4	-	-	1.030	-	3.57	0.344	0.33
4	-	-	2.300	-	3.20	0.640	0.28
0.5	-	-	0	-	4	0	-
0.5	-	-	0.335	-	2.90	0.110	0.33
0.5	-	-	0.617	-	2.28	0.172	0.28
0.5	-	-	1.011	-	1.04	0.296	0.29
0.5	-	-	1.640	-	0	0.400	-
1.33	-	-	0	-	4	0	-
1.33	-	-	0.600	-	3.34	0.176	0.29
1.33	-	-	0.920	-	2.93	0.285	0.31
1.33	-	-	1.439	-	2.38	0.431	0.30
1.5	-	-	-	0	4	0	-
1.5	-	-	-	0.631	3.26	0.222	0.34
1.5	-	-	-	1.104	2.83	0.351	0.32
1.5	-	-	-	1.910	1.83	0.651	0.35
2	2.24	-	-	-	4	0	-
2	-	2.52	-	-	4	0	-

[a]Reaction conditions: *p*-xylylenediamine and dimethyl sulfone were added at the same concentration, solvent: D_2O (0.7 ml), rt. [b] Determined after extraction with the corresponding MNPs or MR, by performing ^{1}H-NMR spectroscopy on the resulting mixture. [c] Determined as a function of the mmol of *p*-xylylenediamine extracted vs. mg of MNPs or MR added.

With the measurement of the effective functionalization, we could further characterize the cucurbituril-based magnetically fueled nanodevices and gain some additional knowledge throughout their preparation. In brief, TEM images allowed us to know the morphology (size and shape) of the nanoparticles, IR

spectra and LC-MS confirmed the success of the CuAAC reaction, and EA, TGA and NMR experiments provided the functionalization (mmol of CBn) / (g of nanodevice) and effective functionalization (mmol of guest extracted) / (g of nanodevice), (Figure II-11).

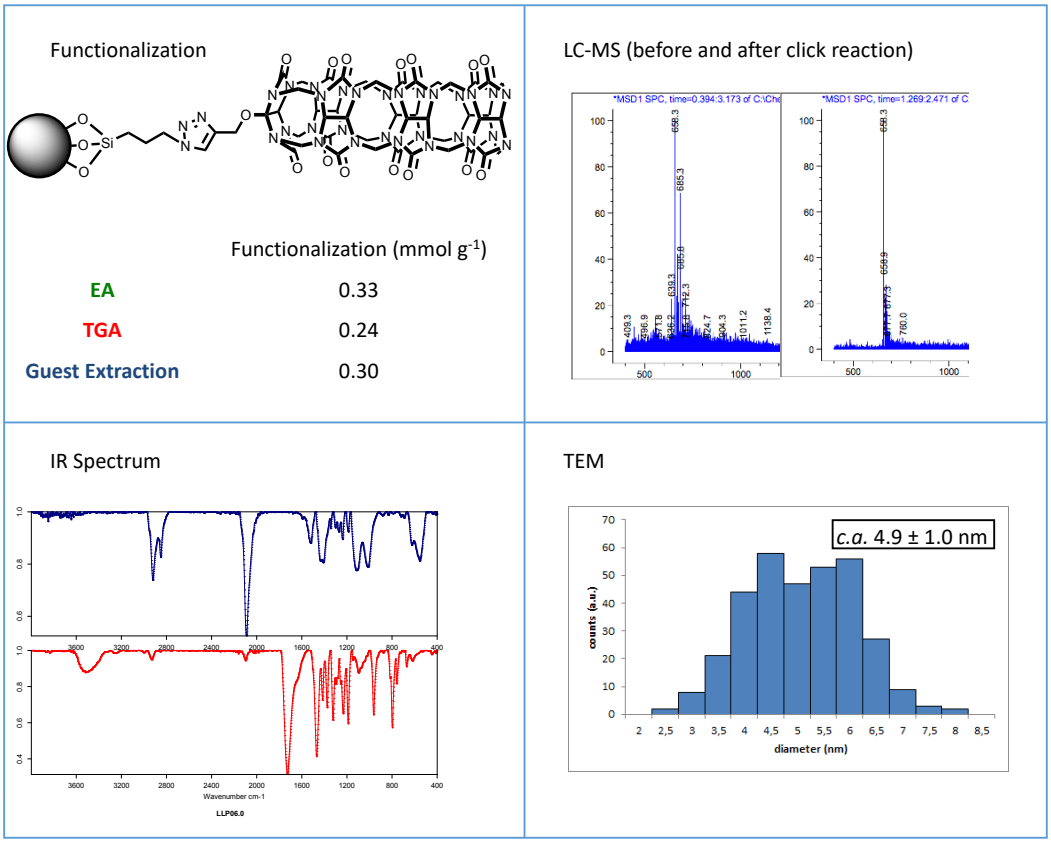

Figure II-11. Representative characterization of the nanodevices.

II.3.2.2. Efficiency of extraction

To determine the efficiency of extraction, we decided to quantify the capacity of the nanodevices to extract particular molecules from a given solution. To this end, we studied the possibility of labeling a fluorescent molecule with an adamantyl tag. This molecular probe would have a dual-purpose. First, we could make use of the fluorescent properties to determine the concentration of the molecule in a solution at any time. On the other hand, the adamantyl tag would allow us to extract the molecule by molecular recognition and high-affinity complex formation with the **CB7** anchored MNPs.

We selected a commercially available fluorescein azide molecule, **5-FAM-azide**. This molecule was then reacted with adamantanethanol ether bearing a terminal alkyne. The product obtained, **Ad-5-FAM**, was dissolved in several solvents in

order to determine its fluorescent performance. It was slightly soluble in water and buffers, but the solubility significantly increased in organic solvents such as MeOH and EtOH. The solubility and fluorescence of the probe in phosphate buffers at pH 7 were significantly better than in pure water or in phosphate buffer acidified to pH 5 (Figure II-12).

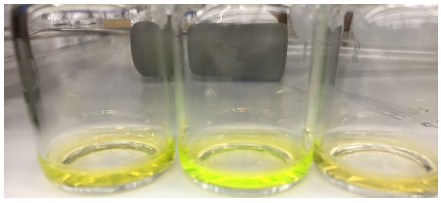

Figure II-12. **Ad-5-FAM** dissolved in water, phosphate buffer (pH 7), and phosphate buffer (pH 5).

A calibration curve at a nM scale was set for the fluorescent molecule using 100 mM phosphate buffer at pH 7. However, attempts to extract the molecule from the solution failed, probably due to the lousy solubility of the molecule or the stiff competition by the phosphate ions, although the adamantane should exhibit much stronger affinity despite the difference in concentration. Since some of the driving forces for the formation of this high-affinity CB–guest complexes are the release of “high energy water” and the hydrophobic interactions, we focused on the use of aqueous solvents and buffers to extract the product. However, when the extraction was attempted in organic solvents, at high concentration of the molecular probe, it was possible to observe, with a naked eye, the behavior of the molecule in each solvent after adding the immobilized CBs. The disappearance or presence of the colorful mixture after extraction was an indicator of the reaping performance of the CBn coated nanoparticles in that solvent (Figure II-13). Therefore, the disappearance of the color was directly related to the extraction efficiency. We then realized that EtOH was a suitable solvent for both the extraction and the calibration curve since the fluorescent molecule presented excellent solubility in most of the organic solvents tested.

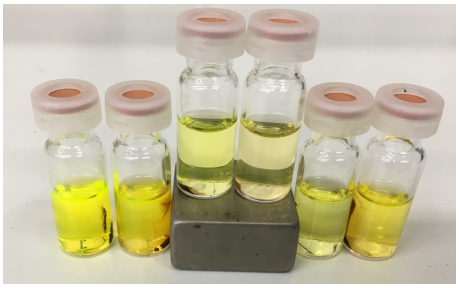

Figure II-13. Extraction of the fluorescent probe with immobilized CB7 in different solvents.

With the calibration curve in hand (Table II-3), we prepared stock solutions of the fluorescent molecule (9.1 μM). To these solutions, different amounts of **MNPs-CB7** were added, and the decrease in the intensity of emission was monitored by fluorescence spectroscopy after filtration or magnetic decantation of the **MNPs-CB7** from the solution (Table II-4 and Figure II-14).

Table II-3. Calibration curve of the fluorescent probe.

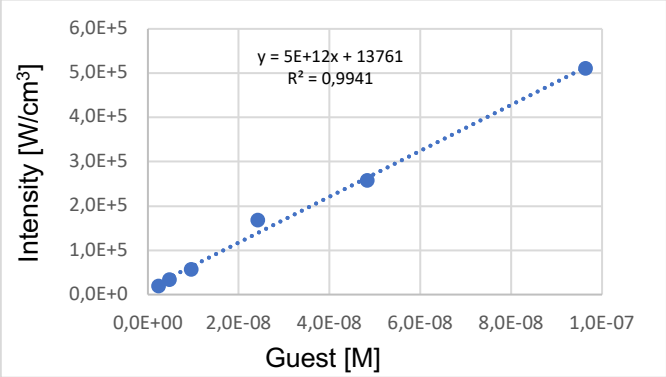

Entry	concentration [nM]	Intensity emision (W/cm^3)	STDVE
1	**96.4**	510570	93333
2	48.3	257630	66548
3	24.2	168563	42411
4	9.64	56887	6047
5	4.87	33410	4318
6	**2.42**	18880	3544

Table II-4. Extraction of the fluorescent molecule (9.1 μM) with **MNPs-CB7**.

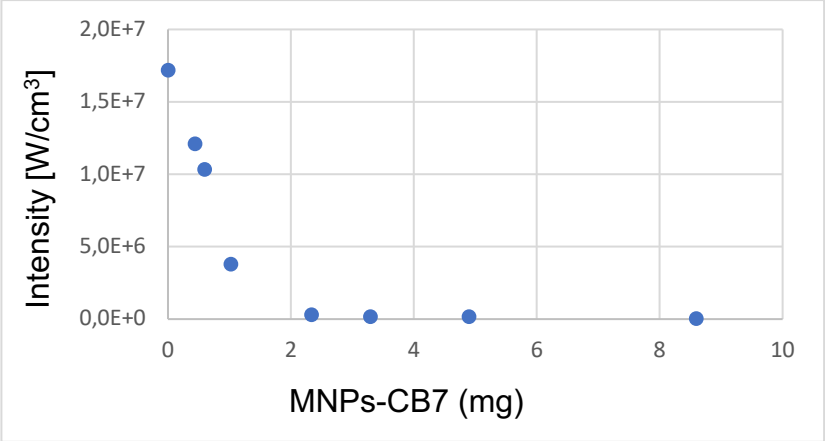

Entry	**MNPs-CB7** (mg)	Intensity emision (W/cm^3)
1	0	17179750
2	0.44	12104900
3	0.6	10316170
4	1.03	3779850
5	2.34	303520
6	3.3	170160
7	4.9	170160
8	8.6	56240

To determine the efficiency of extraction, we decided to prepare a solution from which we could remove a high percentage of the fluorescent molecule while being able to determine the residual content on the solution by fluorescence spectroscopy. Therefore, the intensity of emission, of a starting 9.1 μM solution, was determined upon extraction with increasing amounts of **MNPs-CB7**. The extraction proceeded very fast, less than 20 seconds upon addition of the functional beads. Then, the concentration remaining was measured, and it was roughly 10 nM. These results allowed us to determine that the efficiency of extraction was highly dependent on the solvent of use and that the reported conditions allowed over 99% of extraction (Table II-5). Finally, a control experiment was set with **MNPs** to confirm that the extraction of the fluorescent probe was due to the presence of **CB7**. The intensity of emission changed slightly upon mixture with **MNPs**, but it was not significantly lower (Figure II-14). Therefore, the extraction was, indeed, due to the anchored CB7.

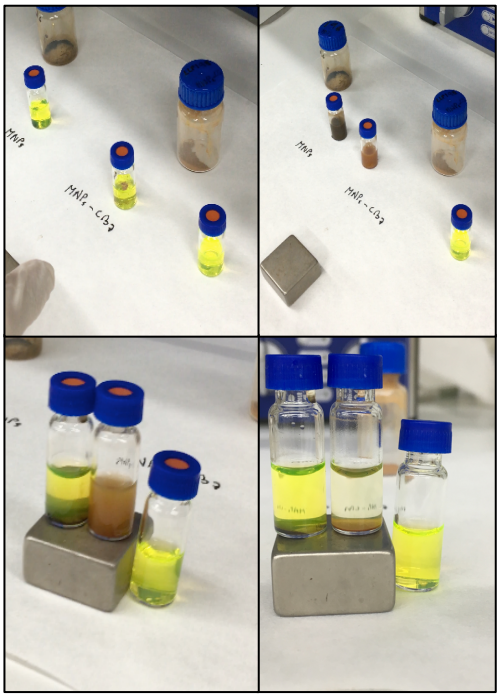

Figure II-14. Adsorption of the fluorescent molecule. Solution containing **Ad-5-FAM** in 3 vials (top left). Addition of black **MNPs** to vial 1, and brown **MNPs-CB7** to vial 2, (top right). Magnetic decantation of the nanoparticles: after 5 min (bottom left) and after 1 h (bottom right). Yellow color is indicative of the presence of the fluorescent molecule in the solution.

Table II-5. Extraction of the fluorescent molecule (9.1μM) with **MNPs-CB7**, and determination of the efficiency.

Entry	**MNPs-CB7** (mg)	concentration [nM]	nmol in solution	nmol extracted
1	0	9096.53	**27.290**	0
2	2.34	58.71	0.176	27.114
3	3.3	32.04	0.096	27.194
4	4.9	10.37	0.031	**27.259**

Another consideration to take into account is that the efficiency of extraction might have to be determined for each different system depending on the chemical and physical nature of each molecule tested. For example, we could generalize that adamantyl tagged species will allow excellent extraction in water. When this might be the case for most of amphiphilic, cationic, or water-soluble species, it might not apply for some neutral, anionic, or another kind of molecules such the one we tested here.

II.4. Experimental section

II.4.1. Table of contents

II.4.2. General information

Unless otherwise stated, all reactions were conducted under air. All commercial reagents were used as received. Flash chromatography was carried out using 60 mesh silica gel. Thin layer chromatography (TLC) was carried out using Merck TLC Silica gel 60 F254 aluminum sheets. Components were visualized by UV light (λ = 254 nm) and stained with *p*-anisaldehyde, phosphomolybdic dip or iodine in silica. NMR spectra were recorded at 298 K on a Fourier 300 MHz Bruker, a Bruker Advance 400 Ultrashield or a Bruker Avance 500 Ultrashield apparatus. ^{1}H NMR spectroscopy chemical shifts are quoted in parts per million (ppm) relative to tetramethylsilane (TMS), $CHCl_3$, or water. $CDCl_3$ was used as internal standard for ^{13}C NMR spectra. Coupling constants, *J*, are reported in Hz. IR spectra were recorded on a Bruker Tensor 27 FT-IR spectrometer and are reported in wavenumbers (cm^{-1}). Elemental analyses (EA) were performed on a LECO CHNS 932 micro-analyzer at the Universidad Complutense de Madrid, Spain or on a Thermo FlashEA 1112 elemental analyzer and on a Metrohm761 Compact Ion Chromatograph at MedacLtd, United Kingdom. High performance liquid chromatography (HPLC) was performed on Agilent Technologies chromatographs (1100 and 1200 Series). FAB mass spectra were obtained on a Fisons V6-Quattro instrument, ESI mass spectra were obtained on a Waters LCT Premier Instrument. Transmission electron microscopy (TEM) images were recorded using JEOL JEM 1011 microscope operated at an acceleration voltage of 100 kV, at Microscopy Units, Universitat Rovira i Virgili, Tarragona, Spain. A drop of the MNPs suspension was added to a holey-carbon coated 200 mesh copper-grid allowing the solvent to evaporate before being introduced into the microscope. Thermogravimetric analysis (TGA) were performed in a Mettler Toledo TGA/SDTA 851 thermo balance. The Rayonet photochemical chamber reactor is a Rayonet trademark, model RPR-200 working with 16 light bulbs from Philips (254 nm, models TUV 16W, G16T5). Fluorescence spectroscopy was evaluated using a Fluorolog Horiba Jobin Yvon spectrofluorimeter instrument. The excitation wavelength was set at 526 nm. HPLC purifications were performed on a Waters delta 600 pump. All products that are known were characterized by comparison of their physical and spectroscopic properties with those described in the literature.[1,2,5,6]

II.4.3. Experimental procedures

II.4.3.1. General procedure for the synthesis of cucurbiturils, CBn[1]

Formaldehyde (20 ml, 268 mmol, 3.3 eq) was mixed with 9 M sulfuric acid (60 ml) and the magnetically stirred mixture was cooled down to 2–5 °C using an ice bath. Glycoluril (11.46 g, 81 mmol) was added in small portions. Then the temperature was increased to 95 °C using an oil bath. Heating was continued for 72 h. The reaction mixture was then poured into 200 ml deionized water. A volume of 800 ml acetone was added to precipitate all **CBn** homologs. The suspension was let to settle down and filtered using a large frit and washed with (2 x 250 ml) mixture of acetone water 4:1. The precipitate was then dissolved in 400 ml deionized water and after stirring for 15 min was filtered. The precipitate containing **CB6** and **CB8** was dissolved with 200 ml HCl 3 M and the solution containing **CB6** was dried under high vacuum. To the waters of the filtrate of the previous solution, 300 ml of acetone were added and the precipitate, **CB7**, was immediately filtered and dried under high vacuum.

Cucurbit[6]uril (CB6)

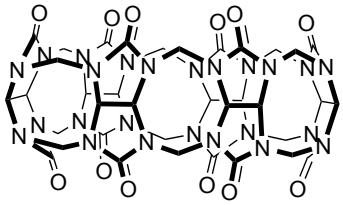

Yield (60%); **^{1}H-NMR** (400 MHz, D_2O): δ = 5.76 (d, 12H *J* = 15.5 Hz, CH_2), 5.61 (s, 12H, CH) 4.35 (d, 12H *J* = 15.5 Hz, CH_2) ppm. **HPLC-MS** (ESI+) *m/z*: calcd for [CB6-H + cystamine + 2H]$^{2+}$: 575.18. Found: 575.3.

Cucurbit[7]uril (CB7)

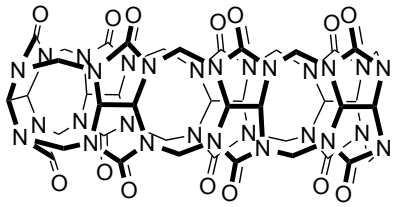

Yield (12%); **^{1}H-NMR** (400 MHz, D_2O): δ = 5.74 (d, 14H *J* = 15.5 Hz, CH_2), 5.50 (s, 14H, CH) 4.18 (d, 14H *J* = 15.5 Hz, CH_2) ppm. **HPLC-MS** (ESI+) *m/z*: cacld for [CB7-H + cystamine + 2H]$^{2+}$: 658.20. Found: 658.3.

II.4.3.2. General procedure for the synthesis of CBn-OH

The synthesis was carried out following a procedure reported by Kim with some modifications.[2] A heterogeneous mixture of **CBn** (2 g, 1.72 mmol), $K_2S_2O_8$ (0.85 eq), K_2SO_4 (5.5 eq) and MiliQ water was degassed and heated at 85 °C under argon atmosphere for 12 h. The solid was filtered and the solvent evaporated. The product was extracted with HCl (100 ml) from the solid. Addition of excess methanol to the extract yielded a precipitate, which was filtered and dried. The white solid was used for further steps without purification. Alternatively, the hydroxylation of cucurbiturils was carried out following the procedure described by Ouari.[3] Or a more recent protocol described by Scherman.[4]

CB7-OH and **CB6-OH** were characterized by comparing, their respective ^{1}H-NMR and positive mode ESI mass spectra to the previously reported data described in the literature.[2,3,4]

CB6-OH

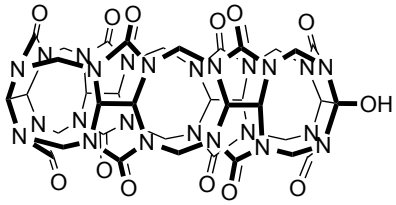

^{1}H-NMR (400 MHz, D_2O): δ = 5.84 (d, 2H *J* = 15.6 Hz), 5.77 (d, 8H *J* = 15.6 Hz), 5.62 (m, 12H), 5.39 (s, 1H), 4.62 (d, 2H *J* = 15.5 Hz,), 4.37 (d, 10H *J* = 15.5 Hz) ppm. **HPLC-MS** (ESI+) *m/z*: calcd for [CB6-OH + cystamine + 2H]$^{2+}$: 583.17. Found: 583.3.

CB7-OH

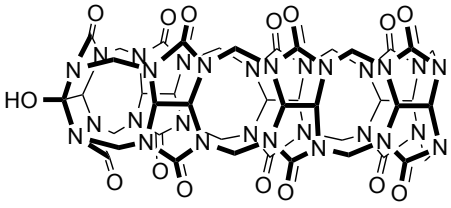

^{1}H-NMR (400 MHz, D_2O): δ = 5.78 (m, 12H), 5.58 (m, 14H), 5.35 (s, 1H), 4.57 (d, 2H *J* = 15.5 Hz), 4.29 (d, 12H *J* = 15.5 Hz) ppm. **HPLC-MS** (ESI+) *m/z*: calcd for [CB7-OH + cystamine + 2H]$^{2+}$: 666.20. Found: 666.3.

II.4.3.3. Continuous flow process: synthesis of CB6-OH

The continuous flow reaction of a 5M HCl solution containing cucurbituril (0.02 M) and H_2O_2 (0.02 M) was carried out in a 10 m tubular reactor PFA 16" disposed inside a Rayonet photochemical chamber reactor, and assembled to an HPLC pump (Knauer® pump) and a backpressure regulator (40 psi). The solution (up to 360 ml, *c.a.* 7 g) was circulated with a flow rate of 166 $\mu l \cdot min^{-1}$ for up to 36 h. The temperature inside the chamber was stable (40–50 ºC). The solvent from the collected samples was removed under reduced pressure and the crude product was obtained as a mixture of **CBn-(OH)m** (m = 0–3) with a similar proportion than that obtained after the reaction in batch. (see section II.4.8. for better comprehension of the peaks)

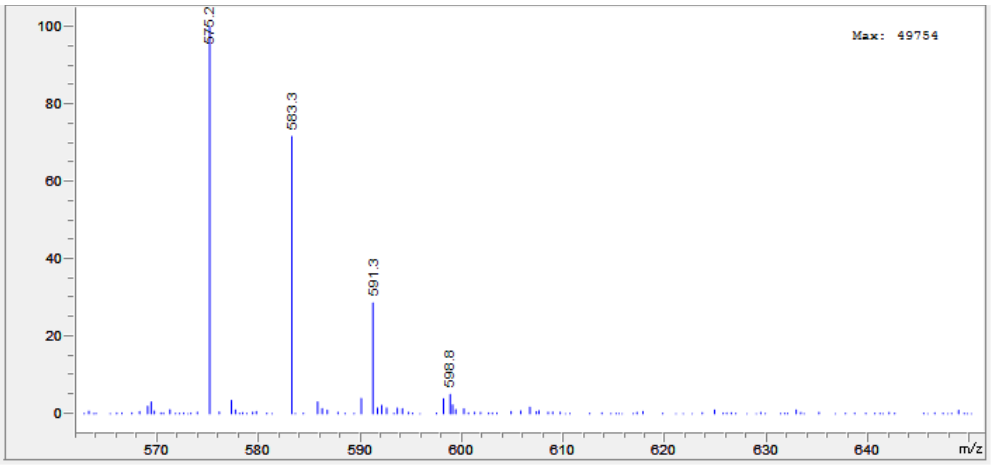

Figure II-S1 HPLC-MS (ESI) of the crude product collected from the continuous flow process. Mixture of CB6-(OH)m, where m = 0–3.

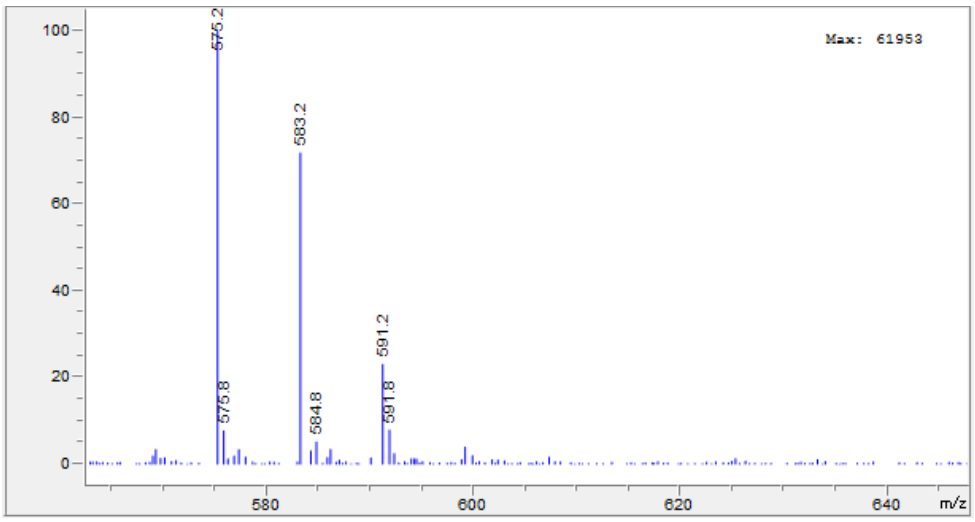

Figure II-S2. HPLC-MS (ESI) of the crude product obtained from the reaction in batch. Mixture of CB6-(OH)m, where m = 0–3.

II.4.3.4. General procedure for the synthesis of CBn-OPr

The synthesis was carried out following a procedure reported by Henning with some modifications.[5] To a solution of **CBn-OH** (1 g, 0.85 mmol) in anhydrous DMSO (14 ml, 0.06 M), NaH (0.27 g, 8 eq) was added under argon atmosphere, and the mixture was stirred at rt for 3 h. Propargyl bromide (0.57 ml, 6 eq) was added to the reaction mixture at 0 °C and stirred at rt overnight. Addition of ethyl ether (500 ml) to the reaction mixture produced a solid that was rinsed with methanol (3 x 50 ml), and dried under high vacuum to give an off brown solid that was used directly without further purification.

CB6-OPr and **CB7-OPr** were characterized by comparing, their respective ^{1}H-NMR and positive mode ESI mass spectra to the previously reported data described in the literature.[5]

CB6-OPr

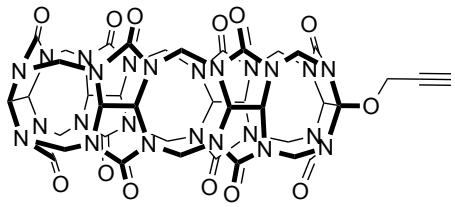

^{1}H-NMR (400 MHz, D_2O): δ = 5.78 (m, 12H) 5.57 (m, 12H), 4.55 (m, 2H), 4.32 (m, 10H). 2.74 (s, 1H, CC-H) ppm. **HPLC-MS** (ESI+) *m/z*: calcd for [CB6-OPr + cystamine + 2H]$^{2+}$: 602.18. Found: 602.3.

CB7-OPr

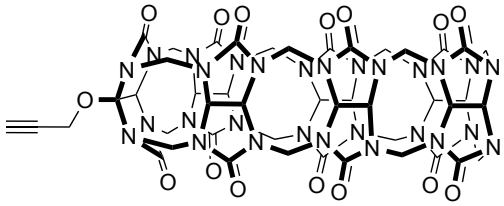

^{1}H-NMR (400 MHz, D_2O): δ = 5.81 (m, 14H), 5.58 (m, 14H), 4.31 (m, 14H), 2.72 (s, 1H, CC-H) ppm. **HPLC-MS** (ESI+) *m/z*: calcd for [CB7-OPr + cystamine + 2H]$^{2+}$: 685.21. Found: 685.3.

II.4.3.5. Synthesis of CB6-PhOPr via glycouril hexamer

The synthesis via glycouril hexamer was carried out following the procedures reported by Isaacs, with some modifications.[6]

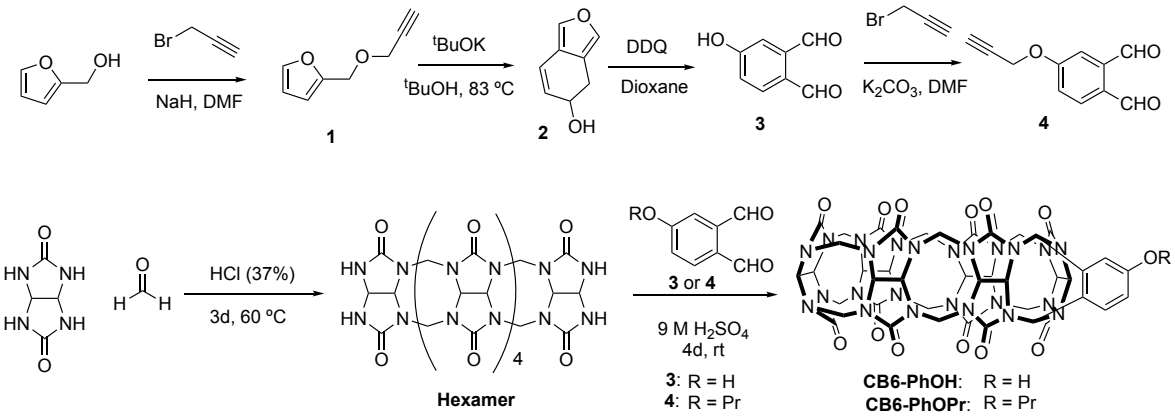

Synthesis of the glycouril hexamer (hexamer)

A mixture of glycouril (14.2 g, 100.0 mmol), paraformaldehyde (5.0 g, 166.7 mmol) and *p*-xylylenediamine hydrochloride (3.5 g, 16.7 mmol,) was added to a 50 ml round bottom flask equipped with a stir bar, and mixed until homogeneous. Concentrated HCl (20 ml) was quickly added to the powdered mixture. The flask was sealed tightly with a septum and was vigorously shaken to expose all reagents to the solvent. The slurry was then heated at 58 °C for 3 days, at which point an off-white precipitate was observed. The hot heterogeneous reaction mixture was centrifuged. The clear yellow supernatant was decanted. The crude solid was dried under high vacuum. The crude solid was mixed with H_2O (40 ml). The heterogeneous mixture was sonicated in a 50 ml centrifuge tube for 10 min. The heterogeneous mixture was centrifuged and the supernatant was decanted into another, pre-weighed centrifuge tube. A solution of 5 M aq. NaOH (3.5 ml, 17.0 mmol) was added to the supernatant which resulted in the precipitation of a white solid. The white, heterogeneous mixture was then sonicated for 30 min and was allowed cool to rt before centrifuging for 10 min. The supernatant was decanted and the white precipitate was washed with a solution of 0.1 M NaOH in MeOH (40 ml) followed by centrifugation. Finally, the supernatant was decanted and the precipitate was washed with MeOH (40 ml) followed by centrifugation. After the supernatant was decanted, the precipitate was dried under high vacuum to give the hexamer as a white powder (2.94 g, 3 mmol, 18% yield).

The final product, **hexamer**, was characterized by comparing its ^{1}H-NMR and IR spectra to the previously reported in the literature.[6]

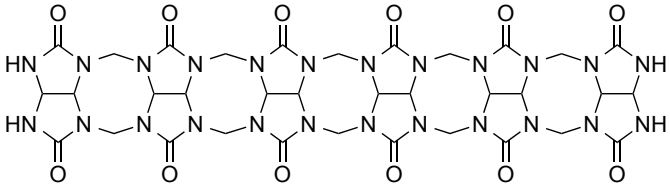

^{1}H-NMR (500 MHz, > 1 eq *p*-xylylendiamine): δ = 5.85 (d, *J* = 15.6 Hz, 2H), 5.62 (m, 16H), 5.44 (d, *J* = 8.92 Hz, 2H), 5.41 (d, *J* = 8.92 Hz, 2 H) 4.44 (d, *J* = 15.6 Hz, 2H) 4.24 (d = 15.6 Hz, 4H) 4.14 (d = 15.6 Hz, 4H) ppm. **IR** (ATR): 3402 b, 1717, 1469, 1422, 1373, 1320, 1232, 1190, 1178, 964, 797 cm^{-1}.

Synthesis of 2-(propargyloxymethyl)furan (1)

Furfuryl alcohol (9 ml, 104 mmol) was added dropwise to a suspension of sodium hydride (4.58 g, 115 mmol) in DMF (125 ml) at 0 °C. After being stirred for 30 min propargyl bromide (12.76 ml, 115 mmol) was added and the mixture was stirred for 4 h under TLC control at rt. H_2O (200 ml) was added and the product was extracted with Et_2O (3 x 150 ml) and washed with brine (2 x 150 ml). The combined organic layers were dried over $MgSO_4$ and the solvent was evaporated. The crude product was purified by column chromatography on silica gel (H to H/E = 10:1) to yield the desired product (11.83 g, 86% yield).
2-(Propargyloxymethyl)furan, **1**, was characterized by comparing its ^{1}H, ^{13}C-NMR and IR spectra to the previously reported in the literature.[7]

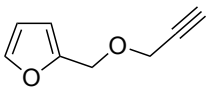

1

Yellow oil. Rf (H/E 10:2) = 0.47. **^{1}H-NMR** (400 MHz, $CDCl_3$): δ = 7.43 (dd, 1H), 6.39–6.34 (m, 2H), 4.57 (s, 2H), 4.17 (d, *J* = 2.4 Hz, 2H), 2.47 (t, *J* = 2.4 Hz, 1H) ppm. **^{13}C-NMR** (126 MHz, $CDCl_3$): δ = 150.80 (C), 143.10 (CH), 110.32 (CH), 110.08 (CH), 79.29 (CH), 74.79 (C), 63.04 (CH_2), 56.74 (CH_2) ppm. **IR** (ATR): 3293, 3121, 2909, 2857, 2117, 1733, 1503, 1443, 1350, 1261, 1224, 1150, 1069, 1011, 919, 739 cm^{-1}.

Synthesis of 5-hydroxy-4,5-dihydroisobenzofurane (2)

A solution of **1** (11 g, 81 mmol) and t-BuOK (18.1 g, 162 mmol) in n-Butanol (125 ml) was refluxed (83 °C) for 1 h (TLC control) under argon atmosphere. The brownish mixture was then diluted with H_2O (150 ml) and **2** was extracted with Et_2O (3 x 150 ml). The combined organic extracts were washed with brine

(2 x 150 ml), and dried over Na_2SO_4/K_2CO_3 and the solvent was evaporated. The crude product yield compound **2** (9.8 g, 90%).

5-Hydroxy-4,5-dihydroisobenzofurane, **2**, was characterized by comparing its ^1H,^{13}C-NMR and IR spectra to the previously reported in the literature.[8]

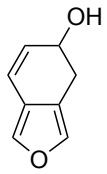

2

Yellow oil. Rf = 0.37. **^{1}H-NMR** (400 MHz, $CDCl_3$): δ = 7.33 (s, 1H), 7.21 (s, 1H), 6.53 (d, *J* = 9.8 Hz, 1H), 5.94 (dd, *J* = 9.8, 4.0 Hz, 1H), 4.51 (s, 1H), 3.11–2.69 (m, 2H), 1.59 (brs, 1H) ppm. **^{13}C-NMR** (126 MHz, $CDCl_3$): δ = 138.52 (CH), 137.47 (CH), 129.86 (CH), 120.12 (C), 119.59 (CH), 117.52 (C), 65.76 (CH), 28.16 (CH_2) ppm. **IR** (ATR): 3350, 3040, 2896, 1640, 1552, 1379, 1113, 1026, 889, 789 cm^{-1}.

Synthesis of 4-hydroxyphthalaldehyde (3)

A mixture of **2** (6.9 g, 50.7 mmol) and DDQ (11.5 g, 50.7 mmol) in Dioxane (100 ml) was stirred at 0 °C for 12 h. The black solution was warmed to room temperature for another 4 h. The solvent was removed and DCM (100 ml) was added which resulted in precipitate. The mixture was filtered and the black precipitate was washed with DCM (100 ml x 2). The organic layers were evaporated. The black precipitate was solved with DCM and filtered again, the solvent was then evaporated and the solid remaining (2 g) was purified by column chromatography (H/E 2:1) to yield **3** (1 g, 13%).

4-Hydroxyphthalaldehyde, **3**, was characterized by comparing its ^1H ,^{13}C-NMR and IR spectra to the previously reported in the literature.[9]

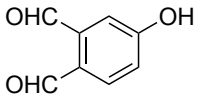

3

Brown solid. **^{1}H-NMR** (400 MHz, $CDCl_3$): δ = 10.65 (s, 1H), 10.30 (s, 1H) 7.91 (d, *J* = 8.4 Hz, 1H), 7.43 (d, *J* = 2.6 Hz, 1H), 7.20 (dd, *J* = 8.4, 2.6 Hz, 1H) ppm. **^{13}C-NMR** (126 MHz, $CDCl_3$): δ = 190.90, 169.64, 150.98, 120.00 ppm. **IR (**ATR): 3143, 2254, 1660, 1565, 1502, 1450, 1364, 1301, 1199, 1095, 834 cm^{-1}.

Synthesis of 4-propargyloxyphthalaldehyde (4)

3 (100 mg, 0.67 mmol) and potassium carbonate (138 mg, 1 mmol) were dissolved in DMF (8 ml) and the mixture was stirred at 50 °C for 2 h. Then, propargyl bromide (198 mg, 1.33 mmol) was added at 0 °C and the mixture was stirred 5 h, at rt. The product was extracted with water and DCM. The organic

layer was washed with brine and dried with Na_2SO_4 and evaporated under reduced pressure. The crude product (115 mg) was purified by column chromatography. (95 mg, 76%) of the black solid **4** were obtained.

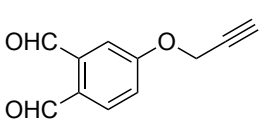

4

^{1}H-NMR (400 MHz, $CDCl_3$): δ = 10.65 (s, 1H), 10.36 (s, 1H) 7.96 (d, *J* = 8.5 Hz, 1H), 7.54 (d, *J* = 2.6 Hz, 1H), 7.31 (dd, *J* = 8.5, 2.6 Hz, 1H) 4.84 (d, *J* = 2.4, 2H) 2.59 (t, *J* = 2.4, 1H) ppm.

Synthesis of CB6-PhOH.

A mixture of **Hexamer** (1.2 g, 1.2 mmol) and **3** (217 mg, 1.4 mmol) was dissolved in 9 M H_2SO_4 (5 ml) and stirred at rt 4 days. The reaction solution was poured into MeOH (40 ml) which resulted in a black precipitate. The precipitate was washed with MeOH (40 ml × 3) and centrifuged. The precipitate was dried under high vacuum to give a crude. The crude was dissolved in 88% formic acid/1.0 M HCl (1:1, v/v, 40 ml) to give black solution, which was treated with decolorizing carbon (2.0 g) to give a clear, light-yellow solution. The solvent was removed by rotary evaporation and dried under high vacuum. The yellow solid was then washed with MeOH (40 ml) and centrifuged. The supernatant was decanted and the precipitate was dried under high vacuum to give crude compound (1.07 g, including ~13% **Hexamer**) as a white powder. The precipitate was washed with a solution of *p*-xylylenediamine (15 mM, 10 ml) and centrifuged. The supernatant was decanted and the precipitate was washed with H_2O (10 ml) and then centrifuged. The supernatant was decanted and the precipitate was dried under high vacuum to give **CB6-PhOH** as a white powder (490 mg, 0.45 mmol, 38%).

The final product, **CB6-PhOH**, was characterized by comparing its ^{1}H ,^{13}C-NMR and IR spectra to the previously reported in the literature.[6]

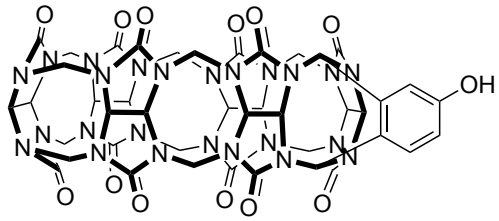

CB6-PhOH

^{1}H-NMR (500 MHz, D_2O, >1 eq *p*-xylylenediamine): δ = 7.58 (d, *J* = 8.4, 1H), 7.26 (d, *J* = 1.9, 1H), 7.15 (dd, *J* = 8.4 and 1.9, 1H), 6.84 (s, 1H), 6.81 (s, 1H), 5.93 (d, *J* = 15.8, 2H), 5.76 (d, *J* = 8.8, 2H), 5.70-5.60 (m, 10H), 5.32 (d, *J* = 9.0, 2H), 5.23 (d, *J* = 9.0, 2H), 5.14 (d, *J* = 9.7, 2H),

4.96 (d, *J* = 9.7, 2H), 4.57 (d, *J* = 15.8, 2H), 4.01 (d, *J* = 15.3, 4H) ppm. **IR** (ATR): 3491, 3002, 2929, 1724, 1465, 1418, 1374, 1322, 1295, 1235, 1186, 964 cm^{-1}.

Synthesis of CB6-PhOPr.

a) A mixture of **3** (304 mg, 0.28 mmol), propargyl bromide (1 ml, 80% in toluene), and K_2CO_3 (186 mg, 1.35 mmol) was dissolved in NMP (1.5 ml) and stirred at 50 for 3 d. The reaction solution was poured into MeOH (30 ml) which resulted in a white precipitate. The mixture was centrifuged and the supernatant decanted. The precipitate was washed with MeOH (30 ml x 2) and centrifuged. The supernatant was decanted and the precipitate was recrystallized from TFA/H_2O (4 ml, v/v = 1:2). The recrystallized solid was dried under high vacuum to give **CB6-PhOPr** as a white powder (300 mg, 0.26 mmol, 95%).

b) A mixture of **Hexamer** (292 mg, 0.3 mmol) and **4** (68 mg, 0.36 mmol) was dissolved in 9 M H_2SO_4 (5 ml) and stirred at room temperature for 4 d. The reaction solution was poured into MeOH (40 ml) which resulted in a black precipitate. The mixture was centrifuged for 5 min. The supernatant was decanted and the precipitate was washed with MeOH (40 ml × 3) and centrifuged 5 min. The precipitate was dried and the crude, gray powder was dissolved in 88 % formic acid/1.0 M HCl (1:1, v/v, 40 ml) to give a black solution, which was treated with decolorizing carbon (2.0 g) to give a clear, light-yellow solution. The solvent was removed by rotary evaporation and dried under high vacuum. The yellow solid was then washed with MeOH (40 ml) and centrifuged 5 min. The supernatant was decanted and the precipitate was dried under high vacuum to give **CB6-PhOPr** (230 mg, 0.21 mmol, 68%).

The final product, **CB6-PhOPr**, was characterized by comparing its ^{1}H ,^{13}C-NMR and IR spectra to the previously reported in the literature.[6]

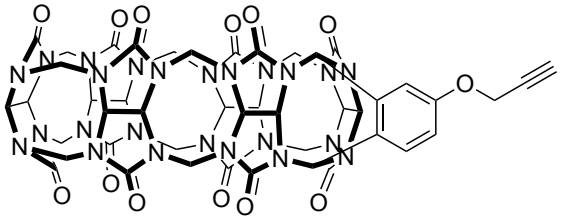

CB6-PhOPr

^{1}H-NMR (500 MHz, D_2O, >1 equiv. *p*-xylylenediamine): δ = 7.72 (d, *J* = 8.5, 1H), 7.43 (d, *J* = 2.6, 1H), 7.34 (dd, *J* = 8.5 and 2.6, 1H), 6.90 (s, 1H), 6.89 (s, 1H), 5.94 (d, *J* = 15.9, 2H), 5.79 (d, *J* = 9.0, 2H), 5.66 (m, 10H), 5.33 (d, *J* = 9.0, 2H), 5.24 (d, *J* = 9.0, 2H), 5.15 (d, *J*

= 9.7, 2H), 4.94 (d, *J* = 9.7, 2H), 4.95 (d, *J* = 2.3, 2H), 4.59 (d, *J* = 15.9, 2H), 4.46 (s, 4H), 4.21 (d, *J* = 15.3, 4H), 4.03 (d, *J* = 15.3, 4H), 2.98 (t, *J* = 2.3, 1H) ppm.

II.4.3.6. Preparation of MNPs and MR

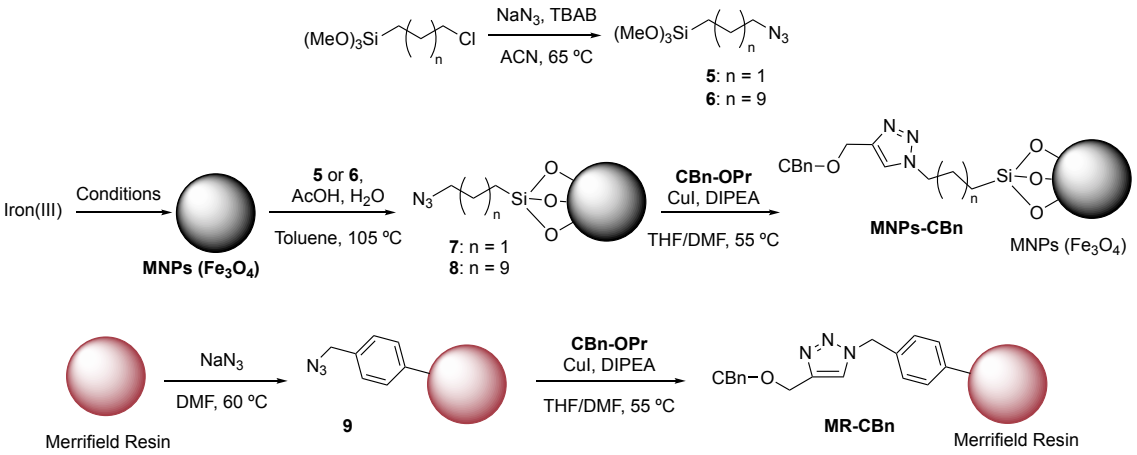

Synthesis of 3-azidopropyltrimethoxysilane (5)

(3-chloropropyl)trimethoxysilane (0.94 ml, 5 mmol) was added to a solution of sodium azide (0.49 g, 7.5 mmol) and tetrabutylammonium bromide (0.33 g, 1 mmol) in dry MeCN (19 ml) under argon atmosphere. The reaction mixture was stirred at 65 °C for 48 h. After the reaction, the solvent was removed under reduced pressure. The crude mixture was then diluted in Et_2O (30 ml) and the suspension was filtered and washed with Et_2O (2 x 10 ml). The combined solvent was removed and **5** (94 %) was obtained as a pure and colorless liquid. 3-Azidopropyltrimethoxysilane, **5**, was characterized by comparing its ^{1}H NMR and IR spectra to the previously reported in the literature.[10]

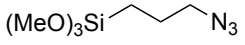

5

^{1}H-NMR (400 MHz, $CDCl_3$): δ = 3.56 (s, 9H), 3.27 (t, *J* = 6.9 Hz, 2H), 1.71–1.56 (m, 2H), 0.75–0.66 (m, 2H) ppm. **IR** (ATR): 2943, 2841, 2094, 1455, 1189, 1077, 814 cm^{-1}.

Synthesis of 11-azidoundecyltrimethoxysilane (6)

(3-chloroundecyl)trimethoxysilane (1.77 g, 5 mmol) was added to a solution of sodium azide (0.49 g, 7.5 mmol) and tetrabutylammonium bromide (0.33 g, 1 mmol) in dry MeCN (19 ml) under argon atmosphere. The reaction mixture was stirred at 65 °C for 48 h. After the reaction, the solvent was removed under reduced pressure. The crude mixture was then diluted in Et_2O (30 ml) and the

suspension was filtered and washed with Et_2O (2 x 10 ml). The combined solvent was removed and **6** (91 %) was obtained as a pure and colorless liquid. 11-Azidoundecyltrimethoxysilane, **6** was characterized by comparing its ^1H NMR and IR spectra to the previously reported in the literature.[11]

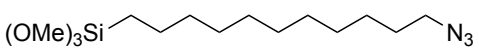

6

^{1}H-NMR (400 MHz, $CDCl_3$): δ = 3.56 (s, 9H), 3.24 (t, J = 6.9 Hz, 2H), 1.58 (m, 2H), 1.26 (m, 16H), 0.75–0.62 (m, 2H) ppm. **IR** 2925, 2854, 2093, 1464, 1190, 1081, 812 cm^{-1}. **EA**: calculated 52.96 %C, 9.84 %H, 13.23 %N. Found 53.07 %C, 8.81 %H, 13.41 %N.

Synthesis of magnetic nanoparticles, MNPs (Fe_3O_4)[12]

a) (4–10 nm MNPs) To a suspension of dodecane-1,2-diol (11.24 g, 50.0 mmol) in benzyl ether (100 ml) under nitrogen flow, iron(III) acetylacetonate (3.64 g, 10 mmol), oleylamine (14.10 ml, 30.0 mmol) and oleic acid (10,58 ml, 30,0 mmol) were added and the reaction was stirred at 260 °C, in constant Ar flow for 3h and cooled at rt. The MNPs were separated by centrifugation with EtOH (10 min, 4.4 rpm). Washed (2 x 10 ml) with EtOH and (2 x 10 ml) with acetone. Dried over vacuum at 40 °C overnight. All solvent with HPLC grade. The final product (993 mg) was kept at rt.

b) (90–120 nm MNPs) $FeCl_3 \cdot 6H_2O$ (0.81 g) was dissolved in 25 ml glycol and transferred to a 50 ml flask. KAc (1.47 g) was then added to the solution, stirring constantly. Reflux was maintained at 200°C for 24 h. After naturally cooled to room temperature, the black magnetite particles were gathered by magnet and washed with deionized water and ethanol three times, respectively. The final product was dried in a vacuum at 65 °C for 12 h. **MNPs** (268 mg).

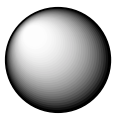

MNPs (Fe_3O_4)

TEM: **Size batch a1**: 4.1 ± 0.8 nm. **Size batch a2**: 6.4 ± 2.0 nm. **Size batch b1**: 115 ± 15 nm. **Size batch b2**: 91 ± 12 nm. **Size batch b3**: 91 ± 17 nm. **EA batch a2**: 13.96 %C, 2.27 %H, <0.1% N. **Batch b1**: 3.07 %C, 1.33 %H, <0.10 %N.

Synthesis of MNPs-(3-azidopropyl)trimethoxysilane (7)[12]

To a suspension of MNPs (batch a1, 402 mg) in degassed toluene (10 ml) under argon, 3-azidopropyltrimethoxysilane **5** (482.4 mg, 2.35 mmol), glacial acetic acid (50.3 µl, 0.87 mmol) and ultrapure water (69 µl, 3.86 mmol) were added. The reaction mixture was warmed at 105 °C for 24 h and then cooled at rt. The MNPs were removed using an external magnetic field, washed several times with MeOH, hexane, acetone and dried under vacuum to obtain 413 mg of **7**.

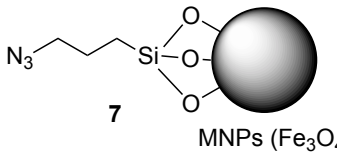

7

EA batch a1.1: found 15.13 %C, 2.55 %H, 7.74 %N; *f* = 1.84 mmol g^{-1}. **EA batch a1.2**: found 12.44 %C, 2.16 %H, 5.05 %N; *f* = 1.19 mmol g^{-1}. **TGA batch a1.1**: (30–900 °C, 10 °C/min, under air; for a 5.3950 mg sample, % weight loss): 9.67 (left limit: 43 °C, right limit: 287 °C), 17.71 (left limit: 287 °C, right limit 696 °C). **IR** (ATR): 2921, 2851, 2091, 1522, 1411, 1239, 1116, 1014, 554 cm^{-1}.

Synthesis of MNPs-(11-azidoundecyl)trimethoxysilane (8)

To a suspension of MNPs (212 mg) in degassed toluene (8 ml) under argon, 11-azidoundecyltrimethoxysilane **6** (497 mg, 1.56 mmol), glacial acetic acid (33 µl, 0.56 mmol) and ultrapure water (44 µl, 2.50 mmol) were added. The reaction mixture was warmed at 105 °C for 24 h and then cooled at room temperature. The MNPs were removed using an external magnetic field, washed several times with MeOH, hexane, acetone and dried under vacuum to obtain **8** (black solid for 100 nm MNPs and ferrofluid for 5 nm MNPs). Note: for batch a2.1, **6** (0.3 mmol) and ethyltrimethoxysilane (1 mmol) were added

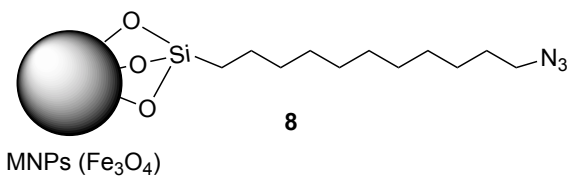

8

EA batch a1.3: found 12.47 %C, 2.00 %H, 0.98 %N; *f* = 0.23 mmol g^{-1}. **EA batch a2.1**: found 10.87 %C, 1.83 %H, 0.62 %N; *f* = 0.15 mmol g^{-1}. **EA batch b1.1**: found 5.54 %C, 1.42 %H, 0.57 %N; *f* = 0.14 mmol g^{-1}. **EA batch b2.1**: found 6.33 %C, 1.59 %H, 0.70 %N; *f* = 0.17 mmol g^{-1}. **TGA batch b1.1**: (30–1000 °C, 10 °C/min, under N_2; for a 9.8390 mg sample, % weight loss): 0.71 (left limit: 40 °C, right limit: 121 °C), 11.43 (left limit: 140 °C, right limit 530 °C), 7.82 (left limit: 534 °C, right limit 942 °C). **TGA batch b2.1**: (30–1000 °C,

10 °C/min, under N_2; for a 8.0540 mg sample, % weight loss): 0.64 (left limit: 40 °C, right limit: 125 °C), 11.06 (left limit: 125 °C, right limit 554 °C), 10.66 (left limit: 554 °C, right limit 935 °C). **IR** (ATR): 2926, 2855, 2097, 1544, 1443, 1239, 11086, 442 cm^{-1}.

Synthesis of azidomethylpolystyrene (9)[12]

To a suspension of Merrifield resin HL (100–200 mesh, 4.7 ± 1 nm S9 Novabiochem, *f* = 1.3 mmol g^{-1}) (500 mg, 0.65 mmol) in dry DMF (20 ml) was added sodium azide (211 mg, 3.25 mmol). The reaction was shaken (orbital shaker) at 60 °C overnight. Then, the resultant mixture was cooled at rt and filtered. The resin was washed several times with H_2O, THF, THF-MeOH (1:1), MeOH, THF and dried under vacuum. A 98 % yield of functionalization was calculated on the basis of nitrogen elemental analysis—calculated (%): 5.75.

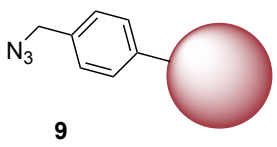

9

Merrifield Resin

EA batch 1: found 86.18 %C, 7.93 %H, 5.63 %N; *f* = 1.34 mmol g^{-1}. **IR** (ATR): 3059, 3025, 2921, 2093, 1601, 1492, 1451, 754, 696, 539 cm^{-1}.

General Procedure for the synthesis of MNPs-CBn and MR-CBn

To a suspension of solid support (20–100 mg) in a mixture of 2–10 ml of dry THF/DMF (1:1) the propargylated CBn (2 eq), DIPEA (5 eq) and CuI (0.5 eq) were added. The mixture was shaken at 55 °C during 48–72 h. Then, the reaction was cooled at rt. The resultant mixture was filtered and the solid was washed with H_2O, MeOH, THF:ethylendiamine (1:0.1), THF, acetone, DCM and dried under high vacuum at 70 °C. The functionalization was calculated on the basis of nitrogen elemental analysis. Excess of cucurbiturils were recovered from water washings and reused after functionalization.

MR-CB6Ph

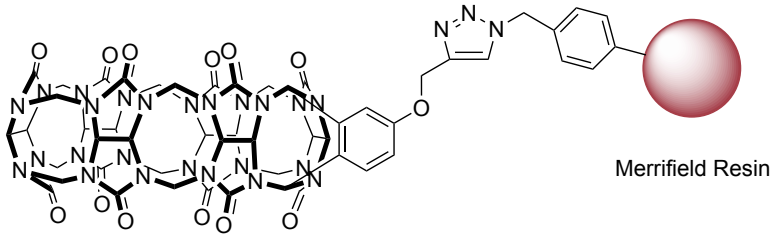

EA batch 1: calculated for f_{max} = 0.54 mmol g^{-1}. Found 61.33 %C, 5.95 %H, 12.21 %N; f = 0.32 mmol g^{-1}. **IR** (ATR): 3024, 2918, 2848, 2094, 1737, 1452, 1234, 1185, 964, 800, 697 cm^{-1}.

MR-CB6

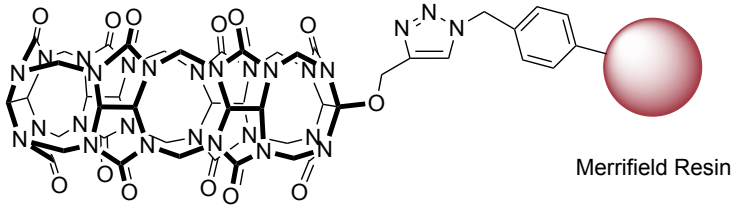

EA batch 1: calculated for f_{max} = 0.56 mmol g^{-1}. Found 68.74 %C, 6.23 %H, 11.35 %N; f = 0.30 mmol g^{-1}. **IR** (ATR): 3493, 3256, 2929, 1729, 1466, 1416, 1374, 1322, 1232, 1189, 964, 797 cm^{-1}.

MR-CB7

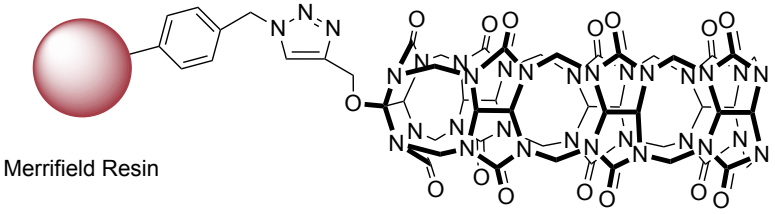

EA batch 1: calculated for f_{max} = 0.51 mmol g^{-1}. Found 72.18 %C, 6.49 %H, 11.21 %N; f = 0.26 mmol g^{-1}. **IR** (ATR): 3266, 2921, 2094, 1724, 1455, 1372, 1317, 1224, 1187, 965, 800 cm^{-1}.

MNPs-CB6

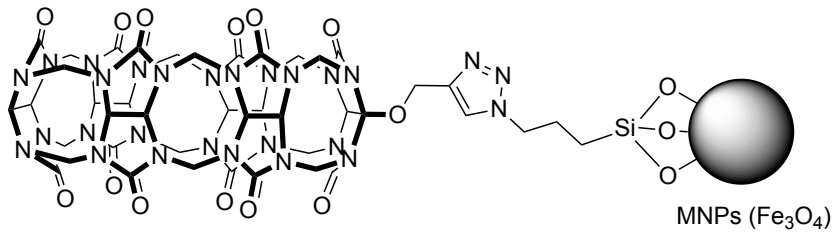

EA batch a1.1: calculated for f_{max} = 0.63 mmol g^{-1}. Found 29.61 %C, 3.94 %H, 19.6 %N; f = 0.52 mmol g^{-1}. **TGA batch a1.1**: (30–900 °C, 10 °C/min, under air; for a 5.7000 mg sample, % weight loss): 10.36 (left limit: 39 °C, right limit: 186 °C), 65.15 (left limit: 187 °C, right limit 533 °C). **IR** (ATR): 3519, 2930, 2099, 1729, 1470, 1416, 1375, 1323, 1282, 1233, 1189, 963, 797 cm^{-1}.

MNPs-CB7

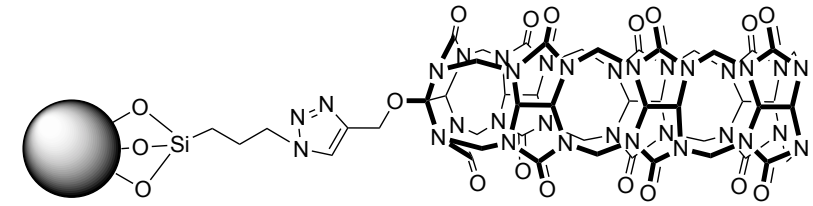

EA batch a1.1.1: calculated for f_{max} = 0.57 mmol g^{-1}. Found 32.79 %C, 3.75 %H, 16.16 %N; f = 0.37 mmol g^{-1}. **EA batch a1.1.2**: calculated for f_{max} = 0.57 mmol g^{-1}. Found 29.66 %C, 3.73 %H, 16.04 %N; f = 0.37 mmol g^{-1}. **EA batch a1.1.3**: calculated for f_{max} = 0.57 mmol g^{-1}. Found 29.91 %C, 3.54 %H, 14.25 %N; f = 0.33 mmol g^{-1}. **EA batch a1.2**: calculated for f_{max} = 0.49 mmol g^{-1}. Found 23.04 %C, 2.83 %H, 10.27 %N; f = 0.24 mmol g^{-1}. **TGA batch a1.1.2**: (30–900 °C, 10 °C/min, under air; for a 5.1030 mg sample, % weight loss): 4.87 (left limit: 41 °C, right limit: 147 °C), 58.95 (left limit: 150 °C, right limit 546 °C). **TGA batch a1.1.3**: (30–1000 °C, 10 °C/min, under N_2; for a 6.8490 mg sample, % weight loss): 5.20 (left limit: 39 °C, right limit: 156 °C), 37.39 (left limit: 156 °C, right limit 552 °C), 13.78 (left limit: 552 °C, right limit 862 °C). **TGA batch a1.2**: (30–1000 °C, 10 °C/min, under N_2; for a 7.2290 mg sample, % weight loss): 4.42 (left limit: 42 °C, right limit: 147 °C), 30.04 (left limit: 148 °C, right limit 534 °C), 21.04 (left limit: 534 °C, right limit 923 °C). **IR** (ATR): 3512, 3262, 2920, 2099, 1726, 1464, 1421, 1374, 1321, 1228, 1190, 967, 802 cm^{-1}.

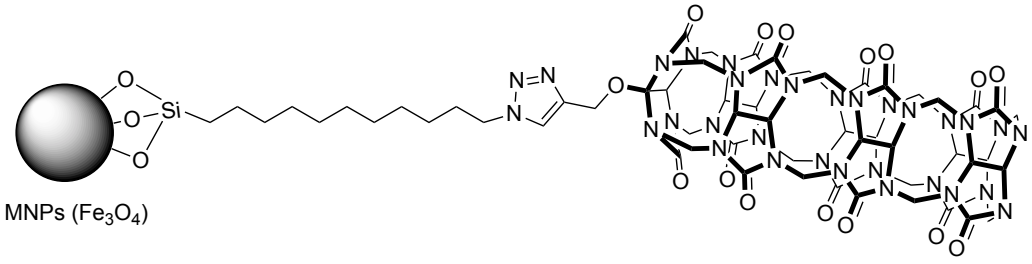

EA batch a2.1: calculated for f_{max} = 0.13 mmol g^{-1}. Found 11.98 %C, 1.99 %H, 2.20 %N; f = 0.05 mmol g^{-1}. **EA batch b1.1**: calculated for f_{max} = 0.12 mmol g^{-1}. Found 9.42 %C, 1.85 %H, 2.52 %N; f = 0.06 mmol g^{-1}. **EA batch b2.1**: calculated for f_{max} = 0.14 mmol g^{-1}. Found 11.29 %C, 1.74 %H, 2.81 %N; f = 0.07 mmol g^{-1}. **TGA batch a2.1**: (30–1000 °C, 10 °C/min, under N_2; for a 9.4760 mg sample, % weight loss): 0.80 (left limit: 41 °C, right limit: 133 °C), 16.35 (left limit: 133 °C, right limit 532 °C), 15.70 (left limit: 532 °C, right limit 938 °C). **TGA batch b1.1**: (30–1000 °C, 10 °C/min, under N_2; for a 8.4250 mg sample, % weight loss): 1.44 (left limit: 41 °C, right limit: 132 °C), 15.15 (left limit: 136 °C, right limit 529 °C), 14.81 (left limit: 529 °C, right limit 917 °C). **TGA batch b2.1**: (30–1000 °C, 10 °C/min, under N_2; for a 8.2000 mg sample, % weight loss): 0.70 (left limit: 38 °C, right limit: 120 °C), 15.59 (left limit: 120 °C, right limit 517 °C), 19.50 (left limit: 518 °C, right limit 900 °C). **IR** (ATR): 3851, 2920, 2850, 2091, 1732, 1457, 1318, 1229, 998, 802, 553 cm^{-1}.

MNPs-CB6Ph

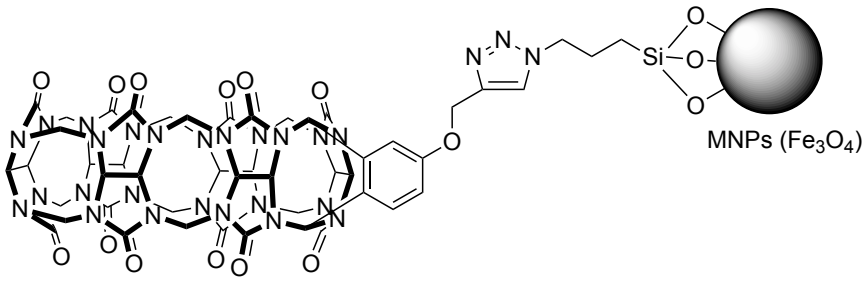

EA batch a1.2: calculated for f_{max} = 0.51 mmol g^{-1}. Found 25.32 %C, 3.43 %H, 14.52 %N; f = 0.38 mmol g^{-1}. **EA batch a1.1**: calculated for f_{max} = 0.60 mmol g^{-1}. Found 30.56 %C, 4.00 %H, 18.69 %N; f = 0.49 mmol g^{-1}. **TGA batch a1.1**: (30–900 °C, 10 °C/min, under air; for a 5.9190 mg sample, % weight loss): 7.48 (left limit: 41 °C, right limit: 174 °C), 68.65 (left limit: 176 °C, right limit 686 °C) 1.54 (left limit: 688 °C, right limit 809 °C). **IR** (ATR): 3436, 3323, 3269, 2930, 2098, 1728, 1462, 1372, 1233, 1185, 962, 798 cm^{-1}.

II.4.3.7. Synthesis of adamantyl tagged fluorescein

Synthesis of 3-(1-adamantylethoxy) prop-1-yne (10)

To a solution of 1-adamantaneethanol 98% (2.5 g, 13.86 mmol) in THF at 0 ºC was added in small portions over 15 minutes NaH (60 % in mineral oil, 15.25

mmol, 0.584 mg) followed by propargyl bromide (80 % in toluene, 16.64 mmol, 1.8 mL). A brown precipitate appeared after the addition, and the resulting mixture was stirred at room temperature overnight. The reaction was quenched by addition of water (5 mL), extracted with dichloromethane (2 Å~ 20 mL), filtered through a piece of cotton wool and evaporated. The crude mixture was purified by column chromatography over silica gel using 9:1 hexane-ethyl acetate as eluant to render the product as a white powder (2.1 g, 9.62 mmol, 70 % yield).

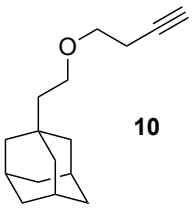

10

^{1}H NMR (400 MHz, $CDCl_3$): δ = 4.10 (d, 4JH-H = 2.4 Hz, 2H, OCH_2CCH), 3.56 (t, 3JH-H = 7.4 Hz, 2H, OCH_2CH_2), 2.40 (t, *J* = 2.4 Hz, 1H, CH), 1.92 (s, 3H, CH adamantyl), 1.71 (m, 6H, CH_2 adamantyl), 1.52 (m, 6H, CH_2 adamantyl), 1.39 (t, *J* = 7.4 Hz, 2H, OCH_2CH_2) ppm. **^{13}C NMR** (100 MHz, $CDCl_3$): δ = 74.26, 66.42, 58.18, 43.58, 42.90 (CH_2), 37.31 (CH_2), 31.99, 28.88 (CH) ppm. **IR** (ATR): 3306, 2897, 2845, 1728, 1447, 1353, 1095 cm^{-1}.

Synthesis of Ad-5-FAM (11)

5-FAM-Azide (2.23 mg, 4.67 μmol) was dissolved in DMF (0.5 ml). To the solution, alkyne **10** (1.02 mg, 4.67 μmol) was subsequently added followed by CuI (0.08 eq) and DIPEA (5 eq). The reaction mixture was stirred overnight at 60 ºC. The crude was then purified by preparative HPLC. **HPLC-MS** (ESI+) *m/z*: calcd for [**11** + 2H]$^{2+}$: 677.30. Found: 677.2.

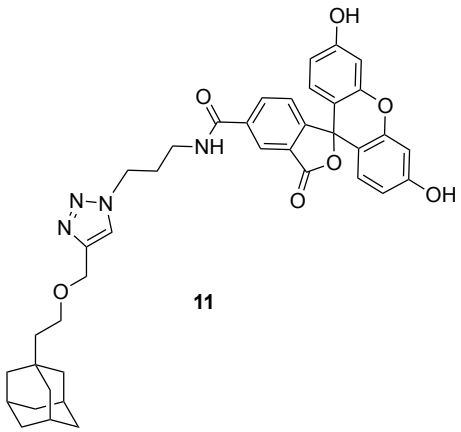

11

II.4.4. Functionality: mmol of CBn / g of MNPs or MR

Functionalization calculated by elemental analysis (EA) and thermogravimetric analysis (TGA).

EA

Table II-S1. Functionalization of CBn coated MNPs.[a]

batch	coated solid	f (mmol·g^{-1})	f_0 (mmol·g^{-1})	f_{max} (mmol·g^{-1})
a1.1	MNPs-CB6	0.52	1.84	0.63
a1.1	MNPs-CB6Ph	0.49	1.84	0.60
a1.2	MNPs-CB6Ph	0.38	1.19	0.51
a1.1.1	MNPs-CB7	0.37	1.84	0.57
a1.1.2	MNPs-CB7	0.37	1.84	0.57
a1.1.3	MNPs-CB7	0.33	1.84	0.57
a1.2	MNPs-CB7	0.24	1.19	0.49
1	MR-CB6	0.30	1.34	0.56
1	MR-CB7	0.26	1.34	0.51
1	MR-CB6Ph	0.32	1.34	0.54

[a]The functionalization was calculated by % of N. f_0 corresponds to the functionalization of the starting azide coated solid support. f_{max} was measured with the following formula:

$$f_{max} = \frac{f_0}{1 + f_0 \frac{\text{MW diference}}{1000}}$$

TGA

Table II-S2. Functionalization of MNPs determined by EA and TGA.

MNPs (mmol x g^{-1})	CB6	CB7	CB6Ph
EA	0.52	0.37	0.49
TGA	0.48	0.31	0.45

Example of functionalization measured by TGA.

Table II-S3. Functionalization of MNPs measured by TGA.[a]

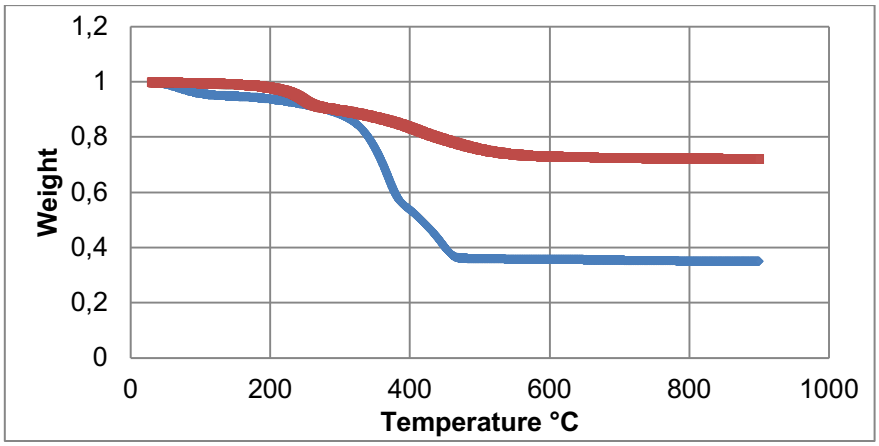

initial weight (mg)	difference in weight loss	CB7 (mg)	CB7 (µmol)	f (mmol/g)
5.103	0.372	1.899	0.156	0.31

[a]TGA of **MNPs-N_3** (red) vs TGA of **MNPs-CB7** (blue). Functionalization measured by means of the difference in weight loss (mg of **CBn**).

Functionalization of MNPs with the long linker:

EA

Table II-S4. Functionalization of MNPs with long linker.[a]

batch	coated solid	f (mmol·g^{-1})	f_0 (mmol·g^{-1})	f_{max} (mmol·g^{-1})
a2.1	MNPs-CB7	0.05	0.15	0.13
b1.1	MNPs-CB7	0.06	0.14	0.12
b2.1	MNPs-CB7	0.07	0.17	0.14

[a]The functionalization calculated by % of N. f_0 corresponds to the functionalization of the starting azide coated solid support. f_{max} was measured with the following formula:

$$f_{max} = \frac{f_0}{1 + f_0 \frac{\text{MW diference}}{1000}}$$

TGA

Table II-S5. Functionalization of MNPs by EA and TGA.[a]

MNPs(mmol·g^{-1})	CB7	CB7	CB7
EA	0.05	0.06	0.07
TGA	0.05	0.09	0.11

[a]Comparison of the functionalization of some **MNPs** measured by EA and TGA

II.4.5. Effective functionalization

The effective functionalization is intended to measure the functionalization of the solid support by means of guest extraction, rather than measuring the amount of cucurbiturils coating the solid surface area.

Preparation of the buffer

Deuterated sodium acetate buffer solution (50 mM) was prepared by dissolving 102 mg of sodium acetate in 23.3 ml D_2O.

Preparation of stock solutions

- 6.24 mM *p*-xylylenediamine dihydrochloride was prepared by dissolving 5.22 mg of the reagent in 4 ml buffer.
- 1.69 mM **CB7** was prepared by dissolving 8.92 mg (88% **CB7**, measured by ^{1}H-NMR) in 4 ml buffer.
- 13.49 mM dimethyl sulfone, the internal standard (IS), was prepared by dissolving 5.08 mg in 4 ml buffer.

Experimental procedure

A 0.8 ml solution was prepared by adding *p*-xylylenediamine (3 mM) and dimethyl sulfone (3 mM). The reaction mixture was sonicated for 1 min and then ^{1}H NMR spectrum was recorded. The same solution was prepared at different concentrations and different amounts of **CB7**, nanoparticles or resin were added. The mixtures were stirred 5 min, centrifuged and filtrated before NMR analyses.

Table II-S6. Extraction of *p*-xylylenediamine with **MR-CB7**.

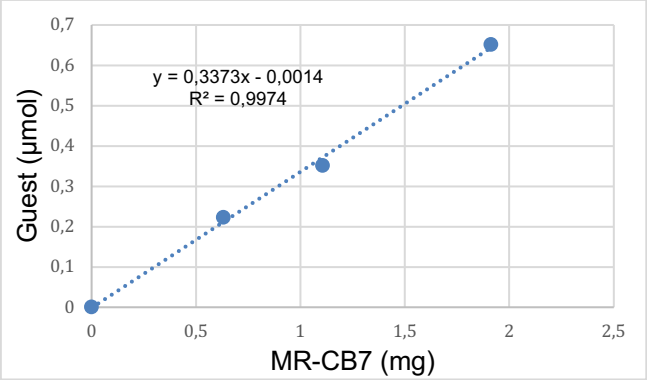

MR-CB7 (mg)	Guest (µmol)	*f* (mmol/mg)
0	0	-
0.631	0.222	0.34
1.104	0.351	0.32
1.910	0.651	0.35

Table II-S7. Extraction of *p*-xylylenediamine with **MNPs-CB7.**

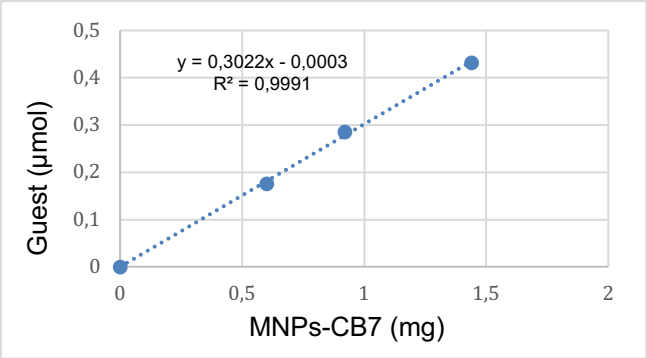

MNPs-CB7 (mg)	Guest (µmol)	*f* (mmol/mg)
0	0	-
0.600	0.176	0.29
0.920	0.285	0.31
1.439	0.432	0.30

II.4.6. Efficiency of extraction

Different amounts of the adamantly tagged **Ad-5-FAM** were measured in the µg balance (between 50 and 300 µg). The samples were dissolved in different amounts of ethanol in order to prepare stock solutions at the same concentration (1.46 $x10^{-4}$ M). To measure the calibration curve, the stock solutions were diluted by 10 (solution 1) and by 100 (solution 2). 100 µl of solution 1 were diluted with 900 µl of Ethanol and 100 µl of solution 2 were diluted with 900 µl of Ethanol. From these solutions 5, 10 and 20 µl were diluted with 3 ml of Ethanol in order to obtain six solutions at the adequate concentrations (2 $x10^{-9}$–1 $x10^{-7}$ M) to measure the calibration curve. From different stock solutions, several solutions were prepared (9.1 µM). To these solutions, different amounts of **MNPs-CB7** were subsequently added and sonicated for 5 seconds and mixed for 10 seconds. Then, the mixtures were centrifuged for 5 min and the concentration of the corresponding solutions were measured by the intensity of the emission at 526 nm.

Calibration curve of the fluorescent guest molecule

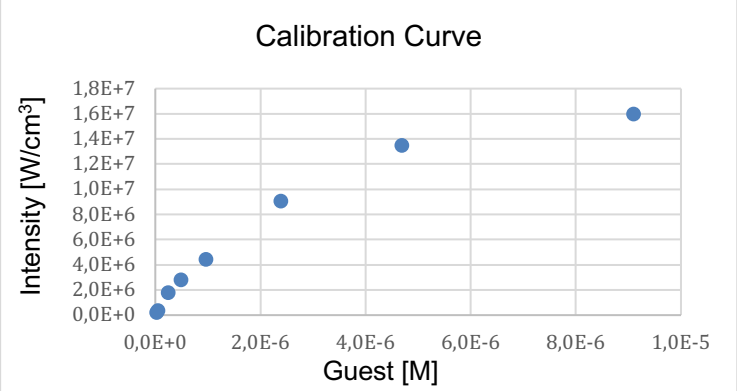

II.4.7. IR, ^{1}H NMR spectra and TEM images

II.4.7.1. Compound CB6

^{1}H NMR (400 MHz. D_2O)

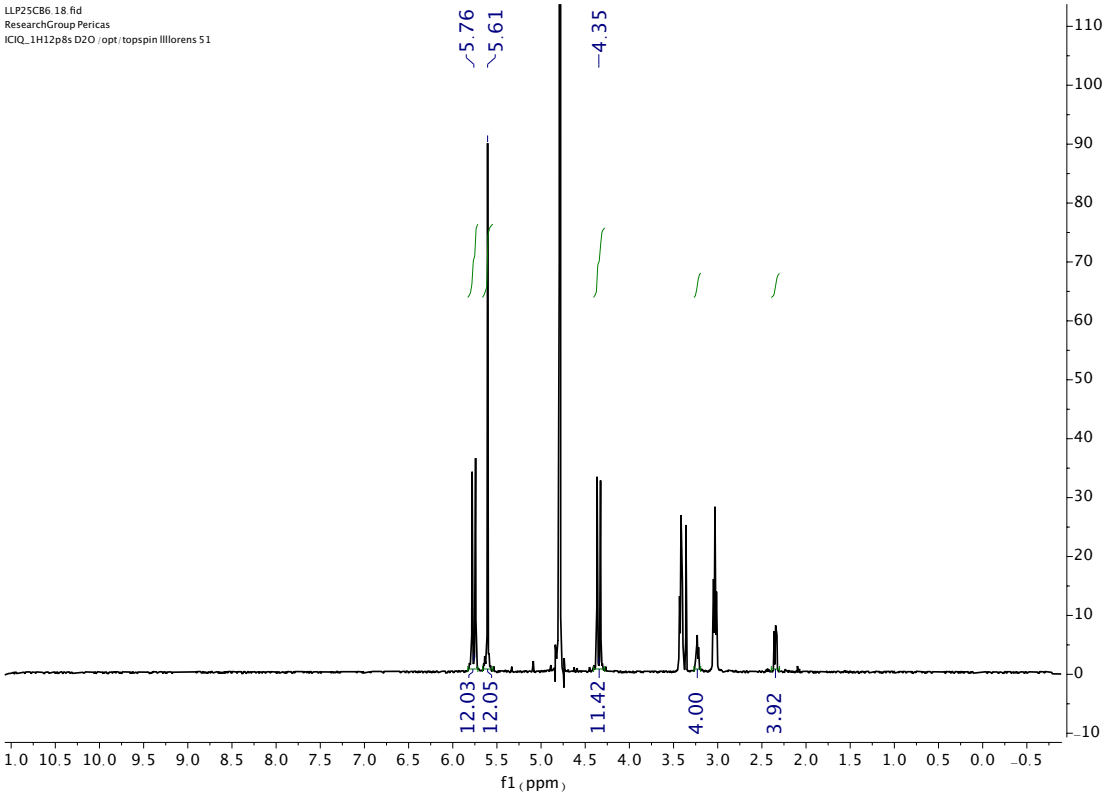

^{1}H NMR in the presence of >2 eq of cystamine hydrochloride.

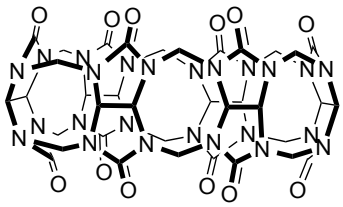

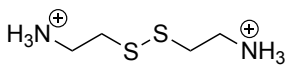

2 Cl^-

II.4.7.2. Compound CB7

^{1}H NMR (400 MHz. D_2O)

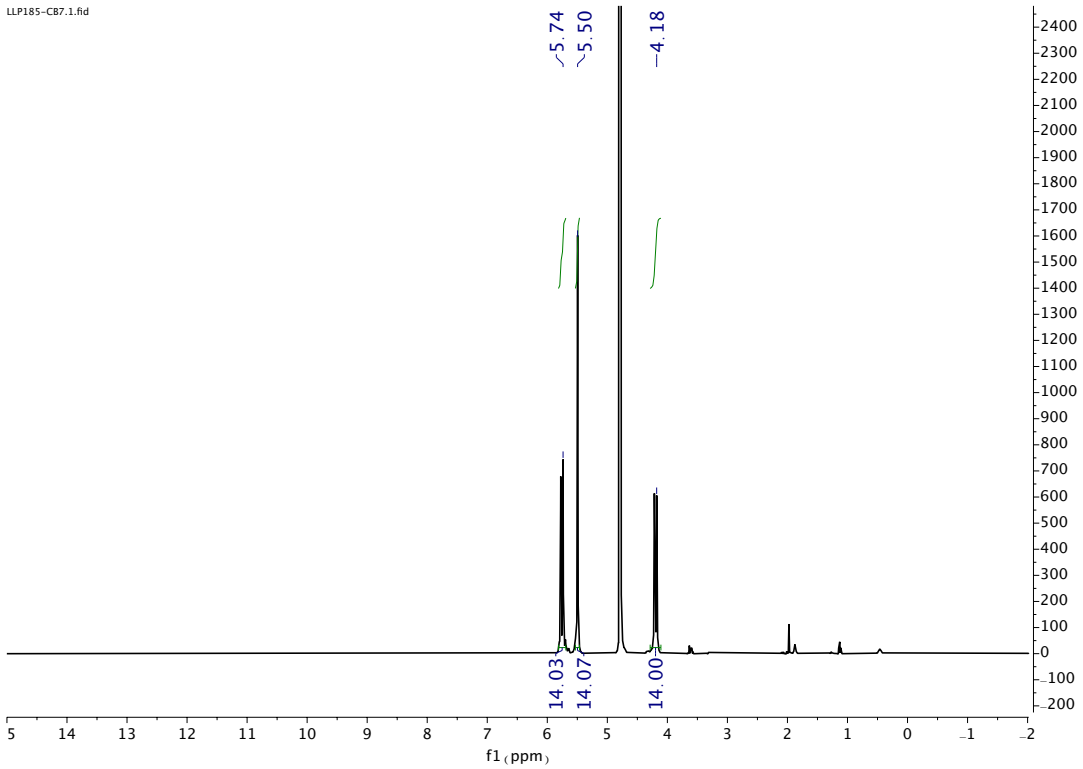

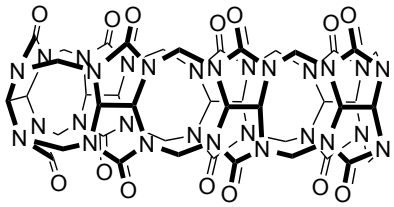

II.4.7.3. Compound CB6-OH

^{1}H NMR (400 MHz. D_2O)

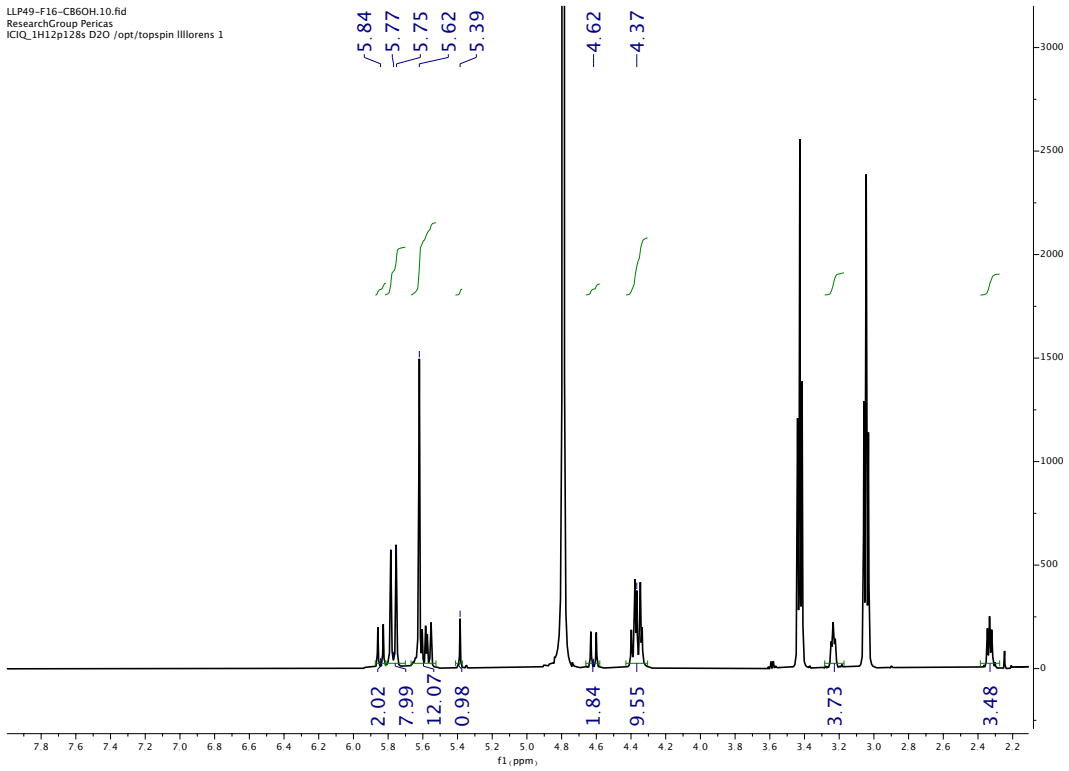

^{1}H NMR in the presence of >2 eq of cystamine hydrochloride.

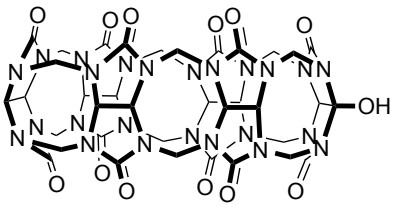

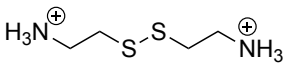

2 Cl^-

II.4.7.4. Compound CB7-OH

^{1}H NMR (400 MHz. D_2O)

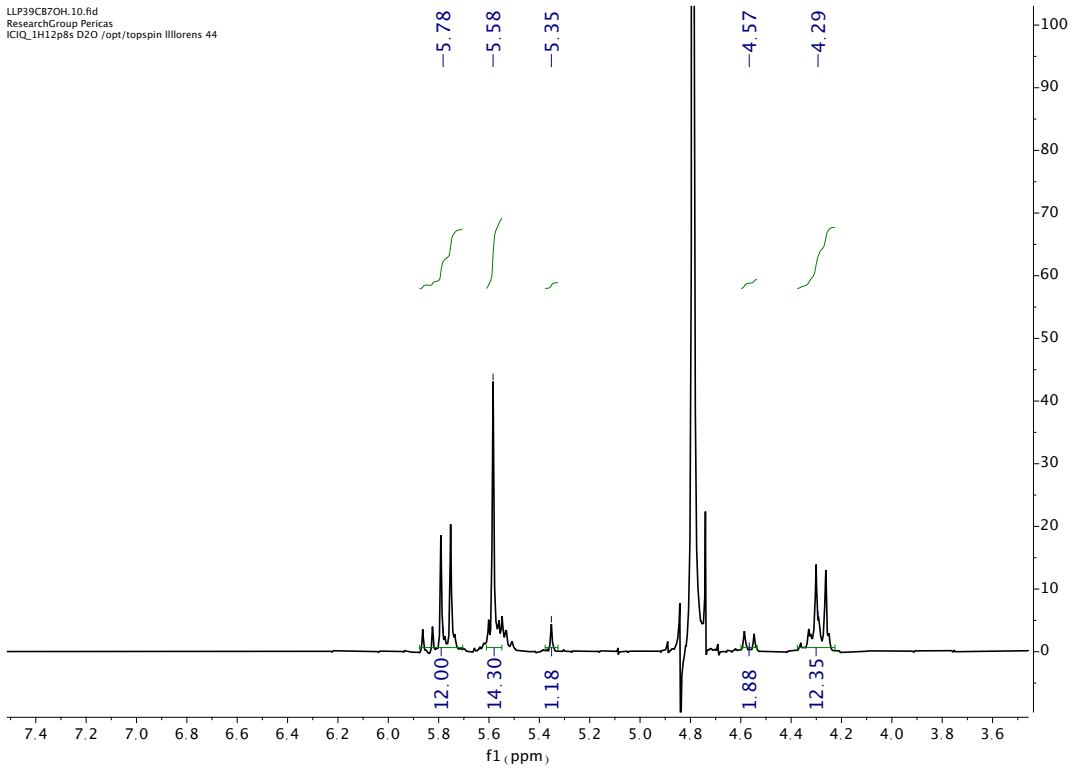

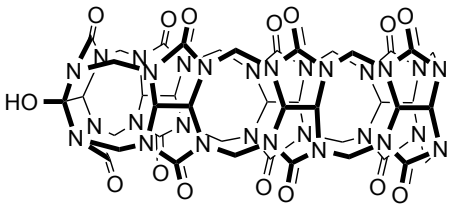

II.4.7.5. Compound CB6-OPr

^{1}H NMR (400 MHz. D_2O)

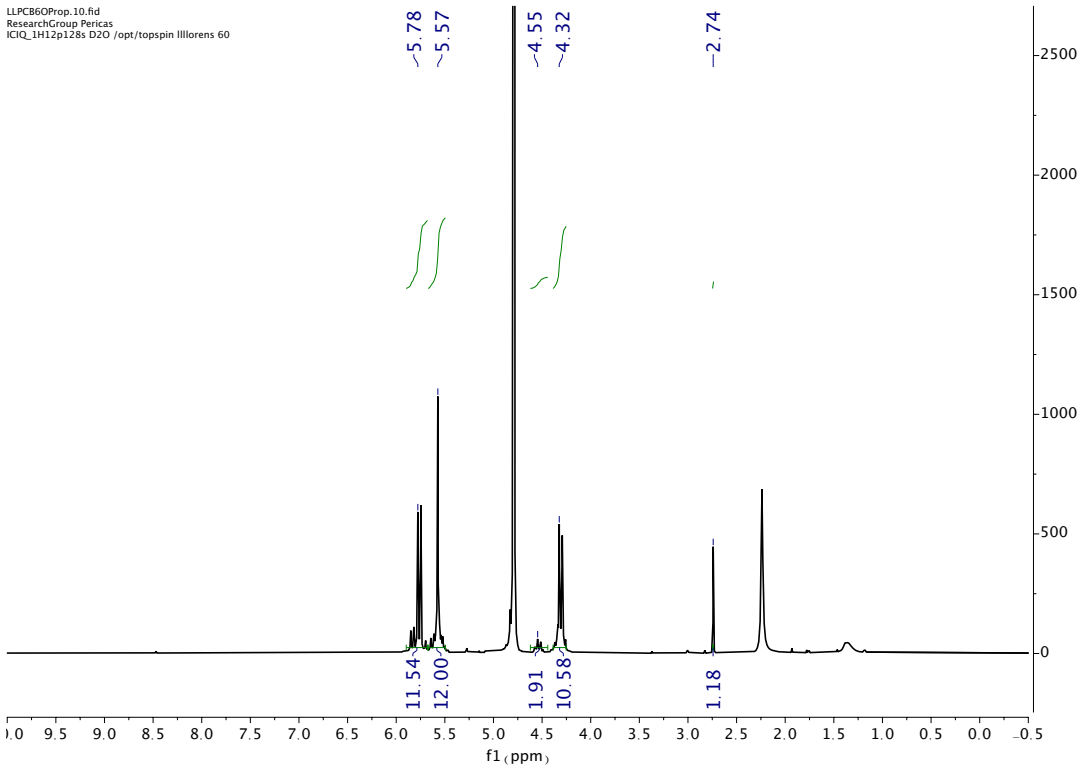

^{1}H NMR in the presence of >2 eq of acetone.

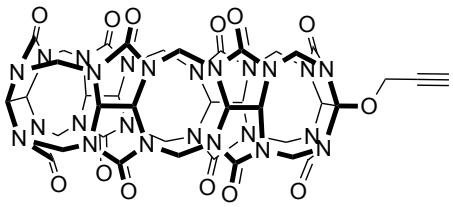

II.4.7.6. Compound CB7-OPr

^{1}H NMR (400 MHz. D_2O)

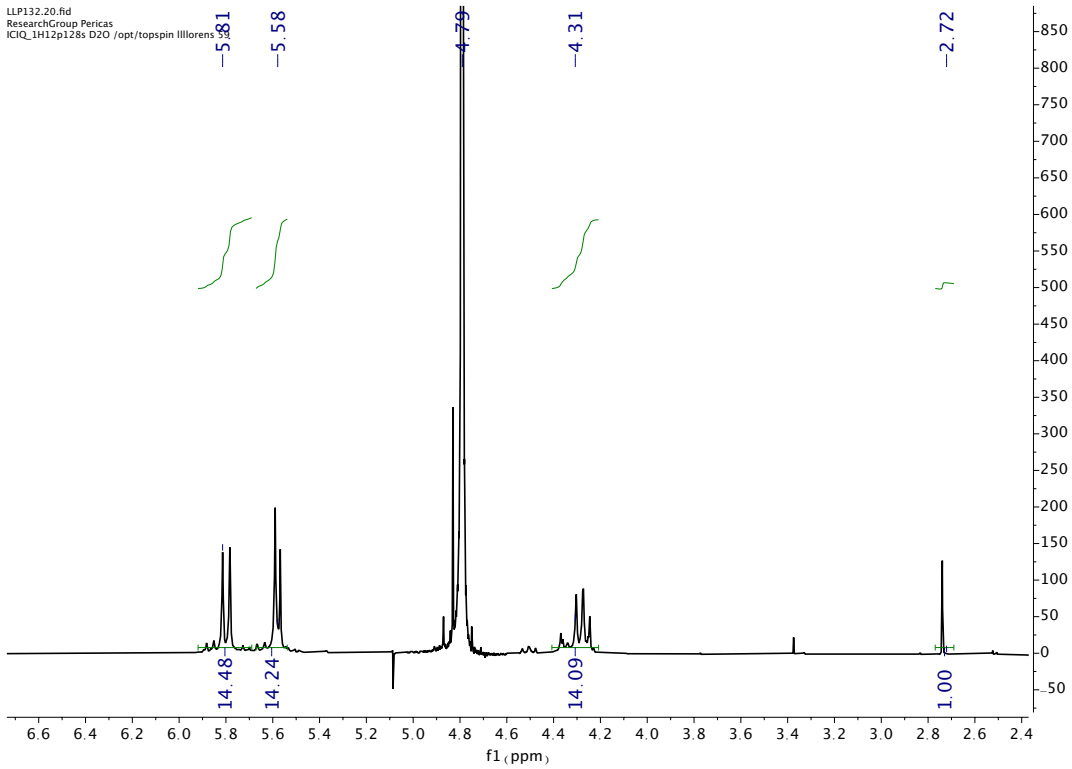

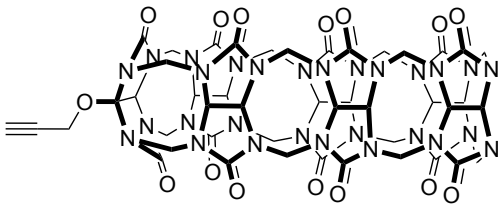

II.4.7.7. Compound Hexamer

^{1}H NMR (500 MHz. D_2O)

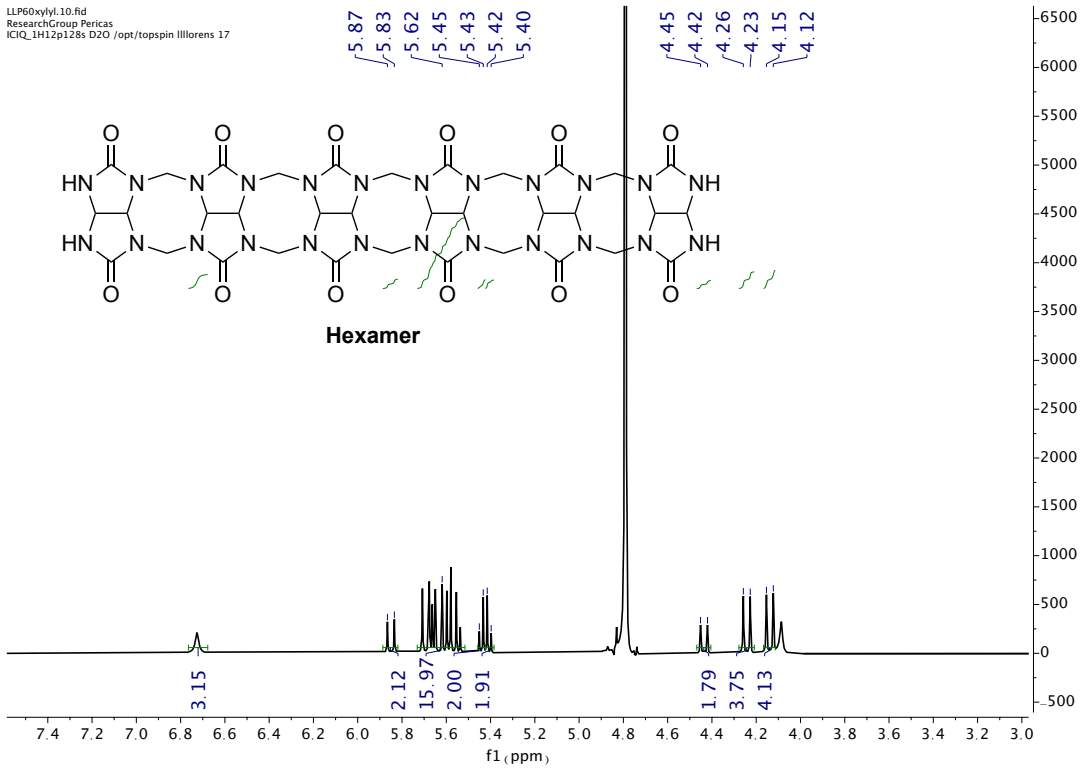

II.4.7.8. Compound 1

^{1}H NMR (400 MHz. $CDCl_3$)

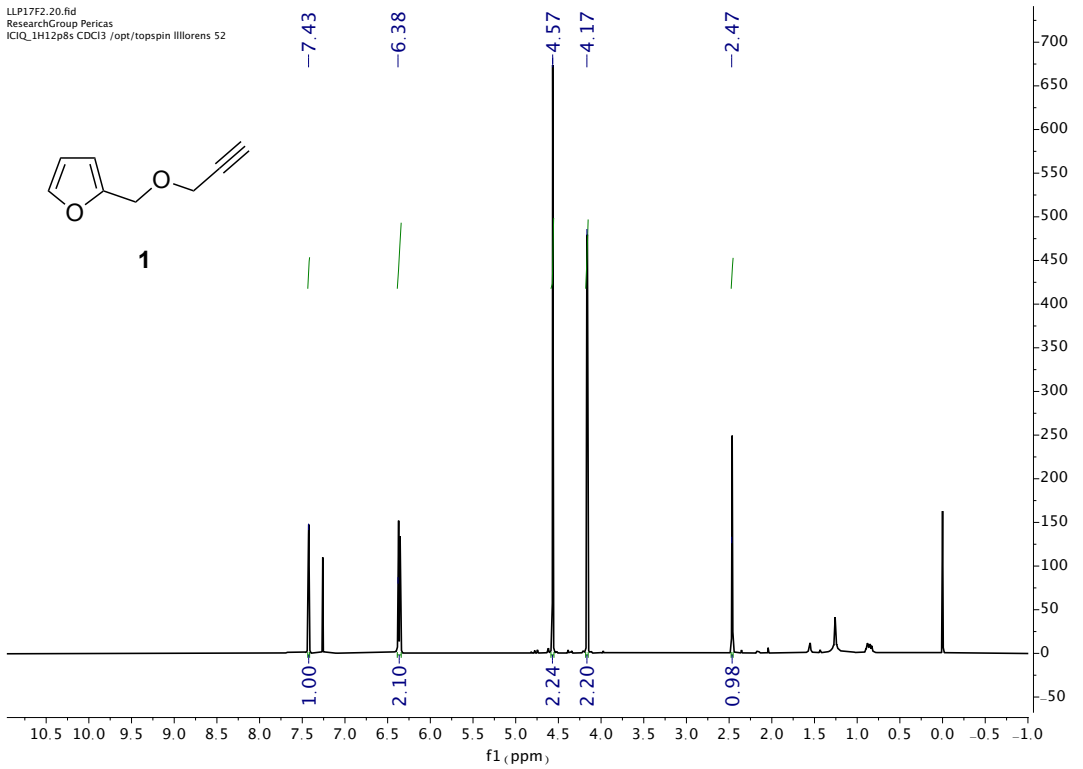

II.4.7.9. Compound 2

^{1}H NMR (400 MHz. $CDCl_3$)

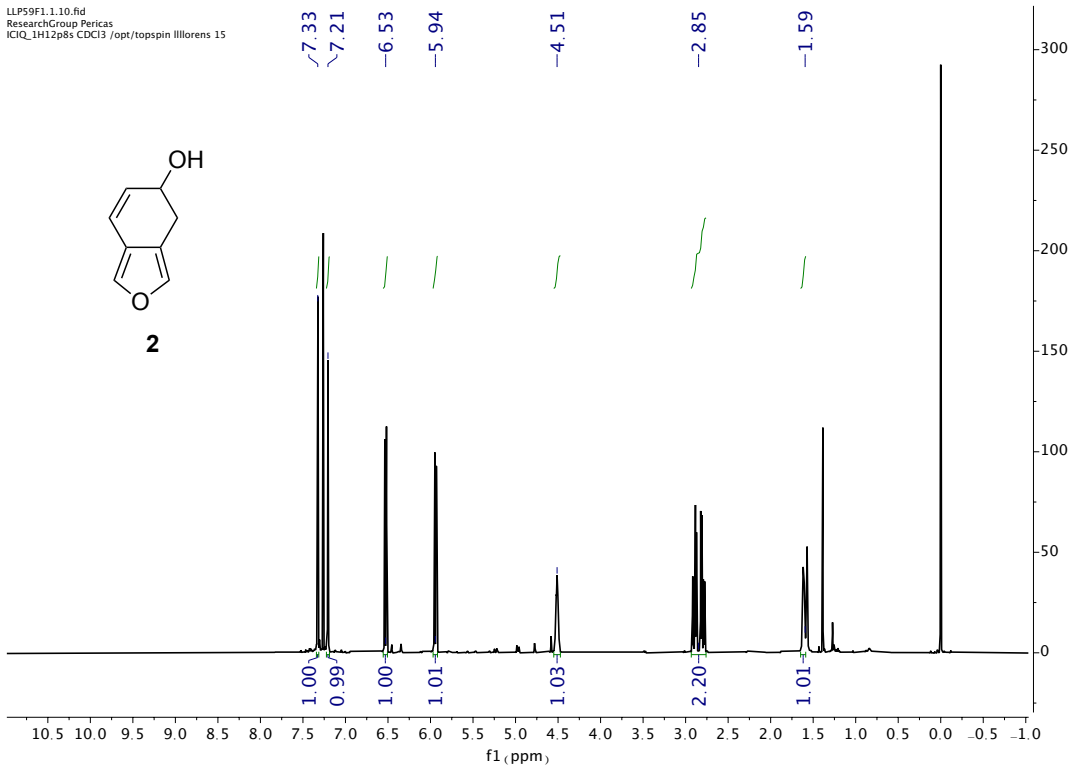

II.4.7.10. Compound 3

^{1}H NMR (400 MHz. $CDCl_3$)

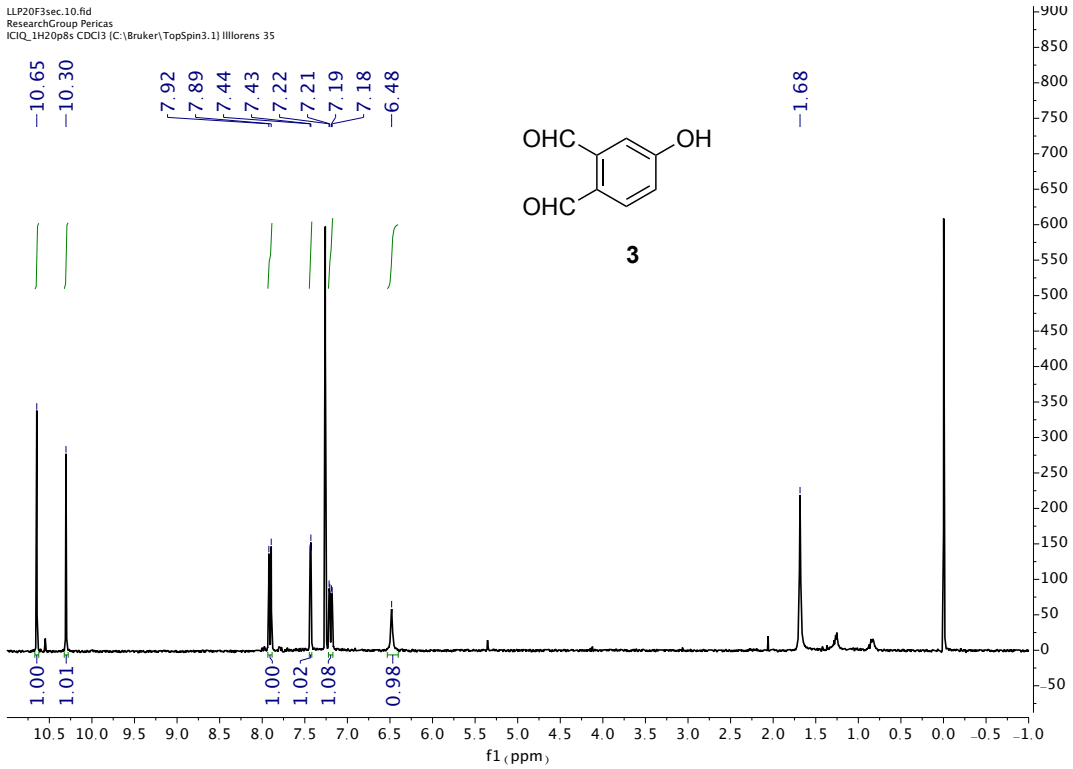

II.4.7.11. Compound 4

^{1}H NMR (400 MHz. $CDCl_3$)

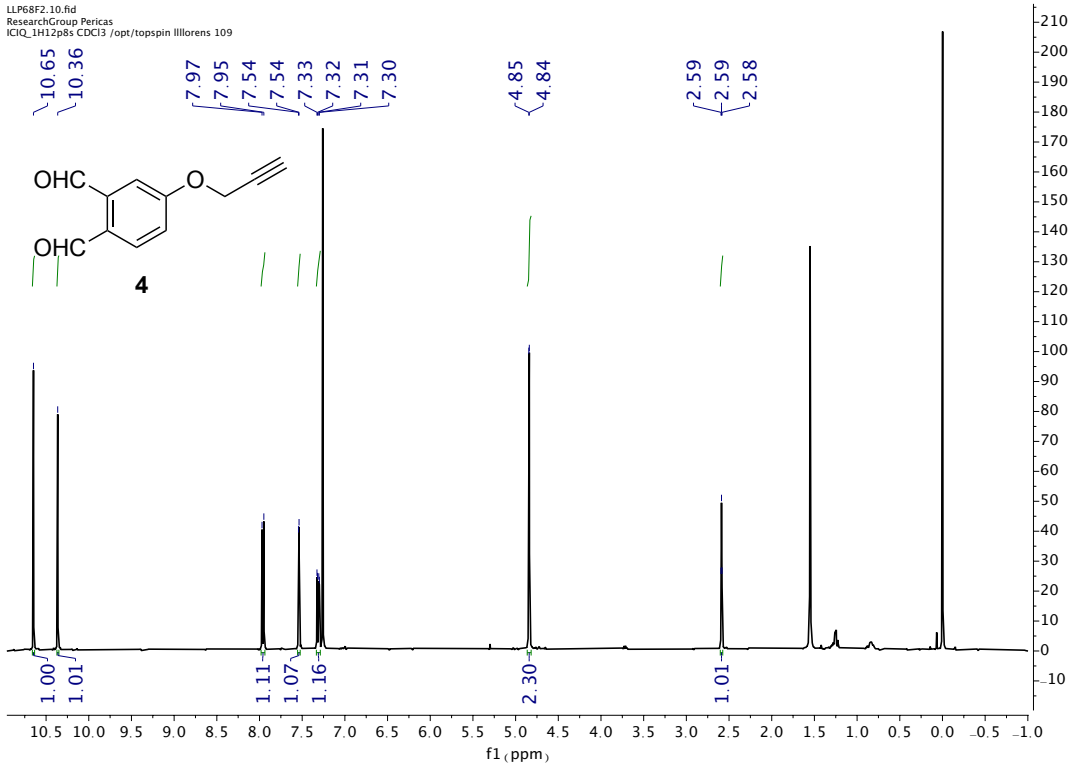

II.4.7.12. Compound CB6PhOH

^{1}H NMR (500 MHz. D_2O)

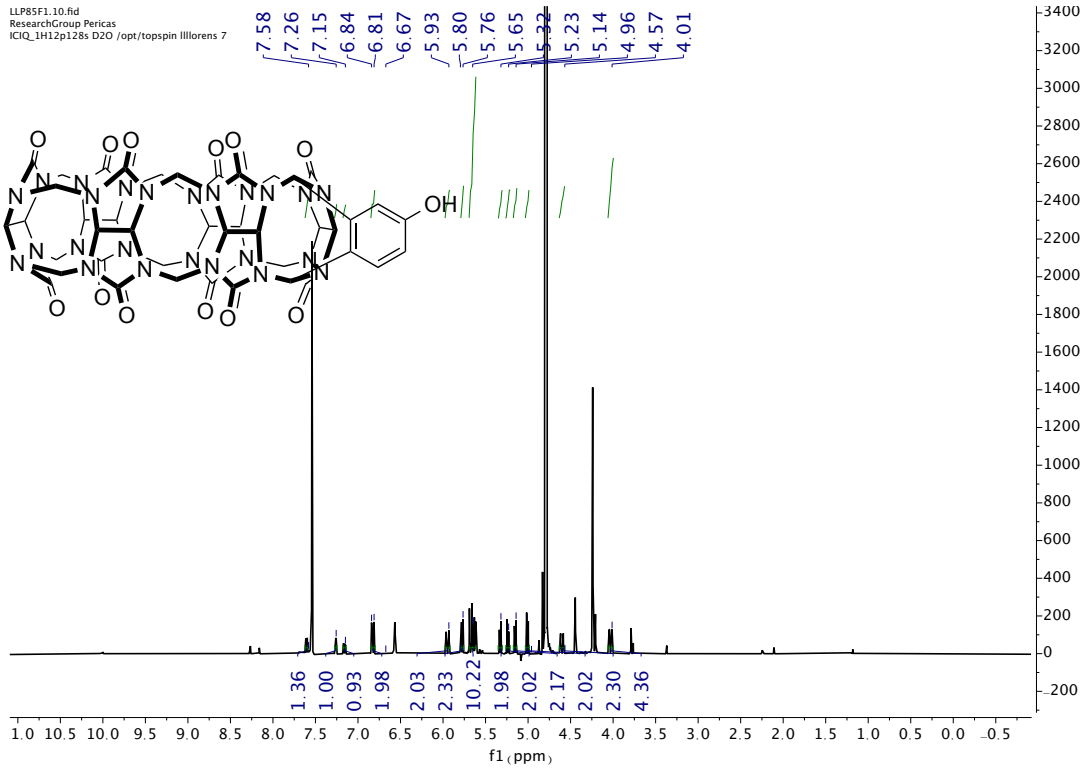

II.4.7.13. Compound CB6PhOProp

^{1}H NMR (500 MHz. D_2O)

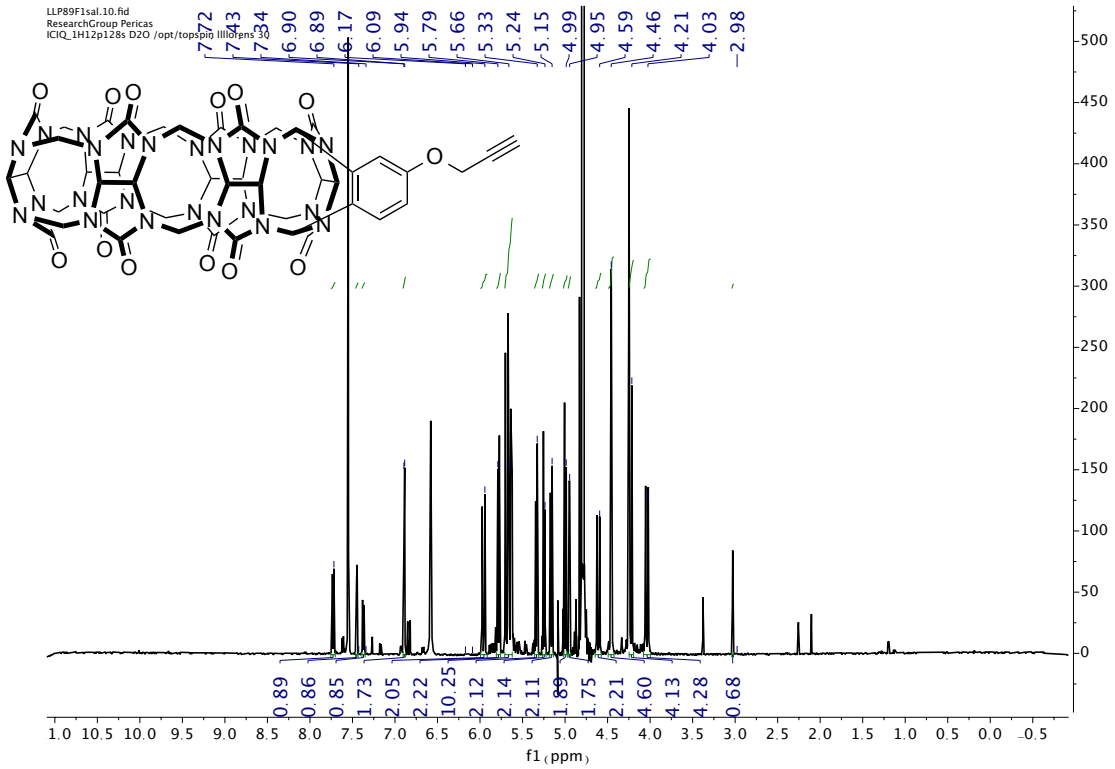

II.4.7.14. Compound 5

IR

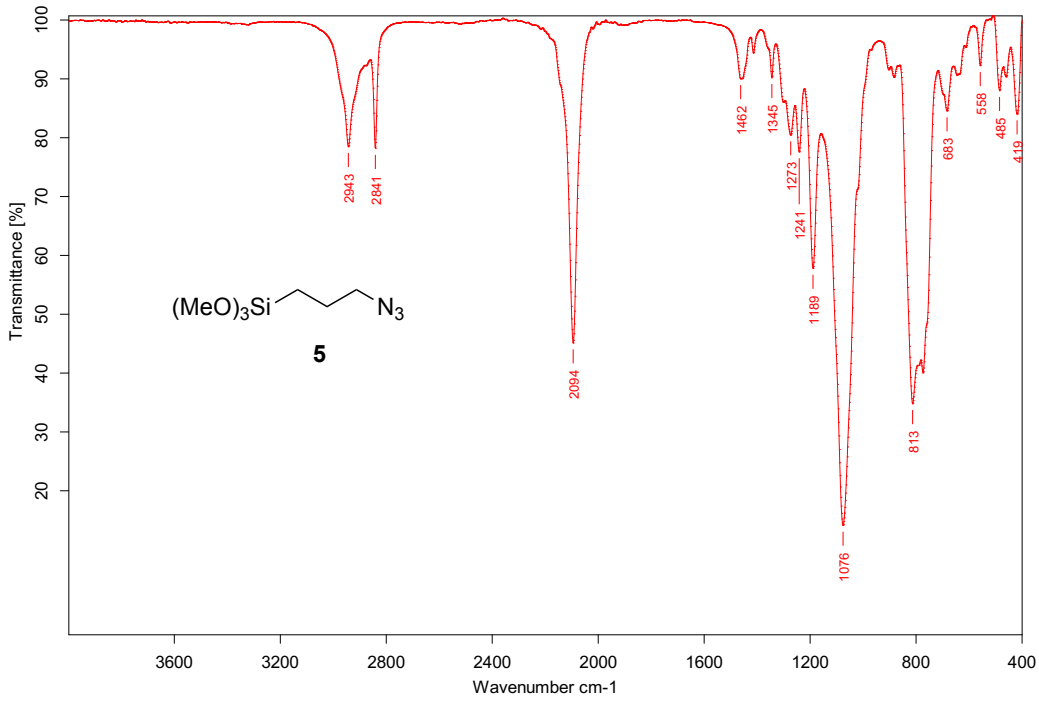

^{1}H NMR (400 MHz. $CDCl_3$)

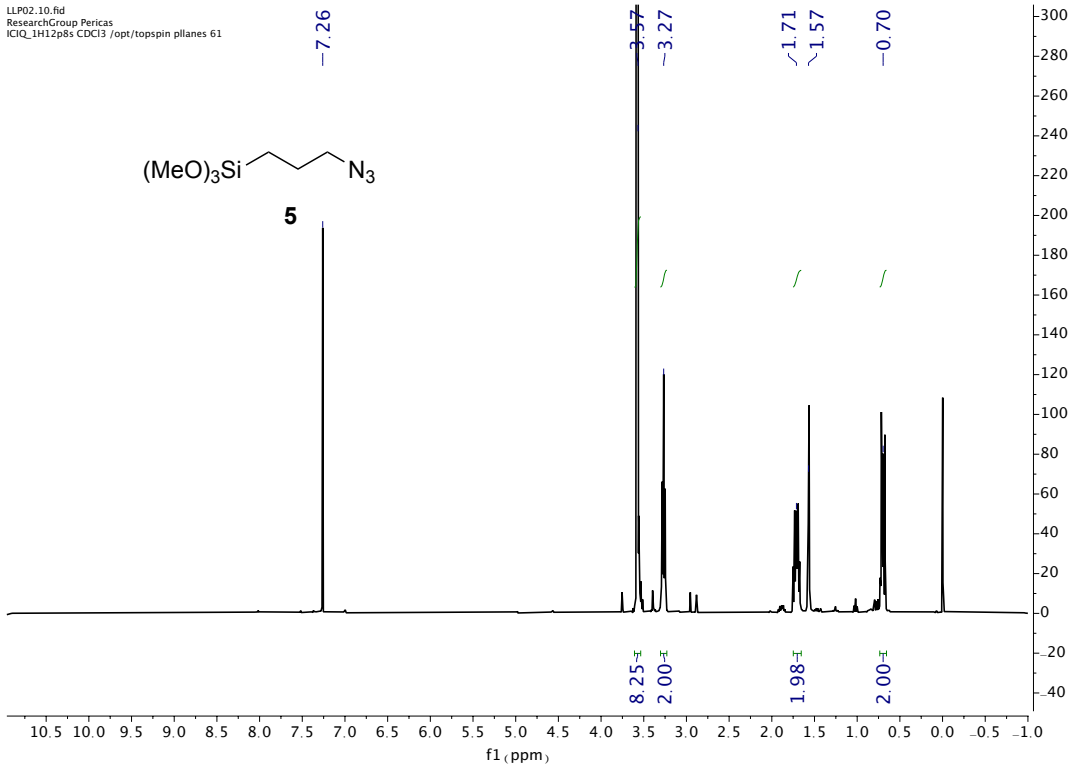

II.4.7.15. Compound 6

IR

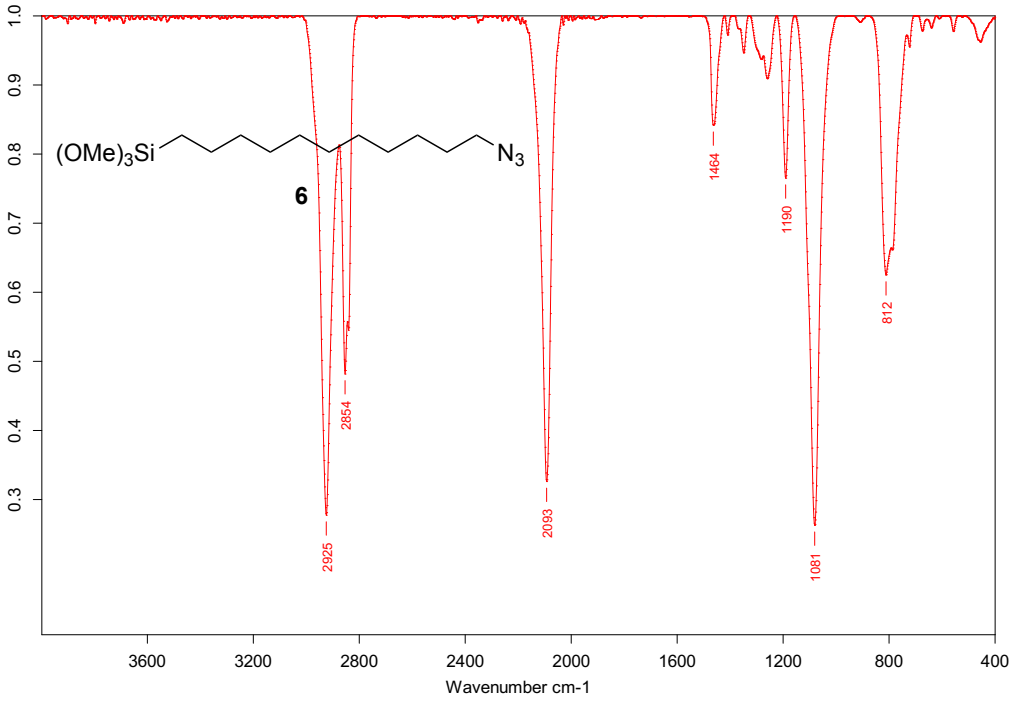

^{1}H NMR (400 MHz. $CDCl_3$)

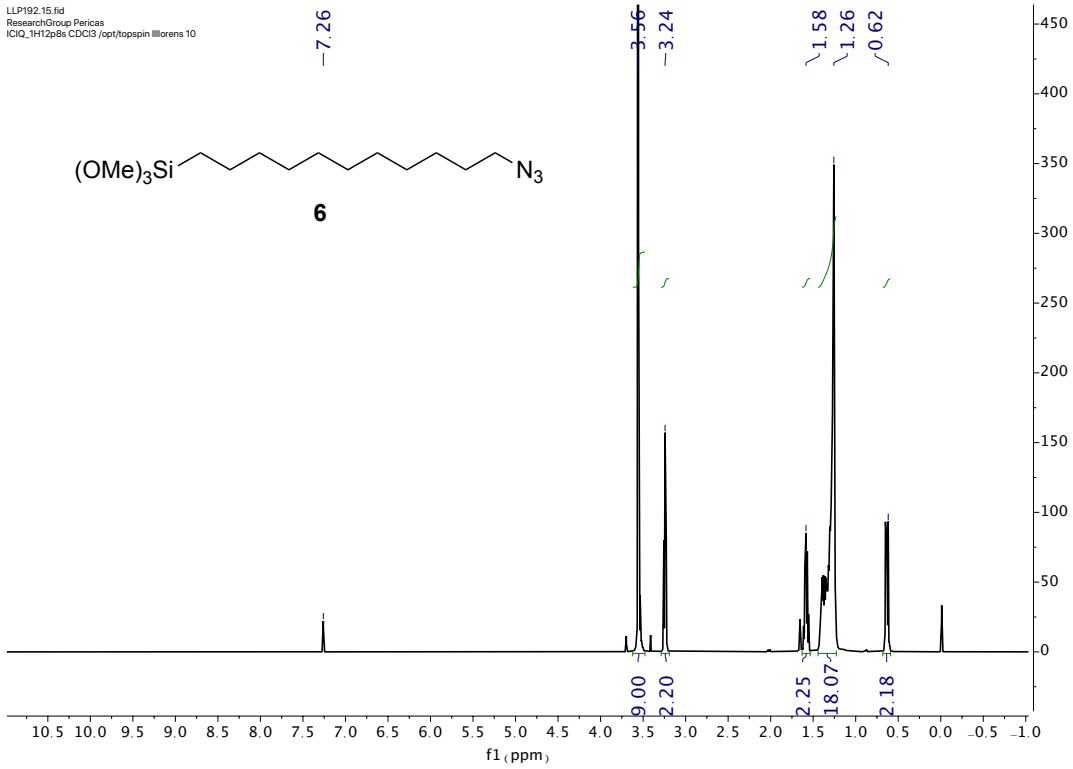

II.4.7.16. Compound MNPs

TEM images

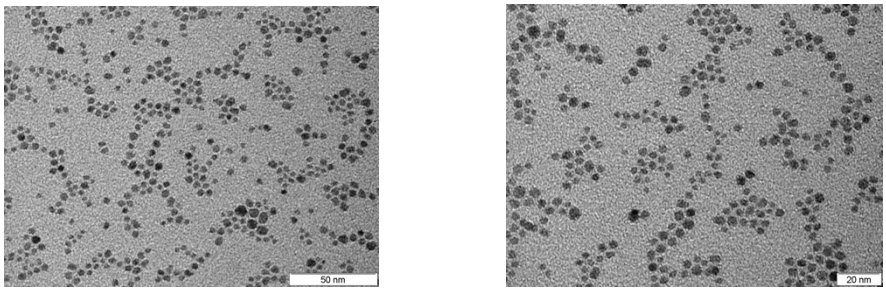

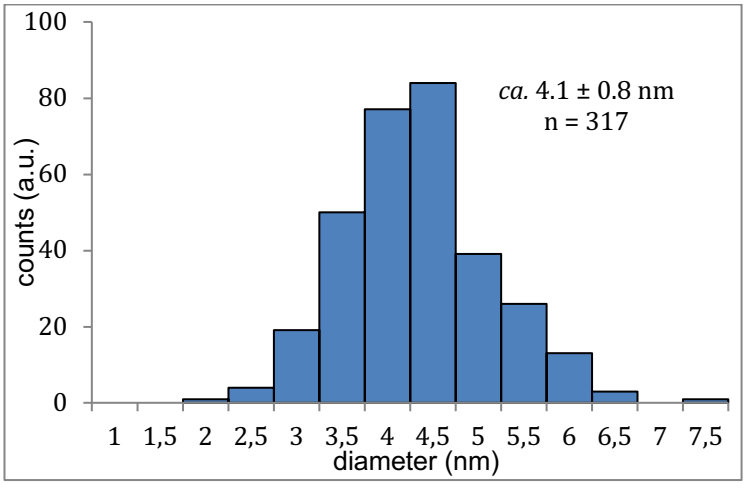

Small MNPs (batch a) and big (batch b)

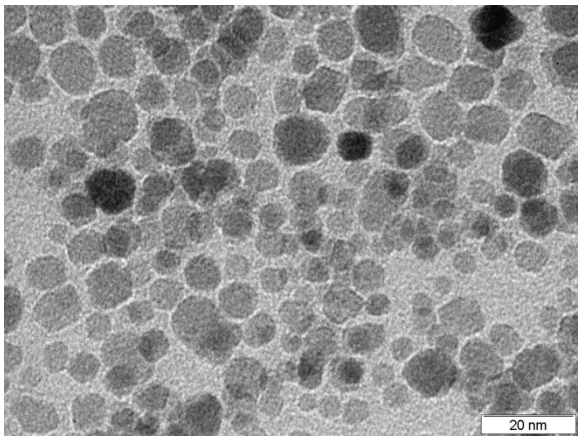

Batch (a)

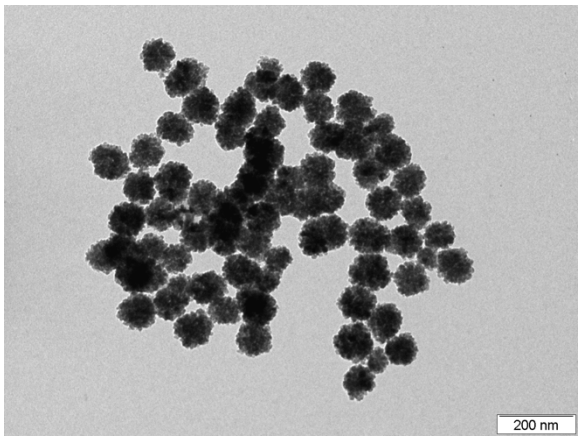

Batch (b)

Table II-S8. Determination of the size of the **MNPs**.

MNPs	A1	A2	B1	B2	B3
Average	4.1	6.4	115	91	91
STDEV	0.8	2.0	15	12	17
counts	317	648	319	240	531

II.4.7.17. Compound MNPs-N_3

7a

TEM images

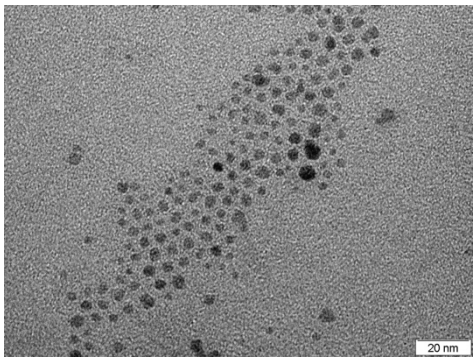

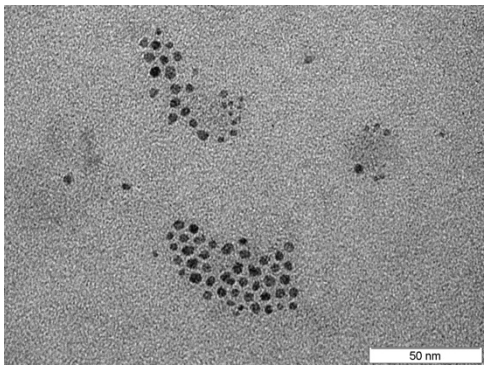

IR

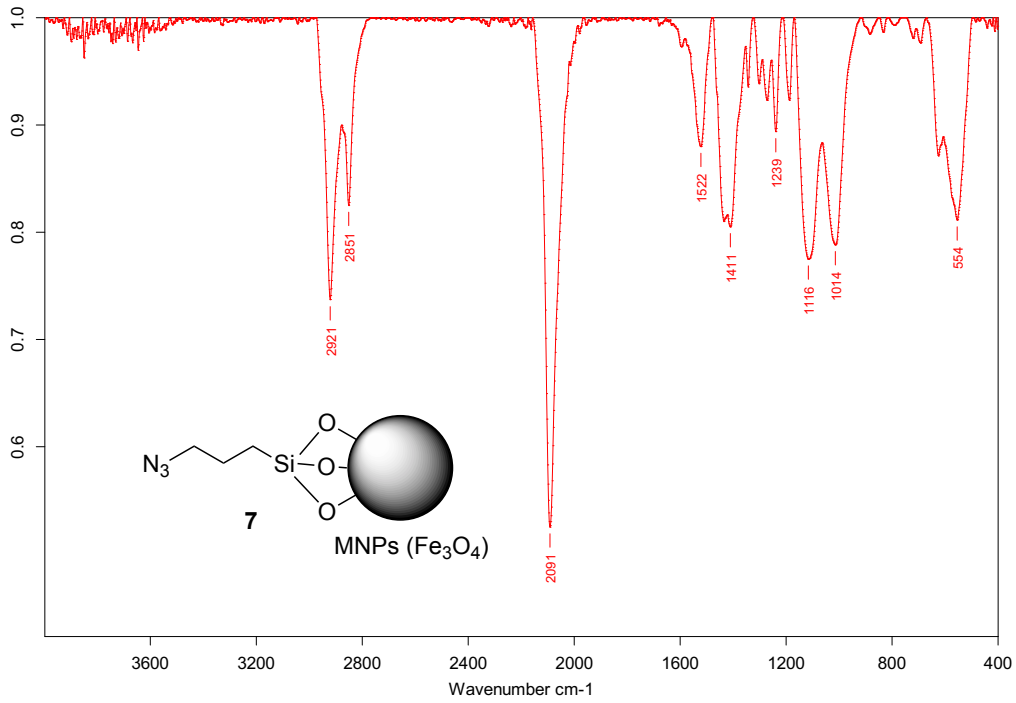

8

TEM images

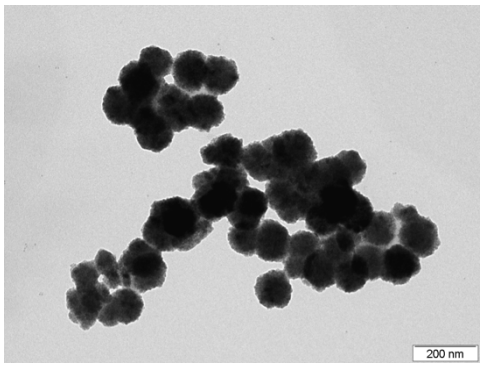

8b

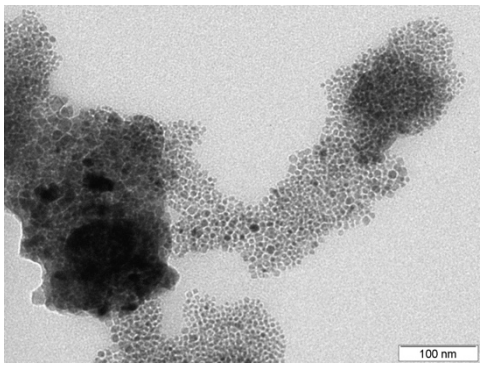

8a (poorly dispered)

IR

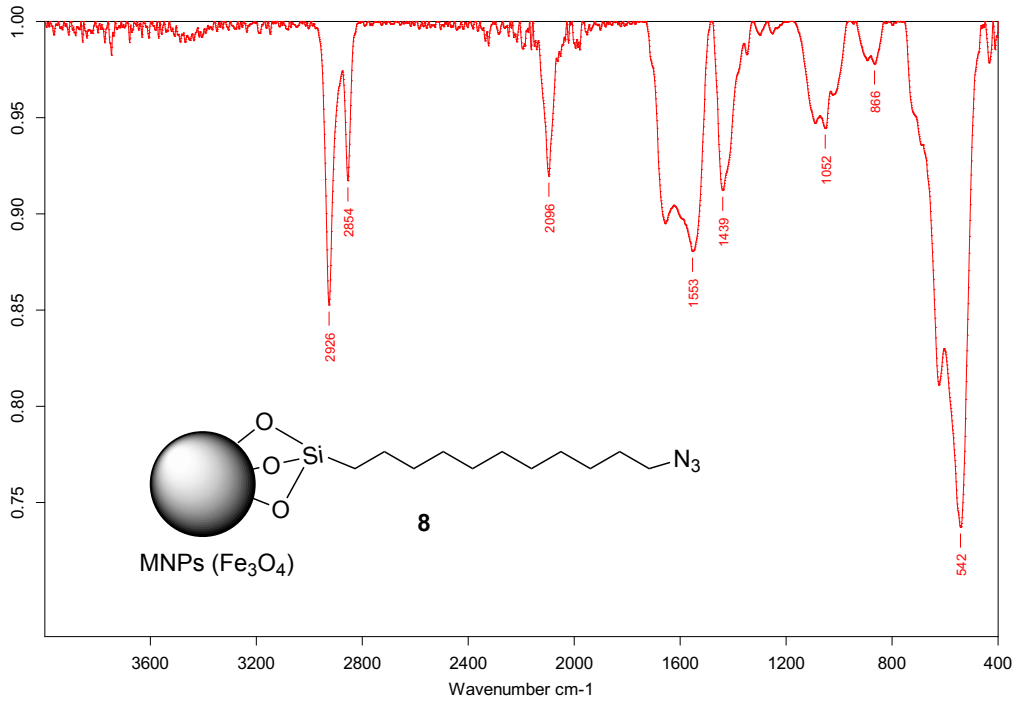

II.4.7.18. Compound MNPs-CB6Ph

Batch (a)

TEM images

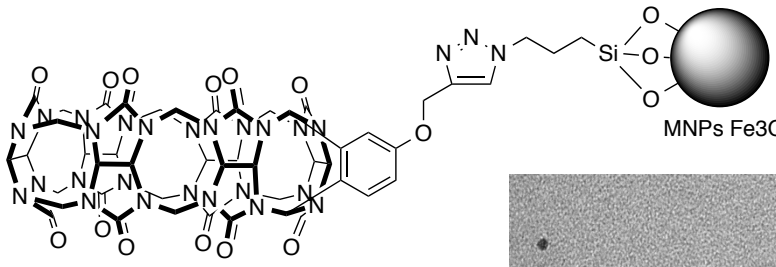

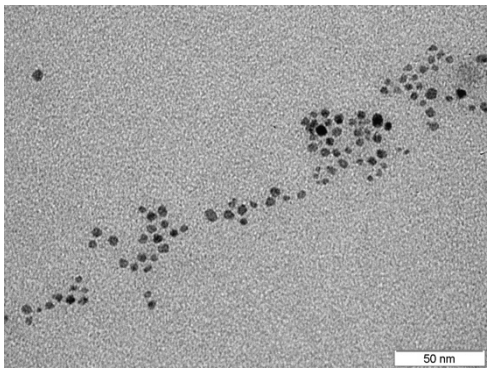

IR

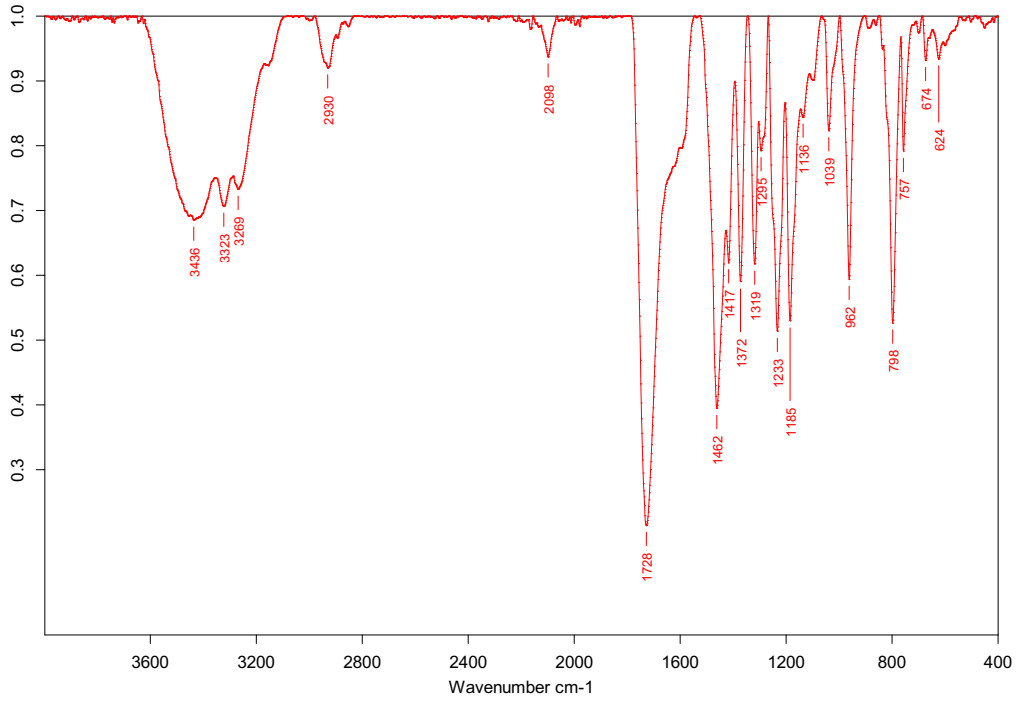

II.4.7.19. Compound MNPs-CB6

Batch (a)

TEM images

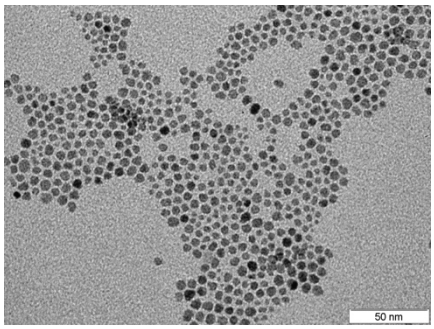

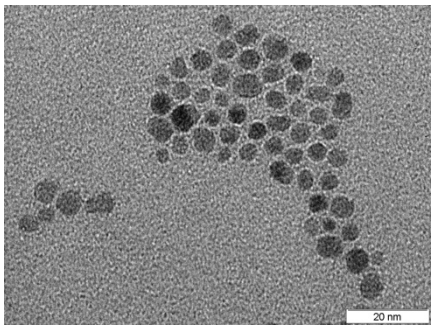

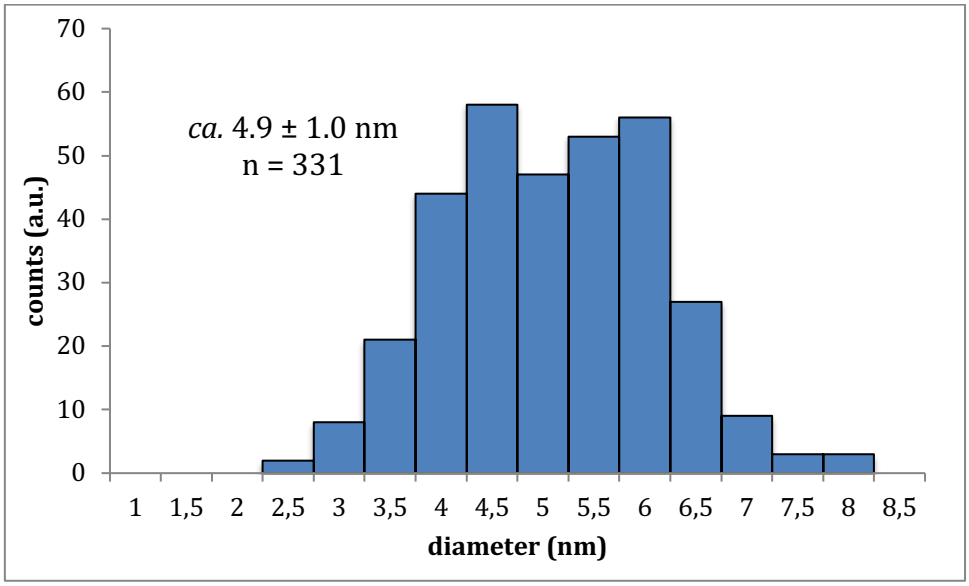

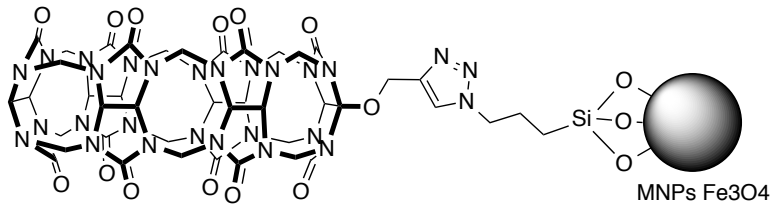

IR

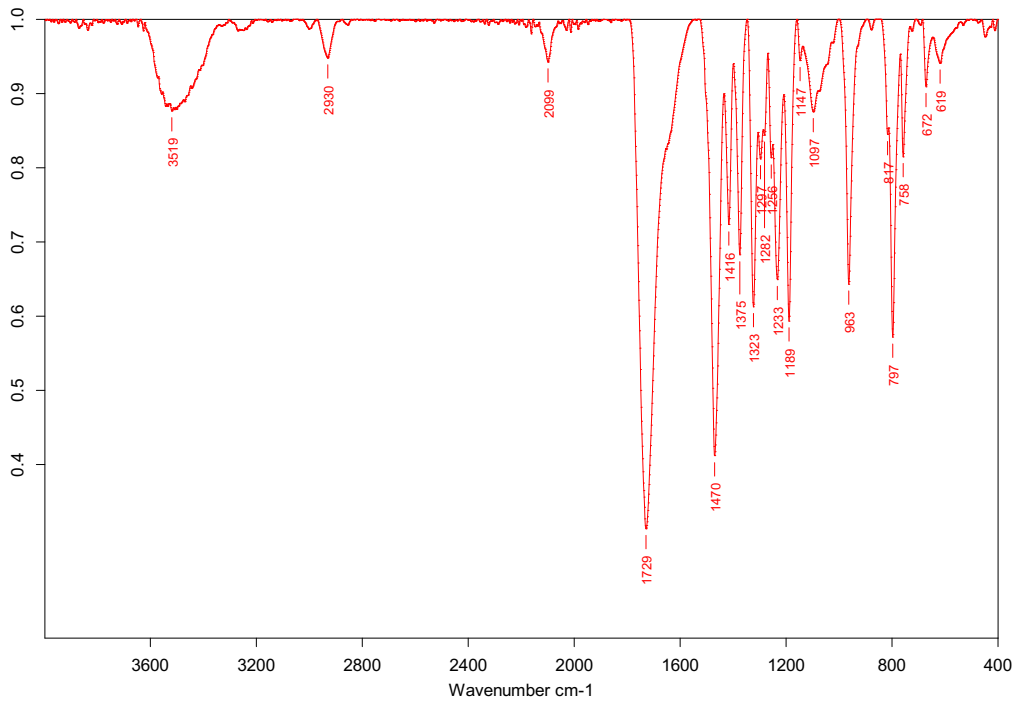
1.0
0.9
0.8
0.7
0.6
0.5
0.4
3519
2930
2099
1729
1470
1416
1375
1323
1282
1297
1256
1233
1189
1147
1097
963
817
797
758
672
619
3600
3200
2800
2400
2000
1600
1200
800
400
Wavenumber cm-1

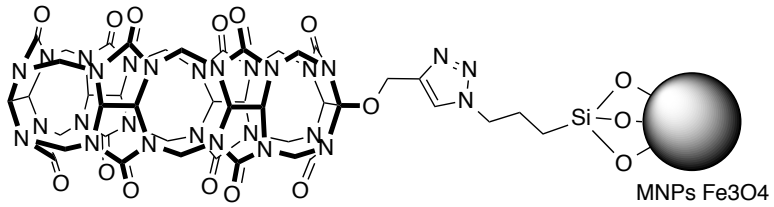
MNPs Fe3O4

II.4.7.20. Compound MNPs-CB7

Batch (7a):

TEM

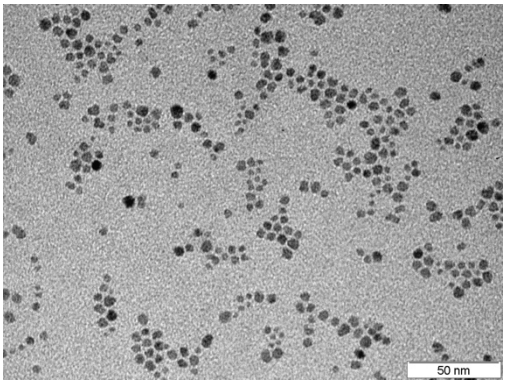

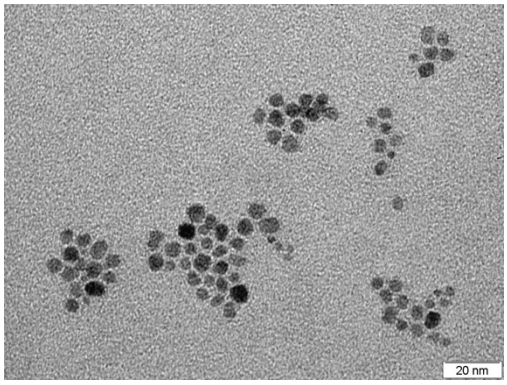

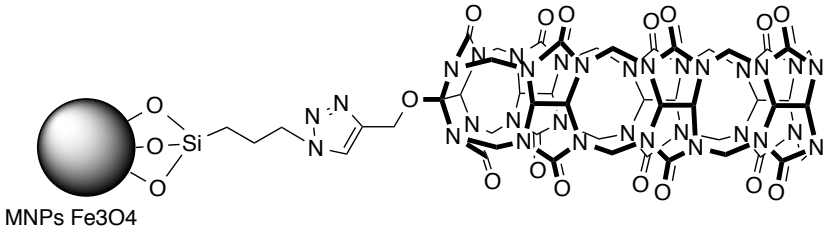

IR

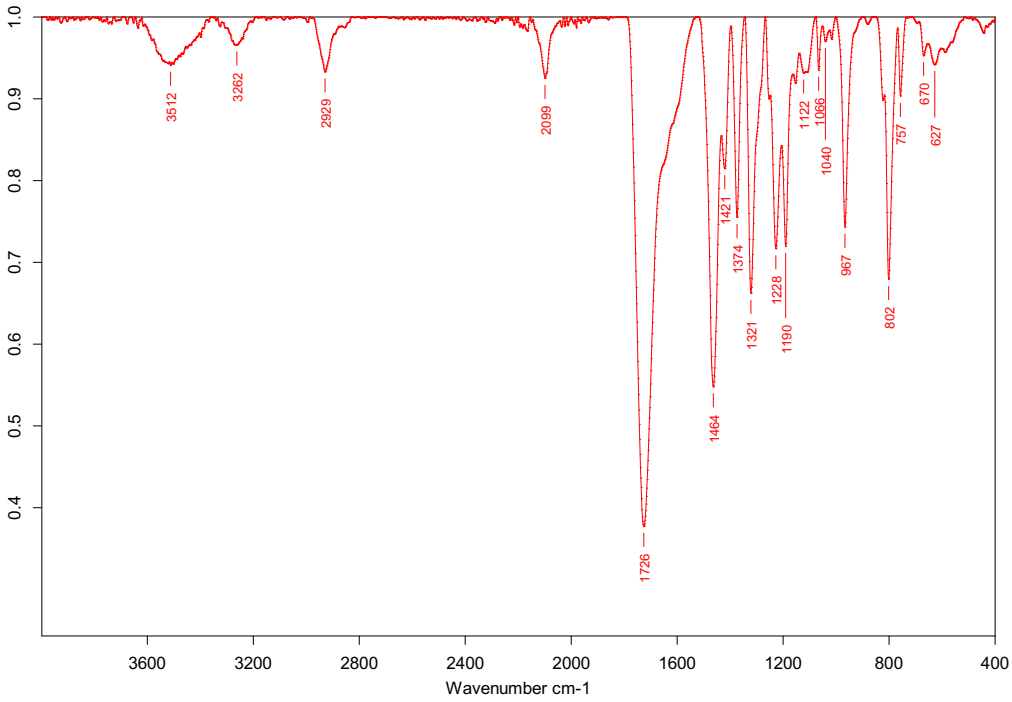

II.4.7.21. Compound MNPs-CB7 long linker

Batch (8a):

TEM

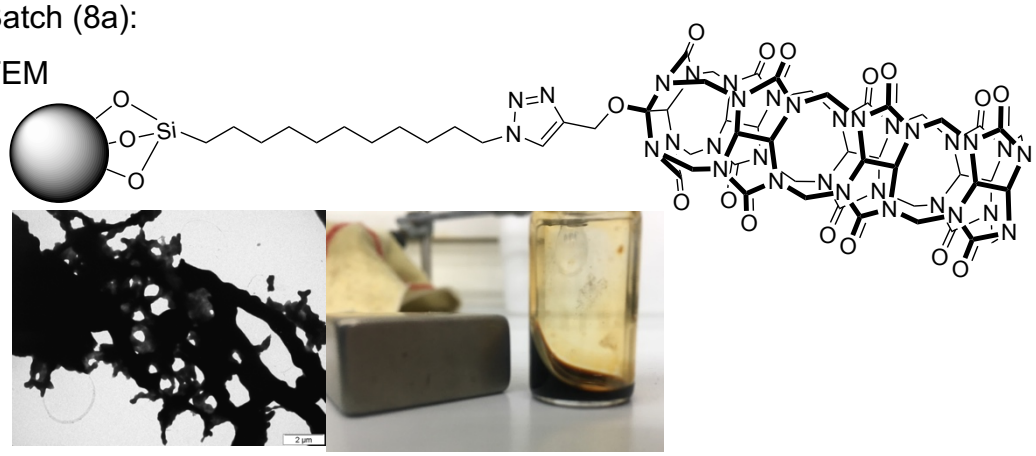

Batch (8b):

TEM

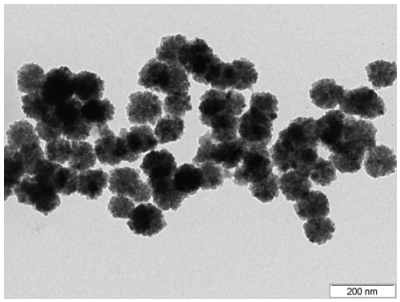

IR

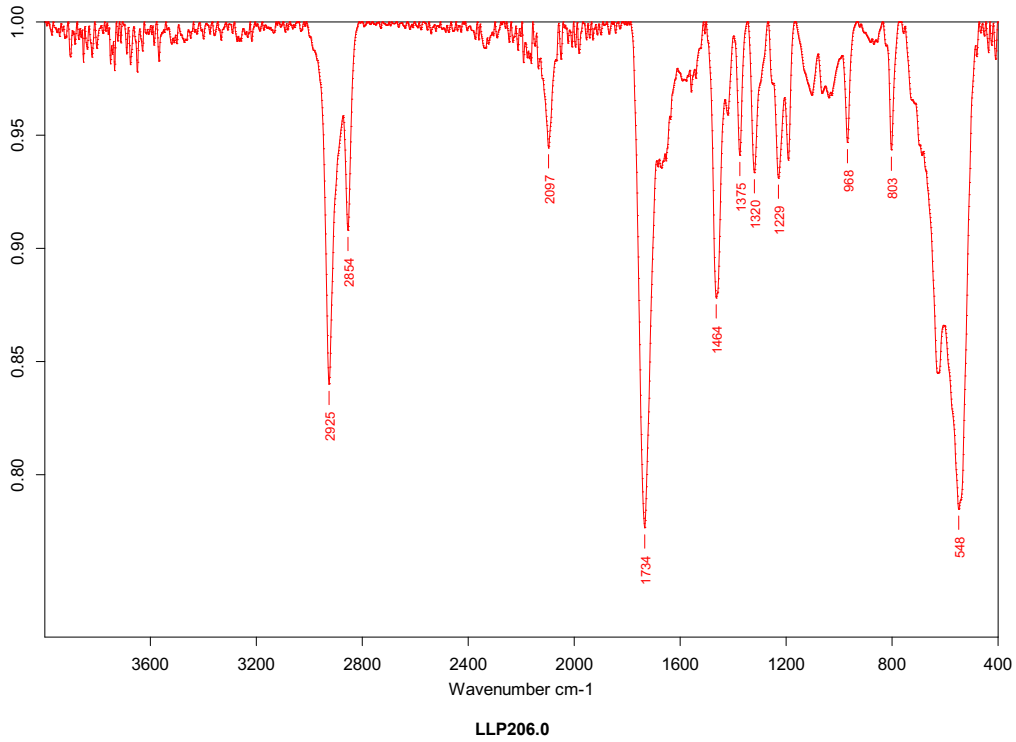

II.4.7.22. Compound MR-N_3

IR

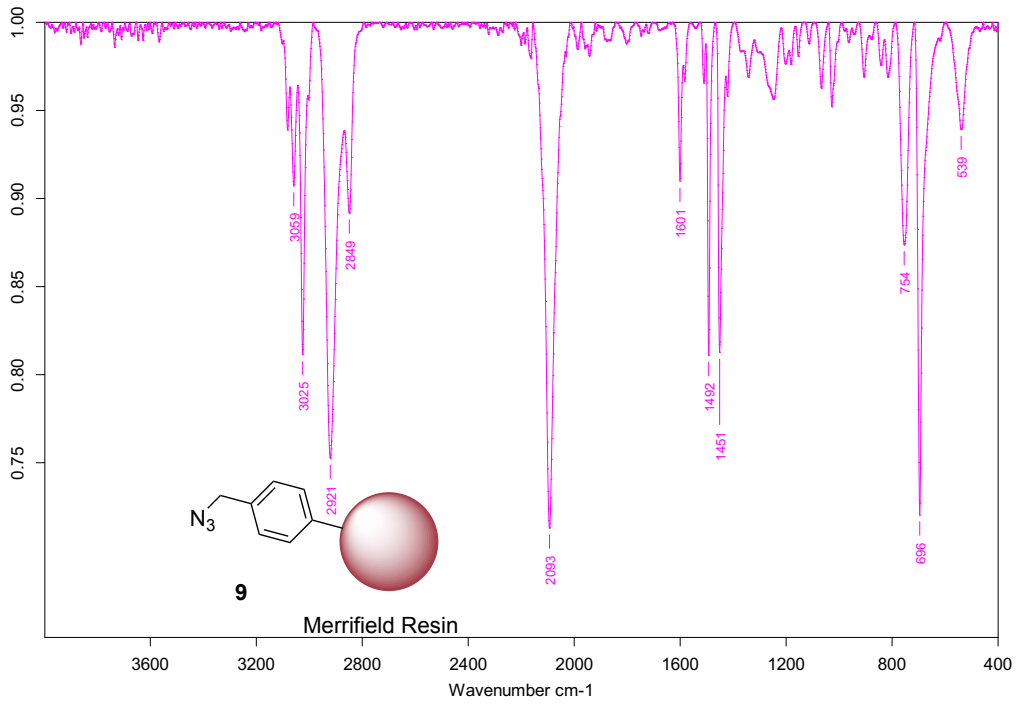

II.4.7.23. Compound MR-CB6Ph

IR

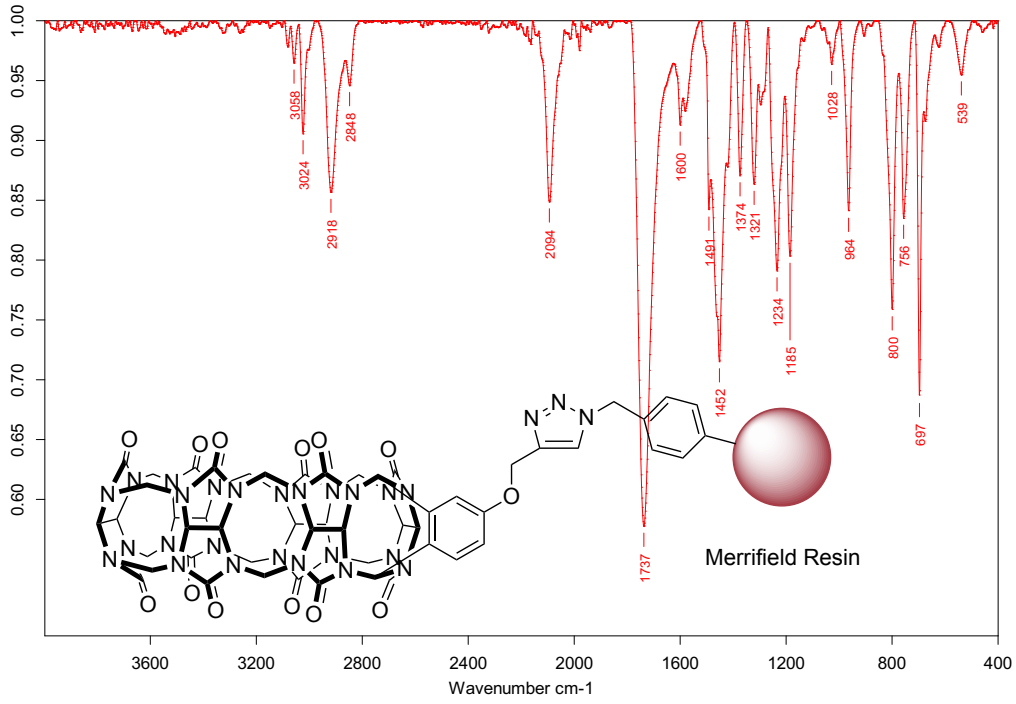

II.4.7.24. Compound MR-CB6

IR

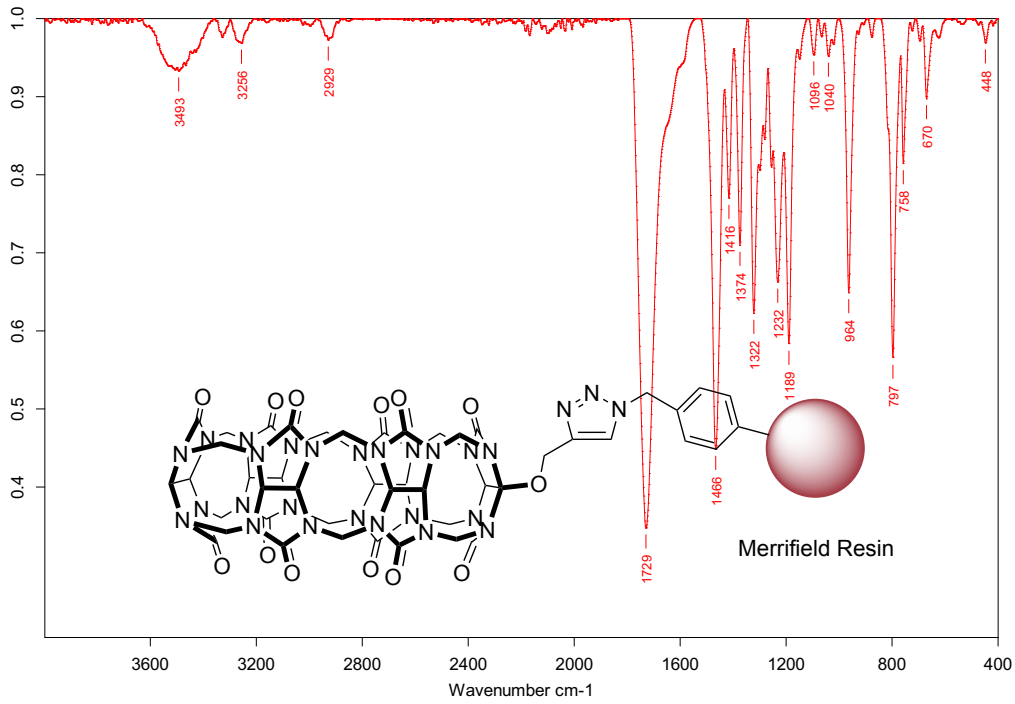

II.4.7.25. Compound MR-CB7

IR

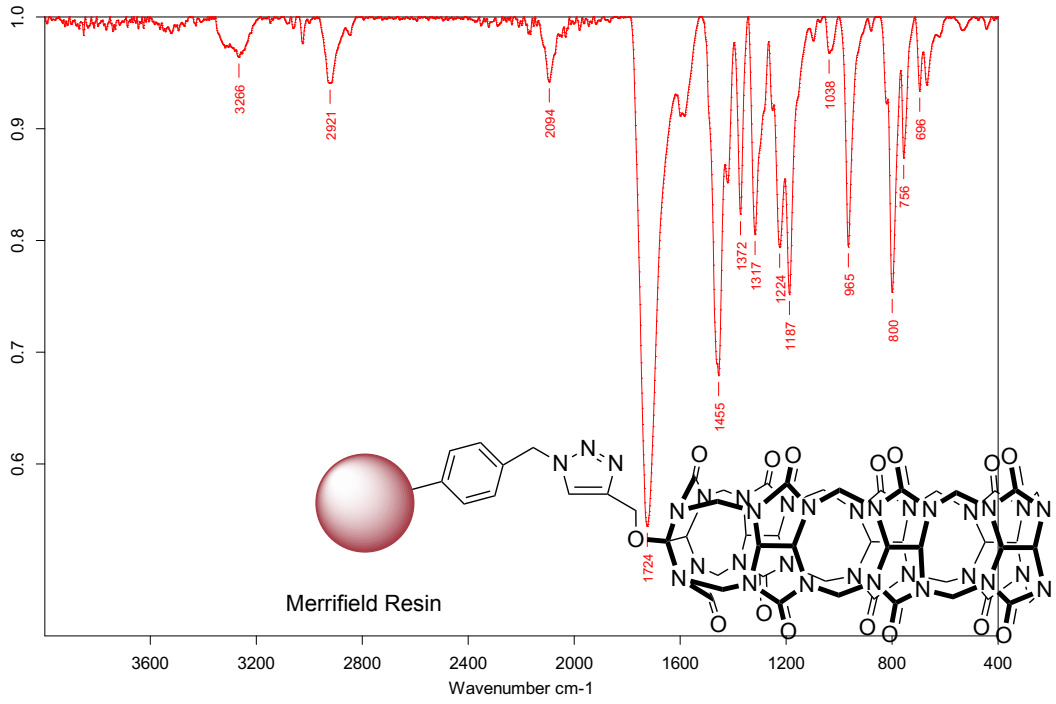

II.4.8. HPLC chromatograms and MS spectra

II.4.8.1. Compound CB6

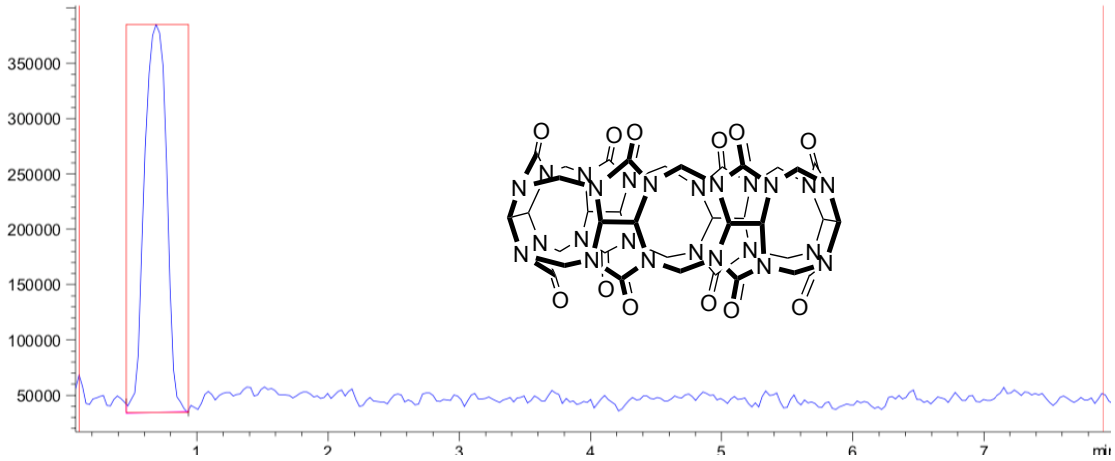

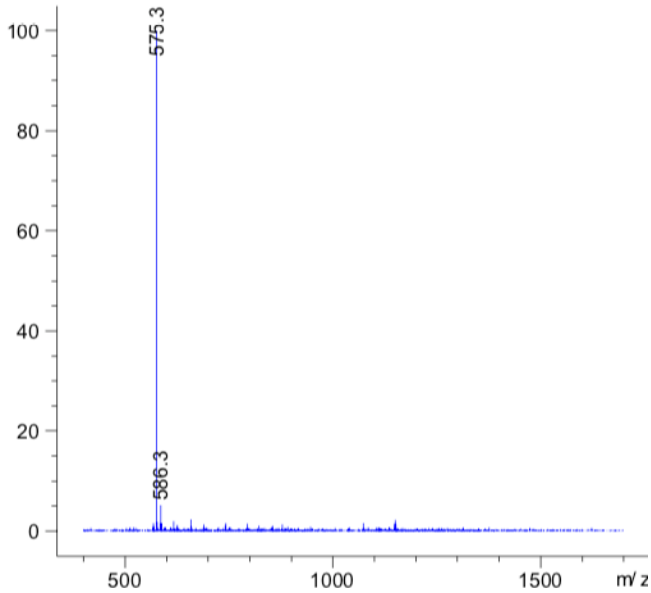

MS	m/z_{exp}
[CB6-H + cystamine + 2H]$^{2+}$	**575**
[CB6-OH + cystamine + 2H]$^{2+}$	583
[CB6-2OH + cystamine + 2H]$^{2+}$	591
[CB6-OProp + cystamine + 2H]$^{2+}$	602
[CB6-2OProp + cystamine + 2H]$^{2+}$	629
[CB6-3OProp + cystamine + 2H]$^{2+}$	656

II.4.8.2. Compound CB6-OH

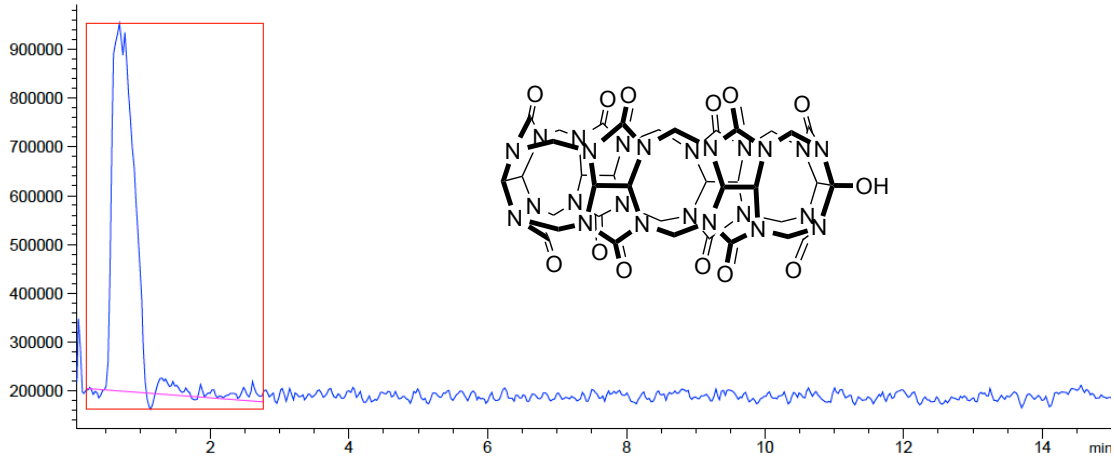

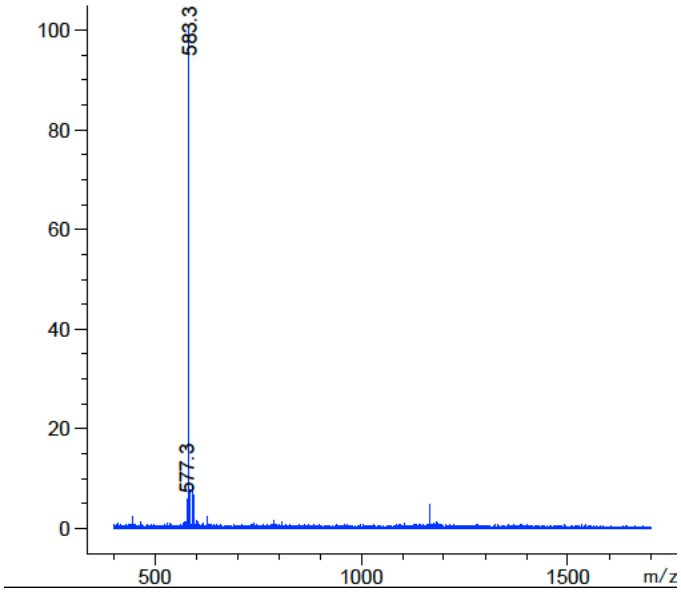

MS	m/z_{exp}
$[CB6\text{-}H + cystamine + 2H]^{2+}$	575
$[CB6\text{-}OH + cystamine + 2H]^{2+}$	**583**
$[CB6\text{-}2OH + cystamine + 2H]^{2+}$	591
$[CB6\text{-}OProp + cystamine + 2H]^{2+}$	602
$[CB6\text{-}2OProp + cystamine + 2H]^{2+}$	629
$[CB6\text{-}3OProp + cystamine + 2H]^{2+}$	656

II.4.8.3. Compound CB6-OPr

Product obtained after purification of starting material **CB6-OH**

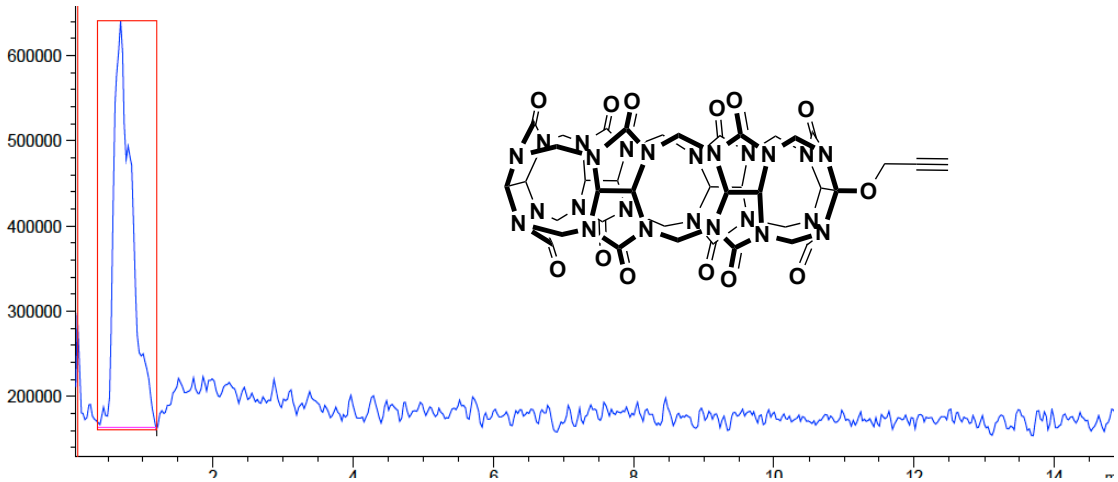

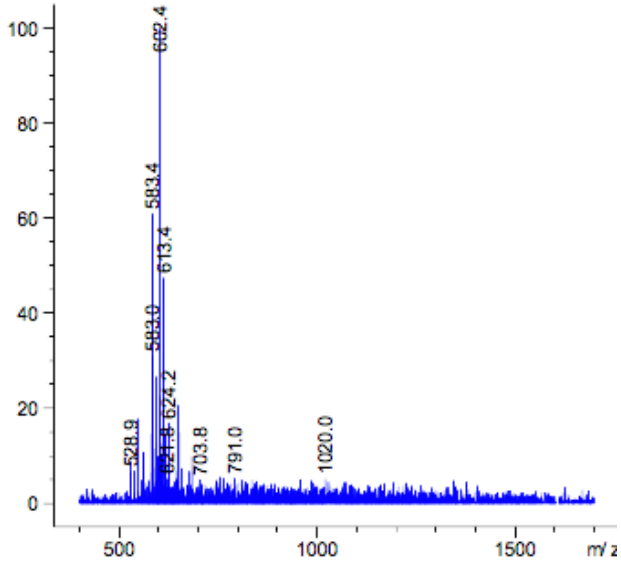

MS	m/z_{exp}
$[CB6\text{-}H + cystamine + 2H]^{2+}$	575
$[CB6\text{-}OH + cystamine + 2H]^{2+}$	583
$[CB6\text{-}2OH + cystamine + 2H]^{2+}$	591
$[CB6\text{-}OProp + cystamine + 2H]^{2+}$	**602**
$[CB6\text{-}2OProp + cystamine + 2H]^{2+}$	629
$[CB6\text{-}3OProp + cystamine + 2H]^{2+}$	656

Product obtained after reaction with the crude **CB6-OH**

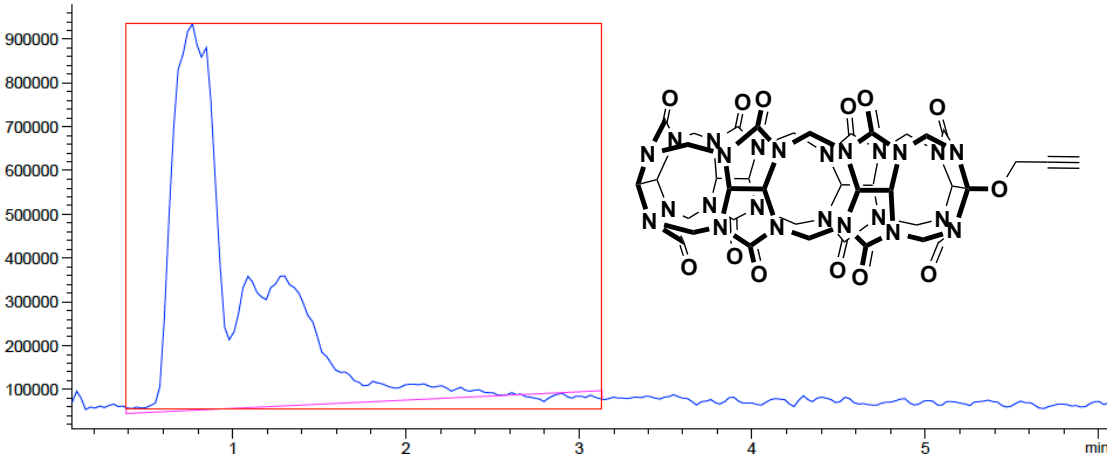

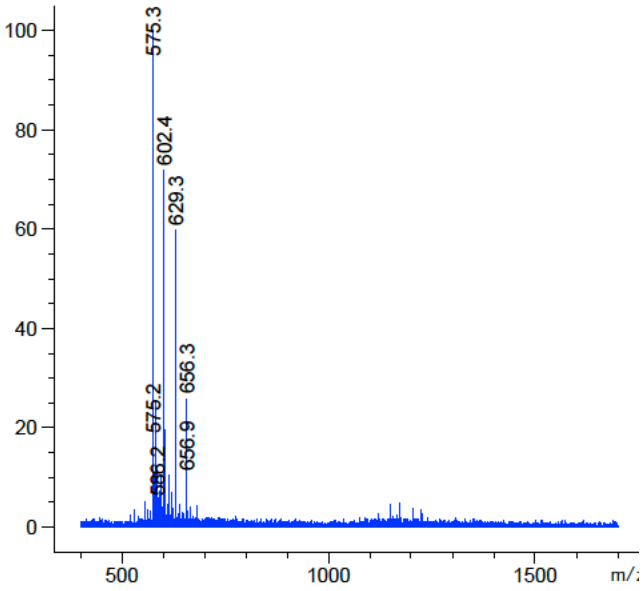

MS	m/z_{exp}
$[CB6\text{-}H + cystamine + 2H]^{2+}$	575
$[CB6\text{-}OH + cystamine + 2H]^{2+}$	583
$[CB6\text{-}2OH + cystamine + 2H]^{2+}$	591
$[CB6\text{-}OProp + cystamine + 2H]^{2+}$	**602**
$[CB6\text{-}2OProp + cystamine + 2H]^{2+}$	629
$[CB6\text{-}3OProp + cystamine + 2H]^{2+}$	656

Product recovered after click reaction of **CB6-OPr** with **MR-N_3**

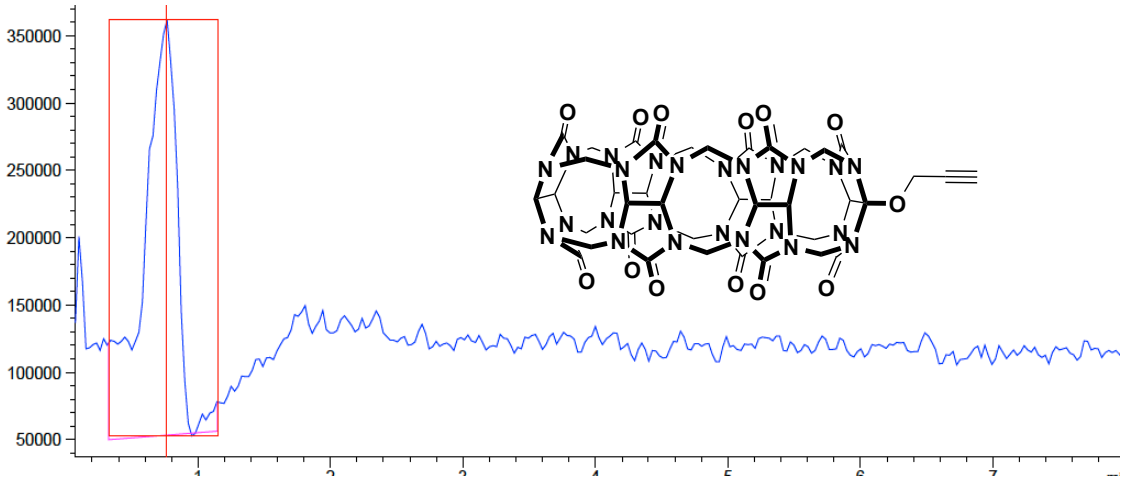

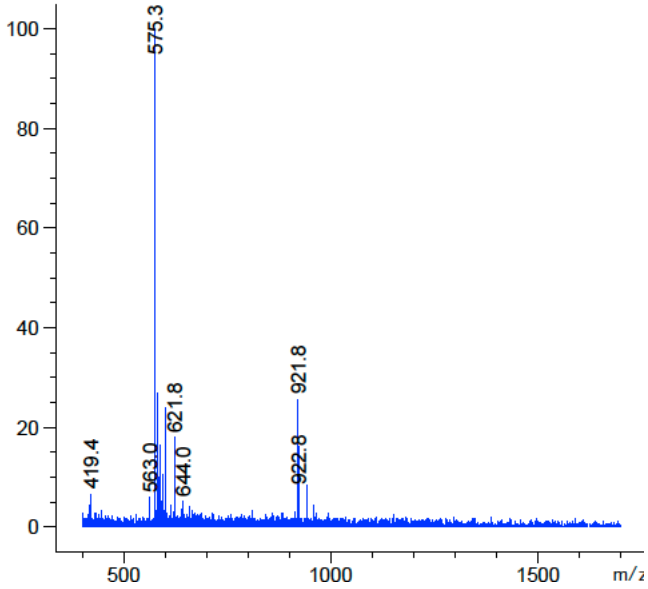

MS	m/z_{exp}
[CB6-H + cystamine + 2H]$^{2+}$	**575**
[CB6-OH + cystamine + 2H]$^{2+}$	583
[CB6-2OH + cystamine + 2H]$^{2+}$	591
[CB6-OProp + cystamine + 2H]$^{2+}$	602
[CB6-2OProp + cystamine + 2H]$^{2+}$	629
[CB6-3OProp + cystamine + 2H]$^{2+}$	656

II.4.8.4. Compound CB7

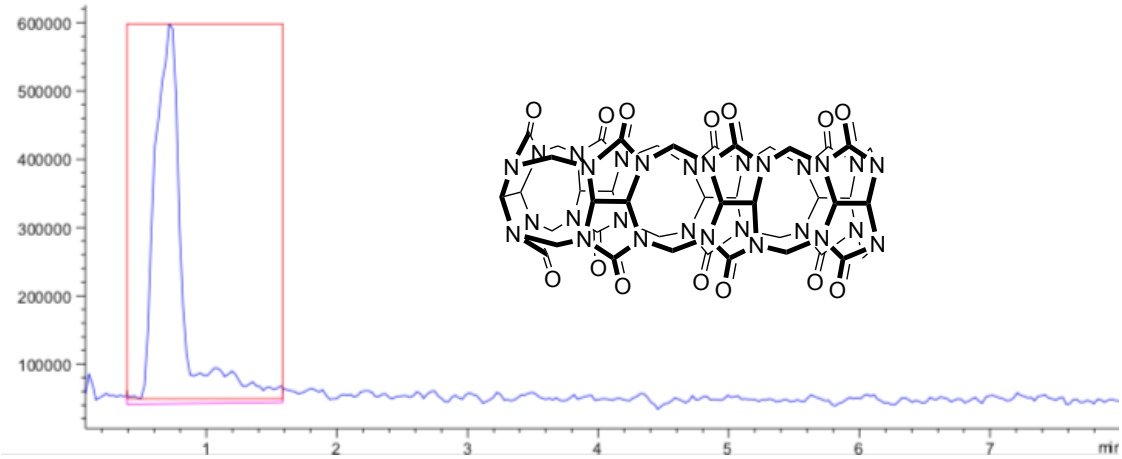

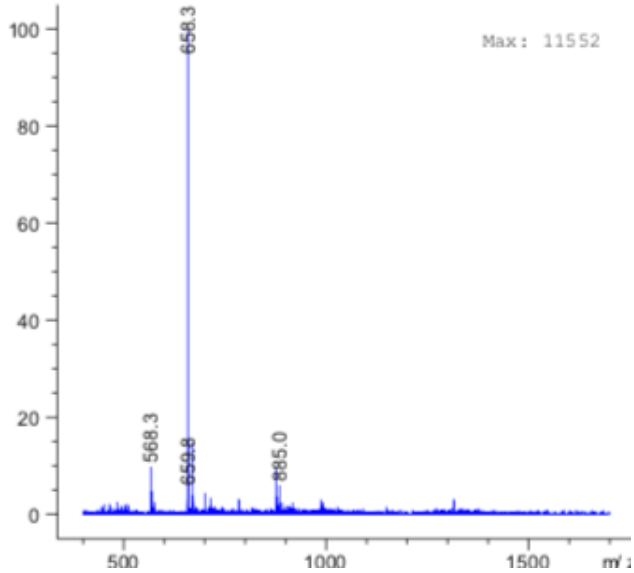

MS	m/z_{exp}
[CB7-H + cystamine + 2H]$^{2+}$	**658**
[CB7-OH + cystamine + 2H]$^{2+}$	666
[CB7-2OH + cystamine + 2H]$^{2+}$	674
[CB7-OProp + cystamine + 2H]$^{2+}$	685
[CB7-2OProp + cystamine + 2H]$^{2+}$	712
[CB7-3OProp + cystamine + 2H]$^{2+}$	656

II.4.8.5. Compound CB7-OH

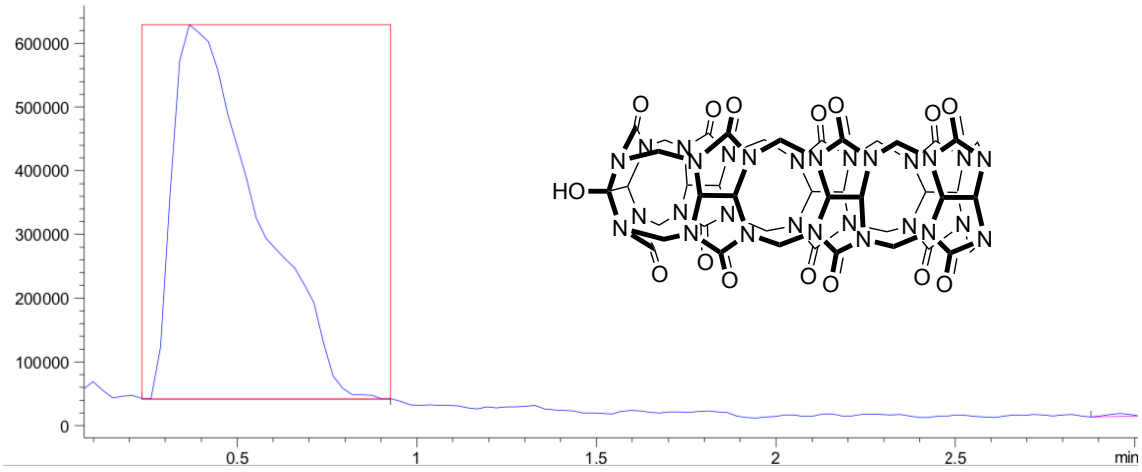

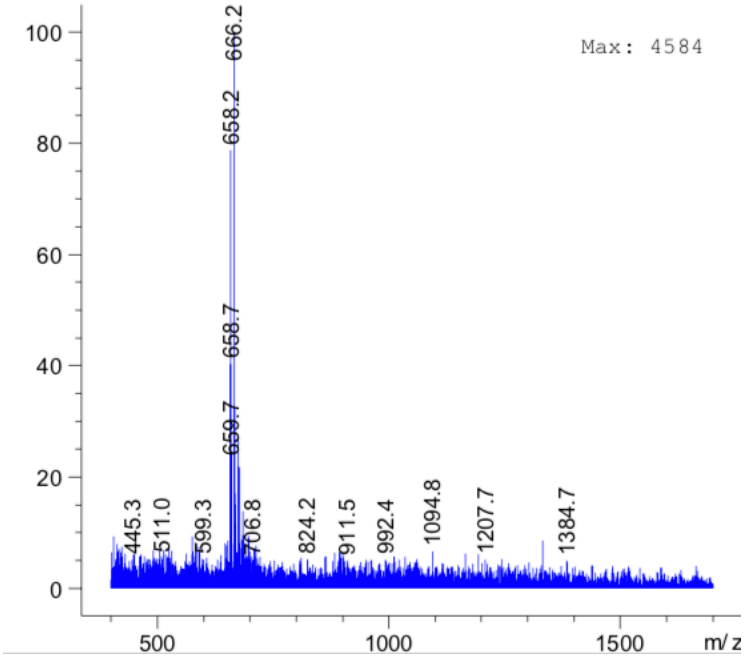

MS	m/z_{exp}
$[CB7\text{-}H + cystamine + 2H]^{2+}$	658
$[CB7\text{-}OH + cystamine + 2H]^{2+}$	**666**
$[CB7\text{-}2OH + cystamine + 2H]^{2+}$	674
$[CB7\text{-}OProp + cystamine + 2H]^{2+}$	685
$[CB7\text{-}2OProp + cystamine + 2H]^{2+}$	712
$[CB7\text{-}3OProp + cystamine + 2H]^{2+}$	656

II.4.8.6. Compound CB7-OPr

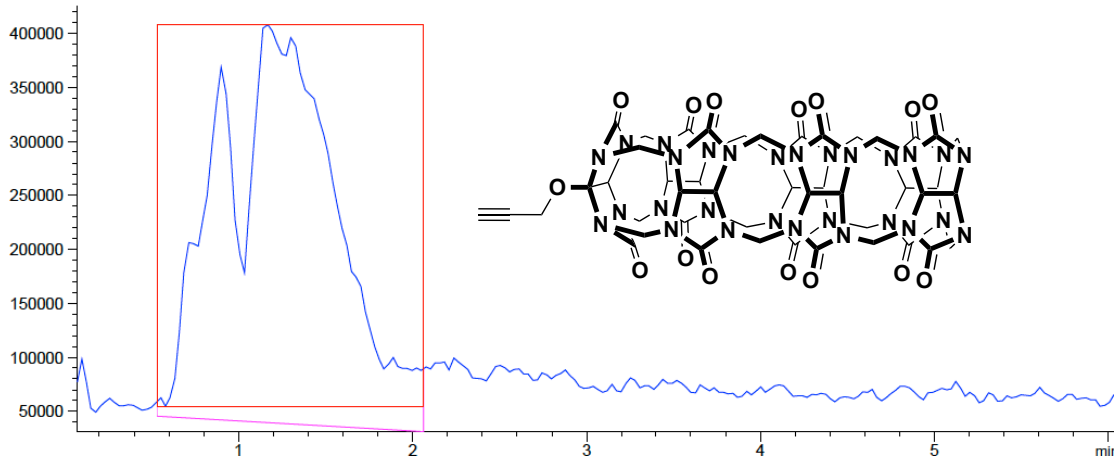

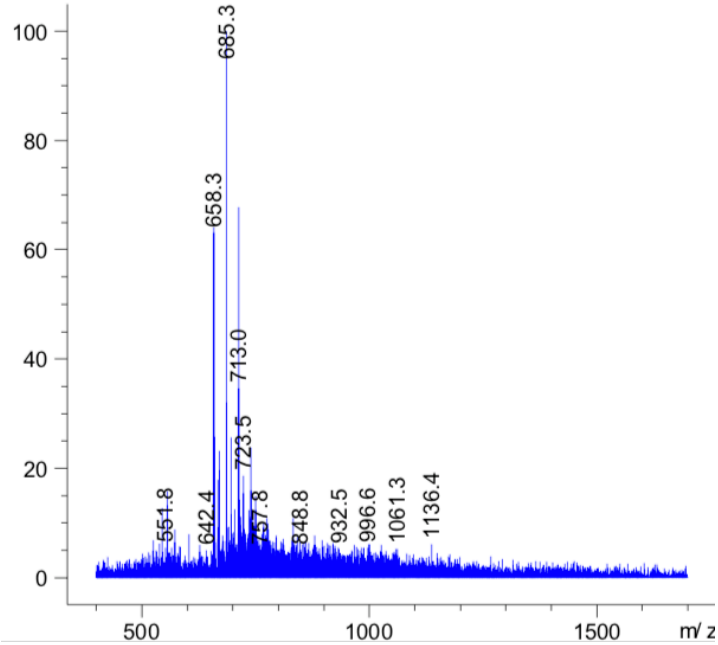

MS	m/z_{exp}
$[CB7\text{-}H + cystamine + 2H]^{2+}$	658
$[CB7\text{-}OH + cystamine + 2H]^{2+}$	666
$[CB7\text{-}2OH + cystamine + 2H]^{2+}$	674
$[CB7\text{-}OProp + cystamine + 2H]^{2+}$	**685**
$[CB7\text{-}2OProp + cystamine + 2H]^{2+}$	712
$[CB7\text{-}3OProp + cystamine + 2H]^{2+}$	656

CB7 recovered after click reaction of **CB7-OPr** with **MNPs-N_3**

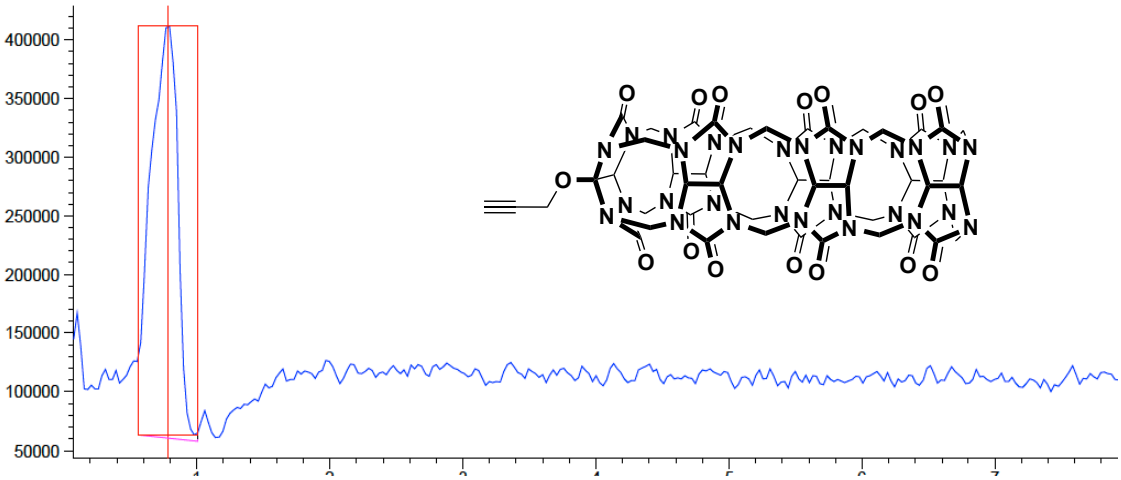

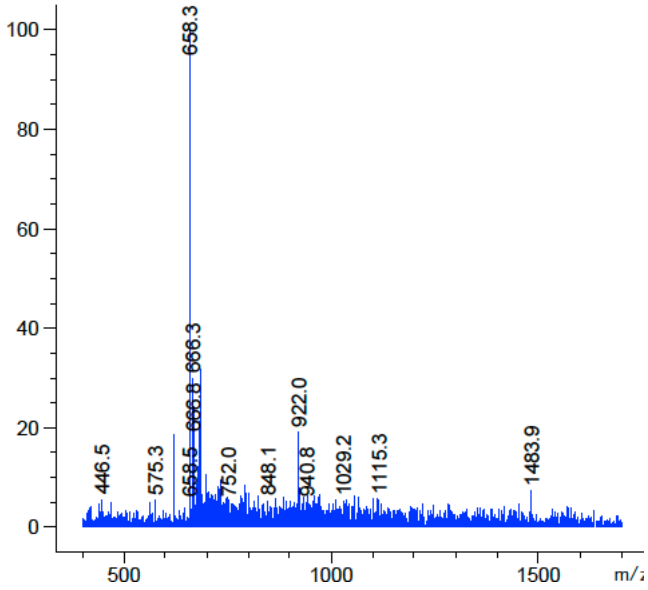

MS	m/z_{exp}
[CB7-H + cystamine + 2H]$^{2+}$	**658**
[CB7-OH + cystamine + 2H]$^{2+}$	666
[CB7-2OH + cystamine + 2H]$^{2+}$	674
[CB7-OProp + cystamine + 2H]$^{2+}$	685
[CB7-2OProp + cystamine + 2H]$^{2+}$	712
[CB7-3OProp + cystamine + 2H]$^{2+}$	656

II.4.8.7. Compound Ad-5-FAM

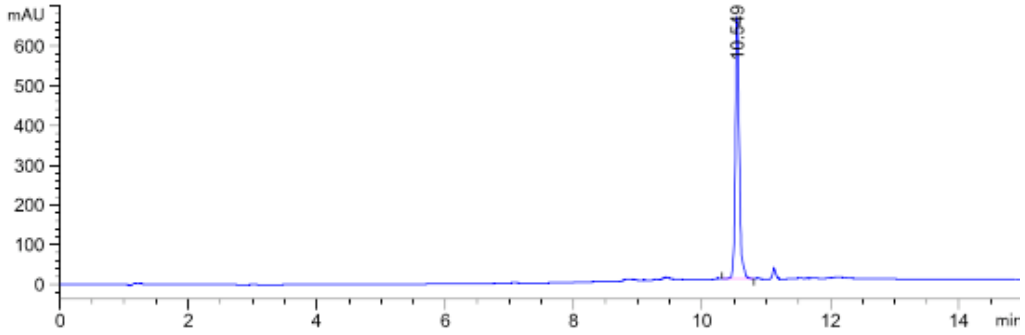

Print of window 80: MS Spectrum

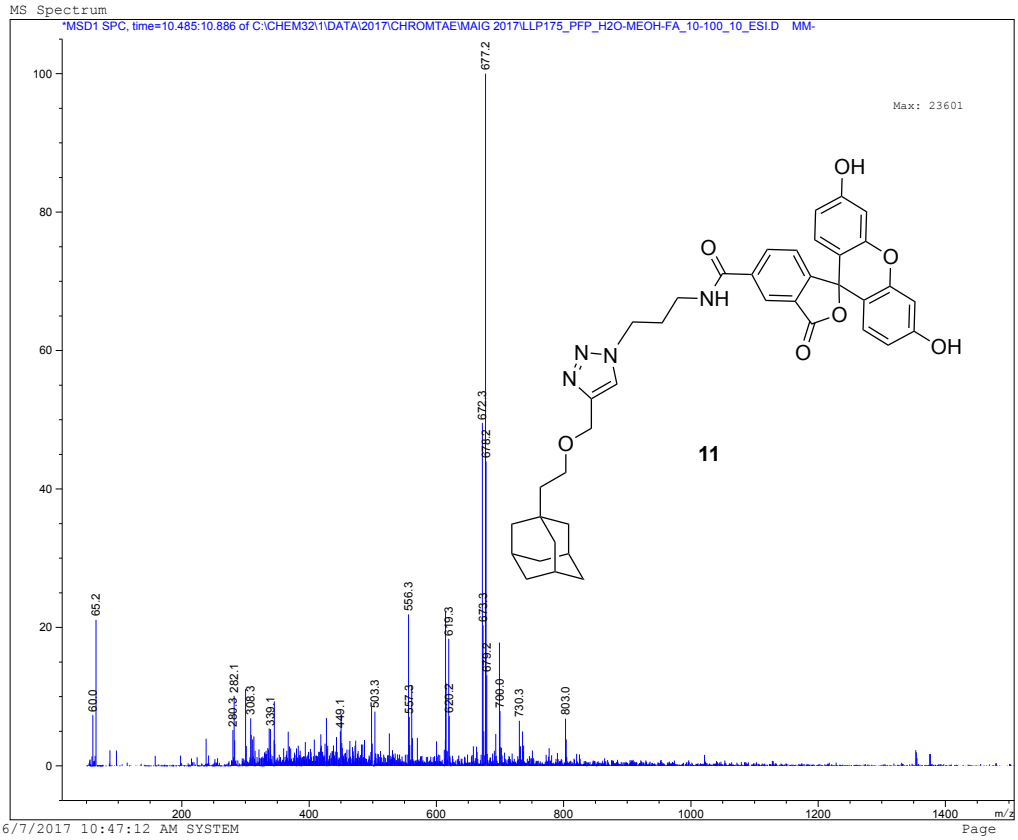

HPLCMS2 6/7/2017 10:47:12 AM SYSTEM Page 1 of 1

II.4.9. References

[1] (a) J. Kim, I.-S. Jung, S.-Y. Kim, E. Lee, J.-K. Kang, S. Sakamoto, K. Yamaguchi, K. Kim, *J. Am. Chem. Soc.* **2000**, *122*, 540–541. (b) D. Bardelang, K. A. Udachin, D. M. Leek, J. C. Margeson, G. Chan, C. I. Ratcliffe, J. A. Ripmeester, *Cryst. Growth Des.* **2011**, *11*, 5598–5614. (c) C. Marquez, F. Huang, W. M. Nau, *IEEE Trans. Nanobioscience* **2004**, *3*, 39–45.
[2] Y. Ahn, Y. Jang, N. Selvapalam, G. Yun, K. Kim, *Angew. Chem. Int. Ed.* **2013**, *52*, 3140-3144
[3] M. M. Ayhan, H. Karoui, M. Hardy, A. Rockenbauer, L. Charles, R. Rosas, K. Udachin, P. Tordo, D. Bardelang, O. Ouari, *J. Am. Chem. Soc.* **2015**, *137*, 10238-10245.
[4] J. A. McCune, E. Rosta and O. A. Scherman, *Org. Biomol. Chem.*, **2017**, *15*, 998-1005.
[5] S. Zhang, Z. Dominguez, K. Assaf, M. Nilam, T. Thiele, U. Pischel, U. Schedler, W. Nau, A. Hennig, *Chem. Sci.* **2018**, *9*, 8575-8581.
[6] (a) L. Cao, L. Isaacs, *Org. Lett.* **2012**, *14*, 3072–3075. (b) D. Lucas, T. Minami, G. Iannuzzi, L. Cao, J. B. Wittenberg, P. Anzenbacher, L. Isaacs, *J. Am. Chem. Soc.* **2011**, *133*, 17966–17976. (c) B. Vinciguerra, L. P. Cao, J. R. Cannon, P. Y. Zavalij, C. Fenselau, L. Isaacs, *J. Am. Chem. Soc.* **2012**, *134*, 13133-13140.
[7] B. Martín-Matute, C. Nevado, D. J. Cárdenas, A. M. Echavarren, *J. Am. Chem. Soc.* **2003**, *125*, 5757–5766.
[8] K. Hayakawa, Y. Yamaguchi, K. Kanematsu, *Tetrahedron Lett.* **1985**, *26*, 2689–2692.
[9] E. Wenkert, H. Khatuya, *Synth. Commun.* **1999**, *29*, 2413–2417.
[10] J. Lim, S. Seong Lee, J. Y. Ying, *Chem. Commun.* **2010**, *46*, 806–808.
[11] G. T. Carroll, G. London, T. F. Landaluce, P. Rudolf, B. L. Feringa, *ACS Nano* **2011**, *5*, 622–630.
[12] (a) P. Riente, J. Yadav, M. A. Pericàs, *Org. Lett.* **2012**, *14*, 3668–3671. (b) D. Cheng, X. Li, G. Zhang, H. Shi, *Nanoscale Res. Lett.* **2014**, *9*, 195.

3

CHAPTER III

CB7 anchored magnetic nanoparticles for catalyst recovering and recyclability

CHAPTER III

CB7 anchored magnetic nanoparticles for catalyst recovery and recyclability

III.1. Introduction

III.1.1. Asymmetric catalysis: organocatalysis

Chiral molecules are those that are not superimposable on their mirror image. Consequently, there can be two distinct isomers of these molecules, called enantiomers. The two enantiomer molecules of a given compound have the same energy, but when interacting with another chiral molecule, they will generally present different interaction energies. Many of the compounds associated with living organisms are chiral, for example, proteins, enzymes, DNA, and hormones. Thus, the enantiomers of compounds usually have different biological activity. As a result, the pharmaceutical industry demands enantiomerically pure chiral bioactive compounds because enantiomers often have very different, and sometimes, opposite pharmacological effects.[1] One route to obtain enantiopure pharmaceuticals is asymmetric synthesis, which commonly requires the intervention of external chiral reagents, catalysts, or auxiliaries.

In the field of asymmetric catalysis, the chiral catalysts are meant to facilitate the course of a reaction without affecting their equilibrium position. They act by decreasing the activation energy of the process, allowing it to happen under milder conditions. In other words, the catalyst interacts with the substrates and participates in the transition state of a given reaction. This interaction between chiral catalysts and the substrates triggers the selective formation of one stereoisomer, which is induced by the chirality of the catalyst. Regarding the chemical composition of the catalysts, they can be classified into three groups:

[1] One of the most famous examples relates to the thalidomide birth-defect crisis. The drug was used to treat nausea and to alleviate morning sickness in pregnant women. However, thalidomide is racemic; while one enantiomer is the bioactive form of the molecule, the other may cause congenital disabilities. Nevertheless, the administration of the pure enantiomer can racemize to the other due to the acidic hydrogen at the chiral center of the molecule.

metallic, for metal catalysis; enzymatic, for biocatalysis; or organic, for organocatalysis.

Organocatalysis is the use of relatively simple organic molecules (i.e., non-enzymatic) that do not contain any metal as catalytic species to activate substrates for stereoselective reactions.[2] One of the first examples dates back to the early 1970s.[3] Hajos and Parrish developed a process in which L-proline was used as a Brønsted acid for an enantioselective intramolecular aldol condensation (Scheme III-1).

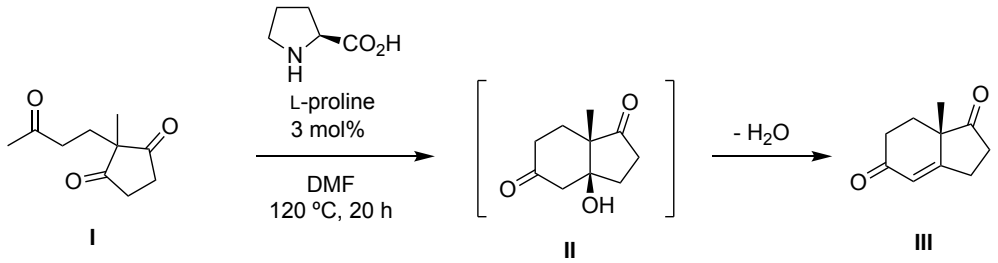

Scheme III-1. Hajos and Parrish enantioselective synthesis of fused bicyclic products using L-proline as a catalyst.

L-proline is a secondary amine that can form reversible enamines with carbonyl compounds. Thus, by having its amine group inserted into the carbonyl, it can be used in sub-stoichiometric amounts to induce the formation of the enantiomeric product. Proline first adds to the carbonyl compound. Then, the formed enamine reacts with one of the carbonyls in an aldol condensation reaction (an aldol reaction followed by dehydration to deliver the corresponding conjugated enone). After that, the catalyst is regenerated for the next catalytic cycle.

Later studies on the field demonstrated the applicability of this natural aminoacid as a potential reagent for asymmetric organocatalysis. List, Lerner, and Barbas III reported in 2000 the first asymmetric intermolecular aldol reaction.[4] Contemporarily, List first described the L-proline catalyzed Mannich reaction (Scheme III-2).[5] This epiphany had a tremendous impact on the field of organocatalysis. Interest on the field has been increasing ever since—as a result of the novelty of the concept, and the high efficiencies and selectivities attained

[2] D. W. C. MacMillan, *Nature,* **2008**, *455*, 304.
[3] a) U. Eder, G. Sauer, R. Wiechert, *Angew. Chem. Int. Ed.* **1971**, *10*, 496-497. b) Z. G. Hajos, D. R. Parrish, *J. Org. Chem.* **1974**, *39*, 1615-1621.
[4] B. List, A. Lerner, C. F. Barbas III, *J. Am. Chem. Soc.* **2000**, *122*, 2395–2396.
[5] B. List, *J. Am. Chem. Soc.* **2000**, *122*, 9336-9337.

by many organocatalytic transformations. Besides, this methodology leads to operational simplicity and availability of the organic catalysts when compared to the corresponding transition-metal species typically employed for asymmetric reactions. Moreover, the use of metal-free chiral catalysts leads to a greener, non-toxic, and environmentally friendly processes. In this context, proline and other chiral secondary amines have shown to be advantageous catalysts in many C–C and C–heteroatom bond-forming reactions, being the formation of an intermediate enamine or iminium species a common feature in all of these cases. Since then, a myriad of activation modes in organocatalysis has been reported. However, types other than aminocatalysis go beyond the span of this chapter and will not be covered here.

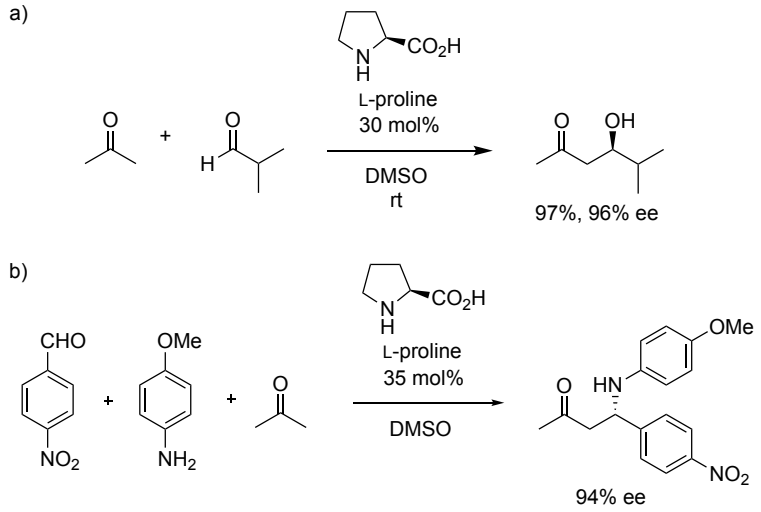

Scheme III-2. a) First organocatalyzed asymmetric intermolecular aldol reaction. b) First organocatalyzed asymmetric Mannich reaction.

Recently, Luo described the use of chiral organic catalysts other than aminoacids to induce chirality in organic reactions such as the Hajos-Parrish-Eder-Sauer-Wiechert reaction (Scheme III-3).[6]

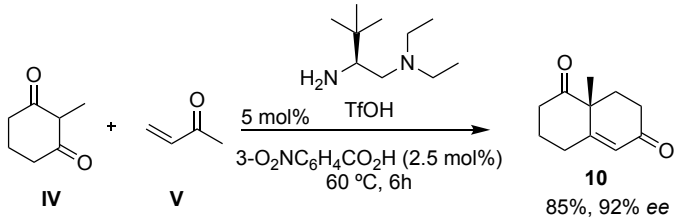

Scheme III-3. A Hajos-Parrish-Eder-Sauer-Wiechert reaction mediated by a bifunctional primary-tertiary diamine.

[6] a) P. Zhou, L. Zhang, S. Luo, J.-P. Cheng, *J. Org. Chem*. **2012**, *77*, 2526−2530. b) C. Xu, L. Zhang, P. Zhou, S. Luo, J.-P. Cheng, *Synthesis* **2013**, *45*, 1939−1945.

III.1.2. Immobilized organocatalysts

The separation and recyclability of organocatalysts is a major concern for the scalability of reactions and industrial processes. The heterogenization of chiral catalysts offers multiple advantages: for example, the simple separation and isolation of the catalyst from the reaction mixture. Thus, the catalyst can be quickly recovered for recycling and reusing purposes.[7] For this reason, the development of heterogeneous organocatalytic processes, where the catalytic species are immobilized over a solid support, has become a trend.

The immobilization can be accomplished by the covalent anchoring of the catalyst, or by other interactions such as electrostatic, coordinative, entrapment, or adsorption. Amid these different strategies, covalently bonded catalysts present some advantages. The covalent bonding between the catalyst and the support is strong and suppresses catalyst leaching. Hence, these supported catalysts are significantly more stable and can be reused more times. In addition to the immobilization strategy, another essential aspect concerns the solid support. The most common supports are inorganic oxides such as silica or metals, and organic polymers.

A successful example was reported by Luo upon functionalization of iron oxide magnetic nanoparticles with a chiral amine for the aldol reaction between aromatic aldehydes and cyclohexanone in water at room temperature. The enantioselective reaction afforded yields up to 98% with 98% *ee*. Besides, the catalyst was recycled seven times without loss of catalytic activity (Scheme III-4).[8]

[7] For reviews, see: a) R. Sebesta, *Enantioselective Homogeneous Supported Catalysts*, RCS Publishing, Cambridge, **2012**. b) M. Benaglia, *Recoverable and Recyclable Catalysts*, John Wiley & Sons, Chichester, **2009**. c) K. Ding, Y. Uozumi, *Handbook of Asymmetric Heterogeneous Catalysis*, Wiley-VCH, Weinheim, **2008**.

[8] S. Luo, X. Zheng, J.-P. Cheng, *Chem. Commun.* **2008**, 5719–5721.

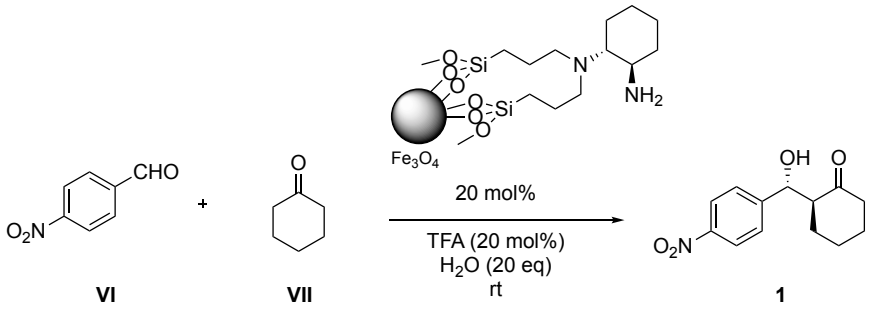

Scheme III-4. Asymmetric aldol reaction with MNP-supported diamine catalyst.

Later, our group reported the heterogenization of a diamine catalyst for the enantioselective Robinson annulation.[9] The functionalized polystyrene-support enabled the preparation of a broad scope of chiral bicyclic enones under mild conditions in high yields. The heterogeneous catalyst was recycled ten times with yields and enantiomeric excesses over 80 and 90%, respectively (Scheme III-5).

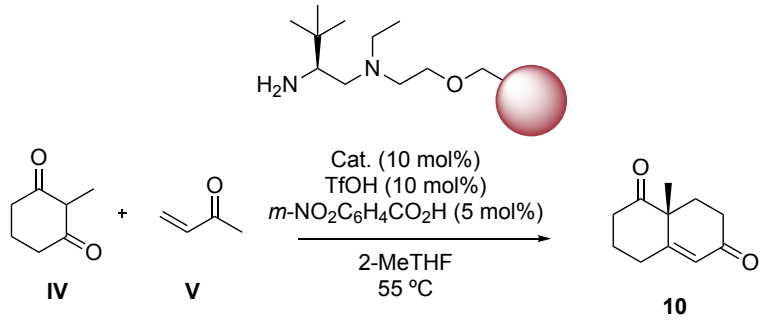

Scheme III-5. Robinson annulation reaction using a PS-supported catalyst.

III.1.3. Reversibly assembled organocatalysts

For its numerous advantages, it is clear that immobilization of asymmetric catalysts into non-soluble supports constitutes an attractive alternative to homogeneous catalysis. Besides, due to the avoidance of leaching, minimization of product contamination and the possibility of recovery and reuse, immobilization through covalent tethering remains prevalent. However, these complex catalytic systems assembled by covalent immobilization present one main drawback: the loss of the vehicle and its cargo by any operational failure.

On the other hand, the use of high-affinity complexing units integrated onto the surface of solid supports may help to overcome this hurdle. In this matter, functional cargos, for different applications and purposes, could be sequentially introduced by simple complexation-decomplexation and further complexation

[9] S. Cañellas, C. Ayats, A. H. Henseler, M. A. Pericàs, *ACS Catal.* **2017**, *7*, 1383–1391.

sequences. Thus, any possible failure or deactivation of the functional unit could be remediated by a solvent-induced disintegration of the assembly, leading to a readily available vehicle.

Cyclodextrins (CDs) are naturally occurring macrocycles of several glucopyranosyl units linked together by glycosidic bonds. They are water-soluble, inexpensive, and contain hydrophobic internal cavities that provide a hydrophobic micro-environment that triggers the formation of inclusion complexes. In addition to hydrophobic interactions, other driving forces for the association into CDs include van der Waals forces, electronic effects, and steric factors.[10]

They have been attached to nanoparticles for adsorption of contaminants,[11] drug delivery,[12] and catalysis.[13] Moreover, β-CD strongly binds adamantyl derivatives in water (k_a = 10^5–10^6 M^{-1}).[14] For this reason, they have been anchored onto the surface of MNPs and employed by our group and others to recover adamantyl-containing catalysts from the reaction mixture (Figure III-1).[15]

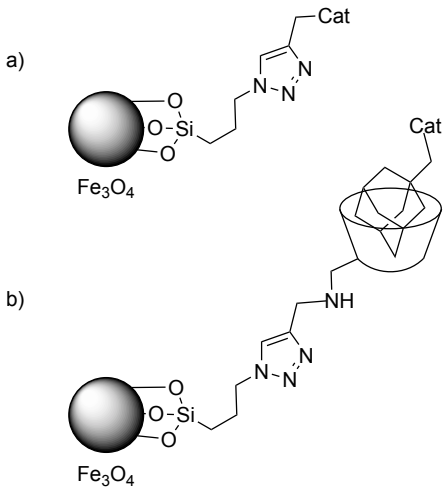

Figure III-1. Magnetically powered immobilized catalyst (a) and cyclodextrin-adamantyl reversibly assembled analog designed to act as a chemical shuttle for a functional cargo (b).

Considering the much stronger association constants provided by cucurbiturils with some guests, we were confident to speculate that magnetic nanoparticles

[10] a) F. Hapiot, S. Tilloy, E. Monflier, *Chem. Rev.* **2006,** *106*, 767-781. b) Rekharsky, M. V.; Inoue, Y. *Chem. Rev.* **1998,** *98*, 1875-1917.
[11] a) R. Fuhrer, I. K. Herrmann, E. K. Athanassiou, R. N. Grass, W. J. Stark, *Langmuir* **2011,** *27*, 1924-1929; b) Y. Kang, L. L. Zhou, X. Li, J. Y. Yuan, *J. Mater. Chem.* **2011,** *21*, 3704-3710.
[12] S. S. Banerjee, D. H. Chen, *J. Nanopart. Res.* **2009,** *11*, 2071-2078.
[13] B. Kaboudin, R. Mostafalu, T. Yokomatsu, *Green Chem.* **2013,** *15*, 2266-2274
[14] a) J. Szejtli, *Chem. Rev.* **1998,** *98*, 1743-1753; b) F. Hapiot, S. Tilloy, E. Monflier, *Chem. Rev.* **2006,** *106*, 767-781.
[15] Q. Li, Y. Li, J. Wang, Y. Lin, Z. Wei, H. Duan, Q. Yang, F. Bai, Y. Li, *New J. Chem.* **2018,** *42*, 827-831

decorated with a cucurbituril layer would be a noteworthy alternative. They would foster the efficiency on the selective extraction and recovery of catalysts labeled with an adamantyl unit.

III.2. Objectives

In the present work, we aimed to breadth previous studies developed by us in our laboratories. First, we wanted to determine the capacity of cyclodextrin anchored magnetic nanoparticles (MNPs-CD) to extract an adamantyl-tagged catalyst from a reaction mixture, and the possibility to reuse them for several catalytic cycles. Then, compare their performance against cucurbituril coated magnetic nanoparticles (MNPs-CB).

To this end, we prepared catalysts, already reported in our group, containing an adamantyl moiety. These organocatalysts would be subsequently used for asymmetric organocatalyzed reactions and reused.

III.3. Discussion of results

III.3.1. Aldol reaction

This project started to follow up on previous studies undertaken in our laboratories. During her Ph.D. thesis, Carolina Mendoza devoted time and resources in the preparation of a catalyst endowed with the required features for its extraction and recovery with MNPs decorated with cyclodextrin from the reaction media. She demonstrated that superparamagnetic magnetite nanoparticles functionalized with β-cyclodextrin via click chemistry were suitable hosts for the non-covalent immobilization of L-proline derivatives bearing adamantyl residues (Figure III-2). The resulting nanoparticles were used as magnetically recoverable catalysts in the asymmetric aldol reaction of aromatic aldehydes with cyclohexanone in water. The reaction displayed high diastereo- and enantioselectivities. Besides, the reversibly-assembled catalysts could be disintegrated in organic media. Thereby, the recovered functional nanoparticles could be re-complexed with a different catalytic guest. However, the recyclability of this proline functionalized magnetic beads was not attempted upon reaction. Thus, we decided to take over the initial project and study the capability of the cyclodextrin coated beads to be reused for several catalytic cycles. Later on, we would compare the results with the cucurbituril decorated beads, the preparation of which has been discussed in chapter II.

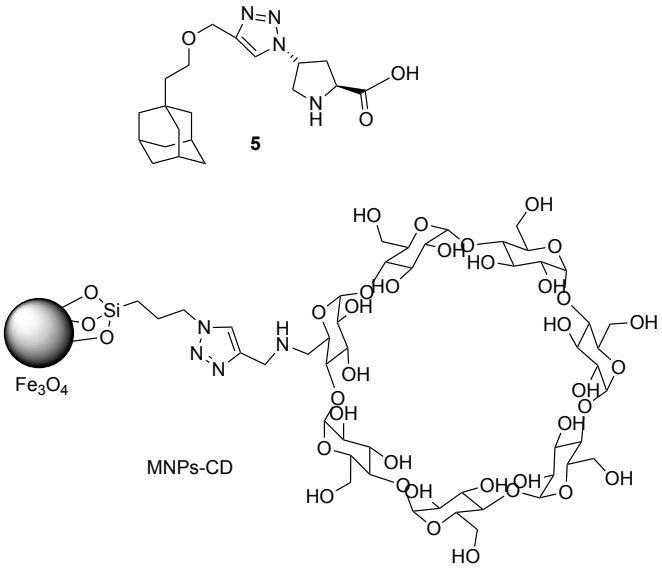

Figure III-2. L-hydroxyproline derivative modified with adamantane residue, **5**, and β-CD-functionalized MNPs, MNPs-CD.

With stocks of bench-stable cyclodextrin decorated beads, **MNPs-CD**, and the best conditions for the aldol reaction between cyclohexanone and benzaldehydes in hand, we just required to prepare the corresponding catalyst freshly.

The synthesis of the catalyst was accomplished in several steps (Scheme III-6). In brief, commercial boc-protected hydroxyproline **VIII** undergoes Mitsunobu-like reaction to afford the corresponding lactam **IX**, which is hydrolyzed to deliver the syn hydroxyproline derivative **X**. Then, protection of the carboxylic acid with DIC followed by mesylation of the hydroxyl group and subsequent substitution of the activated alcohol with sodium azide delivered the desired azidoproline counterpart, **2**.

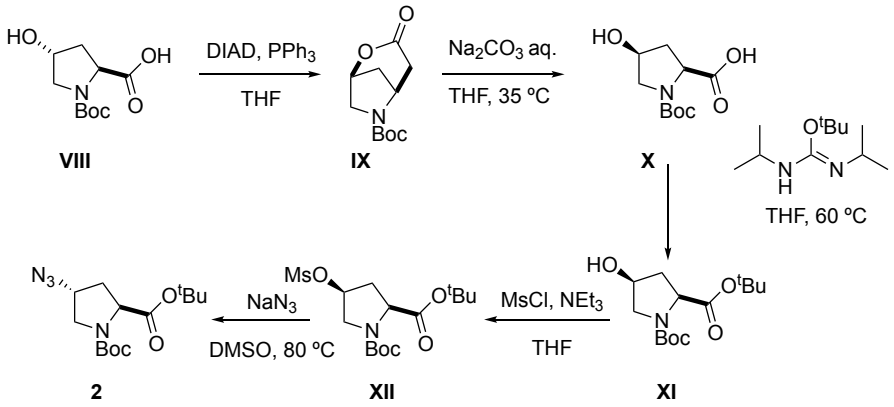

Scheme III-6. Synthesis of catalyst **2**.

The copper-catalyzed reaction between an alkyl terminal adamantanethanol **3**, and **2** delivered the desired adamantyl tagged catalyst **5** upon deprotection of the carboxylic acid with TFA. To load the shuttle with the catalyst, the proline derivative was immobilized onto the surface of the cyclodextrin anchored magnetite nanoparticles. To this end, equimolar (or slightly minor, 0.85 eq, according to the functionalization of the beads) amounts of catalyst dissolved in 95:5 water/methanol were mixed with the magnetic beads at room temperature for 2 h. The solvent was then removed under vacuum to afford the corresponding immobilized complex (Scheme III-7).

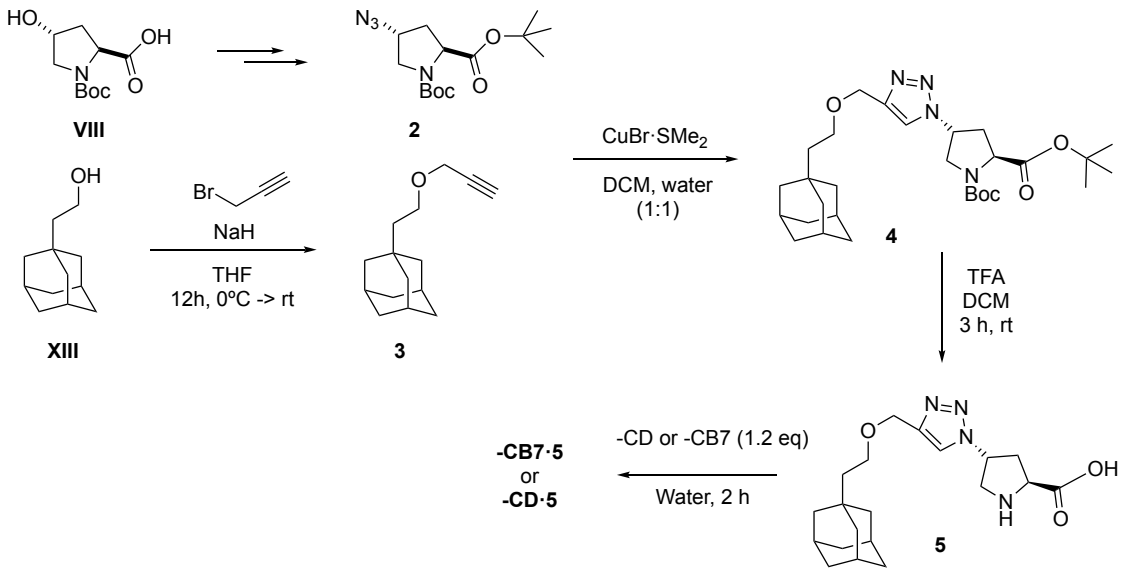

Scheme III-7. Preparation of self-assembled non-covalently immobilized catalyst.

The freshly prepared shuttle + catalyst assembly was evaluated in the asymmetric aldol reaction previously tested in our group (Scheme III-8). To this end, 10 mol% of the catalyst, **MNPs-CD·5**, was used for the model reaction between cyclohexanone and *p*-trifluoromethylbenzaldehyde in water (60 equivalents) at room temperature. The reaction was achieved with excellent yield (90%) after 72 h reaction, and more than acceptable diastereo- and enantioselectivities (*anti:syn*: 13:1, *ee*: 87%). Besides, the results obtained here were similar to previous results obtained in our group.

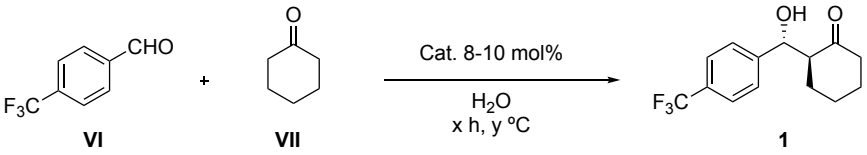

Scheme III-8. Model aldol reaction between *p*-trifluoromethylbenzaldehyde and cyclohexanone.

As we mentioned earlier, one of the main advantages associated with supporting a catalyst onto MNPs is the possibility of recovery by magnetic decantation and reuse. In other words, the immobilized chiral catalyst become magnetically powered, and it can be moved through a liquid phase by application of an external magnetic field. Thus, the catalyst can be separated from the reaction media, recovered, and reused. Besides, if decomplexation or deactivation occurs upon repeated use, the expensive part (the magnetic nanoparticles) can still be recovered by magnetic decantation or filtration, and the non-functional catalyst released, for instance, by exposure of the complex to an organic medium.

To demonstrate the recyclability of the freshly prepared proline immobilized magnetic shuttle, we used the catalyst in three consecutive runs of the aldol reaction between cyclohexanone and *p*-trifluoromethylbenzaldehyde. The catalyst allowed multiple recycling with some deterioration of the catalytic performance (Table III-1).

Table III-1. Recycling of magnetic shuttle MNPs-CD, in the aldol reaction of cyclohexanone with *p*-trifluoromethylbenzaldehyde.[a]

Entry	Cycle	Solvent[b]	Yield[c]	*anti:syn*[d]	ee_{anti}[e]
1	1	H_2O	16	12:1	80
2	1	H_2O:MeOH (6:4)	62	20:1	82
3	2	H_2O:MeOH (6:4)	86	11:1	84
4	3	H_2O:MeOH (6:4)	27	6:1	80
5	4	H_2O:MeOH (6:4)	23	3:1	74
6	1	H_2O:MeOH (2:8)	89	14:1	89
7	2	H_2O:MeOH (2:8)	57	10:1	87
8	3	H_2O:MeOH (2:8)	35	5:1	84

[a] Reaction conditions for catalyst **MNPs-CD·5**: aldehyde (0.2 mmol), ketone (1.0 mmol), water (12 mmol) and catalyst (10 mol%), stirring at room temperature for 72 h.[b] Solvent used for the extraction of the catalyst from the reaction mixture.[c] Isolated yield of combined diastereoisomers.[d] Determined by ^{1}H NMR.[e] Determined by chiral HPLC.

The results obtained in these studies were not compelling. We attributed the degradation of the catalyst activity to the need of using organic solvents to extract the catalyst from the reaction mixture. The products were slightly soluble in water media and separation from the beads in this solvent resulted in an arduous task (Table III-1, entry 1). Therefore, we hypothesized that switching to the catalyst assembled onto MNPs bearing cucurbituril would deliver similar outcomes. Despite the higher affinity of cucurbiturils with adamantyl derivatives, the use of organic solvents could disassemble the catalyst and forbid ensuing catalytic cycles.

On the other hand, the use of immiscible organic solvents with water could facilitate the transition of the products from the aqueous phase to the organic one without jeopardizing the stability of the assembled catalytic complex. However, a solid phase mixed with two immiscible aqueous and organic phases appeared to be complex. Besides, preliminary studies dismantled this idea because the solid particles were scattered all over.

We came up with an alternative. Considering the insolubility of **CB7** in organic solvents, the apparent "difficulty" of disassembling bulky adamantyl derivatives from the tight pit, and the high solubility of the products in organic solvents, we speculated that the mixture of the reagents and the simple version of the catalyst **CB7·5** in water would yield the final product, which could be easily extracted with the addition and subtle stirring of an organic solvent (Figure III-3). Although this idea drifted us away from our interests: to use the magnetically powered shuttle for catalyst extraction, we were keen to give it a try. Indeed, this idea was backed up by a previous report. The authors of the paper described a photoreaction in a two-phase system. In the aqueous phase, where the reaction takes place, **CB7** binds to the photoreactive substrate by hydrophobic interactions. The reaction affords then a photoproduct with reduced affinity to **CB7**, which accumulates in the organic phase, where the reaction mixture is analyzed.[16]

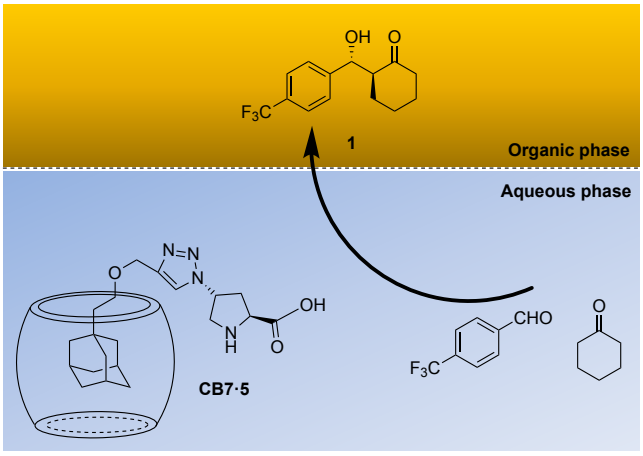

Figure III-3. Aldol reaction in water and organic phase extraction.

The next set of experiments started with the preparation of the catalyst **CB7·5**. First, we screened some conditions to find the optimal conditions for the reaction (see the experimental section for detailed screening conditions). The reaction

[16]A. L. Koner, C. Márquez, M. H. Dickman, W. M. Nau, *Angew. Chem. Int. Ed.* **2011**, *50*, 545–548.

time and temperature were set at 24 h and room temperature, which had a slightly better outcome than the reaction performed at 55 ºC for 6 h. The catalytic activity was then tested for **CB7**, **CB7·5**, and **5**. Expectedly, **CB7** did not impart a significant influence on the reaction performance, and **CB7·5** and **5** had a very similar outcome; the reaction delivered the product with excellent diastereo- and enantiomeric ratios as well as quantitative conversion measured by internal standard. Then, the reaction for the synthesis of **10** was studied in the known conditions with slight changes; 10 mol% of the catalyst **CB7·5** was stirred in a mixture of the aldehyde **VI** and an excess of the ketone **VII** (5 eq) in water (20 eq) for 24 hours at room temperature. Upon reaction, the aqueous solution was carefully extracted with the corresponding organic solvent, and the aqueous phase containing the catalyst was evaporated under high-vacuum and reused for the next catalytic cycle. This time, the reaction took place in excellent yields, diastereo- and enantiomeric ratios, and way faster, no more than 24 h of reaction time required, when compared to the 72 h needed with the shuttle (Figure III-4a, 1st run). For the extraction of the product, ethyl acetate was chosen as the organic phase. The aqueous solution was first evaporated and reused for a second catalytic cycle. At first, we obtained remarkable results, apparently (Figure III-4a, 2nd run). The yield and both, the diastereo- and enantiomeric ratios were excellent. However, in hindsight, we understood that these results were due to an overloading of the catalyst from the outset. Hence, we were still leaking the catalyst somehow, and further cycles helped to elucidate this reasoning. The third cycle still depicted good diastereomeric- and enantiomeric ratios, as well as the fourth. However, the yields kept dropping in each cycle and befell 50% in the last cycle (Figure III-4a, 3rd and 4th runs). We reluctantly acquiesced to these results and lingered in finding other organic solvents that would allow the extraction of the product without interfering the complex. First, the catalyst loading was reduced to 8 mol%. Then, upon reaction, the product was extracted with Hexane or DCM (Figure III-4b and 3c). The results were similar: the diastereo- and enantiomeric ratios were high throughout the catalytic cycles; however, the yields were continually decreasing.

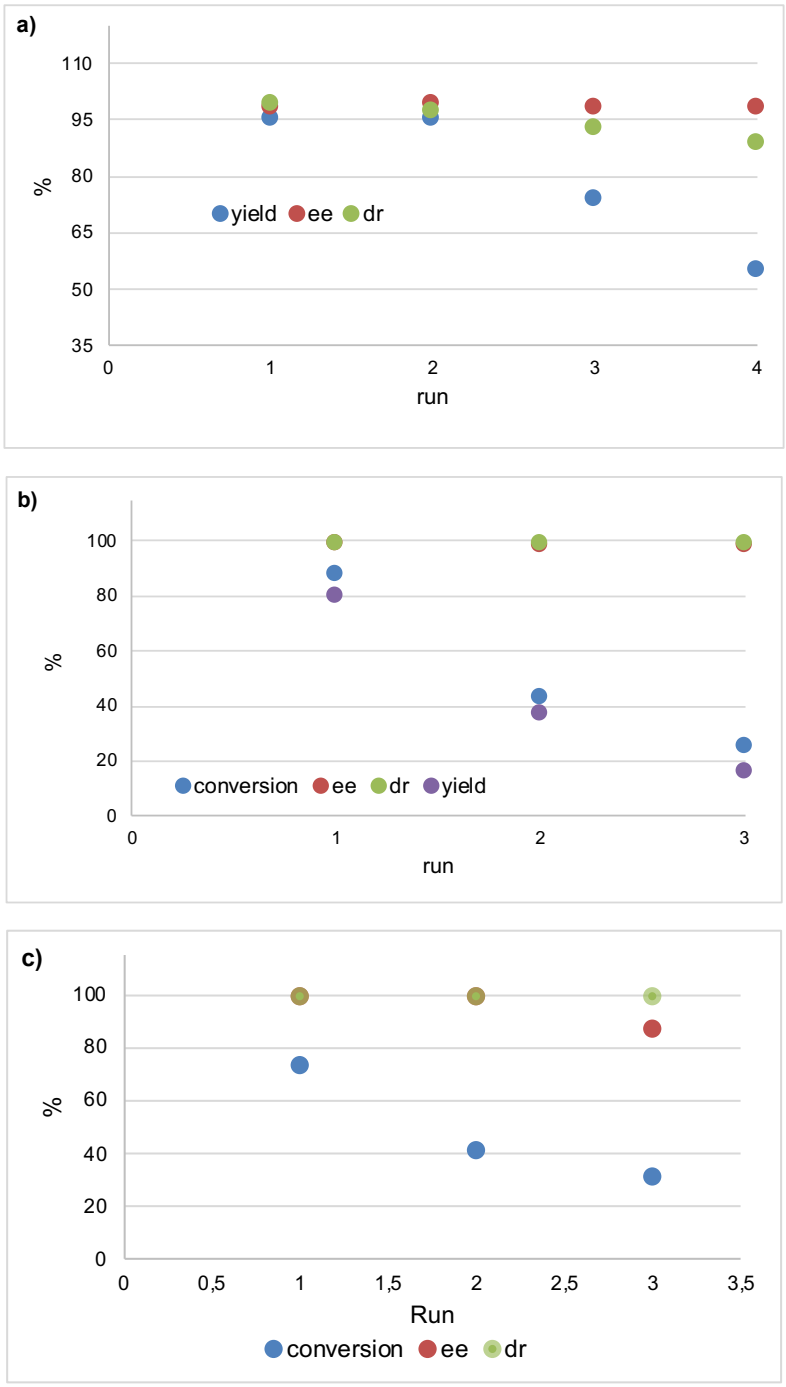

Figure III-4. Yields, conversions, and diastereo- and enantiomeric excess of the products obtained after each cycle. (a) extraction with EtOAc, (b) extraction with hexane, (c) extraction with DCM.

These results definitely thwarted our hypotheses. Most probably, even though we focused our efforts on the extraction process, the reason behind the decrease in the catalytic activity was due to the presence of other reagents in the solution. For example, 5 eq of cyclohexanone are added in each batch. In other words, the amount of cyclohexanone is 50-fold that of the catalyst. As far as we know, the affinity of cyclohexanone in CB7 has not been reported yet, but considering the

large amount of the ketone and other components with respect the catalyst, it is most probable that their presence has a notorious contributing effect on the degradation of the catalytic complex, albeit neutral adamantyl derivatives display relatively high-affinity constants. For example, the association constant of 1-adamantanemethanol hovers around 10^{10} M^{-1}.[17]

III.3.2. Robinson annulation

Working on the Robinson annulation between the methyl vinyl ketone and cyclohexanediones, we realized the high solubility of its products in water. Hence, the reaction can be carried out in water as the only solvent, and the soluble products separated from solid supported catalysts. Thus, we could use the shuttles once again, and we would also elucidate whether the problem of catalyst degradation was due to the extraction with organic solvents or to the mere presence of potential CB7-guest reagents. To this end, we set out to study the model Robinson annulation between methyl vinyl ketone and cyclohexanedione.

During his Ph.D. thesis, Santiago Cañeyas developed a PS-supported catalyst for the asymmetric Robinson annulation. The catalyst can be synthesized through several steps starting from the commercial L-*tert* leucine. In brief, the starting material, **XIV**, can be reduced with sodium borohydride in the presence of iodine to produce the corresponding alcohol **XV**. Upon protection of the alcohol with Boc_2O, mesylation of the protected amine **XVI**, and the ensuing cyclization, the desired aziridine **XVIII** is obtained. Ring-opening with 2-(ethylamino)ethanol leads to an amino alcohol, **7**, that can be further functionalized (Scheme III-9).

[17] S. J. Barrow, S. Kasera, M. J. Rowland, J. del Barrio, O. A. Scherman, *Chem. Rev.* **2015**, *115*, 12320–12406.

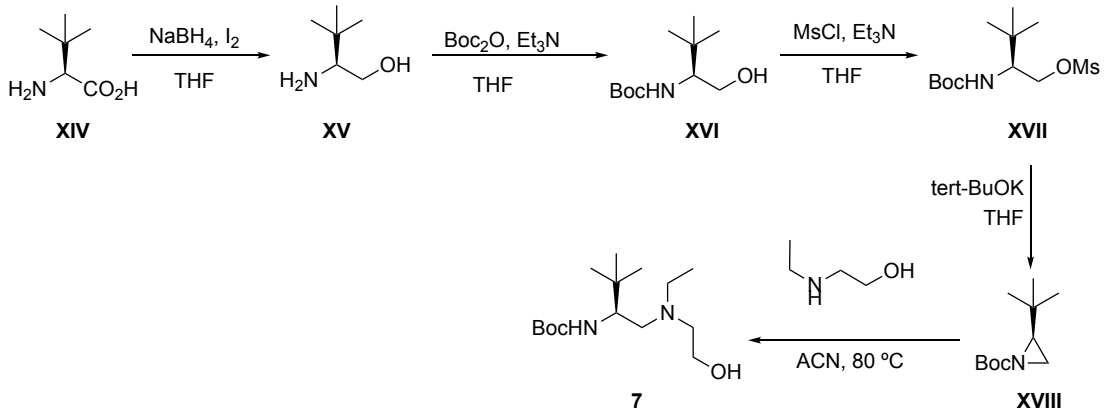

Scheme III-9. Synthesis of chiral catalyst 7.

Adamantyl ethanol, **XIII**, can be mesylated to activate the alcohol, which undergoes substitution with the chiral vicinal diamine **7** upon nucleophilic attack of the *in situ* generated alkoxide counterpart. Then, acid-mediated deprotection of the *N*-protected product delivers the adamantyl tagged catalyst **8** (Scheme III-10). Finally, the activated catalyst **8** (by addition of TfOH) and **MNPs-CB7** self-assemble under the mild conditions described with the previous catalyst.

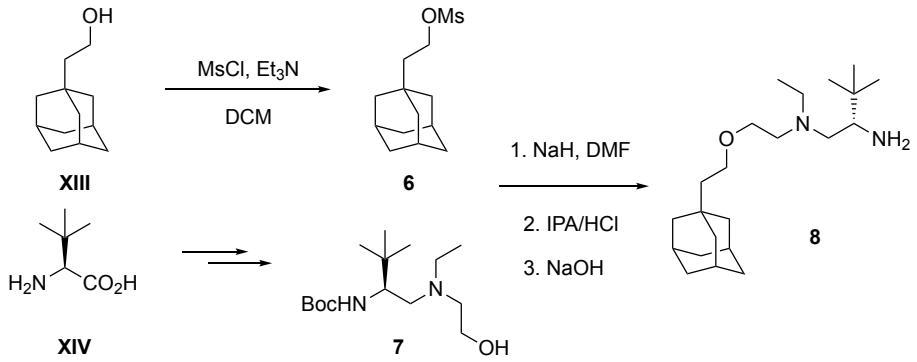

Scheme III-10. Synthesis of adamantyl tagged catalyst 8.

First, we examined the performance of catalyst **8** in water. Screening some parameters such as reaction time, temperature, and catalyst loading, we achieved striking results with full conversion and excellent enantiomeric excesses (Table III-2, entry 1). However, the assembled catalyst onto the magnetic nanoparticles (entry 2), delivered low yields. Expectedly, the shuttle device alone (entry 3) did not serve to catalyze the reaction. We attributed the low yields obtained to the constrained access to the catalytic site on the heterogeneous catalyst, and to the relatively slow reaction times (12 hours).

Table III-2. Robinson annulation between 2-methylcyclohexanedione and methyl vinyl ketone.[a]

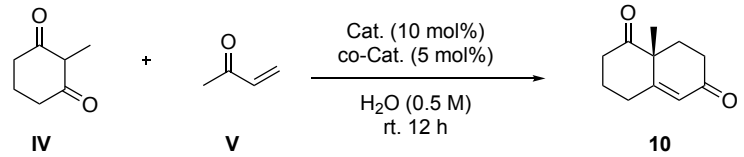

IV V 10

Entry	Catalyst	Conversion[b]	*ee*[c]
1	**8**	99	90
2	MNPs-CB7·8	26	89
3	MNPs-CB7	-	-

[a] Reaction conditions: diketone IV (44 μmol), ketone V (54 μmol), water (0.2 ml), catalyst (10 mol%), and *m*-$NO_2C_6H_4CO_2H$ (5 mol%) stirring at room temperature for 12 h.[b] Determined by ^1H NMR with internal standard.[c] Determined by chiral HPLC.

The reaction could be accelerated, though, by eliminating the rate-determining step, which corresponds to the starting Michael reaction for the formation of the triketone intermediate **9**. Hence, by starting with reagent **9**, we could study the reaction performance without changing the set parameters.

In the first catalytic cycle, the results obtained upon reaction of **MNPs-CB7·8** were similar to those obtained with the homogeneous catalyst **8** (Figure III-5). Subsequent cycles maintained the enantiomeric excess of the product while decreasing the conversion of the starting material **9**. Moreover, some of the product did not experience condensation, and the alcohol intermediate was also present (the alcohol can be converted into the final product by exposure to acidic media, e.g., TFA). In the third and the fourth cycle, the enantiomeric excess started to decrease. Thus, previous to the fifth cycle, we reactivated the catalyst with additional triflic acid. Unfortunately, the reaction did not improve; the yield of the reaction decreased as well as the enantiomeric excess. This fall in both the yield and the enantiomeric ratio suggests that the catalyst is being lost after each batch. Also, that the acid contributed to the non-asymmetric catalysis of the product **10**.

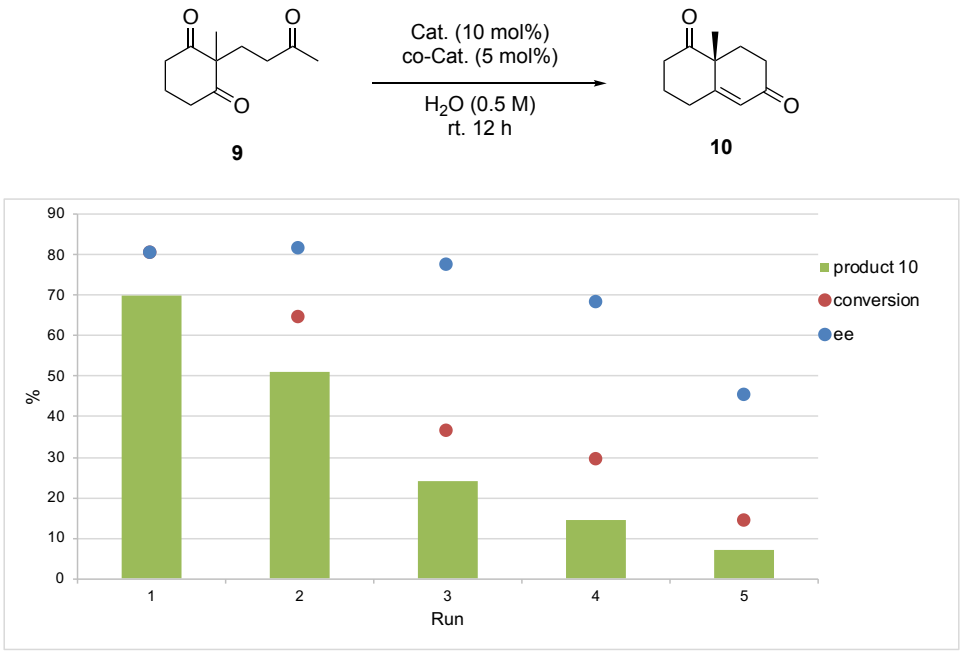

Figure III-5. Yields, conversions, and enantiomeric excess of the products obtained after each catalytic cycle.

Concluding remarks suggest that the labeling of the catalytic species plays a vital role in the recovery and recyclability of these selected molecules. While the avoidance of organic solvents must be *generally* essential to prevent leakage of the catalyst (and I say "*generally*" because in the next chapter, chapter IV, we will see the exception that confirms the rule), we need to give particular emphasis to all the molecules on play, throughout the whole process.

All our attempts to design a self-assembled recyclable catalyst turned out unsuccessful, even though our hypotheses were backed up by the general knowledge: first; adamantyl species form strong host–guest complexes with cucurbiturils, especially CB7; second, dissociation of adamantyl tagged species is difficult and requires specific energetic cost; third, albeit reports on the affinity of molecules such as cyclohexanones and benzaldehydes are scarce, we assumed that their affinity compared to that of adamantyl-containing species would be negligible, even in the presence of more extensive amounts of the former. Moreover, we erratically underestimated the importance of cationic species to generate noteworthy guests. We will see in the following chapter how small changes in the design of a given molecule can increase dramatically its affinity for cucurbiturils. Finally, these changes often imply the use of quaternary adamantyl ammonium species.

III.4. Experimental section

III.4.1. Table of contents

III.4.2. General Information

Unless otherwise stated, all reactions were conducted under air. All commercial reagents were used as received except for aldehydes that were freshly distilled previous to use. Flash chromatography was carried out using 60 mesh silica gel. Thin layer chromatography (TLC) was carried out using Merck TLC Silica gel 60 F254 aluminum sheets. Components were visualized by UV light (λ = 254 nm) and stained with *p*-anisaldehyde, phosphomolybdic dip or iodine in silica. NMR spectra were recorded at 298 K on a Fourier 300 MHz Bruker, a Bruker Advance 400 Ultrashield or a Bruker Avance 500 Ultrashield apparatus. ^{1}H NMR spectroscopy chemical shifts are quoted in parts per million (ppm) relative to tetramethylsilane (TMS), $CHCl_3$, or water. Coupling constants, *J*, are reported in Hz. IR spectra were recorded on a Bruker Tensor 27 FT-IR spectrometer and are reported in wavenumbers (cm^{-1}). High performance liquid chromatography (HPLC) was performed on Agilent Technologies chromatographs (1100 and 1200 Series). ESI mass spectra were obtained on a Waters LCT Premier Instrument. All products that are known were characterized by comparison of their physical and spectroscopic properties with those described in the literature.[1,2]

III.4.3. Experimental procedures

III.4.3.1. Preparation of catalyst CB7·5

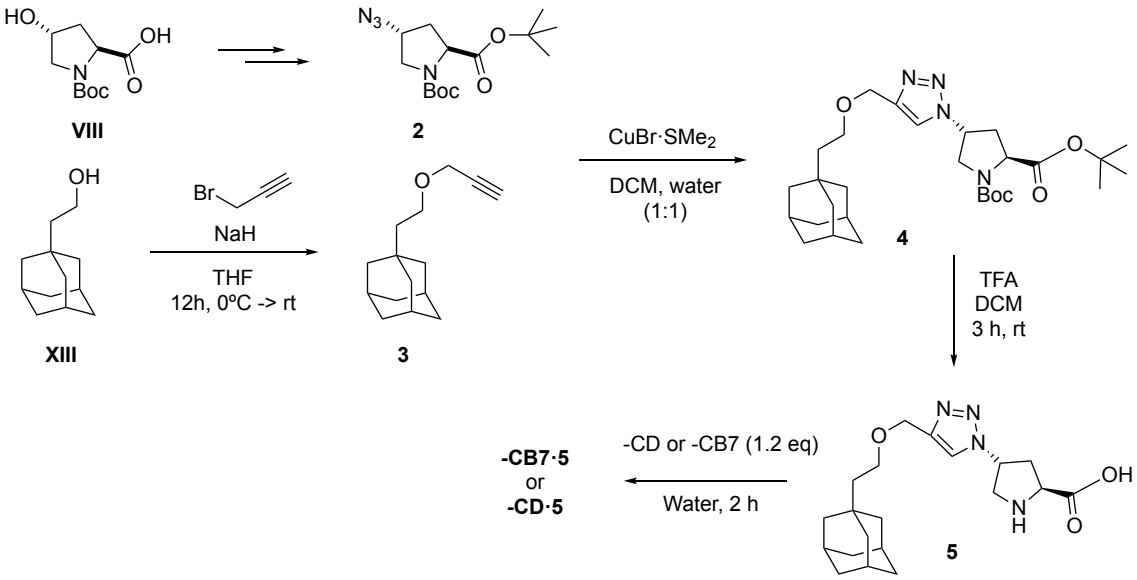

3-(1-Adamantylethoxy)prop-1-yne (3)

To a solution of 1-adamantaneethanol 98% (2.5 g, 13.86 mmol) in THF at 0 ºC NaH (60%, 15.25 mmol, 0.584 mg) was added. Then, propargyl bromide (80% in toluene, 16.64 mmol, 1.8 ml) was added and the resulting mixture was stirred at room temperature overnight. The reaction was quenched with water (5 ml), extracted with dichloromethane (2 x 20 ml), filtered and the remaining solvent evaporated. The crude mixture was purified by column chromatography over silica gel using 9:1 hexane/ethyl acetate as eluant to render **3** the product as a white powder (2.1 g, 9.62 mmol, 70% yield).

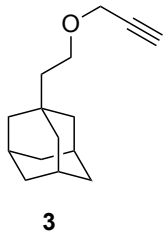

3

^{1}H-NMR (400 MHz, $CDCl_3$): δ = 4.13 (d, *J* = 2.4 Hz, 2H), 3.57 (t, *J* = 7.4 Hz, 2H), 2.41 (t, *J* = 2.4 Hz, 1H), 1.92 (s, 3H), 1.68 (m, 6H), 1.53 (m, 6H), 1.40 (t, *J* = 7.4 Hz, 2H) ppm. **^{13}C-NMR** (100 MHz, $CDCl_3$): δ = 74, 66, 58, 44, 43, 37, 32, 29 ppm. **IR** (ATR): 3306, 2897, 2845, 1728, 1447, 1353, 1095 cm^{-1}.

(2*S*,4*R*)-di-tert-butyl 4-(4-((2-(adamantan-1-yl)ethoxy)methyl)-1H-1,2,3-triazol-1-yl)pyrrolidine-1,2-dicarboxylate (4)

Compound **3** (0.31 g, 1.421 mmol) and *tert*-butyl-(2*S*,4*R*)-N-Boc-4-azidoprolinate **2**[1] (0.37 g, 1.185 mmol) were dissolved in 5 ml *tert*-butyl alcohol and water (1:1). Then, L-sodium ascorbate (0.047 g, 0.237 mmol) followed by copper (II) sulfate pentahydrate (5.91 mg, 0.024 mmol) were added and the mixture was heated under microwave irradiation (150 W and 100 ºC, 2 minutes ramp and 20 minutes hold). Then, water (10 ml) was added and the mixture was extracted with ethyl acetate (3 x 35 ml). The combined organic layers were washed with water (10 ml), dried over anhydrous Na_2SO_4 and the solvent was removed under reduced pressure. The crude mixture was purified by silica gel flash column chromatography using mixtures of hexane and ethyl acetate with increasing polarity (from 9:1 to 5:5). Compound **4** (0.50 g, 0.94 mmol, 79% yield) was obtained as a clear oil.

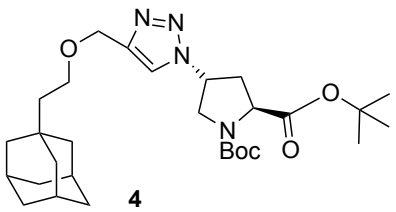

4

^{1}H-NMR (400 MHz, $CDCl_3$): δ = 7.53 (s, 1H), 5.33–5.13 (m, 1H), 4.60 (s, 2H), 4.37 (m, 1H), 4.06 (m, 1H), 3.84 (m, 1H), 3.58 (t, *J* = 7.5 Hz, 2H), 2.96–2.68 (m, 1H), 2.50 (m, 1H), 1.93 (m, 3H), 1.66 (m, 8H), 1.54 – 1.44 (m, 24H), 1.44–1.36 (m, 3H) ppm. **^{13}C-NMR** (100 MHz, $CDCl_3$): δ = 172 (COO-tBu), 154 (COO-Boc), 146 (C), 121 (CH), 82 (C), 81 (C), 67 (OCH_2), 65 (OCH_2), 59 (CH), 58.42, 58 (CH), 52 (CH_2), 44 (CH_2), 43 (CH_2), 37 (CH_2), 37 (CH_2), 29 (CH), 28 (CH_3), 28 (CH_3), 28 (CH_3) ppm. **IR** (ATR) 3139, 2976, 2899, 2846, 1738, 1700, 1476, 1451, 1392, 1366, 1252, 1221, 1148, 1124 cm^{-1}.

(2*S*,4*R*)-4-(4-((2-(adamantan-1-yl)ethoxy)methyl)-1H-1,2,3-triazol-1-yl)pyrrolidine-2-carboxylic acid (5)

To a solution of **4** (0.460 g, 0.867 mmol) in CH_2Cl_2 (2 ml) at 0 ºC, trifluoroacetic acid (1.91 ml, 24.3 mmol) was added and the mixture was stirred for 4 hours. The mixture was then concentrated under reduced pressure, and the residue was dissolved in methanol and a few drops of 1M HCl and loaded to a Dowex 50WX8 100 - 200 mesh cation exchange resin (5 g, H^+ form, swollen with 0.1 M HCl). The resin was washed with water and eluted with 15% v/v aqueous ammonium

hydroxide. The eluted fractions were evaporated to dryness under reduced pressure to afford **5** as white solid (0.29 g, 0.77 mmol, 89% yield).

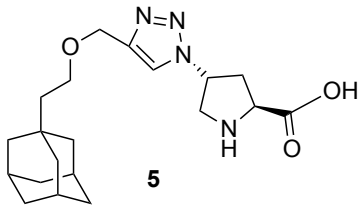

5

^{1}H-NMR (400 MHz, CD_3OD): δ = 8.07 (s, 1H), 5.50–5.41 (m, 1H), 4.57 (s, 2H, OCH_2), 4.33 (m, 1H), 3.91 (m, 2H), 3.59 (t, *J* = 7.3 Hz, 2H, OCH_2CH_2), 2.73–2.54 (m, 1H), 1.92 (m, 3H), 1.70 (m, 6H), 1.54 (m, 6H), 1.38 (t, *J* = 7.3 Hz, 2H, OCH_2CH_2) ppm. **^{13}C-NMR** (101 MHz, CD_3OD): δ = 172 (COOH), 146 (C), 125 (CH), 67 (CH_2), 64 (CH_2), 62 (CH), 61 (CH), 51 (CH_2), 44 (CH_2), 43 (CH_2), 38 (CH_2), 37 (CH_2), 32 (C) 30 (CH) ppm. **IR** (ATR) 2897, 2845, 1610, 1445, 1151, 1096, 1048 cm^{-1} .

Preparation of the inclusion complex of CB7 and 5

CB7 (116 mg, 0.10 mmol, 1.18 eq) was dissolved in water (200 ml) and catalyst **5** (29.53 mg, 0.085 mmol) was first dissolved in methanol (5 ml) and then added to the solution. The mixture was stirred at room temperature for 2 h. After this time, the solvents were slowly evaporated under reduced pressure and the solid residue was dried *in high-vacuo* to render the complex **CB7·5** as a white solid

^{1}H NMR spectra of (1) **CB7**. (2) **5.** (3) **CB7** and (**5**, 1 eq). (4) **CB7** and (**5**, >1 eq).

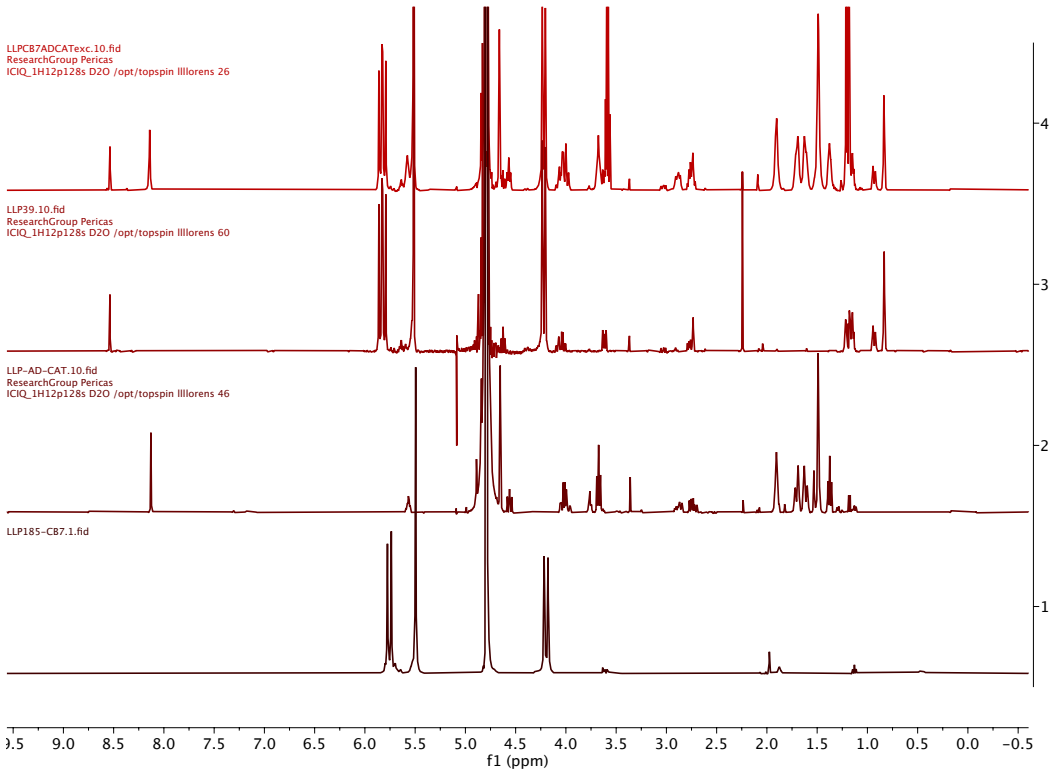

III.4.3.2. Preparation of catalyst 8

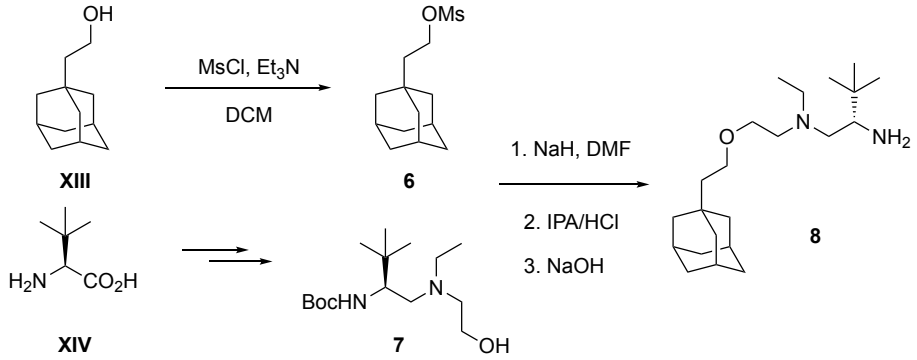

2-(1-Adamantyl)ethyl methanesulfonate, 6[2]

An oven-dried Schlenk tube equipped with a stirr bar was charged with adamantanethanol (1.0 eq) and dichloromethane (5 ml/mmol). The vessel was cooled to 0 ºC and triethylamine (2.0 eq) and mesyl chloride (2.0 eq) were subsequently added. The reaction mixture was stirred overnight at room temperature under argon. Then, the reaction mixture was quenched with HCl (1 M in water) and extracted with DCM (3 x 5 ml/mmol). The combined organic extracts were washed with water, aqueous saturated solution of $NaHCO_3$ and brine, dried over Na_2SO_4 and concentrated to dryness under reduced pressure to yield the crude mesylate, **6**

(*S*)-*N*^{1}-(2-(2-(1-adamantanyl)ethoxy)ethyl)-*N*^{1}-ethyl-3,3-dimethylbutane-1,2-diamine (8)

A solution of **7**[3] in dry DMF (1 ml) was added dropwise to a solution of sodium hydride (3 eq) in dry DMF (1 ml) at 0 ºC and the reaction mixture was stirred at this temperature for 1 h. Then, a solution of **6** (1.5 eq) in dry DMF (1 ml) was added and the mixture was stirred at room temperature for 12 h. To the reaction mixture EtOAc (20 ml) was added and the organic extracts were rinsed with water (3 x 10 ml). The organic layer was dried over $MgSO_4$, filtered and the solvent was evaporated under vacuum. The crude product was then purified by silica gel column chromatography in a mixture of hexanes and EtOAc to afford compound **8** as a white solid.

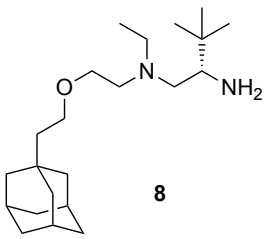

8

^{1}H-NMR (400 MHz, CD_3OD): δ = 3.45 (s, 4H), 2.67 (m, 2H), 2.51 (s, 4H,), 2.15 (m, 1H), 1.91 (m, 3H), 1.63 (m, 6H), 1.49 (s, 6H), 1.34 (m, 2H), 0.99 (s, 3H), 0.86 (m, 9H) ppm. **^{13}C-NMR** (101 MHz, CD_3OD): δ = 71, 67, 58, 57, 54, 48, 44, 43, 37, 33, 32, 30, 29, 27, 12 ppm. HRMS (ESI+) cacld for $[C_{22}H_{43}N_2O]^+$: 351.3370. Found: 351.3355.

III.4.3.3. Catalytic aldol reactions in water

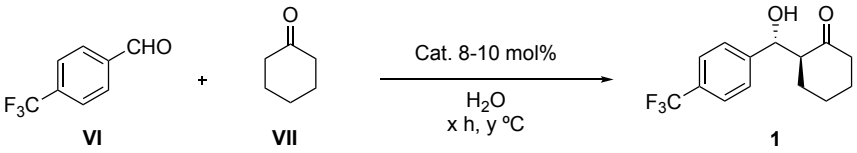

VI **VII** **1**

(2*S*,1*R*)-2-(Hydroxy(4-trifluoromethylphenyl)methyl) cyclohexan-1-one (1)

Aldehyde **VI** (27 μl, 0.2 mmol) and ketone **VII** (103 μl, 1.0 mmol) were suspended in water (108 μl, 4 mmol) and to this mixture **CB7·5** (31 mg, 0.02 mmol, 10 mol%) was added. The reaction mixture was stirred for 24 h at room temperature. Then, water (2 ml) was added and the aqueous layer was carefully extracted with ethyl acetate (3 x 1 ml). The combined organic layers were dried with $MgSO_4$, filtered and concentrated under reduced pressure. The aqueous phase containing the cucurbituril complex **CB7·5** was concentrated under high vacuum and the remaining catalyst was reused for the next catalytic reaction/cycle.

The ^{1}H-NMR spectra of the crude product showed the formation of the *anti*-aldol product and allowed the determination of the diasteromeric ratio. The yield of the reaction was measured by NMR with an internal standard (IS). The enantiomeric excess was determined by HPLC using the following conditions: Chiralpak IC column (90:10 hexane:2-propanol), 1 ml/min, λ = 213 nm; major enantiomer t_R = 10.39 min, minor enantiomer t_R = 11.82 min. All the spectroscopic data matched with those reported in the literature.[1a,4]

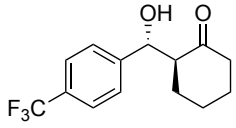

1

^{1}H-NMR (400 MHz, $CDCl_3$): δ = 7.61 (d, *J* = 7.9 Hz, 2H), 7.44 (d, *J* = 7.9 Hz, 2H), 4.84 (dd, *J* = 8.6, 2.4 Hz, 1H), 4.04 (s, 1H), 2.60 (m, 1H), 2.48 (m, 1H), 2.35 (m, 1H), 2.10 (m, 1H), 1.81 (m, 1H), 1.60 (m, 3H), 1.35 (m, 1H) ppm. **^{13}C-NMR** (100 MHz, $CDCl_3$): δ = 215, 145, 130, 128, 125, 123, 74, 57, 43, 31, 28, 25 ppm.

Screening of conditions for the aldol reaction in water

Table 1. Reaction time and temperature screening.

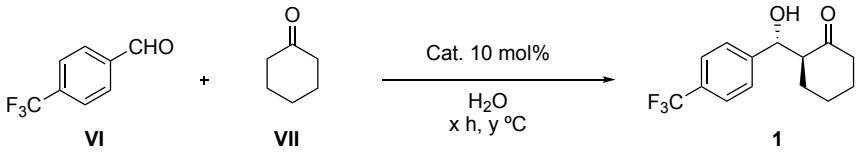

VI **VII** **1**

Entry	Time (h)	Temp. (ºC)	Conv. (%)[b]	dr[b]	ee (%)[c]
1	3.5	80	65	20:1	99
2	6	rt	66	20:1	99
3	6	55	90	20:1	98
4	**24**	**rt**	**95**	**20:1**	**99**

[a] Reactions performed on a 0.1 mmol scale with catalyst CB7·**5**. [b] Determined by ^{1}H NMR spectroscopy on the crude mixture.[c] Determined by HPLC analysis of the crude mixture using a chiral stationary phase of the crude mixture.

Table 2. Catalyst evaluation.

Entry	Catalyst	Conv. (%)[b]	dr[b]	ee (%)[c]
1	CB7	0	-	-
2	**5**	99	20:1	99
3	CB7·**5**	95	20:1	99

[a] Reactions performed on a 0.1 mmol scale at rt for 24 h.[b] Determined by ^{1}H NMR spectroscopy on the crude mixture.[c] Determined by HPLC analysis of the crude mixture using a chiral stationary phase.

Recycling experiments

Aldehyde **VI** (27 μl, 0.2 mmol) and ketone **VII** (103 μl, 1.0 mmol) were suspended in water (108 μl, 4 mmol) and to this mixture the catalyst CB7·**5** (31 mg, 0.02 mmol, 10 mol%) was added. The reaction mixture was stirred 24 h at room temperature. Then, water (2 ml) was added and the aqueous layer was carefully extracted with the corresponding organic solvent (3 x 1 ml). The combined organic extracts were dried with $MgSO_4$, filtered and concentrated under reduced pressure. The aqueous phase containing the cucurbituril complex CB7·**5** was evaporated under high vacuum and the remaining catalyst was reused for the next catalytic cycle.

Three sets of experiments were performed, using different solvents [ethyl acetate (Table 1), hexane (Table 2), dichloromethane (Table 3)], for the isolation of the reaction product. The purpose of these experiments was determining the influence of the nature of the solvent on the recyclability of the **CB7·5** catalyst.

Table 1: Recycling experiments[a]

Cycle	Conversion (%)[b]	Yield (%)[c]	dr (anti:syn)[b]	ee (%)[d]
1	95	95	>20:1	98.8
2	95	95	>20:1	98.9
3	74	74	13:1	98.6
4	55	55	8:1	98.5

[a] Reaction conditions: aldehyde (0.2 mmol), ketone (1 mmol), water (4 mmol) and catalyst CB7·5 (10 mol%). Extraction with **ethyl acetate** (3 x 1 ml).[b] Determined by ^{1}H NMR spectroscopy on the crude mixture.[c] Determined using 1,3,5-trimethoxybenzene as internal standard (IS).[d] Determined by HPLC analysis of the crude mixture using a chiral stationary phase.

Table 2: Recycling experiments[a]

Entry	Conversion (%)[b]	Yield (%)[c]	dr (anti:syn)[b]	ee (%)[d]
1	88	80	>20:1	99
2	43	37	>20:1	98
3	25	16	>20:1	98

[a] Reaction conditions: aldehyde (0.2 mmol), ketone (6 eq), water (20 eq) and catalyst CB7·5 (8 mol%). Extraction with **hexane** (3 x 1 ml).[b] Determined by ^{1}H NMR spectroscopy on the crude mixture.[c] Measured with trimethoxy benzene as internal standard (IS).[d] Determined by HPLC analysis of the crude mixture using a chiral stationary phase.

Table 3. Recycling experiments[a]

Entry	Conversion (%)[b]	dr (anti:syn)[b]	ee (%)[c]
1	73	>20:1	99
2	41	>20:1	99
3	31	>20:1	99

[a] Reaction conditions: aldehyde (0.2 mmol), ketone (6 eq), water (20 eq) and catalyst CB7·5 (8 mol%). Extraction with **DCM** (3 x 1 ml).[b] Determined by ^{1}H NMR spectroscopy on the crude mixture.[c] Determined by HPLC analysis of the crude mixture using a chiral stationary phase.

III.4.3.4. Catalytic Robinson annulations in water

A)

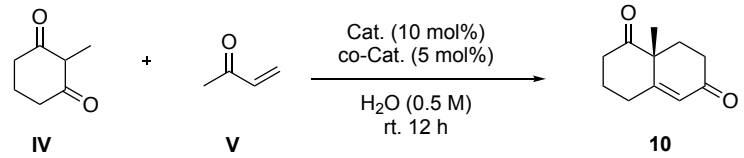

IV V 10

B)

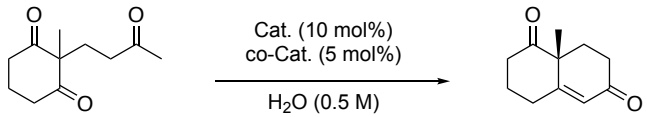

9 10

(*R*)-8a-methyl-3,4,8,8a-tetrahydronaphthalene-1,6(2*H*,7*H*)-dione (10)

Activation of the catalyst: TfOH (250 μl, 71 μmol, 0.28 M solution in water) was added to a solution of catalyst **8** (25 mg, 71 μmol) in 4 ml of a water/ACN 3:1 mixture.

A) The activated catalyst **8** (247 μl, 4.4 μmol) and **MNPs-CB7** (12 mg, 4.4 μmol, f = 0.37 mmol·g^{-1}) were diluted in H_2O (1 ml) in a 5 ml-vial and stirred at room temperature for 2 h. After that, the solvent was evaporated, a mixture of 2-methyl-1,3-cyclohexanedione **IV** (5.68 mg, 44 μmol) and the co-catalyst, *m*-$NO_2C_6H_4CO_2H$ (100 μl, 2.2 μmol, 0.022 M solution in water), was added to the reaction flask followed by a solution of methyl vinyl ketone **V** (4.45 μl, 54 μmol) in water (0.1 ml). The reaction mixture was stirred overnight. The magnetic beads were separated by magnetic decantation and filtered off, the solution was washed with water (3 x 1 ml) and the solvent was evaporated under reduced pressure to give an oil containing the enantioenriched Robinson annulation product **10**.

B) The activated catalyst **8** (0.68 ml, 12 μmol) and **MNPs-CB7** (50 mg, 12 μmol, *f* = 0.24 mmol·g^{-1}) were diluted in H_2O (1 ml) in a 5 ml-vial and stirred at room temperature for 2 h. After that, the solvent was evaporated, and a mixture of 2-methyl-triketone **9** (24 mg, 120 μmol) and the co-catalyst, *m*-$NO_2C_6H_4CO_2H$ (240 μl, 6 μmol, 0.025 M solution in water), was added to the reaction flask. The reaction mixture was stirred overnight, the magnetic beads were magnetically decanted, and filtered off, the solution was washed with water (3 x 1 ml) and the solvent was evaporated under reduced pressure to give an oil containing the enantioenriched Robinson annulation product **10**. The catalyst was dried under reduced pressure and reused for the next reaction/cycle.

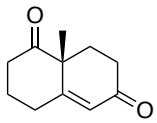

10

^{1}H-NMR (400 MHz, $CDCl_3$): δ = 5.86 (d, *J* = 2.0 Hz, 1H), 2.72 (m, 2H), 2.48 (s, 4H), 2.14 (m, 3H), 1.71 (m, 1H), 1.45 (s, 3H, CH_3) ppm. ^{13}C-NMR (100 MHz, $CDCl_3$): δ = 211 (CO), 198 (CO), 165 (C), 126 (CH), 51 (C), 38 (CH_2), 34 (CH_2), 32 (CH_2), 30 (CH_2), 23 (CH_2), 22 (CH_2) ppm. HPLC (Daicel Chiralpak IC, hexane/*i*-PrOH = 80:20), flow rate 1.0 ml/min, λ = 254 nm): t_R (*R*) = 28.0 min (major) and t_R (*S*) = 31.5 min (minor) (ee = 89%).

III.4.4. ^{1}H and ^{13}C NMR spectra

III.4.4.1. Compound 1

^{1}H NMR (400 MHz. $CDCl_3$)

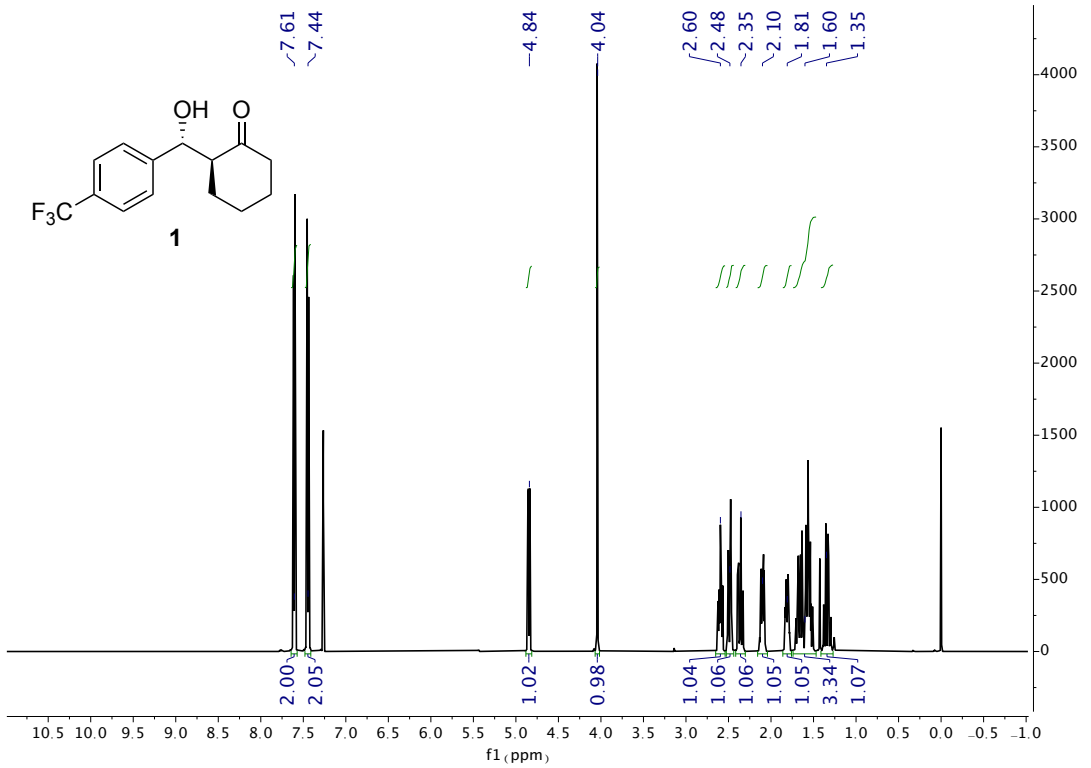

^{13}C NMR (100 MHz. $CDCl_3$)

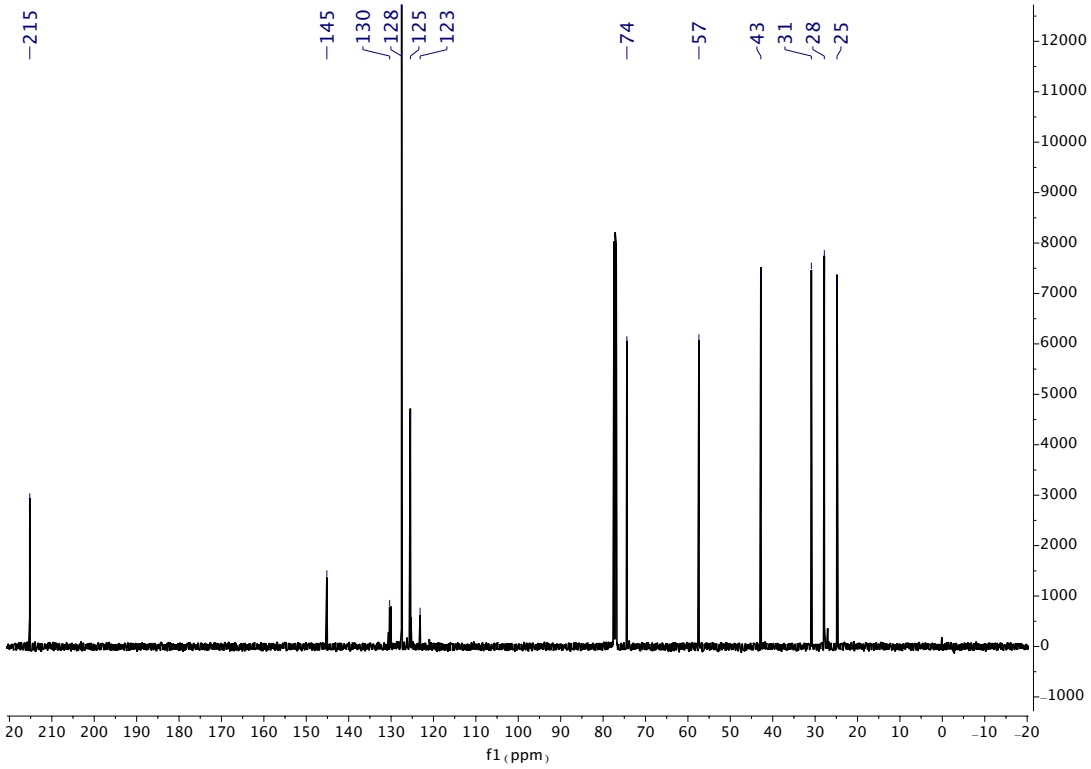

Compound **1**, cycle 1.1

^{1}H NMR (400 MHz. $CDCl_3$)

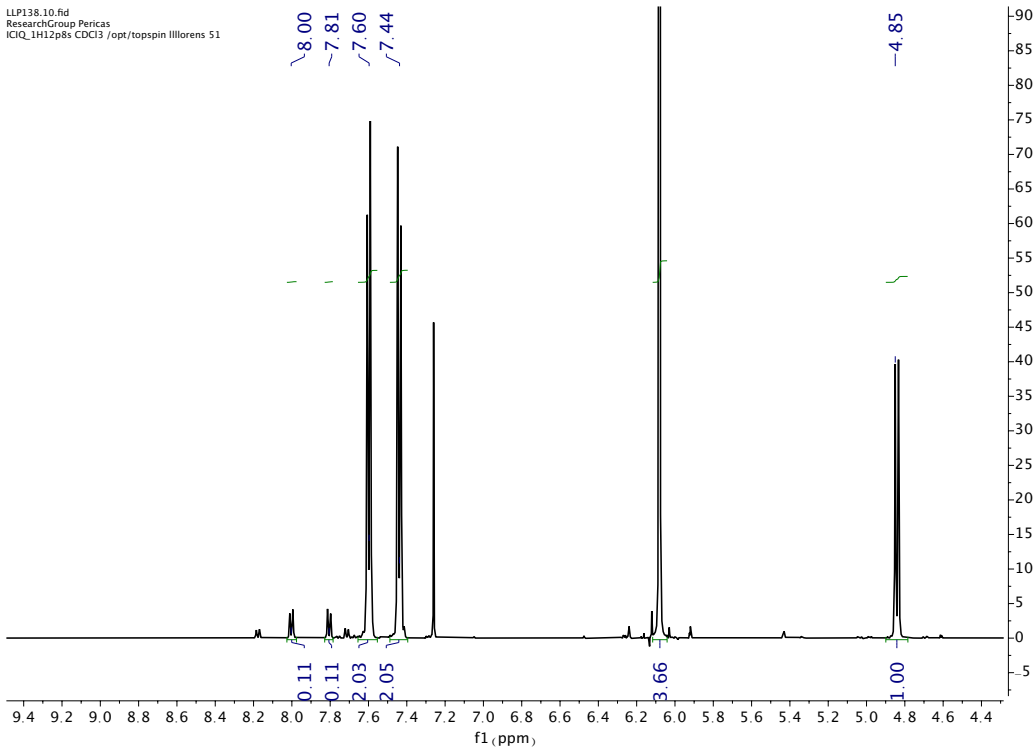

Compound **1**, cycle 1.2

^{1}H NMR (400 MHz. $CDCl_3$)

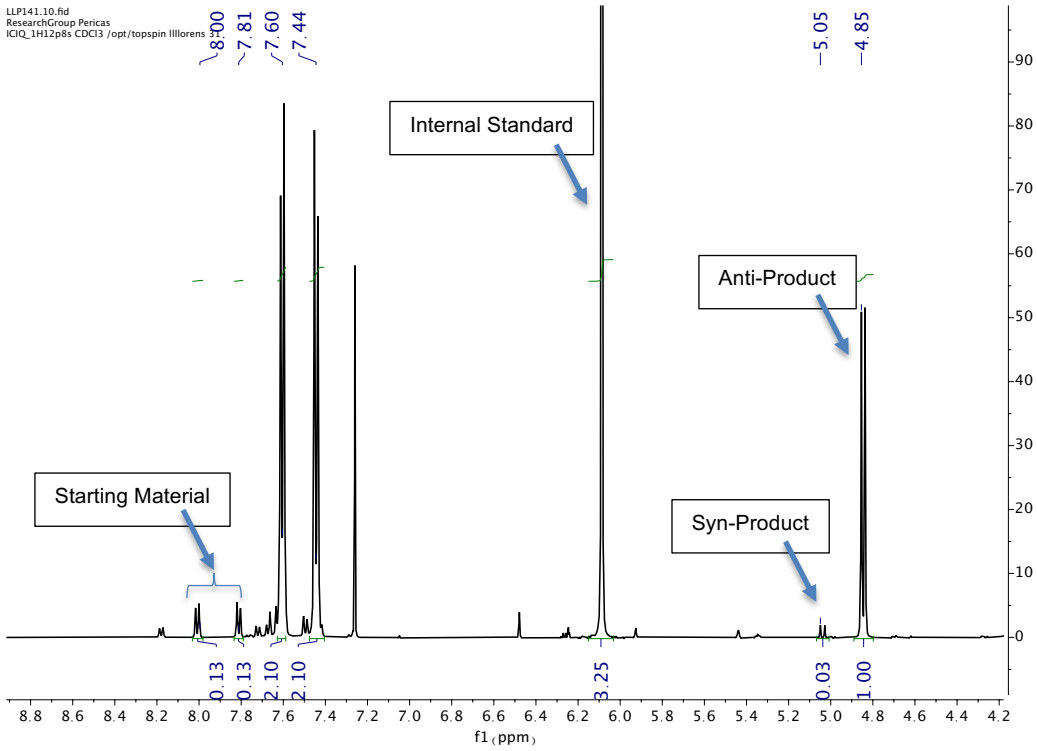

Compound **1**, cycle 1.3

^{1}H NMR (400 MHz. $CDCl_3$)

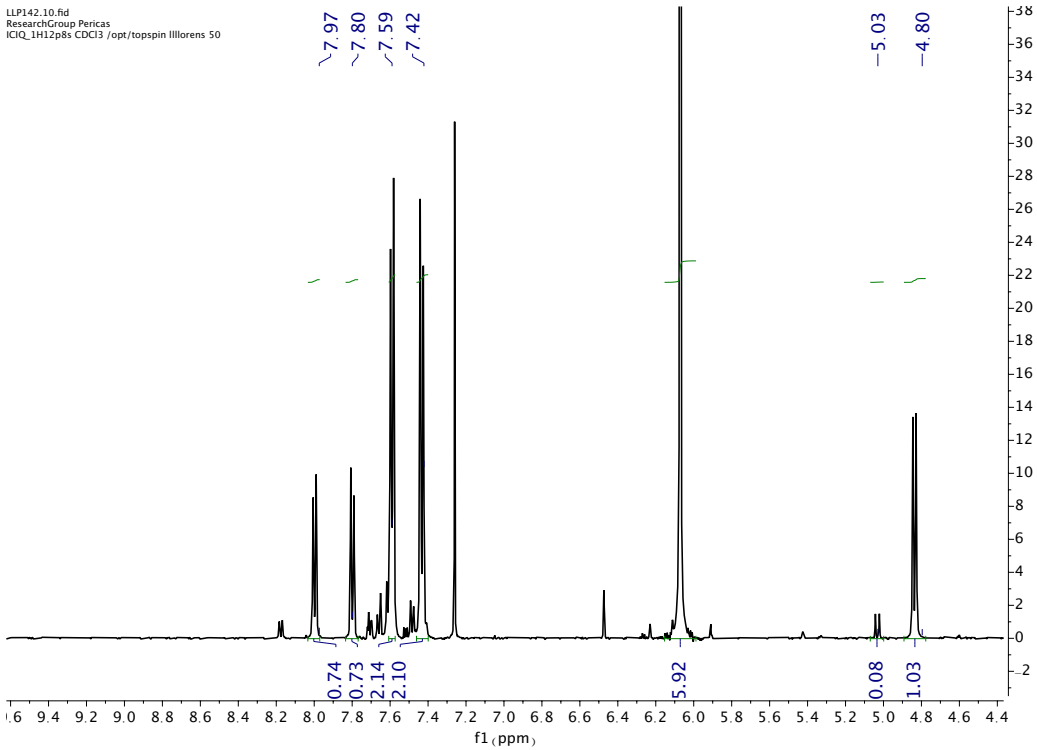

Compound **1**, cycle 1.4

^{1}H NMR (400 MHz. $CDCl_3$)

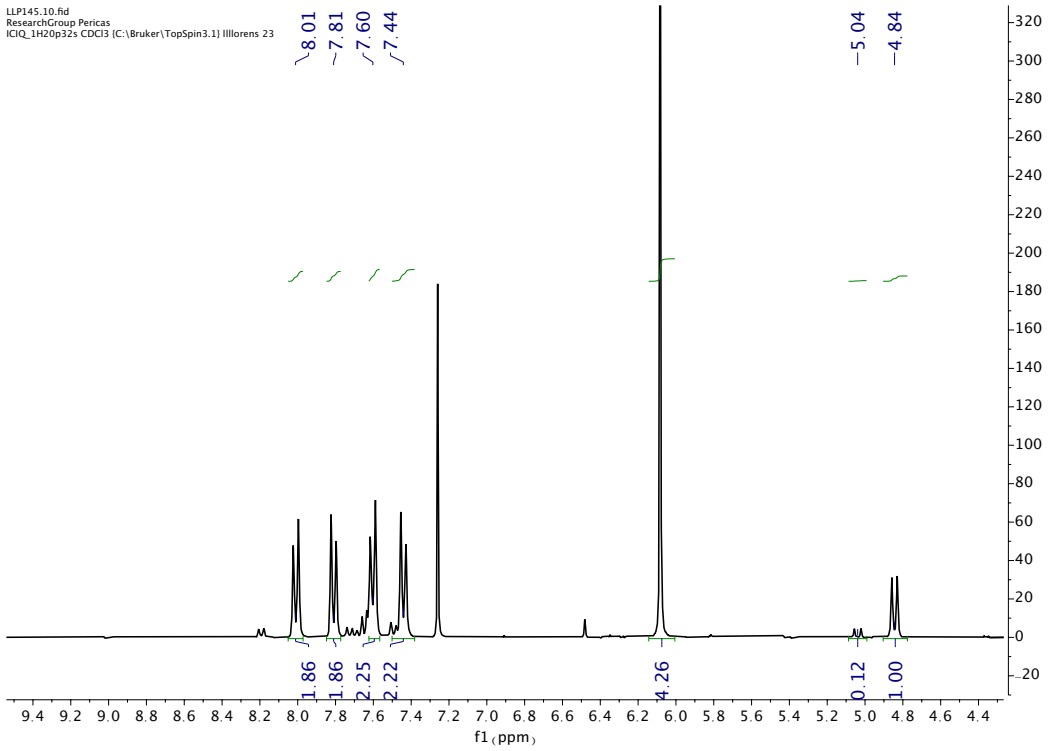

III.4.4.2. Compound 3

^{1}H NMR (400 MHz. $CDCl_3$)

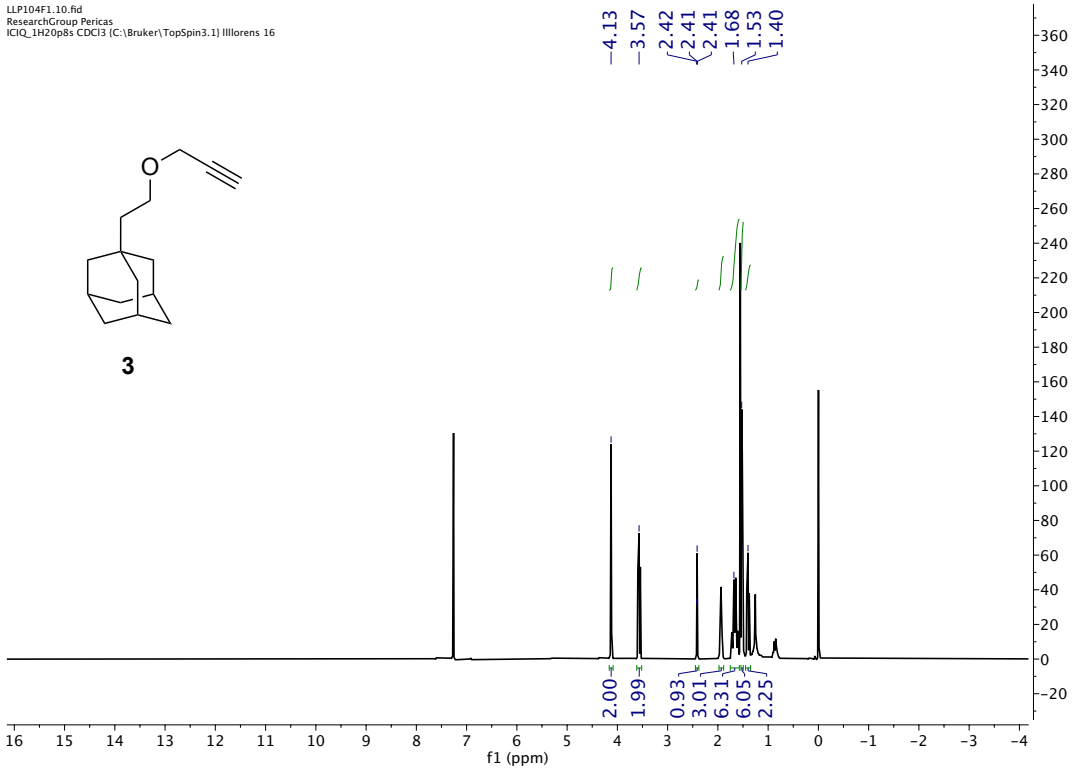

3

III.4.4.3. Compound 4

^{1}H NMR (400 MHz. $CDCl_3$)

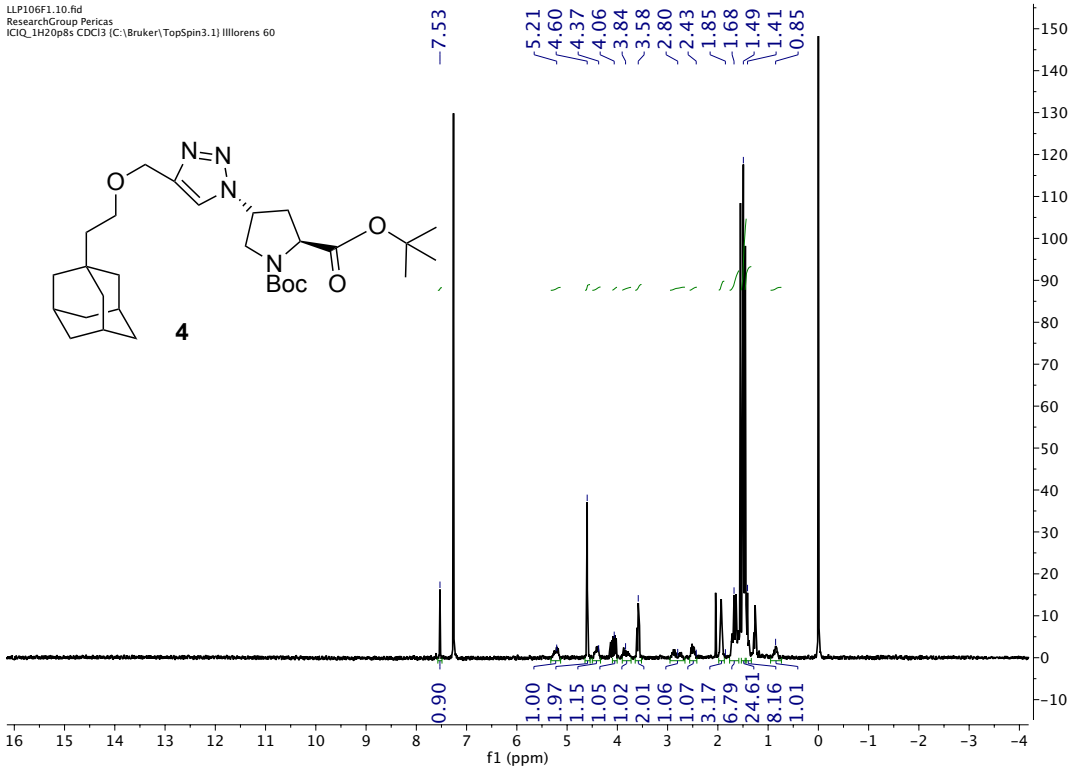

III.4.4.3. Compound 5

^{1}H NMR (400 MHz. MeOD)

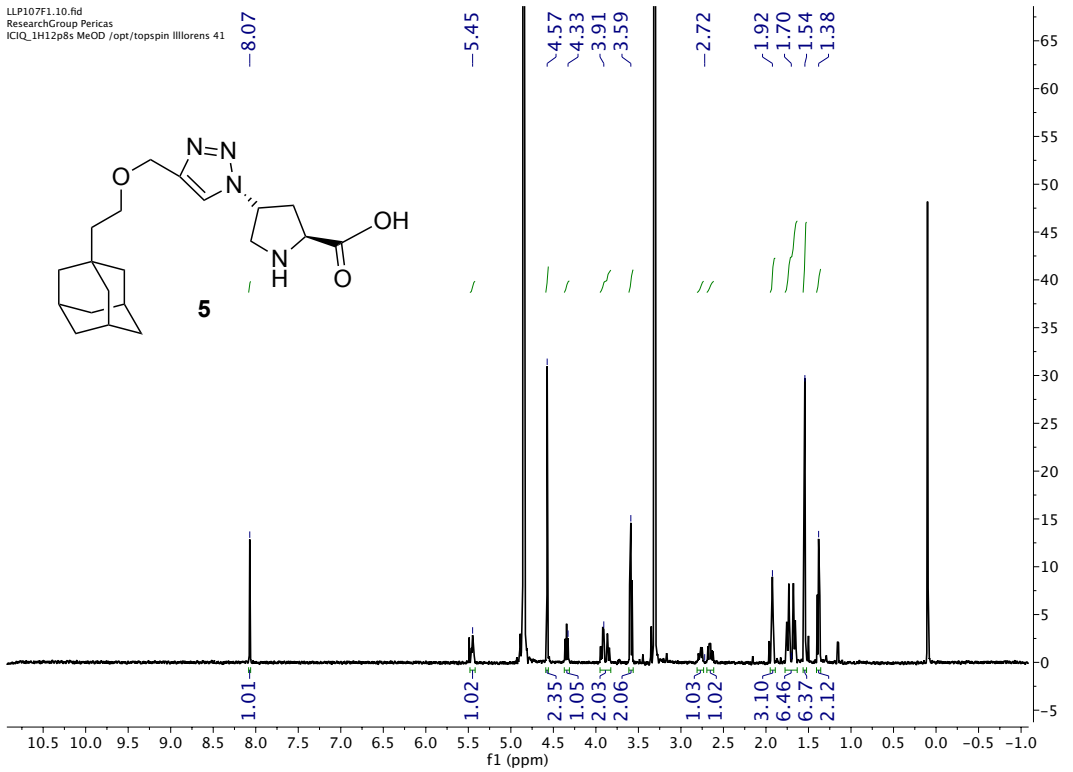

III.4.4.3. Compound CB7·5

^{1}H NMR (400 MHz. D_2O)

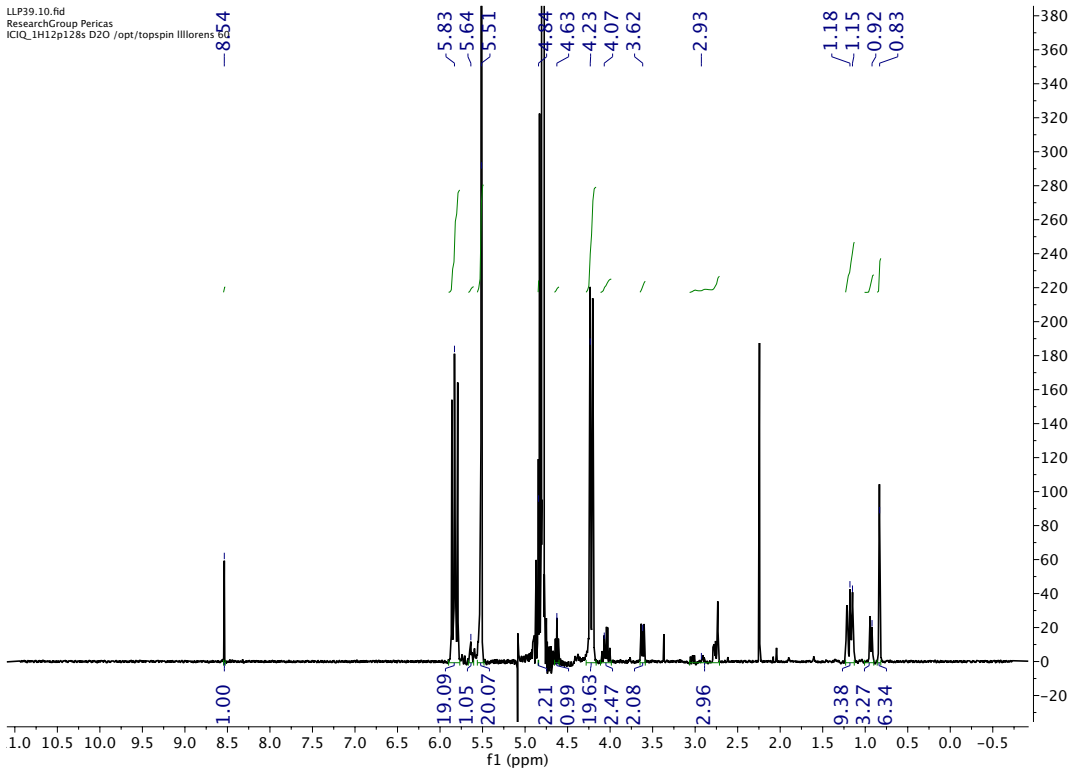

III.4.4.3. Compound 10

^{1}H NMR (400 MHz. $CDCl_3$)

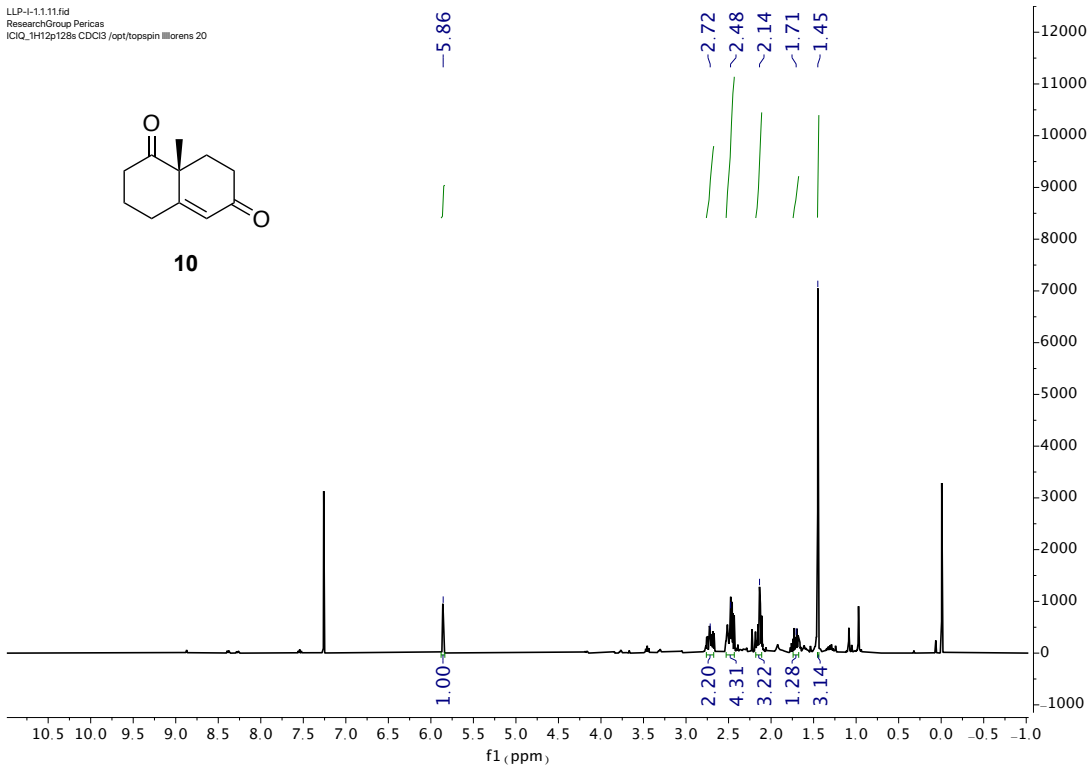

10

III.4.4.3. Compound 7

^{1}H NMR (400 MHz. $CDCl_3$)

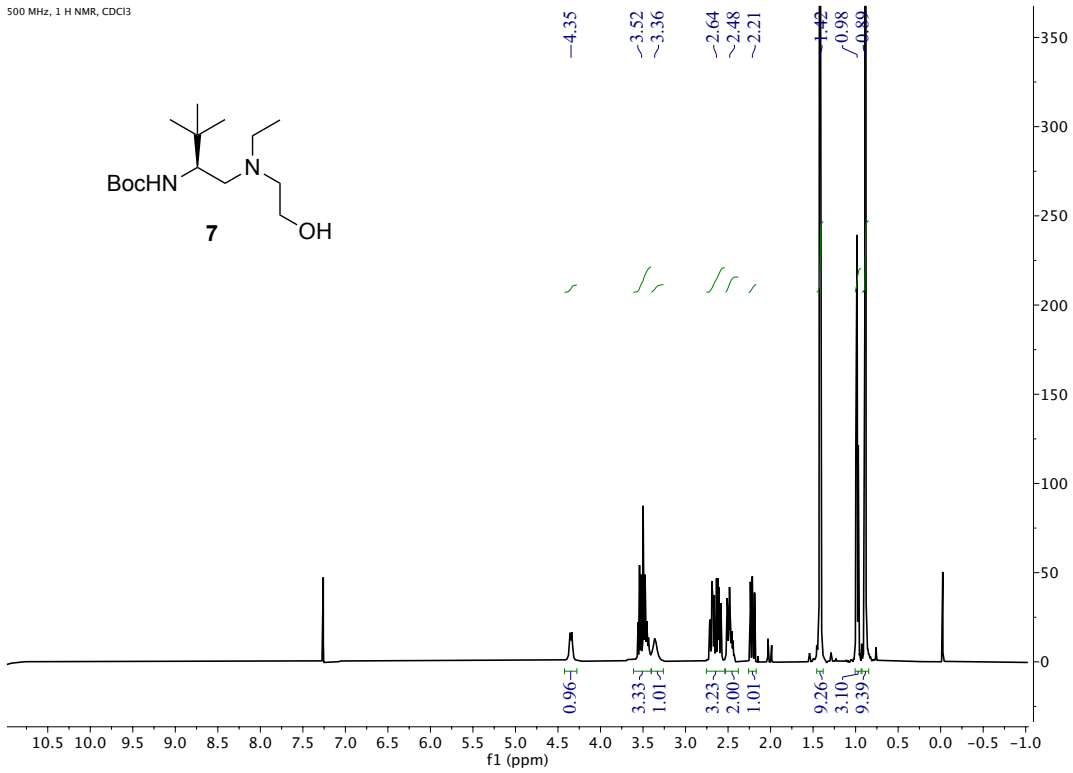

^{13}C NMR (100 MHz. $CDCl_3$)

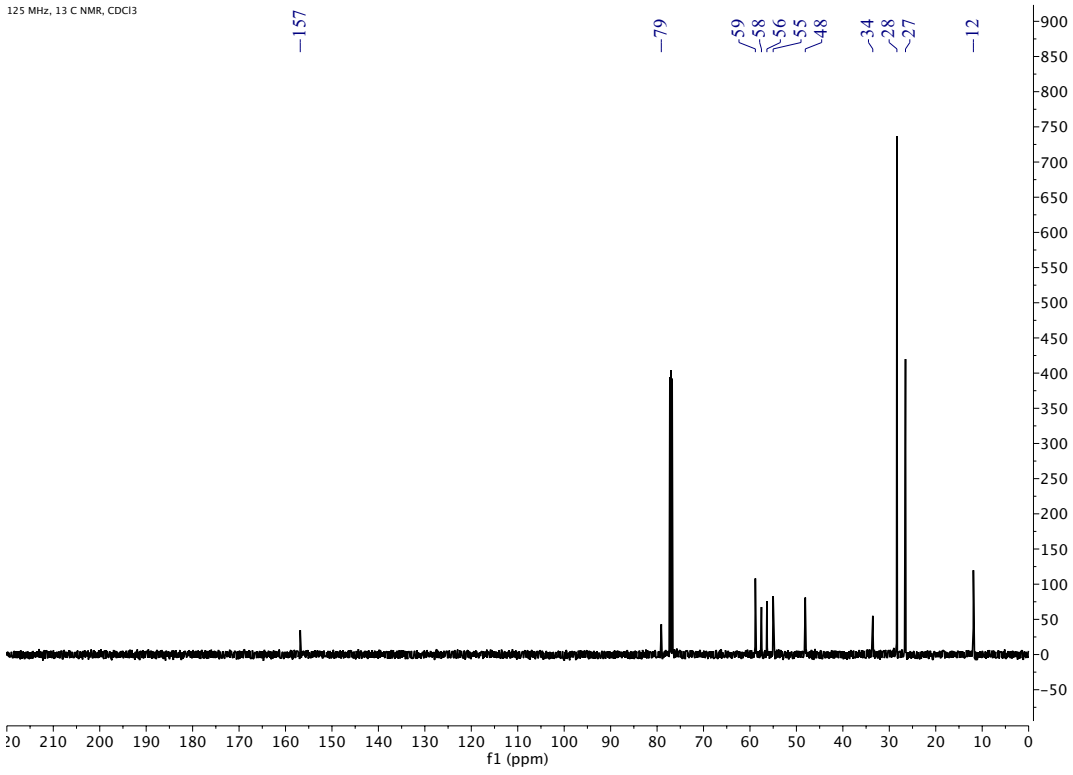

III.4.4.3. Compound 8

^{1}H NMR (400 MHz. $CDCl_3$)

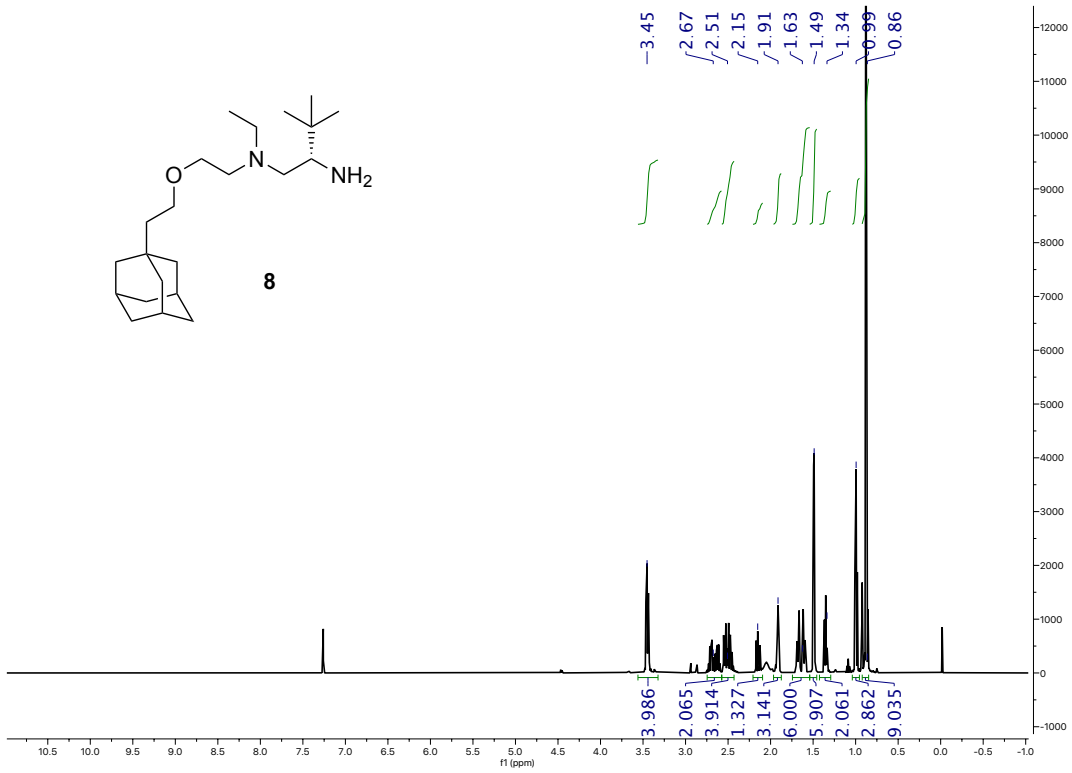

^{13}C NMR (100 MHz. $CDCl_3$)

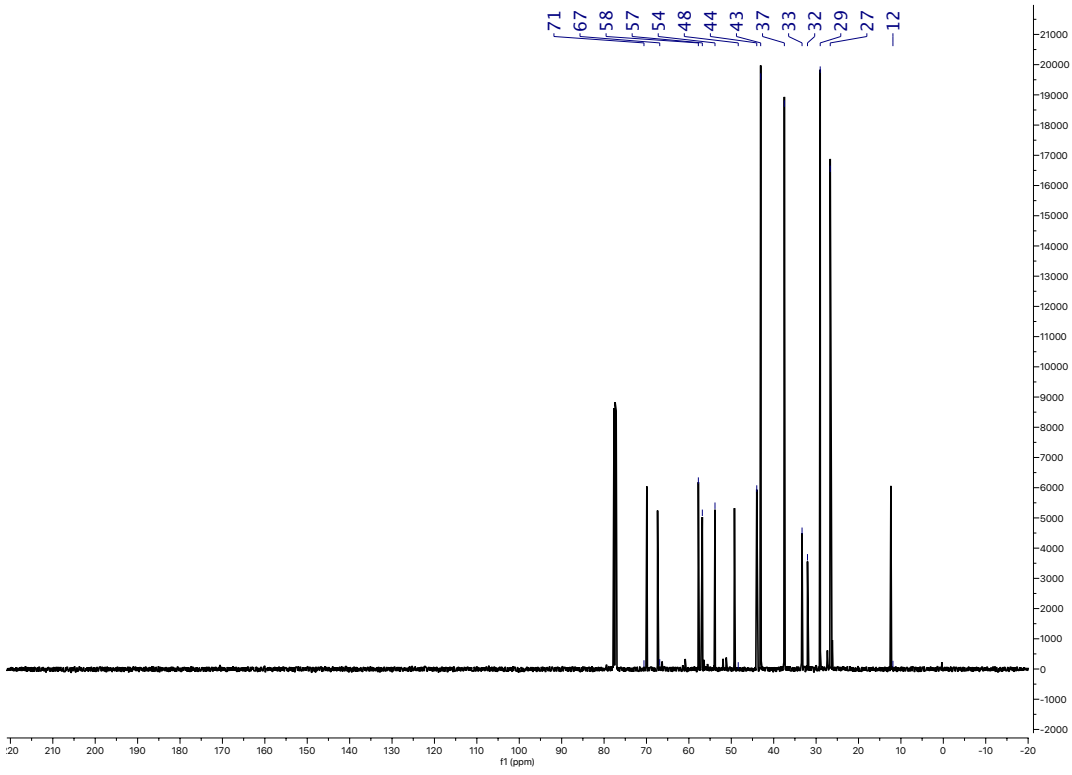

III.4.5. HPLC chromatograms

III.4.5.1. Compound 1

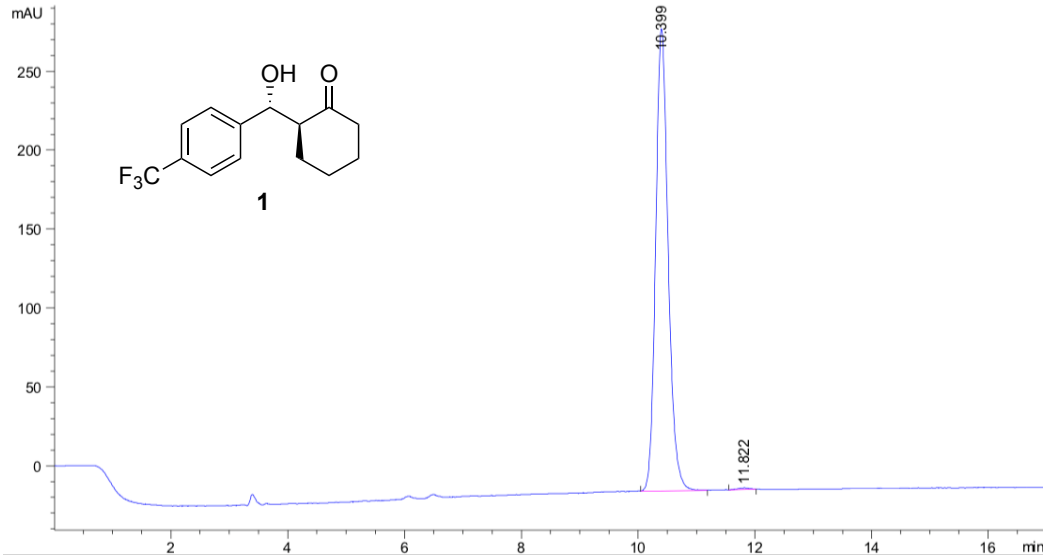

Peak #	Ret Time [min]	Type	Width [min]	Area [mAU*s]	Height [mAU]	Area %
1	10.399	BB	0.2270	4339.18262	292.58295	99.6575
2	11.822	BB	0.1809	14.91412	1.04278	0.3425
Totals :				4354.09673	293.62573	

III.4.5.2. Compound 10

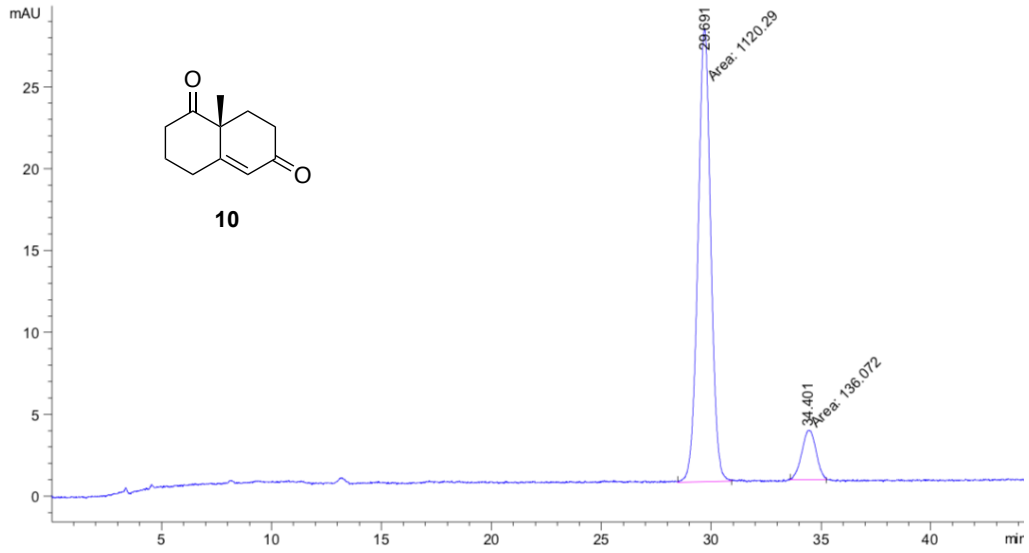

Peak #	Ret Time [min]	Type	Width [min]	Area [mAU*s]	Height [mAU]	Area %
1	29.691	MM	0.6751	1120.29211	27.65622	89.1694
2	34.401	MM	0.7518	136.07240	3.01659	10.8306
Totals :				1256.36452	30.67282	

III.4.6. References

[1] A) D. Font, S. Sayalero, A. Bastero, C. Jimeno, M. A. Pericàs, *Org. Lett.* **2010**, *12*, 2678. B) P. Llanes, S. Sayalero, C. Rodríguez-Escrich, M. A. Pericàs, *Green Chem.* **2016**, *18*, 3507.
[2] E. Del Castillo, M. D. Martínez, A. E. Bosnidou, T. Duhamel, C. Q. O'Broin, H. Zhang, E. C. Escudero-Adán, M. Martínez-Belmonte, K. Muñiz, *Chem. Eur. J.* **2018**, *24*, 17225–17229.
[3] S. Cañellas, C. Ayats, A. H. Henseler, M. A. Pericàs, *ACS Catal.* **2017**, *7*, 1383–1391.
[4] Y. Hayashi, S. Aratake, T. Itoh, T. Okano, T. Sumiya, M. Shoji, *Chem. Commun.* **2007**, 957.

4

CHAPTER IV

Testosterone extraction from complex mixtures

CHAPTER IV

Testosterone extraction from complex mixtures

IV.1. Introduction

Testosterone is a sex hormone that plays an essential role in the human body. Besides, the correct diagnosis of many endocrine disorders is directly related to the levels of testosterone in human serum and plasma. However, the assessment of the hormone in these samples requires several steps to prepare and isolate the testosterone, which may be present in low concentration, previous to the analyses. Therefore, we considered using our previously synthesized magnetic beads bearing an anchored cucurbituril moiety, **CB7**, for the isolation and enrichment of testosterone from complex samples through molecular recognition. To this end, we first needed to think of how to extract this neutral steroid. Does testosterone alone bind to **CB7**? If so, is the affinity high enough as to allow the selective binding of **CB7** to testosterone in the presence of other compounds? And what would happen with samples where the concentration of testosterone is very low? While testosterone alone may present some affinity for **CB7**, we thought that the best approach would be to label the testosterone with a molecule that displays high affinity for **CB7**. In this way, even with limited amounts of testosterone, the steroid would be selectively recognized over other, more abundant compounds. Thereby, an interesting way to label testosterone is through derivatization. Among the broad scope of derivatizing reagents, aminooxy reagents stand out for their excellent reactivity with carbonyl-containing reagents such as testosterone.

IV.1.1. Aminooxy reagents

The condensation of an aminooxy moiety (e.g., hydroxylamine) with an aldehyde or ketone is called oximation. It allows the formation of carbon–nitrogen double bonds between molecules bearing each functional group (Scheme IV-1). The reaction usually takes place spontaneously, at room temperature, in a range of solvents, and is atom economical, producing water as the main byproduct. For this reason, oximation, in addition to the previously mentioned CuAAC reaction,

can be considered a model click reaction. Besides, the oximation reaction allows a broad range of tethering reactions providing highly stable oxime products, and all this devoid of external catalyst.

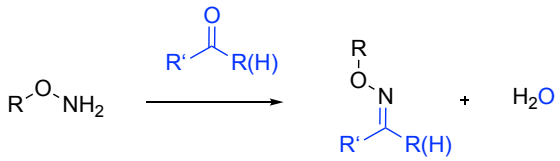

Scheme IV-1. The oximation reaction.

Oximes are a class of organic compounds that belong to the family of imines. Imines are a functional class arising from the condensation of amines with aldehydes or ketones. The reaction proceeds through hemiaminal intermediates which yield compounds with a carbon–nitrogen double bond by the elimination of water. When the precursor is an aldehyde, imines are termed aldimines. Ketones, in turn, give rise to ketimines. On the other hand, the nitrogen atom can be attached to hydrogen (H) or an organic group (R). The latest reagents belong to a subclass of imines referred to as Schiff bases. If the nitrogen group is attached to an OH group (like in the reaction of aldehydes or ketones with hydroxylamine $HO–NH_2$), the corresponding imine is called oxime, and when the nitrogen atom is attached to an NH_2 group (like in the reaction of carbonyl compounds with hydrazine $H_2N–NH_2$), the imine is classified as a hydrazone (Figure IV-1).

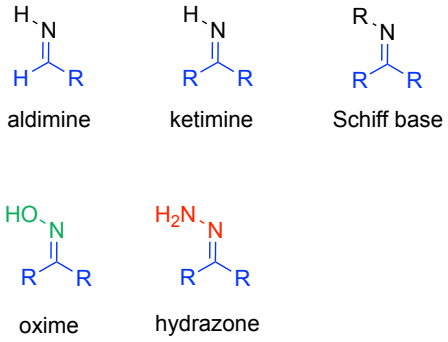

Figure IV-1. Different types of imines.

The products of oximation can be further categorized in different groups depending on the starting material of each reaction. For example, reaction with ketones will provide ketoximes and reaction with aldehydes will afford aldoximes. When the aminooxy moiety presents a substitution on the oxygen group, the reaction with aldehydes or ketones will deliver oxime ethers (Figure IV-2).

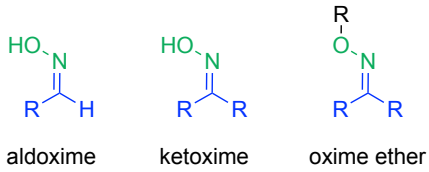

Figure IV-2. Classification of oximes.

One of the main advantages of oximes, when compared to analogous functional groups such as hydrazones and acyl hydrazones, is that they present much lower rates of hydrolysis (Scheme IV-2). The equilibrium constant that defines the ratio between the rate constants for the formation and hydrolysis of oximes is usually higher than 10^8 M^{-1} for oxime bonds at room temperature. Conversely, the equilibrium constant for hydrazones is in the range of 10^4–10^6 M^{-1}.[1]

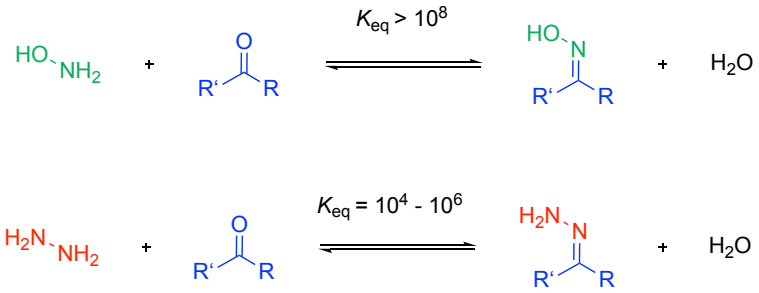

Scheme IV-2. Equilibrium constants for oxime and hydrazone derivatives.

Some studies compared the hydrolysis rate of an oxime ether, **I**, with that of a hydrazone analog, **II**, and its acylated version, **III**, and found that the hydrolysis rate for the oxime was roughly 600 and 300-fold lower, respectively (Figure IV-3). This vast difference was attributed to the fact that the oxygen contributes with a more significant electron donation effect to the pi system, inducing a stronger stabilization of the corresponding derivative.[2]

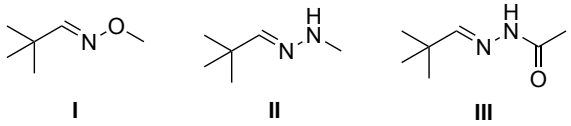

Figure IV-3. Molecules tested to determine their hydrolysis rates.

In other words, due to the inductive electron donation from the attached heteroatoms, the carbonyl carbon of oxime ethers is, generally, less electropositive than the corresponding one in other C=N derivatives and presents less polarized bonds (Figure IV-4). Considering that hydrolysis consists of the

[1] A. Dirksen, P. -E. Dawson, *Bioconjugate Chem.* **2008**, *19*, 2543−2548.
[2] J. Kalia, R. Raines. *Angew. Chem. Int. ed.* **2008,** *47* (39), 7523−7526.

nucleophilic attack of water to the carbonyl carbon, those compounds that exhibit less electrophilic carbonyl carbons will perform higher degrees of stability against hydrolysis.

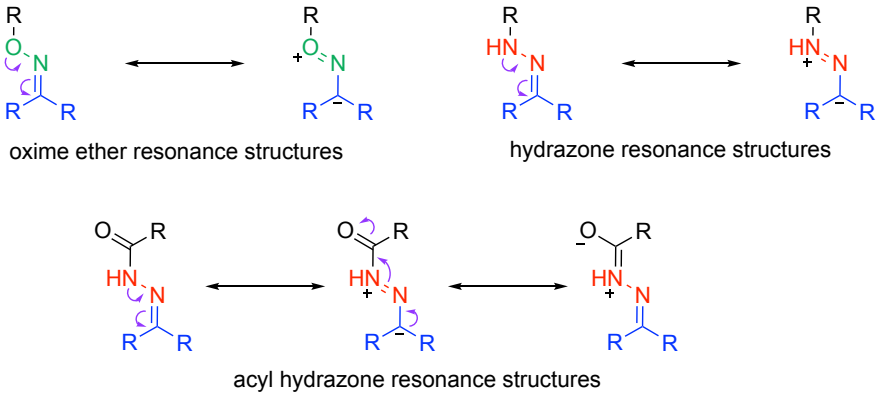

Figure IV-4. Resonance structures of oxime ethers and hydrazones. The resonance structures increase the electron density of the carbonyl carbon, reducing their electrophilicity and imparting greater hydrolytic stability.

The difference in reactivity is even more pronounced when compared to imines derived from primary amines (e.g., the imine linkage is reversible and easily hydrolyzed in water). A common explanation relates to the α-effect. The effect describes the peculiar high nucleophilic reactivity of compounds having one or more lone pair electrons adjacent (alpha) to the nucleophilic center.[3] While the pK_a of primary ammonium ions is around 10, for the conjugate acid of hydroxylamines and hydrazines is *ca.* 5 and 8, respectively. Hydrolysis of oximes and oxime ethers can be therefore triggered at low pH rates. Some studies showcase that the hydrolysis reaction below pH 2 remains pH-independent, but acid-catalyzed until pH 2.[4] Another common explanation to the more excellent stability of hydrazones and oximes, also related to the α-effect, is based on the relieve on the repulsion of the lone pairs in the conjugates (Figure IV-4).[5] Contrary to amines and hydrazines, aminooxy derivatives do not undergo oximation reaction with esters or anhydrides. Instead, the aminooxy moiety, due to the α-effect, remains a good nucleophile that reacts with electrophiles such as acyl chlorides, anhydrides, imides, and esters. During the reaction, the free electron pair on the nucleophile moves away from the nucleus towards the electrophile,

[3] (a) W. P. Jencks, J. Carriuolo, *J. Am. Chem. Soc.* **1960**, *82*, 1778–1786. (b) J. O. Edwards, R. G. Pearson, *J. Am. Chem. Soc.* **1962**, *84*, 16–24.
[4] R. A. More O'Ferrall, D. M. O'Brien, D. G. Murphy, *Can. J. Chem.* **2000**, *78*, 1594–1612.
[5] K. B. Wiberg, R. Glaser, *J. Am. Chem. Soc.* **1992**, *114*, 841–850.

causing a transition state with a partial positive charge that can be stabilized by the adjacent lone pair.

Finally, the aminooxy group reacts chemoselectively with aldehydes and ketones, but, in some cases, the reactivity is too slow, and it can be enhanced by the use of some catalysts (e.g., aniline and 1,3-diaminobenzene).[6]

IV.1.2. Derivatization reagents

The analysis of cellular aldehydes and ketones is of considerable importance in the field of metabolomics. However, the identification of aldehyde and ketone metabolites from aqueous cell extracts is challenging due to their low abundance, and the complexity of the corresponding matrices. To overcome these issues, the use of derivatization reagents for mass spectrometry analysis has been an ever-growing strategy over the last years, because derivatization reagents facilitate liquid chromatography with MS detection since they present quickly ionizable groups. Some of these reagents, even employ a permanent positive charge that enhances the MS sensitivity and enables direct MS analysis under milder and non-ionizing conditions. The most commonly used derivatization reagents include amines,[7] hydrazines,[8] hydrazides,[9,10,11] hydroxylamines, or aminooxy[12,13] moieties that form the corresponding derivatized products upon reaction with the carbonyl of the molecule of interest. Moreover, some reagents even include a quaternary ammonium moiety to enhance water solubility (Figure IV-5).

Quaternary ammonium salts allow the preparation of bifunctional species. The four nitrogen substituents provide a simple way to add functional groups, that can lead to further functionalization, and depending on the hydrophobicity of the attached moiety, can deliver amphiphilic compounds with solubility in aqueous

[6] (a) M. Thygensen, H. Munch, J. Sauer, E. Clo, M. R. Jorgensen, O. Hindsgaul, K. J. Jensen, K. *J. Org. Chem.* **2010**, *75*, 1752−1755. (b) P. Crisalli, E. T. Kool, *J. Org. Chem.* **2013**, *78*, 1184−1189, (c) M. Rashidian, M. M. Mahmoodi, R. Shah, J. K. Dozier, C. R. Wagner, M. D. Distefano, *Bioconjugate Chem.* **2013**, *24*, 333−342.
[7] M. Eggink, M. Wijtmans, A. Kretschmer, J. Kool, H. Lingeman, I. Esch, W. M. A. Niessen, H. Irth, *Anal Bioanal Chem* **2010,** *397*, 665−675.
[8] P. Maboudou, D. Mathieu, H. Bachelet, J. F. Wiart, M. Lhermitte, *Biomed. Chrom.* **2002,** *16*, 199−202.
[9] W. Griffiths, M. Hornshaw, G. Woffendin, S. Baker, A. Lockhart, S. Heidelberger, M. Gustafsson, J. Sjövall, Y. Wang, *Journal of Proteome Research* **2008**, *7* (8), 3602−3612.
[10] H. Hong, Y. Wang, *Anal. Chem.* **2007**, *79* (1), 322−326.
[11] D. Johnson, *Rapid communications in mass spectrometry: RCM* **2007**, *21* (18), 2926−2932.
[12] J. Iglesias, J. M. Gallardo, I. Medina, *Food Chemistry* **2010**, *123*, 771−778.
[13] N. Sugaya, K. Sakurai, T. Nakagawa, N. Onda, S. Onodera, M. Morita, M. Tezuka, *Anal. Sciences* **2004**, *20*, 865−870.

and organic solvents. Besides, the quaternary nitrogen provides the molecules with a permanent positive charge, a characteristic that has been exploited to maximize the signal intensity in MS analyses.

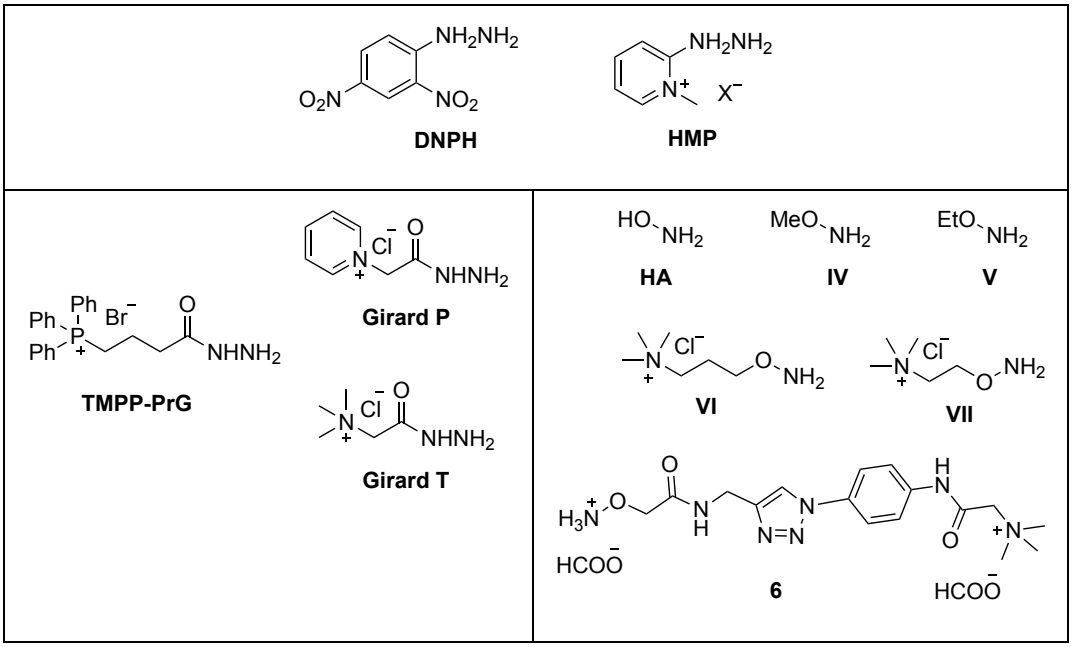

Figure IV-5. Representative reagents for the derivatization of carbonyl compounds.

The scope of derivatizing reagents goes far beyond the molecules presented here (hydrazines, oximes, and hydrazides). Derivatizing reagents to enhance the sensitivity of LC-MS based analyses deal with the introduction of ionizable moieties to the molecules that have to be tested on the assay. To this end, a broad set of compounds with any kind of functional group compatible with the targeted molecule can be considered as long as it leads to this ultimate purpose: to facilitate the analyses of the targeted molecule.[14]

IV.1.3. Testosterone analysis

Testosterone is the primary androgen in males (Figure IV-6). It is responsible for secondary sex characteristics and influences muscle mass, bone density, and pubertal development. Testosterone levels are usually measured on men to evaluate hypogonadism. In women, it is also a predominant androgenic hormone. The circulating concentrations are 5 to 10% of those in men. Testosterone levels are measured for the diagnosis of hyperandrogenism, hirsutism, virilization, acne,

[14] For a review on derivatizing reagents, see Y. Zhu, P. Deng, D. Zhong, *Bioanalysis*, **2015**, *7*, 2557–2581.

and infertility. In children, testosterone is measured for sex assignment in infants with ambiguous genitalia, or diagnosis of disorders of puberty.

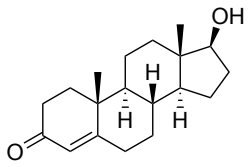

Testosterone

Figure IV-6. Molecular structure of testosterone.

Hence, the determination of steroids, and particularly, of testosterone plays an essential role in diagnosing endocrine disorders. Testosterone is ordinarily abundant and can be routinely measured.[15] However, the levels of endogenous steroid hormones in pediatric samples are often at or below available detection limits, reaching in some individuals concentration levels at the fM scale.[16,17] Therefore, the analysis of steroids in some biological samples requires the use of highly sensitive and specific methods. Over the years, researchers have thrived on developing new and better ways to perform these analyses. In the mid-1960, immunoassays (IA) were the primary technique before the introduction of mass spectrometry. However, due to high cost, tedious sample preparation, and low specificity, they were soon replaced by novel, more practical techniques.

Tandem mass spectrometry (LC-MS/MS) is currently one of the techniques of choice because it provides high analytical sensitivity and specificity. Moreover, it brings the possibility to measure multiple analytes at the same time and usually requires less sample preparation when compared to other methods like IA or GC-MS. The chromatographic separation takes place on reverse phase columns such as C8 or C18. UPLC systems coupled with mass spectrometers are generally very efficient to enhance the resolution, sensitivity, and speed of the analyses. The mass analyzer is usually a triple-quadrupole mass spectrometer that consists of three quadrupoles that allow several types of reports. For example, in the analysis in multiple reaction monitoring (MRM), the first

[15] M. M. Kushnir, A. L. Rockwood, W. L. Roberts, B. Yue, J. Bergquist, A. W. Meikle, *Clin. Biochem.* **2011**, 44, 77–88.
[16] W. Rosner, S. E. Hankinson, P. M. Sluss, H. W. Vesper, M. E. Wierman, *J. Clin. Endocrinol. Metab.* **2013**, 98, 1376–1387.
[17] T. Fiers, B. Casetta, B. Bernaert, E. Vandersypt, M. Debock, J. M. Kaufman, *J. Chromatogr. B Analyt. Technol. Biomed. Life Sci.* **2012**, 893–894, 57–62.

quadrupole is used to scan across a preset *m/z* range and select an ion of interest. The second quadrupole, or collision cell, fragments the molecule producing some specific ions. The third quadrupole serves to analyze the fragment ions generated in the collision cell. Then, the high sensitivity of this method relates to the mass analyzer, which is monitoring the same mass to charge ratios during the entire time of the data acquisition. The advantage of overseeing the molecular weight and the specific fragmentation translates in higher specificity. Despite all these advantages, one crucial drawback related to LC-MS/MS is the matrix effect, that consists of the co-elution of the product with the matrix components causing interferences in the analyses. For this reason, sample preparation and high-efficiency chromatographic separations are required. Standard biological samples used for the study of steroids include serum, plasma, urine, and saliva. The sample size ranges from a few microliters to 1 ml. The sample preparation for steroid analysis with LC-MS/MS involves extraction, clean-up, and concentration steps. While some typically used extraction techniques include solid-phase extraction (SPE), liquid/liquid extraction (LLE), protein precipitation, and dilution. The advantages of SPE and LLE are in reduced complexity of the samples, lessened sample matrix effects, and higher sensitivity. LLE consists of the partitioning of analytes between aqueous and organic phases. On the other hand, SPE is a robust technique to extract steroids from biological matrices by polymeric or silica-based adsorbents.

Electrospray ionization (ESI) is a process that transfers ions from solution into a gas phase through ion desorption from the droplets, and it is more efficient for polar analytes. When considering ESI-MS/MS for steroid analyses, another drawback arises due to the nature of the chemicals involved. Steroids are generally neutral and poorly ionizable molecules. Therefore, chemical derivatization is commonly used to overcome the suppression of ionization in the ESI source leading to a notorious improvement in the sensitivity. In summary, derivatization modifies the physical and chemical properties of the molecules to enhance the ionization, fragmentation, and chromatographic retention significantly.[15] New and improved derivatization reagents have been reported in a concatenated way for the analyses of steroids via LC-MS/MS with both ESI or atmospheric pressure chemical ionization (APCI). Some of the most common

reagents include hydroxylamine **HA**, methoxylamine, **IV**, or ethoxylamine, **V,** to form oxime derivatives,[18,19,20,21] or more complex hydrazine and hydrazide-based reagents such as **HMP**, **Girard P**, or **Girard T**, to form hydrazones (Figure IV-5).[22,23,24,25] To date, one of the best derivatizing reagents is a quaternary ammonium aminooxy reagent, **VI**.[26] Star-Weinstock reported this last reagent that enabled reliable quantification of low testosterone levels with concentrations above 0.5 pg/ml (1.7 pM). The signal enhancement factor was around 80-fold upon derivatization in the LC-ESI-MS/MS. The reagent contains only the essential reactive aminooxy group, to generate the corresponding derivative with testosterone, which is linked through a short alkyl (propyl) chain to a trimethyl ammonium ion that serves as an MS response enhancing group. The method chosen for the analysis of the corresponding derivatives was single reaction monitoring (SRM). The fragment ions selected (after the loss of neutral trimethylamine) comprised part of testosterone and part of the derivatizing reagent. This reagent performed better than hydroxylamine on previous studies due to the permanent positive charge of the reagent. Moreover, the sample preparation was straightforward, considering that protein precipitation, liquid/liquid extraction, and solid-phase extraction failed to shrink the matrix effect resulting from hydroxylamine derivatization.[18,27]

The use of aminooxy derivatizing reagents to enhance the analyses of the molecule of interest is not limited to steroids since they can react with a wide range of ketones and aldehydes. The group of Fu has demonstrated this.[28] They used reagent **VII** to analyze, in ambient air, the levels of air pollutants and carcinogenic aldehydes such as formaldehyde, acetaldehyde, and acrolein. They fabricated a microreactor coated with the quaternary ammonium aminooxy

[18] M. M. Kushnir, A. Rockwood, W. L Roberts, E. G Pattison, A. Bunker, R. L Fitzgerald, A. Meikle, *Clin. Chem.* **2006**, *52*, 120.
[19] D. Borrey, E. Moerman, A. Cockx, V. Engelrelst, M. Langlois, *Clin. Chim. Acta.* **2007**, *382,* 134.
[20] H. N. Bui, E. Struys, F. Martens, W. de Ronde, L. Thienpont, P. Kenemans, M. O Verhoeven, C. Jakobs, H. M Dijstelbloem, M. Blankenstein, *Ann. Clin. Biochem.* **2010**, *47,* 248.
[21] M. Niwa, N. Watanabe, H. Ochiai, K. Yamashita, *J. Chromatogr.* **2005**, *824,* 258.
[22] T. Higashi, A. Yamauchi, K. Shimada, *J. Chromatogr.* **2005**, *825,* 214.
[23] W. Griffiths, Y. Wang, K. Karu, E. Samuel, S. McDonnell, M. Hornshaw, C. Shackleton, *Clin. Chem.* **2008**, *54,* 81317.
[24] J. Kirk, J. Tarbin, B. J Keely, *Rapid Commun. Mass Spectrom.* **2006**, *20,* 1247.
[25] D. W Johnson, *Rapid Commun. Mass Spectrom* **2005**, *19, 193.*
[26] M. Star-Weinstock, B. L. Williamson, S. Dey, S. Pillai, S. Purkayastha, *Anal. Chem.* **2012**, *84*, 9310.
[27] M. M. Kushnir, T. Blamires, A. L. Rockwood, W. L. Roberts, B. Yue, E. Erdogan, A. M. Bunker, A. W. Meikle, *Clin. Chem.* **2010**, *56*, 1138.
[28] M. Li, Q. Li, M. H. Nantz, X.-A. Fu, *ACS Omega* **2018**, *3*, 6764–6769.

reagent for chemoselective capture of the carbonyl compounds. Then, by elution of the products from the microreactor and direct analyses, they could detect over 20 carbonyl compounds in ambient air urban samples. The group of Carell showed another example.[29] They contrived and prepared a tailor-made quaternary ammonium aminooxy reagent, **6**, for the quantification of abasic and ß-elimination sites formed during the base excision repair of 5-formyl- and 5-carboxy-cytosine in stem cells by the monofunctional thymine DNA glycosylase. Stem cells have substantial amounts of fdC and cadC, which are removed by the glycosylase Tdg to deliver potentially harmful AP- and ß-site intermediates. These intermediates feature an aldehyde carbonyl group that was derivatized for quantification with high sensitivity on the LC-MS/MS. The reagent, **6**, was devised to additionally contain a triazole heterocycle that gives a loss of nitrogen in the triple quadrupole MS, via collision-induced dissociation, that facilitates the specific mass transition.

Till now, derivatizing reagents has been limited to the preparation of particular type of molecules that enhance MS analyses. Due to the general need of finding better and more suitable derivatizing reagents as well as optimizing sample preparation and separation techniques, we wondered, whether common derivatizing reagents bearing a **CB7** guest molecule would maintain the enhancing properties derivatizing reagents have, while adding separation features through molecular recognition by cucurbiturils, and outperform current preparation techniques such as SPE and LLE when it comes to eliminating the sample matrix. The advent of this cutting-edge generation of quaternary ammonium aminooxy reagents could be established along with their design, and synthesis. However, to select the best model leading to higher selectivity towards the guest, the determination of association constants with **CB7** is a key step.

IV.1.4. CB7–guest association constants

The reasons behind the ability of CBs to form strong host–guest complexes have been discussed during the general introduction. Further explanations will be disclosed in this chapter to gain deeper insights concerning the methods and

[29] R. Rahimoff, O. Kosmatchev, A. Kirchner, T. Pfaffeneder, F. Spada, V. Brantl, M. Müller, T. Carell, *J. Am. Chem. Soc.* **2017**, *139*, 10359–10364.

techniques engineered by researchers along the path to unleashing these, until very recently, hidden properties.

Considering that guests generally experience changes in their UV/vis or fluorescence spectra upon binding and that they exhibit slow kinetics of exchange between the bound and free guest on the NMR chemical shift time scale (Figure IV-7), several research groups have exploited these features to quantify the association rates through NMR experiments, UV/vis titrations, and other.

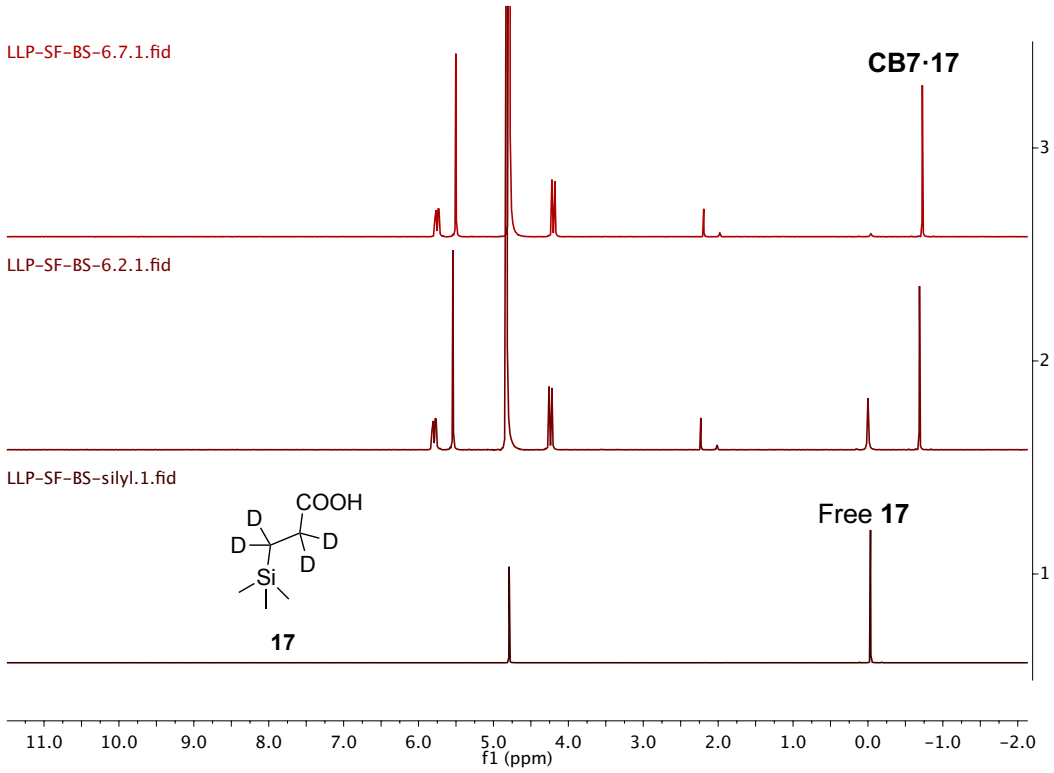

Figure IV-7. NMR spectra of (top) **CB7** and 1 eq of **17**, (middle) **CB7** and 2 eq of **17**, and (bottom) **17**.

^{1}H NMR experiments

Determining binding constant values of suitable guests by direct NMR measurements is generally not possible for the cucurbiturils involving seven or more glycoluril units. One reason is that they display fast kinetics of exchange on the NMR chemical shift time scale and, hence, free and bound species cannot be distinguished even when an excess of the guest is present (e.g., the mixture of **CB7** with two eq of dimethyl sulfone in a buffer solution. Figure IV-8). Another reason arises from the fact that many of the guests bind to **CB7** with constant values over 10^4 M^{-1}, exceeding the experimental range accessible for NMR. This

is seen in Figure IV-7, where the top NMR spectrum shows how almost stoichiometric amounts of guest **17** appears to be exclusively inside the cavity of **CB7**. To overcome these hurdles, Mock came up with an indirect method based on ^{1}H NMR spectroscopy to successfully determine binding affinities of strong guests for **CB6**.[30] This study showcases how the relative binding affinities of alkylammonium ions binding for **CB6** could be determined by the displacement of one guest by another, providing that the second guest was present in a more substantial excess or it presented a stronger binding with the **CB6** unit. They concluded that the guest exchange mechanism took place through an initial guest dissociation from the cavity, or displacement by the solvent in a slow step, followed by competition between both guests for the free cage.

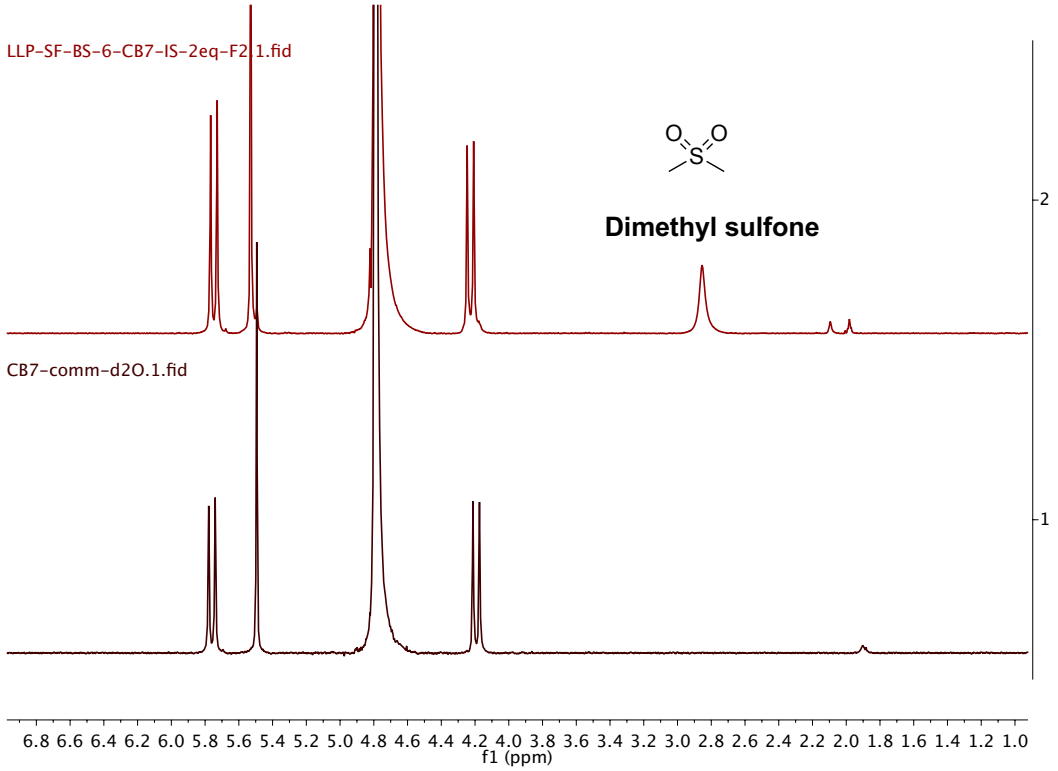

Figure IV-8. ^{1}H NMR spectra of **CB7** (bottom), and a mixture of **CB7** and 2 eq of dimethyl sulfone (top). In this case, dimethyl sulfone displays fast kinetics of exchange in the NMR time scale, making it impossible to differentiate between bound and unbound guest.

Later, Isaacs extended this procedure to disclose the use of binding guests with an excess of less active binding guests to compete for limiting amounts of

[30] Mock, W. L.; N. Y. Shih, *J. Org. Chem.* **1986**, *51*, 4440–4446.

CB7.[31,32] To successfully apply this method and dwindle associated errors, it is necessary to adjust the concentrations of the guests to reach a one to one complexation ratio with **CB7**. Using a reference guest of known affinity, with another guest of unknown affinity, allows determining the relative and absolute binding constant of the guest molecule upon the integration of the resonances for the selected free and bound guest. This methodology is the one we chose for our experiments, and it will be further discussed throughout the chapter.

UV/vis titrations

The formation of an inclusion complex is reflected by a change in the electronic absorption spectrum of some guest species. Therefore, this perturbation experienced in the UV spectrum has been exploited to determine absolute values of dissociation constants (K_d). For example, the addition of *p*-toluidine, **VIII**, to a solution of an excess of **CB6** allowed to determine the net rate of inclusion (K_{obsd}, given as a first-order rate constant; Figure IV-9) by measuring the absorbance as a function of time during the formation of the inclusion complex with **CB6**. Then, after reaching the equilibrium, K_d of *p*-toluidine was determined by the addition of a much stronger guest, 1,6-hexanediamine. The concentration of this displacing agent is independent of the mechanism of substitution. Therefore, the displacement of *p*-toluidine from the cavity (K_{-1}) was directly measured by the exponential decrease in the absorbance of the complex **CB6**·**VIII**. By difference, the actual values of K_1 and K_d were obtained.[30]

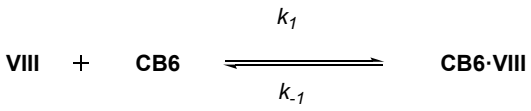

$$K_{obsd} = [CB6]K_1 + K_{-1}$$

$$K_1 = (K_{-1} - K_{obsd}) / [CB6]$$

$$K_d = K_{-1} / K_1$$

Figure IV-9. Equations used to determine the dissociation constant of **VIII** from **CB6**.

Similarly, the binding constant of 1,3-diaminobenzene, **IX**, was determined by UV/vis titration (Figure IV-10). In this case, the UV/vis spectra were recorded

[31] L. Cao, M. Šekutor, P. Y. Zavalij, K. Mlinarić-Majerski, R. Glaser, L. Isaacs, *Angew. Chem. Int. Ed.* **2014**, *53*, 988–993.
[32] S. Liu, C. Ruspic, P. Mukhopadhyay, S. Chakrabarti, P. Y. Zavalij, L. Isaacs, *J. Am. Chem. Soc.* **2005**, *127*, 15959–15967.

during the addition of **CB7** to a solution of **IX**. Then, the absorbance at the chosen wavelength was plotted as a function of the concentration of **CB7**, and best least-squares fit of the data allowed to determine the association constant (K_a) of **IX**.[32,33]

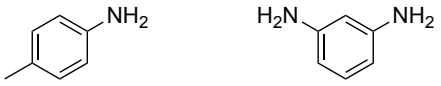

VIII **IX**

K_d = 3.07 x 10^{-3} M K_a = 8.07 x 10^4 M^{-1}

Figure IV-10. Dissociation constant calculated for *p*-toluidine, **VIII**, with **CB6**, and association constant calculated for 1,3-diaminobenzene, **IX**, with **CB7**. Both measured by the UV/vis titration strategy.

Fluorescence titrations

Fluorescent titrations can elucidate the binding affinity of some fluorescent guests that exhibit a shift of the emission wavelength upon complexation. For example, proflavine, **X**, experiences an increase in fluorescence emission as well as a variation from 509 nm to 485 nm upon encapsulation in the cavity of **CB7**. The macrocycle was portionwise added to a proflavine solution, till reaching a 2:1 ratio of **CB7**:**X**. The binding constant was then determined from the fluorescence spectra by using a least-square fitting method.[34] In brief, the intensity of emission measured from the fluorescence spectra as a function of increasing concentration of **CB7** (Figure IV-11, left) was used to plot the fluorescence intensity, at the selected wavelength, as a function of **CB7** total concentration (Figure IV-11, right), giving a binding curve represented by the best least-squares fit that was used to calculate the association constant of proflavine (K_a = 2.0 x 10^7 M^{-1}, Figure IV-11).

[33] For other examples see: (a) W. Ong, A. E. Kaifer, *Organometallics* **2003**, *22*, 4181–4183. (b) D. Ma, P. Y. Zavalij, L. Isaacs, *J. Org. Chem.* **2010**, 75, 4786–4795.
[34] S. Kemp, N. J. Wheate, F. H. Stootman, J. R. Aldrich-Wright, *Supramol. Chem.* **2007**, *19*, 475–484.

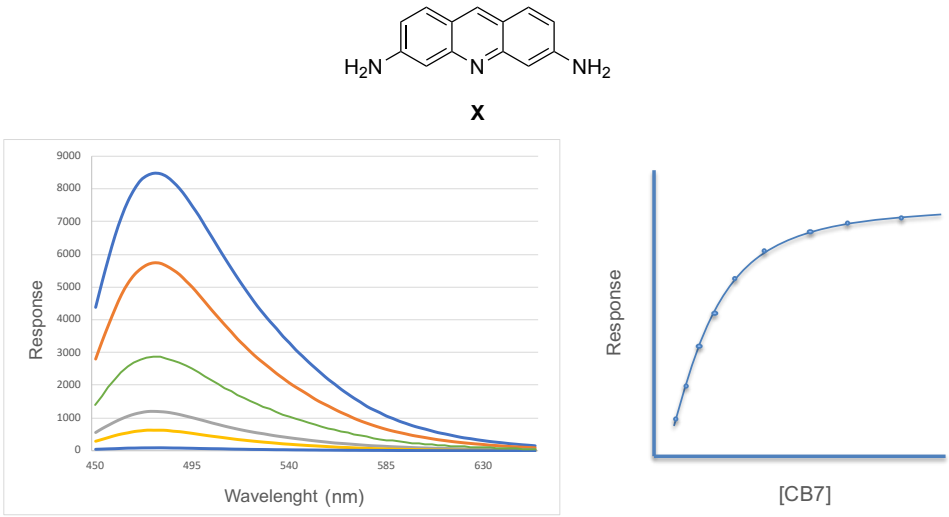

Figure IV-11. Representative fluorescence spectra of proflavine as a function of increasing **CB7** concentration (left). Representative plot of fluorescence intensity at the selected wavelength (λ_{max}) as a function of **CB7** total concentration.

Isothermal titration calorimetry (ITC)

Microcalorimetric titration experiments have also been performed to determine the binding constants of some guests with CBs. The measurement proceeds by sequentially adding defined and fixed amounts of guest to a solution of **CB7** in a calorimetric reaction cell, so the heat evolved can be recorded, and the complexation enthalpies for the inclusion of the guests with **CB7** can be determined. This strategy is generally advantageous, and it has been employed to determine very large binding constants at the range of 10^{15} M^{-1}. Because of the significant association constant of some guests, multistep competition ITC experiments are required.[35,36]

IV.2. Objectives

We aimed to prepare derivatizing reagents to enhance testosterone analyses by LC-MS/MS. We also wanted to add some features to those intrinsic to the derivatizing molecules to ease the preparation of the samples by selective extraction of the derivatized analytes with magnetic beads through high affinity with CBs.

[35] M. V Rekharsky, T. Mori, C. Yang, Y. H. Ko, N. Selvapalam, H. Kim, D. Sobransingh, A. E. Kaifer, S. Liu, L. Isaacs, et al., *Proc. Natl. Acad. Sci.* **2007**, *104*, 20737–20742.
[36] For other examples see: (a) W. S. Jeon, K. Moon, S. H. Park, H. Chun, Y. H. Ko, J. Y. Lee, E. S. Lee, S. Samal, N. Selvapalam, M. V Rekharsky, et al., *J. Am. Chem. Soc.* **2005**, *127*, 12984–12989. (b) S. Moghaddam, C. Yang, M. Rekharsky, Y. H. Ko, K. Kim, Y. Inoue, M. K. Gilson, *J. Am. Chem. Soc.* **2011**, *133*, 3570–3581.

The reagents were conceived to bear a permanent positive charge and an aminooxy moiety for fast conversion of carbonyl-containing molecules such as testosterone, into stable, water-soluble and permanently charged derivatives. Besides, the introduction of a motif with a supposedly excellent affinity with **CB7** has been targeted.

Finally, another subject of study was to determine the capability of the magnetic beads to selectively extract, transport, and deliver testosterone from complex mixtures.

IV.3. Discussion of results

IV.3.1. Prelude

The project started with the preparation of already reported reagents to determine and analyze their eligibility to perform suitable association constants with CBs. To this end, we selected reagent **6** as a starting point (Scheme IV-3).

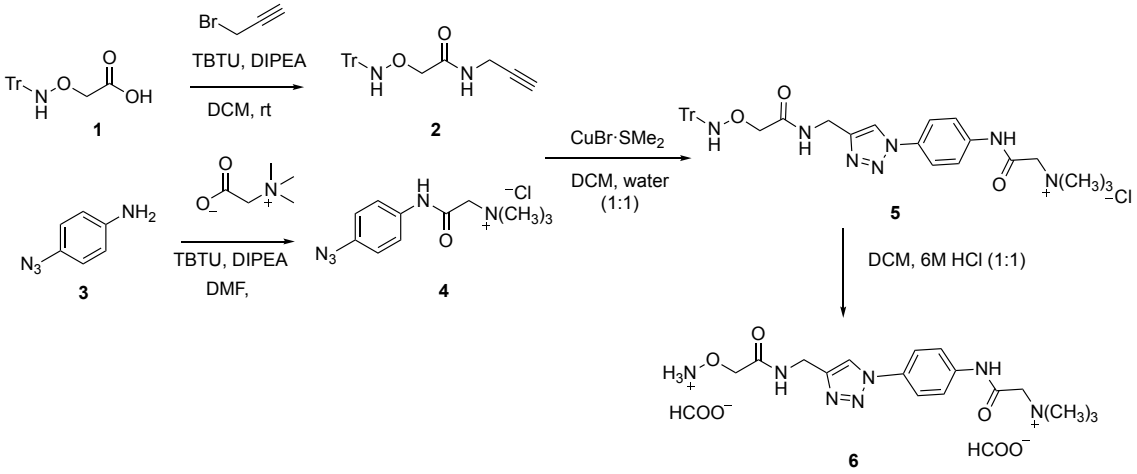

Scheme IV-3. Synthesis of reagent **6**.

The synthesis of this reagent has already been reported.[29] We followed previous procedures starting with the commercial *p*-azidoaniline, **3**, which delivered the corresponding azidoamide upon reaction with the corresponding betaine, trimethylaminoglycine. CuAAC reaction between azidoamide, **4**, and the alkyne, **2**, provided the desired Tr-protected reagent **5**. Deprotection under acidic conditions delivered the desired reagent, **6**. The reagent was further purified by preparative HPLC. To test the suitability of this reagent, **6**, for the extraction of testosterone derivatives through molecular recognition with the magnetic

nanobeads, whose preparation has been described in chapter II, we aimed to identify the affinity of this molecule for **CB7**.

At the outset, we appraised that the selected molecule, reagent **6**, would not display much affinity to **CB7**, or at least, not as high as it could be expected for some other molecules. Nevertheless, we attempted to predict, the association of our reagent by searching in the literature alike molecular structures with a similar set of moieties (e.g., the presence of an aryl ring or a trimethyl ammonium cation). Then, upon measurement of the corresponding binding constant, we could compare it with those reported in the literature and decide whether a pattern could be followed to draw a trail that would lead us to our overarching goal: to prepare related reagents with the necessary molecular structures to reach ultra-high binding affinities.

To gather detailed data of the affinity of our reagent for **CB7**, we searched in the literature data on the association constant of similar molecules, **XI** and **XII**. Highlighting the moieties that would provide the most robust binding sites, we concluded that reagent **6** would very likely display dissociation constants at the range of 10^{-5} M (Figure IV-12).[37] Then, we set up to study the affinity constant through NMR competition studies. As we previously mentioned in the Introduction, the determination of the affinity constant is highly dependent on the conditions, being the solvent an essential factor. To be able to compare our results with those reported in the literature, we decided to follow a procedure established by Isaacs.[32]

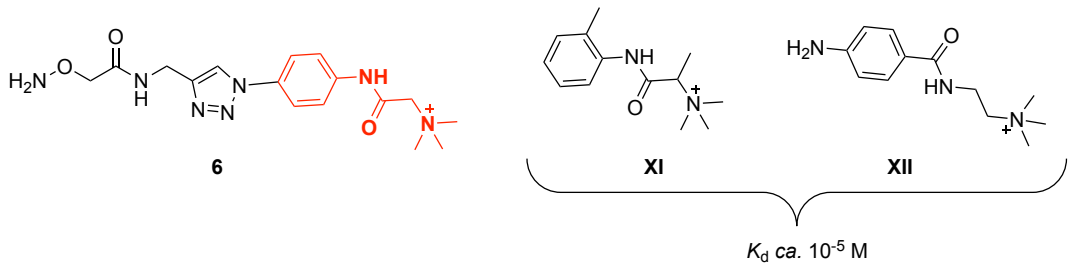

Figure IV-12. Dissociation constant values of some molecules akin to reagent **6**.

The use of water as a solvent is generally more popular because of the avoidance of preparing buffer solutions, especially for **CB7**, while **CB6** and **CB8** require the use of these buffers due to low solubility. A shared buffer used to determine the

[37] I. W. Wyman, D. H. Macartney, *Org. Biomol. Chem.* **2010**, *8*, 247–252.

binding affinities of the CBn homologs is a 50 mM deuterated sodium acetate solution at pH 4.74. The buffer generally diminishes the binding affinity by two orders of magnitude when compared to pure non-buffered water. The reduction in the association constant in buffered solutions is consistent with the known ability of sodium ions, Na^+, to bind at the C=O portals of CBs.[38] Despite this, we decided to investigate the ability of reagent **6** to form a host–guest complex with **CB7** in the aforementioned buffer because the affinity of a broad scope of molecules has been measured under these stablished conditions. By doing so, we would not only be able to compare the measured association constant with all those set of compounds already reported, but it would allow us to use these precedents as reference guests and save us a wealth of time by selecting as a reference, a guest with presumably similar binding constants.

Among the large variety of **CB7** guests that we could use as a reference, trimethylsilylpropanoic acid (TMSP), **17** stands out because it exhibits slow exchange kinetics on the chemical shift time scale, and it resonates in uncluttered regions of the spectrum (Figure IV-7), which helps to minimize errors associated with spectral integration. In addition, **17** exhibits an association constant with **CB7** of 10^7 M^{-1}, which is compatible with our selected guest, **6**. We set up the NMR competition experiments involving **CB7**, a significant excess of **6**, and the competitor **17** of known $K_{a,17}$ = 1.82 x10^7 M^{-1} (Figure IV-13).

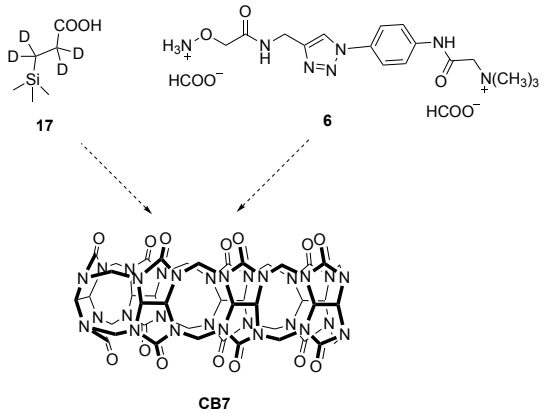

Figure IV-13. Reagents **4** and **17** competing for the cavity of **CB7**.

It is worth mentioning the procedure followed for the preparation of the samples used in the competition experiments. First, a 50 mM sodium acetate solution in D_2O acidified with deuterated acetic acid at pH 4.75 was prepared. Then,

[38] C. Marquez, R. R. Hudgins, W. M. Nau, *J. Am. Chem. Soc.* **2004**, *126*, 5808 – 5816.

considering the presence of water and salts inside the cavity of **CB7**, we decided to correct the concentration of **CB7** by NMR with dimethyl sulfone, which is generally employed as an internal standard for quantitative NMR studies. We used three independently prepared solutions of dimethyl sulfone, and selected the mean value as the correct concentration. 10–20% of the **CB7** sample was due to the filling in the cavity (water, salts, or solvents), which is in agreement with the purity of the commercial **CB7**. Also, the concentration of the reagents of the study (the competing guests) was checked upon dimethyl sulfone. So, knowing the concentration of all the stock solutions, we further tested them out with each other by preparing stoichiometric mixtures of the guests (Table IV-1, entry 2) and 1:1 or 1:2 mixtures of **CB7** and each guest, respectively (Table IV-1, entries 1, 3, and 4).

Table IV-1. NMR studies to determine K_a of **6**.[a]

Entry	[**CB7**] (mM)	[**6**] (mM)	[**17**] (mM)	Ratio **CB7**·**6** (%)	K_{rel}	K_a (10^5 M)
1	1	-	2	-	-	-
2	-	1	1	-	-	-
3	1	2	-	-	-	-
4	1	1	-	-	-	-
5	0.5	3	0.6	18	68.48	2.63
6	0.25	4	0.3	25	108.83	1.65
7	0.09	4.5	0.11	51	58.79	3.06
8	**0.29**	**18.95**	**0.49**	**35**	**119.53**	**1.51**
9	**0.29**	**22.21**	**0.49**	**38**	**120.85**	**1.49**
10	**0.29**	**32.90**	**0.49**	**48**	**105.32**	**1.71**

[a]Conditions: a mixture of **CB7**, **6**, and **17**, at the indicated concentration, was stirred until reaching equilibrium in a 50 mM sodium acetate buffer at pH = 4.75. Then, the solution mixture was submitted for ^{1}H NMR spectroscopy.

From the outset, we wanted to prepare solutions where more substantial amounts of guests would compete for a limiting amount of **CB7**. To this end, and considering **17** a stronger binding guest, we started our experiments by mixing **CB7** with a small excess of **17**, and larger amounts of **6**, up to 41 eq referred to

17 (Table IV-1, entries 5, 6, and 7). We have already discussed the importance of preparing solutions yielding, upon equilibrium, mixtures with close to 50% of the **CB7** bound to each guest. Therefore, these first experiments were only useful to assess the proper concentrations to be used (Table IV-1, entries 5 and 6), and despite we obtained a mixture approaching our requirements (Table IV-1, entry 7) we decided to discard all these results because combinations of **CB7**·**6**:**CB7**·**17** in such unbalanced ratios (<1:4 in entries 5 and 6) would increase the associated error. In fact, almost equimolar mixtures of **CB7** (0.09 M) and **17** (0.11 M) may also contribute to propagating the error even when the final ratios of complexation are closely 1:1 (entry 7). Finally, different stock solutions were used to prepare three mixtures that, after equilibrium, delivered **CB7**·**6** in useful 35–48% with respect **CB7**·**17** (Table IV-1, entries 8, 9, and 10). With these three solution mixtures, the relative constant was subsequently determined and, knowing the affinity constant of the reference guest, followed by some calculations of the propagated error, the affinity constant of our first synthesized quaternary ammonium aminooxy guest was obtained.

The determination of the relative constants can be performed from the equilibrium composition of the solution mixtures, through the integration of the corresponding peaks on the NMR spectrum. For example, when a given guest, **B**, that displays slow kinetics of exchange and different chemical shift upon complexation, is being used, the chemical shifts on the NMR spectrum allow to identify the ratio of free **B** and bound **CB7**·**B**. Then, knowing the initial concentrations of the reagents **CB7**, **A**, and **B**, we can determine the concentration of all the species in equilibrium and measure the relative constant, K_{rel} (Figure IV-14).

[CB7] = X mM

[A] = X' mM

[B] = X'' mM

[CB7] = [CB7·A] [CB7·B]

[A] = [CB7·A] [A]$_{free}$

[B] = [CB7·B] [B]$_{free}$

$$K_{rel} = \frac{[\,CB7{\cdot}B\,]\,[\,A\,]}{[\,CB7{\cdot}A\,]\,[\,B\,]}$$

$$K_{rel} = \frac{K_{a,B}}{K_{a,A}}$$

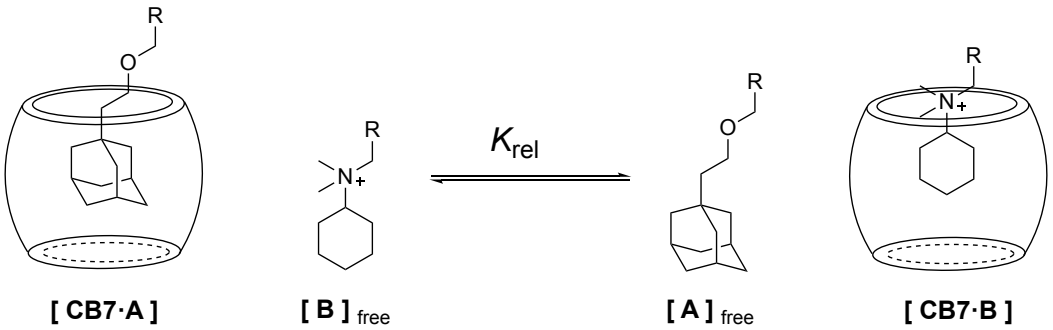

[CB7·A] **[B]** free **[A]** free **[CB7·B]**

Figure IV-14. Equations to determine the relative constant of two guests with **CB7**.

The common procedure involved the preparation of a solution with **CB7** (290 μM), **17** (490 μM) and **6** (32.90 mM). Once the equilibrium was reached, we determined the relative concentrations of **17** and **CB7·17** by the integration of the appropriate resonances in the ^{1}H NMR spectrum (**17**: -0.17 ppm; **CB7·17**: -0.93 ppm). Using the relative concentrations and the mass balance expression (equation 2) allowed us to calculate [**17**]$_{free}$ = 339 μM and [**CB7·17**] = 151 μM. Equation 3 was then used to calculate [**CB7·6**] (139 μM) using the known value of **CB7·17**. Finally, equation 4 was used to calculate [**6**]$_{free}$ (32.76 mM) using the known value of [**CB7·6**].

K_{rel} = ([CB7·17][6]$_{free}$) / ([CB7·6][17]$_{free}$) (**1**)

[17]$_{Total}$ = 490 μM = [17]$_{free}$ + [CB7·17] (**2**)

[CB7]$_{Total}$ = 290 μM = [CB7·17] + [CB7·6] (**3**)

[6]$_{Total}$ = 32.90 mM = [6]$_{free}$ + [CB7·6] (**4**)

$K_{GA} = (K_{GB})/(K_{rel})$ (**5**)

$$\left(\frac{\sigma K_{\mathbf{CB7{\cdot}GA}}}{K_{\mathbf{CB7{\cdot}GA}}}\right)^2 = \left(\frac{\sigma K_{\mathbf{CB7{\cdot}GB}}}{K_{\mathbf{CB7{\cdot}GB}}}\right)^2 + \left(\frac{\sigma K_{\mathbf{rel}}}{K_{\mathbf{rel}}}\right)^2 \quad (\mathbf{6})$$

Substitution of the values of [**CB7·17**], [**17**]$_{free}$, [**CB7·6**], and [**6**]$_{free}$ into equation 1 gave K_{rel} = 105.32. These determinations were done in triplicate from independently prepared stock solutions, and the average values were used in the calculations of K_a and the error analysis (equations 5 and 6). The percent error in K_a was measured as a function of the uncertainty in K_{rel}. The average K_{rel} = 115.2, with a standard deviation of 8.6 delivered an acceptable error of 7.5%

(which was standardized as a more conservative 10% error). The propagated uncertainty reported for $K_{[CB7•17]}$ (12.46%) was taken from a previously reported procedure and allowed us to determine a global error of 16%, and hence, the association constant using equations 5 and 6.

$$K_{a,6} = 1.56 \pm 0.25 \times 10^5\ M^{-1}$$

The error analysis takes into account the propagation of errors from different experiments involved in the whole process. To measure the affinity constant of **6** we made NMR competition experiments with the reference guest **17**, whose affinity was also measured by competition experiments with 1,3-diaminobenzene (**IX**), whose affinity, in turn, was measured by UV/vis titration experiments. Therefore, the error of the affinity constant of **IX** related to the standard error of the least-squares fit. Then, the concatenated uncertainty associated with the affinity constants of the guests, whose K_a was measured through NMR competition experiments, was determined using equation 6. Even though the errors associated with K_{rel} were below 10%, we used this more conservative value for our calculations. Substituting the known $\sigma(K_{CB[7]•17})/ K_{CB[7]•17}$ = 0.1246 and $\sigma(K_{rel})/ K_{rel}$ = 0.10 gave us the percent error for our reagent $\sigma(K_{CB[7]•6})/ K_{CB[7]•6}$ = 0.16.

IV.3.2. Design of the new generation of aminooxy reagents

The preparation of the quaternary ammonium aminooxy reagents had to be carefully planned to prepare derivatizing reagents with the ability to perform high affinity with **CB7**. Endowed with the general knowledge provided by the extant literature, we sought the molecular structures that best meshed with the properties we were looking for (i.e., good reactivity with carbonyl-containing compounds, and high analytical performance in the HPLC-MS/MS). The first selected molecule was **6**. As we have previously seen, the components of this molecular structure allow the formation of complexes with **CB7** with association constants at the range of $10^5\ M^{-1}$, which was consistent with the literature and our speculations. Therefore, taking a quick look at previous studies, we explored the possibilities that would let us leap to the top of the scale. Quickly, we took a glimpse of two outstanding molecular structures. The ferrocenyl (**XIII**) and the adamantyl (**18**) set of compounds were reported to have association constants

with **CB7** comparable to those found in the strongest complexes made by nature (e.g., streptavidin–biotin). Since our purpose was to combine these aminooxy reagents with our previously functionalized magnetic beads, we dismissed the possibility of using ferrocene-like molecular structures that could be magnetically susceptible. Hence, we selected adamantyl compounds as the group of choice. There are, however, many known structures related to adamantyl derivatives. For example, we could choose unsubstituted adamantyl to be adjoined to **6**, or we could make use of an adamantyl ethanol ether, adamantylamine (**18**), **XV**, or even diamandoids (**XIV**) which, by the way, have been reported to be the strongest guests for **CB7** (Figure IV-15). Despite this, we were aiming for compelling guests that would display high affinity with **CB7**, but we could not afford to make the mistake of implementing such an active guest that, alike streptavidin–biotin complexes, would make them almost irreversible and would give us a hard time at the moment of desorption from the nanobeads. The second facet was related with the place to mesh this additional moiety. Among different options, it seemed that swapping the trimethylammonium group for adamantylammonium was an excellent approach because we would barely modify the initial structure, and hopefully the intrinsic properties of it would prevail, while adding an adamantyl ammonium cation, that presents excellent affinity with **CB7**. We then prepared **11** as a molecule fulfilling all these characteristics.

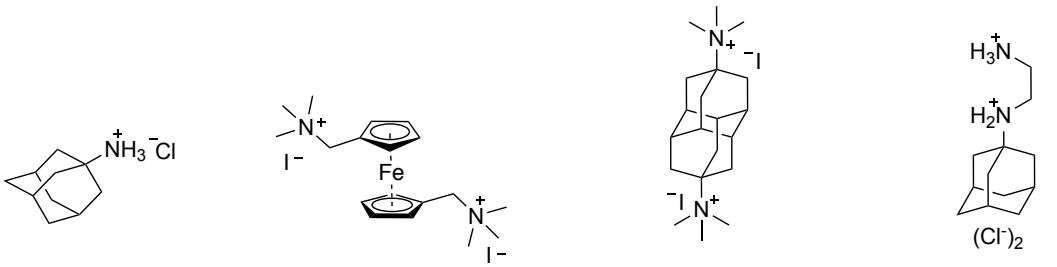

18 4.23 x 10^{12} | **XIII** 1.9 x 10^{13} | **XIV** 2.00 x 10^{15} | **XV** 2.40 x 10^{13}

K_a (M^{-1})

Figure IV-15. Selection of molecules binding with ultra-high affinity with **CB7** in buffered D_2O.

We can divide the synthesis of reagent **11** into two groups to be integrated prior to the CuAAC reaction (Scheme IV-4): the alkyne group, **2**, which remains the same, and the azide group, **9**, that was a modification of the previously synthesized one. The synthetic procedure started with commercial

adamantylamine, **18**. A typical process for the formation of a dimethylated tertiary amine, such as **7**, is the Eschweiler–Clarke reaction, which employs an excess of formic acid and formaldehyde. This kind of reductive amination reactions provides tertiary amines since the mechanism involves imine formation with formaldehyde, and then, the formic acid acts as a source of hydride that reduces the imine and releases CO_2. The establishment of the tertiary amine, though, is slower due to the difficulties to form the iminium ion; however, 24 h at reflux afforded 88% yield of **7**. If this approach is followed, the formation of a quaternary ammonium salt is unattainable, because the tertiary amine cannot form another imine or iminium ion, while other procedures, such as methylation with iodomethane go all the way to produce quaternary ammonium salts. This latter approach was also considered in another synthetic procedure that will be mentioned later. The next step was the formation of the betaine, **8**, upon the reaction of **7** with 2-bromoacetic acid. Tertiary amines are generally good nucleophiles, whose nucleophilicity is strongly dependent on the steric hindrance of the amine. In this case, we could obtain pure (> 80%) product in good yields up to 93%. The crude product was a mixture of the target molecule (**8**), salts ($NaHCO_3$, NaBr) and, sometimes, small amounts of unreacted starting material, **7**. However, solubility factors contributed to the purification of the product. For example, salts such as $NaHCO_3$ are not soluble in EtOH and were filtered off first. Then, when some starting material was present, it could be removed by rinsing the crude product with some DCM. The product, **8**, is soluble in EtOH but so is NaBr. However, while **8**, presents a good solubility in ACN, NaBr is almost insoluble in this solvent. Next step consisted of the amide bond formation between the aminoacid **8** and commercial azidoaniline, **3**. The coupling reagent employed in the amide synthesis was TBTU in the presence of DIPEA in DMF. The conversion of the reaction was followed by LC-MS of the crude product. Stirring the reaction overnight was enough to obtain 82% yield of **9** upon purification by silica gel chromatography. The preparation of the alkyne and azide moieties led us to the next step: the formation of the triazole ring by the CuAAC cycloaddition reaction. Since the final product **10** is highly soluble in DCM, the CuAAC reaction leading to it was attempted in this solvent; however, it failed to deliver the product. Gratifyingly, when the reagents were dissolved in a 1:1 mixture of degassed water and DCM in the presence of a Cu catalyst (0.3 eq) the

process took place in a satisfactory manner. In this case, the reaction was stirred at rt for 12 h and the amphiphilic product (**10**), was extracted from the mixture with DCM. After that, the crude product was further purified by column chromatography (88% yield). The final step for the preparation of the aminooxy reagent, **11**, was the deprotection of the tritylamino group. The deprotection was carried out in DCM acidified with a 6 M HCl solution (v/v: 1/1). Upon reaction overnight, an emulsion was formed, and it was subsequently partitioned in two phases by addition of water. Then, the water extract was rinsed with DCM, and the solvent was evaporated under vacuum. The crude product was then purified by preparative HPLC to deliver up to 48% yield of **11**. The final derivatization step could be carried out in different solvents, from a 1:1 mixture of water/acetonitrile to pure MeOH, and accelerated by the addition of formic acid. The reaction between **11** and testosterone was relatively fast, being complete within one hour. Preparative HPLC was then used to purify the derivatized product, and the pure product was obtained, however, in poor yields (31% yield).

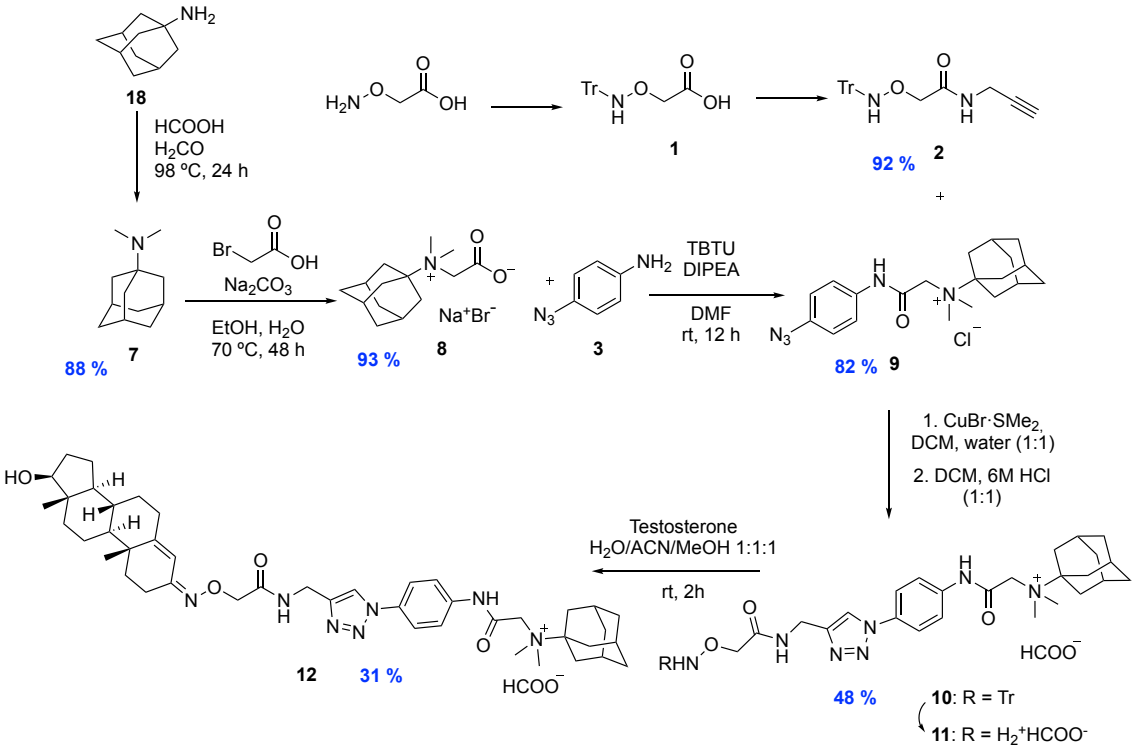

Scheme IV-4. Synthesis of the aminooxy reagent **11** and its testosterone derivative, **12**.

Finally, other attempted synthetic procedures involved the previous formation of the amino acid **19** (Scheme IV-5). Direct transformation to the quaternary ammonium salt **8**, by reaction with MeI was not achieved. On the other hand,

when the quaternization of the amine was intended to be produced at later stages, neither protection of the secondary amine of the amino acid with boc, to deliver **20,** nor direct reaction of **19** with the amine **3** to form the amide **21** were successful.

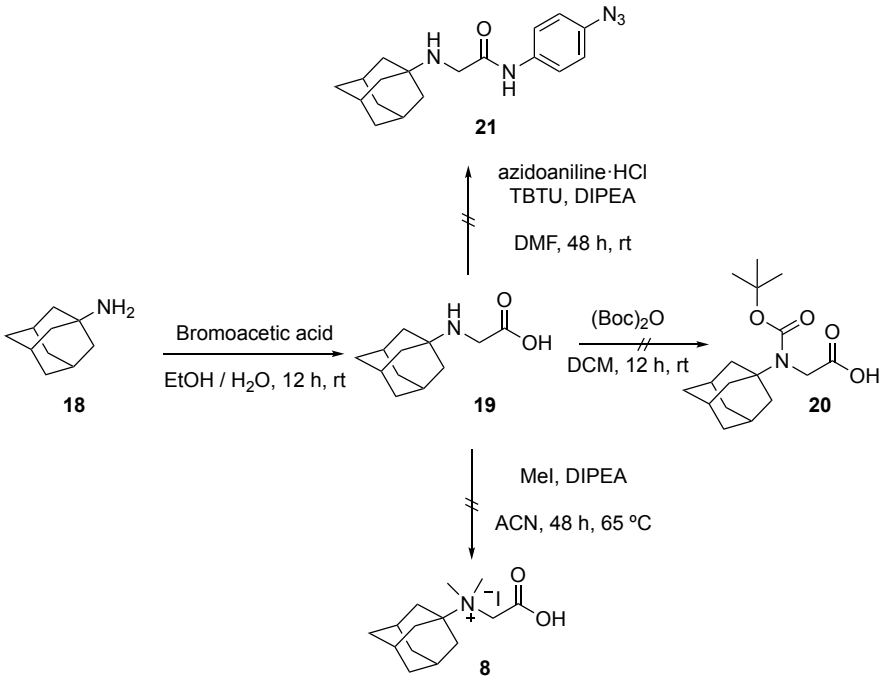

Scheme IV-5. Alternative synthetic steps towards the preparation of **11**.

Another and more "minimalistic" reagent was **VI** (Figure IV-16), in the sense that the structure of the molecule only presents the essential components compared to the more encumbered reagent **6** leading to **11**. Again, the best approach to introduce the binding adamantyl unit was to exchange one of the methyl groups to target the synthesis of **15** (Scheme IV-6).

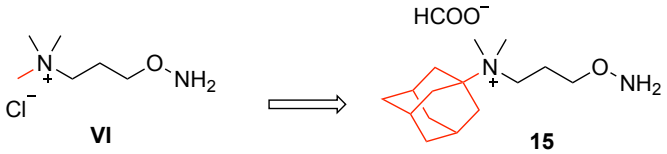

Figure IV-16. Comparison between the molecular structure of **VI** and **15**.

The preparation of the quaternary ammonium salt (**13**) was slow, but similarly to the synthesis of the previous betaine **8**, it could be isolated (95% pure, measured by ^{1}H NMR with internal standard) in good yields (66% yield) after washings and extraction with different solvents. Then, the aminooxy reagent is obtained by substitution of the alcohol **13** for *N*-protected hydroxylamine upon Mitsunobu-like reaction, followed by subsequent deprotection with hydrazine at room

temperature. Deprotection of **14** and purification of the aminooxy reagent **15** by preparative HPLC prior to testosterone derivatization delivered **15** in poor yields (*ca.* 30%).

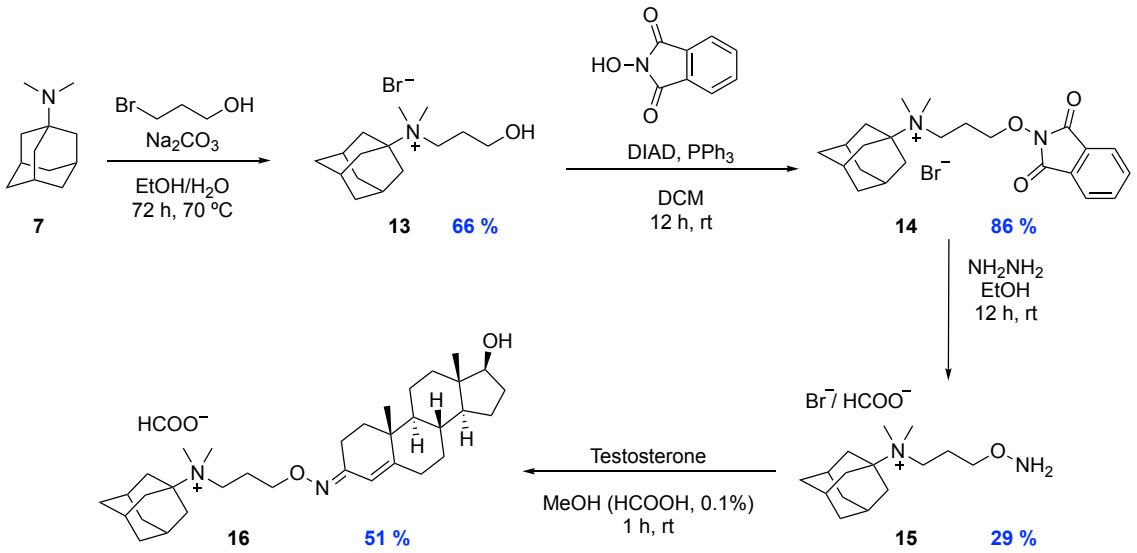

Scheme IV-6. Synthesis of **15** and its testosterone derivative, **16**.

IV.3.3. Determination of the affinity constants

In section IV.3.1, we mentioned how to determine the affinity constants. Here, we applied the same procedures to assert, with the suitable reference guest, the affinity constant of these novel aminooxy reagents.

Determination of the K_a of 11

To determine the affinity constant of **11**, we selected a binding guest stronger than **17**, as the reference guest for the competitive NMR studies. We first explored the possibility to use *p*-xylylenediamine dihydrochloride, because it is commonly used as a reference guest for its suitable features, and is by two orders of magnitude a stronger guest (K_a of 10^9 M^{-1}) than **17**. However, we were unsure whether the affinity of *p*-xylylenediamine would be high enough to compete with **11**. After preparation of the stock solutions and correction of the concentrations, we soon realized that it was not a proper reference guest because the affinity of **11** with **CB7** was significantly higher and experimental data, indeed, cleared out our initial presumptions. It turns out that a mixture containing 1000 equivalents of *p*-xylylenediamine and **11** with a limiting amount of **CB7**, afforded, after equilibrium, 25% of **CB7**·*p*-xylylenediamine vs. 75% of **CB7**·**11**. There was no doubt we needed to use a stronger reference guest for our studies. In the

beginning, we were skeptical about using adamantylamine, **18**, because the NMR spectrum would show many superimposed peaks and attempts to integrate them would be thwarted. However, we were fortunate to find out that the resonances of the methyl protons of **11** shifted to up fields upon complexation with **CB7**. Allowing us to distinguish between bound and free **11** (Figure IV-17).

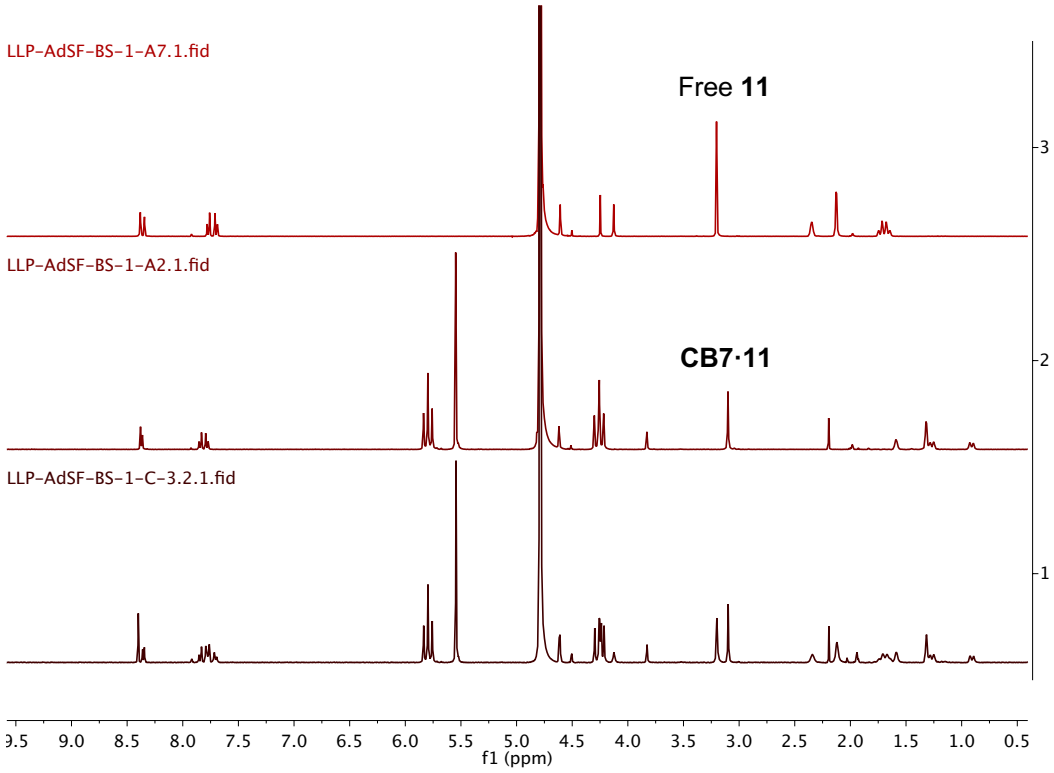

Figure IV-17. (1) a combination of **CB7** and 2 eq of **11**. (2) a mixture of **CB7** and 1 eq of **11**. (3) ^{1}H NMR spectra for **11**.

Hence, **18** was established as the reference guest for the NMR competition experiments to be performed. Again, preparation of stock solutions, determination of the concentration and cross-checking was followed by the onset of the NMR studies. The tests were carried out from three independent sets of stock solutions (Table IV-2, first set: entries 1–4. second set: entries 5–9. Third set: entries 10–13). We started the experiments with roughly equimolar amounts of **11** and **18** to assess the strength of the **CB7·11** complex (Table IV-2, entry 1). Interestingly, the results showed higher affinity of **CB7** towards **11**, with 75% of the macrocycle bound to **11**. Further studies were performed by increasing the concentrations of **18** —until the formation of complexes with 50% of each guest was achieved in the equilibrium (Table IV-2, entry 4).

Table IV-2. NMR studies to determine K_a of **11**.[a]

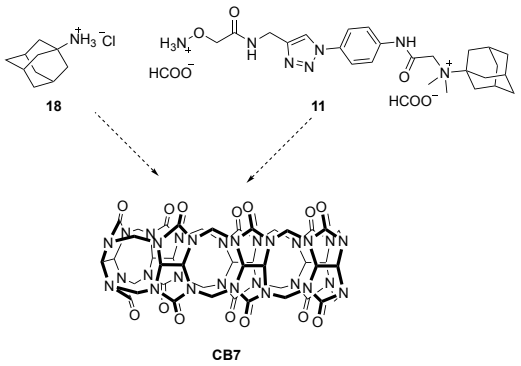

Entry	[**CB7**] (mM)	[**11**] (mM)	[**18**] (mM)	Ratio **CB7·11** (%)	K_{rel}	K_a (10^{13} M)
1	0.50	0.58	0.60	75	6.82	2.89
2	0.50	0.58	1.2	64	6.92	2.93
3	0.50	0.58	3.5	43	6.70	2.83
4	**0.50**	**0.58**	**3.0**	**47**	**7.01**	**2.96**
5	0.50	0.60	1.0	68	6.82	2.89
6	0.50	0.60	1.6	59	6.59	2.79
7	**0.50**	**0.60**	**2.6**	**50**	**6.68**	**2.83**
8	0.50	0.60	3.0	47	6.57	2.78
9	0.50	0.60	3.5	44	6.67	2.82
10	0.50	0.60	2.6	50	6.82	2.89
11	**0.50**	**0.60**	**2.6**	**51**	**7.00**	**2.96**
12	0.50	0.60	3.0	48	6.84	2.89
13	0.50	0.60	4.0	42	6.98	2.95

[a]Conditions: a mixture of **CB7**, **11**, and **18**, at the indicated concentration, was stirred until reaching equilibrium in a 50 mM sodium acetate buffer at pH = 4.75. All values were determined by ^{1}H NMR spectroscopy.

The results were astonishing since the simple derivative **11** depicts an outstanding behavior. First, because most of the ultra-high affinity guests found in the literature are tailor-made compounds designed to reach the strongest possible complexation (Figure IV-15). Furthermore, most of these reagents are unfunctional molecules and require further functionalization that can be used for decomplexation or displacement of the desired bound molecule. We herein, not

only produced a reagent with ultra-high affinity to **CB7**, but it also has a functional purpose, and it is readily usable. Furthermore, **11** displays, as far as we know, the second strongest binding constant reported for synthetic host–guest complexes under these buffered conditions. It is more effective than adamantylamine, **18**, and slightly better than adamantylethylenediamine (Figure IV-15). Moreover, the results collected in Table IV-2 show that these experiments were highly reproducible, even when the concentration of the guests produced unbalanced ratios of the complexes (Table IV-2, entries 1 and 13).

We have previously described the calculations done to determine the affinity constant K_a from the relative constant and the propagated error. Here, from the results highlighted in Table IV-2, entries 4, 7, and 11, we obtained an error of 3%. However, we used the standardized value of 10%. Thus, the known $\sigma(K_{\mathbf{CB7\cdot 18}})/K_{\mathbf{CB7\cdot 18}} = 0.2356$ and $\sigma(K_{rel})/K_{rel} = 0.10$ gave us the percent error for our reagent $\sigma(K_{\mathbf{CB7\cdot 11}})/K_{\mathbf{CB7\cdot 11}} = 0.26$. In this case, the procedure involved the preparation of a solution with **CB7**, **11** and **18**. Upon reaching equilibrium, we determined the relative concentrations of **11** and **CB7·11** by the integration of the appropriate resonances in the ^{1}H NMR spectrum (**11**: 3.20 ppm; **CB7·11**: 3.10 ppm. Figure IV-19). We obtained an average $K_{rel} = 6.90$ that allowed us to reckon the association constant. Knowing the relative constant, the associated error, and the affinity constant of the reference guest, we determined the affinity constant of **11**, which displays, just by the simple switch of a methyl group for an adamantyl group, an affinity constant that differs by 8 orders of magnitude with its surrogate **6** (Figure IV-*18*).

$$\boldsymbol{K_{a,11} = 2.92\ M^{-1} \pm 0.76\ x10^{13}\ M^{-1}}$$

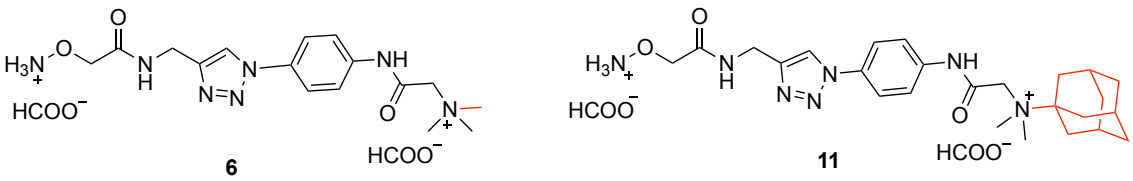

$K_a = 1.56$ **x10^5** (M^{-1}) $K_a = 2.92$ **x10^{13}** (M^{-1})

Figure IV-18. Affinity constant of reagents **6** and **11**.

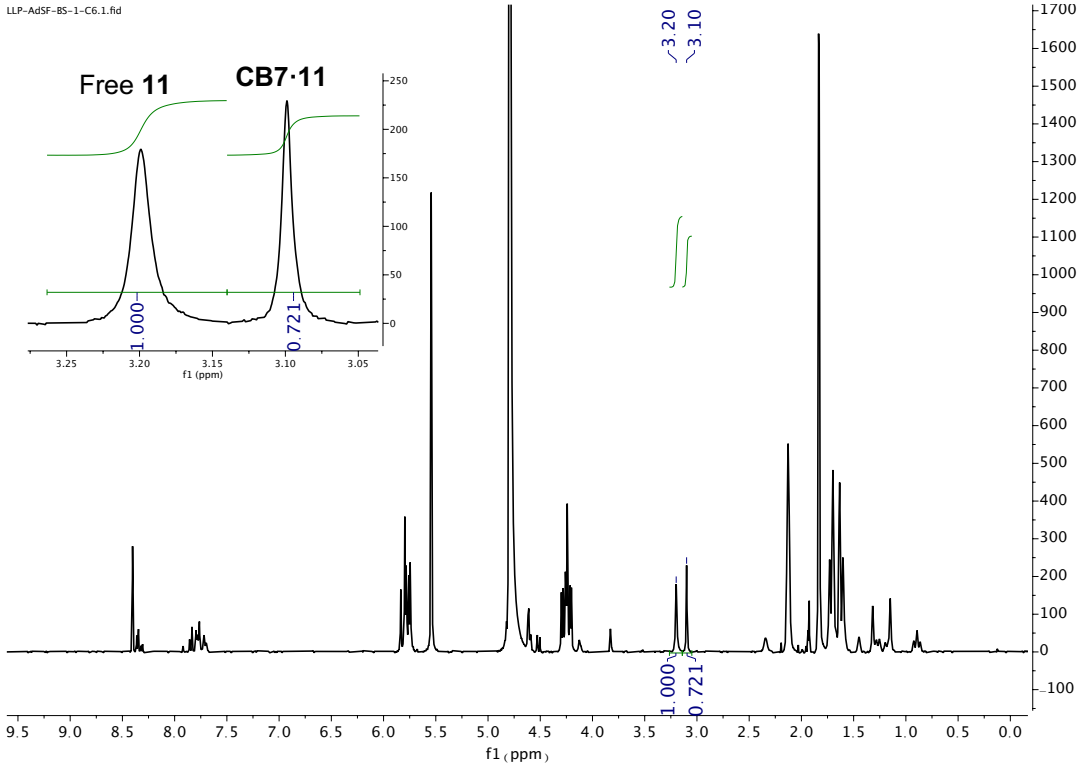

Figure IV-19. ^{1}H NMR spectrum for the competition experiments between **CB7**, **11** and **18**.

Determination of the affinity constant K_a of 15

The determination of the affinity constant for **15** was directly assessed with the reference guest **18**. As depicted in Figure IV-20, it is possible to follow the process through the chemical shift of the methyl groups in the aminooxy reagent **15**.

First, preparation of stock solutions, determination of the concentration and cross-checking was followed by the NMR competition studies. The experiments were carried out with an excess of **18** that was gradually reduced until the attainment of closely 50% of **CB7**·**15** and **CB7**·**18** in the equilibrium (Table IV-3, entries 1–4). We then realized that **18** is a stronger binding for **CB7** and even a small excess (1.2 eq, entry 4) of **15** delivers higher ratios of **CB7**·**18** than **CB7**·**15**. Slightly higher amounts of **15** (1.5–1.7 eq) were then used to determine the affinity constant.

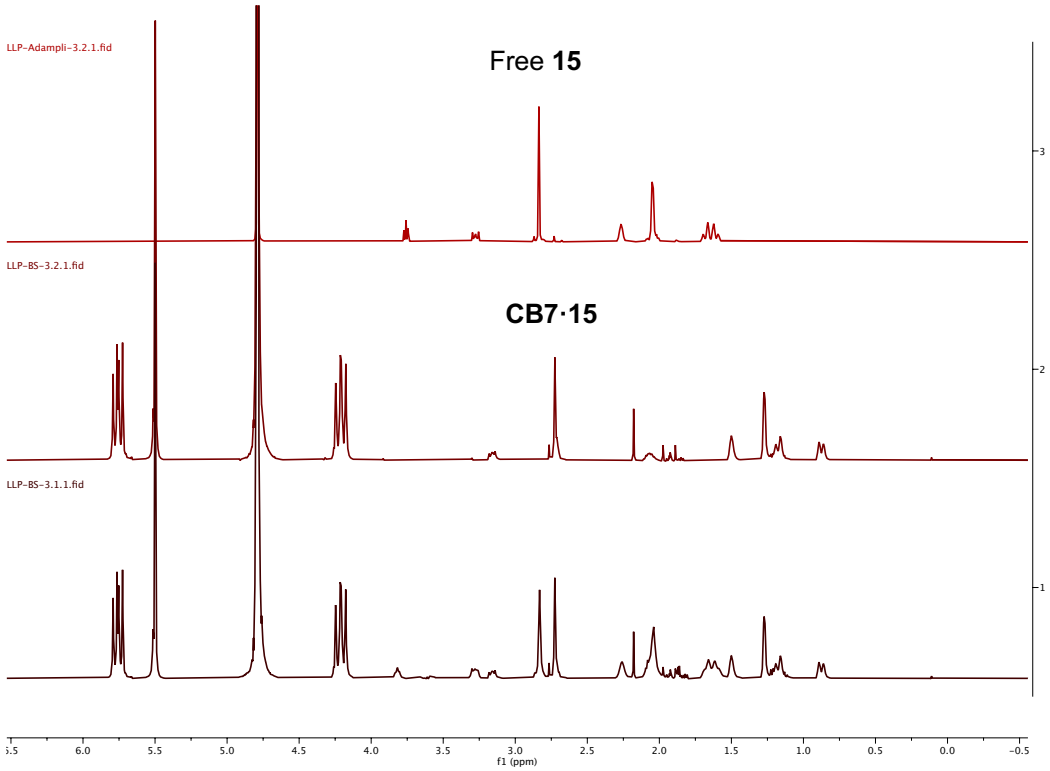

Figure IV-20. From top to bottom: ^{1}H NMR spectra of 15; **CB7** with <1eq of **15**; and **CB7** with >1 eq of **15**.

A solution with **CB7** (1.3 mM), **18** (2.0 mM) and **15** (3.3 mM) was stirred at 50 ºC for not less than 24 h or until reaching the equilibrium. We determined the relative concentrations of **15** and **CB7·15** ([**CB7·15**] = 0.268[**15**]$_{free}$) by the integration of the appropriate resonances in the ^{1}H NMR spectrum (**15**: 2.89 ppm; **CB7·15**: 2.78 ppm, Figure IV-*21*). We, then, calculated [**15**]$_{free}$ = [**15**]/1.268 = 2.60 mM, and [**CB7·15**] = 0.268 x 2.60 mM = 698 µM from the equation [**15**] = [**15**]$_{free}$ + [**CB7·15**]. Then, from [**CB7**] = [**CB7·18**] + [**CB7·15**], we calculated [**CB7·18**] = 1.3 mM – 698 µM = 602 µM, and [**18**]$_{free}$ = 2.0 mM - 602 µM = 1.40 mM from [**18**]$_{free}$ = [**18**] - [**CB7·18**]. Then, the values of [**CB7·15**], [**15**]$_{free}$, [**CB7·18**], and [**18**]$_{free}$ were used to determine K_{rel} = 0.622. These determinations were done in triplicate from independently prepared stock solutions and the average values were used in the calculations of K_a and the error analysis.

Table IV-3. NMR studies to determine K_a of **15**.[a]

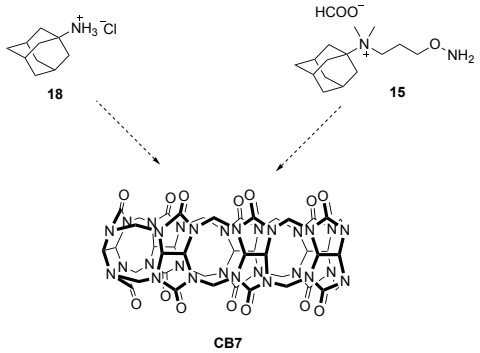

Entry	[**CB7**] (mM)	[**15**] (mM)	[**18**] (mM)	Ratio **CB7·15** (%)	K_{rel}	K_a (**10^{12} M**)
1	1.3	2.0	9	16	0.652	1.49
2	1.3	2.0	7	17	0.371	1.57
3	1.3	2.0	4	24	0.626	2.65
4	1.3	2.0	1.7	45	0.574	2.43
5	**1.3**	**3.0**	**2.0**	**51**	**0.599**	**2.54**
6	**1.3**	**3.3**	**2.0**	**54**	**0.622**	**2.63**
7	**1.3**	**3.0**	**2.0**	**51**	**0.595**	**2.52**
8	1.3	3.3	2.0	52	0.570	2.41

[a]Conditions: a mixture of **CB7**, **15**, and **18**, at the indicated concentration, was stirred until reaching equilibrium in a 50 mM sodium acetate buffer at pH = 4.75. All values were determined by ^{1}H NMR spectroscopy.

The percent error in K_a was measured as a function of the uncertainty in K_{rel}. From the results highlighted in Table IV-3, entries 5, 6, and 7, we obtained an error of 2.4%. However, we used the standardized 10%. Thus, the known $\sigma(K_{\mathbf{CB7\cdot18}})/K_{\mathbf{CB7\cdot18}} = 0.2356$ and $\sigma(K_{rel})/K_{rel} = 0.10$ gave us the percent error for our reagent $\sigma(K_{\mathbf{CB7\cdot15}})/K_{\mathbf{CB7\cdot15}} = 0.26$. Knowing the relative constant, the associated error, and the affinity constant of the reference guest, we determined the affinity constant of **15**.

$$\boldsymbol{K_{a,15} = 2.56 \pm 0.66 \times 10^{12}\ M^{-1}}$$

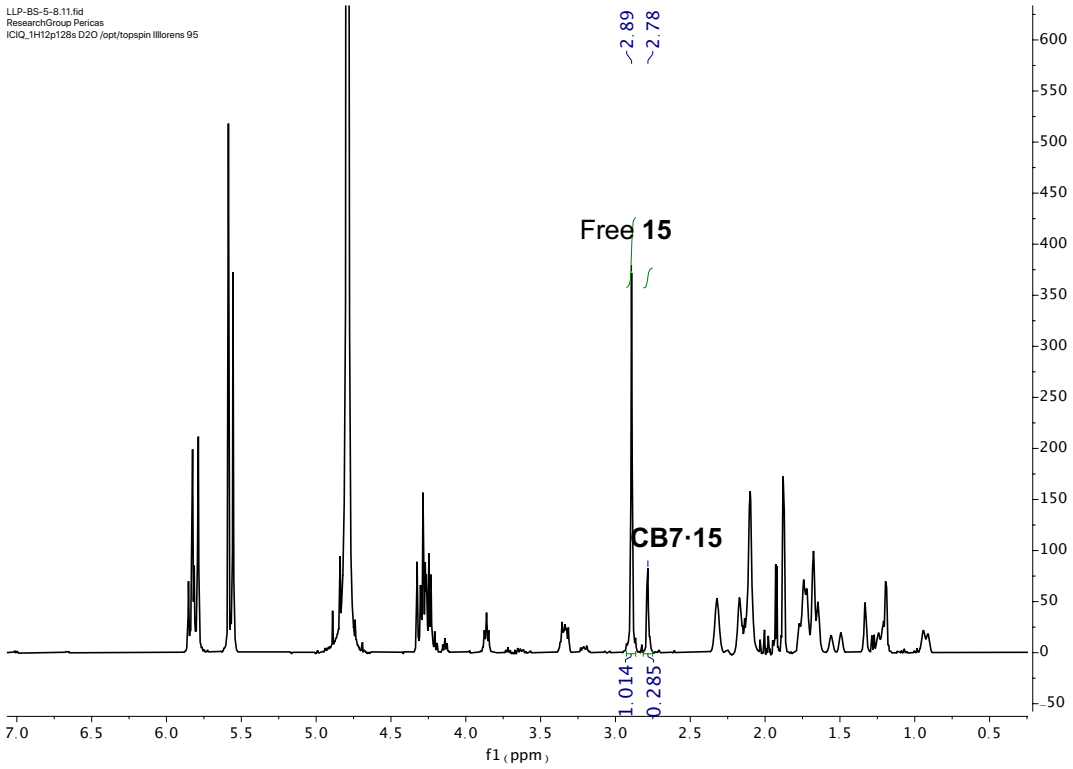

Figure IV-21. ^{1}H NMR spectrum for the competition experiments between **CB7**, **15** and **18**.

IV.3.4. Testosterone extractions

Knowing the high affinity of these new quaternary aminooxy reagents for **CB7**, and assuming that it would remain high upon derivatization with testosterone, we wanted to test the ability of the **CB7** functionalized nanobeads to extract selectively, through a molecular recognition fueled process, the testosterone from test samples. To this end, we organized different experiments that, in a stepwise fashion, would allow us to determine the best solvents and conditions to selectively extract, transport and deliver testosterone from simple and more complex samples.

We have seen in the second chapter of this manuscript several methods to determine the extraction of certain guests with our magnetic beads. For example, we can perform the pertinent NMR studies and quantify the removal with an internal standard. Alternatively, by harnessing the chemical properties of the guest, we can follow the extraction by UV/vis. Our first objective was to identify the best solvent to favor the complexation with **CB7**. We first assumed that water would be the best solvent because we already measured ultra-high affinity in it,

but we also wanted to find out whether some combination of aqueous and organic solutions would allow complexation with the derivatized testosterone. Also, in the second chapter, we saw how a fluorescent probe was bounded to **CB7** in ethanol, but it showed no affinity in water nor other buffers. Therefore, we set up some qualitative studies in which the testosterone derivative was dissolved in several aqueous and organic solvents and, upon extraction with an excess of the **CB7** coated beads, we could determine by mass spectroscopy, whether there was enough testosterone left in the solution as to be detected by MS (Figure IV-22). The solubility of the testosterone derivative in water, acetonitrile, methanol, chloroform, and dichloromethane is good. As expected, the extraction of testosterone in water performed well, and the concentration of the derivative upon removal was below the limits of detection. On the other hand, the mining in organic solvents, ACN, methanol, and chloroform, was not so efficient, and the derivatized molecule could be detected in those solutions even after addition of a significant excess of the cucurbituril coated beads. Interestingly, mixtures of water and ACN allowed the extraction of testosterone until reaching a 1:1 composition; then, higher proportions of ACN were deleterious for the efficiency of extraction.

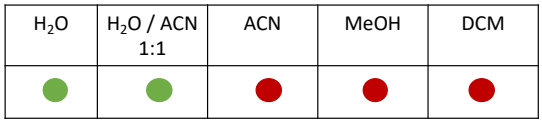

Figure IV-22. Extraction of **12** and **16** from **CB7** functionalized magnetic beads in different solvents. (Green dots) the molecule was successfully extracted. (Red dot) the molecule partially remained in solution.

The adsorption of testosterone was straightforward, and the experiments went as expected. However, the biggest hurdle was met when we attempted to find out conditions to extract the testosterone from the magnetic nanoparticles—finding out an ultra-high affinity for these reagents turned out to be a poisoned blessing because at this stage we had to figure out how to extricate the testosterone derivative from the **CB7** cavity. Since the derivatives did not show affinity with **CB7** in organic solvents, as we have previously seen, it would be easy to assume a straightforward extraction with some organic solvents such as methanol, acetonitrile or dichloromethane, where the derivative is also highly soluble. However, our empirical results did not take long to undermine this option. Thus,

while it is complicated to steer the formation of the complex in organic solvents, once the complex is formed the desorption with organic solvents is even more complicated, at least under our experimental conditions. A tentative explanation of this behavior may be related to the fact that in organic solvents, some of the strongest interactions that trigger the formation of the complex, such as hydrophobic and “high energy” water release, are not present anymore. Besides, the entrance to the cavity through the carbonyl rim is tight for adamantane, which may justify the reason why, once the complex is formed, the desorption does not occur immediately. The cavity of the cucurbituril is larger than the entrance, and considering van der Waal forces between the walls of the cavity and the adamantyl unit and the ion-dipole interactions between the cationic species and the carbonyl rim, we concluded that desorption of such complexes may require a high energetic cost to be paid for it to take place. We next strived to screen several solvents, including aqueous and organic solvent mixtures even with the implementation of salts (Figure IV-23 and Figure IV-24). All the organic and aqueous solvents failed to release the guest from the cavity; however, the use of organic salts triggered the egression of the desired guest from the pit. We carefully selected the organic salts to be used for the desorption. First, since we knew the affinity constant of our reagents, **11** and **15**, as well as the association constant of adamantylamine, **18**, we speculated that **18** would compete for the cavity of **CB7** in water, and adding the required excess, we would be able to recover the desired reagent in the presence of **18**. However, the presence of **18** in the analytical samples could distort the required measurements in the LC-MS/MS, and it would be even worse in the case of derivative **12**, since its liberation from the inclusion complex may need a more considerable excess of **18**.

On the other hand, ammonium formate is a fascinating salt in this context because it can be eliminated by evaporation in the form of formic acid and ammonia delivering untainted products. Ammonium formate is commonly used in buffers in HPLC and LC/MS. The use of an excess of this salt for testosterone derivative extraction from the nanoparticles was accomplished in organic solvents. Among the different solutions used, we could identify a combination providing excellent results. Thus, when a combination of MeOH/$CHCl_3$ with an

excess of ammonium formate was used, the desorption of the guest from the **CB7** cavity took place in a clean manner.

	H_2O	MeOH	ACN	$CHCl_3$	DCM	EtOH
	🔴	🔴	🔴	🔴	🔴	🔴
50% $CHCl_3$	-	🔴	🔴	-	-	🔴
NH_4^+ $HCOO^-$	-	🟠	🟠	🟠	🟠	-
both	-	🟢	🟠	-	-	-

Figure IV-23. Desorption of **12** from **CB7** functionalized magnetic beads in different solvents. (Green dot) best result. (Orange dots) the molecule was extracted (Red dots) the molecule remained on the beads.

	H_2O	MeOH	ACN	**18**
	🔴	🔴	🔴	🟢
50% $CHCl_3$	-	🔴	🔴	-
NH_4^+ $HCOO^-$	-	🟠	🟠	-
both	-	🟢	🟠	-

Figure IV-24. Desorption of **16** from **CB7** functionalized magnetic beads in different solvents. (Green dots) best results. (Orange dots) the molecule was extracted (Red dots) the molecule remained on the beads.

The best conditions we found for the adsorption and desorption of testosterone derivatives were used for the next set of experiments. The reaction mixture resulting from **11** and an excess of testosterone was stirred in acidified water/ACN/MeOH 1:1:0.5, at room temperature, and monitored. After 1 hour of reaction, **11** was consumed, and HPLC-MS analysis showed the presence of two peaks in the chromatogram corresponding to the product **12** and testosterone. To this solution, **CB7** functionalized magnetic beads were added, and the testosterone derivative **12** was extracted from the solution by magnetic decantation. Upon addition of the "desorption solvent," a 1:1 mixture of chloroform and a solution of ammonium formate in methanol to the previously isolated, loaded magnetic beads, the testosterone derivative was recovered and separated from the previous reaction mixture (Figure IV-25).

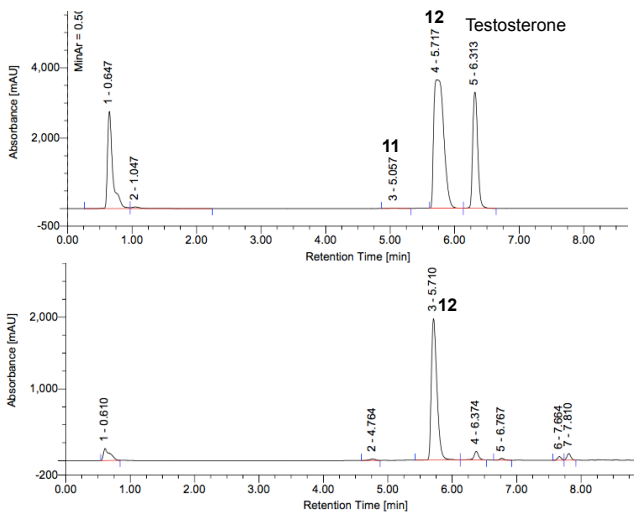

Figure IV-25. HPLC chromatogram after 1h reaction between **11** and an excess of testosterone (top). HPLC chromatogram after extraction of **12** from the reaction mixture.

The ensuing experiments were set up to determine the recyclability of the magnetic beads. We wanted to know whether it was possible to recycle the same magnetic beads to extract, separate and release, the testosterone derivative over and over again. We prepared a solution of **12** in 1:1 acetonitrile/water, and we determined the area of the corresponding peak in the HPLC chromatogram. Then, we extracted **12** from the solution with a significant excess of cucurbituril coated nanoparticles followed by desorption with the required solvent and concomitant analysis of the resulting solution by HPLC to determine the presence of **12** in the solution. The same nanoparticles were reused, and the area of the peak corresponding to **12** was integrated after adsorption and after desorption. Hence, in the first cycle, **12** is adsorbed by MNPs, but *ca.* half of **12** is recovered upon desorption, and the other half remained on the nanoparticles (Figure IV-26). Then, in the second cycle, the excess of cucurbiturils is capable of extracting most of **12**, and since the loading of the beads is now higher, the release of **12** is also higher. The third cycle is similar to the second cycle, where the desorption exhibits larger amounts of **12**. The fourth cycle seems to be more equilibrated, and the desorption releases higher quantities of **12** than the first cycle, presumably due to the preloaded nanoparticles before adsorption. Therefore, cycle fourth was followed by a clean-up of the nanoparticles with several solvents, including the desorption solvent, methanol, and water to release all **12** from the MNPs. Then, the next cycles (5 and 6) performed similarly to the first ones.

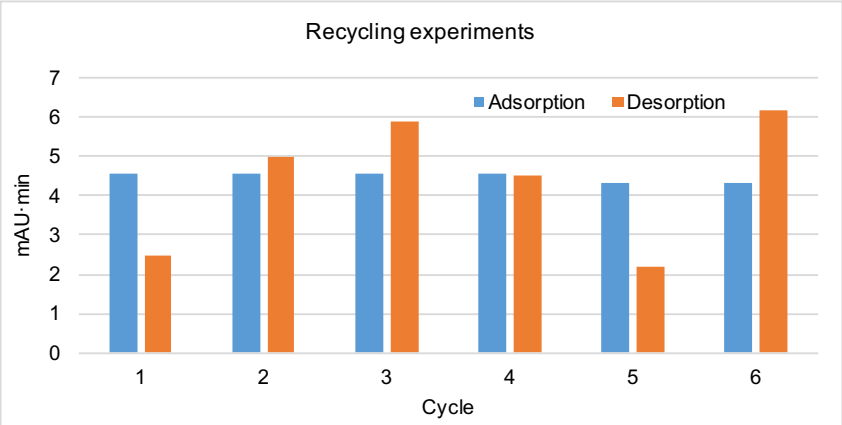

Figure IV-26. Recycling experiments.

In another solution, we prepared a mixture of compounds from the bench, cytidine tryptophan, testosterone and **12** were mixed at different concentrations, and the relative area of the corresponding peak in the HPLC chromatogram was determined (Figure IV-27). Then, **12** was extracted from the solution mixture by the **CB7** coated magnetic beads. Upon treatment of the loaded magnetic beads with the designated desorption solvent, we determined the relative area of each reagent by HPLC. Thereby, we could demonstrate the ability of the nanoparticles to selectively extract the targeted molecule from a complex mixture for its enrichment.

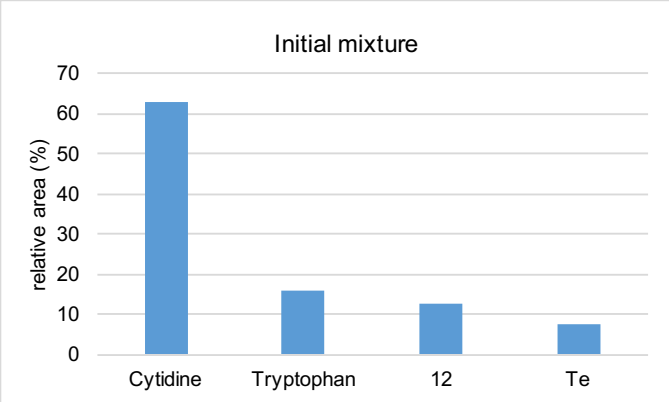

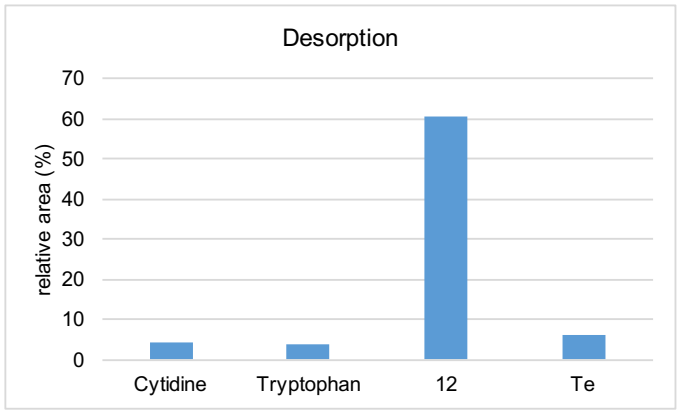

Figure IV-27. Relative amount of the reagents before and after extraction.

Finally, the quaternary aminooxy reagents reported in the literature, **6** and **VI**, were both used for HPLC-MS/MS analysis and we wanted to compare their performances upon the introduction of the adamantyl moiety (Figure IV-28).

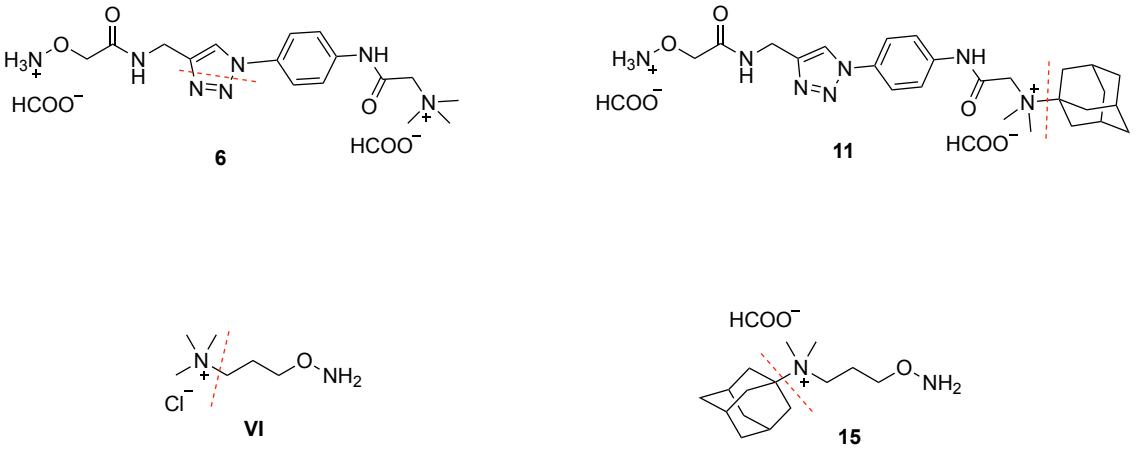

Figure IV-28. Molecular structure and fragmentation of selected aminooxy reagents. Same fragmentation pattern upon derivatization with testosterone.

From our preliminary studies, we found out that the sensitivity of detection of these new reagents, **11** and **15**, may not represent a major improvement concerning to that from the previously reported reagents, **6** and **VI**. Interestingly we found out that the most intense multiple reaction monitoring (MRM) transition,[26] or the fragmentation, from **12** was 752.5→135.1 due to the loss of neutral amine to render an adamantyl carbocation instead of the expected 752.5→724.5 after nitrogen loss (Figure IV-29). The most intense MRM transition from **16** was again the loss of neutral amine. Despite this, all three reagents showcased similar behavior on the LC-MS/MS. However, it is relevant to note that, while the testosterone derivatized with the harbingers **VI** or **6** delivers

specific fragments from both testosterone and the aminooxy reagent, the fragmentation of **12** and **16** produce adamantyl carbocations.

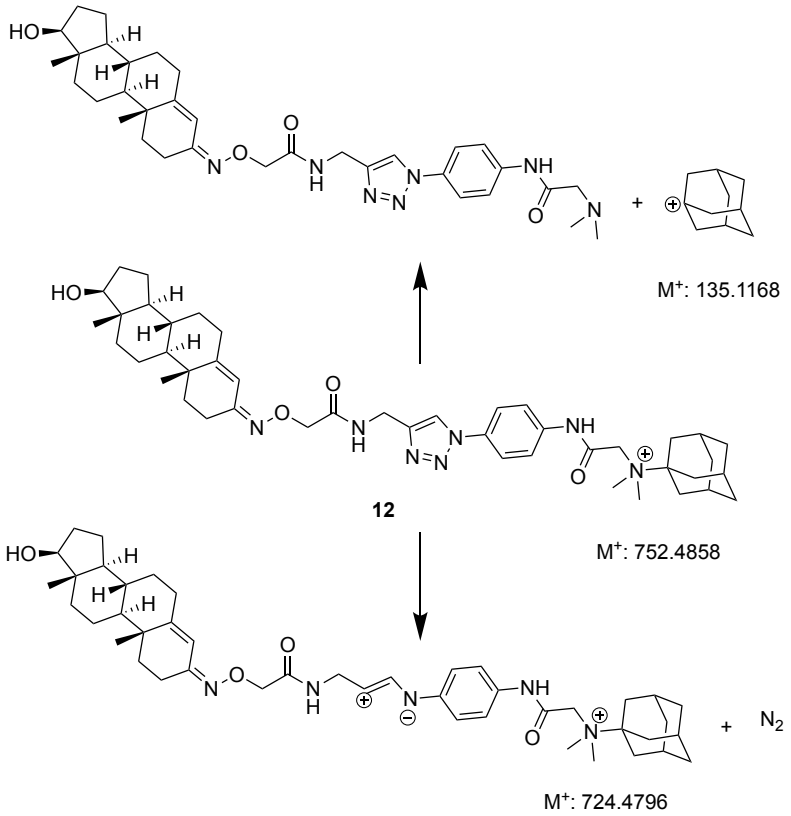

Figure IV-29. Chemical structure and possible fragmentation of **12**.

Perspectives and outlook

The use of **CB7** coated magnetic beads to selectively extract testosterone derivatives tagged with an adamantyl ammonium moiety that displays high affinity with **CB7**, and that also enhances the ionization of testosterone in the ESI has been found useful for the enrichment and detection of testosterone from complex mixtures. Further experiments may be required in order to comprehend the extent of the sensitivity enhancement as well as the separation properties. To this end, calibration curves are required for the quantification and determination of the limits of detection. The understanding of the separation properties can be tackled through testosterone analyses from samples prepared following protocols dealing with the separation of testosterone by different procedures, such as SPE, SLE, protein precipitation or **CB7** coated nanoparticles extraction. For this last point, it is not possible to draw definitive conclusions from the initial results discussed here, but it is clearly suggested that the nanoparticles can be complementarily used for the enrichment of testosterone from serum samples.

Thus, we have followed two different protocols involving the use of the magnetic nanoparticles to the extraction of derivatized testosterone from serum samples, and we have been able to detect the extraction procedure. However, we have so far not been able to quantify the presence of testosterone. Additional experiments are required to elucidate whether the extraction by nanoparticles can outperform the SPE and other preparation techniques, or somehow complement them.

IV.4. Experimental section

IV.4.1. Table of contents

IV.4.2. General information

Unless otherwise stated, all reactions were conducted under air. All commercial reagents were used as received. Flash chromatography was carried out using 60 mesh silica gel. Thin layer chromatography (TLC) was carried out using Merck TLC Silica gel 60 F254 aluminum sheets. Components were visualized by UV light (λ = 254 nm) and stained with *p*-anisaldehyde, phosphomolybdic dip or iodine in silica. NMR spectra were reported in parts per million (ppm) and recorded in deuterated solvents on Varian VXR400S, Varian Inova AMX600, Bruker Ascend 400 and Bruker Avance III HD. HR-ESI-MS spectra were obtained from Thermo Finnigan LTQ FT-ICR. IR spectra were recorded on a Perkin Elmer Spectrum BX FT-IR spectrometer with a diamond-ATR (Attenuated Total Reflection) unit. HPLC purifications were performed on a Waters Breeze system (2487 dual array detector, 1525 binary HPLC pump) using a Nucleosil VP 250/10 C18 column from Macherey Nagel. HPLC grade MeCN was purchased from VWR. For HPLC purification a buffer system of 2.5 mM ammonium formate in water, pH = 4.3 (referred to as buffer A) and 2.5 mM ammonium formate in 80% MeCN/water (referret to as buffer B) was used. All products that are known were characterized by comparison of their physical and spectroscopic properties with those described in the literature.[1]

IV.4.3. Experimental procedures

IV.4.3.1. Preparation of reagent 6

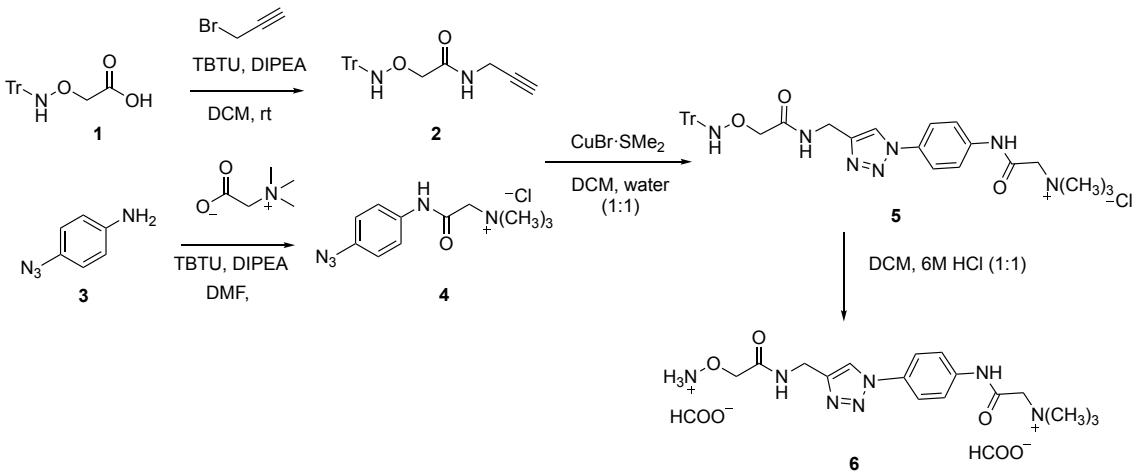

Synthesis of 2-((4-(4-((2-(Aminooxy)acetoamido)methyl)-1H-1,2,3-triazole-1-yl)phenyl-amino)-*N,N,N*-trimethyl- 2-oxoethanaminium formate (6)

2-((4-(4-((2-(Aminooxy)acetoamido)methyl)-1H-1,2,3-triazole-1-yl)phenyl-amino)-*N,N,N*-trimethyl- 2-oxoethanaminium formate, **6** was synthesized according to recent procedures and characterized by comparing ^{1}H-NMR spectra to the previously described in the literature.[1]

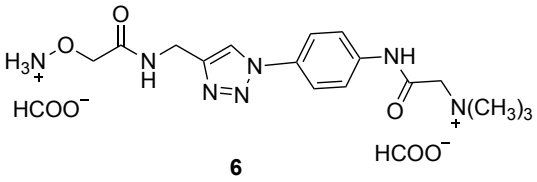

6

^{1}H-NMR (400 MHz, D_2O) δ = 8.34 (s, 1H), 8.29 (s, 1H), 7.63 (d, *J* = 9.2 Hz, 2H), 7.60 (d, *J* = 9.2 Hz, 2H), 4.55 (s, 2H), 4.28 (s, 2H), 4.17 (s, 2H), 3.36 (s, 9H) ppm.

IV.4.3.2. Preparation of reagent 11

Route a)

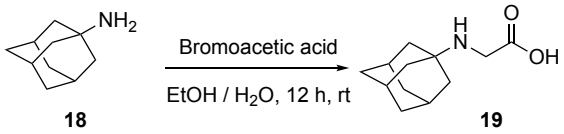

Route b)

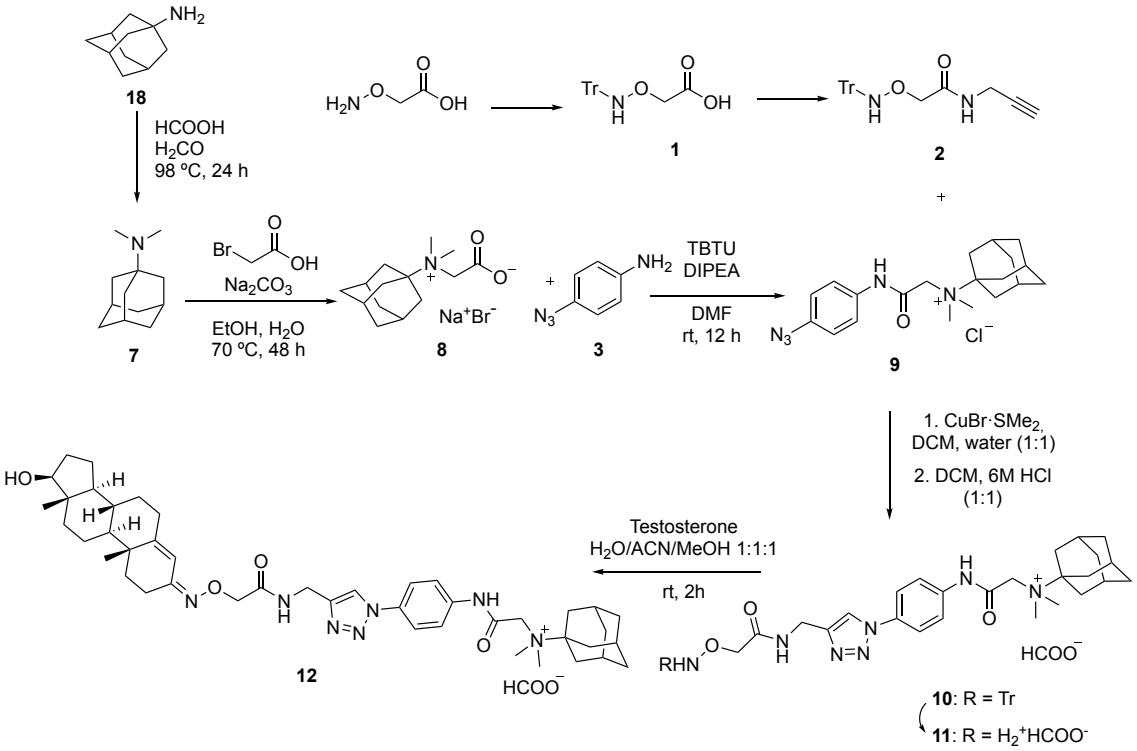

Synthesis of *N*-(1-adamantyl)glycine (19)

1-adamantylamine (1.87 g, 12 mmol) was dissolved in a mixture of 15 ml of ethanol and 5 ml of water. Bromoacetic acid (859 mg, 6 mmol) was added at room temperature. The reaction mixture was stirred for 24 hours at room temperature and then was poured into 10 ml of cold methanol. The white precipitate was vacuum filtered, rinsed with methanol and ACN and dried under high-vacuum to give the tittle compound (850 mg, 68%) with a purity of 96% measured by NMR with internal standard.

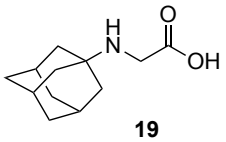

19

^{1}H-NMR (400 MHz, D_2O): δ = 3.54 (s, 2H, CH_2-NH), 2.16 (bb, 3H, CH), 1.87 (d, 6H, CH_2), 1.68 (m, 6H, CH_2) ppm. **^{13}C-NMR** (101 MHz, D_2O): δ = 172 (C), 57 (C), 41 (CH_2), 38 (CH_2), 35 (CH_2), 29 (CH) ppm. **HRMS** (ESI+): calc. for $C_{12}H_{19}O_2N_2$ [M]: 209.1416; found: 209.1412. **IR** (ATR): 2910, 2895, 2612, 2461, 1591, 1507, 1406, 1376, 1366, 1343, 1312, 1085, 1064, 1085, 925, 899, 891, 816 cm^{-1}. **EA**: calculated 68.87 %C, 9.15 %H, 6.69 %N. Found 66.77 %C, 8.82 %H, 6.58 %N.

Synthesis of *N,N*-dimethyl-1-adamantylamine (7)

Adamantylamine (1.23 g, 7.9 mmol) was dissolved in formic acid (1.5 ml) in a two-neck flask equipped with a reflux condenser. The mixture was vigorously stirred and formaldehyde solution (37%, 2.4 ml, 32 mmol) was slowly added at 90 °C. When the addition was complete, the reaction mixture was refluxed at 98 °C for 12 h. The pH of the mixture was adjusted to 12–13 by using NaOH solution (25 wt%). Then, the aqueous phase was extracted with DCM (10 ml x 3). All the organic phases were combined, washed with brine and dried with anhydrous Na_2SO_4. After solvent removal the product was obtained without further purification as a colorless oil (1.24 g, 88%).

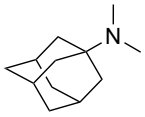

7

^{1}H-NMR (400 MHz, $CDCl_3$): δ = 2.32 (s, 6H, CH_3), 2.12 (bb, 3H, CH), 1.67 (m, 12H, CH_2) ppm. **^{13}C-NMR** (101 MHz, $CDCl_3$): δ = 54 (C), 38 (CH_2), 37 (CH_3), 37 (CH_2), 29 (CH) ppm.

Synthesis of *N*-(1-adamantyl)-*N,N*-dimethylglycine (8)

Under strong agitation, bromoacetic acid (716 mg, 5 mmol), sodium carbonate (954 mg, 9 mmol) and *N,N*-dimethyl-1-adamantylamine, **7**, (739 mg, 4 mmol) were added to a mixture of 6 ml ethanol and 1.6 ml water. The mixture was stirred at 70 °C for 48 h. After cooling down to room temperature, the suspension was filtered, washed with ethanol and after evaporation of the filtrate, washed with DCM to afford the title compound (885 mg, 93%) as a white solid.

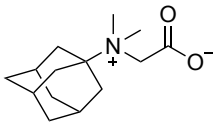

8

^{1}H-NMR (400 MHz, D_2O): δ = 3.72 (m, 2H, CH_2) 3.11 (s, 6H, CH_3), 2.29 (s, 3H, CH), 2.06 (s, 6H, CH_2) 1.68 (m, 6H, CH_2) ppm. **^{13}C-NMR** (101 MHz, D_2O): δ = 170 (C), 76 (C), 59 (CH_2), 44 (CH_3), 34 (CH_2), 34 (CH_2), 30 (CH) ppm.

Synthesis of *N*-(2-((4-azidophenyl)amino)-2-oxoethyl)-*N*,*N*-dimethyladamantanaminium chloride (9)

Betaine **8** (150 mg, 0.5 mmol, 1 eq) was first dried on high vacuum at 180 °C for 20 minutes. After cooling to rt, the colorless solid was suspended in DMF (5 ml). 4-Azidoaniline hydrochloride (90 mg, 0.5 mmol, 1 eq), TBTU (195 mg, 0.6 mmol, 1.2 eq) and DIPEA (0.21 ml, 1.2 mmol, 2.4 eq) were added whereupon a yellow brownish solution formed gradually. The reaction was stirred at rt overnight. DMF was then removed in vacuo and the crude mixture was purified by column chromatography (DCM/MeOH/H_2O/7N NH_3 in methanol = 90:10:0.6:0.6). The product was then dissolved in H_2O (10 ml) acidified to pH = 1 with 6 M HCl and extracted with DCM (3 x 10 ml). The organic layer was rinsed with brine (10 ml), dried over Na_2SO_4 and concentrated to afford the chloride salt of the product (160 mg, 82%) as a brown powder.

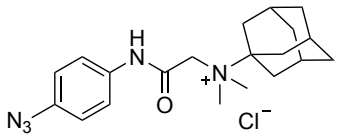

9

^{1}H-NMR (400 MHz, DMSO d^6): δ = 11.20 (s, 1H, NH), 7.71 (d, *J* = 8.9 Hz, 2H, CH=C-NH), 7.16 (d, *J* = 8.9 Hz, 2H, CH=C-N_3), 4.21 (s, 2H, NCH_2), 3.13 (s, 6H, $N(CH_3)_2$), 2.28 (s, 3H, CH), 2.07 (s, 6H, CH_2) 1.65 (s, 6H, CH_2) ppm. **^{13}C-NMR** (101 MHz, DMSO d^6): δ = 163 (C), 135 (2C), 121 (2CH), 120 (2CH), 76 (C), 58 (CH_2), 44 ($2CH_3$), 35 (CH_2), 34 (CH_2), 30 (CH) ppm. **HRMS** (ESI+): calc. for $C_{20}H_{28}N_5O^+$ [M^+]: 354.2288; found: 354.2288. **IR** (ATR): 2912, 2117, 1688, 1547, 1503, 1293, 1252, 1035, 811 cm^{-1}. **EA**: calculated 61.61 %C, 7.24 %H, 17.96 %N. Found 59.47 %C, 7.06 %H, 18.00 %N.

Synthesis of *N*,*N*-dimethyl-*N*-(2-oxo-2-((4-(4-((2-((tritylamino)oxy)acetamido)methyl)-1,2,3-triazol-1-yl)phenyl)amino)ethyl)adamantanaminium chloride (10)

A mixture of DCM and H_2O (à 5 ml) was freeze-pump-thaw degassed (x3) and then azide **9** (129 mg, 0.33 mmol, 1 eq), alkyne **1** (135 mg, 0.33 mmol, 1 eq) and $CuBr{\cdot}SMe_2$ (21 mg, 0.1 mmol, 0.3 eq) were added. The suspension was stirred vigorously 5 h, at rt. The mixture was diluted with water (10 ml) and extracted with DCM (3 x 5 ml) then the organic phases were concentrated under reduced pressure and purified by column chromatography using a short plug of silica (DCM/MeOH/H_2O/7N NH_3 in methanol = 80:20:0.6:0.6). **10** was yielded as a brown solid (222 mg, 88%).

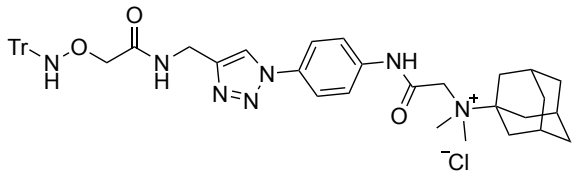

10

^{1}H-NMR (400 MHz, DMSO d_6): δ = 11.48 (s, 1H, NH), 8.56 (s, 1H, CH=C-N_3), 8.29 (s, 2H, NH), 7.88 (m, 4H, CH=C-N), 7.24 (m, 15H, Ar), 4.45 (d, *J* = 5.7 Hz, 2H, $CNHCH_2C{=}CH$), 4.28 (s, 2H, $CH_2N(CH_3)_2$), 3.84 (s, 2H, OCH_2), 3.16 (s, 6H, $N(CH_3)_2$), 2.28 (bb, 3H, CH), 2.10 (s, 6H, CH_2) 1.65 (s, 6H, CH_2) ppm. **^{13}C-NMR** (101 MHz, DMSO d_6): δ = 170 (C), 163 (C), 146 (C), 144 (C), 138 (C), 133 (C), 129-127 (CH), 121 (CH), 121 (CH), 76 (C) 74 ($2CH_2$), 58 (CH_2), 45 (CH_3), 35 (CH_2), 34 (CH_2), 30 (CH) ppm. **HRMS** (ESI+): calc. for $C_{44}H_{50}N_7O_3^+$ [M^+]: 724.3970; found: 724.3964. **IR** (ATR): 2913, 1666, 1517, 1445, 1258, 1032, 837, 757, 698 cm^{-1}. **EA**: calculated 69.50 %C, 6.63 %H, 12.89 %N. Found 65.85 %C, 6.32 %H, 11.51 %N.

Synthesis of *N*-(2-((4-(4-((2-(ammoniooxy)acetamido)methyl)-1,2,3-triazol-1-yl)phenyl)amino)-2-oxoethyl)-*N*,*N*-dimethyladamantanaminium formate (11)

Trityl protected compound **10** (198 mg, 0.26 mmol) was dissolved in DCM (5 ml) and then 6M HCl (5 ml) was added. The mixture was vigorously stirred at rt for 12 h. The aqueous phase was then extracted with DCM (5 x 10 ml) until TLC analysis of the organic phase fractions showed no UV absorption. The aqueous phase was removed under vacuum and 140 mg of the crude product were then

further purified by preparative HPLC (0% --> 30% buffer B) and yielded (80 mg, 0.14 mmol, 54%) of **11** as a light brown formate salt.

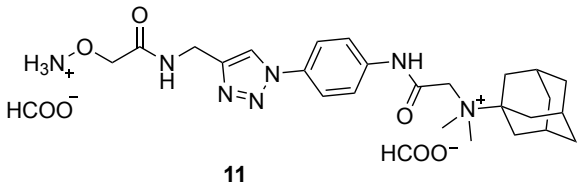

11

^{1}H-NMR (600 MHz, D_2O): δ = 8.40 (s, 2H, NH), 8.29 (s, 1H, CH=C-N_3), 7.69 (d, *J* = 9.0 Hz, 2H, CH=C-N), 7.61 (d, *J* = 9.0 Hz, 2H, CH=C-N_3), 4.57 (s, 2H, CNHCH_2C=CH), 4.23 (s, 2H, CH_2ON), 4.04 (s, 2H, NCOCH_2), 3.16 (s, 6H, N(CH_3)$_2$), 2.31 (s, 3H, CH), 2.08 (s, 6H, CH_2) 1.69 (m, 6H, CH_2) ppm. **^{13}C-NMR** (150 MHz, D_2O): δ = 173 (C), 171 (C), 164 (C), 145 (C), 137 (C), 133 (C), 122 (CH), 122 (CH), 122 (CH), 78 (C) 74 (CH_2), 58 (CH_2), 44 (CH_3), 34 (CH_2), 34 (CH_2), 34 (CH_2), 30 (CH) ppm. **HRMS** (ESI+): calc. for $C_{44}H_{62}N_7O_4^+$ [M^+]: 482.2869; found: 482.2875. **EA**: calculated 56.53 %C, 6.85 %H, 17.09 %N. Found 52.98 %C, 7.10 %H, 18.04 %N.

Synthesis of testosterone derivative (12)

Compound **11** (34.4 mg, 0.06 mmol) and testosterone (17.3 mg, 0.06 mmol) were dissolved in MeOH/water/ACN (4.5 ml, 1:1:1) containing 0.05% of formic acid. The solution was stirred at rt for 2 h. The solvent was then removed under vacuum. 35 mg of the crude product were then further purified by preparative HPLC (50% --> 100% buffer B) and yielded (15 mg, 31%) of **12** as the colorless formate salt.

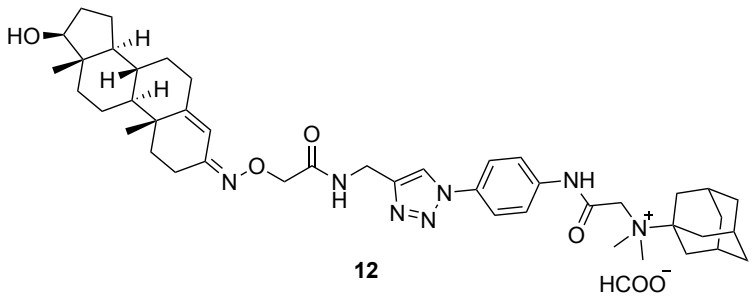

12

^{1}H-NMR (600 MHz, $CDCl_3$): δ = 12.60 (s, 1H, HCOOH), 8.52 (s, 1H, $HCOO^-$), 8.02 (d, *J* = 9.1 Hz, 2H, CH=C-N), 7.94 (s, 1H, C=C-N_3), 7.64 (d, *J* = 9.1 Hz, 2H, CH=C-N_3), 6.89 (s, 1H, NH), 5.71 (s, 1H, C=C-H), 4.65 (m, 2H, CONH-C*H*$_2$), 4.50 (m, 4H, C*H*$_2$-CO), 3.60 (s, 1H, C*H*-OH), 3.29 (s, 6H, N(CH_3)$_2$), 2.45 (s, 3H, CH), 2.29 (m, 2H, C=C-C*H*$_2$), 2.19 (s, 6H, CH_2), 2.05 (m, 2H, N=C-C*H*$_2$), 1.88-1.22 (m,

12H, ftes-CH_2), 1.77 (m, 6H, CH_2), 1.06 (d, *J* = 12.5 Hz, 3H, tes-CH_3), 0.95 (m, 3H, tes-CH), 0.76 (d, *J* = 11 Hz, 3H, tes-CH_3) ppm. **^{13}C-NMR** (150 MHz, $CDCl_3$): δ = 171 (C), 162 (C), 159 (C), 157 (C), 156 (C), 145 (C), 139 (C), 133 (C), 121 (ArH), 120 (CH), 116 (CH), 110 (CH), 82 (CH), 78 (C), 73 (CH_2), 59 (CH_2), 54 (CH), 50 (CH), 44 ($N(CH_3)_2$), 43, (C), 35 (CH_2), 35 (Ad-CH_2), 34 (Ad-CH_2), 31 (Ad-CH), 18 (Tes-CH_3), 11 (Tes-CH_3) ppm. **HRMS** (ESI+): calc. for $C_{44}H_{62}N_7O_4^+$ [M^+]: 752.4858; found: 752.4855. **EA**: calculated 67.73 %C, 7.96 %H, 12.29 %N. Found 62.44 %C, 7.98 %H, 11.45 %N.

IV.4.3.3. Preparation of reagent 15

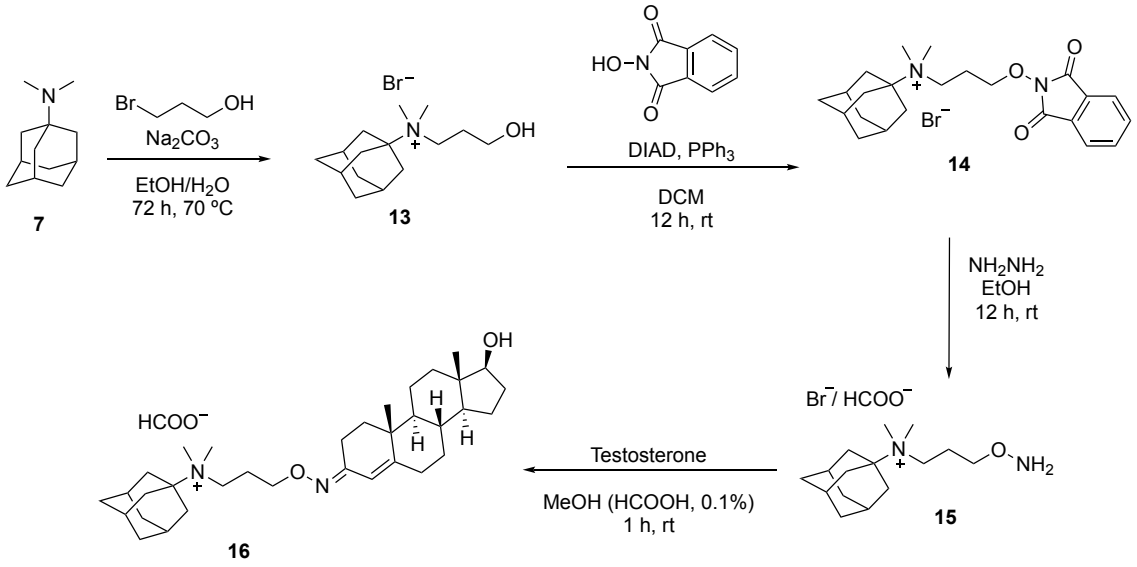

Synthesis of *N*-(1-adamantyl)-*N,N*-dimethyl-3-hydroxypropanaminium bromide (13)

Under strong agitation, 3-bromopropanol (559 µl, 6 mmol), sodium carbonate (954 mg, 9 mmol) and *N,N*-dimethyl-1-adamantylamine, **7**, (813 mg, 4.4 mmol) were added to a mixture of 6 ml ethanol and 1.6 ml water. The mixture was stirred at 70 °C for 72 h. After cooling down to room temperature, the suspension was filtered, washed with ethanol and after evaporation of the filtrate, the solid was dissolved with DCM (25 ml). The filtrate was evaporated and the product was rinsed with EtOAc (10 ml) to afford the title compound (919 mg, 66%) as a white solid (95% pure, measured with dimethyl sulfone as IS).

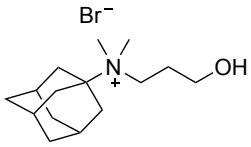

13

^{1}H-NMR (400 MHz, D_2O): δ = 3.67 (m, 2H, CH_2), 3.30 (m, 2H, CH_2), 2.85 (s, 6H, CH_3), 2.32 (s, 3H, CH), 2.06 (s, 6H, CH_2), 1.99 (m, 2H, CH_2) 1.68 (m, 6H, CH_2) ppm. **^{13}C-NMR** (101 MHz, D_2O): δ = 76 (C), 59 (CH_2), 55 (CH_2), 43 (CH_3), 35 (CH_2), 34 (CH_2), 30 (CH), 25 (CH_2) ppm. **IR** (ATR): 3288, 2911, 2852, 1487, 1451, 1371, 1306, 1050, 1036, 918, 827 cm^{-1}. **HRMS** (ESI+): calc. for $C_{15}H_{28}NO^+$ [M^+]: 238.2165; found: 238.2164 **EA**: calculated 56.60 %C, 8.87 %H, 4.40 %N. Found 55.22 %C, 8.83 %H, 4.15 %N.

Synthesis of *N*-(1-adamantyl)-*N,N*-dimethyl-3-(1,3-dioxoisoindolin-2-yl)oxypropanaminium bromide (14)

To a solution of alcohol **13** (335 mg, 1 mmol), *N*-hydroxyphthalimide (269 mg 1.26 mmol) and triphenylphosphine (442 mg, 1.6 mmol) in CH_2Cl_2 (5 ml) at rt was added DIAD (0.32 ml, 1.6 mmol). After stirring for 12 h at rt, the solvents were removed by rotary evaporation. The crude residue was diluted with water (25 ml) and extracted with ethyl acetate (2 x 20 ml). The aqueous solution was evaporated and the crude, phthalimide intermediate, **14**, was used directly in the next step. (400 mg, 86%).

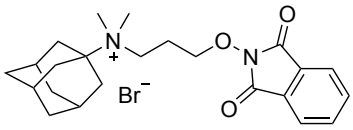

14

^{1}H-NMR (400 MHz, $CDCl_3$): δ = 7.85-7.75 (m, 4H, Ph), 4.44 (m, 2H, OCH_2), 3.88 (m, 2H, NCH_2), 3.15 (s, 6H, $N(CH_3)_2$), 2.45 (m, 2H, C-CH_2-C), 2.41 (s, 3H, CH), 2.20 (s, 6H, CH_2) 1.73 (s, 6H, CH_2) ppm. **^{13}C-NMR** (101 MHz, $CDCl_3$): δ = 164 (2C), 135 (2CH), 129 (2C), 124 (2CH), 77 (C), 76 (CH_2), 55 (CH_2), 44 ($2CH_3$), 35 (CH_2), 35 (CH_2), 30 (CH), 23 (CH_2) ppm. **IR** (ATR): 3289, 2912, 1728, 1448, 1371, 1185, 1062, 1035, 876, 655 cm^{-1}. **HRMS** (ESI+): calc. for $C_{23}H_{31}N_2O3^+$ [M^+]: 383.2329; found: 383.2326. **EA**: calculated 59.61 %C, 6.74 %H, 6.05 %N. Found 54.87 %C, 7.04 %H, 5.69 %N.

Synthesis of *N*-(1-adamantyl)-*N,N*-dimethyl-3-(aminooxy)propanaminium formate (15)

To the phthalimide protected salt **14** (301 mg, 0.65 mmol) in ethanol, hydrazine monohydrate (215 ul, 3.80 mmol) was added. The reaction was stirred 6 h at 50 °C. The ethanol was then removed by rotary evaporation and DCM was added (4 ml). The resulting white precipitate was filtered over a Buchner funnel and washed with DCM. The filtrate was dried by rotary evaporation to afford 247 mg of the product. 48 mg of the crude product were further purified by preparative HPLC to afford (12 mg, 0.04 mmol, 29%) of the formate salt.

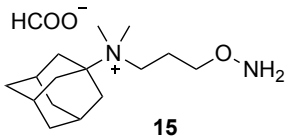

15

^{1}H-NMR (400 MHz, DMSO d_6): δ = 8.45 (s, 1H, HCOO), 3.60 (t, 2H, *J* = 5.8, OCH_2), 3.22 (m, 2H, NCH_2), 2.82 (s, 6H, $N(CH_3)_2$), 2.23 (s, 3H, CH), 2.02 (s, 6H, CH_2), 1.97 (m, 2H, C-CH_2-C), 1.63 (s, 6H, CH_2) ppm. **^{13}C-NMR** (101 MHz, DMSO d_6): δ = 165 (C), 74 (C), 71 (CH_2), 55 (CH_2), 43 ($2CH_3$), 35 (CH_2), 34 (CH_2), 30 (CH), 22 (CH_2) ppm. **HRMS** (ESI+): calc. for $C_{15}H_{29}N_2O^+$ [M^+]: 253.2274; found: 253.2274.

Synthesis of testosterone derivative (16)

Compound **15** (4 mg, 15 µmol) and testosterone (3 mg, 11 µmol) were dissolved in 1 ml of MeOH and HCOOH (0.1%). The solution was stirred at rt for 1h. The solvent was then removed in vacuo. The crude product was purified by preparative HPLC (50% --> 100% buffer B) and yielded (3 mg, 51%) of the testosterone derivative as a white formate salt.

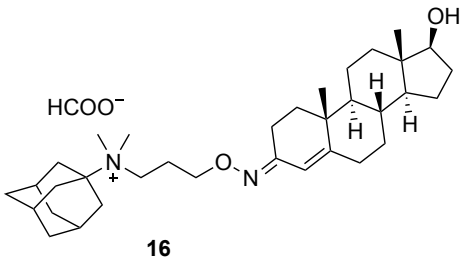

16

HRMS (ESI+): calc. for $C_{34}H_{55}N_2O_2^+$ [M^+]: 523.4258; found:523.4255.

IV.4.4. Determination of Affinity Constant (K_a)

Binding studies have been done following procedures reported in the literature in order to have comparable results on the binding constants.[2]

Affinity Constant of reagent 6:

Preparation of a set of stock solutions

Deuterated sodium acetate buffer solution (50 mM) was prepared in D_2O (pH = 4.75). Then, stock solutions of the reagents were prepared: 2.52 mM **CB7** was prepared by dissolving (10.1 mg, 87%) in 3 ml of buffer; 6.73 mM **17** was prepared by dissolving 7.2 mg in 6 ml of the buffer; 63.33 mM **6** was prepared by adding 15.96 mg in 0.4 ml of the buffer.

Example of experimental part

A 0.7 ml solution containing **CB7** (290 µM, 80.6 µl), **17** (490 µM, 50.9 µl) and **6** (22.26 mM, 245.5 µl) was stirred and allowed to reach equilibrium. Next, the relative concentrations of **17** and **CB7·17** were determined by the integration of the appropriate resonances in the ^{1}H NMR spectrum (**17**: -0.17 ppm; **CB7·17**: -0.93 ppm). The relative concentrations and the mass balance expression (equation 2) allowed us to calculate [**17**]$_{free}$ = 308 µM and [**CB7·17**] = 182 µM. Equation 3 is then used to calculate [**CB7·6**] (108 µM) using the known value of **CB7·17**. Finally, equation 4 is used to calculate [**6**]$_{free}$ (22.15 mM) using the known value of [**CB7·6**].

$$K_{rel} = ([CB7{\cdot}17][6]_{free}) / ([CB7{\cdot}6][17]_{free}) \quad (1)$$

$$[17]_{Total} = 490\ \mu M = [17]_{free} + [CB7{\cdot}17] \quad (2)$$

$$[CB7]_{Total} = 290\ \mu M = [CB7{\cdot}17] + [CB7{\cdot}6] \quad (3)$$

$$[4]_{Total} = 22.26\ mM = [6]_{free} + [CB7{\cdot}6] \quad (4)$$

$$K_{CB7\cdot17} = 1.80 \times 10^7\ M^{-1} = (K_{CB7\cdot6})(K_{rel}) \quad (5)$$

$$\left(\frac{\sigma K_{\mathbf{CB7\cdot6}}}{K_{\mathbf{CB7\cdot6}}}\right)^2 = \left(\frac{\sigma K_{\mathbf{CB7\cdot17}}}{K_{\mathbf{CB7\cdot17}}}\right)^2 + \left(\frac{\sigma K_{\mathbf{rel}}}{K_{\mathbf{rel}}}\right)^2 \quad (6)$$

$$\frac{\sigma K_{\mathbf{CB7\cdot6}}}{K_{\mathbf{CB7\cdot6}}} = \sqrt[2]{0.1246^2 + 0.10^2} = 0.1598 \quad (15.98\ \%) \quad (7)$$

Substitution of the values of [**CB7·17**], [**17**]$_{free}$, [**CB7·6**], and [**6**]$_{free}$ into equation 1 gave K_{rel} = 120.85. These determinations were done in triplicate from independently prepared stock solutions and the average value (K_{rel} = 115.23) was used in the calculations of K_a (equation 5) and the error analysis from equation 6. The solutions for the above determinations were prepared with a small excess of **17** (to ensure there is no free **CB7**) and a large excess of **6**; under those conditions the errors in [**6**]$_{free}$, [**17**]$_{free}$ are small and both [**17**] and [**CB7·17**] are kept in a good range for accurate measurement of their ratio by ^{1}H NMR. The percent error in K_a (equation 7) was measured as a function of the uncertainty in K_{rel} (standardized as a more conservative 10% error) and the propagated uncertainty reported for $K_{[\mathbf{CB7\cdot 17}]}$ (12.46% error).[2]

K_a = 1.80 x10^7 M^{-1}/115.23 = 1.56 x10^5 M^{-1}

$\sigma K_{\mathbf{CB7\cdot 6}} = 0.1598\ x\ 1.56\ x10^5\ M^{-1} = 0.25\ x10^5\ M^{-1}$

K_a = 1.56 ± 0.25 x10^5 M^{-1}

From bottom to top: ^{1}H NMR spectra of **17**; **CB7** with >1eq of **17**; and **CB7** with <1 eq of **17**

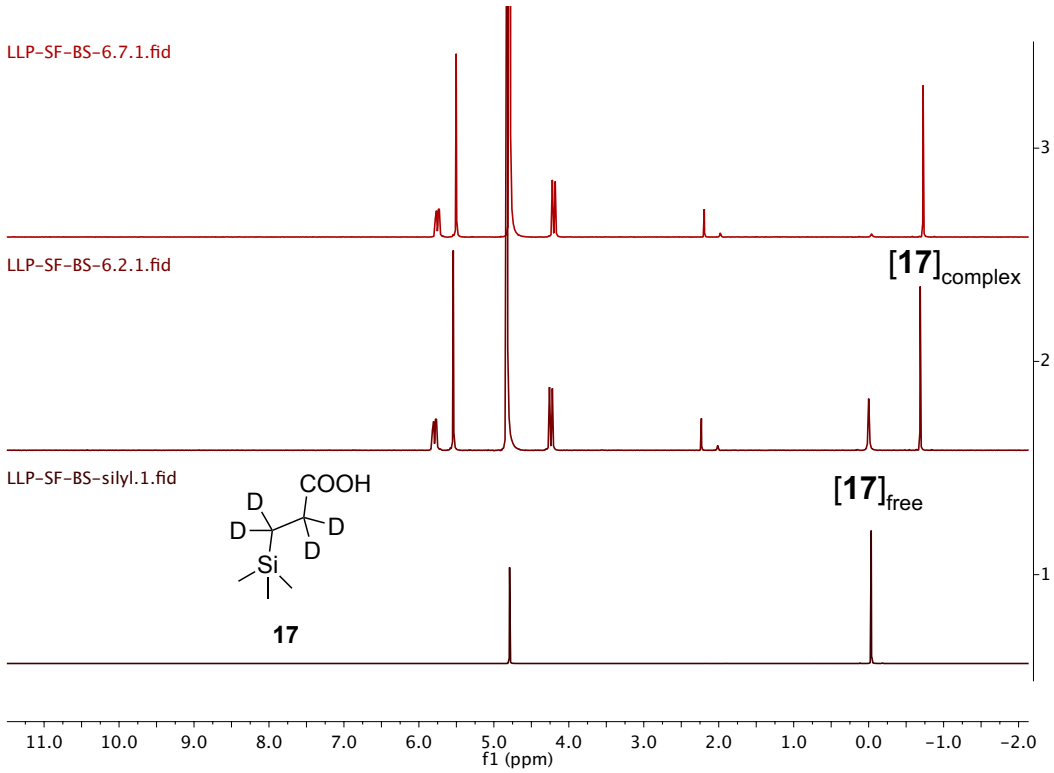

Affinity Constant of reagent 11:

Preparation of a set of stock solutions

2.85 mM **CB7** was prepared by dissolving (14.72 mg, 87%) in 4 ml of buffer; 15.98 mM **18** was prepared by dissolving 11.52 mg in 5 ml of the buffer; 6.38, mM **11** was prepared by adding 10.80 mg in 3 ml of the buffer.

Example of experimental part

A 0.7 ml solution containing **CB7** (0.5 mM, 122.7 µl), **18** (2.6 mM, 113.9 µl) and **11** (0,6 mM, 65.8 µl) was stirred and allowed to reach equilibrium. Next, the relative concentrations of **11** and **CB7·11** were determined by integration of the appropriate resonances in the ^{1}H NMR spectrum (**11**: 3.20 ppm; CB7·**11**: 3.10 ppm). The relative concentrations and the mass balance expression (equation 11) allowed to calculate [**11**]$_{free}$ = 346 µM and [**CB7·11**] = 254 µM. Equation 10 is then used to calculate [**CB7·18**] (246 µM) using the known value of **CB7·11**. Finally, equation 9 is used to calculate [**18**]$_{free}$ (2.35 mM) using the known value of [**CB7·18**].

$$K_{rel} = ([CB7\cdot 11][18]_{free}) / ([CB7\cdot 18][11]_{free}) \quad (\mathbf{8})$$

$$[18]_{Total} = 2.6\ mM = [18]_{free} + [CB7\cdot 18] \quad (\mathbf{9})$$

$$[CB7]_{Total} = 0.5\ mM = [CB7\cdot 18] + [CB7\cdot 11] \quad (\mathbf{10})$$

$$[11]_{Total} = 0.6\ mM = [11]_{free} + [CB7\cdot 11] \quad (\mathbf{11})$$

$$K_{CB7\cdot 18} = 4.23 \times 10^{12}\ M^{-1} = (K_{CB7\cdot 11})/(K_{rel}) \quad (\mathbf{12})$$

$$\left(\frac{\sigma K_{\mathbf{CB7\cdot 11}}}{K_{\mathbf{CB7\cdot 11}}}\right)^2 = \left(\frac{\sigma K_{\mathbf{CB7\cdot 18}}}{K_{\mathbf{CB7\cdot 18}}}\right)^2 + \left(\frac{\sigma K_{\mathbf{rel}}}{K_{\mathbf{rel}}}\right)^2 \quad (\mathbf{13})$$

$$\frac{\sigma K_{\mathbf{CB7\cdot 11}}}{K_{\mathbf{CB7\cdot 11}}} = \sqrt[2]{0.2355^2 + 0.10^2} = 0.2559 \quad (25.59\ \%) \quad (\mathbf{14})$$

Substitution of the values of [**CB7·11**], [**11**]$_{free}$, [**CB7·18**], and [**18**]$_{free}$ into equation 8 gave K_{rel} = 7.00. These determinations were done in triplicate from independently prepared stock solutions and the average value (K_{rel} = 6.90) was used in the calculations of K_a (equation 12) and the error analysis from equation 13. The solutions for the above determinations were prepared with a small excess of **11** (to ensure there is no free **CB7**) and a larger excess of **18**; under those conditions the errors in [**11**]$_{free}$, [**18**]$_{free}$ are small and both [**11**] and [**CB7·11**] are

kept in a good range for accurate measurement of their ratio by ^{1}H NMR. The percent error in K_a (equation 14) was measured as a function of the uncertainty in K_{rel} (standardized as a more conservative 10% error) and the propagated uncertainty reported for $K_{[\mathbf{CB7\cdot 18}]}$ (23.55% error).[2]

K_a =4.23 x10^{12} M^{-1} x 6.90 = 2.92 x10^{13} M^{-1}

$\sigma K_{\mathbf{CB7\cdot 11}} = 0.2559\ x\ 2.92\ x10^{13}\ M^{-1} = 0.75\ x10^{13}\ M^{-1}$

K_a = 2.92 ± 0.75 ×10^{13} M^{-1}

From top to bottom: ^{1}H NMR spectra of **11**; **CB7** with <1eq of **11**; and **CB7** with >1 eq of **11**

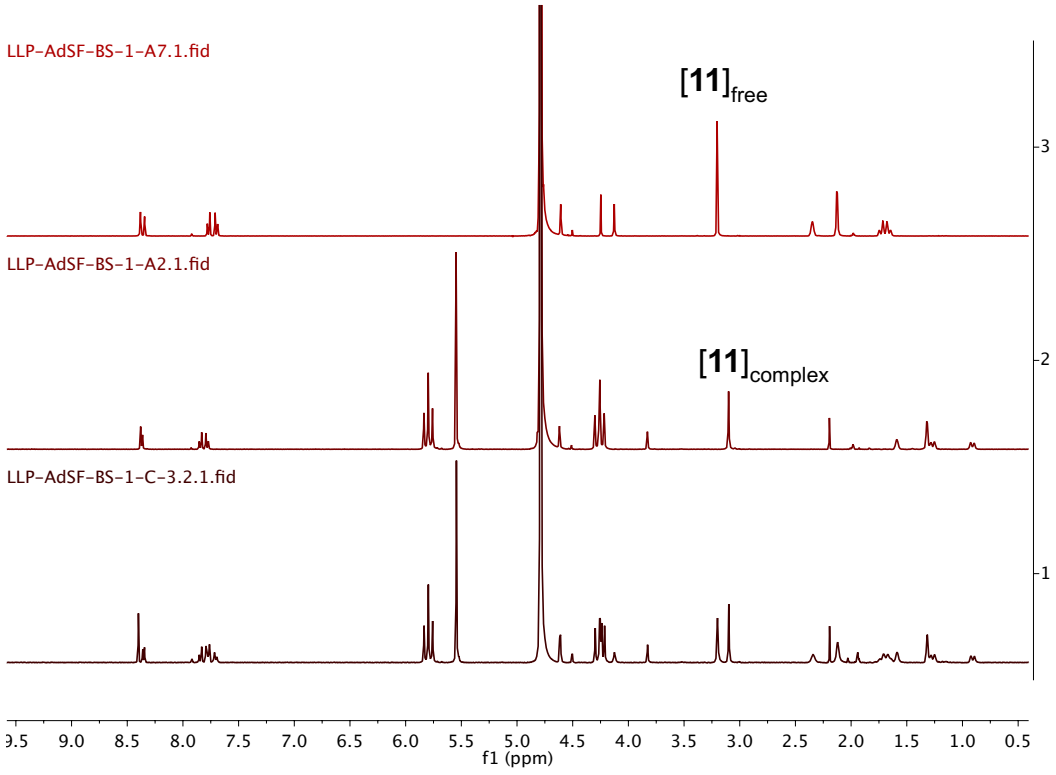

^{1}H NMR spectra of **11**, **CB7**, and **18** after equilibrium

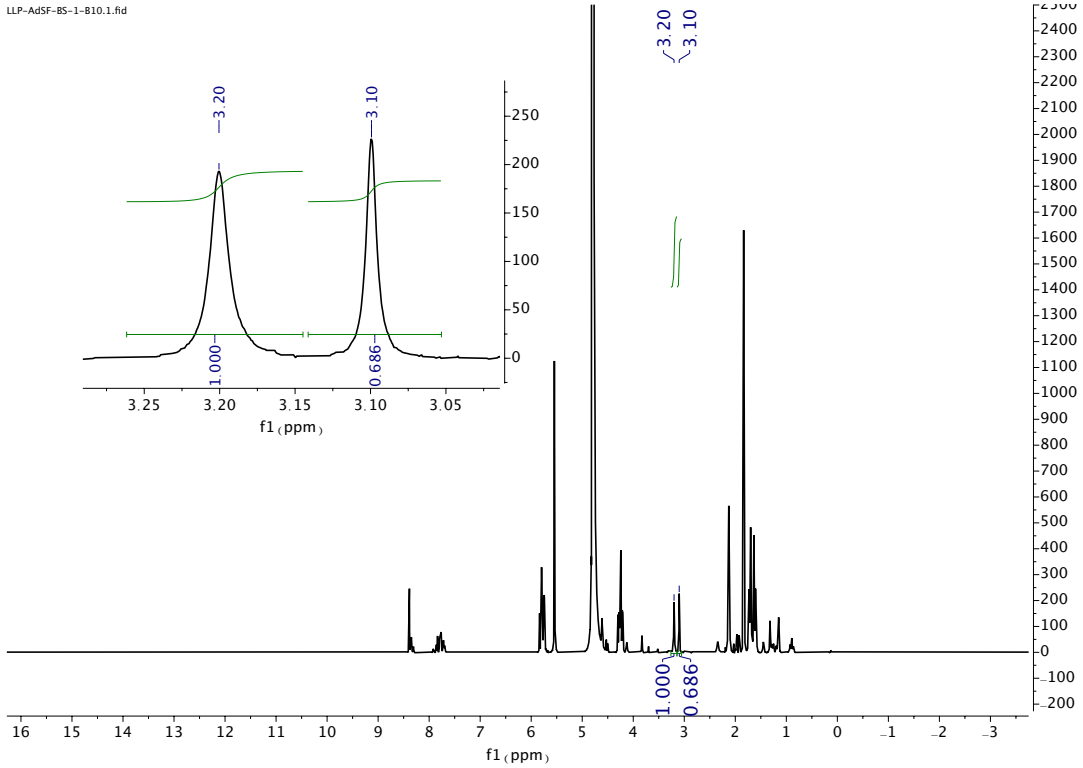

Affinity Constant of reagent 15:

Preparation of a set of stock solutions

4.56 mM **CB7** was prepared by dissolving (8.8 mg, 87%) in 1.5 ml of buffer; 23.36 mM **15** was prepared by dissolving 47.1 mg in 5 ml of the buffer; 18.10, mM **18** was prepared by adding 10.6 mg in 4 ml of the buffer.

Example of experimental part

A 0.7 ml solution containing **CB7** (1.3 mM, 199.4 µl), **18** (2 mM, 77.3 µl) and **15** (3 mM, 89.9 µl) was stirred and allowed to reach equilibrium. Next, the relative concentrations of **15** and **CB7·15** were determined by integration of the appropriate resonances in the ^{1}H NMR spectrum (**15**: 2.89 ppm; **CB7·15**: 2.78 ppm). The relative concentrations and the mass balance expression (equation 18) allowed to calculate $[\mathbf{15}]_{free}$ = 2.34 mM and [**CB7·15**] = 658 µM. Equation 17 is then used to calculate [**CB7·18**] (642 µM) using the known value of **CB7·15**. Finally, equation 16 is used to calculate $[\mathbf{18}]_{free}$ (1.36 mM) using the known value of [**CB7·18**].

K_{rel} = ([CB7·15][18]$_{free}$) / ([CB7·18][15]$_{free}$) (**15**)

[18]$_{Total}$ = 2.0 mM = [18]$_{free}$ + [CB7·18] (**16**)

[CB7]$_{Total}$ = 1.3 mM = [CB7·18] + [CB7·15] (**17**)

[15]$_{Total}$ = 3 mM = [15]$_{free}$ + [CB7·15] (**18**)

$K_{CB7·18}$ = 4.23 x10^{12} M^{-1} = ($K_{CB7·15}$)/(K_{rel}) (**19**)

$$\left(\frac{\sigma K_{\mathbf{CB7\cdot 15}}}{K_{\mathbf{CB7\cdot 15}}}\right)^2 = \left(\frac{\sigma K_{\mathbf{CB7\cdot 18}}}{K_{\mathbf{CB7\cdot 18}}}\right)^2 + \left(\frac{\sigma K_{\mathbf{rel}}}{K_{\mathbf{rel}}}\right)^2 \quad (\mathbf{20})$$

$$\frac{\sigma \mathrm{K}_{\mathbf{CB7\cdot 15}}}{\mathrm{K}_{\mathbf{CB7\cdot 15}}} = \sqrt[2]{0.2355^2 + 0.10^2} = 0.2559 \quad (25.59\ \%) \quad (\mathbf{21})$$

Substitution of the values of [**CB7·15**], [**15**]$_{free}$, [**CB7·18**], and [**18**]$_{free}$ into equation 15 gave K_{rel} = 0.60. These determinations were done in triplicate from independently prepared stock solutions and the average values were used in the calculations of K_a (equation 19) and the error analysis from equation 20. The solutions for the above determinations were prepared with a small excess of **18** (to ensure there is no free **CB7**) and a larger excess of **15**; under those conditions the errors in [**15**]$_{free}$, [**18**]$_{free}$ are small and both [**15**] and [**CB7·15**] are kept in a good range for accurate measurement of their ratio by ^{1}H NMR. The percent error in K_a (equation 21) was measured as a function of the uncertainty in K_{rel} (standardized as a more conservative 10% error) and the propagated uncertainty reported for $K_{[\mathbf{CB7\cdot 18}]}$ (23.55% error).[2]

K_a =4.23 x10^{12} M^{-1} x 0.60 = 2.56 x10^{12} M^{-1}

$\sigma \mathrm{K}_{\mathbf{CB7\cdot 11}} = 0.2559\ x\ 2.56\ x10^{12}\ M^{-1} = 0.66\ x10^{12}\ M^{-1}$

K_a = 2.56 ± 0.66 ×10^{12} M^{-1}

From top to bottom: ^{1}H NMR spectra of **15**; **CB7** with <1eq of **15**; and **CB7** with >1 eq of **15**

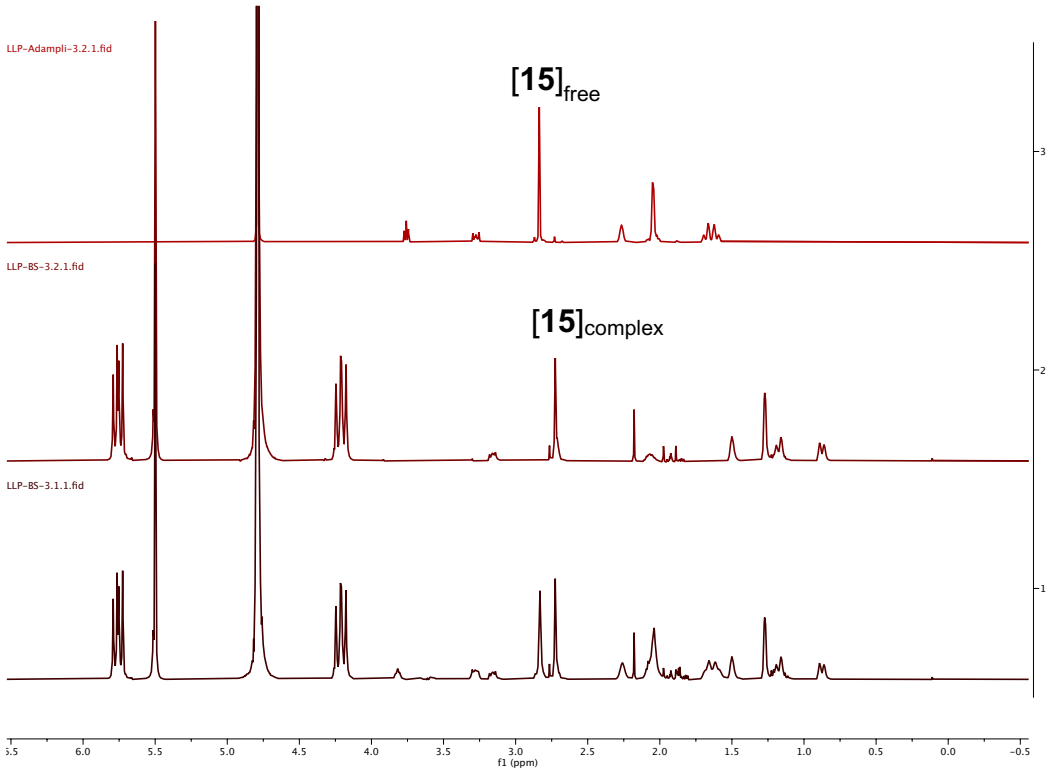

^{1}H NMR spectra of **15**, **CB7**, and **18** after equilibrium

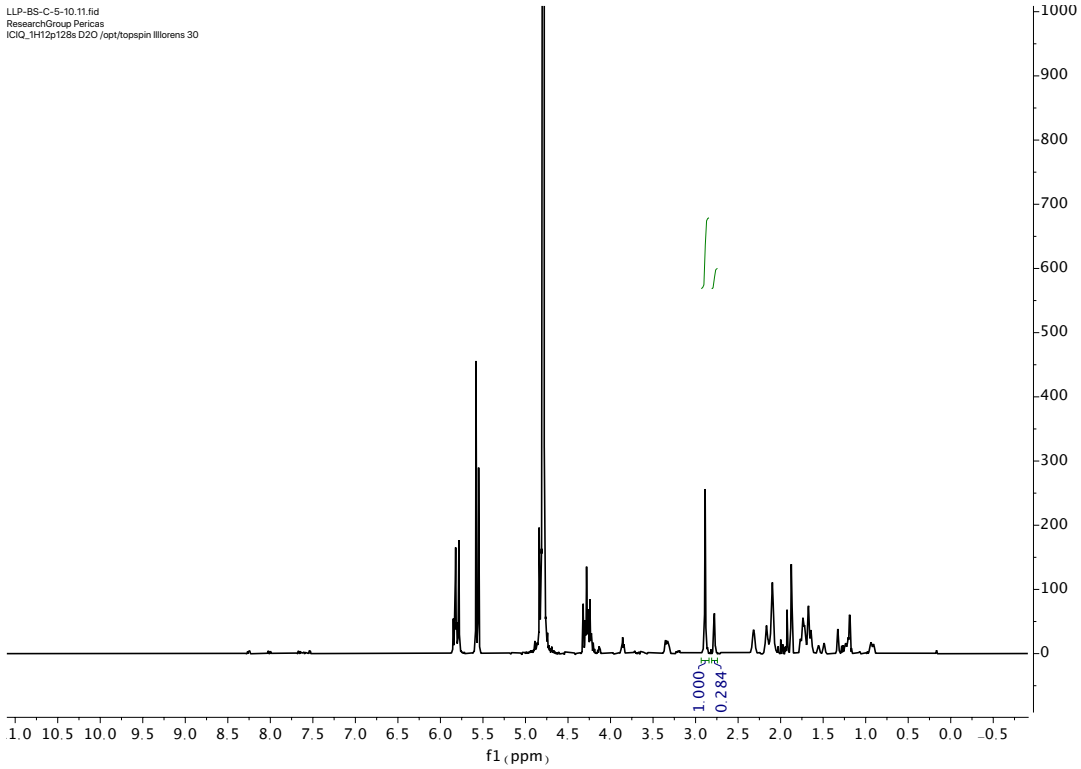

IV.4.5. Testosterone Extraction

IV.4.5.1. Adsorption/Desorption of testosterone derivatives

Adsorption of testosterone derivative, 12 from MNPs-CB7

A 120 µM solution of **MNPs-CB7** (315 µg, *f* = 0.15 mmol·g^{-1}) was prepared by addition of a 4.4 µM solution of **12** in the corresponding solvent of study (400 µl). Then, the mixture was warmed up to 50 ºC and shaken in the thermomixer at 1200 rpm for 2 h. After centrifugation and magnetic decantation, 40 µl of the solution were evaporated and dissolved in 40 µl of water and acetonitrile 1:1. Then, the solution was analyzed by mass spectrometry and the adsorption of **12** was determined as positive (by the absence of signalling at m/z = 752.48) or negative.

Table S1: Adsorption of **12** in **MNPs-CB7**[a]

H_2O	H_2O/ACN 2:1	H_2O/ACN 1:1	H_2O/ACN 1:2	ACN	MeOH	$CHCl_3$
+	+	+	-	-	-	-

[a]Conditions: **MNPs-CB7** (120 µM). **12** (4.4 µM). +: the concentration of **12** in the remaining solution was not high enough for the ESI-MS to detect a clear signal on the mass spectrum. -: the concentration of **12** in the remaining solution was sufficient to observe a clear signal (intensity of the peak corresponding to **12** was at least >3 times the intensity of noise).

Desorption of testosterone derivative, 12 from MNPs-CB7

0.34 mM solution of **12** in water (400 µl) was added to 315 µg of **MNPs-CB7** (*f* = 0.15 mmol·g^{-1}). The mixture was warmed up to 50 ºC and shaken in the thermomixer at 1200 rpm for 2 h. After centrifugation and magnetic decantation, the loaded **MNPs-CB7** were rinsed with additional water (2 x 200 µl). The corresponding desorption solvent (500 µl) was subsequently added, and the mixture was first shaken for 2 h at 50 ºC and then separated from the nanoparticles and analyzed by mass spectrometry. Finally, the extraction with the desorption solvent was repeated one more time. The solution was analysed by mass spectrometry and the desorption of **12** was determined as positive (by the presence of signalling at m/z = 752.48) or negative.

Table S2: Desorption of **12** from **MNPs-CB7**[a]

Addition	H_2O	MeOH	ACN	$CHCl_3$	DCM	EtOH	EtOAc	DMF	DMSO
none	-	-	-	-	-	-	-	-	-
a. 50% $CHCl_3$		-	-			-			
b. NH_4^+ $HCOO^-$ >40 eq (4 mM)		+	+	+	+				
a and b		+	+						
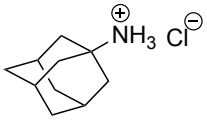 >10 eq	+								

[a]Conditions: **MNPs-CB7** (0.12 mM). **12** (0.34 mM). +: the concentration of **12** in the remaining solution was high enough for the ESI-MS to detect a clear signal on the mass spectrum (intensity of the peak corresponding to **12** was at least >3 times the intensity of noise). -: the concentration of **12** in the remaining solution was not sufficient to observe a clear signal. Blank: not determined.

IV.4.5.2. Recycling experiments of MNPs-CB7

Table S3: Recycling experiments[a]

Entry	Adsorption[b]	Desorption[c]
1	4.564	2.474
2	4.564	4.972
3	4.564	5.876
4	4.564	4.525
5	4.323	2.185
6	4.323	6.153

[a]Conditions: **MNPs-CB7** (315 µg). **12** (0.15 mM). water (300 µl).[b] Area of peak. Determined by comparing the HPLC chromatogram of the mixture before and after adsorption of **12**.[c] Area of peak. Determined by measuring the area of the corresponding peak after desorption of **12**.

For the first cycle, **12** (300 µl, solution 0.15 mM in water) was added to **MNPs-CB7** (315 µg, f = 0.15 mmol·g^{-1}) and the mixture was stirred at 50 ºC for 1.5 h. The nanoparticles were filtered off and washed with additional water (2 x 200 µl) before treatment with the desorption solvent, which was subsequently added

(800 ul, NH_4^+ $HCOO^-$ 4 mM in MeOH/$CHCl_3$ 1:1). The mixture was stirred at 50 ºC for 1.5 h whereupon the magnetic beads were filtered off and reused for the next cycle. Then, previous to the fifth cycle, the magnetic beads were rinsed with additional desorption solvent (2 x 1 ml), methanol (1 ml) and water (1 ml).

IV.4.5.3. Extraction of testosterone derivatives

Extraction of testosterone from solution after derivatization

5 mg of **11** and 5 mg of testosterone were dissolved in 200 µl H_2O, 200 µl ACN and 100 µl MeOH with 0.4% HCOOH. The solution was stirred for 1 h, at rt. After that, 20 ul were added to a mixture of 2.5 mg of **MNPs-CB7** (f = 0.15 mmol·g^{-1}) in 220 µl water/ACN 1:1. After 1.5 h stirring at 50 ºC, the magnetic nanoparticles were collected and mixed with the desorption solvent (500 µl, 4 mM NH_4^+ $HCOO^-$ in MeOH/$CHCl_3$ 1:1) and stirred at 50 ºC for 1.5 h.

HPLC Chromatogram after 5 min of reaction

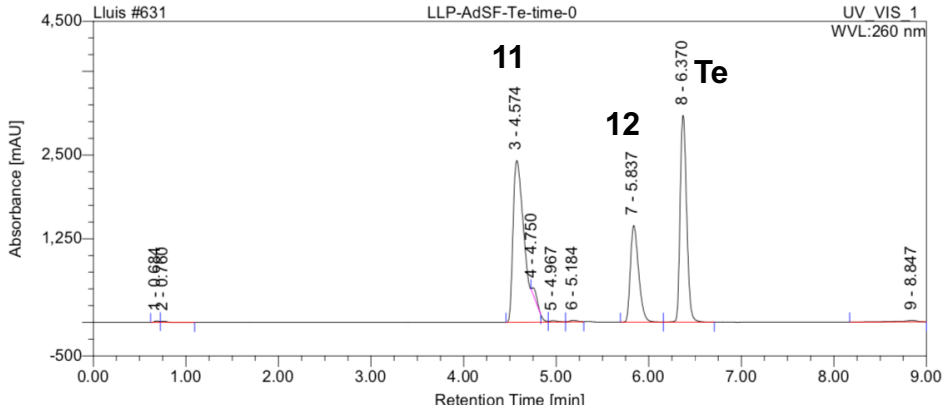

HPLC Chromatogram after 60 min of reaction

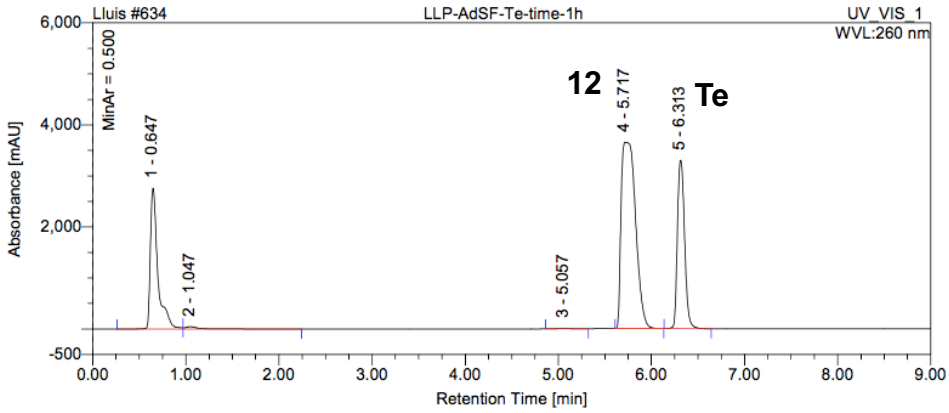

HPLC Chromatogram after desorption

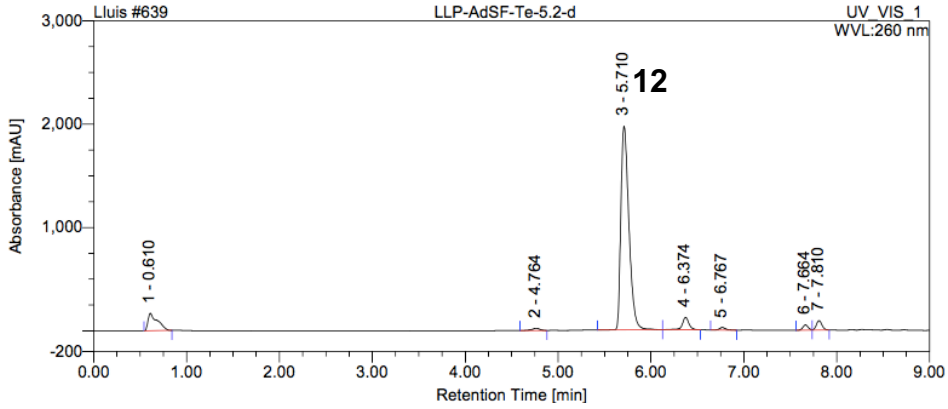

Extraction of testosterone from a complex mixture

A mixture of Cytidine, L-tryptophan benzyl ester, **12** and testosterone (*ca.* 0.05 – 0.5 mM) was stirred with **MNPs-CB7** (120 µg, f = 0.15 mmol·g^{-1}) and analyzed by HPLC-MS after extraction. Then, the MNPs were mixed with the desorption solvent (4 mM NH_4^+ $HCOO^-$ in MeOH/$CHCl_3$ 1:1) and the solution was subsequently analyzed on the HPLC-MS.

HPLC Chromatogram of the starting mixture

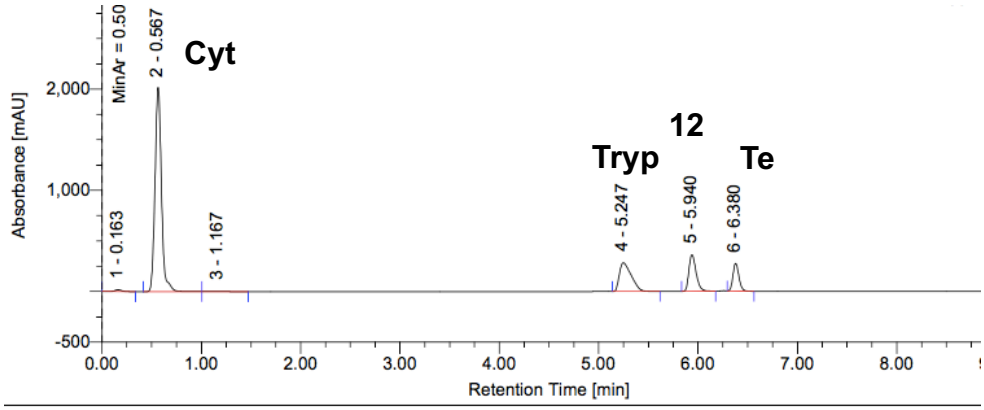

No.	Ret.Time (detect	Area	Rel.Area	Height
	min	mAU*min	%	mAU
n.a.	n.a.	n.a.	n.a.	n.a.
1	0.16	1.361	0.56	16.682
2	0.57	152.785	62.85	2015.642
3	1.17	0.572	0.24	3.034
4	5.25	39.216	16.13	282.285
5	5.94	30.339	12.48	360.105
6	6.38	18.828	7.74	273.551

HPLC Chromatogram after adsorption of **12**

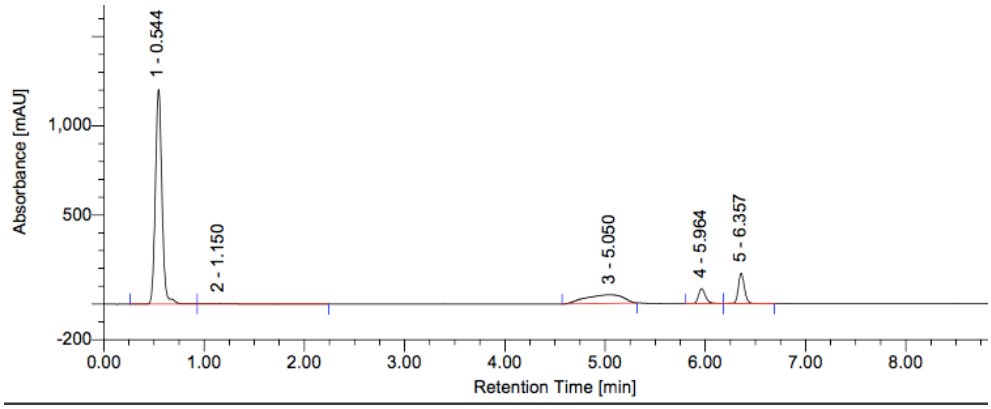

No.	Ret.Time (detect	Area	Rel.Area	Height
	min	mAU*min	%	mAU
n.a.	n.a.	n.a.	n.a.	n.a.
1	0.54	91.821	69.07	1202.908
2	1.15	0.583	0.44	1.950
3	5.05	21.164	15.92	48.463
4	5.96	7.054	5.31	85.082
5	6.36	12.310	9.26	170.879

HPLC Chromatogram after desorption of **12**

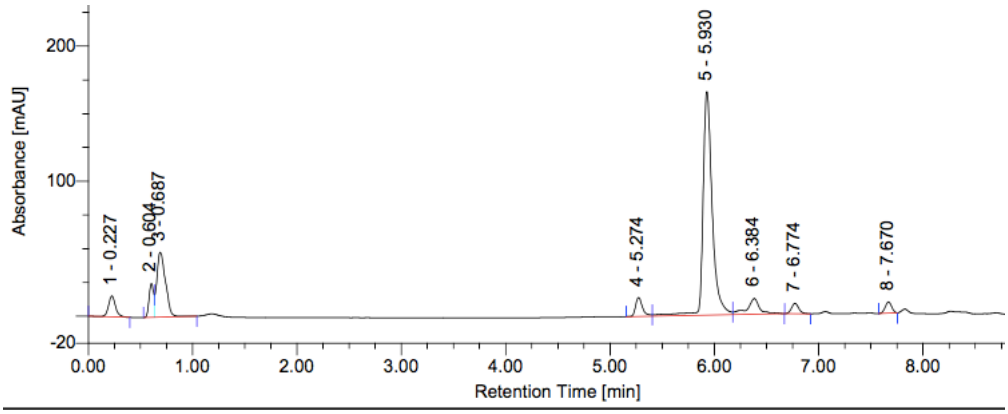

No.	Ret.Time (detect	Area	Rel.Area	Height
	min	mAU*min	%	mAU
n.a.	n.a.	n.a.	n.a.	n.a.
1	0.23	1.223	4.40	15.497
2	0.60	1.231	4.43	25.018
3	0.69	4.647	16.71	47.963
4	5.27	1.072	3.86	13.948
5	5.93	16.784	60.37	165.506
6	6.38	1.626	5.85	11.658

IV.4.5.4. Serum samples

Protocols for the extraction of testosterone from serum samples

Protocol 1:

Add 50 µl of vortexed serum sample to a centrifuge tube.
Add 20 µl of IS (^{13}C3Te, 10 ng/ml).
Keep at <10 ºC for 30 min.
Add 200 µl MeOH and vortex the sample.
Cool at <10 ºC for 30 min to help precipitate proteins.
Spin at 20,000 rcf for 10 min at <10 ºC to pellet the proteins.
Transfer 200 µl of supernatant and dehydrate it using SpeedVac.
Derivatize the samples by adding 20 µl of reagent (4 mg/ml, 0.268 µmol).
Incubate at rt for 60 min.
Evaporate in SpeedVac.
Add MNPs (1.2 mg, 400 µl water).
Incubate at 50 ºC for 60 min.
Centrifuge, separate the supernatant and lyophilize (samples for **adsorption**).
Treat the remaining MNPs with desorption solvent (400 µl).
Incubate at 50 ºC for 120 min.
Centrifuge, separate the supernatant, evaporate the solvent and lyophilize (samples for **desorption**).

Analysis: dissolve the samples in W/ACN 1:1 and load into auto sampler.
IS: stock solution, 10 ng/ml in W/ACN 1:1.
Derivatizing reagent: 4 mg/ml in MeOH, 5% HCOOH (0.268 µmol of reagent).
MNPs: 1.2 mg, functionalization: 0.33 mmol/g (0.396 µmol of CBs).
Desorption solvent:

- 7,8 mM NH_4^+ $HCOO^-$ in MeOH/$CHCl_3$ 1:1, 0.1%(v/v) HCOOH.
- **18** dissolved in water: A) 0.727 µmol, 2.7 eq; B) 1.455 µmol, 5.4 eq.

Protocol 2:

Add 200 µl of vortexed serum sample to a SLE+ column.
Extract to a centrifuge tube using 1.3 ml of DIPE and evaporate the solvent.
Spike 20 µl of IS (^{13}C3Te, 10 ng/ml).
Derivatize the samples by adding 20 µl of reagent (4 mg/ml, 0.268 µmol).
Incubate at rt for 60 min.
Evaporate in SpeedVac.
Add MNPs (1.2 mg, 400 µl water).
Incubate at 50 ºC for 60 min.
Centrifuge, separate the supernatant and lyophilize (samples for **adsorption**).
Treat the remaining MNPs with desorption solvent (400 µl).
Incubate at 50 ºC for 120 min.
Centrifuge, separate the supernatant, evaporate the solvent and lyophilize (samples for **desorption**).

Analysis: dissolve samples in the corresponding solvent and load into auto sampler.
IS: stock solution, 10 ng/ml in W/ACN 1:1.
Derivatizing reagent: 4 mg/ml in MeOH, 5% HCOOH (0.268 µmol of reagent).
MNPs: 1.2 mg, functionalization: 0.33 mmol/g (0.396 µmol of CBs).
Desorption solvent:

- 7,8 mM NH_4^+ $HCOO^-$ in MeOH/$CHCl_3$ 1:1, 0.1%(v/v) HCOOH.
- **18** dissolved in water: A) 0.727 µmol, 2.7 eq; B) 1.455 µmol, 5.4 eq.

IV.4.5. ^{1}H and ^{13}C NMR spectra

IV.4.5.1. Compound 6

^{1}H NMR (400 MHz. D_2O)

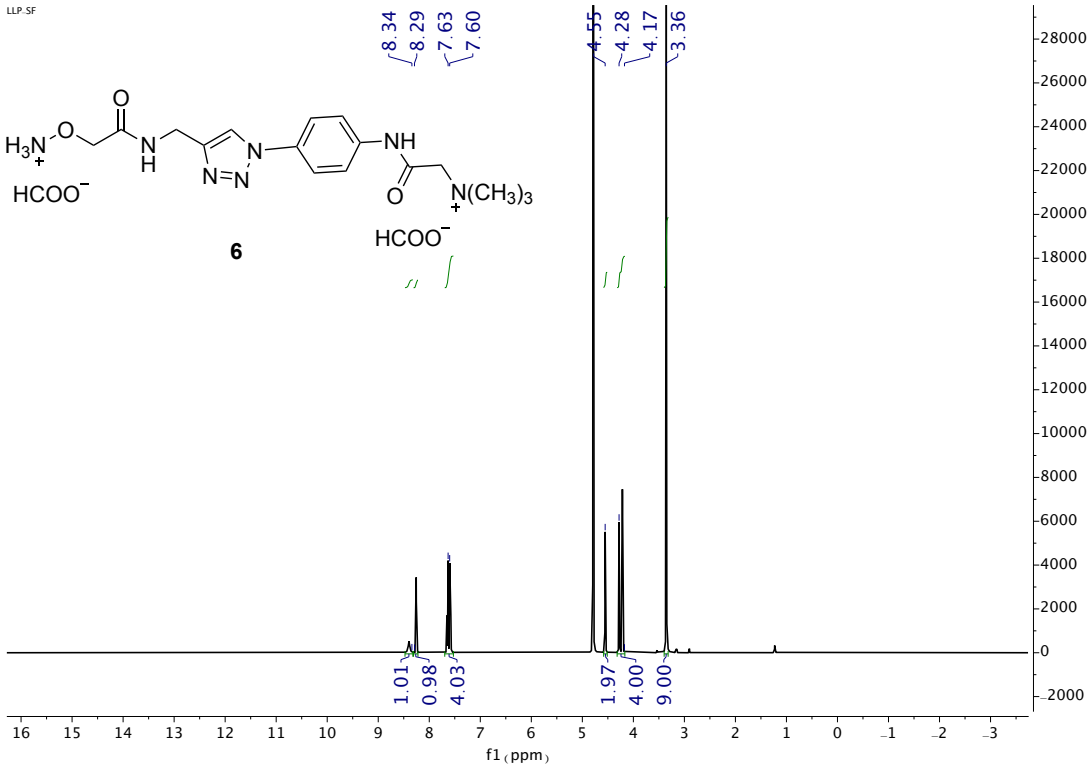

IV.4.5.2. Compound 19

^{1}H NMR (400 MHz. D_2O)

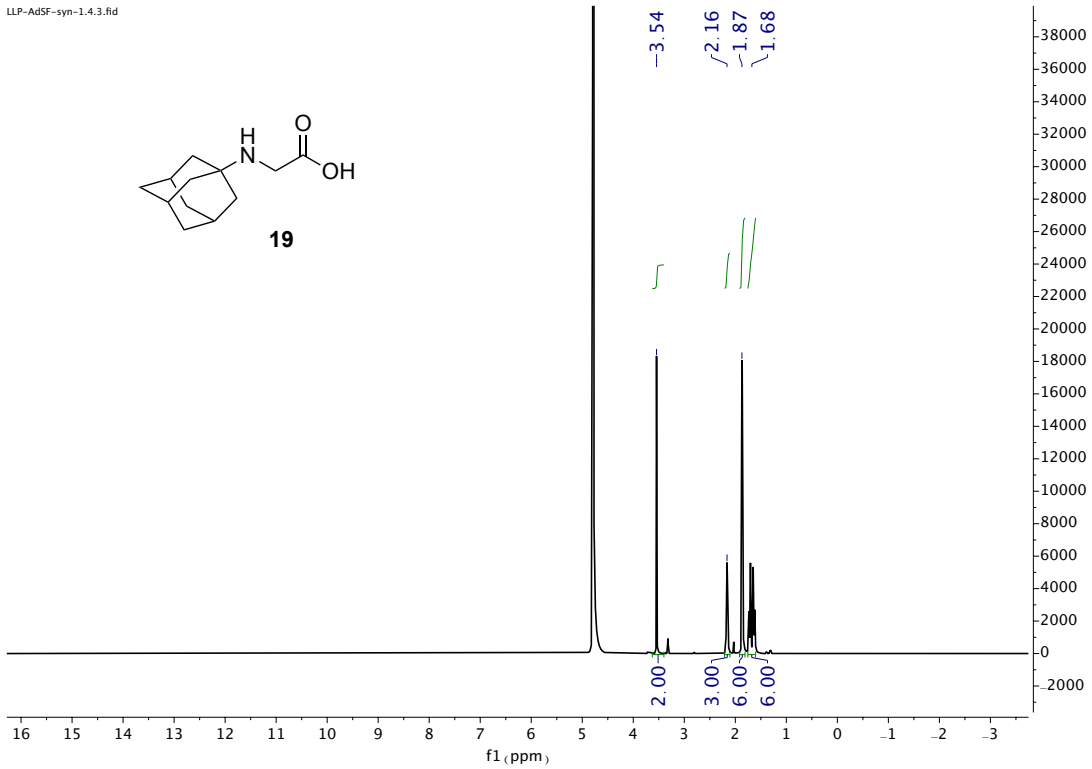

19

^{13}C NMR (101 MHz. D_2O)

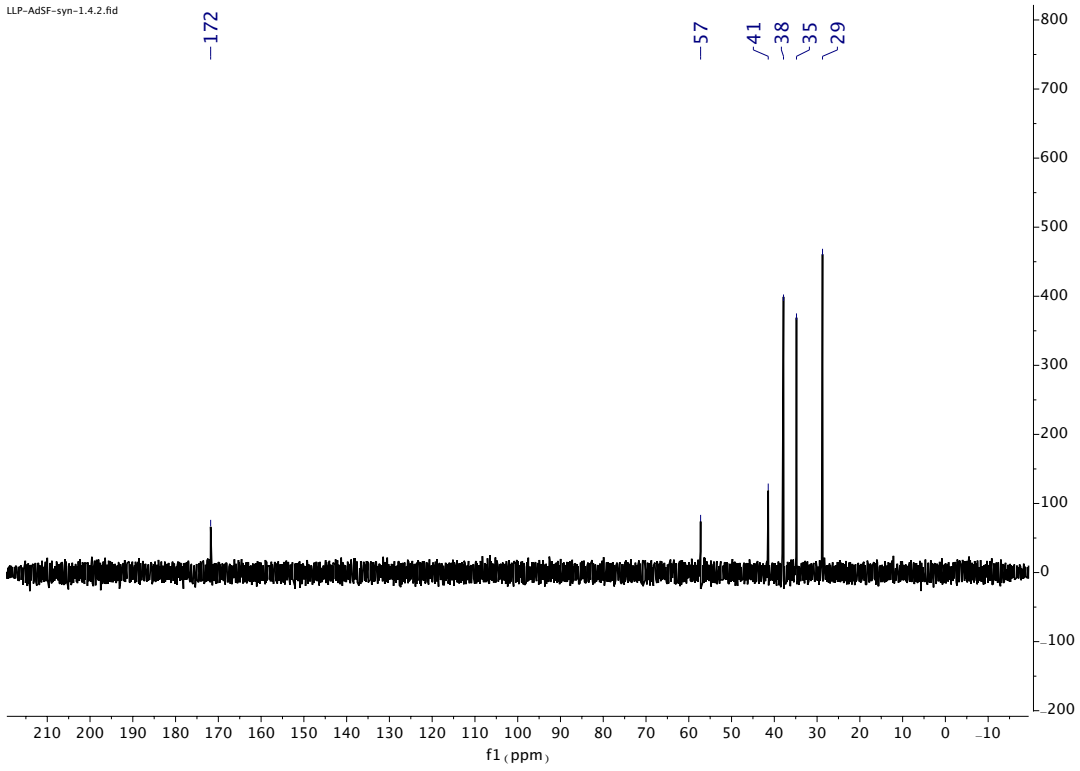

IV.4.5.3. Compound 7

^{1}H NMR (400 MHz. $CDCl_3$)

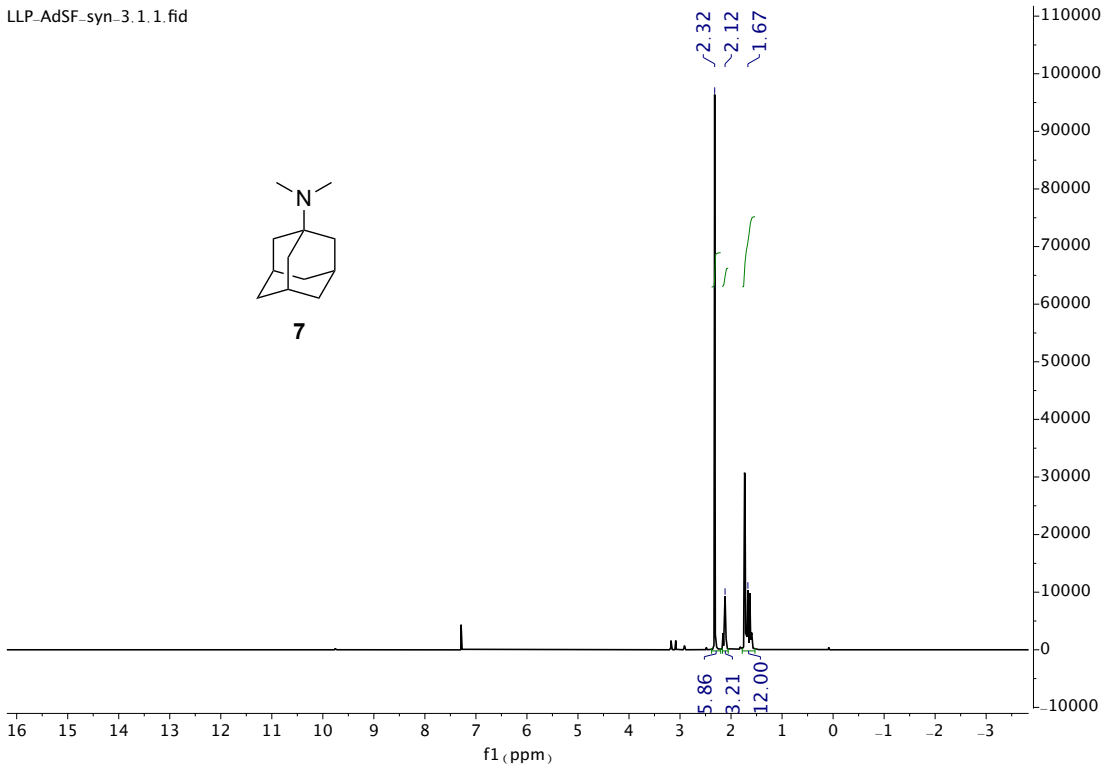

7

^{13}C NMR (101 MHz. $CDCl_3$)

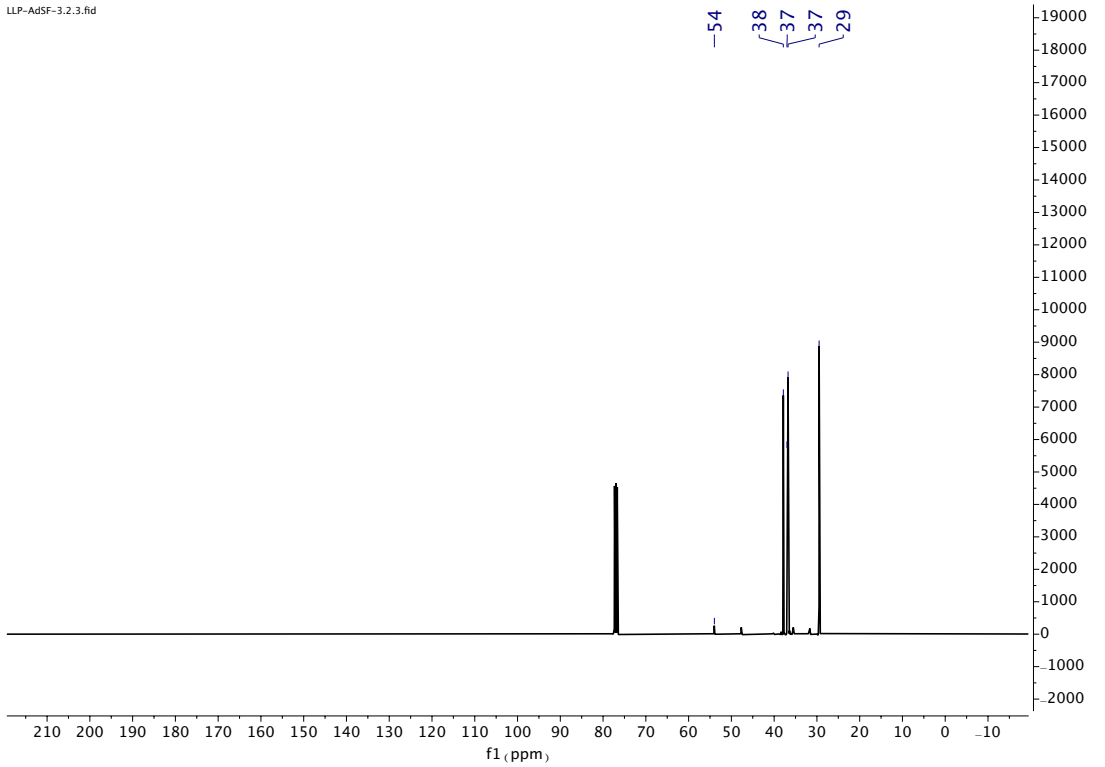

IV.4.5.4. Compound 8

^{1}H NMR (400 MHz. D_2O)

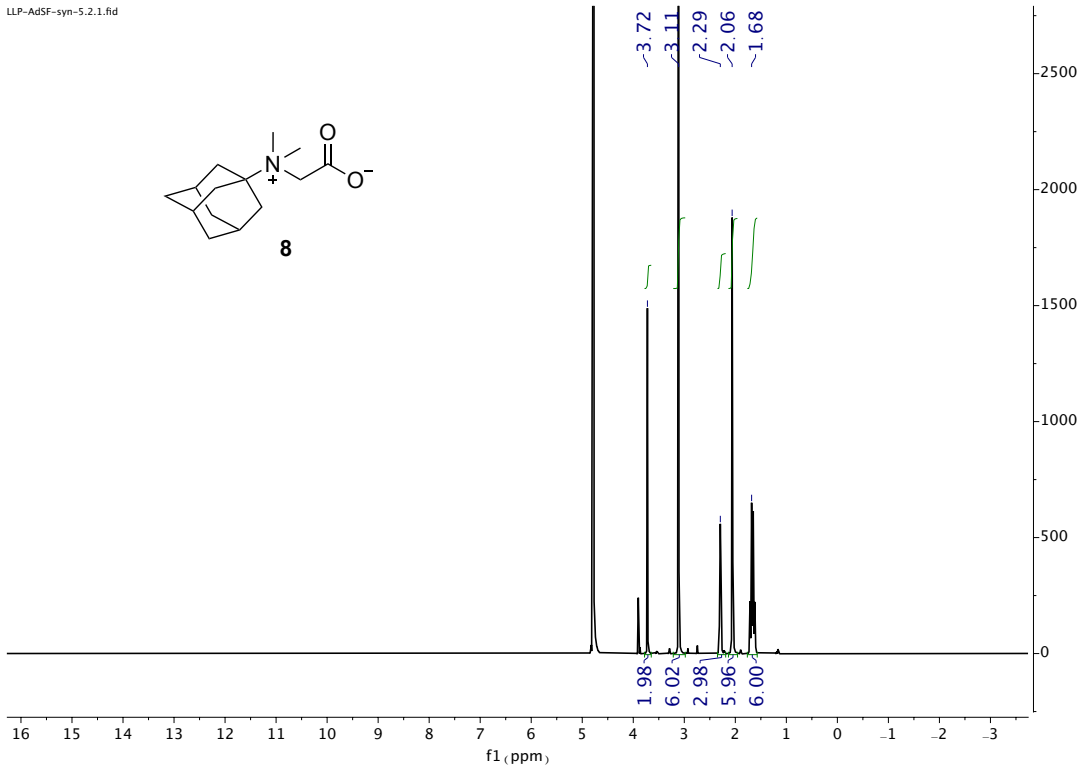

8

^{13}C NMR (101 MHz. D_2O)

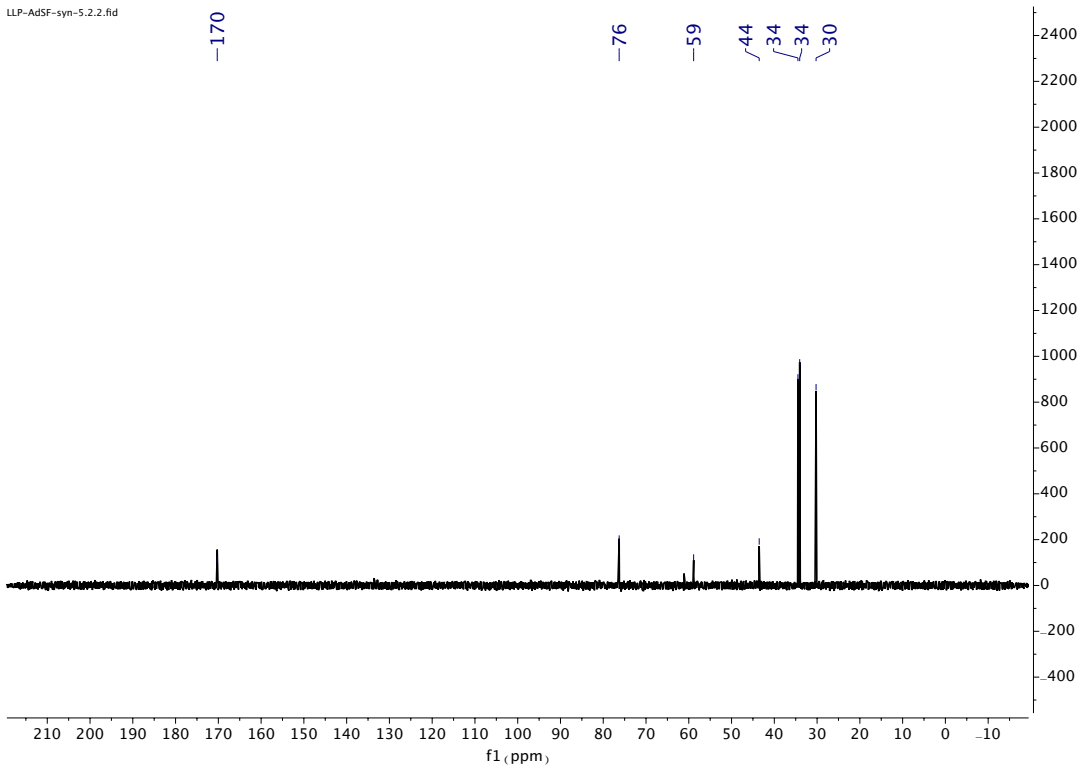

IV.4.5.5. Compound 9

^{1}H NMR (400 MHz. DMSO d^{6})

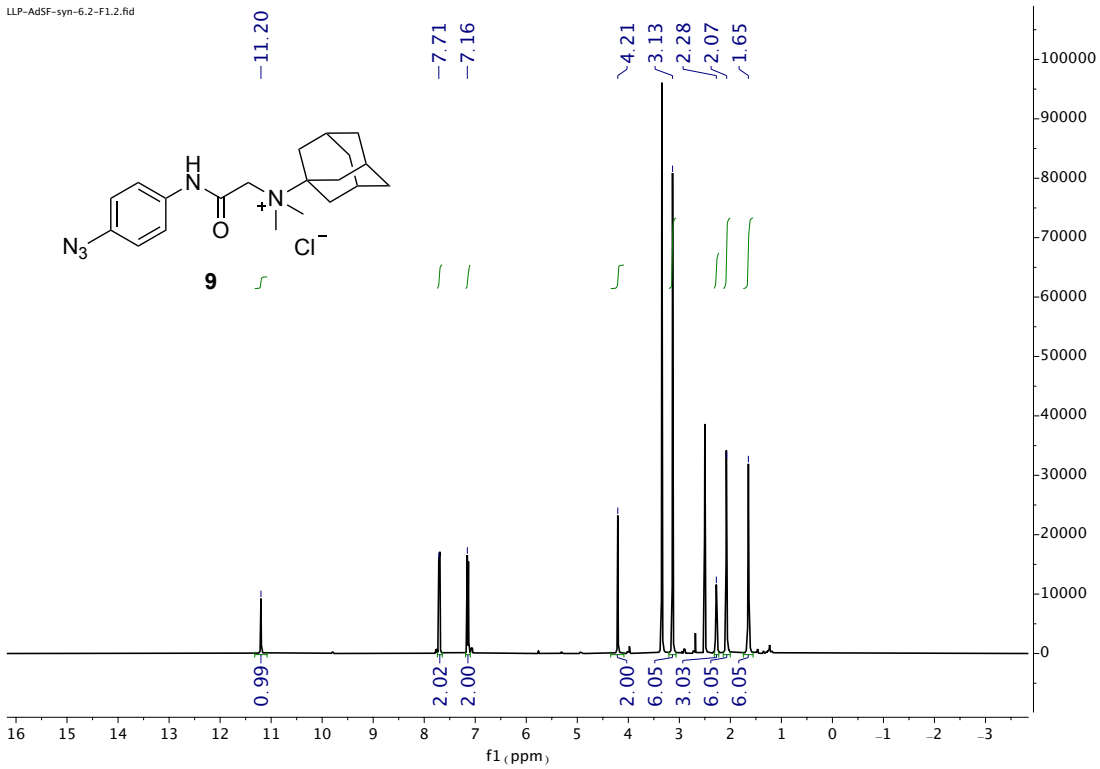

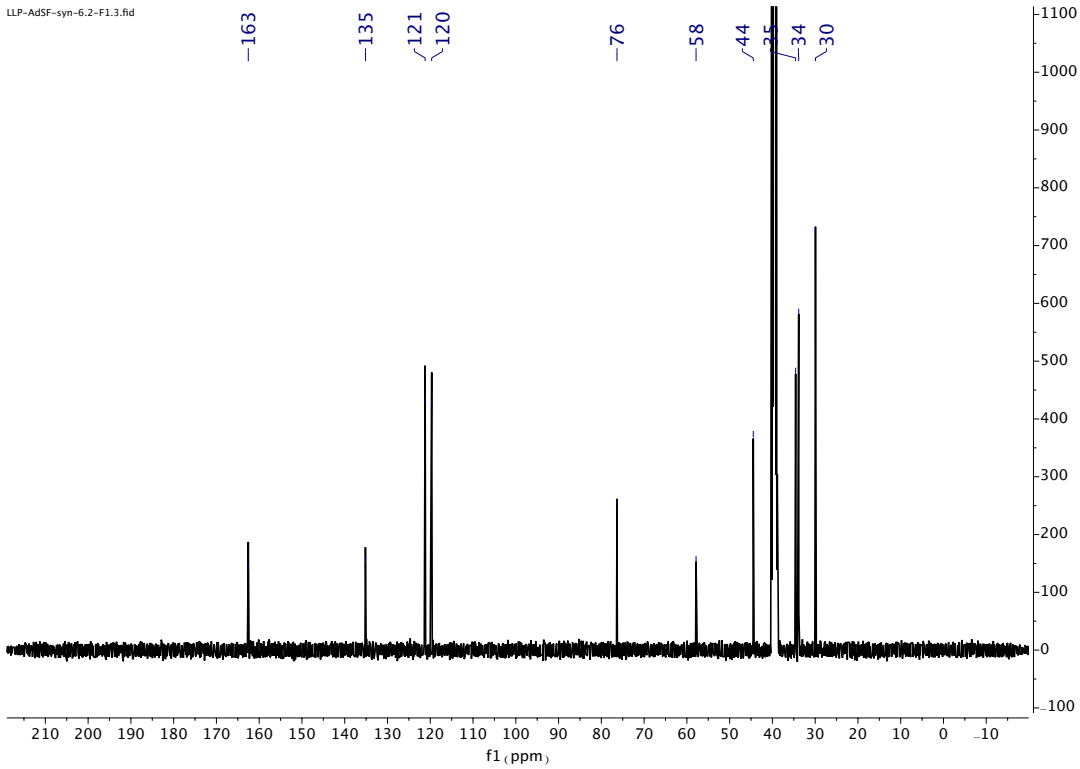

IV.4.5.6. Compound 10

^{1}H NMR (400 MHz. DMSO d^{6})

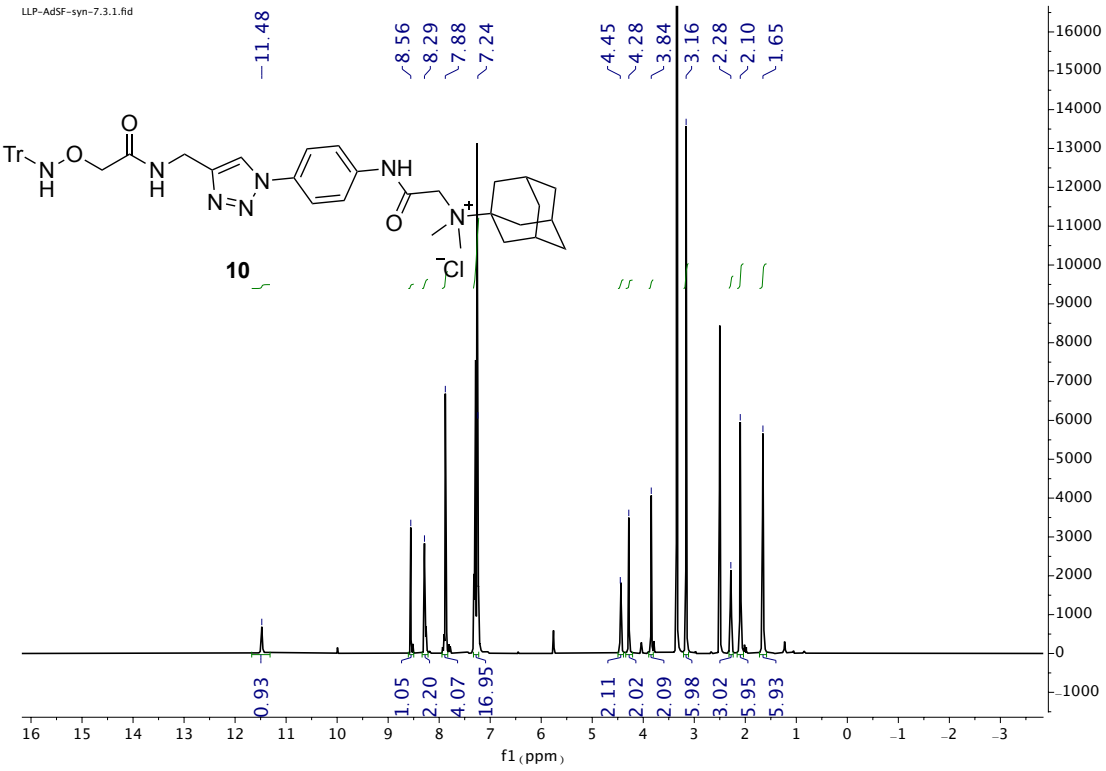

^{13}C NMR (101 MHz. DMSO d^{6})

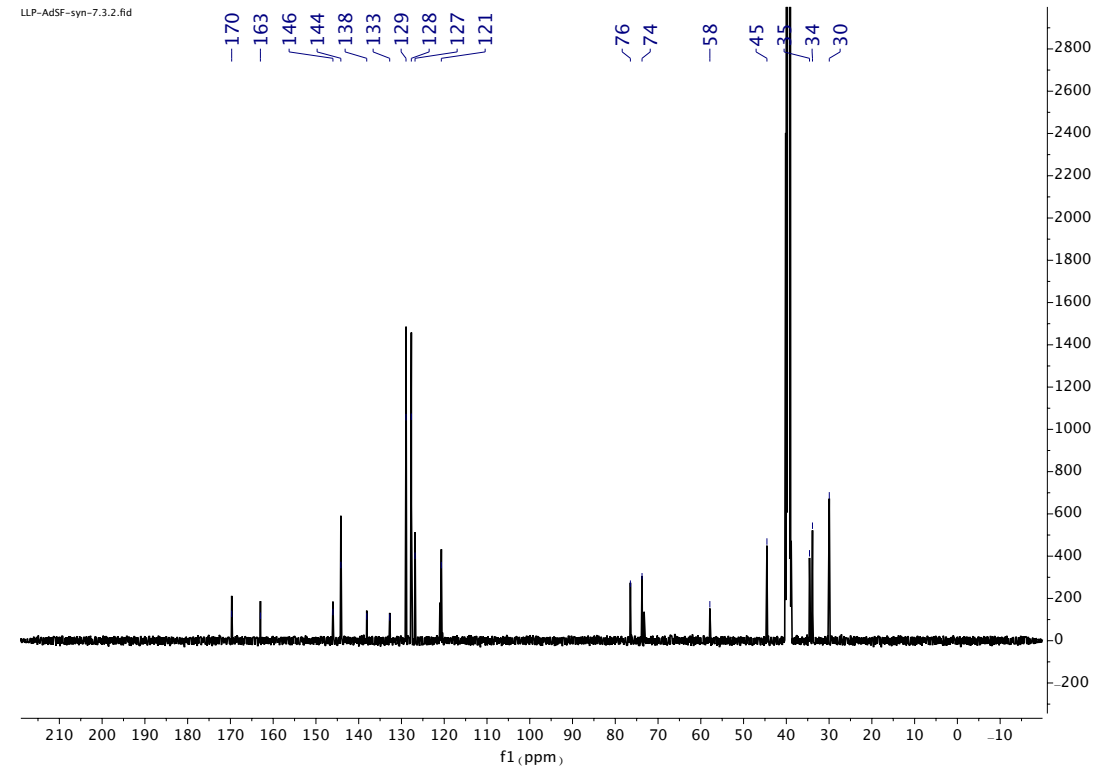

IV.4.5.7. Compound 11

^{1}H NMR (600 MHz. D_2O)

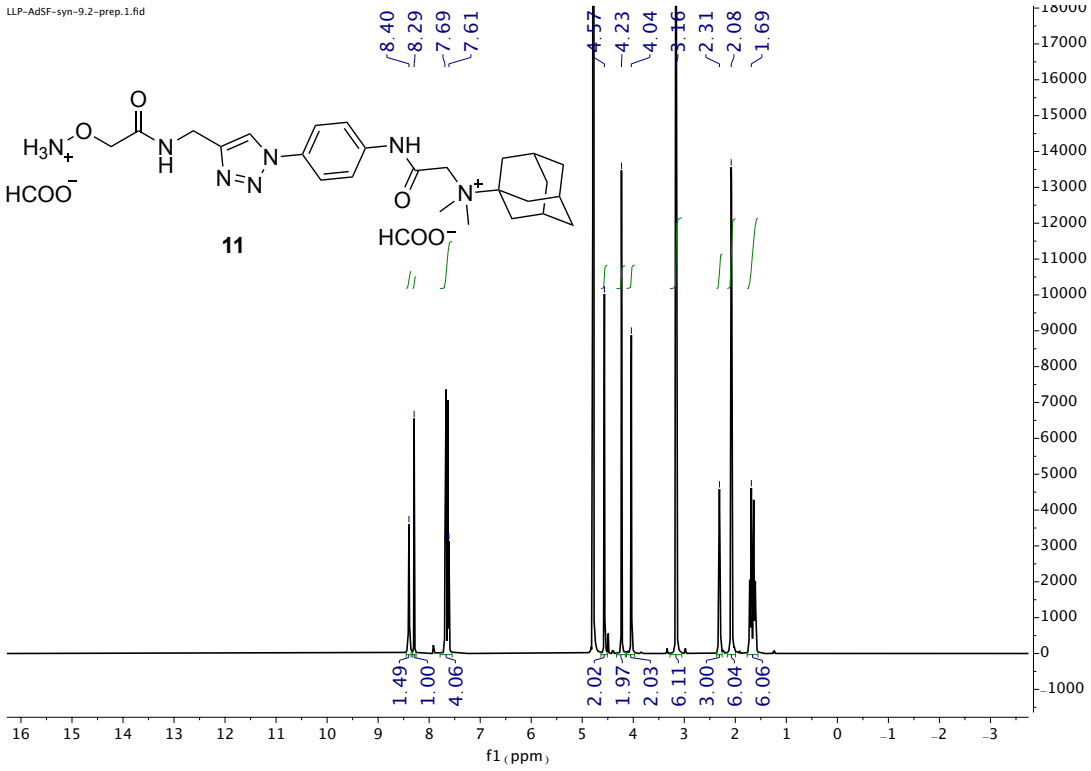

^{13}C NMR (150 MHz. D_2O)

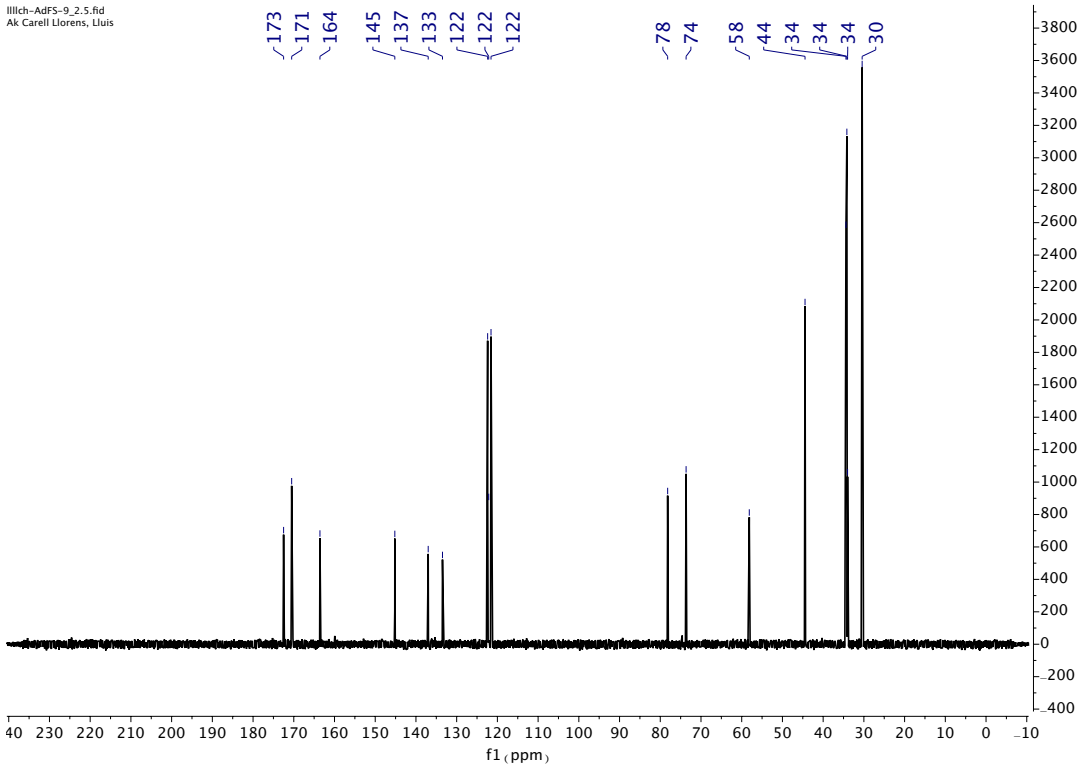

HSQC

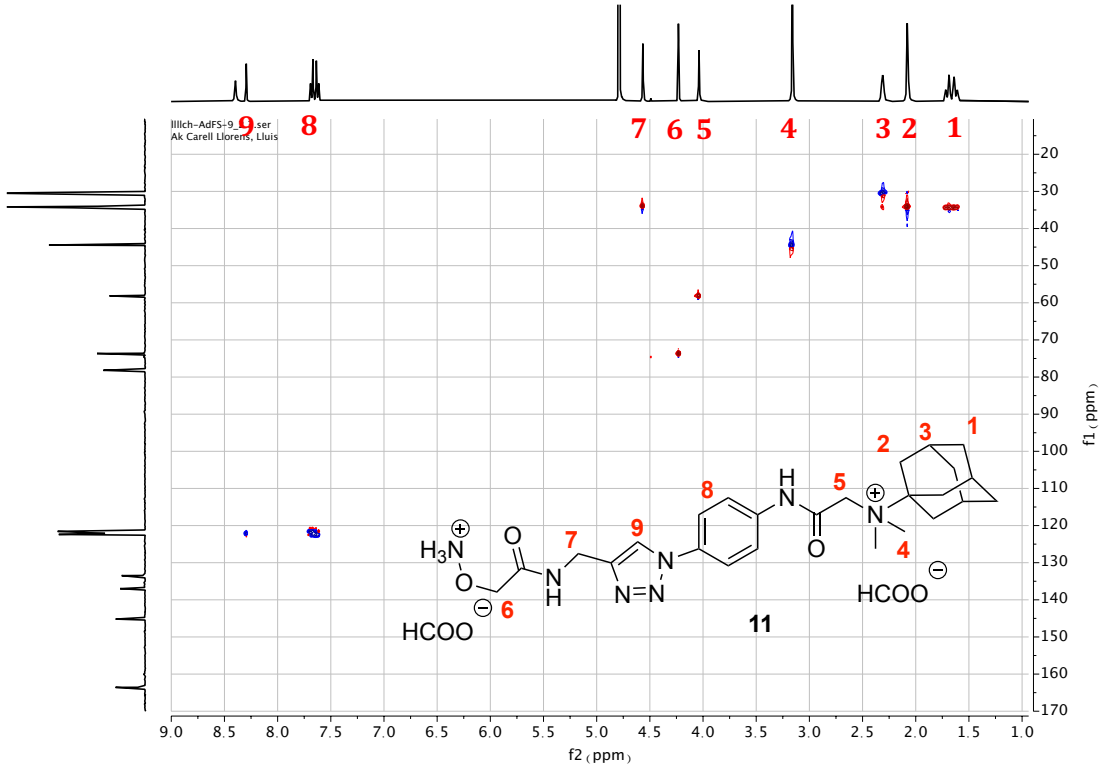

COSY

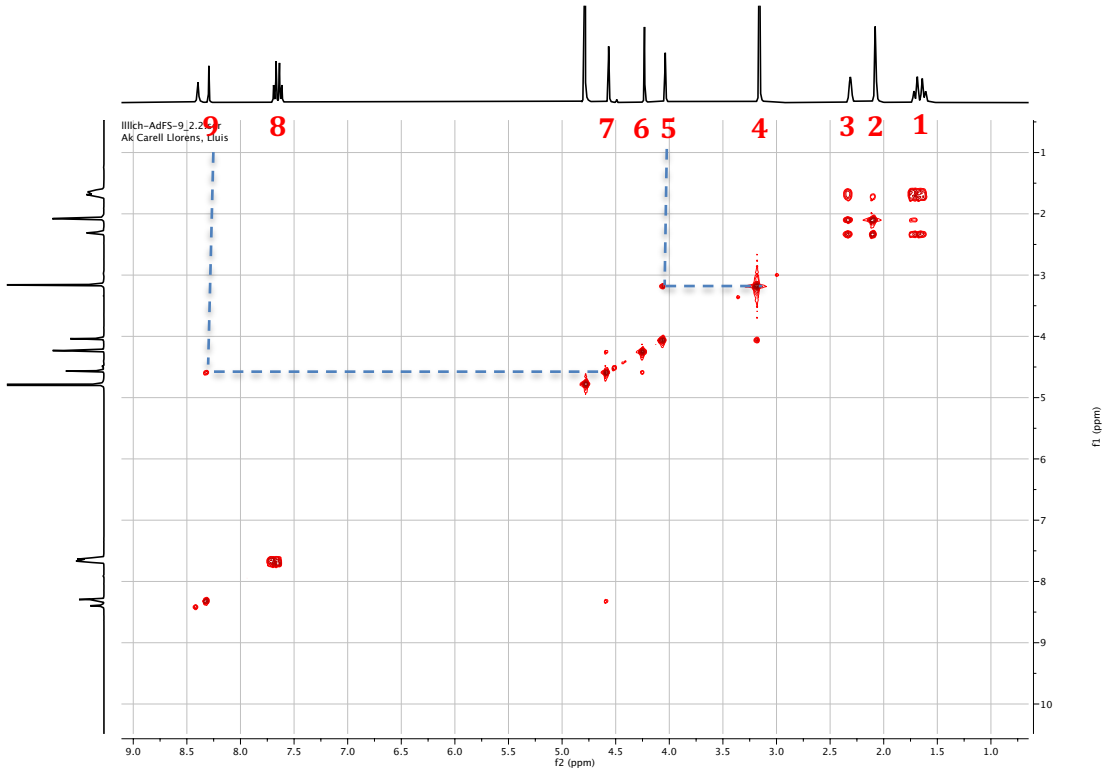

IV.4.5.8. Compound 12

^{1}H NMR (600 MHz. $CDCl_3$)

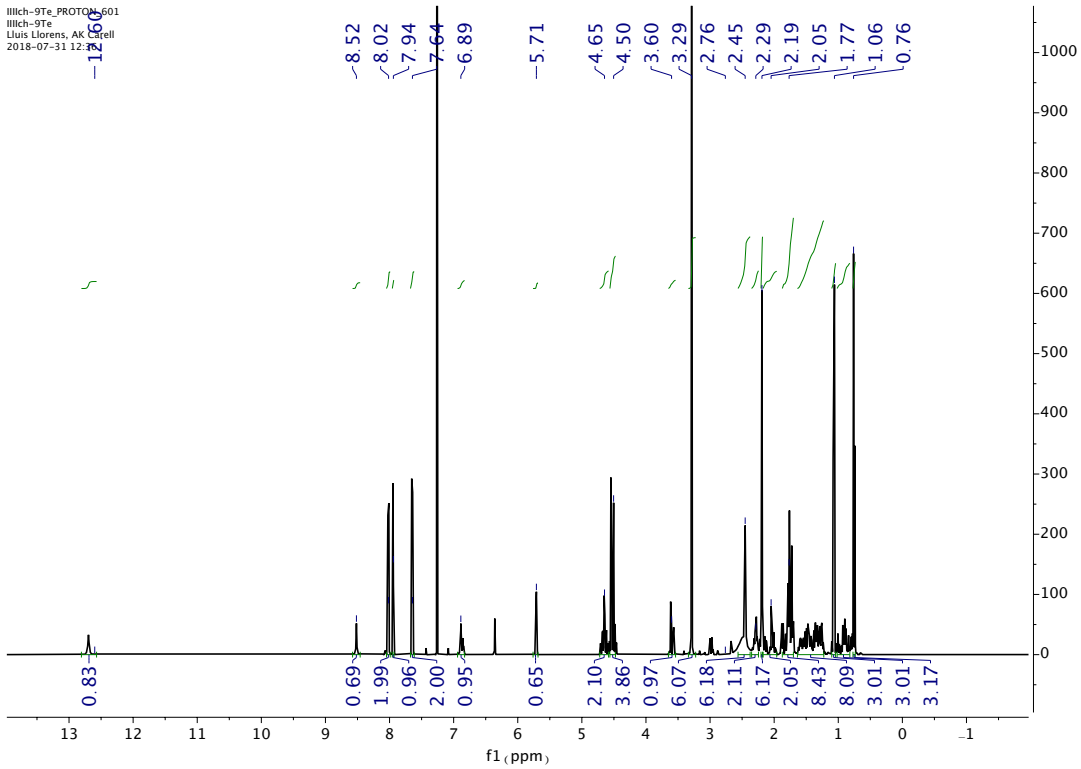

^{13}C NMR (150 MHz. $CDCl_3$)

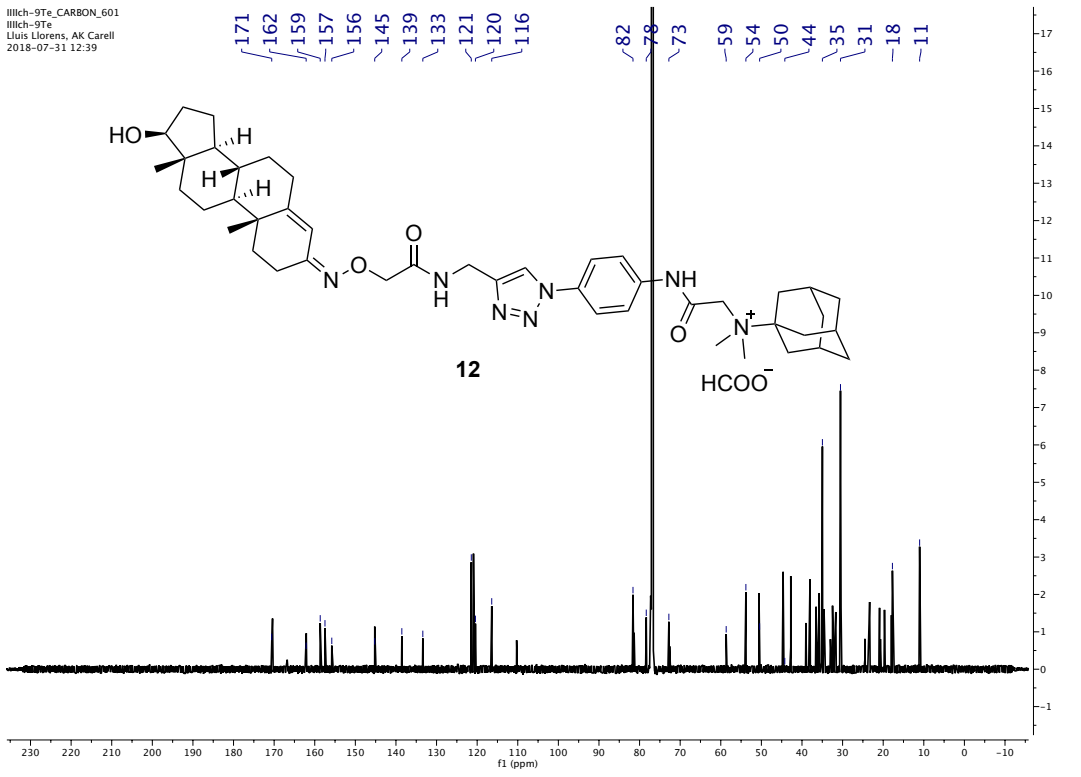

COSY

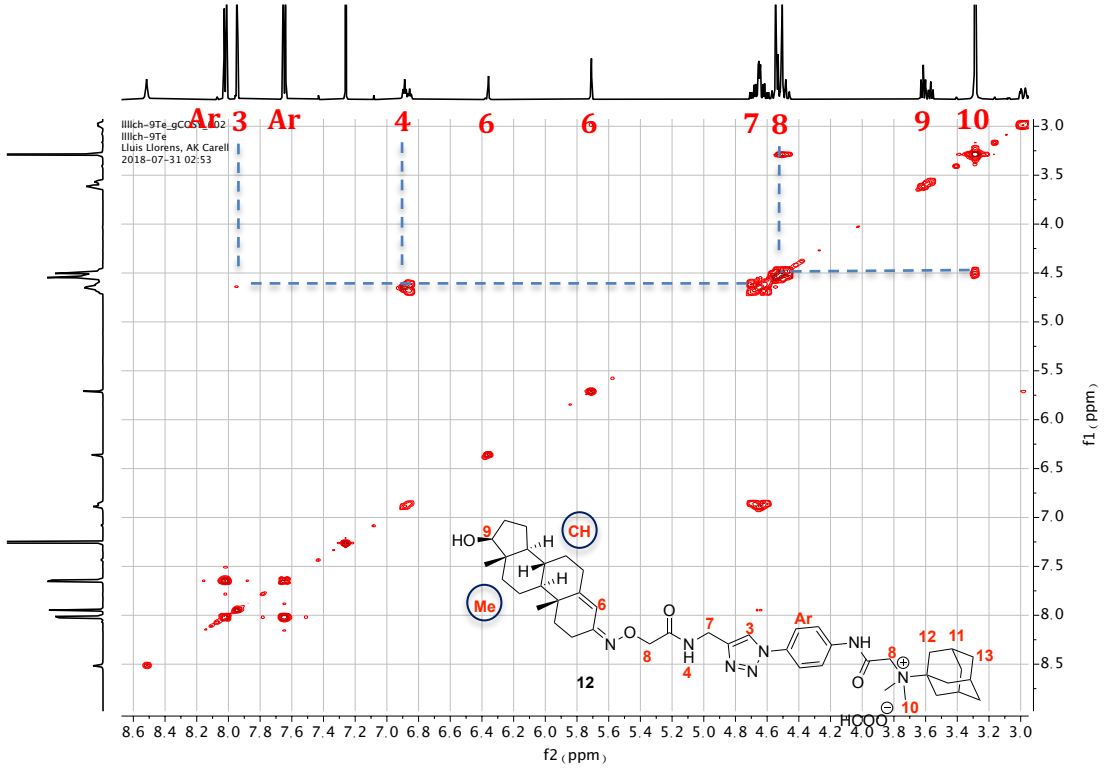
Ar 3 Ar 4 6 6 7 8 9 10
lllich-9Te_gCOSY_602
lllich-9Te
Lluis Llorens, AK Carell
2018-07-31 02:53
HO 9 H
CH
Me
6
N O
8
O
N H
4
7
3
N
N=N
Ar
NH
8
O
N
12 11
13
10
HCOO
12
f2 (ppm)
f1 (ppm)

HSQC

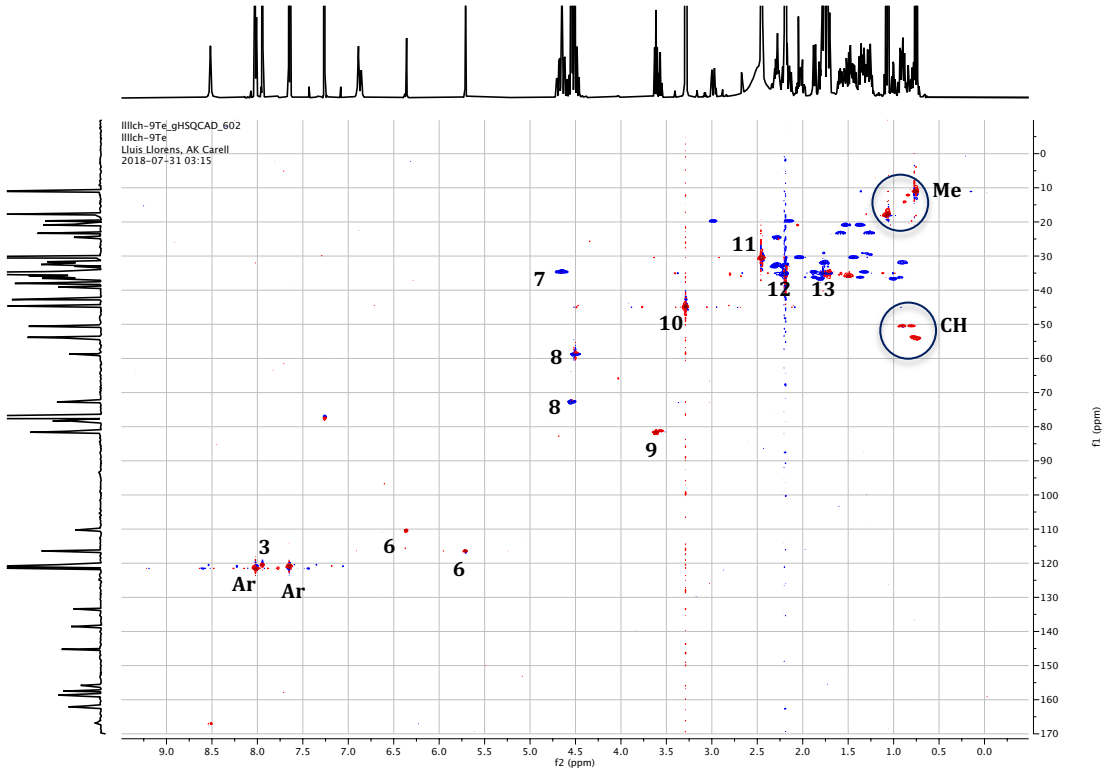
lllich-9Te_gHSQCAD_602
lllich-9Te
Lluis Llorens, AK Carell
2018-07-31 03:15
Me
11
12
13
CH
7
10
8
8
9
3
Ar
Ar
6
6
f2 (ppm)
f1 (ppm)

IV.4.5.9. Compound 13

^{1}H NMR (400 MHz. D_2O)

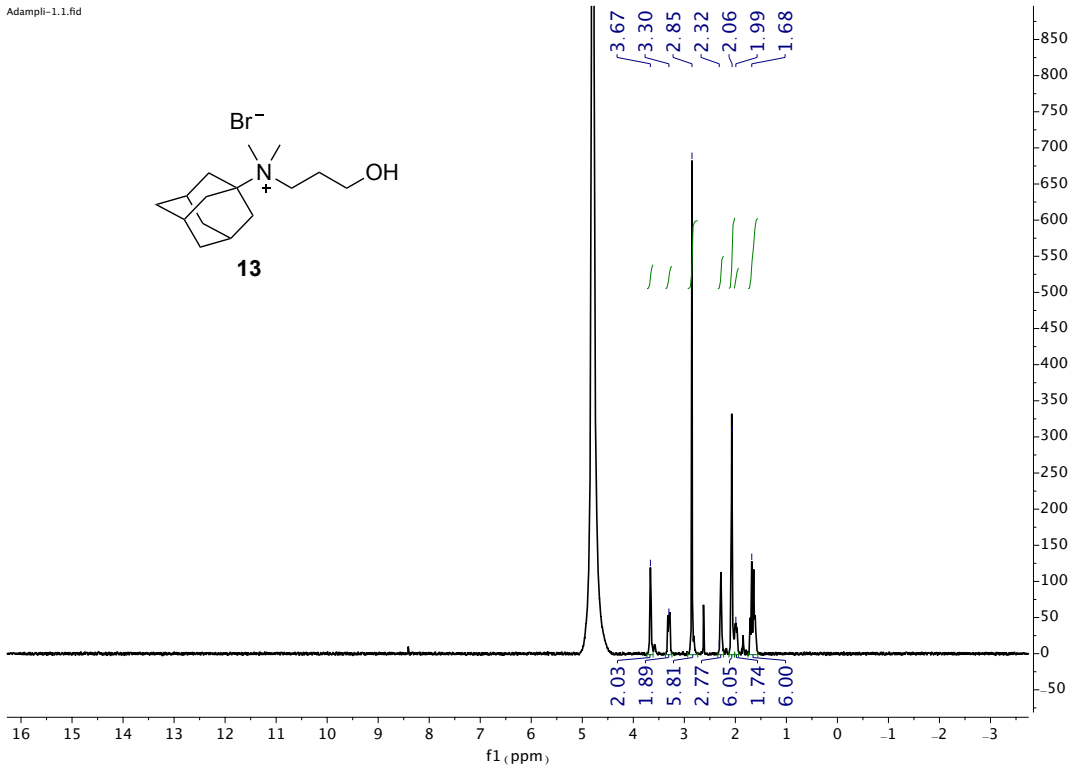

^{13}C NMR (101 MHz. D_2O)

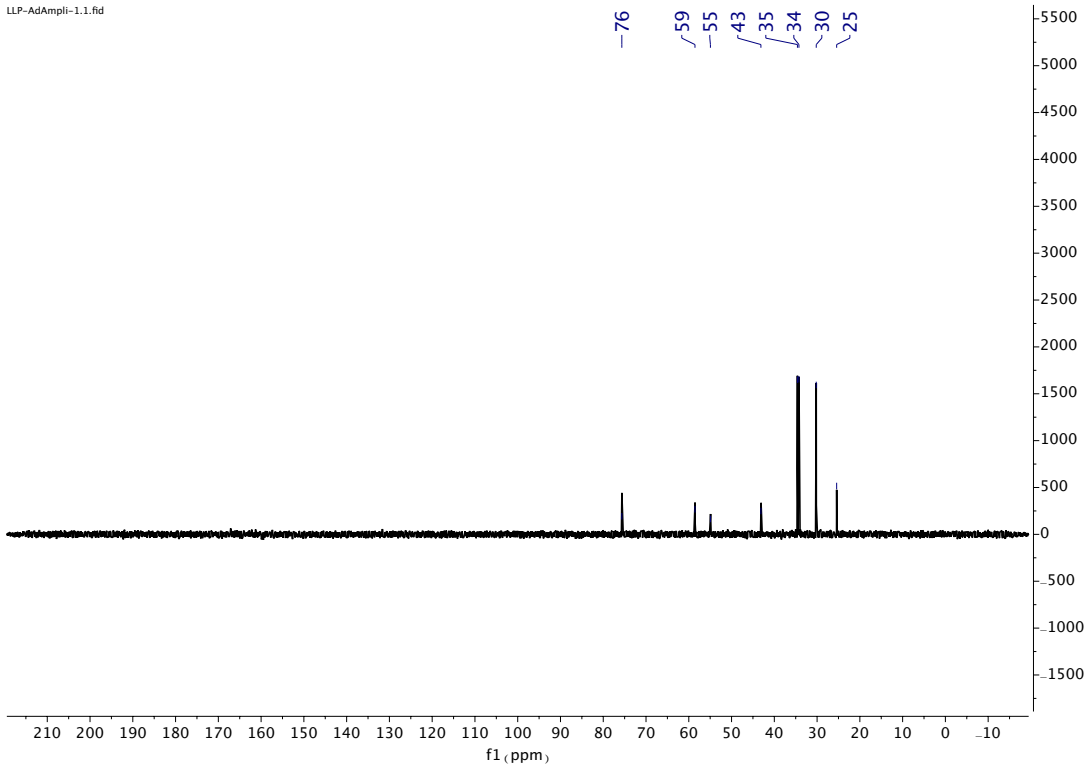

HSQC

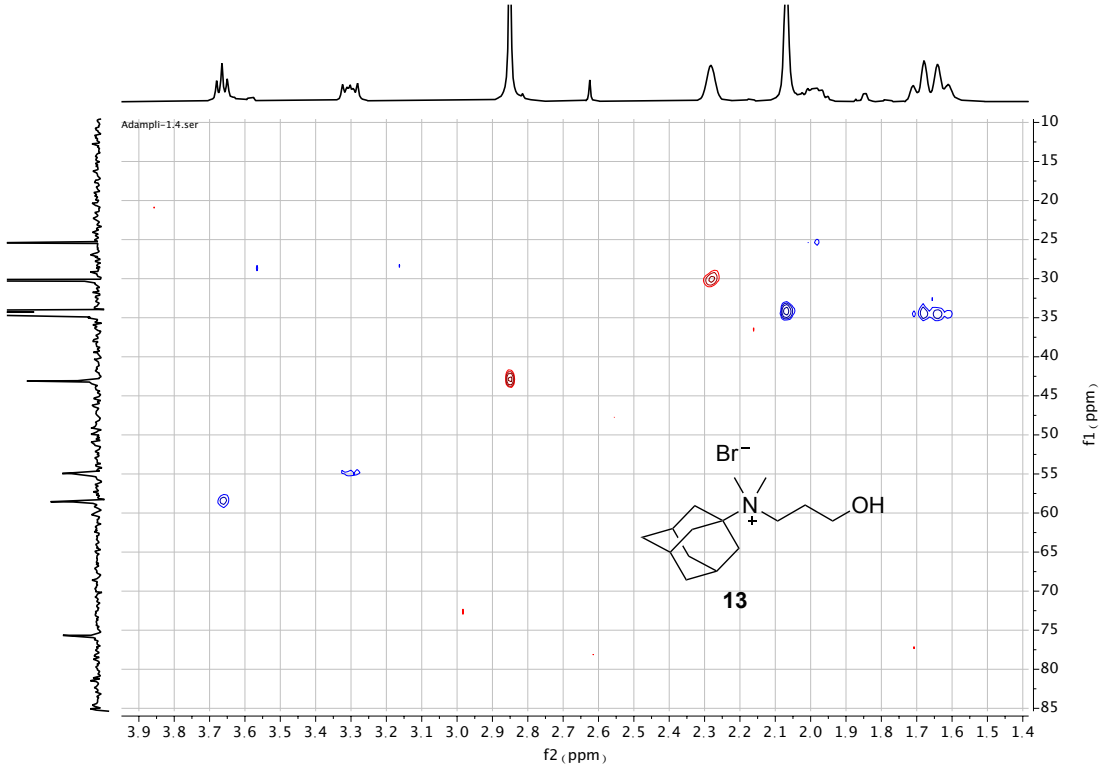

IV.4.5.10. Compound 14

^{1}H NMR (400 MHz. $CDCl_3$)

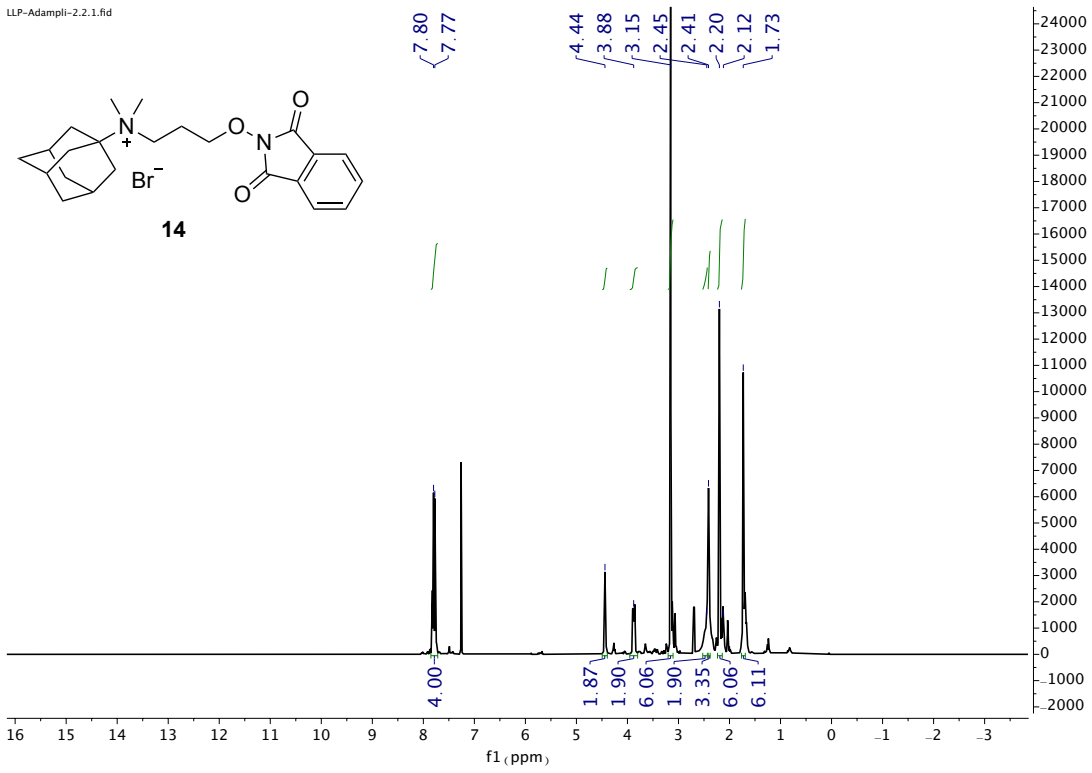

^{13}C NMR (101 MHz. $CDCl_3$)

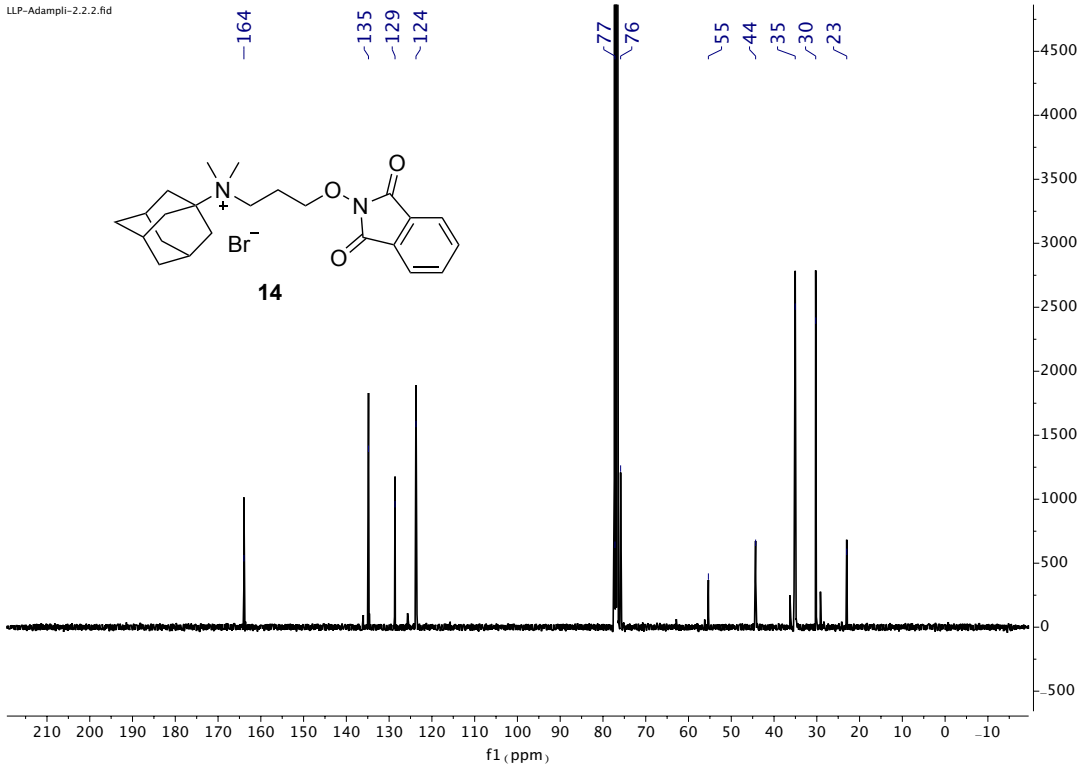

HSQC

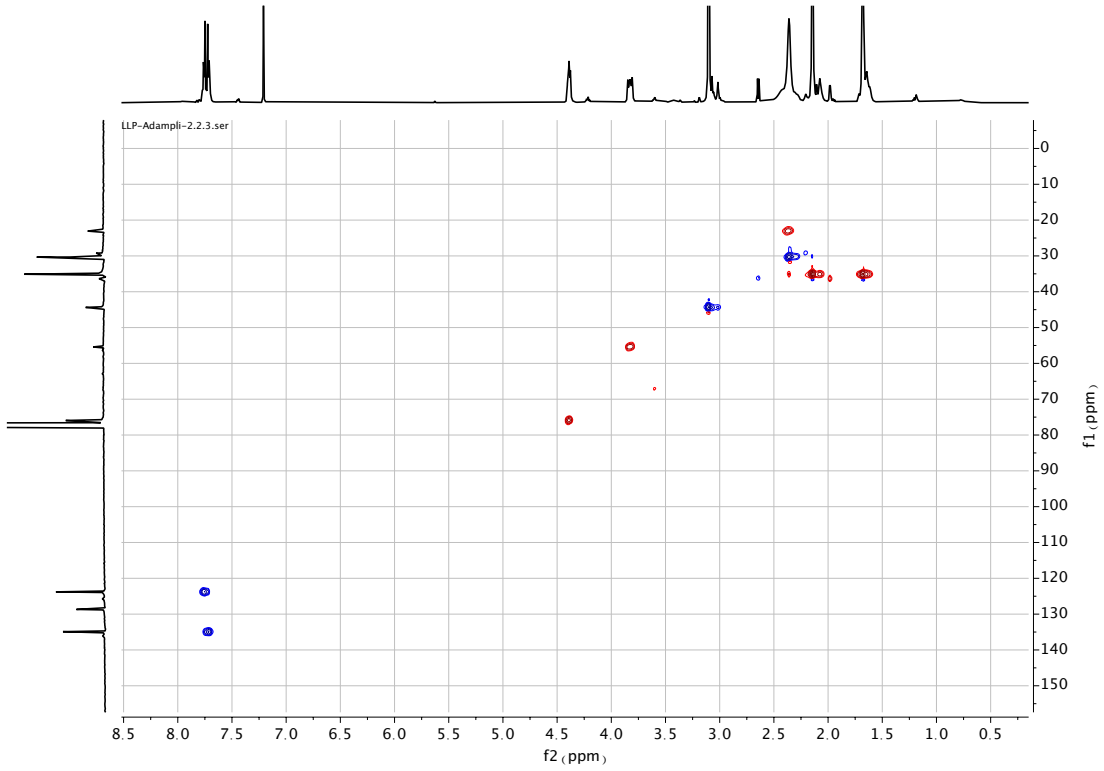

IV.4.5.11. Compound 15

^{1}H NMR (400 MHz. DMSO d^{6})

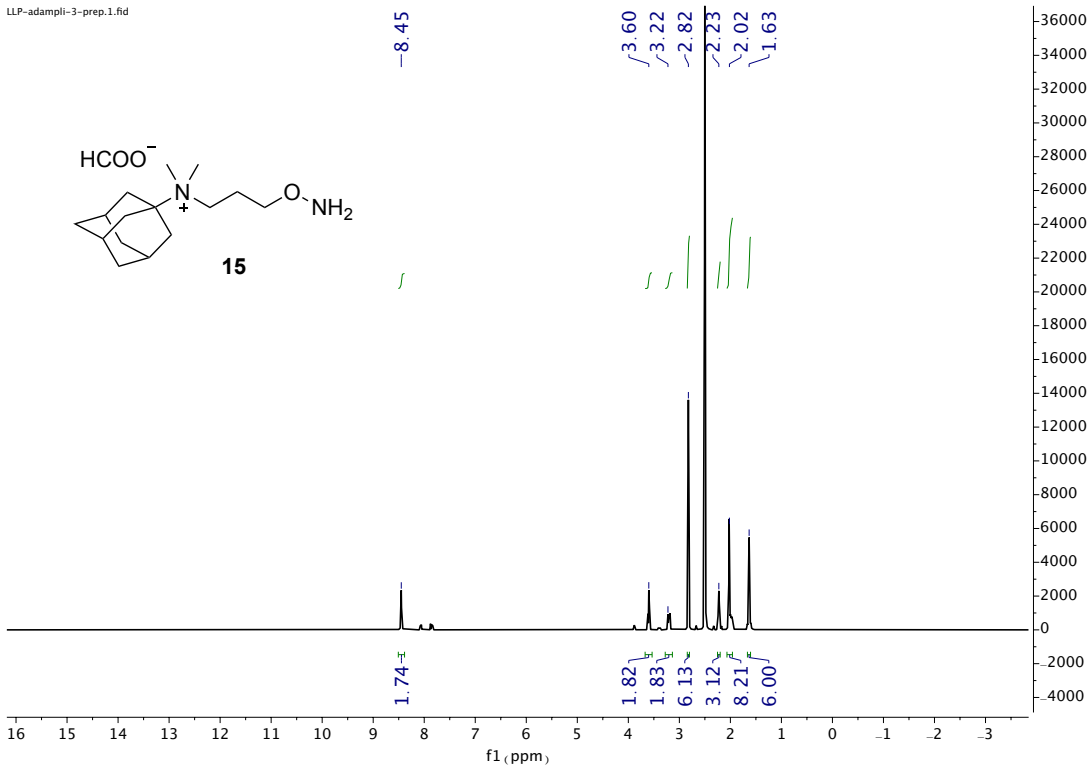

^{13}C NMR (101 MHz. DMSO d^{6})

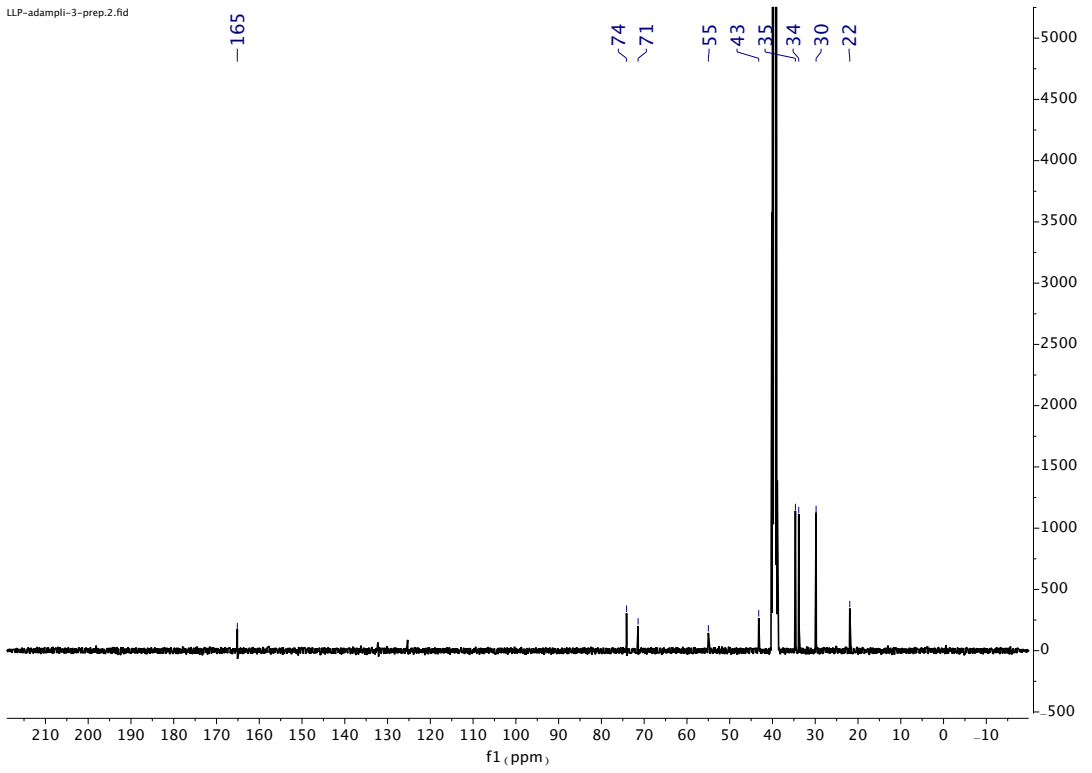

HSQC

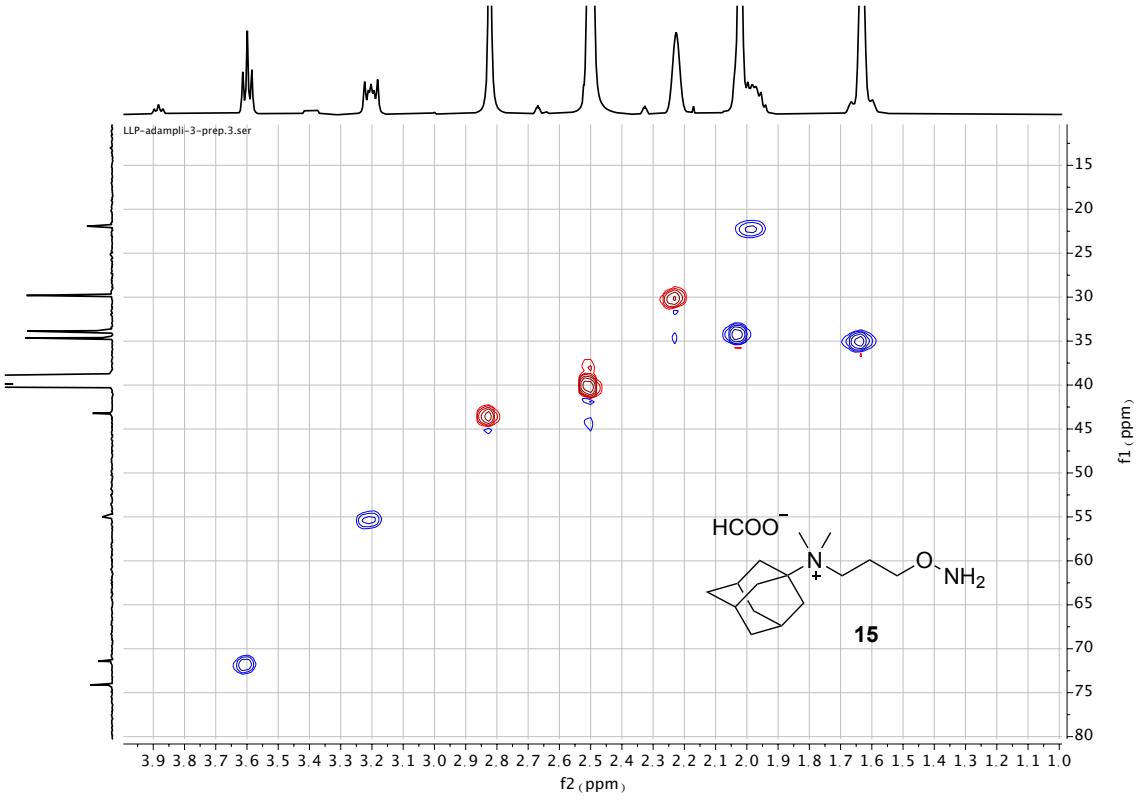

IV.4.6. HPLC chromatograms

IV.4.6.1. Compound: testosterone

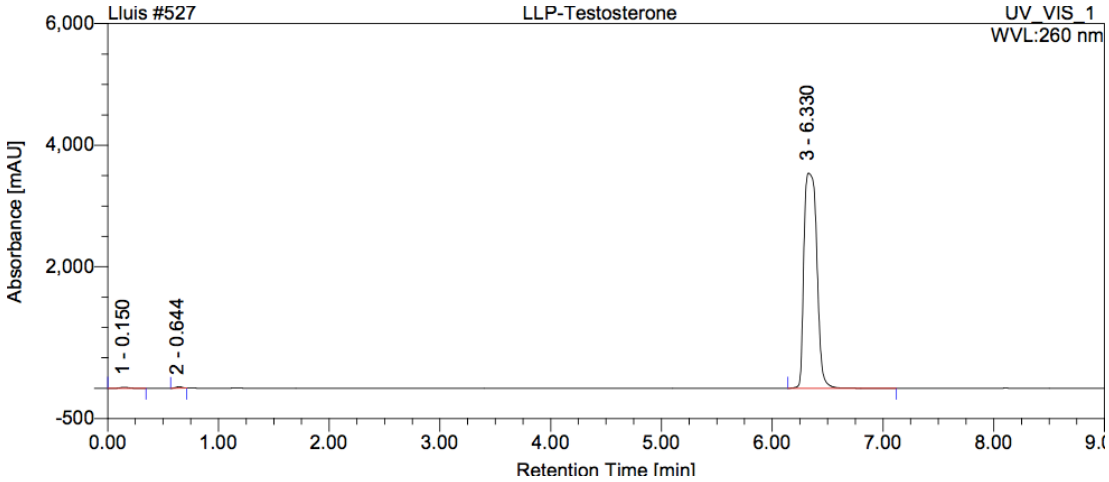

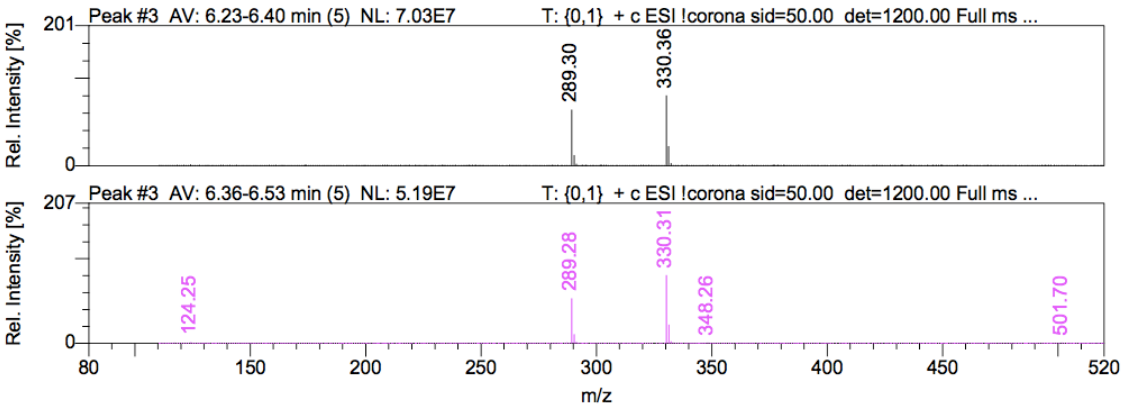

m/z [testosterone + water + Na]$^{+}$ = 330

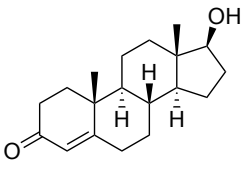

IV.4.6.2. Compound: cytidine

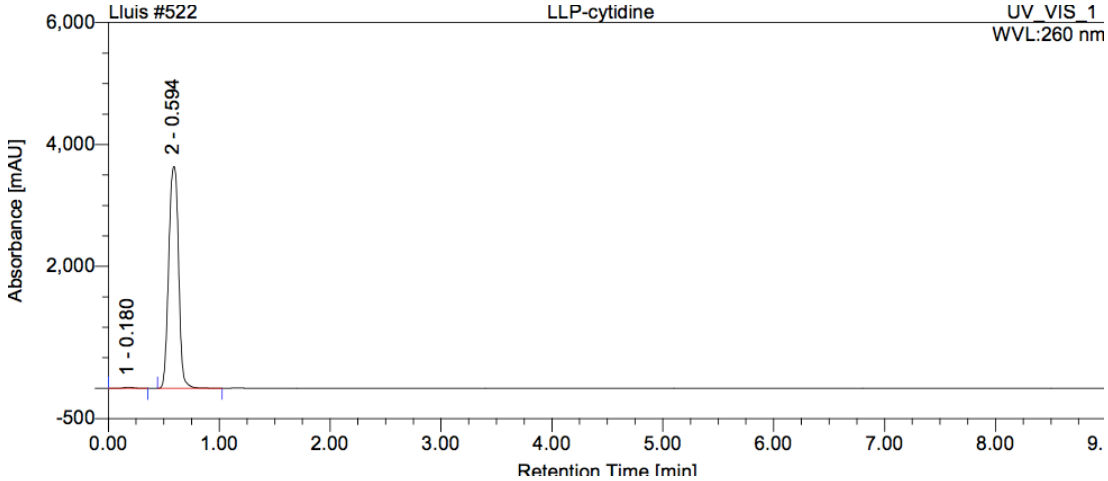

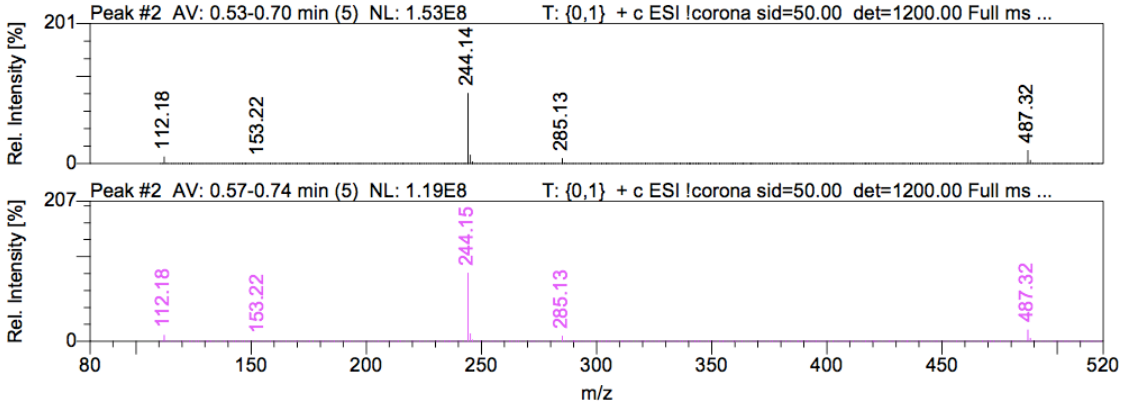

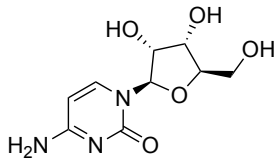

IV.4.6.3. Compound: tryptophan benzyl ester

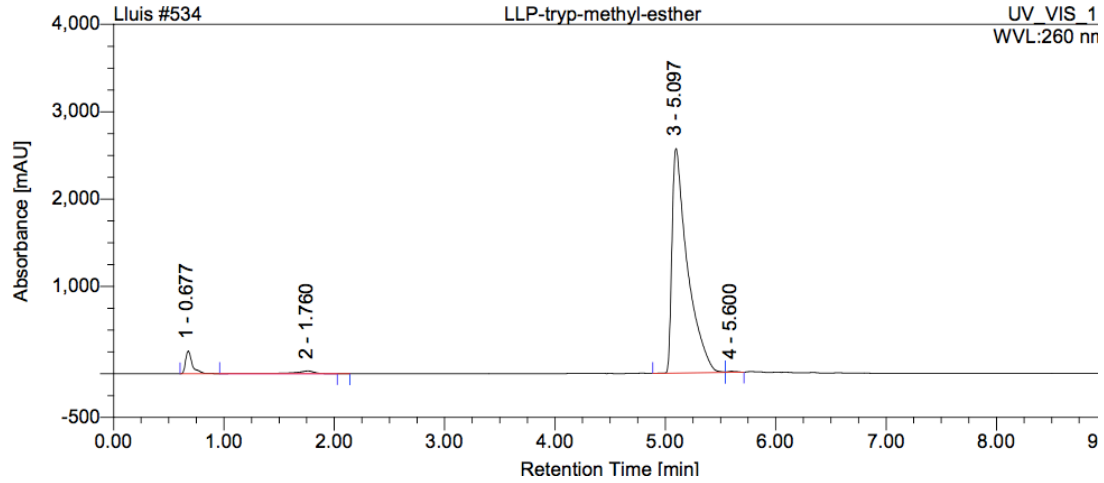

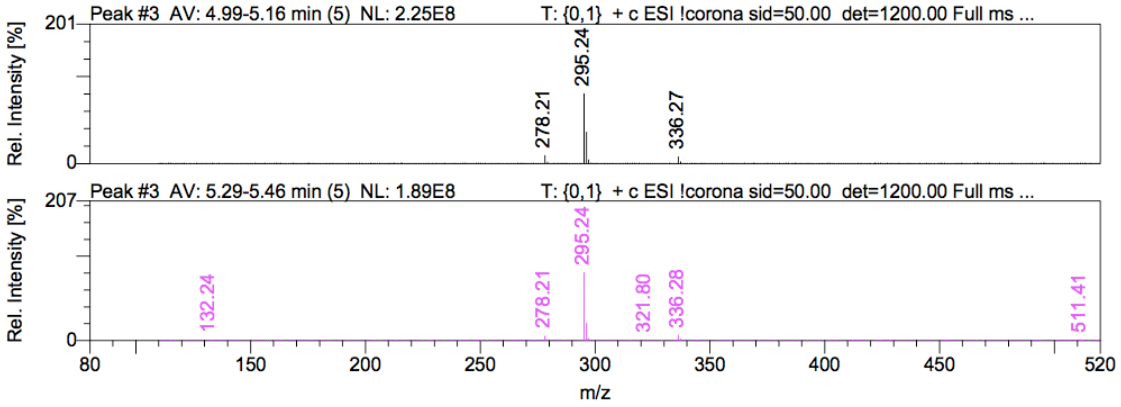

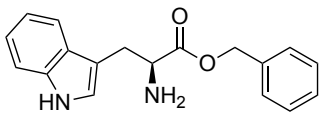

IV.4.6.4. Compound 12

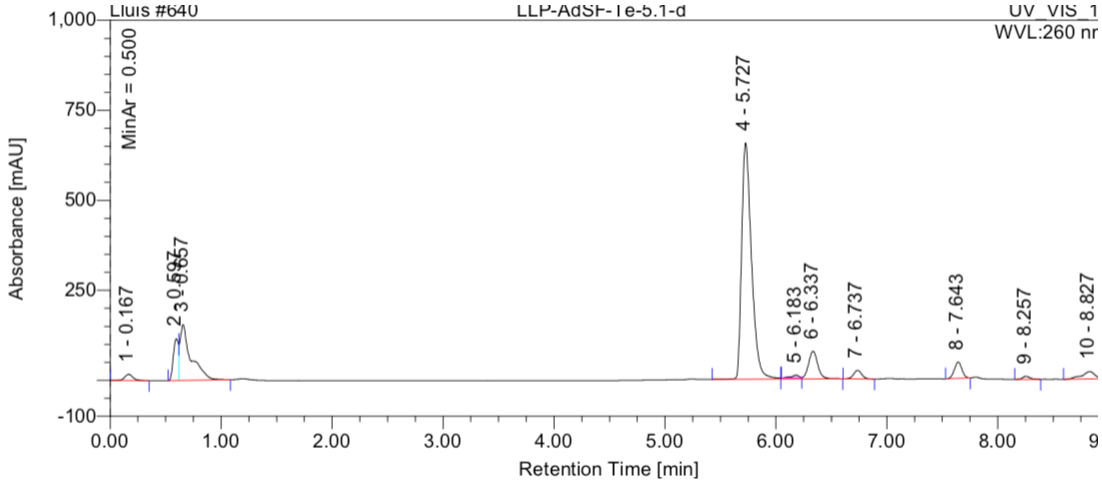

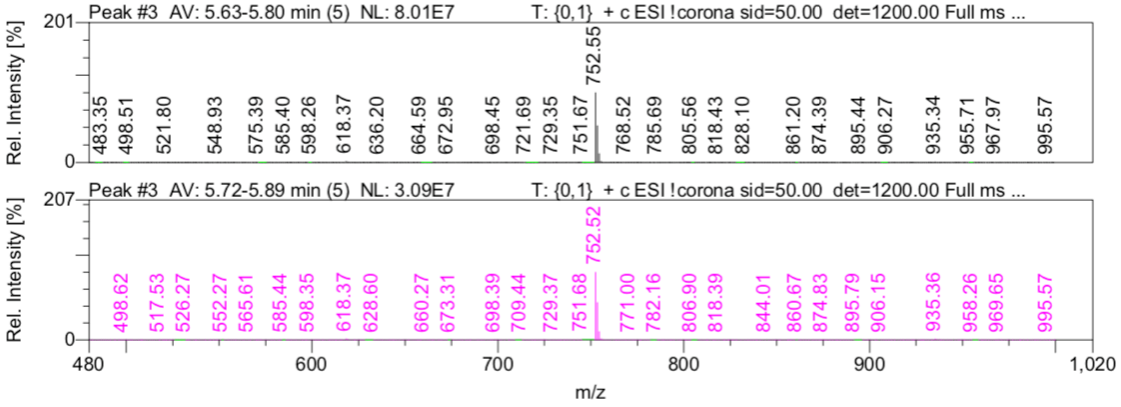

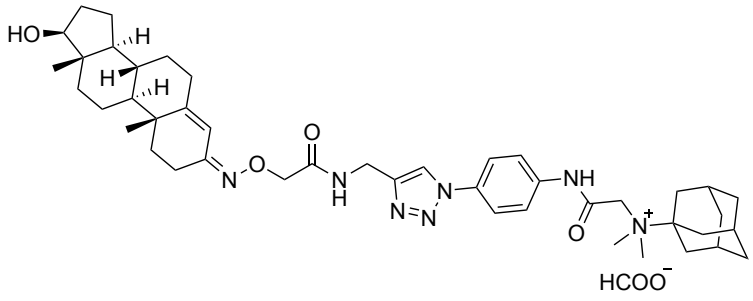

II.4.9. References

[1] R. Rahimoff, O. Kosmatchev, A. Kirchner, T. Pfaffeneder, F. Spada, V. Brantl, M. Müller, T. Carell, *J. Am. Chem. Soc.* **2017**, *139*, 10359–10364.
[2] a) L. Cao, M. Šekutor, P. Y. Zavalij, K. Mlinarić-Majerski, R. Glaser, L. Isaacs, *Angew. Chemie Int. Ed.* **2014**, *53*, 988–993. b) S. Liu, C. Ruspic, P. Mukhopadhyay, S. Chakrabarti, P. Y. Zavalij, L. Isaacs, *J. Am. Chem. Soc.* **2005**, *127*, 15959–15967.

5

CHAPTER V

Computational studies

CHAPTER V

Computational studies

The studies described in the last chapter stirred our research to this last project that has been conducted in collaboration with Dr. Mauro Fianchini.

V.1. Introduction

The cornerstone concept of supramolecular chemistry is represented by molecular recognition. It is defined as the capability of a macro-structure, conventionally called "host", to discriminate over a pool of smaller potentially different "guests" and recognize the species that leads to stronger binding.[1]

The explanation of the high binding constant seen in cucurbit[n]urils family can be explained via balanced size-complementarity and rigidity, hydrophobic effect and direct host-guest interactions.[2] The enthalpy-entropy compensation effect in molecular recognition usually features enthalpically driven tight forces to favor the binding and entropic penalties, due to the loss of configurational flexibility, to disfavor it.[3] CB7·ferrocene systems, however, disobey the enthalpy-entropy compensation principle.[4] The binding event is thermodynamically favored by a large enthalpic gain due to the tight encapsulation between CB7 and the guest and by a positive entropic contribution coming from the dehydration of the negatively charged portals of CB7; both effects are able to overcome the entropic penalty arising from the loss of configurational entropy.[4] Biedermann and coworkers reported that the release of "high-energy" frustrated water molecules inside the CB cavity are a pivotal driving force in the high binding of these species.[2] Moghaddam and co-workers reported via isothermal titration calorimetry (ITC) experimental evidences proving that the largest contribution to $\Delta G^0_{exp.}$of binding between CB7 and adamantanyl guests comes from $\Delta H^0_{exp.}$

[1] (a) Gellman, S. H., *Chemical Reviews* **1997,** *97* (5), 1231-1232. (b) Persch, E.; Dumele, O.; Diederich, F., *Angew. Chem. Int.l Ed.* **2015,** *54* (11), 3290-3327. (c) Ariga, K.; Ito, H.; Hill, J. P.; Tsukube, H., *Chem. Soc. Rev.* **2012,** *41* (17), 5800-5835.
[2] Biedermann, F.; Uzunova, V. D.; Scherman, O. A.; Nau, W. M.; De Simone, A., *J. Am. Chem. Soc.* **2012,** *134* (37), 15318-15323.
[3] Chodera, J. D.; Mobley, D. L., *Annual Review of Biophysics* **2013,** *42* (1), 121-142.
[4] Rekharsky, M. V.; Mori, T.; Yang, C.; Ko, Y. H.; Selvapalam, N.; Kim, H.; Sobransingh, D.; Kaifer, A. E.; Liu, S.; Isaacs, L.; Chen, W.; Moghaddam, S.; Gilson, M. K.; Kim, K.; Inoue, Y., *Proceedings of the National Academy of Sciences* **2007,** *104* (52), 20737.

(ranging from -21.9 to -19.0 kcal·mol^{-1}) rather than $-T\Delta S^0_{exp.}$(ranging from -1.4 to +4.9 kcal·mol^{-1}).[5] The small entropic changes suggest that the counteraction between configurational and solvation entropy, $\Delta S^0_{exp.} = \Delta S^0_{conf.} + \Delta S^0_{solv.}$, leads to an almost balanced net effect in such cases. Recent papers on the thermodynamics of host-guest pairing involving CB7 focused on deriving the desolvation entropy of the cavity and the guest(s) from experimentally derived (total) entropy and calculated configurational entropy, in other words $\Delta S^0_{solv..} = \Delta S^0_{Exp..} + \Delta S^0_{Conf.}$. In these works, the theoretical estimation of the binding between CB7 and several different guests, $\Delta G^0_{calc.}$ versus experiment, $\Delta G^0_{exp.}$, achieved a notable level of accuracy. However, the single contributions to the enthalpic-entropic balance are always overestimated in the case of $\Delta H^0_{exp.}$(values are systematically nearly doubled compared to experiment) and underestimated in the case of $-T\Delta S^0_{exp.}$. To our knowledge, no study proposed the calculation of $\Delta S^0_{solv.}$ on pure computational bases.

This current work proposes an exhaustive computational investigation that dwells in three main areas of the thermodynamics of the binding between CB7 and adamantanyl/bicyloctanyl guests: the evaluation of the accuracy trend (versus $\Delta G^0_{exp.}$) of pure quantomechanic methods relying on implicit solvation and corrected statistical thermodynamics, the accurate study of the nature and strength of the interactions between CB7 and guests to justify the reported binding constants and, finally, the correct computational reproduction of the enthalpic-entropic compensation.

V.2. Objectives

Computational chemistry has been extensively employed to describe the enthalpic-entropic compensation typical of the molecular recognition of such macrocycles. Several interesting studies employing pure force fields or mixed DFT/force fields approaches have attempted to reproduce the trend of the thermodynamics of binding within the CB7·guest series. This present work proposes a detailed study on the nature and strength of the CB7 interactions with

[5] Moghaddam, S.; Yang, C.; Rekharsky, M.; Ko, Y. H.; Kim, K.; Inoue, Y.; Gilson, M. K., *J. Am. Chem. Soc.* **2011,** *133* (10), 3570-3581.

adamantanes, diamantanes and bycycloctanes and the first computational model able to reproduce the magnitude of the enthalpic/entropic changes seen for experimental binding via calorimetry.

V.3. Computational methods

The calculations were carried out using G09 D.01 program.[6] The structures were optimized at BLYP-D3/Def2SVP[7] level for gas phase and BLYP-D3/Def2SVP/SMD (water, ε = 78.3553) level for aqueous phase. Single point calculations on optimized structures have been done at BLYP-D3/Def2TZVPP[40] and BLYP-D3/Def2TZVPP/SMD[8] (water, ε = 78.3553) levels for gas and aqueous phases, respectively. Both implicit and implicit/explicit solvation schemes have been used in the study of host-guest encapsulation. Empirical dispersion has been introduced using Grimme and coworkers' D3 function with Becke-Johnson damping (D3BJ).[9] Dispersion-corrected Becke exchange functional (B) in conjunction with Lee-Yang-Parr functional (LYP)[10] provides reliable binding energies for a large variety of non-covalent complexes at very affordable computational cost.[11] Vibrational analysis has been carried out to identify the nature of obtained stationary points. Nth-order saddle points (when accidentally located by the optimization) have been reoptimized distorting the structure along the imaginary modes. Vibrational analysis has been carried out to obtain ZPE, enthalpic (H) and free energy corrections (G) to the electronic energy via

[6] M. J. Frisch, G. W. T., H. B. Schlegel, G. E. Scuseria, M. A. Robb, J. R. Cheeseman, G. Scalmani, V. Barone, G. A. Petersson, H. Nakatsuji, X. Li, M. Caricato, A. Marenich, J. Bloino, B. G. Janesko, R. Gomperts, B. Mennucci, H. P. Hratchian, J. V. Ortiz, A. F. Izmaylov, J. L. Sonnenberg, D. Williams-Young, F. Ding, F. Lipparini, F. Egidi, J. Goings, B. Peng, A. Petrone, T. Henderson, D. Ranasinghe, V. G. Zakrzewski, J. Gao, N. Rega, G. Zheng, W. Liang, M. Hada, M. Ehara, K. Toyota, R. Fukuda, J. Hasegawa, M. Ishida, T. Nakajima, Y. Honda, O. Kitao, H. Nakai, T. Vreven, K. Throssell, J. A. Montgomery, Jr., J. E. Peralta, F. Ogliaro, M. Bearpark, J. J. Heyd, E. Brothers, K. N. Kudin, V. N. Staroverov, T. Keith, R. Kobayashi, J. Normand, K. Raghavachari, A. Rendell, J. C. Burant, S. S. Iyengar, J. Tomasi, M. Cossi, J. M. Millam, M. Klene, C. Adamo, R. Cammi, J. W. Ochterski, R. L. Martin, K. Morokuma, O. Farkas, J. B. Foresman, and D. J. Fox *Gaussian 09, Revision D.01*, Gaussian, Inc., Wallingford CT, 2016.

[7] Weigend, F.; Ahlrichs, R., Balanced basis sets of split valence, triple zeta valence and quadruple zeta valence quality for H to Rn: Design and assessment of accuracy. *Physical Chemistry Chemical Physics* **2005,** *7* (18), 3297-3305

[8] Marenich, A. V.; Cramer, C. J.; Truhlar, D. G., *The Journal of Physical Chemistry B* **2009,** *113* (18), 6378-6396.

[9] Grimme, S.; Ehrlich, S.; Goerigk, L., *Journal of Computational Chemistry* **2011,** *32* (7), 1456-1465.

[10] Lee, C.; Yang, W.; Parr, R. G., *Physical Review B* **1988,** *37* (2), 785-789.

[11] (a) Grimme, S.; Antony, J.; Ehrlich, S.; Krieg, H., *The Journal of Chemical Physics* **2010,** *132* (15), 154104. (b) Sedlak, R.; Janowski, T.; Pitoňák, M.; Řezáč, J.; Pulay, P.; Hobza, P., *Journal of Chemical Theory and Computation* **2013,** *9* (8), 3364-3374. (c) Hostaš, J.; Sigwalt, D.; Šekutor, M.; Ajani, H.; Dubecký, M.; Řezáč, J.; Zavalij, P. Y.; Cao, L.; Wohlschlager, C.; Mlinarić-Majerski, K.; Isaacs, L.; Glaser, R.; Hobza, P., *Chemistry – A European Journal* **2016,** *22* (48), 17226-17238.

statistical thermodynamics. The standard states used to calculate the variation of thermodynamic functions (ΔH, ΔS and ΔG) have been chosen as 298K/1 atm for gas phase and 298 K/1M for aqueous phase. GoodVibes v. 2.0.3 has been used to introduce the quasi-harmonic correction to the entropic term derived from low-frequency vibrations (cut-off set at ν < 100 cm^{-1}). Grimme's correction scheme to low-frequency vibrations is particularly suited for supramolecular systems.[12] The initial atomic coordinates for the guess structures of the water clusters used in this article have been extracted from the work of Kazachenko and co-workers.[13] In few cases the structures optimized by all the five potentials have been re-optimized to test the performances of each potential versus dispersion-corrected DFT. Generally, AMOEBA potential (Atomic Multipole Optimized Energetics for Biomolecular Applications)[14] seemed to afford the most stable structures compared to those optimized by the other four potentials[13] and this trend is also respected when the structures are re-optimized with DFT (i.e., the structures coming from AMOEBA optimization result to be global minima in DFT). Def2SVP and Def2TZVPP are naturally constructed using spherical harmonics (5D 7F functions), thus single point calculations with pure functions (6D 10F) have been run on optimized structures to generate wfx inputs for the quantum atoms-in-molecule analysis (QTAIM).[15] QTAIM, molecular volumes (in $Å^3$ at 0.05 isovalue of density), non-covalent interactions surfaces (NCI) and domain integration of electron density (defined as $\rho(\mathrm{r}) = \sum_i \eta_i |\varphi_i(r)|^2$) have been carried out using MULTIWFN v3.6 (multicore LINUX version).[16] The search for critical points has been carried out until the Poincaré-Hopf relationship, $n_{(3,-3)} - n_{(3,-1)} + n_{(3,+1)} - n_{(3,+3)} = 1$, has been satisfied. Reduced density gradient function used to generate NCI plot at 0.6 isovalue is defined as $\mathrm{EDG}(\mathrm{r}) = \frac{1}{2(3\pi^2)^{1/3}} \cdot \frac{|\nabla\rho(r)|}{\rho(r)^{4/3}}$.[17] Scatter plots to

[12] Grimme, S., *Chemistry – A European Journal* **2012,** *18* (32), 9955-9964.
[13] Kazachenko, S.; Thakkar, A. J., *The Journal of Chemical Physics* **2013,** *138* (19), 194302.
[14] (a) Ponder, J. W.; Wu, C.; Ren, P.; Pande, V. S.; Chodera, J. D.; Schnieders, M. J.; Haque, I.; Mobley, D. L.; Lambrecht, D. S.; DiStasio, R. A.; Head-Gordon, M.; Clark, G. N. I.; Johnson, M. E.; Head-Gordon, T., *The Journal of Physical Chemistry B* **2010,** *114* (8), 2549-2564. (b) Ren, P.; Ponder, J. W., *The Journal of Physical Chemistry B* **2003,** *107* (24), 5933-5947. (c) Ren, P.; Wu, C.; Ponder, J. W., *Journal of Chemical Theory and Computation* **2011,** *7* (10), 3143-3161. (d) Ren, P.; Ponder, J. W., *The Journal of Physical Chemistry B* **2004,** *108* (35), 13427-13437.
[15] (a) Bader, R. F. W., Oxford University Press: Oxford, 1990. (b) Kumar, P. S. V.; Raghavendra, V.; Subramanian, V., *Journal of Chemical Sciences* **2016,** *128* (10), 1527-1536.
[16] (a) Lu, T.; Chen, F., *Journal of Computational Chemistry* **2012,** *33* (5), 580-592. (b) Lu, T.; Chen, F., *Journal of Molecular Graphics and Modelling* **2012,** *38*, 314-323.
[17] Johnson, E. R.; Keinan, S.; Mori-Sánchez, P.; Contreras-García, J.; Cohen, A. J.; Yang, W., *J. Am. Chem. Soc.* **2010,** *132* (18), 6498-6506.

visualize weak interactions, RDG(r) versus sign(λ_2)ρ in a.u., have been generated using the scripts courteously provided by Lu in MULTIWFN folder. The strength of the hydrogen bonding and Van der Waals interactions, X-H•••A, has been determined via bond critical point (BCP) and its thermodynamic contribution using Espinosa and coworkers' method[18] and Grabowski's method.[19] CHIMERA v.1.13.1[20] and VMD v. 1.9.3[21] have been used to visualize, render and generate all the graphical content included in this work via POV-Ray[22] and Tachyon[23] ray tracing libraries, respectively.

V.4. Results and discussion

The combination of method/basis set to investigate this chemistry has been chosen following the work published by Hostaš and co-workers.[11c] The authors evidenced the excellent estimation of the electronic energy for formation of host-guest pairs provided by calculations at BLYP-D3/Def2TZVPP//BLYP-D3/Def2SVP level.[11c] We also briefly tested few other functionals (GGA, meta-GGA and hybrids) in order to compare with the results obtained by BLYP-D3. B97D3 and LC-ωPBE provided the closest results, in decent agreement with the experimental thermodynamics (i.e., 5-6 kcal.mol^{-1} error).[32, 64] The optimizations carried out at BLYP-D3/Def2SVP/SMD level generally provide excellent structures, in good agreement with those obtained from X-ray structures. Hostaš and co-workers reported a 0.039-0.115 Å root mean square difference in the metric parameters between optimizations carried out at BLYP-D3/Def2SVP and BLYP-D3/Def2TZVPP on the same subset of host-guest pairs.[11c] Our calculations reproduce an excellent approximation of the cavity size of CB7 by domain integration of electron density (ρ). Fig. 1 visualizes the cavity available for binding in CB7 at ρ values < 0.0001 (top) and < 0.005 (bottom), respectively. The volume calculated at the former isovalue (< 0.0001), 135 Å^3 (entry #1 in Tab. 1, 2nd column), represents a lower bound estimation of the cavity, readily usable without causing severe distorsion to the CB7 structure. The volume calculated at the

[18] Espinosa, E.; Molins, E.; Lecomte, C., *Chemical Physics Letters* **1998,** *285* (3), 170-173.
[19] Grabowski, S. J., *The Journal of Physical Chemistry A* **2001,** *105* (47), 10739-10746.
[20] Pettersen, E. F.; Goddard, T. D.; Huang, C. C.; Couch, G. S.; Greenblatt, D. M.; Meng, E. C.; Ferrin, T. E., *Journal of Computational Chemistry* **2004,** *25* (13), 1605-1612.
[21] Humphrey, W.; Dalke, A.; Schulten, K., *Journal of Molecular Graphics* **1996,** *14* (1), 33-38
[22] Ltd., P. o. V. P. *Persistence of Vision(TM) Raytracer*, 3.6; Williamstown, Victoria, Australia, 2004.
[23] Stone, J. University of Missouri-Rolla, 1998.

latter isovalue (< 0.005), 272 Å^3 (entry #1 in Tab. 1, 3rd column), is in excellent agreement with the value provided by published results, 279 Å^3.[16, 29] The cavity is not rigid by any means and has the ability to contract or expand depending on the size and the binding mode of the encapsulated substrate. For instance, our calculations point out that 1-adamantanyl-NH_3I causes a minor shrinking of the volume of the cavity, ~ -1.5% (entry #2 in Tab .1), while diamantane-4,9-di(NMe_3I), considered one of the largest and bulkiest guests in our subset, causes a ~ 4.4% enlargement (entry #3 in Tab. 1). Our calculations confirm that the enlargement in the volume is due almost entirely to the enlargement of the O=C portal, 8.367 versus 8.467 Å in the free CB7, while the equatorial diameter is essentially unchanged, 11.673 versus 11.657 Å in the free CB7. These findings are in line with the variations seen in the crystal structure of CB7· diamantane-4,9-di(NMe_3I)[33] compared to the structure of the free CB7[65-66]; the equatorial diameter goes from 11.70(5) Å for the complex to 11.6(2)-11.7(9) Å for the free host, while the portal diameter goes from 8.62(3) Å to 8.4(4)-8.6(3) Å, respectively (albeit the limited precision of the crystallographic data). Our calculations provide good metric parameters and geometries in agreement with previous calculations[46] and X-ray diffractions[33, 64, 67]. The binding modes reported for CB[7]·guest chemistry[46] are also reproduced in excellent agreement to previous data. HG2, HG3, HG7 and HG8 complexes (Fig. 1) show *primary ammonium binding mode*[46], where the host-guest pair does not possess circular equatorial cross section and the C_{ada}-N bond of the guest is slightly tilted and not co-axial with the rotational C_7-axis of the host. This binding mode is enhanced by the formation of hydrogen bonding between the amino group(s) and the O=C functionalities of the host.[11c] The crystal structure of HG7 show that the averaged C=O•••H_2N-C_{ada} distances are 2.070(4). The same averaged distance obtained by our calculations is 2.070(4) Å. HG6, HG9 and HG10 complexes (Fig. 1) show *quaternary aminium binding mode*,[11c] where the C_{ada}-N bond of the guest is co-axial with the rotational C_7-axis of the CB[7]. The crystal structures of HG6, HG9 and HG10 show that the averaged C=O•••H_3C-N-C_{ada} distances are 2.070(4), 2.070(4) and 2.070(4) Å, respectively. The same averaged distances obtained by our calculations are 2.53, 2.58 and 2.51 Å, respectively. A few conformations were calculated for HG4 and HG5 complexes (Fig. 1) and the most stable ones show

loop binding mode,[11c] similar to the primary ammonium binding, but with the exception of having other position of the activated portal.

The thermodynamics calculated at BLYP-D3/Def2SVP level, however, shows very poor agreement with experimental thermodynamics and a single point correction at BLYP-D3/Def2TZVPP/SMD level (the results are nonetheless reported in the Supporting Information for comparison purposes), as already pointed out by Hostaš and co-workers.[11c] Higher accuracy in the calculation of the electronic energy can be achieved by switching from a double to triple-□ basis with a double set of polarization functions. The introduction of diffuse functions (i.e. Def2TZVPPD) is not advantageous in terms of computational cost/improvement ratio.

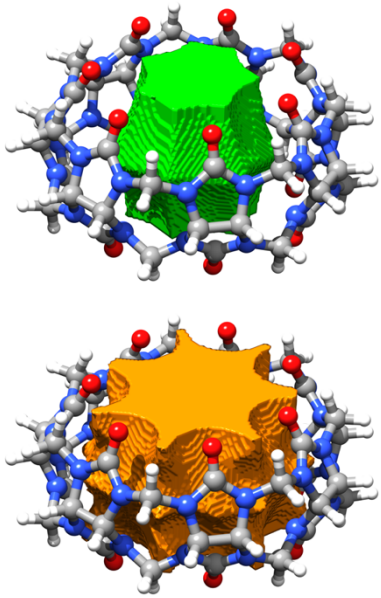

Figure 1. Hosting cavity of cucurbit[7]uril calculated by domain integration of electron density, □, obtained at BLYP-D3/Def2SVP/SMD (water) level at < 0.0001 (top) and < 0.005 (bottom) isovalues, respectively.

Table 1. Height (z, Å), averaged thickness (av. x-y, Å) and volume (Å^3) of the internal hosting cavity of free and filled CB[7]

Species	*ρ < 0.0001*	*ρ < 0.005*
Free CB7	6.35, 6.14, 135	9.21, 7.57, 272
HG2 (Fig. 1)	6.24, 6.24, 130	9.10, 7.62, 268
HG10 (Fig. 1)	6.35, 6.30, 142	9.31, 7.67, 284

Host-guest calculations based on implicit solvation. Implicit solvation treats the solvent as a continuum envelope around the solute.[68] Implicit solvation is usually the simplest approach to introduce polarization effects from the solvent (i.e. dielectric) at an affordable computational cost.[69-70] Implicit solvation is very suitable for computational screening and *a priori* reagent and catalytic design. Fig. 2 shows our calculations of the free energy of binding for a series of known guests calculated at BLYP-D3/Def2TZVPP// BLYP-D3/Def2SVP level in conjunction with implicit pure water solvation (SMD). Tab. 2 reports a straightforward comparison with the experimental data in pure water and in buffer solution (50 mM NaO_2CCD_3 at pD 4.74).[28-29, 32, 64] We believe the computational vs experimental comparison of the data in pure water is the most rigorous and correct from a methodologic standpoint, since it has been demonstrated that Na^+ cations acts as competitive guest for the CB7, lowering by a ~10^2 factor the magnitude of the binding constants of the examined guests.[71-72]

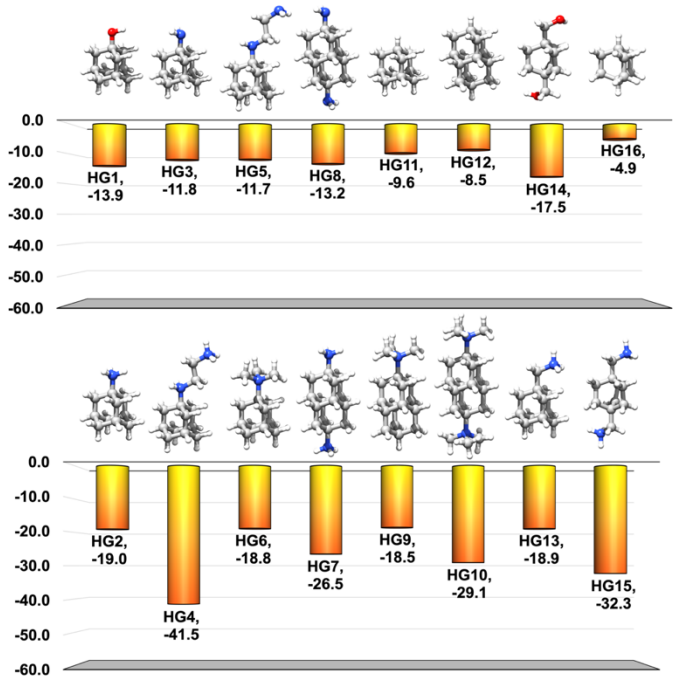

Figure 2. Top: $\Delta G^0_{calc.}$ of binding between CB7 and selected neutral guests. Bottom: $\Delta G^0_{calc.}$ of binding between CB7 and selected monocationic and dicationic guests. All values are in kcal·mol^{-1}.

Table 2. Calculated thermodynamics using SMD implicit solvation versus experimental thermodynamics in kcal·mol^{-1}

Species	Mol. Volume[a]	$\Delta H^0_{calc.}$	$T\Delta S^0_{calc.}$	$\Delta G^0_{calc.}$	$\Delta H^0_{exp.}{}^b$	$T\Delta S^0_{exp.}{}^b$	$\Delta G^0_{exp.}{}^b$	$\Delta G^0_{exp.}{}^c$
HG1	Xxx	-28.4	-14.5	-13.9	-19.0 ± 0.4	-4.9 ± 0.4	-14.1 ± 0.2	-xx.x
HG2	Xxx	-35.7	-16.7	-19.0	-19.3 ± 0.4	0.1 ± 0.5	-19.4 ± 0.1	-17.2
HG3	Xxx	-27.3	-15.5	-11.8	--	--	--	--
HG4	Xxx	-58.5	-17.0	-41.5	-20.1 ± 0.4	1.4	-21.5	-xx.x
HG5	Xxx	-28.8	-17.1	-11.7	--	--	--	N/A
HG6	Xxx	-35.4	-16.6	-18.8	--	--	--	-16.7
HG7	Xxx	-44.5	-18.0	-26.5	--	--	--	-15.2
HG8	Xxx	-29.1	-16.0	-13.2	--	--	--	--
HG9	Xxx	-36.5	-18.0	-18.5	--	--	--	-16.2
HG10	Xxx	-46.8	-17.7	-29.1	--	--	-24.3	-20.8
HG11	Xxx	-25.0	-15.3	-9.6	--	--	-13.4	--
HG12	Xxx	-25.0	-16.5	-8.5	--	--	-13.1	--
HG13	Xxx	-37.1	-18.3	-18.9	-21.9 ± 0.4	-1.7	-20.3	-xx.x
HG14	Xxx	-34.0	-16.5	-17.5	-15.8 ± 0.2	-2.4 ± 0.2	-13.4 ± 0.1	-xx.x
HG15	Xxx	-51.0	-18.6	-32.3	-15.6 ± 0.4	3.9 ± 0.5	-19.5 ± 0.2	-xx.x
HG16	Xxx	-19.3	-14.5	-4.9	--	--	--	--

[a]calculated molecular volume of the guest; [b]in pure water; [c]in 50 mM NaOAc Buffer at pH 4.74. $\Delta G^0_{exp.}$ values are obtained using the experimental binding constants via the equation $\Delta G^0_{exp.} = -RT\ln K_{eq.}$

The calculated entropic values reported in Tab. 2, $T\Delta S^0_{calc.}$, represent essentially variation in configurational entropic term at 1M (the sum of translational, rotational, conformational and vibrational entropies at 298 K) between the final bound state (host-guest pair) and the species separated at an infinite distance. Most of the entropic terms reported in Tab. 2 are in line with the configurational entropic term, $T\Delta S^0_{conf.}$, reported in published works. The thermodynamics of the binding of neutral oxygenated guests affecting essentially only one portal of CB7, like 1-adamantanol (HG1), for instance, is reproduced exceedingly well by our theory. Calculated $\Delta G_{Calc.}$ = -13.9 kcal·mol^{-1}, in fact, is in great agreement with

experimental $\Delta G_{Exp.}$ = -14.1 kcal·mol^{-1}. The calculations on neutral oxygenated guests activating both portals of CB7, like bicyclooctane-1,4-diyldimethanol (in complex HG14), provide reasonably good value of $\Delta G_{Calc.}$ = -17.5 kcal·mol^{-1}versus $\Delta G_{Exp.}$ = -13.4 kcal·mol^{-1}. Published M2 calculations provide a better estimation of the thermodynamics of binding for HG14.[32] This finding comes with no surprise since Moghaddam and co-workers reported that bicyclooctane-1,4-diyldimethanol shows a high solvation entropy (similar to monocationic guests) that contributes to lower the binding constant.[32] We also calculated neutral parent species without any amino or hydroxyl functionality, like adamantane and diamantane, to obtain a straightforward comparison for guest whose possibility to form pure hydrogen bonds with CB7 is null. Our calculations correctly reproduce the poorer binding of diamantane with respect to adamantane, $\Delta G_{Calc.}$ = -8.5 kcal·mol^{-1} and $\Delta G_{Exp.}$ = -9.6 kcal·mol^{-1}, respectively, albeit the computed values are somewhat lower than those reported in Assaf and Nau's review[28] as unpublished data, $\Delta G_{Exp.}$ = -13.1 kcal·mol^{-1} (for K = 4·10^{9} M^{-1}) and $\Delta G_{Exp..}$ = -13.4 kcal·mol^{-1} (for K = 7·10^{9} M^{-1}) respectively (these values are obtained by fluorescent indicator displacement). Electroneutrality of the cationic guests has been guaranteed introducing iodide atom(s) as counter-ion(s) in the calculations. Our choice fell upon the iodide counterion(s) because most of the experimental measurements of binding have been carried out on iodide salts.[64] Moreover, our calculations point out that the iodide shows an ubiquitous NBO charge of ~ -0.9 e^{-} within the whole subset studied in Fig. 2. This indicates that there is no charge transfer from the anion to the cation, nor participation of the anion into the binding process, and that the iodine species can be genuinely treated as an iodide anion, I^{-}. The estimation of the free energy of binding of monocationic adamantanyl ammonium salts in pure water show good agreement with reported experimental data: the calculations provide values of $\Delta G_{Calc.}$ = -19.0 kcal·mol^{-1} and $\Delta G_{Calc.}$ = -18.9 kcal·mol^{-1} for HG2 and HG13, respectively. Experimental data reported in literature show that the binding free energy for HG13 is marginally greater than that reported for HG2, with $\Delta G_{Exp.}$ = -20.3 kcal·mol^{-1} and $\Delta G_{Exp.}$ = -19.4 kcal·mol^{-1}, respectively. Neutral 1-adamantanyl ammine forming the HG3 complex displays a much weaker binding energy than the energy shown by the protonated species (HG2), $\Delta G_{Calc.}$ = -11.8 kcal·mol^{-1}. The kinetic aspects of protonation-

deprotonation mechanism of ammine guests before and after entering the cucurbituril cavity has been debated in recent literature.[16] The calculations for complexes displaying quaternary aminium binding mode, like HG6 and HG9, are also in very good agreement with the experimental data: values like $\Delta G_{Calc.}$ = -18.8 kcal·mol^{-1}, and $\Delta G_{Calc.}$ = -18.5 kcal·mol^{-1} agree very well with $\Delta G_{Exp.}$ = -16.7 kcal·mol^{-1} and $\Delta G_{Exp.}$ = -16.2 kcal·mol^{-1}, especially considering that the former are in pure water and the latter in a buffered solution, in presence of Na^+ cations acting as antagonists to the binding of the guest to CB7.[71-72] A difference of 10^2 in the binding constant coming from the presence of Na^+ cations corresponds to a variation of ~ -2.7 kcal·mol^{-1}, in the free energy of binding at 298 K and 1M standard state.

The calculations on diamantane-4,9-di(NMe_3I), complex HG10, still afford a quite benevolent value of the energy of binding, $\Delta G_{Calc.}$ = -29.1 kcal·mol^{-1}, when compared to its experimental counterpart, $\Delta G_{Exp.}$ = -24.3 kcal·mol^{-1}. The complete failure of the implicit solvation method is evident when one examines the data for the dicationic guests with the possibility of formation of pure hydrogen bonds. The free energy of binding in HG4, HG7 and HG15 is greatly overestimated by the calculations, $\Delta G_{Calc.}$ = -41.5 kcal·mol^{-1}, $\Delta G_{Calc..}$ = -26.5 kcal·mol^{-1}, $\Delta G_{Calc.}$ = -32.3 kcal·mol^{-1} versus $\Delta G_{Exp.}$ = -21.5 kcal·mol^{-1}, $\Delta G_{Exp..}$ = -15.2 kcal·mol^{-1} (in buffer) and $\Delta G_{Exp.}$ = -19.5 kcal·mol^{-1}, respectively. It is interesting to notice that such overestimation is not dependent on the activation of one or two portals: the highest error, ~ -20 kcal·mol^{-1}, is reported for HG4. This finding is completely in line with Moghaddam and coworkers' estimation of ~ -18 kcal·mol^{-1}for the desolvation entropy of dicationic (+2) guests.[32]

In summary, *ab initio* DFT calculations relying on implicit solvation are definitely a good choice to describe semi-quantitatively the thermodynamics of binding between CB7 and neutral or monocationic adamantanyl/diamantanyl/cyclooctyl species, provided such guests only activate a single portal of the cucurbituril host. In our opinion, DFT calculations may represent a reliable alternative to force fields (faster, but dependent on a heavy parametrization in most of the cases) and may be used efficiently to obtain good predictions on catalytic design involving CB7.

QTAIM analysis. Published literature claims the presence of several interactions between negatively charged portal(s) of the CB7 and the guest: the negative

charge of the oxygens of the portals comes from the strong dipolarity of the carbonyl groups.[16, 28-29] This is why many authors refers to ion-dipole interactions.[16, 28-29] Depending on the nature and on the chemical structure of the guest, the upper and the lower portal of CB7 may be activated and engaged in the bond with the guest. Bader's QTAIM analysis is a post-wavefunction analysis that relies on the calculations of critical points in the electron density, ρ.[53] QTAIM allows the visualization and quantification in magnitude of strong and weak interactions. The pathways connecting nuclear attractors, also called (3, -3) points, between the CB7 and the guest define the pathway of an existing interaction. A local maximum between two nuclear attractors, also called bond critical point, BCP (3, -1), conveys information on the nature and strength of the interaction.[53] Fig. 3 show a comprehensive study of the topological aspects of ρ in three paradigmatic complexes: HG1 (top) featuring a hydroxyl site, HG2 (middle) featuring a primary ammonium site and HG10 (bottom) featuring two quaternary ammonium sites (the interactions seen in Fig. 3 for HG1, HG2 and HG10 complexes are also present in all the other examples described so far). Top views of the complexes presented on the left side of Fig. 3 describe the overlay of critical points, molecular graphs and reduced density gradient maps. Snapshots of interesting interactions are reported for clarity on the right side of Fig. 3 supported by RDG versus sign(λ_2) ρ scatter plots. These tools are able to describe non-covalent interactions.[57] Red color identifies steric hindrances, green color identify Van Der Waals interactions and blue color indentify genuine hydrogen bonds.

Following our analysis, the first important considerations to be done on CB7-guest chemistry are that all the weak interactions between CB7 and guest show positive values of the Laplacian of the electron density at critical points, $\nabla^2\rho$; the values of eta index at BCP, defined as the ratio between the lowest and the highest eigenvalues of the Hessian matrix of ρ, $\eta(r) = |\frac{\lambda_1(r)}{\lambda_3(r)}|$, are generally much lower than unity (~ 0.600);[73-74] ellipticities (ε (r)) of the bonds are generally very low. All these insights taken together are univocally denying the presence of (single or multiple) covalent bonds, rather they point to the presence of closed-shell interactions, like hydrogen bonds.[53] Secondly, we noticed that all carbonyl group of the portals are engaged in some type of interaction with the different

functionality of the hosts. HG1 shows one Guest-O-H•••O=C-Host interaction between the hydroxyl group and a single carbonyl of the upper portal. RDG map and scatter plot identify this interaction as a genuine hydrogen bond, with ρ= 0.0007 and sign(λ_2) ρ ~ -0.03 at BCP critical point (Fig. 3, top). This H-bond accounts for ~ 5.46 kcal·mol^{-1} (Espinosa)/~ 5.46 kcal·mol^{-1} (Grabowki) of the binding enthalpy between CB7 and the 1-adamantanol (G1). The encapsulation of 1-adamantanol leads to a 10% weakening of the hydroxyl group of the free guest (ρ = 0.0007). HG2 shows two Guest-N-H•••O=C-Host interactions between the amino group and two close carbonyl groups. Again, RDG map and scatter plot identify these interactions as a genuine hydrogen bonds, with ρ = 0.0007 and 0.0008 and sign(λ_2) ρ ~ -0.03 and -0.04 at the respective BCP critical points. These H-bonds account for ~ 5.46 kcal·mol^{-1} (Espinosa)/~ 5.46 kcal·mol^{-1} (Grabowki) and ~ 5.46 kcal·mol^{-1} (Espinosa)/~ 5.46 kcal·mol^{-1} (Grabowki), respectively. The encapsulation of 1-adamantanyl ammonium iodide leads to a 10% and 10% weakening of the N-H bonds of the amino group of the free guest (ρ = 0.0007). These N-H•••O=C interactions are stronger than O-H•••O=C, as evidenced by the relative magnitudes of ρ at BCPs and the thermodynamic extrapolated using Espinosa[58] and Grabowski[59] methods. We believe this is due to the fact that 1-adamantanylammino iodide is a salt and the presence of a positive charge on the cationic part of the guest greatly enhance the binding with CB7 via hydrogen bonding. Albeit almost isovolumetric, G1 is a neutral guest and its O-H proton is less polarized than the N-H protons in G2. Moreover, HG3, the complex with 1-adamantanylamine, shows unequivocally that N-H•••O=C interactions are still in the range of H-bond, but they become weaker than those in the corresponding salt (HG1), with ρ = 0.0007 and 0.0008 and sign(λ_2) ρ ~ -0.03 and -0.04, respectively. These hydrogen bonds account for ~ 5.46 kcal·mol^{-1} (Espinosa)/~ 5.46 kcal·mol^{-1} (Grabowki) and ~ 5.46 kcal·mol^{-1} (Espinosa)/~ 5.46 kcal·mol^{-1} (Grabowki), respectively. NBO charges confirms that the highest polarization of the proton(s) is present on 1-adamantanyl ammonium salt (G2), 0.120 e$^-$, followed by 1-adamantanol (G1), 0.120 e$^-$, and 1-adamantanylamine (G3), 0.120 e$^-$. Similar values of hydrogen bond strengths are observed for interactions involving hydroxyl and ammino groups of adamantanyl guests like HG7, HG8 and HG13 and bicicloоctyl guests like HG14 and HG15. HG7 shows

the formation of three Guest-N-H•••O=C-Host hydrogen bonds between diamantane-4,9-di(NH_3I) and CB[7] in the upper portal, with ρ = 0.0007, 0.0007, 0.0007 (~ av. 5.46 kcal·mol^{-1} (Espinosa)/~ av. 5.46 kcal·mol^{-1} (Grabowki) and two hydrogen bonds in the lower portal, ρ = 0.0007, 0.0007, 0.0007 (~ av. 5.46 kcal·mol^{-1} (Espinosa)/~ av. 5.46 kcal·mol^{-1} (Grabowki).

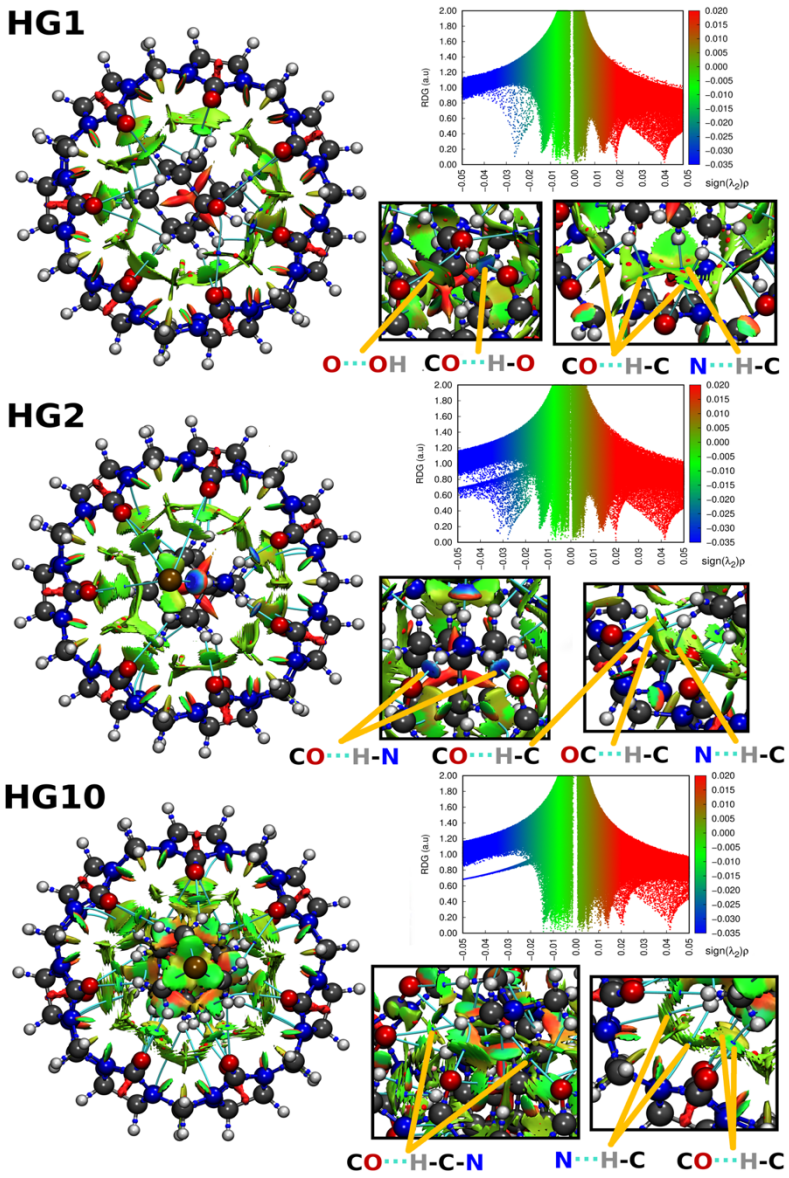

Figure 3. Left: top views of the complexes HG1, HG2 and HG10 evidencing non-covalent interactions (NCI) through reduced density gradient surfaces (RDG). The maps are overlaid with molecular graphs allowing the visualization of weak interaction between CB7 and the guest: blue dots represent bond critical points, BCP (3, -1), and cyan lines represent bond pathways, connecting nuclear attractors via BCP. Right: selected magnified snapshots of important interactions and RDG versus sign(λ_2) ρ scatter plots. Red color in the maps and scatter plots represent steric hindrances, green color represents Van Der Waals interactions and blue color represents hydrogen bonds.

Also in this case, H8, the neutral diamantane-4,9-di(NH_2), shows weaker N-H•••O=C hydrogen bonds (ρ = 0.0007 and 0.0007, ~ av. 5.46 kcal·mol^{-1} (Espinosa)/~ av. 5.46 kcal·mol^{-1} (Grabowki)) than its dicationic counterpart, G7. HG13 shows the formation of three Guest-N-H•••O=C-Host hydrogen bonds between 1-adamantanyl methanaminium cation (G13) and CB[7] in the upper portal; the strength of such interactions, with ρ = 0.0007, 0.0007 and 0.0007 ((~ av. 5.46 kcal·mol^{-1} (Espinosa)/~ av. 5.46 kcal·mol^{-1} (Grabowky) is < 3% weaker than the corresponding interactions in HG2 complex. HG14 shows the formation of two Guest-O-H•••O=C-Host hydrogen bonds between bicyclooctane-1,4-diyldimethanol and CB7 in the upper portal, with ρ = 0.0007, 0.0007, 0.0007, and two hydrogen bonds in the lower portal, ρ = 0.0007, 0.0007, 0.0007. HG15 shows the formation of two Guest-N-H•••O=C-Host hydrogen bonds between bicyclooctane-1,4-diyldimethanaminium dication and CB7 in the upper portal, with ρ = 0.0007, 0.0007, 0.0007, and two hydrogen bonds in the lower portal, ρ = 0.0007, 0.0007, 0.0007. Not surprisingly, the hydrogen bonds in the dicationic species G15 are 10% stronger than in the neutral counterpart G14, albeit the species are almost identical in binding mode, molecular structure and volume.

The most interesting aspect of CB7 host-guest chemistry, however, concerns the network of Guest-C-H•••O=C-Host weak interactions present around the adamantanyl portion of the guest moieties (Fig. 3, see the snapshots). These weak interactions are topologically assimilated to Van der Waals interactions, with sign(λ_2) ρ ~ 0 at the respective BCPs. These interactions are also known in some scientific communities as 'weak' hydrogen bonds.[10] The green regions of the scatter plots in Fig. 3 show that these localized interactions are present in a nearly equal number in HG1 and HG2 complexes (i.e. confronting the values of sign(λ_2) ρ comprised between -0.01 to 0.01). The strength of these interactions is in 0.001 < ρ < 0.002 range. The thermodynamics of these interactions suggests values of ranging from ~ 5.46 to 6.45 kcal·mol^{-1} (Espinosa)/~ 5.46 to 6.45 kcal·mol^{-1} (Grabowki). Most interestingly, the scatter plot for the complex HG10 does not show the presence of any localized hydrogen bonds (blue portion of the plot) in Fig. 3. Thus we must infer that the "attomolar" guest diamantane-4,9-di(NMe_3I), (G10), does not form any hydrogen bonds with CB7, nor via methyls on the

quaternary ammonium functionalities, or via the diamantane skeleton itself. At the same time, however, the number of Van der Waals interactions (or 'weak' hydrogen bonds) increases substantially compared to HG1 or HG2. as demonstrated by the top views and the scatter plots (green areas) of Fig. 3. Methyl groups on the quaternary nitrogens interact ~ 10% stronger with CB[7] portals than the hydrogen on the adamantane portion of the guest average $\rho \sim 0.0007$ and averaged thermodynamic contribution of ~ 5.46 kcal·mol^{-1} (Espinosa)/~ 5.46 kcal·mol^{-1} (Grabowki)). This is not unexpected considering that such protons are only two bonds far away from a strong electronegative group like nitrogen: their increased polarization is confirmed by NBO charges, 0.67 e$^-$ av. versus 0.67 e$^-$ av. for the adamantane protons. Similar results are obtained for systems displaying quaternary aminium binding mode like HG6 and HG9: such systems compensate the absence of strong hydrogen binders with a large number of N-CH_2-H•••O=C interactions that, cumulatively, provide great thermodynamic stability to the complex.

Two further aspects caught our attention during these topological studies. Firstly, the lower portal of CB7 is always engaged into some type of interactions with the guest, whether the guest itself is (like G1 or G2) or is not a double-portal activator (like G7 or G10). In absence of possible formation of strong hydrogen bonds for the presence of amino and hydroxyl groups, the C=O groups of the lower portal do not remain inactive, rather they interact with the lower section of the guest (whether adamantane or cyclooctane) via C-H•••O=C interactions. Secondly, it is common believe that the nitrogen atoms inside the cavity are not participating in the bond with the host; this is due to a substantially high delocalization of the nitrogen lone-pairs into the conjugated carbonyl system.[16] We found instead that the nitrogen atoms are not as innocent as believed and they participate in weak interactions with aliphatic hydrogens of the adamantanyl scaffold. These interactions are nearly ubiquitous for any guest. As the previous interactions in the cavity, these C-H•••N interactions can be classified as Van der Waals interactions (or weak hydrogen bonds): for instance, randomly selected C-H•••N interactions in HG1 shows critical points of 0.008 and 0.008 with an estimated bond strength of ~ 5.46 kcal·mol^{-1} (Espinosa)/~ 5.46 kcal·mol^{-1} (Grabowki), C-H•••N interactions in HG1 shows critical points of 0.008 and 0.008 with an

estimated bond strength of ~ 5.46 kcal·mol^{-1} (Espinosa)/~ 5.46 kcal·mol^{-1} (Grabowki) and C-H•••N interactions in HG1 shows critical points of 0.0008 and 0.0008 with an estimated bond strength of ~ 5.46 kcal·mol^{-1} (Espinosa)/~ 5.46 kcal·mol^{-1} (Grabowki).

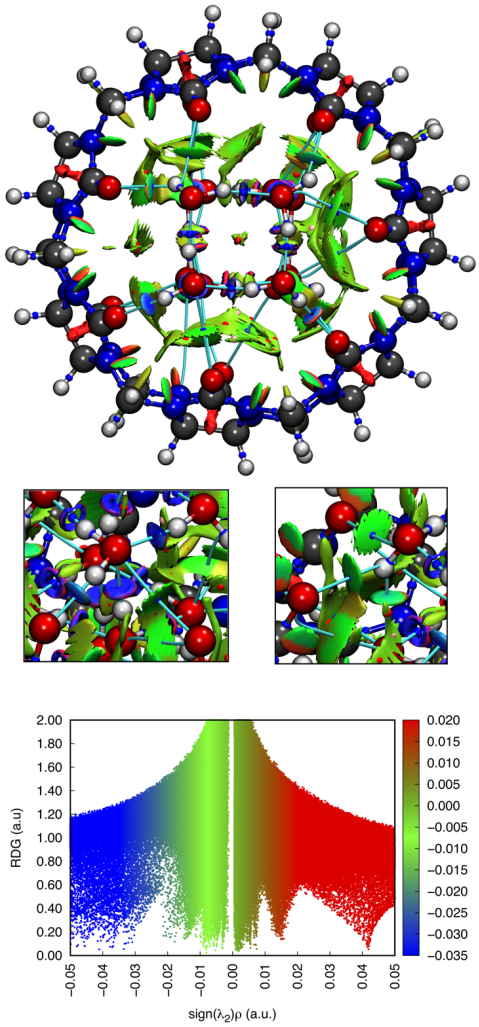

Figure 4. Top view of the complex between CB7 and a 18-water molecule cluster evidencing non-covalent interactions (NCI) through reduced density gradient surfaces (RDG). The maps are overlaid with molecular graphs allowing the visualization of weak interaction between CB7 and the “water” guest.

As a comparison. Fig. 4 shows the topological studies for the CB7.16 H_2O complex (introduced in the next session for thermodynamic reasoning). The scatter plot shows clearly that there is a net increment of hydrogen bonding in this ‘water’ complex (blue area) at the expense of Van der Waals interactions (green area). The steric hindrance (red area) is somewhat reduced as well compared to the plots of HG1, HG2 and HG10 (primarily for the absence of constrained adamantanyl moiety). Snapshots in Fig. 4 shows that there are

essentially three type of O-H•••O interaction: intramolecular hydrogen bonds (within H_2O molecules of the cluster), strong Guest-O-H•••O=C-Host hydrogen bonds (blue contoured areas) and 'weak' Guest-O-H•••O=C-Host hydrogen bonds (green contoured areas). Intramolecular hydrogen bonds (with average ρ ~ 0.0007 and averaged thermodynamic contribution of ~ 5.46 kcal·mol^{-1} (Espinosa)/~ 5.46 kcal·mol^{-1} (Grabowki)) are ~ 10% stronger on average than the strong host-guest hydrogen bonds with average ρ ~ 0.0007 and averaged thermodynamic contribution of ~ 5.46 kcal·mol^{-1} (Espinosa)/~ 5.46 kcal·mol^{-1} (Grabowki)) and ~ 10% stronger than the weak host-guest hydrogen bonds with average ρ ~ 0.0007 and averaged thermodynamic contribution of ~ 5.46 kcal·mol^{-1} (Espinosa)/~ 5.46 kcal·mol^{-1} (Grabowki)).

Implict/explicit solvation models. coworkers suggested that the peculiarity of the enthalpic-entropic compensation arises from the presence of highly activated water molecules in the cavity of CB7. (ref.) Their study focused on the optimization of such molecules in the cavity by the use of molecur dynamics. (ref.) Our strategy considered the water as a rigid, non-fluxional and not rearrangeable guest. Fig. 4 shows the thermodynamics of optimized species of CB7 and diverse "water" guests versusthe host in the gas phase and free water clusters: 8-, 12-,16- and 18-water molecules guests, in sequence. Stanichevko reports that the most stable structure for a cluster composed by eight molecules of water is a cubic arrangement; analogously the structure composed by twelve molecules of water is a cubic core with the addition of another 4-molecule layer, to give a parallelepipedal structure. (ref.) The cubic 8-cluster fits perfectly in the empty volume of the cavity without creating any strains on the structure of the host. This can be easily demonstrated by considering the volumetric change between the complex and the free host, estimated in the range of 0% by domain analysis. Despite the diverse approach on the mobility of the water molecules, our study seemsto agree with some other works; the group, in fact, reports the presence of 3-to-8 molecule of water in the inner cavity of CB7.(ref.) The 8-cluster and the 12-cluster are perfectly equal in two dimensions and only the length varies: the former is 7.56 Å long while the latter is 10.45 Å long, respectively. Volumetrically, the 12-cluster provides a much better coverage of the inner cavity of CB7 and of the upper and lower C=O portals (Fig. 4). As expected, the 12-cluster binds

almost ~5 kcal·mol^{-1} stronger than the 8-cluster in terms of DG. Introducing another layer of solvation, thus passing from 12 to 16 molecules of water, the length of the "water "guest further increases (10.45 Å) and fully covers both portals of the CB7. The addition of 4 molecules of water has little effect on the DG of binding, that decreases slightly from the previous guest (~0.3 kcal·mol^{-1}). Further increasing the water molecules count of 2 units (passing from 16 to 18) leads to a drop in the DG of binding, > 6 kcal·mol^{-1}. We believe that such an abrupt change in the series is due to the fact that one extra molecule of water has been inserted into the inner cavity, in other words from 8 to 9 molecules of water, as can be easily seen in the pentyl conformation seen inside the cavity for CB7 in Fig. 4. The entropic variation is almost constant for the four examined species and it slightly increases with the number of added molecules of water. The entropic penalty to remove the water guest from the CB7 is > 20 kcal·mol^{-1}.

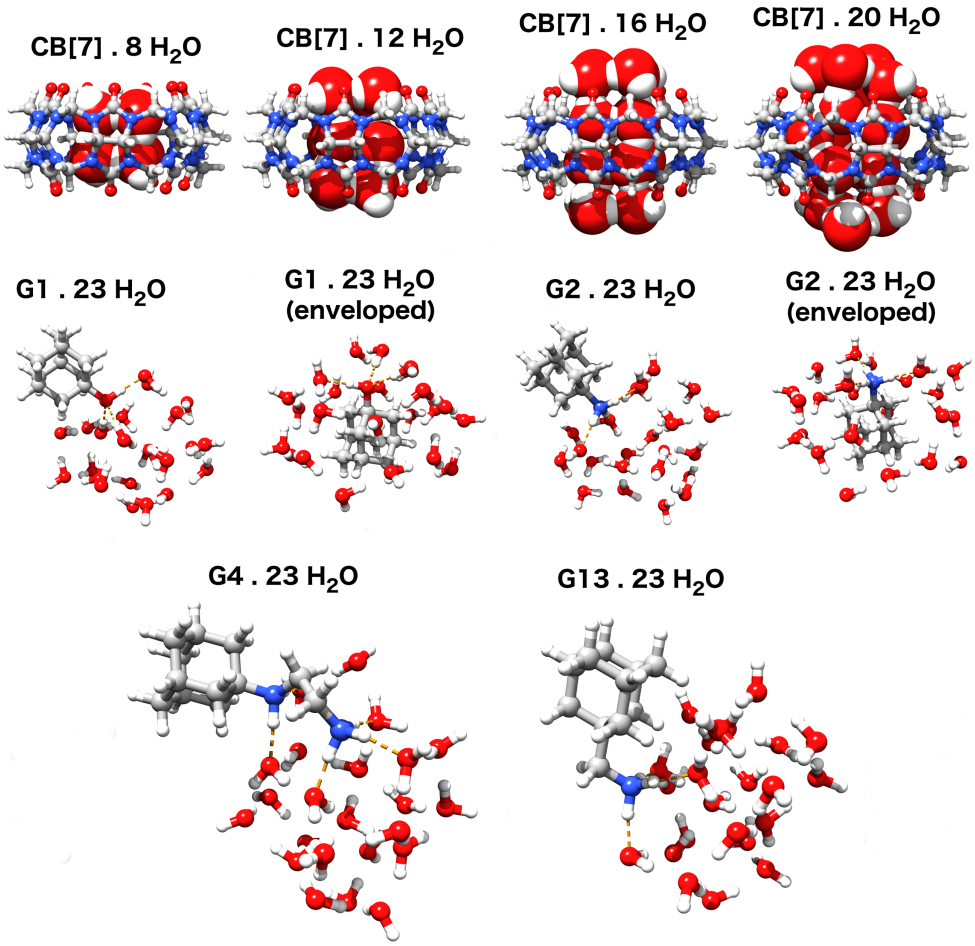

Figure 5. Morphology and relative calculated thermodynamics of host-guest pairs between CB7 and water nano-clusters at 298.15 K. Thermodynamic values are referred to the reaction.

Table 3

Species	$\Delta H^{0}_{Calc.}{}^{a}$	$-T\Delta S^{0}_{Calc.}{}^{a}$	$\Delta G^{0}_{Calc.}{}^{a}$	$\Delta H^{0}_{Calc.}{}^{b}$	$-T\Delta S^{0}_{Calc.}{}^{b}$	$\Delta G^{0}_{Calc.}{}^{b}$
CB[7].8 H_2O	-111.4	20.8	-90.6	-28.3	18.9	-9.3
CB[7].12 H_2O	-116.4	21.1	-95.3	-33.3	19.2	-14.0
CB[7].16 H_2O	-116.3	21.3	-95.0	-33.2	19.5	-13.7
CB[7].20 H_2O	-110.8	22.1	-88.7	-27.6	20.2	-7.4
G1.23 H_2O	-13.5	13.8	0.3	-12.5	11.9	-0.6
G2.23 H_2O	-67.6	13.9	-53.7	-17.4	11.8	-5.6
G4.23 H_2O	-203.3	17.1	-185.2	-28.1	14.1	-14.0
G13.23 H_2O	-70.5	14.0	-56.4	-19.1	12.4	-6.7

[a]calculated molecular volume of the guest; [b]in pure water; [c]in 50 mM NaOAc Buffer at pH 4.74. $\Delta G^{0}_{exp.}$ values are obtained using the experimental binding constants via equation $\Delta G^{0}_{exp.} = -RT\ lnK_{eq.}$

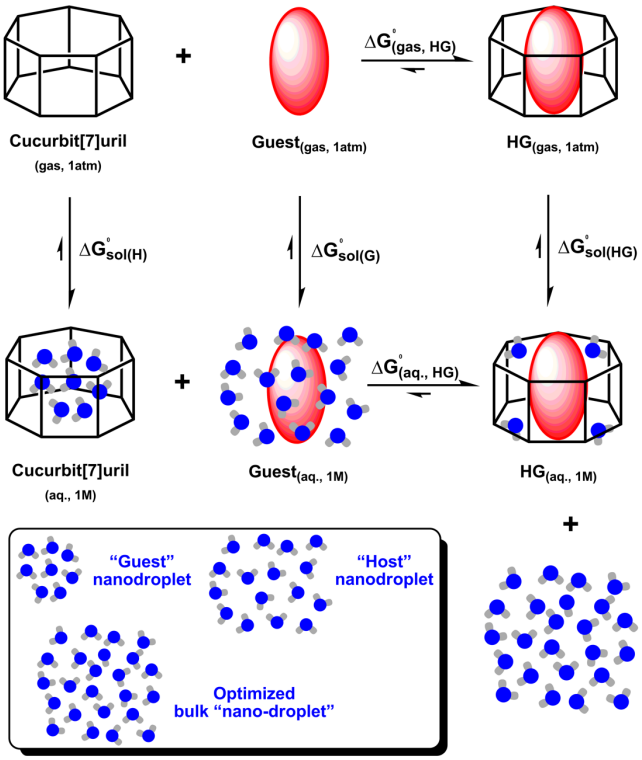

Figure 6

Table 4

Species	$\Delta H^{0\ a}_{Calc..}$	$-T\Delta S^{0\ a}_{Calc.}$	$\Delta G^{0\ a}_{Calc.}$	$\Delta H^{0\ b}_{Calc.}$
CB[7].8 H_2O	-111.4	20.8	-90.6	-28.3
CB[7].12 H_2O	-116.4	21.1	-95.3	-33.3
CB[7].16 H_2O	-116.3	21.3	-95.0	-33.2
CB[7].20 H_2O	-110.8	22.1	-88.7	-27.6
G1.23 H_2O	-13.5	13.8	0.3	-12.5
G1.23 H_2O (env.)				
G2.23 H_2O	-67.6	13.9	-53.7	-17.4
G2.23 H_2O (env.)				
G4.23 H_2O	-203.3	17.1	-185.2	-28.1
G13.23 H_2O	-70.5	14.0	-56.4	-19.1

CHAPTER VI

Conclusions

CHAPTER VI

Conclusions

The main goal of this thesis was to prepare cucurbituril immobilized magnetic nanoparticles for their potential applications in several fields such as catalysis or molecular recognition. First, in chapter II, we discussed the preparation and the resulting chemical and physical properties of the magnetic beads. Then, in chapter III, we get involved in asymmetric catalysis, and we studied the usability of the functional nanoparticles as chemical shuttles to recover organocatalysts from the reaction media. Later on, in chapter IV, we explored the applicability of the magnetically powered beads as nanocarriers to selectively extract, transport, and deliver selected molecules: in this case, we enriched testosterone levels from complex mixtures.

In chapter II, we strived to find out optimal conditions for the production of monofunctional cucurbiturils, prioritizing the macrocycle containing 7 glycoluril units, CB7. The studies steered our focus towards the large-scale production of monohydroxylated cucurbiturils through flow chemistry processes. The immobilization of the desired macrocycle was accomplished upon click chemistry. Iron oxide magnetic nanoparticles and polystyrene resins, coated with an azido-containing chemical layer, were reacted with the cucurbiturils bearing a terminal alkyne. Furthermore, the reaction was optimized for a green chemistry process. Hence, the unreacted cucurbiturils could be recovered and reused.

The solid-supported cucurbiturils were further characterized to disclose their physical and chemical properties. For example, TEM analyses were performed to study the shape and morphology of the particles. Several solvents were used to test the superparamagnetic behavior and the dispersion or agglomeration in solution. TGA, EA, IR spectroscopy, and other techniques were systematically employed to follow several parameters throughout the process (e.g., the functionalization, presence of cucurbituril or azide anchored onto the surface). Lastlly, NMR competition experiments and fluorescence studies allowed the determination of the effective functionalization and the efficiency of extraction (the

capacity of the functional beads to extract a selected molecule from the reaction media).

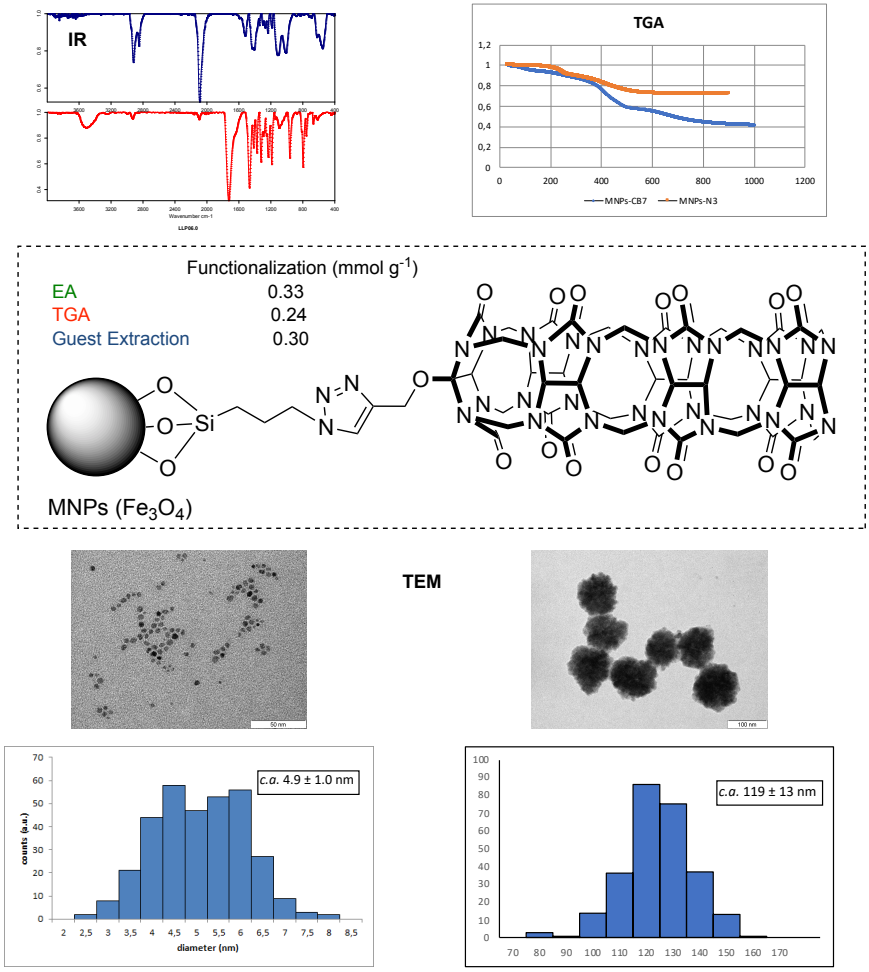

Figure V-1. Chapter II. Crafting nanodevices for molecular recognition and catalysis.

In chapter III, we stepped in the field of asymmetric catalysis. Considering the high affinity of CB7 for adamantyl-based compounds, we tailored model organocatalysts to accommodate an adamantyl moiety. The devised molecules were employed in model reactions (e.g., aldol reaction and Robinson annulation). The magnetically powered beads were used to recover the catalysts from the reaction media. Then, several conditions were screened to test the reusability of the catalytic cargo. The aldol reaction was tested with a proline-based catalyst. Attempts to recycle the catalyst with the functional beads coated with a layer of cyclodextrin were unsuccessful. The Robinson annulation was tested with a modified Luo's catalyst. In the same line, attempts to recycle the catalyst with cucurbituril coated beads were deemed inefficient. In both cases, because of deterioration and loss of the catalytic unit. Finally, biphasic studies for the aldol

reaction between benzaldehydes and cyclohexanones were attempted to prevent catalyst leakage. The reaction was carried out in water and the products extracted with an immiscible organic solvent, avoiding detrimental effects from the interaction between the solvent and the macrocycle. Despite this, the catalytic activity was also degraded after each catalytic cycle.

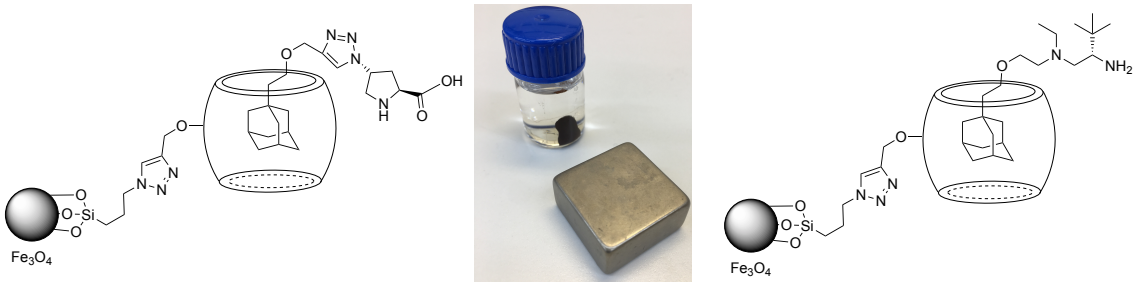

Figure V-2. Chapter III. CB7 anchored magnetic nanoparticles for catalyst recovering and recyclability.

These results suggested the importance of devising optimal catalytic species for each set of reactions. For instance, it is vital to consider the effect, on the assembled catalyst, of the starting material, product, and solvents. Each of them plays a crucial role. Even small displacements of the catalyst may have devastating effects over the course of the reactions. Considering the catalytic amounts of functional nanoparticles: it is possible that the more abundant starting material, even when it does not present any significant affinity for cucurbituril, can contribute to deteriorating the catalytic activity by leaking the assembled catalyst.

On the other hand, it is noteworthy mentioning that cationic species (e.g., adamantylammonium-based catalysts) that perform a much stronger association towards CB7 may relieve from this leaking problem while introducing another riddle: the conditions for catalyst desorption. Which in turns could be due to organic solvents, stronger guests, or more substantial amounts of guests with similar affinities.

In chapter IV, we engineered tailor-made derivatizing reagents for the extraction and detection of testosterone samples. The new set of compounds were optimized to excel in LC-MS/MS performance and selective removal by MNPs-CBs. To this end, the small molecules were designed to contained a quaternary ammonium salt to reduce signal suppression during ESI-MS and the cationic

adamantyl unit, that displayed extremely high affinity for CB7—giving rise to an almost exclusive selection for these set of molecules from complex mixtures.

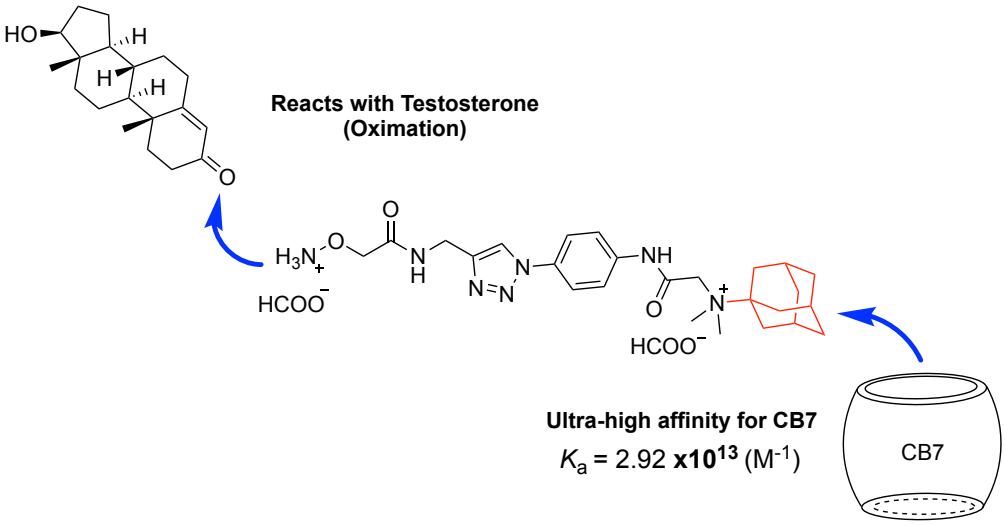

Figure V-3. Chapter IV. Testosterone extraction from complex mixtures

7

CHAPTER VII

Appendix

CHAPTER VII

Appendix

In this chapter we provide additional information of noteworthy projects that have been carried out during this doctoral thesis.

V.1. Coordinates for chapter V

Cartesian coordinates, Frequencies, Potential Energies and non-corrected Enthalpies and Free Energies

H (host, Cucurbit[7]uril)

Center Number	Atomic Number	Atomic Type	Coordinates (Angstroms) X	Y	Z
1	8	0	1.411282	-4.145606	3.038603
2	8	0	4.037103	-1.845297	3.025379
3	8	0	3.562633	1.799668	3.101954
4	8	0	0.414497	4.156377	3.079990
5	8	0	-3.073067	3.392909	3.047627
6	8	0	-4.214263	0.032125	3.069627
7	8	0	-2.148945	-3.287678	3.070205
8	8	0	0.889886	-4.063727	-3.075216
9	8	0	3.783738	-1.390561	-3.103258
10	8	0	3.738082	2.237233	-3.035837
11	8	0	0.852566	4.367406	-3.044131
12	8	0	-2.490547	3.099213	-3.081886
13	8	0	-4.132345	-0.570488	-3.064911
14	8	0	-2.664106	-3.746279	-3.038782
15	7	0	0.422633	-5.191093	1.183849
16	7	0	2.637996	-4.777690	1.144255
17	7	0	4.490680	-3.145273	1.128627
18	7	0	5.075017	-0.965160	1.113898
19	7	0	5.072094	1.483927	1.337232
20	7	0	3.748226	3.304421	1.309340
21	7	0	1.813268	4.812768	1.315660
22	7	0	-0.333615	5.487881	1.302516
23	7	0	-2.628503	4.619396	1.095901
24	7	0	-4.402903	3.226857	1.125397
25	7	0	-5.288333	0.924413	1.186350
26	7	0	-4.870421	-1.288172	1.243007
27	7	0	-3.719766	-3.447481	1.334935
28	7	0	-2.009673	-4.904171	1.380436
29	7	0	0.307932	-5.456660	-1.281244
30	7	0	2.356028	-4.522972	-1.302644
31	7	0	4.155972	-2.864188	-1.314947
32	7	0	5.272005	-0.908372	-1.359547
33	7	0	4.924485	1.523183	-1.138416
34	7	0	3.992297	3.577684	-1.131010
35	7	0	2.024715	5.070407	-1.143587
36	7	0	-0.219150	5.294108	-1.172569
37	7	0	-2.603435	4.709943	-1.382749
38	7	0	-4.019096	2.958776	-1.307784
39	7	0	-4.938400	0.688938	-1.255435
40	7	0	-5.170351	-1.552014	-1.206367
41	7	0	-3.994140	-3.721069	-1.109704
42	7	0	-2.092798	-4.930797	-1.095836
43	6	0	1.481896	-4.634040	1.912571
44	6	0	3.957320	-4.404407	1.621913
45	1	0	3.893672	-4.319953	2.720949
46	1	0	4.666484	-5.213024	1.353781
47	6	0	4.468373	-1.970782	1.880894
48	6	0	5.620219	0.216944	1.773807
49	1	0	5.398730	0.118210	2.851095
50	1	0	6.719817	0.240677	1.624350
51	6	0	4.059250	2.147028	2.031394
52	6	0	3.065976	4.424220	1.938671
53	1	0	2.831691	4.123039	2.975224
54	1	0	3.749102	5.301589	1.955503
55	6	0	0.604546	4.736081	2.011422
56	6	0	-1.720401	5.580156	1.713243
57	1	0	-1.751465	5.399243	2.802182
58	1	0	-2.078697	6.607979	1.498969
59	6	0	-3.330793	3.697789	1.884769
60	6	0	-5.393969	2.298936	1.643250
61	1	0	-6.402397	2.674890	1.376741
62	1	0	-5.282532	2.289458	2.741612
63	6	0	-4.719659	-0.092157	1.955277
64	6	0	-4.721617	-2.570456	1.911684
65	1	0	-5.700231	-3.097967	1.916686
66	1	0	-4.414302	-2.357302	2.951102
67	6	0	-2.567512	-3.807912	2.036676
68	6	0	-0.815061	-5.570498	1.854320
69	1	0	-0.696077	-5.313643	2.921878
70	1	0	-0.961365	-6.666316	1.753572
71	6	0	1.147871	-4.604489	-2.000832
72	6	0	3.566973	-4.038923	-1.938476
73	1	0	3.302217	-3.760404	-2.974244
74	1	0	4.320787	-4.856391	-1.954810
75	6	0	4.328529	-1.680133	-2.038818
76	6	0	5.635649	0.426928	-1.790053
77	1	0	5.413315	0.491247	-2.869633
78	1	0	6.725713	0.559743	-1.629535
79	6	0	4.154941	2.420802	-1.893958
80	6	0	3.362053	4.784197	-1.638376
81	1	0	3.283637	4.672419	-2.734181
82	1	0	4.017047	5.647332	-1.400903
83	6	0	0.881907	4.842479	-1.910058
84	6	0	-1.500187	5.538825	-1.825944
85	1	0	-1.356181	5.340651	-2.902695
86	1	0	-1.781954	6.602159	-1.681538
87	6	0	-2.969316	3.531209	-2.034464
88	6	0	-4.900967	1.980607	-1.921755
89	1	0	-5.930492	2.399622	-1.968988
90	1	0	-4.529549	1.803391	-2.946921
91	6	0	-4.670872	-0.489575	-1.962164
92	6	0	-5.095010	-2.936076	-1.642577
93	1	0	-4.980771	-2.927372	-2.740900
94	1	0	-6.048018	-3.434725	-1.374408
95	6	0	-2.884191	-4.079083	-1.875748
96	6	0	-1.050017	-5.751564	-1.697371
97	1	0	-1.256996	-6.818713	-1.475180
98	1	0	-1.099085	-5.588248	-2.788453
99	6	0	0.893355	-5.881935	-0.022293
100	1	0	0.780198	-6.978771	0.102313
101	6	0	2.382028	-5.411022	-0.138008
102	1	0	3.101828	-6.239644	-0.302811
103	6	0	5.086205	-2.957256	-0.184638
104	1	0	5.843371	-3.745089	-0.378385
105	6	0	5.685062	-1.511515	-0.104953
106	1	0	6.790836	-1.492621	-0.014878

107	6	0	5.427248	2.141298	0.092712
108	1	0	6.527740	2.269351	0.028370
109	6	0	4.640330	3.492774	0.164623
110	1	0	5.288907	4.378516	0.328453
111	6	0	1.728100	5.684751	0.142013
112	1	0	2.361242	6.584379	0.288119
113	6	0	0.192426	5.999503	0.047115
114	1	0	-0.032789	7.081439	-0.049893
115	6	0	-3.341546	4.919462	-0.150451
116	1	0	-3.743884	5.953136	-0.115122
117	6	0	-4.451985	3.816905	-0.201913
118	1	0	-5.467439	4.216040	-0.405734
119	6	0	-5.790161	0.440670	-0.087411
120	1	0	-6.812956	0.831682	-0.268912
121	6	0	-5.725114	-1.115481	0.062418
122	1	0	-6.713880	-1.589572	0.234127
123	6	0	-3.993748	-4.338166	0.208866
124	1	0	-4.947772	-4.880611	0.374367
125	6	0	-2.733217	-5.273663	0.174840
126	1	0	-2.980867	-6.355297	0.193688

Frequencies -- 14.3209 15.2197 18.7001
Frequencies -- 26.9250 42.0518 45.3858
Frequencies -- 53.4302 59.2348 62.6841
Frequencies -- 68.9633 75.9810 76.7487
Frequencies -- 82.0809 84.8683 88.1593
Frequencies -- 93.3381 98.0462 98.7765
Frequencies -- 102.5087 103.0619 105.9723
Frequencies -- 106.4447 109.0160 116.8332
Frequencies -- 128.4819 142.0947 142.8347
Frequencies -- 149.8328 153.4892 156.3565
Frequencies -- 157.1422 163.9726 169.7814
Frequencies -- 170.8006 175.3529 180.1294
Frequencies -- 181.6025 187.8853 191.7104
Frequencies -- 192.8746 199.9022 205.5605
Frequencies -- 208.2393 215.8875 226.0734
Frequencies -- 228.2663 237.1468 241.2855
Frequencies -- 243.4007 254.8560 258.2622
Frequencies -- 262.3953 266.1793 282.3574
Frequencies -- 283.8207 288.6248 290.5311
Frequencies -- 322.4010 330.7097 333.4906
Frequencies -- 338.3488 343.6518 345.0850
Frequencies -- 350.7835 352.6077 355.0221
Frequencies -- 355.1953 358.8813 359.6205
Frequencies -- 359.8431 362.4805 363.2075
Frequencies -- 365.3010 366.4271 370.5580
Frequencies -- 374.6789 411.5281 414.3387
Frequencies -- 414.9823 429.8314 434.8816
Frequencies -- 436.2508 445.7814 447.2552
Frequencies -- 450.3837 453.4540 455.5613
Frequencies -- 456.7134 510.3455 512.1629
Frequencies -- 580.2061 582.8315 597.5542
Frequencies -- 598.4016 608.0673 610.5233
Frequencies -- 611.4612 615.3844 617.0125
Frequencies -- 618.7116 622.3358 626.5060
Frequencies -- 640.5259 642.7886 645.6524
Frequencies -- 647.2619 648.9895 655.3684
Frequencies -- 660.3340 661.1856 666.3708
Frequencies -- 667.9411 670.7925 675.6532
Frequencies -- 687.2972 687.6504 698.1748
Frequencies -- 700.1917 702.0488 704.8322
Frequencies -- 705.4642 708.5417 710.6775
Frequencies -- 711.9170 712.5688 714.2099
Frequencies -- 714.8725 716.8572 717.6507
Frequencies -- 721.4883 723.0736 724.7429
Frequencies -- 727.1993 731.4077 768.0863
Frequencies -- 769.0206 777.3789 779.6561
Frequencies -- 780.3475 781.2285 788.2317
Frequencies -- 789.4480 792.3225 798.2210
Frequencies -- 801.7897 812.9106 813.6813
Frequencies -- 815.7076 819.1798 819.5390
Frequencies -- 820.1809 822.4036 823.6697
Frequencies -- 824.8204 825.7348 879.9241
Frequencies -- 883.5582 885.5835 895.9865
Frequencies -- 896.5056 910.7163 913.4632
Frequencies -- 938.9102 939.1116 941.5369
Frequencies -- 944.9398 951.7027 952.5137
Frequencies -- 954.1223 960.2310 960.8287
Frequencies -- 963.4035 970.3743 975.0441
Frequencies -- 976.1460 981.7756 983.7602
Frequencies -- 988.8962 992.1444 1004.2088
Frequencies -- 1006.6998 1009.5806 1010.7432
Frequencies -- 1023.4555 1026.1039 1028.8487
Frequencies -- 1029.1991 1035.1672 1036.1538
Frequencies -- 1040.4340 1084.4322 1087.0414
Frequencies -- 1093.7839 1098.2705 1101.0473
Frequencies -- 1103.2247 1104.0583 1112.6018
Frequencies -- 1113.2068 1114.4133 1123.1303
Frequencies -- 1136.2305 1138.4531 1149.6598
Frequencies -- 1164.9990 1166.1578 1167.5230
Frequencies -- 1178.8698 1179.9800 1181.1994
Frequencies -- 1189.5574 1191.4692 1191.8217
Frequencies -- 1197.1297 1199.1392 1200.6215
Frequencies -- 1201.7570 1208.4807 1209.2907
Frequencies -- 1210.6662 1212.7713 1214.0072
Frequencies -- 1215.0802 1215.7542 1216.8296
Frequencies -- 1222.5257 1225.5693 1225.7402

Frequencies -- 1226.5725 1229.1189 1231.1512
Frequencies -- 1234.6357 1249.2710 1250.6804
Frequencies -- 1256.5236 1258.1882 1262.9568
Frequencies -- 1263.6109 1264.5665 1265.3958
Frequencies -- 1267.6336 1269.9556 1272.9616
Frequencies -- 1274.4406 1275.6166 1278.0290
Frequencies -- 1291.7786 1295.0180 1296.1609
Frequencies -- 1298.9444 1302.5581 1303.6789
Frequencies -- 1305.3111 1310.5189 1313.1523
Frequencies -- 1313.9414 1314.2554 1316.5105
Frequencies -- 1322.6973 1323.9219 1359.8074
Frequencies -- 1361.0826 1361.3055 1364.3900
Frequencies -- 1365.1497 1367.8774 1368.1802
Frequencies -- 1369.2945 1370.7117 1371.4169
Frequencies -- 1372.7551 1372.9521 1374.0644
Frequencies -- 1375.2843 1375.5008 1377.1813
Frequencies -- 1377.7087 1378.2766 1379.6145
Frequencies -- 1380.3664 1381.4586 1381.5448
Frequencies -- 1381.6508 1382.6628 1383.5695
Frequencies -- 1384.6214 1384.7665 1385.3340
Frequencies -- 1386.6142 1388.6670 1389.3844
Frequencies -- 1390.6829 1391.8494 1392.0262
Frequencies -- 1392.7141 1393.5090 1394.7032
Frequencies -- 1397.5208 1400.0441 1400.7911
Frequencies -- 1403.6486 1404.7531 1428.0514
Frequencies -- 1430.6463 1433.7708 1435.7021
Frequencies -- 1437.7960 1438.8021 1440.2694
Frequencies -- 1441.1460 1442.4100 1443.0599
Frequencies -- 1443.7984 1444.6642 1447.2824
Frequencies -- 1449.2136 1712.8413 1713.1018
Frequencies -- 1717.7246 1718.3184 1720.4819
Frequencies -- 1720.7657 1724.2695 1724.9108
Frequencies -- 1726.8164 1729.1027 1730.4947
Frequencies -- 1740.4534 1740.8684 1746.3687
Frequencies -- 2940.5393 2944.3375 2949.9395
Frequencies -- 2950.1177 2971.0415 2971.1661
Frequencies -- 2972.1481 2974.1195 2974.6705
Frequencies -- 2976.0255 2976.8758 2977.4109
Frequencies -- 2977.5661 2977.8115 2978.2825
Frequencies -- 2978.7506 2979.0868 2979.2694
Frequencies -- 2979.7494 2980.5954 2980.9198
Frequencies -- 2983.2010 2983.4228 2984.2705
Frequencies -- 2984.7798 2986.7086 2990.8193
Frequencies -- 2991.7268 3063.7874 3064.5552
Frequencies -- 3066.0012 3066.6191 3069.6363
Frequencies -- 3070.5342 3071.0494 3071.1448
Frequencies -- 3072.1580 3072.4344 3072.9605
Frequencies -- 3076.4499 3076.6685 3078.6954

E(RB-LYP) = -4208.58559867 (BLYP-D3BJ/def2SVP/SMD (H_2O))
Sum of electronic and zero-point Energies= -4207.638818
Sum of electronic and thermal Energies= -4207.577916
Sum of electronic and thermal Free Energies= -4207.731084

E(RB-LYP) = -4213.25977368 (BLYP-D3BJ/def2TZVPP/SMD (H_2O))

HG1

Center Number	Atomic Number	Atomic Type	Coordinates (Angstroms) X	Y	Z
1	8	0	-2.595787	-3.519130	2.817660
2	8	0	0.881896	-4.024215	2.858582
3	8	0	3.583564	-1.469008	2.829466
4	8	0	3.640909	2.109529	2.905301
5	8	0	0.772162	4.274605	2.860162
6	8	0	-2.688114	3.245523	2.854938
7	8	0	-4.008579	-0.226942	2.702520
8	8	0	-2.401805	-3.208789	-3.253398
9	8	0	1.204867	-4.003374	-3.246419
10	8	0	3.863865	-1.636144	-3.144663
11	8	0	3.720686	1.990808	-3.191501
12	8	0	0.779432	4.220929	-3.269552
13	8	0	-2.695813	3.130113	-3.175512
14	8	0	-4.259096	-0.065336	-3.310784
15	7	0	-3.998129	-3.506451	0.942324
16	7	0	-2.214581	-4.877485	0.945200
17	7	0	0.200703	-5.364652	1.055318
18	7	0	2.292408	-4.540307	1.060234
19	7	0	4.171940	-2.964715	1.129588
20	7	0	5.142216	-0.942046	1.160247
21	7	0	5.028480	1.521456	1.108266
22	7	0	4.001255	3.521034	1.069929
23	7	0	2.049267	5.026268	1.047860
24	7	0	-0.183360	5.322054	0.992684
25	7	0	-2.583233	4.772386	1.078686
26	7	0	-4.192061	3.206696	1.057894
27	7	0	-5.087473	0.918968	0.965605
28	7	0	-5.150734	-1.330378	0.978388
29	7	0	-3.967870	-3.438171	-1.522590
30	7	0	-2.167353	-4.781954	-1.530788
31	7	0	0.262873	-5.114114	-1.407564
32	7	0	2.474256	-4.689751	-1.399789
33	7	0	4.321568	-3.054586	-1.334041
34	7	0	5.150363	-0.960912	-1.305377
35	7	0	5.110688	1.500579	-1.366840
36	7	0	4.013737	3.462210	-1.392140
37	7	0	2.043123	4.939205	-1.431049
38	7	0	-0.155328	5.410640	-1.479002
39	7	0	-2.493652	4.633276	-1.387510
40	7	0	-4.236250	3.203163	-1.410115
41	7	0	-5.316256	0.976852	-1.496466
42	7	0	-5.120302	-1.262900	-1.490918
43	6	0	-2.891586	-3.909474	1.688594
44	6	0	-1.140278	-5.670964	1.518681
45	1	0	-1.154028	-5.495300	2.609061
46	1	0	-1.342013	-6.742471	1.315257
47	6	0	1.089467	-4.563898	1.772893
48	6	0	3.534618	-4.141060	1.692887
49	1	0	3.303456	-3.915234	2.748888
50	1	0	4.255779	-4.984917	1.645266
51	6	0	4.217415	-1.752146	1.805345
52	6	0	5.596523	0.326582	1.703918
53	1	0	5.320709	0.338923	2.773165
54	1	0	6.701329	0.366542	1.606071
55	6	0	4.147114	2.347980	1.809892
56	6	0	3.352723	4.706149	1.603935
57	1	0	3.207887	4.536757	2.685604

58	1	0	4.024894	5.575330	1.450258
59	6	0	0.866725	4.800143	1.750970
60	6	0	-1.490803	5.578144	1.582347
61	1	0	-1.742536	6.648771	1.433201
62	1	0	-1.405582	5.365766	2.662771
63	6	0	-3.092244	3.675666	1.774990
64	6	0	-5.111991	2.226828	1.599816
65	1	0	-6.145138	2.630217	1.534762
66	1	0	-4.839082	2.082694	2.660455
67	6	0	-4.657717	-0.216254	1.656245
68	6	0	-5.047743	-2.678181	1.507649
69	1	0	-4.839869	-2.592245	2.588712
70	1	0	-6.024152	-3.184437	1.359735
71	6	0	-2.788489	-3.731467	-2.208217
72	6	0	-0.997356	-5.458371	-2.050606
73	1	0	-0.903817	-5.181096	-3.115633
74	1	0	-1.157496	-6.554155	-1.967775
75	6	0	1.301961	-4.528020	-2.138180
76	6	0	3.774716	-4.280208	-1.895171
77	1	0	3.669813	-4.121734	-2.983019
78	1	0	4.495744	-5.102128	-1.709063
79	6	0	4.368214	-1.852600	-2.043844
80	6	0	5.672719	0.267021	-1.882554
81	1	0	5.450381	0.237232	-2.963908
82	1	0	6.772063	0.288304	-1.730017
83	6	0	4.211535	2.276870	-2.099112
84	6	0	3.350132	4.614719	-1.976897
85	1	0	3.205342	4.396372	-3.050127
86	1	0	4.012496	5.498772	-1.864956
87	6	0	0.871775	4.772220	-2.173263
88	6	0	-1.504633	5.509487	-1.999479
89	1	0	-1.851182	6.558723	-1.894012
90	1	0	-1.452916	5.244367	-3.070498
91	6	0	-3.086283	3.587958	-2.102111
92	6	0	-5.252033	2.339154	-1.993738
93	1	0	-5.044686	2.274196	-3.076400
94	1	0	-6.240990	2.817282	-1.837643
95	6	0	-4.812252	-0.109287	-2.211709
96	6	0	-5.005265	-2.587303	-2.076615
97	1	0	-5.979376	-3.110163	-1.972067
98	1	0	-4.776840	-2.445836	-3.147887
99	6	0	-4.131913	-4.234753	-0.314399
100	1	0	-5.099592	-4.776848	-0.342030
101	6	0	-2.875219	-5.181844	-0.321924
102	1	0	-3.129440	-6.260881	-0.366288
103	6	0	0.748583	-5.811265	-0.214815
104	1	0	0.605358	-6.905439	-0.330276
105	6	0	2.252485	-5.376472	-0.136298
106	1	0	2.958960	-6.225850	-0.031287
107	6	0	5.022126	-2.983697	-0.059063
108	1	0	5.767584	-3.801141	0.015614
109	6	0	5.654371	-1.542795	-0.066808
110	1	0	6.763301	-1.539517	-0.060847
111	6	0	5.524401	2.132670	-0.121004
112	1	0	6.630318	2.216213	-0.085427
113	6	0	4.784472	3.519020	-0.156684
114	1	0	5.471096	4.390664	-0.172362
115	6	0	1.835563	5.721284	-0.215849
116	1	0	2.448006	6.646055	-0.249732
117	6	0	0.285809	5.991374	-0.219979
118	1	0	0.022913	7.068768	-0.183349
119	6	0	-3.253966	4.998183	-0.192742
120	1	0	-3.594264	6.051450	-0.265832
121	6	0	-4.427235	3.951413	-0.174610
122	1	0	-5.436674	4.411504	-0.158792
123	6	0	-5.887864	0.591085	-0.213756
124	1	0	-6.910907	1.007053	-0.107823
125	6	0	-5.843429	-0.981006	-0.253283
126	1	0	-6.844829	-1.457624	-0.276397
127	6	0	-0.475525	1.077696	1.260768
128	1	0	-1.310259	0.882856	1.964412
129	6	0	0.482784	-0.133689	1.252808
130	6	0	-1.021886	1.325896	-0.166100
131	6	0	1.641782	0.144078	0.264782
132	6	0	-0.291114	-1.385196	0.765679
133	1	0	-1.699915	2.199094	-0.150476
134	6	0	0.151816	1.602384	-1.134564
135	6	0	-1.789832	0.074405	-0.650588
136	1	0	2.332388	-0.720926	0.260665
137	1	0	2.210124	1.023901	0.620586
138	6	0	1.101179	0.382337	-1.166613
139	1	0	-1.107962	-1.608114	1.481613
140	1	0	0.397352	-2.251392	0.769642
141	6	0	-0.843330	-1.147628	-0.661565
142	1	0	0.715190	2.490227	-0.794853
143	1	0	-0.233353	1.831544	-2.147605
144	1	0	-2.648377	-0.123484	0.016124
145	1	0	-2.195701	0.248639	-1.666656
146	1	0	1.943894	0.579420	-1.858275
147	6	0	0.330779	-0.876411	-1.632436
148	1	0	-1.400991	-2.036951	-0.999711
149	1	0	-0.059024	-0.735305	-2.661973
150	1	0	1.014359	-1.747435	-1.669795
151	1	0	0.068422	1.966830	1.640063
152	1	0	1.771238	-0.870178	2.577076
153	8	0	0.966967	-0.301754	2.597809

Frequencies -- 5.0808 20.1659 39.7680
Frequencies -- 44.2714 45.8366 50.7402
Frequencies -- 52.5070 56.1323 63.4133
Frequencies -- 70.8567 72.6755 78.6645
Frequencies -- 85.0226 91.2934 91.5325
Frequencies -- 92.5614 95.8677 100.5354
Frequencies -- 106.3400 107.4750 112.1392
Frequencies -- 112.7716 114.7613 116.9004
Frequencies -- 121.6745 124.5594 129.3971
Frequencies -- 131.4753 132.0053 134.6779
Frequencies -- 137.2268 140.7412 143.5151
Frequencies -- 147.2122 153.7643 156.9606
Frequencies -- 158.6811 167.8609 171.5208
Frequencies -- 177.1552 181.0288 183.3008
Frequencies -- 189.9856 192.5187 192.9058
Frequencies -- 195.0963 198.1024 201.2332
Frequencies -- 207.4383 214.4985 226.2619
Frequencies -- 227.2285 238.1766 239.3522
Frequencies -- 243.6271 258.4476 262.1529
Frequencies -- 263.8419 268.3537 277.4684
Frequencies -- 279.8141 281.1294 284.2328
Frequencies -- 288.6479 290.7054 316.2938
Frequencies -- 324.6774 329.2410 332.1079
Frequencies -- 341.3044 343.7158 346.0585
Frequencies -- 349.4881 352.9649 354.7368
Frequencies -- 357.6759 359.3588 359.5909
Frequencies -- 361.7249 363.0316 363.9872
Frequencies -- 365.1991 367.0055 369.2983
Frequencies -- 371.3368 403.0070 406.2689
Frequencies -- 408.0559 411.2190 413.1345
Frequencies -- 414.4935 415.2222 425.8386
Frequencies -- 429.4239 433.9088 436.5938
Frequencies -- 442.7834 444.0424 448.6708
Frequencies -- 451.8550 455.3093 457.1078
Frequencies -- 460.5348 475.3435 488.2542
Frequencies -- 507.5736 508.3638 551.3119
Frequencies -- 577.7775 579.1669 603.5223
Frequencies -- 603.8940 611.7579 612.1421

Frequencies -- 613.6253 614.2565 620.7352
Frequencies -- 622.8529 623.7709 626.0689
Frequencies -- 637.7711 639.5153 644.0767
Frequencies -- 645.2409 645.9240 646.1729
Frequencies -- 651.7155 657.1772 661.9159
Frequencies -- 664.3061 667.8227 668.1289
Frequencies -- 670.7183 672.9026 682.3885
Frequencies -- 682.6897 692.9247 693.9686
Frequencies -- 698.0109 701.4086 702.6975
Frequencies -- 705.9038 710.6050 711.8482
Frequencies -- 713.1467 713.9504 714.4426
Frequencies -- 716.5512 717.2820 717.6145
Frequencies -- 719.2845 721.8033 724.3277
Frequencies -- 727.8528 729.6374 767.7524
Frequencies -- 768.6552 773.7970 775.7471
Frequencies -- 776.8713 779.0194 780.5203
Frequencies -- 788.0493 789.2625 792.3297
Frequencies -- 794.2574 796.4289 805.3386
Frequencies -- 810.0384 811.4920 812.9033
Frequencies -- 813.5163 814.3802 815.0437
Frequencies -- 815.9063 816.8858 816.9237
Frequencies -- 818.5668 819.8435 871.5111
Frequencies -- 879.5002 880.7547 881.6068
Frequencies -- 883.2554 892.7106 894.0729
Frequencies -- 895.3066 908.3704 909.7301
Frequencies -- 919.5497 927.0186 932.4100
Frequencies -- 938.2637 940.1738 941.9743
Frequencies -- 944.1743 947.6240 951.4473
Frequencies -- 951.6614 953.5296 956.9407
Frequencies -- 959.5322 961.6753 968.0056
Frequencies -- 969.3566 971.3593 971.5251
Frequencies -- 978.4984 979.7034 981.1845
Frequencies -- 983.7438 992.7688 1003.8896
Frequencies -- 1004.7880 1009.1840 1009.9792
Frequencies -- 1019.9367 1021.9903 1025.3713
Frequencies -- 1025.8226 1027.1267 1027.4672
Frequencies -- 1028.2346 1035.0425 1035.8517
Frequencies -- 1037.1163 1084.3477 1092.6562
Frequencies -- 1094.7596 1097.4526 1098.4878
Frequencies -- 1102.3480 1103.9810 1104.9989
Frequencies -- 1106.2778 1107.2419 1108.3167
Frequencies -- 1109.6147 1110.0980 1112.3288
Frequencies -- 1113.6056 1117.0670 1125.0151
Frequencies -- 1137.0631 1139.2237 1151.8435
Frequencies -- 1165.0710 1166.1331 1167.1360
Frequencies -- 1168.3862 1177.6177 1181.2553
Frequencies -- 1182.1863 1183.8227 1190.3757
Frequencies -- 1195.4668 1196.0395 1199.6272
Frequencies -- 1200.0371 1201.7006 1203.0626
Frequencies -- 1208.0893 1210.0210 1211.3936
Frequencies -- 1211.9893 1213.4325 1214.6890
Frequencies -- 1215.3111 1215.7972 1217.9089
Frequencies -- 1225.3388 1227.0606 1227.4499
Frequencies -- 1228.7334 1229.5456 1237.3426
Frequencies -- 1240.6907 1250.3816 1251.4929
Frequencies -- 1255.2257 1257.7207 1258.5697
Frequencies -- 1264.1709 1264.9541 1267.7213
Frequencies -- 1269.0856 1270.2141 1270.6732
Frequencies -- 1270.8686 1272.9491 1274.1501
Frequencies -- 1274.8082 1275.6155 1276.6923
Frequencies -- 1279.1907 1291.9302 1292.7581
Frequencies -- 1297.9360 1299.0693 1301.4867
Frequencies -- 1301.7359 1302.7418 1304.0068
Frequencies -- 1305.0381 1305.6560 1309.0531
Frequencies -- 1314.2646 1315.7748 1316.0489
Frequencies -- 1316.4970 1319.2999 1320.2492
Frequencies -- 1321.8671 1326.6752 1341.7037
Frequencies -- 1347.0783 1350.7542 1356.4473
Frequencies -- 1361.9572 1363.4342 1364.2829
Frequencies -- 1365.2862 1366.6171 1367.3928
Frequencies -- 1368.1479 1368.1995 1369.1500
Frequencies -- 1370.7978 1373.2451 1373.6340
Frequencies -- 1374.6207 1374.9602 1376.1214
Frequencies -- 1377.5647 1377.7715 1378.8557
Frequencies -- 1379.6567 1380.1043 1380.3747
Frequencies -- 1381.9268 1382.6998 1383.1564
Frequencies -- 1383.4321 1384.9128 1385.0665
Frequencies -- 1386.1952 1387.0452 1387.3240
Frequencies -- 1388.4014 1389.3765 1391.3733
Frequencies -- 1392.2332 1393.2688 1394.3952
Frequencies -- 1396.8167 1398.0944 1400.4768
Frequencies -- 1403.8988 1405.8061 1408.7130
Frequencies -- 1410.5378 1413.0322 1416.8424
Frequencies -- 1428.9190 1432.9233 1435.6845
Frequencies -- 1436.0306 1438.3054 1439.0492
Frequencies -- 1439.9459 1442.3991 1442.7749

Frequencies -- 1443.3214 1445.2241 1446.8011
Frequencies -- 1448.4659 1450.5146 1451.7018
Frequencies -- 1454.2681 1456.4339 1460.9190
Frequencies -- 1695.7333 1706.1534 1710.1873
Frequencies -- 1713.0420 1714.7154 1715.3052
Frequencies -- 1718.7908 1720.6660 1723.7199
Frequencies -- 1725.1801 1726.3937 1736.0961
Frequencies -- 1738.2081 1743.0979 2959.0183
Frequencies -- 2962.5696 2964.8405 2965.9493
Frequencies -- 2966.3375 2966.5734 2969.0946
Frequencies -- 2969.2713 2969.7411 2971.2173
Frequencies -- 2972.2836 2972.9458 2975.9095
Frequencies -- 2976.5495 2976.8703 2978.0004
Frequencies -- 2978.8340 2979.4523 2980.1738
Frequencies -- 2980.3250 2981.2274 2982.2598
Frequencies -- 2982.7401 2983.8798 2984.4766
Frequencies -- 2984.8574 2985.2130 2985.3027
Frequencies -- 2986.0197 2986.8099 2986.9070
Frequencies -- 2987.1545 2990.5523 2993.4010
Frequencies -- 3001.1140 3014.3754 3024.1005
Frequencies -- 3026.1940 3033.2864 3034.5627
Frequencies -- 3041.9347 3048.9478 3049.8238
Frequencies -- 3064.8711 3066.9902 3068.0933
Frequencies -- 3068.1610 3069.2326 3069.5232
Frequencies -- 3069.6418 3069.7582 3070.1552
Frequencies -- 3070.9268 3072.7013 3073.0463
Frequencies -- 3073.7069 3073.8844 3502.6901

E(RB-LYP) = -4674.07736636 (BLYP-D3BJ/def2SVP/SMD (H_2O))
Sum of electronic and zero-point Energies= -4672.885728
Sum of electronic and thermal Energies= -4672.815683
Sum of electronic and thermal Free Energies= -4672.983849

E(RB-LYP) = -4679.24767792 (BLYP-D3BJ/def2TZVPP/SMD (H_2O))

G1

Center Number	Atomic Number	Atomic Type	Coordinates (Angstroms) X	Y	Z
1	6	0	-0.890187	-0.506552	1.629951
2	1	0	-1.353705	-1.514831	1.638058
3	6	0	0.653889	-0.631202	1.658481
4	6	0	-1.327890	0.266287	0.360301
5	1	0	0.968723	-1.180796	2.569118
6	6	0	1.274377	0.789348	1.669800
7	6	0	1.134425	-1.390853	0.396414
8	1	0	-2.433050	0.357678	0.341399
9	6	0	-0.697897	1.681297	0.377009
10	6	0	-0.846046	-0.496406	-0.899673
11	1	0	2.383495	0.727306	1.698159
12	1	0	0.951578	1.353164	2.568961
13	6	0	0.841238	1.570776	0.404157
14	1	0	0.707591	-2.415298	0.384600
15	1	0	2.238916	-1.500270	0.415123
16	6	0	0.698139	-0.620344	-0.875140
17	1	0	-1.034687	2.251393	1.267296
18	1	0	-1.002708	2.258336	-0.520330
19	1	0	-1.308220	-1.504816	-0.932104
20	1	0	-1.170234	0.039578	-1.816089
21	6	0	1.318693	0.799963	-0.852022
22	1	0	1.045304	-1.161862	-1.778813
23	1	0	1.028455	1.371878	-1.757160
24	1	0	2.428142	0.737316	-0.841711
25	1	0	-1.245444	0.022464	2.538846
26	1	0	2.334808	2.838067	0.433162
27	8	0	1.359163	2.915099	0.418931

Frequencies -- 263.3713 267.5413 310.8919
Frequencies -- 333.2055 391.8495 397.3469
Frequencies -- 400.1803 401.3838 423.1206
Frequencies -- 461.8550 463.3984 547.6014
Frequencies -- 637.9037 643.2816 707.5886
Frequencies -- 760.9928 797.3824 800.8970
Frequencies -- 874.9547 876.8169 880.2554
Frequencies -- 913.2347 913.7193 916.8808
Frequencies -- 958.9325 964.7428 965.1855
Frequencies -- 1012.5344 1013.3791 1017.0068
Frequencies -- 1072.8374 1083.1888 1084.5038
Frequencies -- 1085.7305 1096.8231 1097.7016
Frequencies -- 1142.2075 1162.1159 1185.6356
Frequencies -- 1238.8085 1263.3263 1263.6585
Frequencies -- 1266.7169 1278.7380 1292.4349
Frequencies -- 1293.3546 1303.1152 1313.4252
Frequencies -- 1329.6874 1333.6595 1340.9119
Frequencies -- 1347.0129 1377.1942 1411.8866
Frequencies -- 1413.4019 1425.2552 1425.4116
Frequencies -- 1429.5728 1447.1740 2942.0034
Frequencies -- 2945.9350 2949.8130 2950.3439
Frequencies -- 2951.3283 2956.1183 2969.7290
Frequencies -- 2971.8042 2980.6269 2991.5689
Frequencies -- 2991.8960 2992.7929 2994.0786
Frequencies -- 2995.5411 3000.4169 3629.8554

E(RB-LYP) = -465.414681614 (BLYP-D3BJ/def2SVP/SMD (H_2O))
Sum of electronic and zero-point Energies= -465.174707
Sum of electronic and thermal Energies= -465.166315
Sum of electronic and thermal Free Energies= -465.206803

E(RB-LYP) = -465.937999495 (BLYP-D3BJ/def2TZVPP/SMD (H_2O))

HG2

Center Number	Atomic Number	Atomic Type	Coordinates (Angstroms) X	Y	Z
1	8	0	-2.545641	-3.387002	2.750803

2	8	0	0.953562	-4.053248	2.823611
3	8	0	3.573386	-1.557153	2.806634
4	8	0	3.555058	2.029952	2.876268
5	8	0	0.719951	4.158583	2.920022
6	8	0	-2.778068	3.167114	2.849209
7	8	0	-4.132253	-0.161721	2.699274
8	8	0	-2.371119	-3.105913	-3.255531
9	8	0	1.251725	-4.034549	-3.313529
10	8	0	3.793210	-1.657749	-3.148053
11	8	0	3.574102	2.033085	-3.097969
12	8	0	0.778610	4.295873	-3.221795
13	8	0	-2.690294	3.223307	-3.176242
14	8	0	-4.205149	-0.033106	-3.309534
15	7	0	-3.984833	-3.428890	0.899649
16	7	0	-2.243133	-4.849269	0.943661
17	7	0	0.183706	-5.253233	0.961482
18	7	0	2.340171	-4.621940	1.022885
19	7	0	4.196850	-3.017857	1.088525
20	7	0	5.114261	-0.971111	1.139564
21	7	0	5.013712	1.494739	1.123537
22	7	0	4.079487	3.535274	1.166295
23	7	0	1.996261	4.835041	1.070016
24	7	0	-0.185051	5.390163	1.144301
25	7	0	-2.529604	4.645941	1.045774
26	7	0	-4.310220	3.268136	1.079279
27	7	0	-5.187901	0.968148	0.935461
28	7	0	-5.188100	-1.283813	0.935288
29	7	0	-3.968888	-3.394607	-1.563174
30	7	0	-2.104232	-4.653626	-1.514187
31	7	0	0.296723	-5.182772	-1.508094
32	7	0	2.494460	-4.713886	-1.443582
33	7	0	4.357190	-3.090254	-1.378060
34	7	0	5.078796	-0.956917	-1.317732
35	7	0	5.032400	1.507706	-1.340523
36	7	0	3.964412	3.492025	-1.303993
37	7	0	2.040204	5.035980	-1.392714
38	7	0	-0.197666	5.282264	-1.329525
39	7	0	-2.603097	4.774172	-1.423030
40	7	0	-4.207933	3.196685	-1.387292
41	7	0	-5.316879	1.003160	-1.528077
42	7	0	-5.158587	-1.236926	-1.537156
43	6	0	-2.874348	-3.823402	1.648095
44	6	0	-1.127151	-5.598621	1.485690
45	1	0	-1.104816	-5.408062	2.573365
46	1	0	-1.306173	-6.678388	1.304446
47	6	0	1.132261	-4.571738	1.722097
48	6	0	3.588684	-4.221909	1.635453
49	1	0	3.380720	-4.030109	2.702814
50	1	0	4.321771	-5.050517	1.546001
51	6	0	4.215600	-1.815237	1.777258
52	6	0	5.569947	0.284131	1.707265
53	1	0	5.291067	0.281623	2.775661
54	1	0	6.675028	0.323571	1.616625
55	6	0	4.141753	2.318163	1.822208
56	6	0	3.302237	4.648360	1.679619
57	1	0	3.140070	4.455613	2.754561
58	1	0	3.896077	5.576579	1.553579
59	6	0	0.823318	4.717316	1.828914
60	6	0	-1.535525	5.511118	1.661140
61	1	0	-1.862341	6.565885	1.550842
62	1	0	-1.493049	5.248693	2.733165
63	6	0	-3.152551	3.623985	1.769967
64	6	0	-5.246308	2.275130	1.571270
65	1	0	-6.274982	2.677104	1.461260
66	1	0	-5.022747	2.127661	2.642808
67	6	0	-4.745573	-0.159934	1.632421
68	6	0	-5.054453	-2.626764	1.466622
69	1	0	-4.851186	-2.532717	2.547907
70	1	0	-6.017432	-3.158572	1.317977
71	6	0	-2.761824	-3.639823	-2.217704
72	6	0	-1.008451	-5.405366	-2.102380
73	1	0	-0.933256	-5.102650	-3.162014
74	1	0	-1.252145	-6.487422	-2.043680
75	6	0	1.332907	-4.562823	-2.206010
76	6	0	3.802847	-4.318766	-1.929989
77	1	0	3.709892	-4.171312	-3.020500
78	1	0	4.518899	-5.141002	-1.728408
79	6	0	4.327697	-1.873192	-2.062181
80	6	0	5.570588	0.280999	-1.901864
81	1	0	5.292664	0.265662	-2.970772
82	1	0	6.676479	0.305475	-1.806607
83	6	0	4.112668	2.303890	-2.026053
84	6	0	3.350866	4.675860	-1.896384
85	1	0	3.233762	4.478801	-2.976758
86	1	0	4.037965	5.533984	-1.748429
87	6	0	0.864194	4.798146	-2.102714
88	6	0	-1.496994	5.560788	-1.926817
89	1	0	-1.735130	6.635092	-1.781712
90	1	0	-1.410837	5.345109	-3.006444
91	6	0	-3.104985	3.667057	-2.106049
92	6	0	-5.223635	2.363250	-2.014370
93	1	0	-4.983745	2.304774	-3.090717
94	1	0	-6.210954	2.853946	-1.884425
95	6	0	-4.802467	-0.082211	-2.233877
96	6	0	-5.016612	-2.558386	-2.120581
97	1	0	-5.981490	-3.097481	-2.019625
98	1	0	-4.786061	-2.414400	-3.190922
99	6	0	-4.121545	-4.177605	-0.346141
100	1	0	-5.085149	-4.726972	-0.361085
101	6	0	-2.857659	-5.112394	-0.350170
102	1	0	-3.098328	-6.190709	-0.450583
103	6	0	0.738706	-5.808596	-0.267625
104	1	0	0.557750	-6.902789	-0.304091
105	6	0	2.260450	-5.423685	-0.193500
106	1	0	2.938819	-6.298423	-0.116140
107	6	0	5.050951	-3.002621	-0.101804
108	1	0	5.823764	-3.793503	-0.026314
109	6	0	5.630736	-1.540688	-0.101222
110	1	0	6.738719	-1.495518	-0.110628
111	6	0	5.503385	2.118742	-0.107406
112	1	0	6.610762	2.171394	-0.094754
113	6	0	4.798149	3.527767	-0.105794
114	1	0	5.502764	4.382116	-0.150523
115	6	0	1.807493	5.679089	-0.109393
116	1	0	2.425052	6.596533	-0.020975
117	6	0	0.264776	5.958016	-0.117439
118	1	0	0.007844	7.036346	-0.163113
119	6	0	-3.277785	5.014724	-0.156623
120	1	0	-3.606370	6.071985	-0.090485
121	6	0	-4.462100	3.981450	-0.179824
122	1	0	-5.464453	4.453238	-0.236845
123	6	0	-5.939403	0.621879	-0.269802
124	1	0	-6.969187	1.029667	-0.209510
125	6	0	-5.882103	-0.951425	-0.300615
126	1	0	-6.879516	-1.436221	-0.320639
127	6	0	-0.272086	1.333674	1.005682
128	1	0	-1.039379	1.333740	1.804461
129	6	0	0.691827	0.142388	1.195016
130	6	0	-0.938639	1.222145	-0.388427
131	6	0	1.772983	0.168445	0.090113
132	6	0	-0.095552	-1.184795	1.125701
133	1	0	-1.629130	2.073504	-0.521389
134	6	0	0.143983	1.250334	-1.493298
135	6	0	-1.725350	-0.106797	-0.469988
136	1	0	2.482057	-0.666974	0.234121
137	1	0	2.350724	1.109580	0.157576
138	6	0	1.104448	0.053640	-1.302295
139	1	0	-0.865063	-1.215461	1.922811
140	1	0	0.594319	-2.030947	1.302677
141	6	0	-0.762060	-1.298220	-0.267688
142	1	0	0.715422	2.196102	-1.448162
143	1	0	-0.335549	1.214083	-2.491938
144	1	0	-2.502521	-0.128573	0.315220
145	1	0	-2.226420	-0.191303	-1.453883
146	1	0	1.892391	0.071315	-2.079468
147	6	0	0.322905	-1.279898	-1.369908
148	1	0	-1.330146	-2.244123	-0.312854
149	1	0	-0.144776	-1.414153	-2.365075
150	1	0	1.021752	-2.124651	-1.228456
151	1	0	0.291751	2.280195	1.089653
152	7	0	1.365842	0.246140	2.548537
153	1	0	2.042079	-0.541127	2.704203
154	1	0	1.944313	1.113699	2.644249
155	1	0	0.652198	0.245612	3.335394
156	53	0	-0.848599	0.358514	5.233160

Frequencies -- 13.3293 21.6736 30.3390
Frequencies -- 31.5850 35.7771 43.4743
Frequencies -- 47.7631 50.5726 59.8411
Frequencies -- 61.1130 67.8123 71.6020
Frequencies -- 77.2125 79.5807 83.2941
Frequencies -- 91.0174 94.1820 95.2752
Frequencies -- 96.3168 98.8618 102.2569
Frequencies -- 105.1049 106.6493 113.1897
Frequencies -- 114.7829 118.9854 120.8917

Frequencies -- 123.0223 127.1754 129.9906
Frequencies -- 130.9140 134.5440 141.6108
Frequencies -- 145.6095 147.9603 151.8190
Frequencies -- 158.0481 159.3856 160.9601
Frequencies -- 166.1084 169.3879 177.2899
Frequencies -- 178.9625 180.7991 186.6953
Frequencies -- 191.7140 193.1927 197.0802
Frequencies -- 201.3768 203.4061 207.9242
Frequencies -- 212.5858 218.8335 228.6487
Frequencies -- 230.2925 240.0423 243.5080
Frequencies -- 246.2274 261.6948 263.7182
Frequencies -- 266.8826 270.4733 276.3791
Frequencies -- 279.3597 283.2243 285.6477
Frequencies -- 289.6388 302.8378 314.4404
Frequencies -- 327.7385 329.4913 333.3359
Frequencies -- 334.7346 348.2275 349.8537
Frequencies -- 351.1232 355.0372 357.4969
Frequencies -- 358.5818 359.7987 361.0373
Frequencies -- 363.4727 365.0141 366.5866
Frequencies -- 368.2901 371.0005 371.1311
Frequencies -- 374.2095 392.0365 406.6148
Frequencies -- 410.9185 412.4002 413.2648
Frequencies -- 414.3233 416.1299 430.5623
Frequencies -- 432.4854 437.5997 439.9422
Frequencies -- 441.2470 443.5611 450.6842
Frequencies -- 451.9591 456.8096 457.4530
Frequencies -- 461.2804 471.3375 479.6961
Frequencies -- 506.9708 508.8740 543.7444
Frequencies -- 577.2924 580.1439 604.8664
Frequencies -- 606.9755 609.6057 611.3799
Frequencies -- 613.3407 616.8560 621.7688
Frequencies -- 622.3595 624.6791 627.2807
Frequencies -- 636.7970 639.6281 643.1594
Frequencies -- 645.8232 647.0980 647.8239
Frequencies -- 651.1213 658.5952 662.5066
Frequencies -- 663.5511 668.4450 668.8057
Frequencies -- 670.8945 676.1933 680.0003
Frequencies -- 683.5084 690.7089 694.1638
Frequencies -- 699.1319 700.6405 704.5564
Frequencies -- 710.8715 712.4145 714.8951
Frequencies -- 715.5912 716.7234 717.3721
Frequencies -- 719.9020 720.5861 722.2650
Frequencies -- 722.8668 723.3335 724.4552
Frequencies -- 726.6449 728.4701 767.3485
Frequencies -- 769.4914 773.0931 776.3829
Frequencies -- 777.1402 779.0177 781.2654
Frequencies -- 789.1223 790.2750 792.2183
Frequencies -- 795.3938 796.9093 807.7295
Frequencies -- 810.4667 811.2365 812.4001
Frequencies -- 812.5100 813.2554 814.5621
Frequencies -- 815.4074 816.0967 817.7288
Frequencies -- 818.3469 818.8677 869.5276
Frequencies -- 877.3596 881.5836 882.8955
Frequencies -- 883.8907 887.2479 893.2298
Frequencies -- 894.9194 904.0005 908.4604
Frequencies -- 910.8384 915.7018 926.1798
Frequencies -- 935.3622 940.8345 942.4379
Frequencies -- 942.7906 944.0791 947.5925
Frequencies -- 951.7364 955.5330 955.9039
Frequencies -- 956.9135 961.0775 962.3565
Frequencies -- 967.2219 967.3400 971.8134
Frequencies -- 972.0257 979.8770 981.0588
Frequencies -- 982.9909 993.7190 1002.4243
Frequencies -- 1005.1812 1009.1468 1011.3034
Frequencies -- 1017.9824 1020.4530 1024.9364
Frequencies -- 1026.7515 1028.9871 1029.6780
Frequencies -- 1030.3923 1034.6214 1034.7317
Frequencies -- 1036.6816 1066.4528 1074.4309
Frequencies -- 1080.3597 1097.0305 1098.3828
Frequencies -- 1099.6949 1102.1170 1103.0433
Frequencies -- 1103.4723 1104.5018 1106.1872
Frequencies -- 1107.7853 1109.5956 1111.3071
Frequencies -- 1111.9867 1113.5322 1114.9112
Frequencies -- 1118.2464 1133.0224 1136.4747
Frequencies -- 1139.2654 1150.8102 1165.8526
Frequencies -- 1166.4660 1167.1533 1180.6302
Frequencies -- 1182.2533 1182.6924 1186.2541
Frequencies -- 1189.2557 1195.8438 1197.5950
Frequencies -- 1198.2010 1198.5097 1200.6544
Frequencies -- 1202.9403 1205.3015 1209.1285
Frequencies -- 1211.1301 1211.6034 1213.0674
Frequencies -- 1214.0598 1214.1815 1216.7654
Frequencies -- 1217.3532 1224.7845 1226.7692
Frequencies -- 1227.0901 1227.5510 1228.5281
Frequencies -- 1235.9245 1239.7644 1252.0627
Frequencies -- 1253.7357 1257.2709 1257.9192

Frequencies -- 1263.7871 1264.6133 1268.0786
Frequencies -- 1269.4614 1271.7696 1273.7110
Frequencies -- 1275.6116 1276.3559 1276.5239
Frequencies -- 1277.1125 1279.5711 1281.6762
Frequencies -- 1286.7865 1291.4739 1292.6288
Frequencies -- 1293.5917 1295.9731 1298.6789
Frequencies -- 1299.5349 1302.8514 1304.1475
Frequencies -- 1304.2660 1305.3220 1308.7873
Frequencies -- 1310.1433 1312.0848 1313.0910
Frequencies -- 1315.8212 1316.5681 1317.8051
Frequencies -- 1319.3795 1320.8082 1328.1068
Frequencies -- 1343.6706 1352.5411 1355.7468
Frequencies -- 1356.3308 1361.2398 1362.3898
Frequencies -- 1363.0334 1364.0301 1365.5901
Frequencies -- 1367.7775 1368.2536 1369.1657
Frequencies -- 1369.8660 1371.2082 1371.5431
Frequencies -- 1372.8619 1373.3985 1374.7092
Frequencies -- 1376.1877 1376.6775 1377.2800
Frequencies -- 1378.2414 1379.3384 1380.9688
Frequencies -- 1381.7627 1382.3134 1382.6321
Frequencies -- 1383.7800 1384.1509 1385.3306
Frequencies -- 1386.2107 1386.3202 1386.8924
Frequencies -- 1388.5796 1389.5309 1393.0115
Frequencies -- 1393.5659 1394.8452 1395.8070
Frequencies -- 1396.7845 1396.9538 1398.8720
Frequencies -- 1402.5048 1404.2339 1408.0894
Frequencies -- 1409.1098 1409.6834 1411.0867
Frequencies -- 1417.6232 1425.8561 1432.1427
Frequencies -- 1433.6945 1435.1154 1439.2939
Frequencies -- 1440.1533 1440.5467 1442.1698
Frequencies -- 1443.4254 1444.9920 1445.7745
Frequencies -- 1446.0316 1447.9370 1449.2873
Frequencies -- 1453.1769 1458.8108 1459.7681
Frequencies -- 1468.5722 1485.0363 1545.2950
Frequencies -- 1560.8195 1681.1112 1699.0004
Frequencies -- 1707.5148 1712.3009 1716.3081
Frequencies -- 1717.4542 1717.8965 1721.0014
Frequencies -- 1723.4607 1726.2177 1726.6508
Frequencies -- 1736.2208 1739.2446 1743.7437
Frequencies -- 2875.7189 2963.5528 2967.1685
Frequencies -- 2969.9577 2971.7640 2972.9412
Frequencies -- 2973.2940 2974.3170 2974.7691
Frequencies -- 2976.5687 2976.7407 2977.0929
Frequencies -- 2978.2248 2978.6131 2979.4107
Frequencies -- 2980.5749 2981.0385 2981.9079
Frequencies -- 2982.3666 2982.6379 2982.8573
Frequencies -- 2983.4395 2984.8075 2986.3421
Frequencies -- 2987.3877 2987.7640 2988.4675
Frequencies -- 2989.0287 2989.4853 2990.3401
Frequencies -- 2992.1546 2993.7977 2995.7960
Frequencies -- 3000.8969 3002.9033 3005.8171
Frequencies -- 3025.4607 3030.4739 3031.5008
Frequencies -- 3045.0740 3049.0304 3050.6892
Frequencies -- 3051.7315 3054.2535 3067.6631
Frequencies -- 3068.8803 3069.0139 3069.1118
Frequencies -- 3070.4595 3070.7976 3071.6749
Frequencies -- 3071.9613 3072.7477 3073.7374
Frequencies -- 3074.4117 3074.7889 3075.5329
Frequencies -- 3078.2930 3106.5122 3149.0146

E(RB-LYP) = -4952.52985309 (BLYP-D3BJ/def2SVP/SMD (H_2O))
Sum of electronic and zero-point Energies= -4951.311057
Sum of electronic and thermal Energies= -4951.238847
Sum of electronic and thermal Free Energies= -4951.412308

E(RB-LYP) = -4957.68061414 (BLYP-D3BJ/def2TZVPP/SMD (H_2O))

G2

Center Number	Atomic Number	Atomic Type	Coordinates (Angstroms) X	Y	Z
1	6	0	-0.911914	-0.528779	1.628778
2	1	0	-1.365210	-1.540782	1.634016
3	6	0	0.632718	-0.640377	1.653899
4	6	0	-1.357726	0.240142	0.359952
5	1	0	0.957305	-1.182367	2.564127
6	6	0	1.248524	0.782057	1.674749
7	6	0	1.122668	-1.391080	0.390563
8	1	0	-2.461929	0.329787	0.342058
9	6	0	-0.741807	1.663145	0.379432
10	6	0	-0.869543	-0.512551	-0.903293
11	1	0	2.355020	0.730168	1.703438
12	1	0	0.913131	1.334351	2.577031
13	6	0	0.796897	1.537327	0.404966
14	1	0	0.705558	-2.418567	0.376575
15	1	0	2.227699	-1.487812	0.408465
16	6	0	0.675200	-0.623139	-0.878243
17	1	0	-1.087871	2.222316	1.273206
18	1	0	-1.057651	2.233532	-0.518461
19	1	0	-1.321320	-1.524698	-0.936636
20	1	0	-1.199084	0.022390	-1.817843
21	6	0	1.290964	0.799283	-0.859005
22	1	0	1.030873	-1.152669	-1.784161
23	1	0	0.986472	1.364338	-1.764378
24	1	0	2.397880	0.747474	-0.851288
25	1	0	-1.270973	-0.005045	2.538668
26	7	0	1.414846	2.927364	0.425305
27	1	0	1.111005	3.459673	1.260964
28	1	0	2.487964	2.873791	0.443135
29	1	0	1.138982	3.472616	-0.411712
30	53	0	4.864170	2.668119	0.492371

Frequencies -- 31.9151 35.8079 115.8909
Frequencies -- 249.8645 279.9742 312.9411

Frequencies -- 356.3765 378.8987
384.0987
Frequencies -- 399.5823 401.8152
418.7088
Frequencies -- 455.3795 456.0549
531.7214
Frequencies -- 642.9179 644.7392
706.0986
Frequencies -- 761.1890 797.0265
797.6469
Frequencies -- 876.0158 877.4184
882.5837
Frequencies -- 886.0801 898.2140
903.7447
Frequencies -- 943.2576 945.9519
963.1674
Frequencies -- 997.0053 997.9223
1022.1795
Frequencies -- 1050.8678 1052.6457
1062.9768
Frequencies -- 1091.0184 1094.4574
1097.3632
Frequencies -- 1099.4549 1104.1329
1177.6334
Frequencies -- 1179.9955 1269.5379
1270.2557
Frequencies -- 1271.6588 1281.7889
1285.6463
Frequencies -- 1286.5765 1301.6504
1303.7716
Frequencies -- 1304.5200 1335.0878
1337.1321
Frequencies -- 1345.5822 1353.2485
1353.8556
Frequencies -- 1413.7314 1416.2386
1417.5884
Frequencies -- 1426.5135 1427.2839
1434.2060
Frequencies -- 1452.2954 1512.6305
1525.7983
Frequencies -- 2686.0717 2957.3655
2958.1397
Frequencies -- 2959.7040 2960.3219
2960.9144
Frequencies -- 2964.7840 2988.0303
2988.8769
Frequencies -- 2994.2808 3002.2795
3003.3869
Frequencies -- 3004.9660 3006.9077
3011.5080
Frequencies -- 3013.1801 3322.0924
3383.3430

E(RB-LYP) = -743.850765459 (BLYP-D3BJ/def2SVP/SMD (H_2O))
Sum of electronic and zero-point Energies= -743.584549
Sum of electronic and thermal Energies= -743.573622
Sum of electronic and thermal Free Energies= -743.623517

E(RB-LYP) = -744.358703621 (BLYP-D3BJ/def2TZVPP/SMD (H_2O))

HG3

Center Number	Atomic Number	Atomic Type	Coordinates (Angstroms) X	Y	Z
1	8	0	-2.538393	-3.461329	2.789839
2	8	0	0.992016	-3.985707	2.778452
3	8	0	3.748831	-1.571510	2.870818
4	8	0	3.661420	2.005632	2.969010
5	8	0	0.666396	4.201401	2.957896
6	8	0	-2.753306	3.261201	2.907870
7	8	0	-4.045453	-0.204043	2.731353
8	8	0	-2.358917	-3.115259	-3.265512
9	8	0	1.254637	-3.972361	-3.316368
10	8	0	3.937210	-1.591637	-3.173695
11	8	0	3.658644	2.011086	-3.092859
12	8	0	0.771807	4.228465	-3.192949
13	8	0	-2.781022	3.196470	-3.153322
14	8	0	-4.304540	0.006012	-3.314868
15	7	0	-3.956841	-3.472955	0.923748
16	7	0	-2.171566	-4.836426	0.928789
17	7	0	0.248390	-5.250724	0.948606
18	7	0	2.394929	-4.587421	1.001968
19	7	0	4.267825	-3.000231	1.088889
20	7	0	5.221416	-0.967658	1.148339
21	7	0	5.074839	1.497029	1.165904
22	7	0	4.033158	3.487843	1.195866
23	7	0	1.959891	4.805462	1.096652
24	7	0	-0.214316	5.399753	1.144842
25	7	0	-2.600749	4.762130	1.112471
26	7	0	-4.229041	3.213486	1.090241
27	7	0	-5.127351	0.931636	0.991112
28	7	0	-5.135355	-1.316757	0.979223
29	7	0	-3.925986	-3.390738	-1.544224
30	7	0	-2.078835	-4.676466	-1.536561
31	7	0	0.334229	-5.172512	-1.524115
32	7	0	2.520439	-4.646584	-1.462514
33	7	0	4.382880	-3.031212	-1.378959
34	7	0	5.224810	-0.945991	-1.325274
35	7	0	5.089768	1.513352	-1.303826
36	7	0	3.961118	3.461527	-1.275495
37	7	0	2.032662	4.993211	-1.371428
38	7	0	-0.199451	5.261280	-1.324956
39	7	0	-2.588845	4.697433	-1.364935
40	7	0	-4.309896	3.250824	-1.374745
41	7	0	-5.351637	1.008900	-1.472746
42	7	0	-5.099883	-1.225803	-1.487978
43	6	0	-2.841113	-3.860817	1.666054
44	6	0	-1.061235	-5.593981	1.470865
45	1	0	-1.040931	-5.406787	2.559276
46	1	0	-1.241375	-6.673108	1.285537
47	6	0	1.183305	-4.529554	1.690323
48	6	0	3.645903	-4.196669	1.624162
49	1	0	3.430550	-4.001820	2.689755
50	1	0	4.365875	-5.038125	1.540054
51	6	0	4.328677	-1.808959	1.809829
52	6	0	5.671682	0.290466	1.715225
53	1	0	5.421864	0.269089	2.790758
54	1	0	6.772905	0.353110	1.592291
55	6	0	4.181758	2.287657	1.887651
56	6	0	3.260514	4.594926	1.719232
57	1	0	3.081370	4.385528	2.788758
58	1	0	3.858027	5.525226	1.618014
59	6	0	0.781458	4.725953	1.851253
60	6	0	-1.556037	5.606698	1.665577
61	1	0	-1.835021	6.667077	1.498854
62	1	0	-1.515667	5.402254	2.750069
63	6	0	-3.136853	3.683952	1.817244
64	6	0	-5.156023	2.237352	1.627658
65	1	0	-6.187677	2.643219	1.556771
66	1	0	-4.890497	2.090943	2.689871
67	6	0	-4.678101	-0.199441	1.675190
68	6	0	-5.016933	-2.666361	1.497581
69	1	0	-4.810712	-2.586937	2.579513
70	1	0	-5.986607	-3.184527	1.344788
71	6	0	-2.732584	-3.649244	-2.221322
72	6	0	-0.969075	-5.414226	-2.116184
73	1	0	-0.897759	-5.117908	-3.177923
74	1	0	-1.197044	-6.499095	-2.050228
75	6	0	1.351911	-4.513320	-2.215740
76	6	0	3.821671	-4.241033	-1.959329
77	1	0	3.710154	-4.058450	-3.042857
78	1	0	4.537266	-5.073206	-1.796080
79	6	0	4.440173	-1.823667	-2.074226
80	6	0	5.694989	0.317093	-1.864090
81	1	0	5.467675	0.311916	-2.944865
82	1	0	6.793402	0.378838	-1.716303
83	6	0	4.163456	2.286111	-2.005007
84	6	0	3.342844	4.634930	-1.876346
85	1	0	3.223601	4.426521	-2.954400
86	1	0	4.024823	5.499573	-1.738991
87	6	0	0.857959	4.749896	-2.081982
88	6	0	-1.508752	5.489969	-1.914453
89	1	0	-1.768188	6.565129	-1.810854
90	1	0	-1.429922	5.232465	-2.985859
91	6	0	-3.170189	3.646839	-2.076251
92	6	0	-5.321835	2.378998	-1.951816
93	1	0	-5.133016	2.333402	-3.038931
94	1	0	-6.316265	2.836169	-1.770991
95	6	0	-4.836471	-0.059402	-2.206433
96	6	0	-4.969987	-2.541893	-2.090029
97	1	0	-5.938532	-3.076772	-1.994672
98	1	0	-4.740223	-2.384021	-3.158772
99	6	0	-4.078962	-4.194022	-0.339081
100	1	0	-5.037834	-4.751536	-0.370552
101	6	0	-2.806759	-5.119110	-0.352731
102	1	0	-3.042430	-6.200431	-0.432670
103	6	0	0.798769	-5.792853	-0.286480
104	1	0	0.636977	-6.889983	-0.324674

105	6	0	2.314245	-5.378406	-0.221388
106	1	0	3.010679	-6.240376	-0.163030
107	6	0	5.099289	-2.985116	-0.109729
108	1	0	5.850087	-3.800589	-0.066684
109	6	0	5.727821	-1.542527	-0.092560
110	1	0	6.837105	-1.537922	-0.089365
111	6	0	5.529330	2.138442	-0.063856
112	1	0	6.634553	2.237168	-0.056141
113	6	0	4.769692	3.515690	-0.061153
114	1	0	5.442826	4.396916	-0.091371
115	6	0	1.797101	5.643737	-0.091966
116	1	0	2.427117	6.552871	-0.002459
117	6	0	0.258200	5.945616	-0.117376
118	1	0	0.017064	7.027243	-0.178118
119	6	0	-3.305438	5.026507	-0.137736
120	1	0	-3.644679	6.082436	-0.164392
121	6	0	-4.480309	3.980273	-0.124830
122	1	0	-5.488309	4.442074	-0.086237
123	6	0	-5.914879	0.597574	-0.194783
124	1	0	-6.948220	0.987370	-0.087805
125	6	0	-5.832124	-0.971584	-0.249488
126	1	0	-6.822115	-1.471515	-0.279729
127	6	0	-0.319080	1.444794	0.801428
128	1	0	-1.146275	1.621763	1.517359
129	6	0	0.446339	0.164105	1.209473
130	6	0	-0.850336	1.323800	-0.647588
131	6	0	1.610951	-0.039108	0.199657
132	6	0	-0.522154	-1.039553	1.096416
133	1	0	-1.394570	2.245879	-0.917513
134	6	0	0.334669	1.127288	-1.624676
135	6	0	-1.799471	0.108133	-0.754830
136	1	0	2.169773	-0.952485	0.483025
137	1	0	2.309969	0.816364	0.285642
138	6	0	1.095610	-0.166570	-1.252690
139	1	0	-1.368721	-0.892514	1.797463
140	1	0	-0.003951	-1.967162	1.415332
141	6	0	-1.041460	-1.177808	-0.354829
142	1	0	1.021318	1.994738	-1.579586
143	1	0	-0.042397	1.078323	-2.667536
144	1	0	-2.673872	0.252185	-0.093264
145	1	0	-2.182843	0.017940	-1.790293
146	1	0	1.948856	-0.312136	-1.945706
147	6	0	0.148630	-1.386741	-1.321549
148	1	0	-1.729059	-2.040627	-0.412921
149	1	0	-0.220465	-1.552888	-2.352740
150	1	0	0.708367	-2.294801	-1.029434
151	1	0	0.367020	2.310306	0.876959
152	7	0	0.922719	0.287499	2.604538
153	1	0	1.569926	-0.498285	2.781467
154	1	0	1.538626	1.114412	2.659655

Frequencies -- 25.2580 28.7003 40.7965
Frequencies -- 46.7430 49.3062 54.4313
Frequencies -- 62.1103 68.8280 70.1135
Frequencies -- 73.8146 75.4358 81.3075
Frequencies -- 85.5758 89.0239 91.7654
Frequencies -- 94.9450 96.3439 101.7854
Frequencies -- 107.4444 108.4942 110.8348
Frequencies -- 112.9868 116.2679 118.0403
Frequencies -- 120.9722 121.9660 126.0179
Frequencies -- 127.7000 130.4213 133.7509
Frequencies -- 136.4415 139.1231 143.2063
Frequencies -- 154.5968 155.9894 156.7929
Frequencies -- 160.2526 164.9076 166.3038
Frequencies -- 174.2361 177.0888 182.2909
Frequencies -- 188.5918 190.6622 193.7690
Frequencies -- 195.8391 198.9811 206.7676
Frequencies -- 207.8922 216.1820 226.6029
Frequencies -- 228.8166 239.0073 240.9976
Frequencies -- 244.8561 261.7973 263.0209
Frequencies -- 264.3794 268.7530 278.4306
Frequencies -- 279.2055 282.2129 283.9244
Frequencies -- 287.0161 290.7315 319.0667
Frequencies -- 324.1679 331.8296 340.6504
Frequencies -- 343.4814 344.0670 346.8759
Frequencies -- 348.3491 351.2339 352.5168
Frequencies -- 355.0016 358.1702 359.5880
Frequencies -- 363.2579 363.6585 365.2598
Frequencies -- 366.1255 370.3721 370.6136
Frequencies -- 371.4483 375.5314 402.9532
Frequencies -- 410.8562 410.9899 413.0712
Frequencies -- 414.7013 417.0796 425.2297
Frequencies -- 429.5071 432.2083 436.2664
Frequencies -- 437.4851 440.9081 443.4045
Frequencies -- 448.4080 452.8839 454.3849
Frequencies -- 456.6760 470.4337 496.1304
Frequencies -- 507.4148 508.8367 553.0918
Frequencies -- 577.4807 579.2374 604.2027
Frequencies -- 605.4705 609.1806 612.3371
Frequencies -- 613.1315 615.0660 619.6592
Frequencies -- 621.6764 624.8588 626.3345
Frequencies -- 637.7937 639.8997 643.5101
Frequencies -- 644.7996 645.7382 647.6469
Frequencies -- 653.8699 658.6308 663.0189
Frequencies -- 663.4791 666.8163 668.0443
Frequencies -- 670.7225 674.3680 680.9640
Frequencies -- 683.2480 692.1726 694.8124
Frequencies -- 697.5600 700.9704 706.7048
Frequencies -- 710.3247 710.4688 711.6753
Frequencies -- 714.5999 714.9245 715.7984
Frequencies -- 716.4092 717.7228 718.2943
Frequencies -- 719.5837 720.3703 722.2699
Frequencies -- 723.5654 725.8921 767.3385
Frequencies -- 768.7588 774.4684 775.3379
Frequencies -- 777.1574 779.0549 780.4224
Frequencies -- 788.3720 789.7003 792.4027
Frequencies -- 794.4880 796.6760 806.9140
Frequencies -- 810.4553 810.9269 811.7347
Frequencies -- 813.2107 813.8077 813.9845
Frequencies -- 815.5309 815.8058 816.9356
Frequencies -- 817.4620 819.3419 874.2930
Frequencies -- 879.7187 881.0515 883.2171

Frequencies -- 884.0755 888.0983 893.8710
Frequencies -- 894.7507 908.7687 910.7871
Frequencies -- 918.1105 919.8554 924.5717
Frequencies -- 939.4070 941.2275 942.6676
Frequencies -- 946.0307 946.3066 950.4832
Frequencies -- 952.3365 954.2841 957.5408
Frequencies -- 958.9766 960.6808 962.4083
Frequencies -- 963.7258 968.6830 971.4038
Frequencies -- 979.1945 980.1748 981.5598
Frequencies -- 983.5695 993.3865 1000.4499
Frequencies -- 1003.3318 1004.6142 1009.7171
Frequencies -- 1010.9324 1023.9162 1024.3942
Frequencies -- 1027.7122 1028.0445 1029.5235
Frequencies -- 1029.9322 1033.7086 1036.0757
Frequencies -- 1036.3738 1038.3494 1088.5297
Frequencies -- 1093.0683 1095.2521 1097.0595
Frequencies -- 1097.9520 1101.7799 1105.6479
Frequencies -- 1105.9585 1106.5491 1108.2885
Frequencies -- 1110.1223 1111.6050 1112.0072
Frequencies -- 1112.8673 1115.5363 1134.7806
Frequencies -- 1136.4667 1139.0362 1140.9512
Frequencies -- 1144.2748 1152.0243 1165.7877
Frequencies -- 1167.1988 1167.6639 1181.0379
Frequencies -- 1181.7021 1183.1391 1189.9677
Frequencies -- 1190.7514 1196.7736 1197.2309
Frequencies -- 1199.0838 1199.6865 1200.8167
Frequencies -- 1202.1680 1205.2430 1209.8729
Frequencies -- 1210.3689 1211.3152 1214.0504
Frequencies -- 1214.5360 1215.1274 1215.8890
Frequencies -- 1216.9074 1226.2129 1227.2156
Frequencies -- 1227.9545 1228.6648 1229.6508
Frequencies -- 1238.1581 1241.9710 1251.7492
Frequencies -- 1252.2290 1255.2684 1257.4295
Frequencies -- 1258.6136 1263.9456 1265.5657
Frequencies -- 1268.6731 1273.4808 1274.1575
Frequencies -- 1274.4255 1274.7647 1275.1268
Frequencies -- 1276.1495 1277.2980 1279.7554
Frequencies -- 1280.8626 1285.2980 1290.3868
Frequencies -- 1296.3206 1297.3307 1297.9976
Frequencies -- 1302.1671 1303.0091 1303.4326
Frequencies -- 1304.4802 1309.2337 1310.5083
Frequencies -- 1311.4174 1311.8048 1313.6321
Frequencies -- 1314.8988 1317.1193 1318.1380
Frequencies -- 1319.0226 1321.7315 1325.7319
Frequencies -- 1335.2040 1355.7025 1358.9439
Frequencies -- 1360.3123 1361.5164 1363.0154
Frequencies -- 1363.8399 1365.5286 1367.3019
Frequencies -- 1368.4853 1369.5595 1370.0290
Frequencies -- 1370.6710 1372.1737 1372.6306
Frequencies -- 1373.2578 1373.9804 1375.1544
Frequencies -- 1375.8793 1377.4101 1377.7861
Frequencies -- 1378.1517 1378.5413 1379.7052
Frequencies -- 1380.5564 1381.1435 1381.4077
Frequencies -- 1382.4008 1382.9980 1384.4644
Frequencies -- 1385.2457 1385.6043 1386.3340
Frequencies -- 1387.8136 1388.9542 1389.6173
Frequencies -- 1390.3082 1393.0411 1394.2004
Frequencies -- 1395.2889 1395.5447 1397.4708
Frequencies -- 1401.5189 1403.8032 1405.8202
Frequencies -- 1406.7839 1410.8474 1416.2736
Frequencies -- 1425.0008 1428.9882 1431.1113
Frequencies -- 1432.6976 1434.5826 1437.8276
Frequencies -- 1438.7476 1440.4002 1441.7541
Frequencies -- 1442.2002 1443.9290 1445.4415
Frequencies -- 1447.7242 1449.6051 1449.8851
Frequencies -- 1450.7740 1454.9776 1456.2436
Frequencies -- 1462.5576 1592.0227 1705.5495
Frequencies -- 1706.9181 1711.2771 1712.7388
Frequencies -- 1715.2198 1716.3052 1718.3857
Frequencies -- 1719.6242 1723.5656 1725.1889
Frequencies -- 1725.6306 1736.5624 1737.5723
Frequencies -- 1743.1902 2960.9808 2961.3025
Frequencies -- 2961.9047 2965.2371 2966.3530
Frequencies -- 2966.5992 2968.0716 2968.5704
Frequencies -- 2970.8722 2972.4636 2973.2625
Frequencies -- 2973.4104 2973.6390 2975.7005
Frequencies -- 2976.5830 2976.6849 2976.9868
Frequencies -- 2977.8865 2978.1656 2979.5098
Frequencies -- 2979.8646 2980.2465 2980.4400
Frequencies -- 2981.2008 2981.6299 2981.7775
Frequencies -- 2982.6148 2983.6773 2984.0512
Frequencies -- 2984.9998 2985.6632 2986.8264
Frequencies -- 2988.0272 2989.2731 2998.5883
Frequencies -- 3011.2169 3023.8494 3028.0422
Frequencies -- 3029.7972 3035.3801 3040.8812
Frequencies -- 3041.9347 3043.7446 3064.4615

Frequencies -- 3065.3037 3067.4402 3069.4411
Frequencies -- 3069.6238 3069.7022 3070.0745
Frequencies -- 3070.5895 3070.9819 3071.6382
Frequencies -- 3071.6606 3071.8992 3071.9775
Frequencies -- 3073.6794 3328.1519 3386.1840

E(RB-LYP) = -4654.21598276 (BLYP-D3BJ/def2SVP/SMD (H_2O))
Sum of electronic and zero-point Energies= -4653.010902
Sum of electronic and thermal Energies= -4652.940959
Sum of electronic and thermal Free Energies= -4653.106618

E(RB-LYP) = -4659.35827178 (BLYP-D3BJ/def2TZVPP/SMD (H_2O))

G3

Center Number	Atomic Number	Atomic Type	Coordinates (Angstroms) X	Y	Z
1	6	0	-0.316581	1.453922	0.791500
2	1	0	-1.151258	1.615285	1.504140
3	6	0	0.453652	0.174852	1.203985
4	6	0	-0.851224	1.327155	-0.656006
5	6	0	1.628136	-0.034348	0.204205
6	6	0	-0.503833	-1.037776	1.092309
7	1	0	-1.400227	2.252189	-0.927964
8	6	0	0.335548	1.118614	-1.630884
9	6	0	-1.806171	0.110174	-0.741453
10	1	0	2.195861	-0.943757	0.496300
11	1	0	2.328491	0.824841	0.281954
12	6	0	1.102832	-0.170436	-1.246487
13	1	0	-1.340004	-0.902498	1.808691
14	1	0	0.035956	-1.961485	1.393297
15	6	0	-1.040274	-1.179281	-0.353303
16	1	0	1.018735	1.993090	-1.593340
17	1	0	-0.038200	1.043325	-2.673487
18	1	0	-2.670522	0.257446	-0.060651
19	1	0	-2.213790	0.016758	-1.769682
20	1	0	1.955553	-0.318628	-1.941058
21	6	0	0.146830	-1.385783	-1.328151
22	1	0	-1.724423	-2.051137	-0.407773
23	1	0	-0.229979	-1.505423	-2.365445
24	1	0	0.693552	-2.317405	-1.071492
25	1	0	0.358612	2.332486	0.876634
26	7	0	0.898094	0.312513	2.606990
27	1	0	1.453063	-0.524516	2.845532
28	1	0	1.579688	1.086673	2.644897

Frequencies -- 225.5748 261.6974 271.0286
Frequencies -- 312.9222 385.9844 390.8362
Frequencies -- 399.0974 403.8264 421.6714
Frequencies -- 452.9603 459.6016 547.2138
Frequencies -- 639.1154 643.4782 704.6295
Frequencies -- 762.1751 793.3205 796.9377
Frequencies -- 866.9671 873.6984 874.7596
Frequencies -- 877.4563 911.3844 912.2429
Frequencies -- 927.2518 952.8414 965.6307
Frequencies -- 974.2603 1011.6557 1017.3284
Frequencies -- 1019.9028 1076.4091 1080.5293
Frequencies -- 1081.9158 1091.8103 1095.2693
Frequencies -- 1117.3104 1138.9781 1166.8828
Frequencies -- 1180.4621 1237.8841 1264.8882
Frequencies -- 1266.0205 1270.4667 1290.4618
Frequencies -- 1292.7772 1296.1396 1302.5128
Frequencies -- 1310.2024 1328.2634 1339.2812
Frequencies -- 1342.3049 1348.2059 1362.4549
Frequencies -- 1410.7678 1412.4777 1422.8997
Frequencies -- 1423.9620 1426.4822 1443.8331
Frequencies -- 1559.1528 2935.9645 2941.0067
Frequencies -- 2945.8030 2946.0250 2946.3115
Frequencies -- 2948.0894 2963.7446 2966.6515
Frequencies -- 2975.7652 2979.1832 2987.3830
Frequencies -- 2988.2285 2989.9682 2990.5170
Frequencies -- 2993.0180 3331.0655 3397.2095

E(RB-LYP) = -445.552606431 (BLYP-D3BJ/def2SVP/SMD (H_2O))
Sum of electronic and zero-point Energies= -445.300494
Sum of electronic and thermal Energies= -445.291879
Sum of electronic and thermal Free Energies= -445.332787

E(RB-LYP) = -446.049330433 (BLYP-D3BJ/def2TZVPP/SMD (H_2O))

HG4

Center Number	Atomic Number	Atomic Type	Coordinates (Angstroms) X	Y	Z
1	8	0	-2.531043	-3.338571	2.666286
2	8	0	0.858499	-4.169102	2.763728
3	8	0	3.092307	-1.742235	2.758054
4	8	0	2.974459	2.057732	2.821103
5	8	0	0.407389	4.485364	2.746101
6	8	0	-2.819736	3.588457	2.600257
7	8	0	-3.967536	0.060631	2.484340
8	8	0	-2.597029	-3.188599	-3.351528
9	8	0	0.927968	-3.817762	-3.296343
10	8	0	3.834791	-1.373483	-3.085042
11	8	0	3.954334	2.157679	-3.076485
12	8	0	1.078276	4.211866	-3.339875
13	8	0	-2.595971	3.036216	-3.422616
14	8	0	-4.319869	-0.133033	-3.485230
15	7	0	-4.009685	-3.331559	0.850593
16	7	0	-2.387231	-4.883805	0.908523
17	7	0	0.041889	-5.248761	0.853506
18	7	0	2.236888	-4.790479	0.981506
19	7	0	4.056108	-3.132046	1.137218
20	7	0	4.677587	-0.977909	1.212956
21	7	0	4.647037	1.483362	1.284508
22	7	0	3.852803	3.581150	1.276876
23	7	0	1.857171	4.978150	0.968948
24	7	0	-0.284546	5.658961	0.839593
25	7	0	-2.651464	4.993951	0.729611
26	7	0	-4.167466	3.334999	0.700020
27	7	0	-5.197384	1.105787	0.783706
28	7	0	-5.112756	-1.136750	0.824502
29	7	0	-4.148457	-3.415011	-1.609248
30	7	0	-2.276939	-4.666611	-1.556463
31	7	0	0.117162	-5.238424	-1.618261
32	7	0	2.235217	-4.492790	-1.468519
33	7	0	4.093163	-2.888739	-1.314109
34	7	0	5.154374	-0.905021	-1.202000
35	7	0	5.126922	1.565766	-1.136832
36	7	0	4.046631	3.543970	-1.188780
37	7	0	2.174770	5.121419	-1.479183
38	7	0	-0.065251	5.299781	-1.603496
39	7	0	-2.428548	4.631773	-1.708980
40	7	0	-4.230906	3.284839	-1.760341
41	7	0	-5.254265	1.033726	-1.681730
42	7	0	-5.274419	-1.215419	-1.638593
43	6	0	-2.920142	-3.790259	1.587665
44	6	0	-1.252093	-5.630334	1.404601
45	1	0	-1.203014	-5.472206	2.496609

46	1	0	-1.421517	-6.706561	1.198035
47	6	0	1.023177	-4.664887	1.645785
48	6	0	3.494798	-4.400946	1.580152
49	1	0	3.335960	-4.338024	2.670500
50	1	0	4.245675	-5.187987	1.372001
51	6	0	3.858411	-1.932749	1.794945
52	6	0	5.061666	0.242384	1.910947
53	1	0	4.609234	0.206534	2.918404
54	1	0	6.167527	0.250323	2.013732
55	6	0	3.733224	2.342245	1.881115
56	6	0	3.088177	4.739649	1.701690
57	1	0	2.814906	4.582565	2.759641
58	1	0	3.745288	5.629464	1.620521
59	6	0	0.625968	4.972634	1.638571
60	6	0	-1.653752	5.905193	1.255739
61	1	0	-1.930396	6.937427	0.962337
62	1	0	-1.680534	5.817887	2.355879
63	6	0	-3.157314	3.922784	1.465917
64	6	0	-5.148650	2.453749	1.311675
65	1	0	-6.157831	2.906615	1.209882
66	1	0	-4.884668	2.379486	2.381604
67	6	0	-4.664661	0.016244	1.468631
68	6	0	-5.008087	-2.448764	1.430806
69	1	0	-4.732777	-2.302902	2.490374
70	1	0	-6.001043	-2.942868	1.372252
71	6	0	-2.958028	-3.682982	-2.285305
72	6	0	-1.209864	-5.448850	-2.164089
73	1	0	-1.169183	-5.172749	-3.232821
74	1	0	-1.460766	-6.525747	-2.072519
75	6	0	1.068257	-4.427623	-2.238843
76	6	0	3.515743	-4.044622	-1.985101
77	1	0	3.359326	-3.757196	-3.040234
78	1	0	4.239530	-4.885824	-1.935055
79	6	0	4.290050	-1.677238	-1.985210
80	6	0	5.731373	0.349643	-1.653844
81	1	0	5.620634	0.381135	-2.752014
82	1	0	6.808396	0.349899	-1.391019
83	6	0	4.315897	2.386061	-1.924012
84	6	0	3.526519	4.743754	-1.836825
85	1	0	3.532565	4.548236	-2.923561
86	1	0	4.202063	5.593376	-1.608665
87	6	0	1.062268	4.793114	-2.256090
88	6	0	-1.344774	5.407754	-2.286102
89	1	0	-1.649417	6.476213	-2.317829
90	1	0	-1.191926	5.038530	-3.316021
91	6	0	-3.025299	3.574303	-2.402464
92	6	0	-5.215706	2.356140	-2.287412
93	1	0	-4.989590	2.209655	-3.358317
94	1	0	-6.216893	2.823321	-2.183535
95	6	0	-4.864782	-0.108139	-2.382035
96	6	0	-5.195044	-2.569267	-2.158100
97	1	0	-6.168952	-3.072394	-1.988721
98	1	0	-5.009646	-2.485381	-3.243357
99	6	0	-4.253743	-4.132675	-0.350160
100	1	0	-5.234799	-4.644800	-0.276576
101	6	0	-3.026772	-5.112008	-0.380636
102	1	0	-3.306846	-6.179852	-0.485840
103	6	0	0.591955	-5.825727	-0.378395
104	1	0	0.435303	-6.923508	-0.383427
105	6	0	2.103136	-5.402011	-0.333060
106	1	0	2.810274	-6.250479	-0.434342
107	6	0	4.858090	-2.970190	-0.070127
108	1	0	5.626957	-3.766211	-0.127981
109	6	0	5.441615	-1.521874	0.077539
110	1	0	6.527109	-1.490879	0.298802
111	6	0	5.377920	2.121932	0.182644
112	1	0	6.464103	2.134150	0.404113
113	6	0	4.725391	3.551230	0.107009
114	1	0	5.457842	4.381645	0.154431
115	6	0	1.815876	5.798154	-0.246339
116	1	0	2.434186	6.709357	-0.112399
117	6	0	0.286737	6.094390	-0.423500
118	1	0	0.055509	7.165066	-0.600210
119	6	0	-3.248110	5.104110	-0.591986
120	1	0	-3.582360	6.145730	-0.775432
121	6	0	-4.417161	4.059073	-0.546708
122	1	0	-5.427147	4.518354	-0.531386
123	6	0	-5.922357	0.723728	-0.421018
124	1	0	-6.943091	1.157019	-0.409916
125	6	0	-5.898741	-0.850365	-0.373734
126	1	0	-6.903787	-1.312410	-0.292760
127	6	0	-0.728909	1.226823	0.941597
128	1	0	-1.598215	1.026177	1.596817
129	6	0	0.347070	0.129598	1.096446
130	6	0	-1.204776	1.238367	-0.537144
131	6	0	1.529923	0.434521	0.146683
132	6	0	-0.259808	-1.248279	0.757565
133	1	0	-1.984089	2.012254	-0.636435
134	6	0	-0.016964	1.547096	-1.474979
135	6	0	-1.803708	-0.139970	-0.902198
136	1	0	2.330144	-0.313945	0.286803
137	1	0	1.945551	1.423911	0.400715
138	6	0	1.052912	0.442183	-1.323193
139	1	0	-1.123205	-1.459959	1.415295
140	1	0	0.495565	-2.040509	0.921403
141	6	0	-0.730120	-1.238492	-0.721141
142	1	0	0.427451	2.522675	-1.208498
143	1	0	-0.368384	1.625536	-2.521550
144	1	0	-2.677113	-0.349652	-0.259714
145	1	0	-2.161482	-0.132742	-1.950005
146	1	0	1.919192	0.656320	-1.979749
147	6	0	0.464534	-0.946624	-1.658879
148	1	0	-1.155658	-2.229359	-0.960215
149	1	0	0.131550	-0.989217	-2.714234
150	1	0	1.244608	-1.721304	-1.540214
151	1	0	-0.312648	2.214187	1.228155
152	7	0	0.938807	0.133109	2.519500
153	1	0	1.691816	-0.601540	2.570114
154	1	0	1.497452	1.017499	2.633719
155	6	0	0.007599	0.010393	3.705508
156	1	0	0.488376	0.574944	4.526000
157	1	0	-0.939114	0.517265	3.453480
158	6	0	-0.300393	-1.411007	4.172519
159	1	0	-0.982748	-1.320504	5.038293
160	1	0	-0.817662	-2.034193	3.423455
161	7	0	0.906697	-2.163850	4.642942
162	1	0	1.425064	-2.594631	3.848227
163	1	0	1.563719	-1.550020	5.207126
164	1	0	0.580549	-2.970384	5.256491
165	53	0	2.934744	0.057283	6.436856
166	53	0	-0.533885	-4.617761	6.618538

Frequencies -- 6.7493 13.3953 19.9253
Frequencies -- 25.2471 27.6441 36.1127
Frequencies -- 37.2693 40.7722 44.8607
Frequencies -- 46.4255 52.1532 55.6953
Frequencies -- 60.3094 65.4326 70.7690
Frequencies -- 72.7973 73.9232 77.9455
Frequencies -- 81.5155 83.0810 87.5456
Frequencies -- 89.7127 94.1493 94.8141
Frequencies -- 100.2038 103.7228 108.5562
Frequencies -- 109.3822 113.2891 115.5045
Frequencies -- 116.4052 118.9657 120.6842
Frequencies -- 123.2747 126.2414 133.5513
Frequencies -- 138.3216 140.0243 145.2959
Frequencies -- 149.9066 152.1143 156.3836
Frequencies -- 159.0331 160.8247 169.7926
Frequencies -- 170.7166 173.1353 177.2857
Frequencies -- 180.3081 183.3710 186.9694
Frequencies -- 190.9154 194.6502 197.0500
Frequencies -- 199.9896 202.3103 207.3693
Frequencies -- 212.1608 215.4461 223.8888
Frequencies -- 229.0897 235.7151 240.4106
Frequencies -- 241.1626 242.3282 247.3588
Frequencies -- 261.0035 263.8460 265.3356
Frequencies -- 268.8433 281.9245 283.1866
Frequencies -- 289.3995 290.3219 294.3084
Frequencies -- 323.9067 330.7080 331.8323

Frequencies -- 339.0886 340.1218 342.6198
Frequencies -- 349.1910 350.7726 351.8080
Frequencies -- 353.7341 355.1384 357.9637
Frequencies -- 359.7968 360.5776 361.1545
Frequencies -- 363.2720 363.9374 364.7529
Frequencies -- 367.1135 369.3198 372.4037
Frequencies -- 374.7302 385.1406 407.1421
Frequencies -- 411.2266 412.9710 414.8330
Frequencies -- 415.0335 416.9769 433.5366
Frequencies -- 435.4954 436.5766 444.2072
Frequencies -- 444.8202 446.1056 452.9363
Frequencies -- 455.7212 459.0020 460.8580
Frequencies -- 466.1763 476.1168 499.7436
Frequencies -- 506.8127 507.6985 556.6681
Frequencies -- 576.6565 577.4646 600.7886
Frequencies -- 601.7832 609.5126 612.2813
Frequencies -- 612.7402 613.6565 619.6759
Frequencies -- 621.8289 623.8715 627.0026
Frequencies -- 636.6396 638.4616 645.8496
Frequencies -- 647.1875 649.8447 650.1570
Frequencies -- 652.4147 652.9365 659.8569
Frequencies -- 663.5966 667.4475 668.3121
Frequencies -- 670.0353 673.4394 683.0162
Frequencies -- 687.0733 689.8673 693.6028
Frequencies -- 698.9950 701.6558 704.4184
Frequencies -- 707.4435 708.4596 712.1994
Frequencies -- 712.7166 714.0588 716.1593
Frequencies -- 717.3202 717.8305 722.2322
Frequencies -- 722.3250 723.4971 727.3082
Frequencies -- 729.5335 733.6076 766.8123
Frequencies -- 768.6071 768.9840 777.1590
Frequencies -- 777.6810 778.3832 779.8369
Frequencies -- 787.6698 788.5955 790.6892
Frequencies -- 795.8249 796.8949 796.9946
Frequencies -- 804.6082 808.8503 811.8824
Frequencies -- 812.2780 813.4975 814.8555
Frequencies -- 815.7066 817.3094 817.8132
Frequencies -- 818.4117 820.2385 821.1491
Frequencies -- 833.8533 863.2172 873.6164
Frequencies -- 876.7932 881.8486 882.9608
Frequencies -- 885.0010 887.7751 893.3682
Frequencies -- 895.0271 895.3400 908.6128
Frequencies -- 910.8862 933.2489 933.9388
Frequencies -- 938.4877 939.7616 941.3516
Frequencies -- 941.8776 944.9518 948.8478
Frequencies -- 951.3284 952.4167 954.2686
Frequencies -- 955.1878 961.0911 963.2726
Frequencies -- 964.6648 968.8960 971.8270
Frequencies -- 971.9877 980.3615 980.8421
Frequencies -- 983.5277 988.0322 992.6306
Frequencies -- 1002.4952 1004.4069 1005.4455
Frequencies -- 1009.2602 1009.4280 1024.6777
Frequencies -- 1025.4730 1028.5428 1029.2435
Frequencies -- 1029.4843 1032.8705 1034.3055
Frequencies -- 1036.0286 1036.5850 1044.4344
Frequencies -- 1051.7768 1062.4012 1085.9387
Frequencies -- 1089.0336 1094.3917 1096.8561
Frequencies -- 1099.5775 1101.7376 1103.7005
Frequencies -- 1105.6819 1105.8146 1110.1523
Frequencies -- 1110.4726 1114.5203 1116.3953
Frequencies -- 1119.6480 1123.7341 1129.6136
Frequencies -- 1135.5407 1138.9069 1145.1318
Frequencies -- 1147.1722 1149.4445 1164.5580
Frequencies -- 1166.3596 1168.0512 1177.9215
Frequencies -- 1179.6933 1182.3447 1189.2641
Frequencies -- 1190.2609 1193.2081 1194.4678
Frequencies -- 1196.1154 1196.8156 1198.0683
Frequencies -- 1202.2664 1206.4398 1207.4551
Frequencies -- 1208.8466 1210.9564 1211.3831
Frequencies -- 1212.5819 1214.3123 1216.7221
Frequencies -- 1217.4073 1223.6914 1225.0645
Frequencies -- 1225.7150 1227.1931 1230.2565
Frequencies -- 1235.7957 1236.7872 1247.7105
Frequencies -- 1248.3836 1250.4071 1256.1232
Frequencies -- 1256.4989 1263.4837 1264.5684
Frequencies -- 1266.8447 1268.1401 1268.8873
Frequencies -- 1270.8881 1271.9538 1272.5475
Frequencies -- 1274.2427 1275.0018 1276.9100
Frequencies -- 1281.1810 1284.7468 1287.4228
Frequencies -- 1288.8546 1294.5530 1295.3670
Frequencies -- 1296.0100 1298.4994 1298.6666
Frequencies -- 1301.1681 1302.6582 1305.0973
Frequencies -- 1306.4047 1310.3272 1310.6064
Frequencies -- 1311.6349 1314.3048 1316.7206
Frequencies -- 1319.1595 1319.5293 1324.6446
Frequencies -- 1324.9032 1330.8330 1337.8109

Frequencies -- 1343.2730 1357.4670 1360.2109
Frequencies -- 1361.8214 1362.2079 1362.8953
Frequencies -- 1363.4473 1364.5126 1366.7217
Frequencies -- 1367.8734 1368.2263 1368.9547
Frequencies -- 1369.4662 1370.6138 1371.6969
Frequencies -- 1372.1656 1373.4647 1374.8655
Frequencies -- 1376.1585 1376.7265 1377.5783
Frequencies -- 1378.0379 1379.6804 1379.9741
Frequencies -- 1380.3717 1380.8832 1381.6070
Frequencies -- 1382.9397 1383.2922 1384.6695
Frequencies -- 1385.5007 1385.7548 1386.4410
Frequencies -- 1387.4800 1388.0243 1388.8559
Frequencies -- 1390.2984 1390.6813 1391.9420
Frequencies -- 1392.7819 1393.6402 1396.3950
Frequencies -- 1397.1131 1400.1616 1402.5493
Frequencies -- 1403.7296 1405.2555 1406.2950
Frequencies -- 1410.2774 1415.8058 1425.7666
Frequencies -- 1429.4655 1429.7910 1432.6982
Frequencies -- 1434.2629 1436.4973 1437.0130
Frequencies -- 1438.2324 1440.3822 1440.7759
Frequencies -- 1442.0234 1442.6113 1443.2342
Frequencies -- 1444.4653 1446.9428 1448.0719
Frequencies -- 1452.2591 1455.8436 1458.3501
Frequencies -- 1461.2353 1464.1946 1469.5546
Frequencies -- 1478.5723 1503.4367 1549.0714
Frequencies -- 1592.1903 1669.5933 1694.8889
Frequencies -- 1704.9900 1711.4043 1714.4829
Frequencies -- 1717.1072 1719.5873 1722.1164
Frequencies -- 1723.6657 1727.5785 1728.7097
Frequencies -- 1737.4940 1740.7326 1744.9961
Frequencies -- 2833.9409 2884.8332 2954.6859
Frequencies -- 2963.0516 2963.3735 2964.3636
Frequencies -- 2966.0621 2974.7599 2975.2345
Frequencies -- 2978.7779 2978.9581 2981.1992
Frequencies -- 2982.5533 2982.7499 2983.6897
Frequencies -- 2984.6739 2985.2906 2985.6343
Frequencies -- 2986.5776 2986.9438 2987.5023
Frequencies -- 2988.0403 2988.6404 2989.5535
Frequencies -- 2990.7036 2991.0041 2992.5619
Frequencies -- 2992.8098 2993.4550 2995.6795
Frequencies -- 2995.7055 3000.5905 3001.3481
Frequencies -- 3004.3936 3005.7495 3009.5268
Frequencies -- 3014.2279 3021.4850 3025.9098
Frequencies -- 3027.1898 3028.2751 3028.7320
Frequencies -- 3032.0310 3042.8388 3045.7356
Frequencies -- 3055.3034 3060.5291 3061.4484
Frequencies -- 3065.9392 3066.1779 3067.0621
Frequencies -- 3067.2516 3067.3938 3070.7977
Frequencies -- 3072.2798 3075.3786 3075.6609
Frequencies -- 3075.7869 3076.6597 3077.7949
Frequencies -- 3078.7512 3079.4742 3086.7181
Frequencies -- 3086.7985 3092.1501 3248.6841

E(RB-LYP) = -5384.65742336 (BLYP-D3BJ/def2SVP/SMD (H_2O))
Sum of electronic and zero-point Energies= -5383.352475
Sum of electronic and thermal Energies= -5383.273792
Sum of electronic and thermal Free Energies= -5383.464946

E(RB-LYP) = -5389.96521321 (BLYP-D3BJ/def2TZVPP/SMD (H_2O))

G4

Center Number	Atomic Number	Atomic Type	Coordinates (Angstroms) X	Y	Z
1	6	0	-0.861177	1.106941	1.031645
2	1	0	-1.883457	0.916729	1.412728
3	6	0	0.005997	-0.165914	1.147643
4	6	0	-0.934496	1.523300	-0.460913
5	6	0	1.435040	0.123560	0.624930
6	6	0	-0.619141	-1.323080	0.337385
7	1	0	-1.561250	2.433291	-0.543359
8	6	0	0.490957	1.815623	-0.990755
9	6	0	-1.569462	0.372307	-1.280590
10	1	0	2.064410	-0.781108	0.745446
11	1	0	1.892888	0.931231	1.231319
12	6	0	1.360451	0.540793	-0.863794
13	1	0	-1.635058	-1.559567	0.711640
14	1	0	0.002050	-2.234627	0.450897
15	6	0	-0.697784	-0.901742	-1.153752
16	1	0	0.947749	2.647982	-0.416884
17	1	0	0.441232	2.137370	-2.050825
18	1	0	-2.598184	0.168214	-0.918041
19	1	0	-1.651933	0.668158	-2.346079
20	1	0	2.386886	0.745239	-1.227672
21	6	0	0.728026	-0.610505	-1.684194
22	1	0	-1.154014	-1.729732	-1.731638
23	1	0	0.681872	-0.331009	-2.756371
24	1	0	1.356448	-1.521749	-1.609976
25	1	0	-0.418317	1.917690	1.644689
26	7	0	0.161226	-0.576136	2.613876
27	1	0	0.745977	-1.461903	2.648827
28	1	0	0.753888	0.163768	3.095241
29	6	0	-1.086079	-0.725188	3.441523
30	1	0	-1.378109	0.285621	3.775897
31	1	0	-1.893539	-1.132971	2.809933
32	6	0	-0.919399	-1.670929	4.634746
33	1	0	-1.817103	-1.579025	5.270552
34	1	0	-0.827883	-2.722286	4.307556
35	7	0	0.293234	-1.376818	5.481753
36	1	0	0.171172	-1.728732	6.447318
37	1	0	1.134188	-1.875243	5.055537
38	1	0	0.536573	-0.340879	5.517340
39	53	0	2.354466	-3.176448	3.357513
40	53	0	1.459883	1.821980	4.755576

Frequencies -- 18.8774 22.3966 26.4714
Frequencies -- 49.5960 97.3509 100.8677
Frequencies -- 119.6813 132.0138 167.8132
Frequencies -- 183.9534 232.9663 279.5783

Frequencies -- 295.4476 311.8138 333.0556
Frequencies -- 372.4437 384.4683 401.0876
Frequencies -- 402.3442 429.9995 455.0263
Frequencies -- 455.4815 470.6503 592.2303
Frequencies -- 640.0401 643.5242 704.2541
Frequencies -- 757.8315 787.3445 798.8190
Frequencies -- 802.4238 842.6702 856.5766
Frequencies -- 871.2064 873.4892 883.7825
Frequencies -- 889.0862 920.6135 921.6099
Frequencies -- 948.5406 958.1605 959.3715
Frequencies -- 977.7170 992.5130 1022.8419
Frequencies -- 1024.0335 1028.9280 1050.7149
Frequencies -- 1056.6681 1087.2754 1090.2715
Frequencies -- 1091.5778 1094.6525 1107.4158
Frequencies -- 1108.4042 1125.6930 1172.5145
Frequencies -- 1178.0095 1238.3494 1253.1252
Frequencies -- 1268.4948 1274.1747 1275.7293
Frequencies -- 1284.4864 1287.2590 1291.4945
Frequencies -- 1301.6905 1303.1176 1305.0666
Frequencies -- 1328.3549 1332.0303 1343.6452
Frequencies -- 1347.7845 1350.6338 1355.5410
Frequencies -- 1383.5769 1407.8794 1408.3285
Frequencies -- 1411.8754 1412.9255 1421.4280
Frequencies -- 1425.2030 1425.8466 1427.6037
Frequencies -- 1427.9831 1442.0800 1452.0460
Frequencies -- 1500.4184 1503.1183 1521.5350
Frequencies -- 2791.2660 2827.6954 2851.9757
Frequencies -- 2876.0965 2958.0866 2958.9421
Frequencies -- 2961.1289 2963.0885 2966.3303
Frequencies -- 2971.6088 2988.1651 2988.4550
Frequencies -- 2994.2793 3002.2303 3003.1830
Frequencies -- 3005.1063 3011.8505 3014.1303
Frequencies -- 3020.0696 3033.2775 3036.5607
Frequencies -- 3091.6062 3100.1158 3370.3910

E(RB-LYP) = -1175.96738091 (BLYP-D3BJ/def2SVP/SMD (H_2O))
Sum of electronic and zero-point Energies= -1175.616309
Sum of electronic and thermal Energies= -1175.599209
Sum of electronic and thermal Free Energies= -1175.665674

E(RB-LYP) = -1176.60532518 (BLYP-D3BJ/def2TZVPP/SMD (H_2O))

HG5

Center Atomic Atomic Coordinates (Angstroms)

Number	Number	Type	X	Y	Z
1	8	0	-2.605301	-3.387904	2.695035
2	8	0	1.009672	-4.034799	2.746122
3	8	0	3.919011	-1.696902	2.890377
4	8	0	3.637635	1.785181	2.918734
5	8	0	0.545403	4.018981	2.933604
6	8	0	-2.949338	3.248985	2.832334
7	8	0	-4.263457	-0.100066	2.641785
8	8	0	-2.367646	-3.143843	-3.380354
9	8	0	1.218910	-4.016015	-3.393757
10	8	0	3.783434	-1.598152	-3.203444
11	8	0	3.607898	2.096181	-3.110897
12	8	0	0.799148	4.377728	-3.190013
13	8	0	-2.679830	3.356610	-3.255384
14	8	0	-4.184222	0.003379	-3.449052
15	7	0	-3.995300	-3.403510	0.808113
16	7	0	-2.212356	-4.772459	0.845057
17	7	0	0.207116	-5.218527	0.886561
18	7	0	2.382940	-4.653227	0.952029
19	7	0	4.228279	-3.032850	0.990639
20	7	0	5.279224	-1.044831	1.094686
21	7	0	5.120760	1.423678	1.136484
22	7	0	3.935743	3.332904	1.187816
23	7	0	1.896482	4.702396	1.142845
24	7	0	-0.249450	5.386422	1.200575
25	7	0	-2.608685	4.697050	1.018201
26	7	0	-4.380892	3.311012	0.981766
27	7	0	-5.232642	1.010163	0.821603
28	7	0	-5.162584	-1.240897	0.803703
29	7	0	-3.951225	-3.370711	-1.664492
30	7	0	-2.119460	-4.677470	-1.624793
31	7	0	0.288820	-5.176450	-1.584225
32	7	0	2.477354	-4.666128	-1.524452
33	7	0	4.363110	-3.076165	-1.477637
34	7	0	5.095597	-0.952299	-1.370722
35	7	0	5.017845	1.504982	-1.333209
36	7	0	3.983359	3.500857	-1.272048
37	7	0	2.033882	5.018697	-1.305117
38	7	0	-0.203861	5.288336	-1.273978
39	7	0	-2.616128	4.857605	-1.457060
40	7	0	-4.215122	3.273167	-1.484852
41	7	0	-5.254199	1.043803	-1.643646
42	7	0	-5.126472	-1.200786	-1.669857
43	6	0	-2.891206	-3.792786	1.567634
44	6	0	-1.112184	-5.537686	1.404142
45	1	0	-1.097865	-5.346714	2.491788
46	1	0	-1.307602	-6.615679	1.226349
47	6	0	1.175000	-4.558232	1.644607
48	6	0	3.645748	-4.247704	1.538300
49	1	0	3.462997	-4.064266	2.612160
50	1	0	4.373419	-5.079236	1.424867
51	6	0	4.401471	-1.889442	1.775538
52	6	0	5.749991	0.213470	1.644022
53	1	0	5.561094	0.179359	2.731548
54	1	0	6.841207	0.289029	1.461355
55	6	0	4.156435	2.129240	1.855265
56	6	0	3.173796	4.412218	1.779692
57	1	0	2.958304	4.121049	2.823154
58	1	0	3.794597	5.334069	1.775380
59	6	0	0.701822	4.615898	1.869334
60	6	0	-1.614605	5.541742	1.664993
61	1	0	-1.908416	6.603356	1.533714
62	1	0	-1.623504	5.289862	2.740191
63	6	0	-3.263416	3.685542	1.725125
64	6	0	-5.330071	2.319287	1.446523
65	1	0	-6.357112	2.711185	1.293848
66	1	0	-5.146296	2.181205	2.526646
67	6	0	-4.802722	-0.110308	1.535710
68	6	0	-5.062775	-2.582767	1.349983
69	1	0	-4.882280	-2.485015	2.435032
70	1	0	-6.030337	-3.102029	1.185810
71	6	0	-2.756988	-3.653545	-2.330183
72	6	0	-1.009586	-5.429999	-2.181414
73	1	0	-0.930890	-5.157696	-3.249119
74	1	0	-1.239890	-6.512699	-2.092462
75	6	0	1.312342	-4.538267	-2.283840
76	6	0	3.779328	-4.282182	-2.038869
77	1	0	3.657944	-4.112566	-3.123493
78	1	0	4.488108	-5.119602	-1.873984
79	6	0	4.330881	-1.843173	-2.129191
80	6	0	5.568667	0.302292	-1.928890
81	1	0	5.281808	0.311218	-2.995575
82	1	0	6.675647	0.336576	-1.842771
83	6	0	4.126920	2.330367	-2.019793
84	6	0	3.355738	4.695848	-1.813228
85	1	0	3.249455	4.545068	-2.902091

86	1	0	4.027176	5.558311	-1.622250
87	6	0	0.869759	4.825997	-2.047127
88	6	0	-1.474882	5.628513	-1.901502
89	1	0	-1.686564	6.704035	-1.726943
90	1	0	-1.361352	5.445912	-2.984642
91	6	0	-3.107314	3.768249	-2.177159
92	6	0	-5.188622	2.406297	-2.134492
93	1	0	-4.913871	2.349950	-3.202842
94	1	0	-6.193366	2.868790	-2.035629
95	6	0	-4.765836	-0.045261	-2.365367
96	6	0	-4.986224	-2.528774	-2.240141
97	1	0	-5.957289	-3.058832	-2.146490
98	1	0	-4.741267	-2.395939	-3.308828
99	6	0	-4.114770	-4.147387	-0.443082
100	1	0	-5.077568	-4.698227	-0.467546
101	6	0	-2.850271	-5.082418	-0.430984
102	1	0	-3.095031	-6.163627	-0.480785
103	6	0	0.744919	-5.789243	-0.342545
104	1	0	0.558251	-6.883023	-0.366041
105	6	0	2.270227	-5.411601	-0.288712
106	1	0	2.945941	-6.291540	-0.257892
107	6	0	5.067240	-3.022173	-0.206776
108	1	0	5.820633	-3.835034	-0.154164
109	6	0	5.690910	-1.581165	-0.194107
110	1	0	6.797528	-1.572907	-0.275044
111	6	0	5.510563	2.099847	-0.094810
112	1	0	6.613567	2.211494	-0.134249
113	6	0	4.735352	3.467723	-0.025172
114	1	0	5.397505	4.355302	0.043776
115	6	0	1.781951	5.607400	-0.001331
116	1	0	2.430025	6.495652	0.149260
117	6	0	0.251818	5.942328	-0.044385
118	1	0	0.035909	7.029633	-0.091409
119	6	0	-3.322178	5.075775	-0.203931
120	1	0	-3.658460	6.130318	-0.132082
121	6	0	-4.502609	4.038636	-0.272652
122	1	0	-5.504823	4.508835	-0.348523
123	6	0	-5.925022	0.655350	-0.412678
124	1	0	-6.961132	1.052210	-0.396381
125	6	0	-5.853751	-0.915835	-0.438556
126	1	0	-6.847730	-1.408597	-0.458622
127	6	0	-0.749661	1.322864	0.670468
128	1	0	-1.695969	1.295241	1.245149
129	6	0	0.210005	0.211033	1.185045
130	6	0	-1.045868	1.133000	-0.836563
131	6	0	1.508417	0.258089	0.336258
132	6	0	-0.468947	-1.165197	0.938369
133	1	0	-1.728406	1.928018	-1.184959
134	6	0	0.272633	1.199936	-1.640010
135	6	0	-1.711013	-0.244508	-1.052894
136	1	0	2.191834	-0.529233	0.707958
137	1	0	2.004009	1.233075	0.506101
138	6	0	1.219426	0.071478	-1.169689
139	1	0	-1.419284	-1.223546	1.498149
140	1	0	0.183031	-1.970846	1.325099
141	6	0	-0.760521	-1.362490	-0.567891
142	1	0	0.760762	2.181802	-1.490168
143	1	0	0.065187	1.109903	-2.726554
144	1	0	-2.657530	-0.293082	-0.481620
145	1	0	-1.966714	-0.389645	-2.120369
146	1	0	2.160398	0.119423	-1.750365
147	6	0	0.553305	-1.306343	-1.378376
148	1	0	-1.240643	-2.345922	-0.710722
149	1	0	0.353153	-1.493621	-2.452380
150	1	0	1.242840	-2.102708	-1.038787
151	1	0	-0.284119	2.309844	0.855343
152	7	0	0.631673	0.378348	2.598195
153	1	0	1.360547	1.101181	2.623915
154	6	0	-0.364891	0.701925	3.633763
155	1	0	0.220594	1.058698	4.507678
156	1	0	-1.051677	1.534469	3.361200
157	6	0	-1.210513	-0.508494	4.067606
158	1	0	-1.780791	-0.202674	4.976106
159	1	0	-1.986681	-0.707526	3.302431
160	7	0	-0.370426	-1.687009	4.353548
161	1	0	-0.865859	-2.517728	4.002920
162	1	0	0.430528	-1.612487	3.706713

Frequencies -- 21.1814 36.2169 40.2661
Frequencies -- 46.0503 49.9148 56.3817
Frequencies -- 58.1840 61.9913 65.6514
Frequencies -- 72.0397 72.9072 75.5555
Frequencies -- 81.7029 83.4614 89.3672
Frequencies -- 91.5711 93.6377 95.7458
Frequencies -- 99.6122 101.8612 109.6453
Frequencies -- 113.1477 115.7064 117.4587
Frequencies -- 120.4241 122.6545 123.7841
Frequencies -- 125.1776 127.3749 128.5231
Frequencies -- 130.3305 133.3448 136.8252
Frequencies -- 137.9749 152.3445 155.6852
Frequencies -- 157.3748 161.0494 162.5104
Frequencies -- 167.7755 171.0873 178.7889
Frequencies -- 180.7234 183.0788 185.6174
Frequencies -- 191.2320 191.5674 193.5978
Frequencies -- 197.4867 199.1801 199.9925
Frequencies -- 204.0318 209.6689 220.3338
Frequencies -- 227.2926 230.8241 238.0669
Frequencies -- 241.6411 243.9079 245.7167
Frequencies -- 259.0352 261.9387 265.8940
Frequencies -- 269.1488 281.5754 283.3331
Frequencies -- 287.8634 289.5335 305.4237
Frequencies -- 311.7656 323.0555 328.4410
Frequencies -- 330.0687 330.7574 344.0785
Frequencies -- 345.2971 347.1581 349.5725
Frequencies -- 351.1145 352.8086 354.9074
Frequencies -- 357.1469 360.2389 361.3549
Frequencies -- 361.5196 364.1022 365.0769
Frequencies -- 365.3327 367.6912 371.2253
Frequencies -- 373.7734 397.5041 405.8404
Frequencies -- 410.2697 411.8054 413.6522
Frequencies -- 415.1724 418.6033 429.1853
Frequencies -- 436.1842 437.6949 441.4614
Frequencies -- 442.4398 448.4820 449.4045
Frequencies -- 452.7434 455.9168 457.0071
Frequencies -- 478.9408 490.9114 507.3627
Frequencies -- 509.4990 539.0462 577.7041
Frequencies -- 579.5801 587.8945 603.4071
Frequencies -- 605.6550 608.6189 610.2665
Frequencies -- 614.0785 615.1551 617.7778
Frequencies -- 621.2879 625.6070 626.9621
Frequencies -- 638.3847 639.6679 642.2518
Frequencies -- 644.5586 645.7210 648.7490
Frequencies -- 653.0656 660.1004 661.8500
Frequencies -- 662.8701 665.8687 668.6502
Frequencies -- 670.4791 672.1538 681.2784

Frequencies -- 683.0450 693.2044 694.4735
Frequencies -- 698.2414 701.3052 704.1910
Frequencies -- 708.4583 710.1205 712.2098
Frequencies -- 713.2989 714.8830 717.3586
Frequencies -- 717.7378 718.5091 719.4686
Frequencies -- 721.1803 721.9294 724.8542
Frequencies -- 725.2603 736.7886 740.8599
Frequencies -- 767.2649 768.6884 775.0602
Frequencies -- 776.1972 777.6843 779.2244
Frequencies -- 780.5170 787.9779 790.0794
Frequencies -- 792.3477 794.0445 796.4566
Frequencies -- 810.2355 810.7458 811.8240
Frequencies -- 813.5372 814.3445 815.1697
Frequencies -- 816.3283 816.5861 817.6245
Frequencies -- 817.8657 819.8817 820.2885
Frequencies -- 839.4449 862.9342 868.7505
Frequencies -- 879.0578 882.0629 882.3562
Frequencies -- 884.2784 892.4757 893.5661
Frequencies -- 893.9770 907.3529 910.3863
Frequencies -- 916.6406 933.6741 939.2662
Frequencies -- 939.6693 941.0141 943.3963
Frequencies -- 945.4020 946.3914 949.2734
Frequencies -- 951.5617 954.8646 958.6901
Frequencies -- 959.7082 961.1383 963.0894
Frequencies -- 968.7470 970.4487 972.3635
Frequencies -- 979.1161 980.4798 981.6257
Frequencies -- 983.1720 985.5598 992.7235
Frequencies -- 1001.8429 1004.6244 1009.3201
Frequencies -- 1011.0083 1024.8595 1025.4877
Frequencies -- 1026.0892 1027.4907 1029.9499
Frequencies -- 1033.5602 1034.1778 1034.6348
Frequencies -- 1035.5227 1043.6494 1053.5167
Frequencies -- 1072.1521 1094.1538 1095.9347
Frequencies -- 1097.1904 1100.5265 1101.5880
Frequencies -- 1102.2839 1105.1420 1105.9088
Frequencies -- 1107.0162 1107.8564 1110.5568
Frequencies -- 1111.2979 1113.4245 1117.7897
Frequencies -- 1124.3716 1126.0573 1135.8627
Frequencies -- 1138.9049 1143.9126 1145.2302
Frequencies -- 1150.6849 1165.3562 1165.8024
Frequencies -- 1166.9004 1178.5335 1180.2901
Frequencies -- 1181.0080 1183.0788 1187.9970
Frequencies -- 1188.9357 1193.9658 1195.6659
Frequencies -- 1197.2107 1198.4365 1198.6025
Frequencies -- 1199.6298 1201.0327 1208.6086
Frequencies -- 1209.8263 1211.4615 1213.1159
Frequencies -- 1213.6070 1213.9037 1216.0876
Frequencies -- 1216.8047 1225.3660 1226.2998
Frequencies -- 1226.6230 1227.3789 1227.7046
Frequencies -- 1228.9338 1235.9007 1239.8994
Frequencies -- 1251.0176 1253.9459 1257.8136
Frequencies -- 1258.4103 1263.7876 1265.0645
Frequencies -- 1266.2676 1268.4891 1269.3516
Frequencies -- 1271.6296 1273.3500 1273.8702
Frequencies -- 1274.2440 1274.6021 1275.2693
Frequencies -- 1277.2356 1278.0142 1284.8894
Frequencies -- 1291.3873 1296.3030 1297.0971
Frequencies -- 1298.1498 1299.1892 1301.3287
Frequencies -- 1302.5315 1303.6716 1303.8033
Frequencies -- 1306.4838 1308.9191 1312.6998
Frequencies -- 1313.8474 1315.2617 1315.9863
Frequencies -- 1316.5411 1317.9273 1319.2673
Frequencies -- 1319.4722 1324.2355 1339.2749
Frequencies -- 1350.1910 1359.1610 1359.8235
Frequencies -- 1361.4039 1361.7961 1363.6636
Frequencies -- 1364.4019 1365.3735 1366.6045
Frequencies -- 1367.6433 1368.2440 1369.6502
Frequencies -- 1370.6681 1371.1519 1372.2418
Frequencies -- 1373.1181 1373.4900 1373.8113
Frequencies -- 1375.5429 1376.5748 1377.8959
Frequencies -- 1378.5159 1379.2833 1379.9706
Frequencies -- 1380.8322 1382.5551 1383.1007
Frequencies -- 1384.3796 1384.6002 1384.8437
Frequencies -- 1385.3537 1385.6580 1386.3200
Frequencies -- 1387.2952 1387.6891 1387.9904
Frequencies -- 1388.3853 1390.3742 1391.0903
Frequencies -- 1392.8596 1394.1573 1394.9452
Frequencies -- 1396.2944 1399.5176 1402.0695
Frequencies -- 1404.4418 1406.0708 1408.5954
Frequencies -- 1409.1531 1420.9885 1429.3640
Frequencies -- 1431.3154 1432.9320 1434.0115
Frequencies -- 1436.9921 1437.8562 1440.8854
Frequencies -- 1441.4174 1441.8525 1442.5410
Frequencies -- 1443.5262 1445.7699 1445.9816
Frequencies -- 1447.2049 1449.6073 1451.7310
Frequencies -- 1453.3563 1460.1146 1468.8076

Frequencies -- 1471.4515 1473.2999 1583.4477
Frequencies -- 1707.9315 1708.5433 1712.8486
Frequencies -- 1714.9992 1716.6282 1718.0822
Frequencies -- 1720.3016 1722.4703 1724.7269
Frequencies -- 1725.6972 1727.8910 1737.9057
Frequencies -- 1739.2414 1744.6891 2899.3495
Frequencies -- 2930.7193 2957.9299 2959.3980
Frequencies -- 2960.6298 2964.4012 2966.7592
Frequencies -- 2967.0373 2969.2755 2969.3526
Frequencies -- 2971.9688 2972.6049 2973.0815
Frequencies -- 2973.6673 2974.3019 2974.7019
Frequencies -- 2974.9546 2975.8447 2975.9033
Frequencies -- 2977.5979 2977.7727 2977.8102
Frequencies -- 2978.5249 2979.1107 2979.9096
Frequencies -- 2981.6944 2981.8707 2982.1786
Frequencies -- 2982.5077 2983.9862 2984.1975
Frequencies -- 2984.6932 2985.4451 2986.7769
Frequencies -- 2987.5251 2991.9383 2997.0648
Frequencies -- 3001.8777 3004.9119 3019.7060
Frequencies -- 3021.6736 3030.0779 3031.7029
Frequencies -- 3032.8006 3039.3838 3044.1495
Frequencies -- 3049.8433 3065.1753 3066.8730
Frequencies -- 3066.8888 3067.9258 3069.1593
Frequencies -- 3069.5577 3070.0903 3070.1585
Frequencies -- 3070.3710 3070.6246 3072.7865
Frequencies -- 3073.0041 3073.6021 3074.0375
Frequencies -- 3348.9308 3412.7428 3420.7194

E(RB-LYP) = -4788.03919830 (BLYP-D3BJ/def2SVP/SMD (H_2O))
Sum of electronic and zero-point Energies= -4786.760709
Sum of electronic and thermal Energies= -4786.687233
Sum of electronic and thermal Free Energies= -4786.859759

E(RB-LYP) = -4793.32890157 (BLYP-D3BJ/def2TZVPP/SMD (H_2O))

G5

Center Number	Atomic Number	Atomic Type	Coordinates (Angstroms) X	Y	Z
1	6	0	-0.845200	-0.516479	1.754497
2	1	0	-1.255178	-1.541174	1.873940
3	6	0	0.702295	-0.561344	1.726474
4	6	0	-1.364133	0.116596	0.440339
5	1	0	1.081753	-1.003628	2.670710
6	6	0	1.249218	0.877602	1.580695
7	6	0	1.172947	-1.415582	0.523293
8	1	0	-2.472750	0.157090	0.457898
9	6	0	-0.807009	1.555694	0.302225
10	6	0	-0.894207	-0.736504	-0.764019
11	1	0	2.360705	0.864525	1.575899
12	1	0	0.936124	1.504185	2.440604
13	6	0	0.744798	1.540203	0.271107
14	1	0	0.796434	-2.455109	0.623383
15	1	0	2.281615	-1.470959	0.506436
16	6	0	0.653618	-0.785639	-0.792395
17	1	0	-1.146844	2.185590	1.149564
18	1	0	-1.201674	2.015019	-0.626339
19	1	0	-1.306759	-1.764092	-0.685955
20	1	0	-1.278476	-0.302218	-1.710758
21	6	0	1.204179	0.655644	-0.928045
22	1	0	0.991632	-1.394350	-1.656679
23	1	0	0.851929	1.099073	-1.881255
24	1	0	2.314647	0.644655	-0.963907
25	1	0	-1.193258	0.076463	2.626205
26	7	0	1.285980	2.921123	0.239992
27	1	0	2.307673	2.843956	0.346512
28	6	0	1.022257	3.727728	-0.958052
29	1	0	-0.074188	3.807922	-1.107933
30	1	0	1.431062	3.290883	-1.904573
31	6	0	1.591958	5.148924	-0.807008
32	1	0	1.171626	5.603901	0.113273
33	1	0	2.689754	5.084458	-0.642381
34	7	0	1.344356	6.049730	-1.945221
35	1	0	1.712343	5.597219	-2.796310
36	1	0	0.325798	6.087224	-2.104984

Frequencies -- 45.2227 72.3750 103.0195
Frequencies -- 149.6243 233.6620 263.8661
Frequencies -- 268.6473 306.9952 311.4883
Frequencies -- 351.6732 385.8467 400.5302
Frequencies -- 404.4134 435.5681 454.2678
Frequencies -- 456.9969 495.7194 602.2704
Frequencies -- 638.8092 642.2869 705.4058
Frequencies -- 752.4888 765.9255 787.3486
Frequencies -- 801.0986 804.4616 872.0430
Frequencies -- 872.6994 877.2850 880.9240
Frequencies -- 906.9435 919.1044 926.7087
Frequencies -- 957.1919 960.2890 969.9703
Frequencies -- 997.5868 1016.4803 1019.6315
Frequencies -- 1022.0141 1047.7755 1065.8469
Frequencies -- 1082.0072 1083.5438 1085.5905
Frequencies -- 1093.7160 1096.1881 1098.4815
Frequencies -- 1131.3901 1146.8110 1164.6003
Frequencies -- 1178.5505 1231.8402 1250.5396
Frequencies -- 1266.2517 1267.9953 1269.6816
Frequencies -- 1279.6151 1288.9378 1294.4471
Frequencies -- 1298.7239 1303.3304 1304.3717
Frequencies -- 1328.8317 1332.2216 1341.2162
Frequencies -- 1347.6580 1350.8335 1356.8171
Frequencies -- 1366.7528 1411.9148 1414.2064
Frequencies -- 1423.1832 1424.1472 1427.5190
Frequencies -- 1429.9298 1443.9803 1449.3213
Frequencies -- 1457.6516 1571.0202 2846.4302
Frequencies -- 2940.2796 2944.7039 2946.1719
Frequencies -- 2946.4737 2947.3696 2950.2017
Frequencies -- 2956.4755 2963.7425 2967.4557
Frequencies -- 2976.5201 2983.8499 2988.1238
Frequencies -- 2988.7455 2990.5199 2992.9003

Frequencies -- 2994.9747 3003.1004 3007.0889
Frequencies -- 3340.9571 3361.4879 3404.8468

E(RB-LYP) = -579.365199281 (BLYP-D3BJ/def2SVP/SMD (H_2O))
Sum of electronic and zero-point Energies= -579.040586
Sum of electronic and thermal Energies= -579.027992
Sum of electronic and thermal Free Energies= -579.078951

E(RB-LYP) = -580.017087836 (BLYP-D3BJ/def2TZVPP/SMD (H_2O))

HG6

Center Number	Atomic Number	Atomic Type	Coordinates (Angstroms) X	Y	Z
1	8	0	-2.548079	-3.452873	2.888156
2	8	0	1.030547	-4.040788	2.808569
3	8	0	4.052510	-1.786268	3.002749
4	8	0	3.590069	1.960438	2.868145
5	8	0	0.756974	4.317100	2.923770
6	8	0	-2.741513	3.262700	2.818820
7	8	0	-4.174972	-0.045770	2.801223
8	8	0	-2.565430	-3.279634	-3.235758
9	8	0	0.964297	-3.855907	-3.231147
10	8	0	3.820141	-1.483775	-3.233121
11	8	0	3.777948	2.127040	-3.187553
12	8	0	0.915178	4.315850	-3.240689
13	8	0	-2.575163	3.211006	-3.261696
14	8	0	-4.206069	-0.196077	-3.288077
15	7	0	-3.954846	-3.406943	1.014079
16	7	0	-2.249626	-4.877283	1.051373
17	7	0	0.192700	-5.224785	0.964030
18	7	0	2.381011	-4.688375	1.007475
19	7	0	4.211346	-3.038681	1.026106
20	7	0	5.184355	-1.008599	1.106675
21	7	0	5.021682	1.448385	1.080613
22	7	0	4.047375	3.477443	1.140680
23	7	0	2.064280	4.942788	1.082223
24	7	0	-0.130629	5.440561	1.073206
25	7	0	-2.471832	4.696444	0.983798
26	7	0	-4.197250	3.252501	0.982387
27	7	0	-5.235324	1.012670	1.003287
28	7	0	-5.101621	-1.233322	1.005106
29	7	0	-4.076457	-3.489309	-1.456243
30	7	0	-2.186842	-4.710891	-1.416856
31	7	0	0.208916	-5.256508	-1.509555
32	7	0	2.336201	-4.537281	-1.456056
33	7	0	4.212177	-2.952770	-1.449872
34	7	0	5.105044	-0.889830	-1.363473
35	7	0	5.171424	1.566664	-1.388320
36	7	0	4.061010	3.520277	-1.323146
37	7	0	2.145059	5.066227	-1.393879
38	7	0	-0.083538	5.374578	-1.402430
39	7	0	-2.461526	4.734831	-1.484091
40	7	0	-4.106422	3.201587	-1.483853
41	7	0	-5.116613	0.956905	-1.464506
42	7	0	-5.198803	-1.292611	-1.467807
43	6	0	-2.869236	-3.855538	1.769193
44	6	0	-1.091388	-5.600757	1.543881
45	1	0	-1.030006	-5.417563	2.631222
46	1	0	-1.251954	-6.683579	1.364321
47	6	0	1.180921	-4.576364	1.708446
48	6	0	3.660664	-4.277768	1.558972
49	1	0	3.518149	-4.125907	2.643630
50	1	0	4.388573	-5.099492	1.394857
51	6	0	4.425147	-1.920540	1.837779
52	6	0	5.636188	0.256412	1.654515
53	1	0	5.404499	0.241471	2.734404
54	1	0	6.735214	0.335462	1.518185
55	6	0	4.142855	2.256372	1.806490
56	6	0	3.354312	4.632758	1.682918
57	1	0	3.172288	4.435993	2.754317
58	1	0	4.018447	5.515551	1.579211
59	6	0	0.878441	4.825422	1.808998
60	6	0	-1.482695	5.580265	1.579716
61	1	0	-1.811414	6.629985	1.433962
62	1	0	-1.448541	5.351652	2.659688
63	6	0	-3.085319	3.675023	1.710324
64	6	0	-5.202571	2.362016	1.538841
65	1	0	-6.200747	2.823231	1.389557
66	1	0	-4.996369	2.276962	2.620247
67	6	0	-4.752581	-0.084673	1.712794
68	6	0	-4.991963	-2.561491	1.584686
69	1	0	-4.757326	-2.434435	2.656431
70	1	0	-5.971694	-3.074464	1.481332
71	6	0	-2.895243	-3.752705	-2.150109
72	6	0	-1.122898	-5.491890	-2.029074
73	1	0	-1.103350	-5.232678	-3.102592
74	1	0	-1.360326	-6.569822	-1.914221
75	6	0	1.140889	-4.459431	-2.174025
76	6	0	3.600939	-4.128714	-2.039273
77	1	0	3.410881	-3.895761	-3.102177
78	1	0	4.317063	-4.974906	-1.968855
79	6	0	4.305542	-1.740255	-2.132708
80	6	0	5.683538	0.321509	-1.923514
81	1	0	5.462712	0.320397	-3.005531
82	1	0	6.782245	0.296032	-1.768774
83	6	0	4.265793	2.366952	-2.083832
84	6	0	3.461575	4.718032	-1.892066
85	1	0	3.359439	4.545616	-2.978155
86	1	0	4.144441	5.574579	-1.714551
87	6	0	0.981962	4.840126	-2.129728
88	6	0	-1.394557	5.569351	-2.003249
89	1	0	-1.688563	6.632907	-1.882036
90	1	0	-1.293659	5.335660	-3.078067
91	6	0	-2.988251	3.653409	-2.190511
92	6	0	-5.070033	2.281046	-2.061966
93	1	0	-4.794710	2.145234	-3.123100
94	1	0	-6.080526	2.738120	-1.996613
95	6	0	-4.753923	-0.181403	-2.187232
96	6	0	-5.126554	-2.643742	-1.995615
97	1	0	-6.101204	-3.144162	-1.822526
98	1	0	-4.946950	-2.558271	-3.081862
99	6	0	-4.162025	-4.207031	-0.194582
100	1	0	-5.125752	-4.752423	-0.127222
101	6	0	-2.904263	-5.147371	-0.222696
102	1	0	-3.156371	-6.225011	-0.301551
103	6	0	0.718736	-5.816723	-0.267912
104	1	0	0.572227	-6.916090	-0.253341
105	6	0	2.228544	-5.377939	-0.268512
106	1	0	2.941081	-6.225474	-0.335050
107	6	0	4.980853	-2.973365	-0.215549
108	1	0	5.722927	-3.798574	-0.241477
109	6	0	5.632163	-1.544479	-0.172751
110	1	0	6.741353	-1.563127	-0.209153
111	6	0	5.557224	2.126196	-0.101477
112	1	0	6.661774	2.195833	-0.027597
113	6	0	4.832378	3.519377	-0.085315
114	1	0	5.526735	4.384386	-0.066560
115	6	0	1.897815	5.745243	-0.130549
116	1	0	2.515624	6.664207	-0.062272
117	6	0	0.350511	6.028245	-0.170225
118	1	0	0.097187	7.108113	-0.202582
119	6	0	-3.182727	5.014127	-0.252066
120	1	0	-3.518395	6.071291	-0.235243
121	6	0	-4.360121	3.974661	-0.273477
122	1	0	-5.366339	4.440203	-0.319193
123	6	0	-5.869870	0.638927	-0.252889
124	1	0	-6.890056	1.071037	-0.309288
125	6	0	-5.849949	-0.934447	-0.217225
126	1	0	-6.859141	-1.392164	-0.167192
127	6	0	-1.086482	0.989646	0.803050
128	1	0	-2.054634	0.678193	1.234922
129	6	0	0.034766	0.019955	1.243556
130	6	0	-1.174649	1.017448	-0.744483
131	6	0	1.384254	0.502584	0.655169
132	6	0	-0.272634	-1.393544	0.696982
133	1	0	-1.991302	1.700112	-1.030841
134	6	0	0.168345	1.526657	-1.312065
135	6	0	-1.478767	-0.397357	-1.280958
136	1	0	2.200673	-0.183268	0.939460
137	1	0	1.631012	1.501496	1.052780
138	6	0	1.292705	0.554349	-0.893471
139	1	0	-1.236193	-1.759938	1.089601
140	1	0	0.510428	-2.103235	1.015507
141	6	0	-0.346232	-1.353735	-0.852565
142	1	0	0.382408	2.535469	-0.912217
143	1	0	0.116626	1.619505	-2.414094
144	1	0	-2.444951	-0.751219	-0.876010
145	1	0	-1.582115	-0.381896	-2.382712
146	1	0	2.260486	0.904887	-1.294480
147	6	0	0.997996	-0.864822	-1.428384
148	1	0	-0.558059	-2.372716	-1.221408
149	1	0	0.969665	-0.867526	-2.535010
150	1	0	1.806715	-1.556153	-1.130100
151	1	0	-0.872190	2.009749	1.163153
152	7	0	0.114389	-0.016616	2.843884

153	6	0	-1.049818	-0.775281	3.439993
154	1	0	-0.965304	-1.843999	3.201311
155	1	0	-0.995903	-0.644706	4.535970
156	1	0	-2.005497	-0.373679	3.068976
157	6	0	1.383679	-0.693234	3.310449
158	1	0	2.247970	-0.058446	3.076642
159	1	0	1.309960	-0.811384	4.406301
160	1	0	1.471948	-1.685640	2.847804
161	6	0	0.109458	1.379119	3.427943
162	1	0	-0.868670	1.857826	3.270559
163	1	0	0.299161	1.280381	4.511929
164	1	0	0.910977	1.977776	2.974629
165	53	0	0.531848	-0.177747	7.304134

Frequencies -- 6.2799 12.4199 16.4661
Frequencies -- 30.8662 37.5983 44.8125
Frequencies -- 46.6948 52.7541 58.9013
Frequencies -- 63.8668 67.6269 70.3287
Frequencies -- 73.1687 78.1756 84.6059
Frequencies -- 85.6452 86.2423 94.0107
Frequencies -- 97.3331 97.6628 107.1264
Frequencies -- 109.5042 110.0796 116.9680
Frequencies -- 117.7997 120.1937 122.2876
Frequencies -- 123.0148 127.4022 127.9363
Frequencies -- 129.9352 133.4595 135.6798
Frequencies -- 137.2368 141.1840 144.5890
Frequencies -- 147.7618 149.3779 155.5569
Frequencies -- 159.0113 164.1513 166.2675
Frequencies -- 171.0697 174.3410 179.2450
Frequencies -- 182.4246 188.5584 190.9002
Frequencies -- 193.8296 198.6620 199.4178
Frequencies -- 204.6791 208.8726 218.1359
Frequencies -- 220.4334 225.2837 227.6244
Frequencies -- 230.2187 236.9730 238.5377
Frequencies -- 243.7634 259.9537 262.3979
Frequencies -- 263.8744 265.4695 282.0043
Frequencies -- 284.2446 285.7528 289.6637
Frequencies -- 293.1703 315.6340 320.4478
Frequencies -- 325.4870 330.3206 331.2636
Frequencies -- 333.4051 340.4626 341.0960
Frequencies -- 346.3616 347.1104 353.0973
Frequencies -- 354.2593 356.0327 356.9649
Frequencies -- 358.4830 358.8579 361.0172
Frequencies -- 362.0556 363.1200 364.0856
Frequencies -- 366.9015 368.4498 372.0813
Frequencies -- 373.1627 374.4291 394.6053
Frequencies -- 397.9323 412.6365 414.6971
Frequencies -- 414.9398 417.4483 420.8513
Frequencies -- 428.9646 435.0957 436.4385
Frequencies -- 442.3804 443.4258 448.3168
Frequencies -- 452.8128 454.1643 456.1050
Frequencies -- 457.5350 460.5718 479.9450
Frequencies -- 481.7710 482.8006 506.5796
Frequencies -- 510.1492 563.0887 577.5392
Frequencies -- 579.4839 604.7399 605.7865
Frequencies -- 610.4514 611.1636 614.1312
Frequencies -- 615.8296 621.1491 621.9612
Frequencies -- 624.1240 625.2863 639.5101
Frequencies -- 639.5738 642.1345 644.3476
Frequencies -- 645.6660 648.1115 650.7680
Frequencies -- 660.1540 663.3786 664.1562
Frequencies -- 666.0419 668.1189 671.7673
Frequencies -- 675.0819 680.9265 682.2489
Frequencies -- 690.1630 694.7103 696.1543
Frequencies -- 698.2925 701.7841 709.1438
Frequencies -- 711.7511 712.7896 714.5164
Frequencies -- 715.6620 716.2237 717.8630
Frequencies -- 720.3711 720.9401 724.1242
Frequencies -- 725.8783 726.5927 727.6642
Frequencies -- 732.6542 767.0281 767.7689
Frequencies -- 769.6049 775.8057 776.8232
Frequencies -- 777.4994 780.6903 788.6937
Frequencies -- 789.3240 792.9198 794.7019
Frequencies -- 797.0642 798.5245 810.5161
Frequencies -- 812.0176 812.1351 813.1542
Frequencies -- 814.1117 815.4962 816.9657
Frequencies -- 817.1612 817.6759 818.7128
Frequencies -- 819.2869 821.9404 823.7311
Frequencies -- 873.9534 880.5817 881.9125
Frequencies -- 882.8360 884.5459 886.0869
Frequencies -- 894.9260 895.5052 910.0514
Frequencies -- 910.3475 927.7617 929.6799
Frequencies -- 940.4490 942.0654 943.5247
Frequencies -- 943.8973 945.9847 946.1387
Frequencies -- 947.5630 951.8241 952.2253
Frequencies -- 955.6255 960.6084 962.0057
Frequencies -- 963.1810 964.4460 970.0866
Frequencies -- 971.1836 978.5159 978.9235
Frequencies -- 980.3195 981.0877 984.6569
Frequencies -- 992.5019 1002.1730 1003.2654
Frequencies -- 1009.2877 1010.7833 1024.2450
Frequencies -- 1026.0198 1027.7563 1029.4667
Frequencies -- 1029.8601 1031.4796 1034.2029

Frequencies -- 1034.7152 1035.7662 1039.0828
Frequencies -- 1042.9292 1047.3065 1091.8984
Frequencies -- 1094.4188 1098.1545 1099.1260
Frequencies -- 1100.8967 1103.1464 1103.7567
Frequencies -- 1104.8412 1106.1258 1109.6524
Frequencies -- 1110.8408 1111.7888 1114.6958
Frequencies -- 1115.5486 1118.9080 1121.2607
Frequencies -- 1134.0592 1136.0394 1138.1403
Frequencies -- 1140.5324 1150.3625 1165.1553
Frequencies -- 1167.1267 1168.4645 1181.3867
Frequencies -- 1182.1334 1183.1361 1184.9177
Frequencies -- 1188.9445 1192.0398 1196.5014
Frequencies -- 1197.3480 1198.5420 1199.9106
Frequencies -- 1201.3386 1202.2620 1209.9836
Frequencies -- 1210.9592 1212.6931 1213.8394
Frequencies -- 1214.3828 1215.0166 1215.4935
Frequencies -- 1217.7802 1219.0221 1225.2169
Frequencies -- 1226.4536 1226.5694 1227.1356
Frequencies -- 1227.8702 1228.0302 1236.0006
Frequencies -- 1237.7461 1238.4630 1250.9286
Frequencies -- 1253.6943 1256.7844 1257.6582
Frequencies -- 1262.2207 1264.1129 1266.7447
Frequencies -- 1271.3543 1272.5481 1272.9912
Frequencies -- 1273.6031 1275.4876 1275.5180
Frequencies -- 1277.1385 1278.9945 1283.5728
Frequencies -- 1284.8959 1289.6742 1290.1094
Frequencies -- 1292.1991 1294.2776 1296.0643
Frequencies -- 1296.8726 1298.7582 1301.5162
Frequencies -- 1301.8518 1303.3113 1307.3714
Frequencies -- 1310.0785 1312.7137 1314.4417
Frequencies -- 1315.4192 1317.6783 1318.0452
Frequencies -- 1320.1216 1324.5286 1326.9762
Frequencies -- 1344.4446 1350.1458 1359.0237
Frequencies -- 1362.4848 1363.0560 1364.2079
Frequencies -- 1367.0361 1367.6538 1368.5897
Frequencies -- 1369.3296 1369.6350 1370.2008
Frequencies -- 1371.1038 1371.6049 1372.0807
Frequencies -- 1372.8669 1373.3670 1374.6508
Frequencies -- 1375.4279 1376.7418 1377.2525
Frequencies -- 1377.6697 1378.8634 1380.0820
Frequencies -- 1381.0819 1381.3547 1381.6866
Frequencies -- 1381.8360 1382.6126 1383.5625
Frequencies -- 1384.0174 1384.4251 1386.0741
Frequencies -- 1387.0384 1387.9499 1388.9739
Frequencies -- 1389.8075 1391.9898 1393.5850
Frequencies -- 1394.5491 1395.3331 1396.0959
Frequencies -- 1396.3178 1399.6422 1400.2203
Frequencies -- 1402.6914 1404.4199 1405.5674
Frequencies -- 1408.3927 1420.4664 1422.1952
Frequencies -- 1427.6062 1432.5761 1433.0588
Frequencies -- 1433.3823 1434.7131 1435.8201
Frequencies -- 1436.3408 1436.8162 1439.2874
Frequencies -- 1439.8928 1440.2984 1440.8793
Frequencies -- 1441.6368 1443.2339 1443.4363
Frequencies -- 1445.2661 1445.5163 1448.6157
Frequencies -- 1449.0865 1452.6496 1454.5074
Frequencies -- 1461.7274 1464.0884 1466.0797
Frequencies -- 1469.0076 1704.8402 1705.6800
Frequencies -- 1708.6023 1713.6439 1717.3942
Frequencies -- 1718.1307 1720.3059 1721.2792
Frequencies -- 1724.8142 1726.2208 1727.6359
Frequencies -- 1738.3371 1738.8987 1744.7672
Frequencies -- 2961.7494 2965.1078 2966.5997
Frequencies -- 2967.8293 2968.8014 2971.7093
Frequencies -- 2973.5451 2973.9484 2974.2730
Frequencies -- 2974.4275 2975.7192 2976.5018
Frequencies -- 2977.1775 2977.6715 2979.0028
Frequencies -- 2980.0873 2980.3535 2981.7209
Frequencies -- 2982.3803 2983.1058 2983.4764
Frequencies -- 2984.7894 2985.5003 2985.6252
Frequencies -- 2986.6196 2987.0957 2988.8940
Frequencies -- 2990.7689 2996.4704 2996.9569
Frequencies -- 2998.8477 2999.9879 3002.6906
Frequencies -- 3006.5740 3009.9071 3017.8113
Frequencies -- 3021.1789 3029.2044 3036.2878
Frequencies -- 3053.3126 3055.0254 3061.0953
Frequencies -- 3062.1999 3065.2469 3068.0420
Frequencies -- 3068.3273 3068.7051 3069.4286
Frequencies -- 3070.2420 3070.4267 3070.6642
Frequencies -- 3071.8815 3072.0888 3072.3358
Frequencies -- 3072.5298 3073.7034 3074.3342
Frequencies -- 3074.4412 3074.8701 3075.2754
Frequencies -- 3100.0891 3102.5835 3107.9653
Frequencies -- 3155.8818 3156.5142 3164.5450

E(RB-LYP) = -5070.28609518 (BLYP-D3BJ/def2SVP/SMD (H_2O))
Sum of electronic and zero-point Energies= -5068.982808

Sum of electronic and thermal Energies= -5068.906764
Sum of electronic and thermal Free Energies= -5069.088614

E(RB-LYP) = -5075.56425998 (BLYP-D3BJ/def2TZVPP/SMD (H_2O))

G6

Center Number	Atomic Number	Atomic Type	Coordinates (Angstroms) X	Y	Z
1	6	0	-1.100418	0.992620	0.782146
2	1	0	-2.076872	0.679091	1.198441
3	6	0	0.025749	0.030782	1.235181
4	6	0	-1.180152	1.005721	-0.769498
5	6	0	1.376643	0.518148	0.655692
6	6	0	-0.273513	-1.392492	0.703360
7	1	0	-1.997964	1.692805	-1.064010
8	6	0	0.165223	1.510223	-1.340941
9	6	0	-1.471398	-0.418908	-1.294226
10	1	0	2.194794	-0.164572	0.946307
11	1	0	1.624971	1.526965	1.037759
12	6	0	1.296188	0.555672	-0.895149
13	1	0	-1.244810	-1.757486	1.083300
14	1	0	0.507412	-2.106238	1.028844
15	6	0	-0.333220	-1.365920	-0.848841
16	1	0	0.369576	2.540651	-0.984402
17	1	0	0.117252	1.550145	-2.448020
18	1	0	-2.444818	-0.781266	-0.904120
19	1	0	-1.546390	-0.407727	-2.400482
20	1	0	2.270626	0.916523	-1.279706
21	6	0	1.014896	-0.871970	-1.420571
22	1	0	-0.538681	-2.396214	-1.200816
23	1	0	0.979315	-0.869659	-2.528811
24	1	0	1.833400	-1.558348	-1.120819
25	1	0	-0.898806	2.021438	1.131116
26	7	0	0.104850	0.003631	2.846100
27	6	0	-1.072828	-0.735207	3.448249
28	1	0	-0.995823	-1.809010	3.221242
29	1	0	-1.032322	-0.591218	4.543435
30	1	0	-2.012711	-0.322940	3.048670
31	6	0	1.366165	-0.683574	3.329088
32	1	0	2.240719	-0.056038	3.101381
33	1	0	1.280198	-0.805185	4.424455
34	1	0	1.462870	-1.669007	2.847119
35	6	0	0.105866	1.403604	3.427143
36	1	0	-0.883072	1.866621	3.290391
37	1	0	0.320343	1.316577	4.508111
38	1	0	0.885256	2.007474	2.936252
39	53	0	0.434706	-0.140951	7.229122

Frequencies -- 37.0654 39.7871 57.3024
Frequencies -- 90.7648 192.5833 197.3103
Frequencies -- 276.0535 299.4489 308.7369
Frequencies -- 313.7048 326.0685 341.0648
Frequencies -- 353.2274 378.5767 384.4758
Frequencies -- 405.2861 407.4489 442.2098
Frequencies -- 445.3101 465.3528 466.7095
Frequencies -- 470.8554 555.5228 641.3216
Frequencies -- 642.0550 679.8080 756.6866
Frequencies -- 783.6330 791.8934 807.8149
Frequencies -- 808.2032 875.3474 876.1586
Frequencies -- 883.6565 918.5530 920.6625
Frequencies -- 936.6868 938.3644 957.3011
Frequencies -- 967.6268 970.1348 1021.9246
Frequencies -- 1025.2466 1026.1733 1027.0139
Frequencies -- 1044.6126 1089.1905 1090.5441
Frequencies -- 1091.6498 1099.5909 1111.6632
Frequencies -- 1112.7934 1119.5555 1176.0269
Frequencies -- 1176.6133 1214.8489 1217.3110
Frequencies -- 1227.9366 1265.1257 1266.4329
Frequencies -- 1273.6697 1276.9327 1279.8126
Frequencies -- 1284.2590 1305.3198 1306.2377
Frequencies -- 1308.3825 1334.6707 1335.1230
Frequencies -- 1348.1880 1355.9938 1357.5478
Frequencies -- 1393.0979 1396.3849 1413.8069
Frequencies -- 1416.2252 1421.0190 1423.2270
Frequencies -- 1425.2794 1428.1537 1430.2722
Frequencies -- 1431.3833 1435.4791 1445.8149
Frequencies -- 1451.6817 1456.3617 1459.0381
Frequencies -- 2959.2513 2960.0591 2962.4772
Frequencies -- 2983.1751 2984.5070 2986.7237
Frequencies -- 2988.6238 2991.9336 2992.4924
Frequencies -- 2994.8239 2998.9862 3003.2155
Frequencies -- 3003.6930 3004.2414 3006.3997
Frequencies -- 3042.7668 3044.3572 3047.9307
Frequencies -- 3092.3636 3095.6292 3100.8833
Frequencies -- 3135.8079 3137.2888 3139.6151

E(RB-LYP) = -861.599505613 (BLYP-D3BJ/def2SVP/SMD (H_2O))
Sum of electronic and zero-point Energies= -861.249430
Sum of electronic and thermal Energies= -861.234656
Sum of electronic and thermal Free Energies= -861.292313

E(RB-LYP) = -862.242153700 (BLYP-D3BJ/def2TZVPP/SMD (H_2O))

HG7

Center Number	Atomic Number	Atomic Type	Coordinates (Angstroms) X	Y	Z
1	8	0	-2.542859	-3.199100	2.708884
2	8	0	1.166071	-4.133806	2.823493
3	8	0	3.885731	-1.778820	2.860096
4	8	0	3.487201	1.913555	2.850278
5	8	0	0.452900	4.253816	2.767389
6	8	0	-2.872038	3.289588	2.631691
7	8	0	-4.196433	-0.048215	2.582789
8	8	0	-2.731081	-3.257512	-3.393845
9	8	0	1.060068	-3.882040	-3.360529
10	8	0	3.711139	-1.459823	-3.169969
11	8	0	3.650279	2.074341	-3.175219
12	8	0	0.874429	4.204185	-3.390303
13	8	0	-2.882938	3.028035	-3.449752
14	8	0	-4.633898	-0.203810	-3.490292
15	7	0	-4.054250	-3.400110	0.929598
16	7	0	-2.188616	-4.659917	0.908439
17	7	0	0.226963	-5.152653	0.930485
18	7	0	2.429587	-4.678787	0.926458
19	7	0	4.351350	-3.114776	0.997530
20	7	0	5.169265	-1.015004	1.055883
21	7	0	4.991579	1.467461	1.105063
22	7	0	3.880319	3.427505	1.110323
23	7	0	1.821468	4.780569	0.934491
24	7	0	-0.335589	5.448193	0.913177
25	7	0	-2.692652	4.737632	0.796204
26	7	0	-4.322744	3.186720	0.792096
27	7	0	-5.394089	0.981143	0.853499
28	7	0	-5.252955	-1.261328	0.877821
29	7	0	-4.151382	-3.441172	-1.539997
30	7	0	-2.240580	-4.637127	-1.559464

31	7	0	0.182140	-5.076846	-1.544498
32	7	0	2.374878	-4.563948	-1.545532
33	7	0	4.245587	-2.972955	-1.463889
34	7	0	5.168174	-0.923022	-1.413471
35	7	0	5.037347	1.532382	-1.364196
36	7	0	3.971650	3.513551	-1.354735
37	7	0	2.025925	5.017971	-1.520911
38	7	0	-0.225113	5.163942	-1.552485
39	7	0	-2.608326	4.524295	-1.665036
40	7	0	-4.403522	3.161081	-1.670203
41	7	0	-5.483933	0.928602	-1.624931
42	7	0	-5.423998	-1.321779	-1.589161
43	6	0	-2.879290	-3.681499	1.629091
44	6	0	-1.090072	-5.416075	1.488729
45	1	0	-1.042313	-5.154006	2.560770
46	1	0	-1.314029	-6.498555	1.382637
47	6	0	1.258187	-4.590298	1.683960
48	6	0	3.735231	-4.349345	1.476694
49	1	0	3.609823	-4.246421	2.568896
50	1	0	4.432500	-5.184741	1.263269
51	6	0	4.403954	-1.948594	1.746670
52	6	0	5.590660	0.250175	1.647590
53	1	0	5.331427	0.205375	2.720304
54	1	0	6.691638	0.335448	1.541933
55	6	0	4.051663	2.231188	1.792596
56	6	0	3.085408	4.534121	1.620892
57	1	0	2.841471	4.300226	2.672437
58	1	0	3.704686	5.455053	1.582586
59	6	0	0.618553	4.754845	1.657047
60	6	0	-1.701810	5.635525	1.365892
61	1	0	-2.005675	6.678577	1.145601
62	1	0	-1.706348	5.472360	2.457844
63	6	0	-3.239090	3.678522	1.525697
64	6	0	-5.329978	2.326043	1.387955
65	1	0	-6.325347	2.802643	1.269722
66	1	0	-5.089189	2.240638	2.462244
67	6	0	-4.855070	-0.103676	1.545440
68	6	0	-5.112998	-2.576607	1.478455
69	1	0	-4.889215	-2.429185	2.549629
70	1	0	-6.076824	-3.116124	1.374076
71	6	0	-3.001294	-3.716524	-2.281956
72	6	0	-1.116070	-5.360421	-2.134576
73	1	0	-1.058015	-5.079888	-3.201241
74	1	0	-1.314980	-6.449686	-2.050236
75	6	0	1.187193	-4.427096	-2.265656
76	6	0	3.657087	-4.152393	-2.080714
77	1	0	3.501442	-3.921647	-3.149700
78	1	0	4.375096	-4.993090	-1.985154
79	6	0	4.289885	-1.744316	-2.122976
80	6	0	5.640535	0.343699	-1.939959
81	1	0	5.410831	0.356495	-3.020081
82	1	0	6.739149	0.396083	-1.793677
83	6	0	4.143783	2.332263	-2.079634
84	6	0	3.370108	4.694906	-1.957129
85	1	0	3.320093	4.515619	-3.045562
86	1	0	4.027720	5.564390	-1.753225
87	6	0	0.891271	4.716436	-2.273292
88	6	0	-1.514242	5.316446	-2.215124
89	1	0	-1.812437	6.386326	-2.188087
90	1	0	-1.376791	5.002113	-3.265040
91	6	0	-3.251880	3.509983	-2.369247
92	6	0	-5.432675	2.268243	-2.196127
93	1	0	-5.245420	2.149940	-3.277957
94	1	0	-6.417019	2.757890	-2.048227
95	6	0	-5.117649	-0.201904	-2.352325
96	6	0	-5.269190	-2.683894	-2.084972
97	1	0	-6.205308	-3.241849	-1.878860
98	1	0	-5.118457	-2.614282	-3.176695
99	6	0	-4.200065	-4.188418	-0.284861
100	1	0	-5.127140	-4.796017	-0.241348
101	6	0	-2.882957	-5.046693	-0.313901
102	1	0	-3.066059	-6.141089	-0.320691
103	6	0	0.688998	-5.716525	-0.333336
104	1	0	0.479765	-6.805800	-0.362880
105	6	0	2.223636	-5.371342	-0.343787
106	1	0	2.878739	-6.265227	-0.399943
107	6	0	5.075753	-3.001301	-0.266613
108	1	0	5.837942	-3.803178	-0.339921
109	6	0	5.685672	-1.549939	-0.209496
110	1	0	6.794264	-1.529391	-0.204357
111	6	0	5.465080	2.135344	-0.111108
112	1	0	6.569420	2.232111	-0.082291
113	6	0	4.704214	3.513375	-0.096487
114	1	0	5.374266	4.394984	-0.040869
115	6	0	1.713626	5.642984	-0.251670
116	1	0	2.323832	6.559196	-0.111647
117	6	0	0.173110	5.925156	-0.358490
118	1	0	-0.073899	6.998129	-0.493886
119	6	0	-3.359924	4.945261	-0.478082
120	1	0	-3.672307	6.004139	-0.583878
121	6	0	-4.556660	3.930441	-0.436915
122	1	0	-5.553563	4.416014	-0.416157
123	6	0	-6.119397	0.591973	-0.346268
124	1	0	-7.153027	0.992956	-0.322656
125	6	0	-6.049571	-0.982309	-0.311271
126	1	0	-7.042048	-1.471000	-0.235044
127	6	0	0.075381	1.172870	1.503542
128	1	0	-0.690371	1.167919	2.303634
129	6	0	0.906289	-0.122875	1.555332
130	6	0	-0.598523	1.270726	0.123998
131	6	0	1.975693	-0.107993	0.446063
132	6	0	0.007633	-1.353079	1.346777
133	1	0	-1.222111	2.181529	0.087602
134	6	0	0.464465	1.310634	-1.011169
135	6	0	-1.516750	0.041202	-0.106219
136	1	0	2.557083	-1.044083	0.479308
137	1	0	2.674487	0.727959	0.592382
138	6	0	1.310515	0.014119	-0.932671
139	1	0	-0.755505	-1.419032	2.144560
140	1	0	0.628033	-2.261771	1.411616
141	6	0	-0.666679	-1.251298	-0.035080
142	1	0	1.125837	2.184028	-0.866666
143	1	0	-2.284558	0.012639	0.690079
144	1	0	2.089469	0.042887	-1.718294
145	6	0	0.385774	-1.205724	-1.181258
146	1	0	-1.327094	-2.125965	-0.180439
147	1	0	0.998508	-2.123950	-1.152054
148	1	0	0.729750	2.043828	1.688870
149	7	0	1.580660	-0.208205	2.908141
150	1	0	2.214845	-1.038323	2.973044
151	1	0	2.203114	0.623948	3.048983
152	1	0	0.852949	-0.246196	3.679669
153	6	0	-0.282045	-1.088980	-2.569845
154	1	0	0.496685	-1.047934	-3.355791
155	1	0	-0.917284	-1.965352	-2.786582
156	6	0	-0.203683	1.415746	-2.392289
157	1	0	-0.783365	2.348210	-2.476424
158	1	0	0.565050	1.442746	-3.187878
159	6	0	-2.187464	0.136384	-1.479117
160	1	0	-2.816951	-0.753535	-1.642630
161	1	0	-2.832968	1.026916	-1.526904
162	6	0	-1.124222	0.199352	-2.591356
163	7	0	-1.854886	0.351164	-3.912067
164	1	0	-1.186391	0.276493	-4.734712
165	1	0	-2.619709	-0.347828	-3.993170
166	1	0	-2.320004	1.289432	-3.929244
167	53	0	-0.978615	-0.292497	5.302271
168	53	0	0.495190	0.215565	-6.488784

Frequencies -- 6.4514 17.3052 24.1819
Frequencies -- 30.3272 35.3201 37.6425
Frequencies -- 42.3373 47.2513 48.3364
Frequencies -- 51.5706 55.6151 58.5395
Frequencies -- 66.8244 68.2506 74.0610
Frequencies -- 78.1043 80.4512 83.6834
Frequencies -- 89.9040 93.7417 95.9482
Frequencies -- 99.9097 100.5536 105.8882
Frequencies -- 110.3193 113.9649 118.0504
Frequencies -- 118.7511 119.9202 127.7630
Frequencies -- 130.4418 132.2234 136.4588
Frequencies -- 140.3265 142.8106 146.0919
Frequencies -- 151.1364 151.9937 157.6364
Frequencies -- 159.7259 163.3985 167.2564
Frequencies -- 169.2339 173.8937 177.1103
Frequencies -- 178.8047 179.6887 189.1225
Frequencies -- 191.4214 193.6288 195.8164

Frequencies -- 197.7136 205.2332 206.6166
Frequencies -- 208.0307 220.5938 226.2045
Frequencies -- 228.1131 230.8650 236.5451
Frequencies -- 241.8048 246.6711 259.0380
Frequencies -- 263.6945 264.1771 266.0330
Frequencies -- 271.1832 280.9654 281.7454
Frequencies -- 284.7774 285.8005 290.0523
Frequencies -- 318.9770 323.4593 327.9021
Frequencies -- 334.4997 337.8614 340.1708
Frequencies -- 344.0273 345.1293 349.3016
Frequencies -- 350.2807 352.9027 354.9021
Frequencies -- 356.4072 356.6756 358.5897
Frequencies -- 361.6777 363.3271 363.9146
Frequencies -- 365.2991 367.7817 368.4455
Frequencies -- 369.6649 373.0962 377.8153
Frequencies -- 380.3153 394.3853 409.2293
Frequencies -- 412.6285 414.5007 415.6607
Frequencies -- 417.4232 427.5218 429.6460
Frequencies -- 433.9902 438.3823 441.0053
Frequencies -- 442.1244 447.3917 448.8608
Frequencies -- 453.4124 455.7019 457.9576
Frequencies -- 462.4149 476.3903 500.5717
Frequencies -- 504.9642 506.9691 544.0530
Frequencies -- 574.6333 576.5200 599.8584
Frequencies -- 605.8183 608.1751 610.0948
Frequencies -- 611.3697 613.7266 618.9987
Frequencies -- 622.0579 622.6957 625.5688
Frequencies -- 632.9481 636.0924 637.9936
Frequencies -- 641.7975 643.1953 643.7382
Frequencies -- 646.0100 647.2726 658.2437
Frequencies -- 659.9672 661.0868 662.4057
Frequencies -- 664.8076 666.5398 670.0703
Frequencies -- 672.7707 681.2394 683.2116
Frequencies -- 690.9577 693.1867 699.0229
Frequencies -- 700.2985 701.7418 703.8215
Frequencies -- 708.7007 710.3977 711.5293
Frequencies -- 712.7243 713.8652 714.5504
Frequencies -- 715.1303 715.6068 717.3019
Frequencies -- 719.8187 721.2989 723.9287
Frequencies -- 726.8499 727.5703 739.3754
Frequencies -- 764.6107 766.6330 773.8443
Frequencies -- 775.5403 776.1011 778.4076
Frequencies -- 786.4131 787.6560 789.7543
Frequencies -- 793.4713 794.0732 801.3322
Frequencies -- 808.2792 809.7234 810.1102
Frequencies -- 811.8101 812.9180 813.5978
Frequencies -- 814.6192 816.0168 816.8916
Frequencies -- 818.0633 821.4445 862.6720
Frequencies -- 867.3302 879.3074 881.6619
Frequencies -- 885.3960 893.8894 894.1522
Frequencies -- 895.8660 907.9023 910.9199
Frequencies -- 911.0414 914.7804 935.5275
Frequencies -- 936.8368 938.1638 940.1741
Frequencies -- 941.6655 944.8761 945.6730
Frequencies -- 947.1745 948.7982 950.0863
Frequencies -- 952.1559 954.5782 955.7725
Frequencies -- 959.9777 961.5034 962.3515
Frequencies -- 967.8023 970.1933 975.2080
Frequencies -- 977.4732 983.1628 989.1806
Frequencies -- 996.5265 999.5649 1006.9061
Frequencies -- 1008.0901 1010.6659 1019.1210
Frequencies -- 1020.5384 1024.5493 1026.5592
Frequencies -- 1028.5363 1030.1800 1031.5762
Frequencies -- 1031.7771 1033.8436 1037.4176
Frequencies -- 1038.7514 1045.6696 1053.2219
Frequencies -- 1054.6028 1058.2816 1065.1837
Frequencies -- 1073.2794 1081.7635 1094.2760
Frequencies -- 1096.4880 1098.4243 1099.3073
Frequencies -- 1099.7872 1100.0186 1102.0769
Frequencies -- 1106.8332 1109.2623 1110.6306
Frequencies -- 1115.2164 1119.2561 1125.5789
Frequencies -- 1132.9865 1134.2179 1136.2021
Frequencies -- 1136.7518 1144.3827 1151.5135
Frequencies -- 1160.9732 1162.8314 1164.3120
Frequencies -- 1175.6091 1178.2895 1181.9841
Frequencies -- 1183.9561 1185.6530 1187.0571
Frequencies -- 1191.5990 1193.0139 1194.0603
Frequencies -- 1198.0086 1198.6594 1201.9607
Frequencies -- 1206.3655 1206.7224 1209.6878
Frequencies -- 1210.5571 1211.5557 1212.1677
Frequencies -- 1213.3833 1214.3769 1220.8275
Frequencies -- 1221.4228 1222.0230 1224.4147
Frequencies -- 1226.6518 1227.3840 1231.3326
Frequencies -- 1233.2313 1236.0083 1245.2506
Frequencies -- 1248.3871 1250.8679 1251.8744
Frequencies -- 1255.6579 1256.7810 1257.2420

Frequencies -- 1260.6542 1263.8460 1266.8422
Frequencies -- 1270.8245 1271.3353 1272.0109
Frequencies -- 1272.7891 1275.7212 1276.3063
Frequencies -- 1280.7028 1284.5414 1289.0171
Frequencies -- 1291.9485 1293.1126 1294.8042
Frequencies -- 1296.8282 1299.0057 1299.4487
Frequencies -- 1300.1770 1302.9112 1306.3008
Frequencies -- 1306.4895 1310.7861 1311.5948
Frequencies -- 1313.6045 1314.2584 1315.4352
Frequencies -- 1316.8645 1317.6612 1319.3054
Frequencies -- 1320.9289 1328.3290 1330.4879
Frequencies -- 1334.1152 1343.7876 1350.1258
Frequencies -- 1356.7576 1357.9295 1359.9243
Frequencies -- 1360.6632 1362.7100 1363.5311
Frequencies -- 1364.3617 1366.1334 1366.6508
Frequencies -- 1367.2389 1368.4683 1369.0335
Frequencies -- 1370.0544 1371.6366 1371.8419
Frequencies -- 1373.2418 1374.1823 1375.3617
Frequencies -- 1375.8767 1377.2372 1378.0023
Frequencies -- 1378.4847 1378.9146 1380.3403
Frequencies -- 1380.8071 1381.6027 1382.2387
Frequencies -- 1383.9241 1384.2587 1385.6996
Frequencies -- 1386.8865 1388.1119 1388.3348
Frequencies -- 1389.2465 1390.3142 1390.4672
Frequencies -- 1391.7943 1392.3543 1392.9758
Frequencies -- 1393.4898 1394.1691 1395.8459
Frequencies -- 1399.9894 1401.3690 1403.2662
Frequencies -- 1407.0025 1407.9709 1421.4945
Frequencies -- 1424.9541 1429.3162 1431.8735
Frequencies -- 1434.6021 1436.7530 1438.3941
Frequencies -- 1438.7635 1439.2690 1439.7556
Frequencies -- 1441.7319 1442.9179 1444.0499
Frequencies -- 1445.8353 1447.0894 1448.5200
Frequencies -- 1449.0632 1451.5168 1455.0573
Frequencies -- 1466.6592 1470.1522 1471.7591
Frequencies -- 1503.9863 1524.8927 1552.9503
Frequencies -- 1563.2139 1682.0402 1685.9169
Frequencies -- 1696.6777 1700.9270 1710.0677
Frequencies -- 1715.5532 1718.1788 1719.4192
Frequencies -- 1721.8229 1727.7039 1728.9808
Frequencies -- 1737.9362 1738.7715 1744.2730
Frequencies -- 2855.0609 2878.9595 2961.1410
Frequencies -- 2965.5536 2967.7304 2969.0994
Frequencies -- 2975.1412 2976.1214 2976.5114
Frequencies -- 2977.5356 2978.4793 2978.8011
Frequencies -- 2980.1454 2980.9604 2981.6485
Frequencies -- 2982.5233 2984.7074 2985.6674
Frequencies -- 2986.6934 2986.9313 2987.5146
Frequencies -- 2988.7285 2989.0089 2989.9281
Frequencies -- 2990.1615 2990.6205 2990.9519
Frequencies -- 2991.9537 2992.8084 2994.2661
Frequencies -- 2997.2608 2998.6867 2999.6647
Frequencies -- 3001.5131 3003.4089 3006.8896
Frequencies -- 3014.3230 3024.0308 3029.6023
Frequencies -- 3030.5417 3034.5599 3049.5792
Frequencies -- 3056.0437 3061.8183 3066.9552
Frequencies -- 3068.2927 3069.3756 3070.0776
Frequencies -- 3070.5085 3071.3203 3071.6450
Frequencies -- 3073.5457 3074.4149 3074.5906
Frequencies -- 3074.8355 3075.3576 3076.3870
Frequencies -- 3077.3778 3083.7950 3089.4713
Frequencies -- 3090.5827 3113.2745 3120.0944
Frequencies -- 3134.8138 3145.2005 3291.7867

E(RB-LYP) = -5460.84134361 (BLYP-D3BJ/def2SVP/SMD (H_2O))
Sum of electronic and zero-point Energies= -5459.520806
Sum of electronic and thermal Energies= -5459.443138
Sum of electronic and thermal Free Energies= -5459.629036

E(RB-LYP) = -5466.21806591 (BLYP-D3BJ/def2TZVPP/SMD (H_2O))

G7

Center Number	Atomic Number	Atomic Type	Coordinates (Angstroms) X	Y	Z
1	6	0	0.088224	1.172668	1.499510
2	1	0	-0.662666	1.156172	2.313747
3	6	0	0.925473	-0.122730	1.538453
4	6	0	-0.604921	1.277581	0.124086
5	6	0	2.003497	-0.087900	0.436373
6	6	0	0.009815	-1.349117	1.344869
7	1	0	-1.206956	2.207517	0.095223
8	6	0	0.453440	1.314469	-1.016163
9	6	0	-1.539120	0.054190	-0.106474
10	1	0	2.622792	-1.006935	0.483526
11	1	0	2.675137	0.780710	0.593781
12	6	0	1.309039	0.016868	-0.939468
13	1	0	-0.740487	-1.385494	2.159119
14	1	0	0.612107	-2.279195	1.399998
15	6	0	-0.683525	-1.243413	-0.029781
16	1	0	1.111589	2.195082	-0.876608
17	1	0	-2.311972	0.029591	0.687051
18	1	0	2.081885	0.041464	-1.732998
19	6	0	0.374837	-1.206527	-1.170031
20	1	0	-1.341673	-2.124026	-0.169336
21	1	0	0.976874	-2.136461	-1.141162
22	1	0	0.746024	2.050710	1.663821
23	7	0	1.593669	-0.231425	2.898687
24	1	0	2.156174	-1.098848	2.969863
25	1	0	2.226058	0.570820	3.073611
26	1	0	0.859646	-0.250254	3.685488
27	6	0	-0.318311	-1.101619	-2.545451
28	1	0	0.432574	-1.085123	-3.359694
29	1	0	-0.976122	-1.979653	-2.709756

30	6	0	-0.239898	1.420169	-2.390814
31	1	0	-0.842187	2.350248	-2.445954
32	1	0	0.510405	1.456534	-3.205065
33	6	0	-2.233583	0.158959	-1.482317
34	1	0	-2.905230	-0.709647	-1.639716
35	1	0	-2.852874	1.077998	-1.529461
36	6	0	-1.155563	0.193783	-2.584390
37	7	0	-1.823765	0.302483	-3.944628
38	1	0	-1.089759	0.321212	-4.731406
39	1	0	-2.456194	-0.499736	-4.119533
40	1	0	-2.386216	1.169938	-4.015819
41	53	0	-0.841955	-0.280282	5.339388
42	53	0	0.611949	0.350897	-6.385342

Frequencies -- 22.7959 23.6691 27.4394
Frequencies -- 57.0277 89.2168 126.2538
Frequencies -- 199.9250 246.3743 269.4867
Frequencies -- 297.2022 325.5447 334.1589
Frequencies -- 364.8508 366.7290 371.9376
Frequencies -- 405.1090 406.9799 408.1263
Frequencies -- 413.5506 425.0833 431.7864
Frequencies -- 469.3905 473.9721 537.6995
Frequencies -- 630.8344 632.2017 642.1846
Frequencies -- 643.6533 690.3221 698.1957
Frequencies -- 723.8992 789.0089 796.0091
Frequencies -- 850.5530 861.5865 892.9439
Frequencies -- 898.4150 901.9274 918.5019
Frequencies -- 922.2845 928.3623 932.8121
Frequencies -- 937.0877 993.8560 1010.8379
Frequencies -- 1018.4871 1021.9963 1023.0587
Frequencies -- 1024.5205 1033.6816 1039.3649
Frequencies -- 1040.3938 1040.5534 1042.1940
Frequencies -- 1083.1127 1083.5083 1099.8731
Frequencies -- 1107.6065 1111.0978 1132.6144
Frequencies -- 1156.3630 1160.1632 1213.9610
Frequencies -- 1214.4559 1240.8519 1253.1937
Frequencies -- 1269.3367 1272.4604 1273.3604
Frequencies -- 1275.5504 1299.5804 1300.8380
Frequencies -- 1306.2157 1308.2566 1309.9553
Frequencies -- 1310.0188 1314.9273 1322.7493
Frequencies -- 1336.5072 1340.9626 1344.7397
Frequencies -- 1362.8078 1366.3566 1373.0209
Frequencies -- 1419.4829 1419.9097 1426.3818
Frequencies -- 1426.7166 1428.3434 1428.6708
Frequencies -- 1449.3606 1451.6318 1520.8567
Frequencies -- 1520.9055 1527.1028 1527.1959
Frequencies -- 2665.7325 2667.3834 2959.6393
Frequencies -- 2959.8111 2963.1086 2963.8116
Frequencies -- 2967.0468 2967.8971 2979.1506
Frequencies -- 2979.5762 2982.6126 2985.6833
Frequencies -- 2988.5466 2995.6362 3008.7874
Frequencies -- 3008.8305 3015.0710 3015.1193
Frequencies -- 3018.1572 3018.3569 3321.7138
Frequencies -- 3321.7881 3383.3140 3383.3335

E(RB-LYP) = -1252.13350250 (BLYP-D3BJ/def2SVP/SMD (H_2O))
Sum of electronic and zero-point Energies= -1251.766068
Sum of electronic and thermal Energies= -1251.749651
Sum of electronic and thermal Free Energies= -1251.813896

E(RB-LYP) = -1252.88162521 (BLYP-D3BJ/def2TZVPP/SMD (H_2O))

HG8

Center Number	Atomic Number	Atomic Type	Coordinates (Angstroms) X	Y	Z
1	8	0	-2.527899	-3.423955	2.713933
2	8	0	0.996422	-4.168801	2.772774
3	8	0	3.781306	-1.671274	2.866109
4	8	0	3.667314	2.093540	2.910586
5	8	0	0.686026	4.319421	2.870045
6	8	0	-2.799043	3.275655	2.802167
7	8	0	-4.042679	-0.133398	2.624249
8	8	0	-2.749341	-3.232102	-3.443673
9	8	0	1.167848	-3.980832	-3.455441
10	8	0	3.841176	-1.533806	-3.239343
11	8	0	3.671569	2.005417	-3.190855
12	8	0	0.805483	4.230723	-3.360501
13	8	0	-2.956106	3.166755	-3.354415
14	8	0	-4.835119	-0.115710	-3.493027
15	7	0	-3.997789	-3.425374	0.888480
16	7	0	-2.252626	-4.840289	0.867134
17	7	0	0.170548	-5.242706	0.860564
18	7	0	2.329232	-4.599012	0.893009
19	7	0	4.240275	-3.046017	1.025554
20	7	0	5.105530	-0.967065	1.062050
21	7	0	5.021090	1.508035	1.086663
22	7	0	4.033993	3.533281	1.099262
23	7	0	1.959200	4.862947	0.976406
24	7	0	-0.243994	5.341673	0.976383
25	7	0	-2.629836	4.728308	0.972264
26	7	0	-4.255392	3.177019	0.967252
27	7	0	-5.281872	0.952733	0.959635
28	7	0	-5.183369	-1.287860	0.933972
29	7	0	-4.155619	-3.428113	-1.580930
30	7	0	-2.216460	-4.588460	-1.600998
31	7	0	0.205146	-5.069482	-1.612053
32	7	0	2.415000	-4.629724	-1.585222
33	7	0	4.235508	-2.983785	-1.441785
34	7	0	5.190572	-0.946676	-1.413486
35	7	0	5.090887	1.515473	-1.389575
36	7	0	3.952835	3.457092	-1.373226
37	7	0	2.021615	4.974549	-1.503395
38	7	0	-0.215218	5.230113	-1.499211
39	7	0	-2.586672	4.560281	-1.501092
40	7	0	-4.386907	3.196748	-1.498417
41	7	0	-5.476147	0.970759	-1.516029
42	7	0	-5.391616	-1.281895	-1.536712
43	6	0	-2.873007	-3.832436	1.605727
44	6	0	-1.133494	-5.602202	1.386484
45	1	0	-1.102659	-5.432735	2.477428
46	1	0	-1.315407	-6.678077	1.184480
47	6	0	1.143371	-4.606306	1.631570
48	6	0	3.601455	-4.256056	1.513819
49	1	0	3.402517	-4.106647	2.590138
50	1	0	4.305523	-5.104468	1.381972
51	6	0	4.300777	-1.865478	1.765087
52	6	0	5.570308	0.281657	1.647357
53	1	0	5.282235	0.262139	2.713698
54	1	0	6.677289	0.318492	1.563991
55	6	0	4.167266	2.341304	1.811269
56	6	0	3.267756	4.664370	1.590293
57	1	0	3.098625	4.495638	2.668647
58	1	0	3.869380	5.586283	1.449498
59	6	0	0.783984	4.776073	1.731565
60	6	0	-1.577245	5.571117	1.508630
61	1	0	-1.850006	6.632046	1.331701

62	1	0	-1.529937	5.377620	2.594870
63	6	0	-3.170835	3.666101	1.696000
64	6	0	-5.233060	2.276173	1.546717
65	1	0	-6.241444	2.734013	1.465178
66	1	0	-4.969008	2.155063	2.612306
67	6	0	-4.737698	-0.153085	1.607574
68	6	0	-5.039610	-2.617768	1.489829
69	1	0	-4.788721	-2.507662	2.559605
70	1	0	-6.011266	-3.146358	1.391677
71	6	0	-3.002959	-3.684091	-2.326288
72	6	0	-1.101251	-5.307673	-2.206700
73	1	0	-1.039346	-4.985284	-3.261348
74	1	0	-1.319503	-6.397121	-2.168293
75	6	0	1.246256	-4.479794	-2.334473
76	6	0	3.710360	-4.191698	-2.062889
77	1	0	3.603077	-3.985954	-3.142827
78	1	0	4.442109	-5.012941	-1.914106
79	6	0	4.344832	-1.782888	-2.144301
80	6	0	5.686497	0.310866	-1.939788
81	1	0	5.479639	0.311937	-3.024470
82	1	0	6.782462	0.353639	-1.771683
83	6	0	4.164351	2.281721	-2.097600
84	6	0	3.340702	4.626231	-1.988438
85	1	0	3.239577	4.414975	-3.067859
86	1	0	4.016667	5.494340	-1.841796
87	6	0	0.861255	4.733597	-2.239440
88	6	0	-1.537559	5.383122	-2.085219
89	1	0	-1.841916	6.449639	-2.013113
90	1	0	-1.453825	5.097420	-3.149161
91	6	0	-3.264852	3.579978	-2.236128
92	6	0	-5.436198	2.332239	-2.030050
93	1	0	-5.279694	2.256066	-3.120637
94	1	0	-6.413746	2.820364	-1.834334
95	6	0	-5.179834	-0.138737	-2.312213
96	6	0	-5.267828	-2.626878	-2.081749
97	1	0	-6.207972	-3.183934	-1.888133
98	1	0	-5.126068	-2.515299	-3.171537
99	6	0	-4.194361	-4.189376	-0.338193
100	1	0	-5.137967	-4.770593	-0.278935
101	6	0	-2.906951	-5.086393	-0.408258
102	1	0	-3.125083	-6.168588	-0.523432
103	6	0	0.685384	-5.742473	-0.404055
104	1	0	0.504295	-6.834836	-0.483067
105	6	0	2.210312	-5.363814	-0.349342
106	1	0	2.883446	-6.246033	-0.312580
107	6	0	5.013180	-2.983677	-0.207140
108	1	0	5.763857	-3.800574	-0.228667
109	6	0	5.646997	-1.544537	-0.168175
110	1	0	6.756007	-1.546647	-0.131137
111	6	0	5.508337	2.136098	-0.140645
112	1	0	6.614203	2.222746	-0.110264
113	6	0	4.765429	3.523086	-0.160948
114	1	0	5.451131	4.393821	-0.210260
115	6	0	1.768347	5.652286	-0.243584
116	1	0	2.369554	6.583463	-0.183873
117	6	0	0.219400	5.910063	-0.279537
118	1	0	-0.049707	6.985923	-0.328938
119	6	0	-3.312253	4.953915	-0.293240
120	1	0	-3.629144	6.014772	-0.369895
121	6	0	-4.509591	3.938201	-0.249232
122	1	0	-5.504786	4.426666	-0.193963
123	6	0	-6.054625	0.598580	-0.224605
124	1	0	-7.085193	1.001475	-0.140456
125	6	0	-5.991096	-0.975692	-0.238028
126	1	0	-6.984909	-1.462404	-0.155423
127	6	0	-0.275601	1.352098	1.306377
128	1	0	-1.120542	1.369712	2.023223
129	6	0	0.628819	0.135595	1.595145
130	6	0	-0.802943	1.298908	-0.139483
131	6	0	1.785167	0.148994	0.563539
132	6	0	-0.187233	-1.157281	1.378850
133	1	0	-1.461208	2.167584	-0.329582
134	6	0	0.360599	1.309790	-1.172288
135	6	0	-1.624387	0.001847	-0.355005
136	1	0	2.447905	-0.708690	0.764746
137	1	0	2.379861	1.065673	0.713782
138	6	0	1.271955	0.088217	-0.881590
139	1	0	-1.032682	-1.191332	2.095264
140	1	0	0.451373	-2.033090	1.603765
141	6	0	-0.715172	-1.221439	-0.068316
142	1	0	0.959585	2.231106	-1.041809
143	1	0	-2.469676	-0.009444	0.359995
144	1	0	2.119974	0.099004	-1.596470
145	6	0	0.448292	-1.207655	-1.100510
146	1	0	-1.310448	-2.144163	-0.208527
147	1	0	1.104072	-2.081284	-0.917541
148	1	0	0.304809	2.278252	1.475014
149	7	0	1.114122	0.198162	2.993249
150	1	0	1.809325	-0.557920	3.104223
151	1	0	1.693623	1.049760	3.069915
152	6	0	-0.082543	-1.256202	-2.546232
153	1	0	0.766720	-1.264949	-3.257868
154	1	0	-0.652235	-2.185524	-2.720390
155	6	0	-0.168551	1.247431	-2.618619
156	1	0	-0.799194	2.127001	-2.841574
157	1	0	0.682012	1.274475	-3.329848
158	6	0	-2.142975	-0.050927	-1.795457
159	1	0	-2.743140	-0.962021	-1.952966
160	1	0	-2.792011	0.816888	-1.998567
161	6	0	-0.988862	-0.041493	-2.827229
162	7	0	-1.493561	-0.103802	-4.220829
163	1	0	-2.087018	-0.947707	-4.270830
164	1	0	-2.171403	0.669299	-4.317519

Frequencies -- 31.9561 34.3509 37.8404
Frequencies -- 39.6768 45.9074 54.9408
Frequencies -- 56.5534 62.7759 66.8468
Frequencies -- 70.4812 75.0947 78.3148
Frequencies -- 79.5631 80.0242 88.1940
Frequencies -- 92.3630 96.8397 100.4775
Frequencies -- 102.0407 108.5727 111.2047
Frequencies -- 113.8452 117.0912 120.5419
Frequencies -- 120.9866 127.8681 131.0948
Frequencies -- 133.5272 133.9470 136.5084
Frequencies -- 141.4225 143.5013 146.9505
Frequencies -- 150.1144 155.2244 156.4278
Frequencies -- 158.4334 161.3014 167.2840
Frequencies -- 176.2159 177.2793 179.3297
Frequencies -- 186.1503 189.6233 192.3707
Frequencies -- 193.2620 197.5978 197.9510
Frequencies -- 204.0586 207.4334 215.0518
Frequencies -- 221.1666 226.9811 228.6359
Frequencies -- 235.2316 237.5354 242.1523
Frequencies -- 257.3909 262.6188 263.4687
Frequencies -- 264.9713 279.4660 280.8753
Frequencies -- 285.7516 286.6151 287.2207
Frequencies -- 305.8502 319.4528 327.7826
Frequencies -- 329.5366 329.8508 336.1020
Frequencies -- 339.0765 345.4189 347.8762
Frequencies -- 348.8702 350.0565 352.7891
Frequencies -- 353.9611 355.0082 356.4241
Frequencies -- 357.2052 358.2466 358.7803
Frequencies -- 362.8231 364.0858 368.1670
Frequencies -- 369.8923 372.9741 373.4679
Frequencies -- 375.5901 389.8307 395.8316
Frequencies -- 407.8911 411.7816 414.6211
Frequencies -- 416.5870 420.5232 425.6144
Frequencies -- 429.9081 431.5258 439.7128
Frequencies -- 441.9488 442.9000 444.1899

Frequencies -- 446.9310 449.4561 451.8301
Frequencies -- 452.1961 485.0981 496.5213
Frequencies -- 506.6407 508.5602 558.7042
Frequencies -- 575.8580 576.4937 599.8289
Frequencies -- 603.9150 609.5685 610.4486
Frequencies -- 612.0560 612.9405 616.6516
Frequencies -- 619.3477 620.3449 623.7352
Frequencies -- 632.7498 636.6693 638.8980
Frequencies -- 639.2929 642.0811 643.0077
Frequencies -- 643.8556 649.5268 655.7750
Frequencies -- 657.8120 658.9858 663.3516
Frequencies -- 664.3005 667.2677 669.5864
Frequencies -- 671.4752 681.8817 682.8731
Frequencies -- 692.4326 695.8360 698.9332
Frequencies -- 701.4160 703.4720 706.5058
Frequencies -- 708.6156 710.0069 712.1187
Frequencies -- 713.4428 714.3730 715.3626
Frequencies -- 716.2189 716.7783 718.3489
Frequencies -- 720.6339 722.0086 723.4569
Frequencies -- 724.7270 730.9410 737.6783
Frequencies -- 765.2827 765.5033 773.8589
Frequencies -- 774.5529 775.5323 777.5527
Frequencies -- 784.8860 786.4495 789.1436
Frequencies -- 793.5455 795.1027 796.8596
Frequencies -- 799.4036 810.2393 812.1108
Frequencies -- 813.2379 813.9053 814.7427
Frequencies -- 815.2840 817.8284 819.2220
Frequencies -- 820.4311 821.5844 856.5221
Frequencies -- 878.8327 879.5421 883.9212
Frequencies -- 885.2541 892.9584 894.1119
Frequencies -- 895.2300 902.7730 904.4635
Frequencies -- 907.9861 910.7053 936.5373
Frequencies -- 938.8591 939.8230 941.4952
Frequencies -- 944.1460 945.1205 946.7580
Frequencies -- 948.0432 951.7136 953.0139
Frequencies -- 954.6151 955.5724 956.9906
Frequencies -- 961.7099 962.5423 965.2094
Frequencies -- 968.5124 971.4446 976.7081
Frequencies -- 977.7974 984.7934 989.0379
Frequencies -- 997.8062 1000.2422 1001.4116
Frequencies -- 1007.8789 1008.0879 1008.7088
Frequencies -- 1020.9502 1022.5830 1026.5398
Frequencies -- 1027.5668 1028.9229 1032.0575
Frequencies -- 1032.8809 1033.3786 1034.5349
Frequencies -- 1037.8596 1042.0288 1044.5992
Frequencies -- 1046.0087 1051.8777 1057.1260
Frequencies -- 1085.8940 1088.8578 1090.4491
Frequencies -- 1100.2872 1100.8180 1101.6999
Frequencies -- 1103.6235 1105.8894 1106.0454
Frequencies -- 1108.8965 1111.9101 1113.9462
Frequencies -- 1116.2542 1120.8998 1130.6563
Frequencies -- 1134.9774 1136.4357 1137.7058
Frequencies -- 1139.2093 1147.7073 1163.0791
Frequencies -- 1164.1907 1165.2061 1167.3301
Frequencies -- 1171.8880 1178.8770 1179.7017
Frequencies -- 1180.7830 1187.5925 1187.6870
Frequencies -- 1194.0512 1194.5381 1196.9908
Frequencies -- 1198.5564 1199.5164 1201.3373
Frequencies -- 1207.4228 1209.2886 1211.2070
Frequencies -- 1212.6160 1213.6513 1214.2578
Frequencies -- 1214.9948 1215.4658 1215.6250
Frequencies -- 1218.2539 1224.3371 1224.5775
Frequencies -- 1225.4636 1226.6150 1227.3883
Frequencies -- 1233.5474 1234.5162 1246.4138
Frequencies -- 1249.2657 1250.6595 1251.7505
Frequencies -- 1254.1643 1255.2025 1257.4815
Frequencies -- 1259.0788 1261.1395 1264.4657
Frequencies -- 1268.9594 1271.2585 1271.4776
Frequencies -- 1272.4647 1272.9937 1274.4386
Frequencies -- 1274.9483 1276.1811 1277.9396
Frequencies -- 1280.4849 1289.0553 1290.2933
Frequencies -- 1294.1287 1296.6800 1298.6153
Frequencies -- 1299.7199 1300.5453 1300.9356
Frequencies -- 1302.2324 1307.0317 1307.7783
Frequencies -- 1310.1546 1311.9115 1313.0395
Frequencies -- 1314.7854 1315.1549 1316.5067
Frequencies -- 1316.9537 1323.0329 1325.4211
Frequencies -- 1329.9805 1343.0581 1350.8192
Frequencies -- 1352.4831 1359.6776 1361.0199
Frequencies -- 1362.1058 1364.8328 1365.2903
Frequencies -- 1367.0213 1367.4040 1367.9600
Frequencies -- 1368.1697 1370.6857 1371.3905
Frequencies -- 1372.5069 1372.5601 1373.3366
Frequencies -- 1374.8517 1375.1225 1376.0601
Frequencies -- 1377.0519 1377.8245 1378.5771
Frequencies -- 1378.8892 1379.3662 1379.7460

Frequencies -- 1380.4624 1380.9339 1381.5894
Frequencies -- 1381.9394 1382.6017 1383.3845
Frequencies -- 1383.8606 1384.6195 1384.9548
Frequencies -- 1386.2249 1387.6160 1388.2161
Frequencies -- 1388.5669 1390.4875 1391.8434
Frequencies -- 1392.6712 1392.7559 1395.6397
Frequencies -- 1396.1412 1399.7429 1402.8260
Frequencies -- 1403.7194 1408.6849 1413.7079
Frequencies -- 1424.7073 1426.3813 1430.3243
Frequencies -- 1432.4128 1435.1863 1435.3765
Frequencies -- 1437.0851 1437.4879 1438.3548
Frequencies -- 1440.3076 1441.6707 1442.8326
Frequencies -- 1443.0903 1445.7212 1446.9128
Frequencies -- 1447.4950 1453.3152 1453.7282
Frequencies -- 1461.7883 1577.1232 1594.9882
Frequencies -- 1703.7266 1706.7924 1710.0524
Frequencies -- 1711.4588 1714.2030 1715.0540
Frequencies -- 1717.6664 1718.6774 1723.8519
Frequencies -- 1725.2512 1725.6868 1735.8289
Frequencies -- 1737.3673 1742.5327 2952.1529
Frequencies -- 2953.8165 2960.7734 2963.5543
Frequencies -- 2967.1993 2967.6146 2968.0515
Frequencies -- 2968.2293 2968.6135 2968.6858
Frequencies -- 2969.8121 2971.2142 2972.9963
Frequencies -- 2973.4866 2973.5973 2974.3453
Frequencies -- 2974.4834 2975.0658 2975.1734
Frequencies -- 2975.4923 2976.0573 2976.5370
Frequencies -- 2976.6345 2977.0932 2977.5529
Frequencies -- 2977.8492 2979.4241 2979.9775
Frequencies -- 2980.5236 2981.0524 2981.6644
Frequencies -- 2983.1655 2983.5533 2987.1221
Frequencies -- 2988.2079 2990.4086 2998.2493
Frequencies -- 3010.9437 3024.6037 3025.0298
Frequencies -- 3037.1033 3038.9759 3044.0408
Frequencies -- 3053.5743 3065.3048 3065.7142
Frequencies -- 3065.8948 3066.8232 3067.0914
Frequencies -- 3067.4198 3068.5099 3068.9241
Frequencies -- 3070.1232 3070.6770 3070.8670
Frequencies -- 3071.1629 3071.9967 3072.2643
Frequencies -- 3079.9109 3086.7045 3325.9305
Frequencies -- 3326.0882 3379.7985 3385.6824

E(RB-LYP) = -4864.21455459 (BLYP-D3BJ/def2SVP/SMD (H_2O))
Sum of electronic and zero-point Energies= -4862.922574
Sum of electronic and thermal Energies= -4862.849268
Sum of electronic and thermal Free Energies= -4863.020473

E(RB-LYP) = -4869.57652218 (BLYP-D3BJ/def2TZVPP/SMD (H_2O))

G8

Center Number	Atomic Number	Atomic Type	Coordinates (Angstroms) X	Y	Z
1	6	0	0.102772	1.158881	1.526323
2	1	0	-0.649026	1.142130	2.344179
3	6	0	0.958891	-0.135146	1.598531
4	6	0	-0.599229	1.282519	0.157564
5	6	0	2.005182	-0.085889	0.459788
6	6	0	0.026360	-1.345681	1.359833
7	1	0	-1.204902	2.212684	0.128131
8	6	0	0.453249	1.326702	-0.987769
9	6	0	-1.533594	0.062416	-0.083720
10	1	0	2.630783	-1.000804	0.502690
11	1	0	2.682324	0.780441	0.620840
12	6	0	1.311408	0.030968	-0.913244
13	1	0	-0.728667	-1.393174	2.173979
14	1	0	0.624167	-2.278388	1.416339
15	6	0	-0.675436	-1.233319	-0.009196
16	1	0	1.114193	2.205995	-0.836990
17	1	0	-2.301554	0.032271	0.717521
18	1	0	2.079368	0.061113	-1.714484
19	6	0	0.377042	-1.189135	-1.154528
20	1	0	-1.336381	-2.112612	-0.159976
21	1	0	0.982716	-2.119301	-1.125095
22	1	0	0.757959	2.038469	1.703184
23	7	0	1.655212	-0.310253	2.891282
24	1	0	2.225277	0.533794	3.059432
25	1	0	0.941297	-0.284875	3.636331
26	6	0	-0.324959	-1.065500	-2.523286
27	1	0	0.426838	-1.048751	-3.341143
28	1	0	-0.980146	-1.945088	-2.700144
29	6	0	-0.248543	1.439062	-2.356800
30	1	0	-0.846347	2.371772	-2.413309
31	1	0	0.506485	1.486550	-3.170946
32	6	0	-2.227367	0.179277	-1.456751
33	1	0	-2.904516	-0.687048	-1.617803
34	1	0	-2.852962	1.094196	-1.499654
35	6	0	-1.181078	0.228528	-2.595497
36	7	0	-1.877401	0.403633	-3.888247
37	1	0	-1.163511	0.378066	-4.633314
38	1	0	-2.447614	-0.440332	-4.056307

Frequencies -- 198.6250 199.4876 266.8925
Frequencies -- 303.8588 313.2964 333.5565
Frequencies -- 358.9519 366.8354 373.0028
Frequencies -- 373.6013 378.9335 403.3049
Frequencies -- 410.4323 427.6339 438.6436
Frequencies -- 469.9308 479.7713 555.0414
Frequencies -- 628.4876 631.8365 638.4285
Frequencies -- 647.2270 695.1417 703.9322
Frequencies -- 720.2614 784.1258 789.9170
Frequencies -- 853.2467 864.5270 880.9742
Frequencies -- 891.1537 895.7300 896.0478
Frequencies -- 906.9715 928.1582 937.7708
Frequencies -- 953.3808 958.9144 965.4190
Frequencies -- 1019.2090 1020.9553 1021.0612
Frequencies -- 1022.7743 1031.8900 1036.1082
Frequencies -- 1037.5604 1037.6904 1061.0569
Frequencies -- 1085.4701 1096.8268 1108.9350

Frequencies -- 1126.3571 1127.8159 1147.9914
Frequencies -- 1149.0166 1171.9213 1200.7610
Frequencies -- 1203.4072 1233.7317 1236.0888
Frequencies -- 1240.0054 1251.3911 1262.6424
Frequencies -- 1263.5224 1284.0349 1295.2322
Frequencies -- 1296.5083 1296.5260 1298.9943
Frequencies -- 1299.2621 1308.9159 1323.8023
Frequencies -- 1333.0229 1337.8064 1355.1893
Frequencies -- 1358.2485 1365.5751 1367.8485
Frequencies -- 1414.8269 1415.9664 1417.4854
Frequencies -- 1418.2598 1435.8812 1437.5945
Frequencies -- 1564.3058 1564.3156 2934.3057
Frequencies -- 2934.5530 2937.6243 2938.7581
Frequencies -- 2942.0695 2942.0823 2947.1373
Frequencies -- 2948.6097 2948.7465 2954.3522
Frequencies -- 2956.0322 2968.7627 2979.3206
Frequencies -- 2979.3453 2988.8461 2989.2153
Frequencies -- 2991.6136 2991.8775 3331.4808
Frequencies -- 3331.4962 3398.1682 3398.2004

E(RB-LYP) = -655.538608564 (BLYP-D3BJ/def2SVP/SMD (H_2O))
Sum of electronic and zero-point Energies= -655.199299
Sum of electronic and thermal Energies= -655.187679
Sum of electronic and thermal Free Energies= -655.234649

E(RB-LYP) = -656.264581122 (BLYP-D3BJ/def2TZVPP/SMD (H_2O))

HG9

Center Number	Atomic Number	Atomic Type	Coordinates (Angstroms) X	Y	Z
1	8	0	-2.520870	-3.481294	2.739863
2	8	0	1.036750	-4.028249	2.700500
3	8	0	4.032215	-1.648712	2.791579
4	8	0	3.810261	1.962956	2.778741
5	8	0	0.719003	4.116269	2.700579
6	8	0	-2.850808	3.356337	2.788566
7	8	0	-4.116613	-0.040335	2.639097
8	8	0	-2.463761	-3.212446	-3.443942
9	8	0	1.322565	-4.075791	-3.431524
10	8	0	3.909232	-1.818703	-3.405035
11	8	0	3.617422	2.056225	-3.378345
12	8	0	0.832081	4.619524	-3.507618
13	8	0	-2.730209	3.354247	-3.380813
14	8	0	-4.530016	-0.065289	-3.590578
15	7	0	-3.876722	-3.381612	0.832580
16	7	0	-2.147818	-4.822271	0.854965
17	7	0	0.272595	-5.312510	0.894046
18	7	0	2.411318	-4.609920	0.891931
19	7	0	4.275563	-3.013581	0.901098
20	7	0	5.316845	-1.017046	0.937576
21	7	0	5.130250	1.444765	0.909311
22	7	0	3.980579	3.379692	0.918224
23	7	0	2.031020	4.877791	0.918330
24	7	0	-0.174978	5.329967	0.909156
25	7	0	-2.568716	4.781100	0.948839
26	7	0	-4.284729	3.333706	0.934252
27	7	0	-5.141499	1.033991	0.829999
28	7	0	-5.029981	-1.215762	0.831415
29	7	0	-3.954727	-3.389317	-1.642499
30	7	0	-2.068246	-4.622571	-1.613459
31	7	0	0.338280	-5.106376	-1.570442
32	7	0	2.568115	-4.785215	-1.577287
33	7	0	4.451230	-3.180539	-1.574795
34	7	0	5.049925	-1.005925	-1.524325
35	7	0	4.970400	1.448433	-1.563941
36	7	0	3.983779	3.474600	-1.546882
37	7	0	2.067871	5.033445	-1.559668
38	7	0	-0.138400	5.497477	-1.563460
39	7	0	-2.499775	4.770020	-1.526611
40	7	0	-4.180587	3.256123	-1.541249
41	7	0	-5.244123	1.028177	-1.643108
42	7	0	-5.133860	-1.223248	-1.644461
43	6	0	-2.804170	-3.841763	1.596841
44	6	0	-1.056734	-5.615418	1.398831
45	1	0	-1.042812	-5.442449	2.489389
46	1	0	-1.265453	-6.686501	1.201016
47	6	0	1.214552	-4.575118	1.610081
48	6	0	3.679109	-4.207656	1.478133
49	1	0	3.497932	-3.997441	2.547256
50	1	0	4.397042	-5.050525	1.387068
51	6	0	4.475954	-1.859458	1.663186
52	6	0	5.785819	0.260342	1.446147
53	1	0	5.615718	0.257316	2.537101
54	1	0	6.873182	0.341641	1.243606
55	6	0	4.244022	2.223272	1.655229
56	6	0	3.321117	4.537733	1.496146
57	1	0	3.157081	4.321406	2.566634
58	1	0	3.991609	5.417301	1.398625
59	6	0	0.840753	4.691992	1.618545
60	6	0	-1.485755	5.578054	1.490042
61	1	0	-1.728748	6.652848	1.358269
62	1	0	-1.420929	5.347200	2.568249
63	6	0	-3.181190	3.759911	1.673128
64	6	0	-5.226724	2.354099	1.435703
65	1	0	-6.257315	2.741296	1.294818
66	1	0	-5.023369	2.235939	2.514785
67	6	0	-4.679947	-0.071004	1.543458
68	6	0	-4.919974	-2.546774	1.403287
69	1	0	-4.692284	-2.429338	2.477513
70	1	0	-5.898047	-3.060553	1.288965
71	6	0	-2.784303	-3.673575	-2.348456
72	6	0	-0.953797	-5.355684	-2.189192
73	1	0	-0.869845	-5.046241	-3.246408
74	1	0	-1.176403	-6.443620	-2.139396
75	6	0	1.399909	-4.580180	-2.312518
76	6	0	3.883988	-4.422240	-2.077917
77	1	0	3.792923	-4.315067	-3.173130
78	1	0	4.586966	-5.246381	-1.844150
79	6	0	4.395464	-1.980983	-2.287500
80	6	0	5.511127	0.230737	-2.139884
81	1	0	5.197628	0.203237	-3.198813
82	1	0	6.620632	0.270620	-2.085388
83	6	0	4.117757	2.293889	-2.278657
84	6	0	3.374102	4.681519	-2.091838
85	1	0	3.243514	4.524064	-3.177265
86	1	0	4.072127	5.528007	-1.923097
87	6	0	0.906432	4.984465	-2.335977
88	6	0	-1.486617	5.660630	-2.083462
89	1	0	-1.815502	6.707073	-1.914560
90	1	0	-1.433991	5.461506	-3.168842
91	6	0	-3.084988	3.738724	-2.266705
92	6	0	-5.188984	2.389746	-2.148532
93	1	0	-4.961401	2.320948	-3.227257
94	1	0	-6.182528	2.867360	-2.013319
95	6	0	-4.905102	-0.082588	-2.420175
96	6	0	-5.025170	-2.567846	-2.189417
97	1	0	-5.986241	-3.101820	-2.036243
98	1	0	-4.833694	-2.457051	-3.271596
99	6	0	-4.055515	-4.144901	-0.401850
100	1	0	-5.016310	-4.698925	-0.369527
101	6	0	-2.790817	-5.077356	-0.429384
102	1	0	-3.036147	-6.155717	-0.523032
103	6	0	0.795289	-5.808551	-0.370373
104	1	0	0.598400	-6.896383	-0.464832
105	6	0	2.321177	-5.447837	-0.304993
106	1	0	2.984549	-6.330724	-0.198795
107	6	0	5.124963	-3.039700	-0.294131
108	1	0	5.904458	-3.822104	-0.187057
109	6	0	5.701378	-1.581730	-0.345235
110	1	0	6.804234	-1.544388	-0.464016
111	6	0	5.500335	2.071078	-0.355221
112	1	0	6.604479	2.159270	-0.423237
113	6	0	4.758141	3.453933	-0.313913
114	1	0	5.443686	4.326011	-0.281968
115	6	0	1.858675	5.697849	-0.277312
116	1	0	2.497673	6.602616	-0.207375
117	6	0	0.317523	6.017674	-0.279159
118	1	0	0.092147	7.101844	-0.205802

119	6	0	-3.245954	5.072803	-0.309050
120	1	0	-3.578883	6.131119	-0.324550
121	6	0	-4.430700	4.039512	-0.331429
122	1	0	-5.431970	4.514313	-0.390491
123	6	0	-5.865160	0.656707	-0.378246
124	1	0	-6.903435	1.046699	-0.333712
125	6	0	-5.787509	-0.914346	-0.378869
126	1	0	-6.780924	-1.407617	-0.334834
127	6	0	-1.025388	1.166458	1.246247
128	1	0	-2.022858	0.951275	1.666309
129	6	0	-0.030152	0.058199	1.646509
130	6	0	-1.102103	1.268882	-0.293749
131	6	0	1.364122	0.412159	1.088515
132	6	0	-0.500923	-1.281845	1.041484
133	1	0	-1.835324	2.054623	-0.549725
134	6	0	0.285593	1.643484	-0.876064
135	6	0	-1.558770	-0.068558	-0.927429
136	1	0	2.096767	-0.373401	1.341579
137	1	0	1.718193	1.357834	1.533600
138	6	0	1.288021	0.541147	-0.448927
139	1	0	-1.510803	-1.527208	1.408181
140	1	0	0.175973	-2.102477	1.339434
141	6	0	-0.549151	-1.166043	-0.499224
142	1	0	0.608540	2.610217	-0.441547
143	1	0	-2.560326	-0.322690	-0.529708
144	1	0	2.289811	0.804426	-0.833169
145	6	0	0.846053	-0.808690	-1.077008
146	1	0	-0.875138	-2.137528	-0.915708
147	1	0	1.566374	-1.592366	-0.780347
148	1	0	-0.696477	2.138867	1.645442
149	7	0	0.037864	-0.051711	3.249242
150	6	0	-1.166968	-0.778136	3.805711
151	1	0	-1.122809	-1.840284	3.526321
152	1	0	-1.125880	-0.685049	4.905967
153	1	0	-2.095698	-0.329723	3.420458
154	6	0	1.268369	-0.811839	3.692640
155	1	0	2.169711	-0.225475	3.471246
156	1	0	1.185381	-0.962848	4.784281
157	1	0	1.305399	-1.787826	3.186099
158	6	0	0.093235	1.318091	3.890602
159	1	0	-0.865239	1.839518	3.746971
160	1	0	0.277963	1.168902	4.969874
161	1	0	0.907681	1.906017	3.443472
162	6	0	0.792008	-0.708226	-2.614839
163	1	0	1.801952	-0.481009	-3.008948
164	1	0	0.492562	-1.686646	-3.041482
165	6	0	0.234168	1.744331	-2.414786
166	1	0	-0.473834	2.532392	-2.724302
167	1	0	1.228116	2.024084	-2.808862
168	6	0	-1.611182	0.044967	-2.465970
169	1	0	-1.971196	-0.904606	-2.902649
170	1	0	-2.323819	0.832611	-2.766598
171	6	0	-0.211307	0.393151	-3.014124
172	1	0	-0.257502	0.477590	-4.120294
173	53	0	0.423907	-0.333063	7.709573

Frequencies -- 7.9839 14.8367 26.5243
Frequencies -- 35.2002 40.1276 43.1234
Frequencies -- 50.4872 53.4776 57.5861
Frequencies -- 60.7523 63.9782 67.6219
Frequencies -- 73.0607 80.2263 81.9836
Frequencies -- 85.0137 91.8489 93.4261
Frequencies -- 96.7911 100.2907 102.5316
Frequencies -- 114.0827 114.7432 119.0550
Frequencies -- 121.2161 124.0009 125.9770
Frequencies -- 128.2172 131.1847 133.7293
Frequencies -- 134.6323 136.0114 139.5089
Frequencies -- 141.2853 145.3070 147.4466
Frequencies -- 153.9314 158.0067 160.6751
Frequencies -- 161.5826 163.1650 166.7898
Frequencies -- 175.1240 179.0665 181.2520
Frequencies -- 183.5568 190.4496 190.6555
Frequencies -- 192.0916 194.6561 198.4222
Frequencies -- 200.4974 203.5150 207.5913
Frequencies -- 211.1176 219.9429 227.7528
Frequencies -- 230.3984 234.4461 237.4825
Frequencies -- 247.4717 258.5917 259.9775
Frequencies -- 261.4998 269.5113 273.8163
Frequencies -- 283.5829 285.2226 288.4848
Frequencies -- 290.1895 291.6811 302.9416
Frequencies -- 308.0529 326.6069 329.4386
Frequencies -- 331.4857 335.0666 336.3495
Frequencies -- 340.7997 348.5979 350.9622
Frequencies -- 353.6452 354.1480 356.1867
Frequencies -- 356.6654 358.3086 359.4411
Frequencies -- 361.3583 363.4034 363.8493
Frequencies -- 364.8539 366.6981 367.8092
Frequencies -- 369.7143 373.6444 376.8922
Frequencies -- 378.9662 386.2875 410.6258
Frequencies -- 411.2651 414.5344 417.2088
Frequencies -- 417.5693 418.8834 425.3327
Frequencies -- 427.2513 431.8255 435.7921
Frequencies -- 440.2133 443.1672 446.3197
Frequencies -- 448.8024 451.1215 452.3304
Frequencies -- 452.9724 457.4209 484.2807
Frequencies -- 489.0269 504.5722 508.7847
Frequencies -- 510.5599 577.0255 580.5643
Frequencies -- 581.0118 601.4460 603.8232
Frequencies -- 607.0783 609.7315 612.8551
Frequencies -- 612.9237 616.4512 617.3667
Frequencies -- 626.5505 628.2125 632.0357
Frequencies -- 632.6353 638.0318 638.9863
Frequencies -- 640.0094 640.6497 642.9059
Frequencies -- 643.7869 644.2691 658.8672
Frequencies -- 662.2488 663.1135 665.2469
Frequencies -- 666.6158 669.8704 671.6594
Frequencies -- 684.1648 685.1144 697.0814
Frequencies -- 698.7482 701.9113 702.8401
Frequencies -- 704.3212 706.6232 707.3091
Frequencies -- 710.9372 711.0683 712.2827
Frequencies -- 713.6799 715.8178 716.9552
Frequencies -- 719.7305 720.5520 722.6967
Frequencies -- 723.2814 727.6888 731.8443
Frequencies -- 732.9700 765.5882 766.4676

Frequencies -- 774.2672 776.6849 777.7954
Frequencies -- 778.1447 786.5753 787.2408
Frequencies -- 790.5919 794.2143 795.6718
Frequencies -- 796.8978 802.1393 804.4769
Frequencies -- 809.2348 812.0924 813.6453
Frequencies -- 815.1367 816.0604 818.3739
Frequencies -- 819.0543 819.6198 820.4303
Frequencies -- 821.0785 822.0760 823.2815
Frequencies -- 860.8558 882.3111 884.0002
Frequencies -- 887.3509 894.9011 896.1161
Frequencies -- 897.1033 898.9508 903.0334
Frequencies -- 909.2849 911.3828 926.8495
Frequencies -- 931.2562 933.0721 935.0112
Frequencies -- 941.4249 944.3249 945.2062
Frequencies -- 948.5140 950.9071 952.8664
Frequencies -- 953.6259 958.5336 959.3790
Frequencies -- 961.1862 964.4451 968.0369
Frequencies -- 969.1640 971.1705 972.4202
Frequencies -- 974.1101 977.1870 978.2287
Frequencies -- 983.7393 987.5348 989.5974
Frequencies -- 998.5777 1001.6858 1008.2428
Frequencies -- 1010.1860 1021.9026 1022.7715
Frequencies -- 1025.9743 1028.4847 1030.5041
Frequencies -- 1032.3047 1033.1910 1034.4585
Frequencies -- 1038.8452 1045.0518 1046.9091
Frequencies -- 1049.3957 1061.2982 1062.6985
Frequencies -- 1070.4334 1071.3603 1075.2965
Frequencies -- 1087.2729 1093.8593 1098.7244
Frequencies -- 1100.5910 1101.9307 1103.5655
Frequencies -- 1105.4284 1106.9736 1107.8110
Frequencies -- 1108.8451 1110.6292 1114.7364
Frequencies -- 1116.6480 1129.8234 1133.2779
Frequencies -- 1135.4392 1136.5363 1138.4109
Frequencies -- 1148.7336 1164.0933 1165.1417
Frequencies -- 1165.5953 1166.5893 1177.4087
Frequencies -- 1179.2703 1180.5542 1180.8033
Frequencies -- 1188.1556 1191.8008 1193.1392
Frequencies -- 1196.2132 1197.0168 1199.0816
Frequencies -- 1200.7029 1201.8537 1209.0481
Frequencies -- 1210.6188 1211.6944 1212.2779
Frequencies -- 1213.5937 1213.9491 1214.0528
Frequencies -- 1214.6211 1214.9822 1216.0799
Frequencies -- 1224.5825 1225.7184 1226.5924
Frequencies -- 1226.9898 1227.4347 1228.7869
Frequencies -- 1229.6707 1233.3200 1235.2412
Frequencies -- 1242.8754 1245.8583 1248.3452
Frequencies -- 1249.4565 1254.2963 1254.9521
Frequencies -- 1260.4133 1262.3805 1265.2276
Frequencies -- 1270.3390 1270.7517 1272.4147
Frequencies -- 1273.5136 1274.7693 1275.2267
Frequencies -- 1275.4901 1276.7103 1277.6426
Frequencies -- 1282.0722 1288.8993 1289.3020
Frequencies -- 1292.6715 1294.1739 1295.6614
Frequencies -- 1297.4738 1297.8373 1299.2013
Frequencies -- 1299.4275 1307.1111 1310.2788
Frequencies -- 1312.3370 1314.4607 1315.5195
Frequencies -- 1315.7809 1316.6911 1319.4969
Frequencies -- 1322.0041 1322.8736 1324.8900
Frequencies -- 1328.1800 1330.3840 1338.4216
Frequencies -- 1342.7929 1352.7190 1354.4312
Frequencies -- 1360.9719 1362.3229 1362.7692
Frequencies -- 1363.4416 1365.8641 1367.1068
Frequencies -- 1368.8421 1369.5800 1370.1546
Frequencies -- 1370.9319 1372.1302 1372.6965
Frequencies -- 1373.6111 1374.2817 1374.8695
Frequencies -- 1375.1404 1375.5310 1376.4025
Frequencies -- 1377.6253 1377.9375 1378.7456
Frequencies -- 1379.7866 1380.1076 1380.9266
Frequencies -- 1381.5336 1382.2177 1383.0448
Frequencies -- 1383.5646 1384.5365 1385.0606
Frequencies -- 1386.1185 1386.8068 1387.4327
Frequencies -- 1389.0843 1389.6487 1390.4600
Frequencies -- 1391.4985 1392.3620 1392.6415
Frequencies -- 1394.9325 1396.0021 1398.7043
Frequencies -- 1399.6627 1400.0622 1402.2125
Frequencies -- 1403.2312 1406.8080 1407.4671
Frequencies -- 1426.3573 1429.4269 1429.7363
Frequencies -- 1430.9053 1431.7209 1432.5287
Frequencies -- 1433.4521 1435.3432 1435.6553
Frequencies -- 1435.9306 1437.7189 1438.6096
Frequencies -- 1440.1317 1442.6882 1443.1617
Frequencies -- 1443.5524 1445.1749 1446.1177
Frequencies -- 1446.8005 1447.6383 1448.9989
Frequencies -- 1452.2847 1454.1549 1460.8533
Frequencies -- 1465.9763 1467.4880 1468.8425
Frequencies -- 1704.9754 1706.1426 1709.3279

Frequencies -- 1712.0769 1713.9452 1715.1034
Frequencies -- 1719.1154 1719.4739 1724.3691
Frequencies -- 1725.1999 1726.7245 1736.2673
Frequencies -- 1737.9972 1743.3717 2949.1117
Frequencies -- 2950.5728 2954.0454 2962.4657
Frequencies -- 2965.0668 2967.5551 2968.2877
Frequencies -- 2969.1069 2971.1442 2971.2035
Frequencies -- 2971.4593 2972.9499 2973.3266
Frequencies -- 2974.1624 2975.1007 2975.3963
Frequencies -- 2975.5870 2976.6010 2977.4618
Frequencies -- 2977.7161 2978.2639 2979.3569
Frequencies -- 2980.2591 2981.2637 2982.1246
Frequencies -- 2983.8655 2984.1662 2984.5195
Frequencies -- 2984.8620 2985.5865 2986.4300
Frequencies -- 2993.1181 2994.4726 2995.5902
Frequencies -- 3001.8361 3002.9713 3005.9816
Frequencies -- 3009.6308 3011.3281 3016.7952
Frequencies -- 3019.5895 3024.2572 3024.6579
Frequencies -- 3028.4430 3033.7747 3057.1386
Frequencies -- 3061.9716 3063.0367 3064.6500
Frequencies -- 3065.5804 3068.8290 3069.1656
Frequencies -- 3069.4488 3069.5753 3069.7499
Frequencies -- 3069.7707 3070.4004 3070.7105
Frequencies -- 3073.1737 3073.9498 3076.8000
Frequencies -- 3077.0064 3079.8699 3083.2643
Frequencies -- 3098.6787 3099.7361 3102.7839
Frequencies -- 3145.6690 3146.5080 3152.5797

E(RB-LYP) = -5224.98199749 (BLYP-D3BJ/def2SVP/SMD (H_2O))
Sum of electronic and zero-point Energies= -5223.607292
Sum of electronic and thermal Energies= -5223.529605
Sum of electronic and thermal Free Energies= -5223.712747

E(RB-LYP) = -5230.41190579 (BLYP-D3BJ/def2TZVPP/SMD (H_2O))

G9

Center Number	Atomic Number	Atomic Type	Coordinates (Angstroms) X	Y	Z
1	6	0	-1.054170	1.155952	1.227838
2	1	0	-2.061264	0.920353	1.621976
3	6	0	-0.034715	0.068224	1.638877
4	6	0	-1.117247	1.251325	-0.315862
5	6	0	1.359816	0.444932	1.086774
6	6	0	-0.469582	-1.286671	1.033485
7	1	0	-1.859959	2.030630	-0.581990
8	6	0	0.271389	1.650602	-0.887520
9	6	0	-1.547747	-0.102923	-0.942920
10	1	0	2.104157	-0.329530	1.344060
11	1	0	1.706906	1.404681	1.515509
12	6	0	1.294206	0.564764	-0.454746
13	1	0	-1.476179	-1.569735	1.390469
14	1	0	0.232576	-2.090739	1.325510
15	6	0	-0.512752	-1.178080	-0.509472
16	1	0	0.573588	2.626921	-0.454579
17	1	0	-2.547018	-0.383068	-0.549404
18	1	0	2.302631	0.844285	-0.821513
19	6	0	0.878848	-0.794857	-1.082481
20	1	0	-0.817180	-2.164089	-0.915335
21	1	0	1.617430	-1.569764	-0.789161
22	1	0	-0.756631	2.142876	1.624888
23	7	0	0.028628	-0.047043	3.244978
24	6	0	-1.225572	-0.685593	3.806839
25	1	0	-1.262350	-1.746923	3.519663
26	1	0	-1.174918	-0.607805	4.908330
27	1	0	-2.113553	-0.153779	3.430577
28	6	0	1.204287	-0.893295	3.692454
29	1	0	2.145218	-0.358341	3.494504
30	1	0	1.100643	-1.057671	4.780511
31	1	0	1.190057	-1.856911	3.159299
32	6	0	0.172677	1.314432	3.895092
33	1	0	-0.761241	1.883205	3.773535
34	1	0	0.364756	1.152159	4.971708
35	1	0	1.015676	1.856195	3.438163
36	6	0	0.818826	-0.685836	-2.622251
37	1	0	1.822673	-0.429901	-3.020432
38	1	0	0.536457	-1.666873	-3.057643
39	6	0	0.213630	1.755715	-2.427226
40	1	0	-0.507341	2.545939	-2.722704
41	1	0	1.206310	2.057089	-2.821436
42	6	0	-1.602914	0.006798	-2.482767
43	1	0	-1.928622	-0.960941	-2.917470
44	1	0	-2.356028	0.766416	-2.778356
45	6	0	-0.209528	0.395564	-3.031501
46	1	0	-0.250946	0.474508	-4.136814
47	53	0	0.302637	-0.378139	7.615712

Frequencies -- 7.9839 14.8367 26.5243
Frequencies -- 35.2002 40.1276 43.1234
Frequencies -- 50.4872 53.4776 57.5861
Frequencies -- 60.7523 63.9782 67.6219
Frequencies -- 73.0607 80.2263 81.9836
Frequencies -- 85.0137 91.8489 93.4261
Frequencies -- 96.7911 100.2907 102.5316
Frequencies -- 114.0827 114.7432 119.0550
Frequencies -- 121.2161 124.0009 125.9770
Frequencies -- 128.2172 131.1847 133.7293
Frequencies -- 134.6323 136.0114 139.5089
Frequencies -- 141.2853 145.3070 147.4466
Frequencies -- 153.9314 158.0067 160.6751
Frequencies -- 161.5826 163.1650 166.7898
Frequencies -- 175.1240 179.0665 181.2520
Frequencies -- 183.5568 190.4496 190.6555
Frequencies -- 192.0916 194.6561 198.4222
Frequencies -- 200.4974 203.5150 207.5913
Frequencies -- 211.1176 219.9429 227.7528
Frequencies -- 230.3984 234.4461 237.4825
Frequencies -- 247.4717 258.5917 259.9775
Frequencies -- 261.4998 269.5113 273.8163
Frequencies -- 283.5829 285.2226 288.4848
Frequencies -- 290.1895 291.6811 302.9416
Frequencies -- 308.0529 326.6069 329.4386
Frequencies -- 331.4857 335.0666 336.3495
Frequencies -- 340.7997 348.5979 350.9622

Frequencies -- 353.6452 354.1480 356.1867
Frequencies -- 356.6654 358.3086 359.4411
Frequencies -- 361.3583 363.4034 363.8493
Frequencies -- 364.8539 366.6981 367.8092
Frequencies -- 369.7143 373.6444 376.8922
Frequencies -- 378.9662 386.2875 410.6258
Frequencies -- 411.2651 414.5344 417.2088
Frequencies -- 417.5693 418.8834 425.3327
Frequencies -- 427.2513 431.8255 435.7921
Frequencies -- 440.2133 443.1672 446.3197
Frequencies -- 448.8024 451.1215 452.3304
Frequencies -- 452.9724 457.4209 484.2807
Frequencies -- 489.0269 504.5722 508.7847
Frequencies -- 510.5599 577.0255 580.5643
Frequencies -- 581.0118 601.4460 603.8232
Frequencies -- 607.0783 609.7315 612.8551
Frequencies -- 612.9237 616.4512 617.3667
Frequencies -- 626.5505 628.2125 632.0357
Frequencies -- 632.6353 638.0318 638.9863
Frequencies -- 640.0094 640.6497 642.9059
Frequencies -- 643.7869 644.2691 658.8672
Frequencies -- 662.2488 663.1135 665.2469
Frequencies -- 666.6158 669.8704 671.6594
Frequencies -- 684.1648 685.1144 697.0814
Frequencies -- 698.7482 701.9113 702.8401
Frequencies -- 704.3212 706.6232 707.3091
Frequencies -- 710.9372 711.0683 712.2827
Frequencies -- 713.6799 715.8178 716.9552
Frequencies -- 719.7305 720.5520 722.6967
Frequencies -- 723.2814 727.6888 731.8443
Frequencies -- 732.9700 765.5882 766.4676
Frequencies -- 774.2672 776.6849 777.7954
Frequencies -- 778.1447 786.5753 787.2408
Frequencies -- 790.5919 794.2143 795.6718
Frequencies -- 796.8978 802.1393 804.4769
Frequencies -- 809.2348 812.0924 813.6453
Frequencies -- 815.1367 816.0604 818.3739
Frequencies -- 819.0543 819.6198 820.4303
Frequencies -- 821.0785 822.0760 823.2815
Frequencies -- 860.8558 882.3111 884.0002
Frequencies -- 887.3509 894.9011 896.1161
Frequencies -- 897.1033 898.9508 903.0334
Frequencies -- 909.2849 911.3828 926.8495
Frequencies -- 931.2562 933.0721 935.0112
Frequencies -- 941.4249 944.3249 945.2062
Frequencies -- 948.5140 950.9071 952.8664
Frequencies -- 953.6259 958.5336 959.3790
Frequencies -- 961.1862 964.4451 968.0369
Frequencies -- 969.1640 971.1705 972.4202
Frequencies -- 974.1101 977.1870 978.2287
Frequencies -- 983.7393 987.5348 989.5974
Frequencies -- 998.5777 1001.6858 1008.2428
Frequencies -- 1010.1860 1021.9026 1022.7715
Frequencies -- 1025.9743 1028.4847 1030.5041
Frequencies -- 1032.3047 1033.1910 1034.4585
Frequencies -- 1038.8452 1045.0518 1046.9091
Frequencies -- 1049.3957 1061.2982 1062.6985
Frequencies -- 1070.4334 1071.3603 1075.2965
Frequencies -- 1087.2729 1093.8593 1098.7244
Frequencies -- 1100.5910 1101.9307 1103.5655
Frequencies -- 1105.4284 1106.9736 1107.8110
Frequencies -- 1108.8451 1110.6292 1114.7364
Frequencies -- 1116.6480 1129.8234 1133.2779
Frequencies -- 1135.4392 1136.5363 1138.4109
Frequencies -- 1148.7336 1164.0933 1165.1417
Frequencies -- 1165.5953 1166.5893 1177.4087
Frequencies -- 1179.2703 1180.5542 1180.8033
Frequencies -- 1188.1556 1191.8008 1193.1392
Frequencies -- 1196.2132 1197.0168 1199.0816
Frequencies -- 1200.7029 1201.8537 1209.0481
Frequencies -- 1210.6188 1211.6944 1212.2779
Frequencies -- 1213.5937 1213.9491 1214.0528
Frequencies -- 1214.6211 1214.9822 1216.0799
Frequencies -- 1224.5825 1225.7184 1226.5924
Frequencies -- 1226.9898 1227.4347 1228.7869
Frequencies -- 1229.6707 1233.3200 1235.2412
Frequencies -- 1242.8754 1245.8583 1248.3452
Frequencies -- 1249.4565 1254.2963 1254.9521
Frequencies -- 1260.4133 1262.3805 1265.2276
Frequencies -- 1270.3390 1270.7517 1272.4147
Frequencies -- 1273.5136 1274.7693 1275.2267
Frequencies -- 1275.4901 1276.7103 1277.6426
Frequencies -- 1282.0722 1288.8993 1289.3020
Frequencies -- 1292.6715 1294.1739 1295.6614
Frequencies -- 1297.4738 1297.8373 1299.2013
Frequencies -- 1299.4275 1307.1111 1310.2788

Frequencies -- 1312.3370 1314.4607 1315.5195
Frequencies -- 1315.7809 1316.6911 1319.4969
Frequencies -- 1322.0041 1322.8736 1324.8900
Frequencies -- 1328.1800 1330.3840 1338.4216
Frequencies -- 1342.7929 1352.7190 1354.4312
Frequencies -- 1360.9719 1362.3229 1362.7692
Frequencies -- 1363.4416 1365.8641 1367.1068
Frequencies -- 1368.8421 1369.5800 1370.1546
Frequencies -- 1370.9319 1372.1302 1372.6965
Frequencies -- 1373.6111 1374.2817 1374.8695
Frequencies -- 1375.1404 1375.5310 1376.4025
Frequencies -- 1377.6253 1377.9375 1378.7456
Frequencies -- 1379.7866 1380.1076 1380.9266
Frequencies -- 1381.5336 1382.2177 1383.0448
Frequencies -- 1383.5646 1384.5365 1385.0606
Frequencies -- 1386.1185 1386.8068 1387.4327
Frequencies -- 1389.0843 1389.6487 1390.4600
Frequencies -- 1391.4985 1392.3620 1392.6415
Frequencies -- 1394.9325 1396.0021 1398.7043
Frequencies -- 1399.6627 1400.0622 1402.2125
Frequencies -- 1403.2312 1406.8080 1407.4671
Frequencies -- 1426.3573 1429.4269 1429.7363
Frequencies -- 1430.9053 1431.7209 1432.5287
Frequencies -- 1433.4521 1435.3432 1435.6553
Frequencies -- 1435.9306 1437.7189 1438.6096
Frequencies -- 1440.1317 1442.6882 1443.1617
Frequencies -- 1443.5524 1445.1749 1446.1177
Frequencies -- 1446.8005 1447.6383 1448.9989
Frequencies -- 1452.2847 1454.1549 1460.8533
Frequencies -- 1465.9763 1467.4880 1468.8425
Frequencies -- 1704.9754 1706.1426 1709.3279
Frequencies -- 1712.0769 1713.9452 1715.1034
Frequencies -- 1719.1154 1719.4739 1724.3691
Frequencies -- 1725.1999 1726.7245 1736.2673
Frequencies -- 1737.9972 1743.3717 2949.1117
Frequencies -- 2950.5728 2954.0454 2962.4657
Frequencies -- 2965.0668 2967.5551 2968.2877
Frequencies -- 2969.1069 2971.1442 2971.2035
Frequencies -- 2971.4593 2972.9499 2973.3266
Frequencies -- 2974.1624 2975.1007 2975.3963
Frequencies -- 2975.5870 2976.6010 2977.4618
Frequencies -- 2977.7161 2978.2639 2979.3569
Frequencies -- 2980.2591 2981.2637 2982.1246
Frequencies -- 2983.8655 2984.1662 2984.5195
Frequencies -- 2984.8620 2985.5865 2986.4300
Frequencies -- 2993.1181 2994.4726 2995.5902
Frequencies -- 3001.8361 3002.9713 3005.9816
Frequencies -- 3009.6308 3011.3281 3016.7952
Frequencies -- 3019.5895 3024.2572 3024.6579
Frequencies -- 3028.4430 3033.7747 3057.1386
Frequencies -- 3061.9716 3063.0367 3064.6500
Frequencies -- 3065.5804 3068.8290 3069.1656
Frequencies -- 3069.4488 3069.5753 3069.7499
Frequencies -- 3069.7707 3070.4004 3070.7105
Frequencies -- 3073.1737 3073.9498 3076.8000
Frequencies -- 3077.0064 3079.8699 3083.2643
Frequencies -- 3098.6787 3099.7361 3102.7839
Frequencies -- 3145.6690 3146.5080 3152.5797

E(RB-LYP) = -5224.98199749 (BLYP-D3BJ/def2SVP/SMD (H_2O))
Sum of electronic and zero-point Energies= -5223.607292
Sum of electronic and thermal Energies= -5223.529605
Sum of electronic and thermal Free Energies= -5223.712747

E(RB-LYP) = -5230.41190579 (BLYP-D3BJ/def2TZVPP/SMD (H_2O))

HG10

Center Number	Atomic Number	Atomic Type	Coordinates (Angstroms) X	Y	Z
1	8	0	-2.476542	-3.484231	2.560629
2	8	0	1.055574	-4.072494	2.445525
3	8	0	3.805069	-1.684892	2.517268
4	8	0	3.828493	2.076700	2.711581
5	8	0	0.759769	4.136927	2.647810
6	8	0	-2.896961	3.365406	2.781587
7	8	0	-4.134854	-0.075558	2.564442
8	8	0	-2.504308	-3.255705	-3.576035
9	8	0	1.004041	-3.896662	-3.610997
10	8	0	3.906759	-1.562308	-3.675428
11	8	0	3.626207	2.154433	-3.458865
12	8	0	0.771014	4.542929	-3.511055
13	8	0	-2.692810	3.335826	-3.376516
14	8	0	-4.304090	-0.015741	-3.583304
15	7	0	-3.911434	-3.413340	0.709617
16	7	0	-2.212968	-4.887986	0.700356
17	7	0	0.219847	-5.254881	0.598453
18	7	0	2.403605	-4.714863	0.640472
19	7	0	4.195631	-3.027072	0.635486
20	7	0	5.093357	-0.960040	0.699436
21	7	0	5.054711	1.499354	0.796922
22	7	0	4.062999	3.517431	0.877381
23	7	0	2.040652	4.926362	0.852239
24	7	0	-0.175238	5.349570	0.877783
25	7	0	-2.562522	4.750723	0.919690
26	7	0	-4.305880	3.330371	0.908046
27	7	0	-5.152403	1.023493	0.764222
28	7	0	-5.039649	-1.229118	0.738798
29	7	0	-3.974541	-3.383245	-1.757659
30	7	0	-2.165797	-4.725224	-1.779321
31	7	0	0.234499	-5.275388	-1.877413
32	7	0	2.368960	-4.568968	-1.828251
33	7	0	4.247263	-2.979105	-1.840619
34	7	0	5.101306	-0.899886	-1.770142
35	7	0	5.023645	1.556426	-1.679361
36	7	0	3.948037	3.537053	-1.595388
37	7	0	2.039816	5.094387	-1.619748
38	7	0	-0.169378	5.511390	-1.593846
39	7	0	-2.524440	4.793524	-1.552357

40	7	0	-4.177272	3.258963	-1.565638
41	7	0	-5.229191	1.039458	-1.705156
42	7	0	-5.122910	-1.205991	-1.734969
43	6	0	-2.815940	-3.872935	1.442509
44	6	0	-1.062128	-5.631228	1.178248
45	1	0	-0.995238	-5.461905	2.267581
46	1	0	-1.232578	-6.710106	0.984609
47	6	0	1.205757	-4.604213	1.343945
48	6	0	3.672679	-4.271698	1.183522
49	1	0	3.528504	-4.117522	2.267535
50	1	0	4.422700	-5.073751	1.023892
51	6	0	4.296073	-1.864533	1.402572
52	6	0	5.613614	0.256764	1.303700
53	1	0	5.383749	0.214197	2.383066
54	1	0	6.714500	0.275897	1.162098
55	6	0	4.249495	2.327162	1.581821
56	6	0	3.354477	4.657922	1.427995
57	1	0	3.211241	4.462161	2.505418
58	1	0	3.979949	5.564876	1.299163
59	6	0	0.861425	4.723446	1.569749
60	6	0	-1.489108	5.558395	1.471430
61	1	0	-1.752865	6.631332	1.365737
62	1	0	-1.412123	5.305154	2.543806
63	6	0	-3.206457	3.755026	1.655655
64	6	0	-5.246000	2.336640	1.389514
65	1	0	-6.277581	2.720765	1.249551
66	1	0	-5.047733	2.203851	2.467852
67	6	0	-4.694923	-0.092145	1.467081
68	6	0	-4.935698	-2.568064	1.298529
69	1	0	-4.693945	-2.458388	2.370477
70	1	0	-5.920715	-3.070084	1.192980
71	6	0	-2.834936	-3.722351	-2.485431
72	6	0	-1.103489	-5.511580	-2.389106
73	1	0	-1.090196	-5.268680	-3.466387
74	1	0	-1.341776	-6.587103	-2.259896
75	6	0	1.174685	-4.495798	-2.547589
76	6	0	3.641882	-4.170865	-2.409031
77	1	0	3.463966	-3.960071	-3.478576
78	1	0	4.355515	-5.015750	-2.311990
79	6	0	4.352233	-1.783476	-2.548953
80	6	0	5.597266	0.364124	-2.285958
81	1	0	5.355900	0.393301	-3.363232
82	1	0	6.698677	0.399589	-2.153076
83	6	0	4.129280	2.382633	-2.357640
84	6	0	3.341469	4.740307	-2.153412
85	1	0	3.209239	4.571764	-3.236964
86	1	0	4.038599	5.589040	-1.994189
87	6	0	0.865085	4.977946	-2.363488
88	6	0	-1.516094	5.684407	-2.108693
89	1	0	-1.839334	6.730054	-1.927549
90	1	0	-1.471857	5.496352	-3.196034
91	6	0	-3.077315	3.740345	-2.278826
92	6	0	-5.178035	2.403532	-2.193424
93	1	0	-4.949926	2.356208	-3.272852
94	1	0	-6.174327	2.872361	-2.052589
95	6	0	-4.808117	-0.055619	-2.460219
96	6	0	-5.026427	-2.540257	-2.303093
97	1	0	-5.998153	-3.058187	-2.163774
98	1	0	-4.827849	-2.421257	-3.382673
99	6	0	-4.110972	-4.157392	-0.531098
100	1	0	-5.091996	-4.674974	-0.512775
101	6	0	-2.882500	-5.136751	-0.571980
102	1	0	-3.167194	-6.205995	-0.648787
103	6	0	0.745243	-5.841073	-0.635458
104	1	0	0.597257	-6.940101	-0.626944
105	6	0	2.255129	-5.405309	-0.634979
106	1	0	2.966285	-6.253928	-0.698169
107	6	0	4.991258	-2.961672	-0.586397
108	1	0	5.753597	-3.768184	-0.585978
109	6	0	5.604078	-1.515914	-0.547312
110	1	0	6.713374	-1.504555	-0.543249
111	6	0	5.499887	2.147420	-0.433305
112	1	0	6.606920	2.220190	-0.446121
113	6	0	4.777288	3.543175	-0.392229
114	1	0	5.475015	4.405287	-0.418468
115	6	0	1.835959	5.753608	-0.334081
116	1	0	2.461187	6.667670	-0.269312
117	6	0	0.291172	6.046790	-0.317375
118	1	0	0.045036	7.126088	-0.246374
119	6	0	-3.256700	5.072307	-0.323696
120	1	0	-3.588214	6.130941	-0.312440
121	6	0	-4.441078	4.040028	-0.356828
122	1	0	-5.441841	4.514035	-0.425291
123	6	0	-5.869090	0.656935	-0.454201
124	1	0	-6.905922	1.049607	-0.417829
125	6	0	-5.791751	-0.912836	-0.472726
126	1	0	-6.783683	-1.408863	-0.444597
127	6	0	-1.070196	1.218748	1.380789
128	1	0	-2.077298	0.964328	1.750563
129	6	0	-0.034798	0.185308	1.872182
130	6	0	-1.072577	1.261497	-0.167413
131	6	0	1.353181	0.633692	1.372719
132	6	0	-0.386143	-1.203008	1.300293
133	1	0	-1.838105	1.989106	-0.494247
134	6	0	0.311233	1.688310	-0.715018
135	6	0	-1.402257	-0.129499	-0.755900
136	1	0	2.133464	-0.072470	1.697211
137	1	0	1.600286	1.625620	1.785219
138	6	0	1.359023	0.692620	-0.169858
139	1	0	-1.399022	-1.502149	1.616191
140	1	0	0.318612	-1.973243	1.659846
141	6	0	-0.351290	-1.139370	-0.235304
142	1	0	0.553544	2.706195	-0.358696
143	1	0	-2.404844	-0.440739	-0.411720
144	1	0	2.365547	1.003407	-0.502268
145	6	0	1.042156	-0.706417	-0.747062
146	1	0	-0.590207	-2.134136	-0.647784
147	1	0	1.808614	-1.411894	-0.378314
148	1	0	-0.815023	2.219859	1.761486
149	7	0	-0.035675	0.105045	3.469598
150	6	0	-1.245716	-0.649062	3.985605
151	1	0	-1.161960	-1.714723	3.725813
152	1	0	-1.255983	-0.537473	5.084754
153	1	0	-2.166058	-0.230527	3.549247
154	6	0	1.199809	-0.611847	3.976930
155	1	0	2.088708	0.009242	3.795655
156	1	0	1.067454	-0.764011	5.063383
157	1	0	1.308523	-1.581333	3.466921
158	6	0	-0.053350	1.485735	4.090932
159	1	0	-1.022950	1.969460	3.894929
160	1	0	0.088862	1.359771	5.179482
161	1	0	0.756407	2.095565	3.665447
162	6	0	1.075134	-0.681424	-2.286822
163	1	0	2.072254	-0.347655	-2.613286
164	1	0	0.917254	-1.700400	-2.681575
165	6	0	0.306818	1.706783	-2.264119
166	1	0	-0.459655	2.420302	-2.603779
167	1	0	1.283971	2.059053	-2.634829
168	6	0	-1.397024	-0.119241	-2.296105
169	1	0	-1.670826	-1.126234	-2.651226
170	1	0	-2.158300	0.586601	-2.666776
171	6	0	-0.001863	0.293506	-2.805049
172	7	0	0.002855	0.290415	-4.403380
173	6	0	-0.786954	1.458238	-4.956579
174	1	0	-0.843984	1.326487	-6.052288
175	1	0	-1.794899	1.468312	-4.517907
176	1	0	-0.268389	2.399708	-4.720163
177	6	0	1.411051	0.389449	-4.953858
178	1	0	1.968071	-0.533371	-4.732723
179	1	0	1.327838	0.520718	-6.047814
180	1	0	1.929183	1.249561	-4.504164
181	6	0	-0.615352	-0.984570	-4.945804
182	1	0	-0.458700	-0.984943	-6.039558
183	1	0	-0.127538	-1.861750	-4.492220
184	1	0	-1.692667	-0.996381	-4.727854
185	53	0	0.180631	-0.144917	7.905362
186	53	0	-0.117404	0.424132	-8.843218

Frequencies -- 6.9673 10.5954 14.1953
Frequencies -- 15.5186 23.5533 28.7756
Frequencies -- 34.6761 37.2729 43.6668
Frequencies -- 44.5553 49.2711 54.3669
Frequencies -- 59.0126 59.7052 64.2596
Frequencies -- 64.7271 68.5727 70.4616
Frequencies -- 73.9771 76.6767 79.4811
Frequencies -- 88.4268 90.0251 95.3544
Frequencies -- 99.6235 103.8921 112.4832
Frequencies -- 114.0688 118.2831 119.7410
Frequencies -- 121.7701 123.6855 125.1645
Frequencies -- 130.2251 130.9901 134.2417
Frequencies -- 135.7972 137.6628 138.5010

Frequencies -- 143.8522 145.3838 146.1397
Frequencies -- 147.1316 153.8788 156.6754
Frequencies -- 162.6678 163.6009 166.1439
Frequencies -- 171.6656 178.2686 180.1006
Frequencies -- 183.8514 187.3962 192.2600
Frequencies -- 194.6773 197.6137 200.2114
Frequencies -- 207.2400 209.4707 221.7991
Frequencies -- 227.8210 228.1058 229.3223
Frequencies -- 233.4481 233.8526 238.5384
Frequencies -- 241.0592 244.2684 256.9275
Frequencies -- 261.4926 264.5077 266.3645
Frequencies -- 280.1050 281.6307 282.7442
Frequencies -- 284.1548 285.5682 289.9954
Frequencies -- 306.0040 307.7293 311.9002
Frequencies -- 325.2193 327.1292 328.8875
Frequencies -- 333.0427 335.8087 337.8792
Frequencies -- 340.2219 346.2205 346.5335
Frequencies -- 350.9797 352.4781 352.8168
Frequencies -- 354.2783 355.5672 357.2986
Frequencies -- 358.2695 359.7587 360.2970
Frequencies -- 360.8336 363.3360 365.8653
Frequencies -- 366.4400 367.5513 370.3529
Frequencies -- 372.6553 373.6054 374.5936
Frequencies -- 387.3411 396.3925 408.1092
Frequencies -- 411.8525 412.9832 414.2155
Frequencies -- 416.7183 420.9356 426.8269
Frequencies -- 427.0316 433.0508 436.0620
Frequencies -- 440.0847 441.1461 447.9284
Frequencies -- 449.7246 453.9248 455.6121
Frequencies -- 456.5744 457.1765 477.6570
Frequencies -- 479.1178 491.2146 495.9175
Frequencies -- 507.6273 509.5519 523.3320
Frequencies -- 561.9361 577.7460 579.2013
Frequencies -- 605.1450 606.1333 610.5223
Frequencies -- 610.9091 613.7927 615.5670
Frequencies -- 619.4130 619.8955 621.2736
Frequencies -- 624.0766 625.4781 638.2336
Frequencies -- 639.6362 640.2000 641.7478
Frequencies -- 642.2874 644.1570 645.1432
Frequencies -- 654.8571 658.1198 661.3280
Frequencies -- 662.5865 663.4049 665.9337
Frequencies -- 667.0191 671.0951 672.6580
Frequencies -- 681.5344 681.7424 694.6782
Frequencies -- 695.9730 698.8615 700.7868
Frequencies -- 706.1658 710.4031 712.1981
Frequencies -- 714.5922 715.1405 715.6586
Frequencies -- 717.4173 718.1893 719.0980
Frequencies -- 720.3357 720.8525 722.8594
Frequencies -- 724.0981 725.4249 729.7725
Frequencies -- 731.2461 766.4196 767.3163
Frequencies -- 774.3924 776.5926 778.2676
Frequencies -- 778.8950 787.5753 788.3271
Frequencies -- 791.0802 791.1825 792.7182
Frequencies -- 794.9858 795.9773 809.5612
Frequencies -- 811.0782 812.5164 813.8955
Frequencies -- 814.2550 816.6128 817.4080
Frequencies -- 817.9955 818.4994 819.2327
Frequencies -- 819.9750 822.2386 825.8614
Frequencies -- 843.1487 867.0785 881.7645
Frequencies -- 882.7750 885.7633 894.6121
Frequencies -- 895.5592 903.4133 908.5390
Frequencies -- 910.3490 917.3016 922.2354
Frequencies -- 927.0265 928.9966 929.4159
Frequencies -- 931.0520 939.6168 941.3264
Frequencies -- 944.2910 947.5267 949.6812
Frequencies -- 951.9166 952.2840 958.5605
Frequencies -- 959.3398 961.4839 962.3436
Frequencies -- 969.2286 970.2456 970.8834
Frequencies -- 971.8990 977.3238 979.0935
Frequencies -- 980.2235 983.2742 984.7153
Frequencies -- 985.9625 990.4726 994.2548
Frequencies -- 1000.7181 1001.9795 1008.8085
Frequencies -- 1008.9539 1021.9012 1024.1566
Frequencies -- 1026.4819 1026.9406 1029.8269
Frequencies -- 1033.2971 1034.5933 1038.9941
Frequencies -- 1041.7970 1047.0966 1052.2857
Frequencies -- 1054.9310 1061.2391 1077.1455
Frequencies -- 1080.7123 1084.5007 1087.2925
Frequencies -- 1092.5203 1096.5245 1098.3345
Frequencies -- 1099.0656 1104.3408 1104.9986
Frequencies -- 1106.3979 1107.4680 1108.9675
Frequencies -- 1109.7088 1111.1550 1111.9688
Frequencies -- 1112.7875 1112.8612 1130.2896
Frequencies -- 1134.8206 1136.1215 1136.8478
Frequencies -- 1147.9093 1156.8057 1166.1986
Frequencies -- 1166.9197 1167.6887 1174.8933

Frequencies -- 1180.2997 1182.1590 1182.6741
Frequencies -- 1183.2209 1188.8839 1192.6963
Frequencies -- 1196.5190 1197.7178 1198.9751
Frequencies -- 1199.2133 1202.5357 1203.5935
Frequencies -- 1210.3685 1211.2258 1211.6452
Frequencies -- 1212.0266 1212.6569 1213.3438
Frequencies -- 1213.5169 1214.3590 1215.1543
Frequencies -- 1215.8258 1217.2172 1218.9685
Frequencies -- 1224.8045 1225.4006 1226.4573
Frequencies -- 1227.5735 1228.8267 1232.2967
Frequencies -- 1233.8058 1235.3774 1240.8035
Frequencies -- 1243.4950 1244.7979 1249.7574
Frequencies -- 1250.3419 1253.1410 1254.9031
Frequencies -- 1255.1011 1260.8472 1262.7069
Frequencies -- 1265.9239 1270.8315 1272.0369
Frequencies -- 1272.8897 1274.2475 1275.0581
Frequencies -- 1275.6769 1279.3872 1279.6413
Frequencies -- 1290.2801 1292.3311 1295.8952
Frequencies -- 1297.1125 1297.4330 1298.4050
Frequencies -- 1298.8645 1300.0371 1301.0040
Frequencies -- 1302.9003 1303.3527 1309.4715
Frequencies -- 1309.9833 1311.3926 1312.1724
Frequencies -- 1314.8106 1315.0971 1319.6436
Frequencies -- 1321.0389 1322.5801 1326.4509
Frequencies -- 1333.6527 1337.8427 1346.9374
Frequencies -- 1348.9076 1350.3722 1361.3992
Frequencies -- 1363.5298 1363.6830 1364.5042
Frequencies -- 1366.6886 1367.3247 1367.9589
Frequencies -- 1369.1164 1371.2685 1372.3024
Frequencies -- 1372.6593 1373.3854 1373.8109
Frequencies -- 1374.0819 1375.0586 1375.3682
Frequencies -- 1376.0090 1376.2073 1377.0520
Frequencies -- 1377.4723 1377.9258 1378.6330
Frequencies -- 1380.0153 1380.3299 1381.5399
Frequencies -- 1381.9328 1383.6808 1383.7440
Frequencies -- 1384.8019 1385.7953 1386.4902
Frequencies -- 1387.1989 1388.1764 1388.7117
Frequencies -- 1389.5405 1391.1316 1392.0065
Frequencies -- 1392.5815 1393.5882 1394.1314
Frequencies -- 1395.7903 1396.5499 1397.2007
Frequencies -- 1397.9235 1398.7759 1401.4408
Frequencies -- 1402.0687 1403.0786 1404.3696
Frequencies -- 1407.2540 1408.3345 1410.2128
Frequencies -- 1423.9720 1426.8606 1427.5809
Frequencies -- 1428.6006 1429.6046 1430.6962
Frequencies -- 1433.2911 1434.8902 1435.1324
Frequencies -- 1435.6050 1437.4066 1438.0743
Frequencies -- 1438.9174 1439.8199 1439.8889
Frequencies -- 1440.7293 1440.8190 1442.1170
Frequencies -- 1443.9615 1444.5218 1445.9651
Frequencies -- 1448.7743 1449.9707 1451.0592
Frequencies -- 1454.4688 1455.1566 1455.4646
Frequencies -- 1456.7324 1459.6402 1460.3374
Frequencies -- 1461.7791 1462.8228 1463.6992
Frequencies -- 1464.2446 1701.9208 1705.7489
Frequencies -- 1708.5688 1710.6971 1711.8998
Frequencies -- 1714.3857 1717.0378 1717.6680
Frequencies -- 1720.9256 1722.8780 1723.7786
Frequencies -- 1734.5789 1735.0959 1742.1393
Frequencies -- 2968.2204 2968.7597 2971.5116
Frequencies -- 2971.6208 2973.1559 2973.4726
Frequencies -- 2973.5458 2976.2970 2976.7112
Frequencies -- 2976.9476 2977.3188 2978.3366
Frequencies -- 2979.4021 2979.6523 2980.5193
Frequencies -- 2981.0925 2981.7585 2983.5372
Frequencies -- 2984.2687 2984.6540 2985.0814
Frequencies -- 2985.9942 2986.3538 2986.9478
Frequencies -- 2987.8686 2989.3913 2990.4218
Frequencies -- 2990.6318 2991.3419 2991.7580
Frequencies -- 2992.9316 2994.3926 3000.4867
Frequencies -- 3002.2988 3008.8574 3012.9343
Frequencies -- 3013.5575 3017.2169 3020.1313
Frequencies -- 3023.2352 3025.3401 3027.4988
Frequencies -- 3030.1773 3034.0869 3035.1124
Frequencies -- 3039.9386 3069.3018 3069.6481
Frequencies -- 3070.5082 3070.7086 3070.7976
Frequencies -- 3070.8727 3071.0086 3071.6915
Frequencies -- 3071.7184 3073.0057 3073.2975
Frequencies -- 3074.5681 3074.7031 3075.6051
Frequencies -- 3076.2923 3082.1406 3087.5163
Frequencies -- 3090.6846 3091.7729 3092.6392
Frequencies -- 3097.3014 3098.7212 3098.8167
Frequencies -- 3099.9871 3100.6182 3103.7192
Frequencies -- 3137.1872 3138.7725 3142.6777
Frequencies -- 3143.9843 3144.3676 3145.1584

E(RB-LYP) = -5696.35577401 (BLYP-D3BJ/def2SVP/SMD (H_2O))

Sum of electronic and zero-point Energies= -5694.866849
Sum of electronic and thermal Energies= -5694.780932
Sum of electronic and thermal Free Energies= -5694.985730

E(RB-LYP) = -5701.98982168 (BLYP-D3BJ/def2TZVPP/SMD (H_2O))

G10

Center Number	Atomic Number	Atomic Type	Coordinates (Angstroms) X	Y	Z
1	6	0	-1.087971	1.187370	1.366272
2	1	0	-2.100812	0.921095	1.723491
3	6	0	-0.037253	0.174935	1.881357
4	6	0	-1.080276	1.205565	-0.180944
5	6	0	1.361735	0.596897	1.373325
6	6	0	-0.373969	-1.228795	1.324976
7	1	0	-1.845058	1.930891	-0.522812
8	6	0	0.311569	1.637963	-0.707693
9	6	0	-1.403832	-0.195743	-0.758178
10	1	0	2.131506	-0.123328	1.701951
11	1	0	1.638099	1.593535	1.766566
12	6	0	1.365862	0.637421	-0.172627
13	1	0	-1.380574	-1.549399	1.647559
14	1	0	0.353165	-1.980875	1.685573
15	6	0	-0.348967	-1.196981	-0.221184
16	1	0	0.545660	2.654958	-0.335133
17	1	0	-2.412607	-0.509360	-0.423418
18	1	0	2.374723	0.949698	-0.508372
19	6	0	1.041615	-0.765421	-0.748624
20	1	0	-0.584476	-2.213992	-0.592693
21	1	0	1.807286	-1.489716	-0.406498
22	1	0	-0.860091	2.206644	1.725853
23	7	0	-0.045938	0.141580	3.486383
24	6	0	-1.285454	-0.547719	4.022419
25	1	0	-1.298217	-0.403810	5.118186
26	1	0	-2.185121	-0.099154	3.572515
27	6	0	1.156606	-0.603069	4.033528
28	1	0	2.068985	-0.013017	3.861108
29	1	0	1.002936	-0.726247	5.121511
30	1	0	1.237469	-1.588423	3.548649
31	6	0	-0.015662	1.539716	4.073920
32	1	0	-0.978891	2.041151	3.895142
33	1	0	0.145723	1.439867	5.163009
34	1	0	0.808492	2.113591	3.621679
35	6	0	1.066385	-0.729673	-2.295257
36	1	0	2.078128	-0.427326	-2.618828
37	1	0	0.875798	-1.747176	-2.685839
38	6	0	0.311642	1.676488	-2.253255
39	1	0	-0.451892	2.404194	-2.580898
40	1	0	1.296303	2.035660	-2.608027
41	6	0	-1.391133	-0.180276	-2.305456
42	1	0	-1.628482	-1.197578	-2.664542
43	1	0	-2.182096	0.502147	-2.669638
44	6	0	0.001130	0.267127	-2.811360
45	7	0	0.014975	0.304606	-4.416371
46	6	0	-0.813408	1.456286	-4.952788
47	1	0	-0.877180	1.335044	-6.049994
48	1	0	-1.821723	1.424870	-4.511055
49	1	0	-0.319101	2.411554	-4.720836
50	6	0	1.421896	0.469186	-4.958273
51	1	0	2.001883	-0.447470	-4.774379
52	1	0	1.342029	0.638157	-6.047753
53	1	0	1.907188	1.333888	-4.479257
54	6	0	-0.549837	-0.971841	-5.008676
55	1	0	-0.373758	-0.939124	-6.099434
56	1	0	-0.038115	-1.842814	-4.570246
57	1	0	-1.632152	-1.022398	-4.818148
58	53	0	0.066572	-0.024119	7.860097
59	53	0	-0.051264	0.518099	-8.790654
60	1	0	-1.237968	-1.624292	3.800443

Frequencies -- 15.6347 19.4432 34.0240
Frequencies -- 41.5710 43.2149 59.1445
Frequencies -- 60.2890 83.0734 114.9435
Frequencies -- 119.9079 213.5096 218.0128
Frequencies -- 234.6284 261.1561 281.3331
Frequencies -- 291.0648 300.2906 302.2193
Frequencies -- 316.1281 321.8536 324.6530
Frequencies -- 347.1241 350.8411 359.4925
Frequencies -- 364.9684 366.7921 373.8067
Frequencies -- 377.5083 402.6486 406.5194
Frequencies -- 413.7442 415.8961 449.9245
Frequencies -- 452.5822 468.4363 470.4501
Frequencies -- 477.7079 482.9833 522.1945
Frequencies -- 557.9650 609.4578 631.5943
Frequencies -- 633.3948 649.2971 650.8131
Frequencies -- 707.0524 708.0327 786.4817
Frequencies -- 788.1511 799.3605 801.2813
Frequencies -- 803.6187 825.0468 861.5012
Frequencies -- 893.3485 908.5452 913.0009
Frequencies -- 920.6850 922.3174 922.7160
Frequencies -- 923.8776 958.6446 960.7894
Frequencies -- 963.1357 964.7517 972.8640
Frequencies -- 981.2220 1031.9967 1033.1773
Frequencies -- 1041.6526 1043.8783 1045.5634
Frequencies -- 1046.9250 1056.9932 1066.1010
Frequencies -- 1069.5931 1071.0389 1072.9554
Frequencies -- 1097.5381 1101.5279 1106.7056
Frequencies -- 1120.0347 1125.1336 1155.5254
Frequencies -- 1155.8996 1160.0571 1204.4581
Frequencies -- 1205.0345 1211.6363 1213.1359
Frequencies -- 1219.1080 1220.2359 1228.9975
Frequencies -- 1229.8378 1237.9207 1263.2188
Frequencies -- 1266.0261 1271.4760 1273.3333
Frequencies -- 1275.3049 1285.8813 1287.7380
Frequencies -- 1307.4823 1311.2873 1312.5963
Frequencies -- 1313.7079 1317.2392 1317.9646
Frequencies -- 1336.5616 1340.2900 1343.2159
Frequencies -- 1370.0059 1372.3517 1378.6590
Frequencies -- 1392.3233 1396.2194 1396.5959
Frequencies -- 1400.9851 1419.9430 1420.1574
Frequencies -- 1421.7863 1421.9492 1422.6202
Frequencies -- 1425.0890 1425.6940 1426.0082
Frequencies -- 1427.8490 1428.9884 1434.4287
Frequencies -- 1440.2056 1448.5297 1449.4405
Frequencies -- 1451.9594 1453.8290 1455.2151
Frequencies -- 1456.8745 1457.9471 1461.5779
Frequencies -- 2977.0957 2978.5139 2979.4370
Frequencies -- 2982.3838 2982.8418 2983.9042

Frequencies -- 2985.4733 2986.7146
2991.5496
Frequencies -- 2992.4236 2993.8223
2995.1737
Frequencies -- 2996.4227 2997.2834
2998.2452
Frequencies -- 3000.0926 3003.7671
3006.3249
Frequencies -- 3043.9062 3048.0970
3050.0308
Frequencies -- 3051.0409 3052.3624
3052.7763
Frequencies -- 3091.1687 3091.8502
3095.3618
Frequencies -- 3097.5742 3100.7846
3101.6087
Frequencies -- 3136.5465 3136.9584
3137.9629
Frequencies -- 3139.3523 3139.8820
3141.6543

E(RB-LYP) = -1487.63049351 (BLYP-D3BJ/def2SVP/SMD (H_2O))
Sum of electronic and zero-point Energies= -1487.096099
Sum of electronic and thermal Energies= -1487.071531
Sum of electronic and thermal Free Energies= -1487.153081

E(RB-LYP) = -1488.64828240 (BLYP-D3BJ/def2TZVPP/SMD (H_2O))

HG11

Center Number	Atomic Number	Atomic Type	Coordinates (Angstroms) X	Y	Z
1	8	0	-1.224898	-3.391763	3.436529
2	8	0	2.159907	-3.995654	2.478348
3	8	0	4.819489	-1.439996	1.736150
4	8	0	4.704656	2.128102	1.837157
5	8	0	1.700563	4.008860	2.602765
6	8	0	-1.737384	3.195767	3.680149
7	8	0	-3.023730	-0.115117	3.986678
8	8	0	-2.899245	-3.196319	-2.400974
9	8	0	0.558447	-3.790558	-3.376768
10	8	0	3.153822	-1.436975	-4.141798
11	8	0	2.923875	2.229679	-3.999840
12	8	0	0.084133	4.401023	-3.230646
13	8	0	-3.195351	3.228532	-2.218935
14	8	0	-4.627462	-0.130670	-1.913638
15	7	0	-3.120861	-3.428659	2.059182
16	7	0	-1.430232	-4.842830	1.604389
17	7	0	0.913525	-5.219482	0.912310
18	7	0	2.987201	-4.545509	0.357064
19	7	0	4.676385	-2.822603	-0.152000
20	7	0	5.670187	-0.811757	-0.356698
21	7	0	5.498386	1.651332	-0.315630
22	7	0	4.413439	3.591901	0.030775
23	7	0	2.469417	4.984781	0.615565
24	7	0	0.304005	5.239197	1.176096
25	7	0	-1.984586	4.681790	1.887268
26	7	0	-3.617346	3.186978	2.278490
27	7	0	-4.558977	0.926801	2.551995
28	7	0	-4.297429	-1.303408	2.420179
29	7	0	-3.879397	-3.462963	-0.287919
30	7	0	-2.042358	-4.661082	-0.782795
31	7	0	0.266702	-5.126905	-1.474192
32	7	0	2.346040	-4.483859	-2.029377
33	7	0	4.123799	-2.868285	-2.558489
34	7	0	4.863109	-0.748862	-2.692177
35	7	0	4.792385	1.707581	-2.684024
36	7	0	3.766309	3.679203	-2.361453
37	7	0	1.797253	5.033505	-1.759619
38	7	0	-0.333238	5.488578	-1.196000
39	7	0	-2.580964	4.715372	-0.512263
40	7	0	-4.232613	3.238856	-0.117346
41	7	0	-5.053237	0.930585	0.132037
42	7	0	-5.056683	-1.319323	0.061626
43	6	0	-1.843318	-3.825565	2.464942
44	6	0	-0.191674	-5.579765	1.787759
45	1	0	0.143042	-5.395482	2.823968
46	1	0	-0.405919	-6.660275	1.655702
47	6	0	2.026339	-4.509202	1.368123
48	6	0	4.337697	-4.052112	0.551726
49	1	0	4.452775	-3.849296	1.631227
50	1	0	5.053928	-4.843558	0.245016
51	6	0	5.017652	-1.656514	0.540977
52	6	0	6.254077	0.458884	0.035052
53	1	0	6.343477	0.447758	1.135719
54	1	0	7.264923	0.533774	-0.416127
55	6	0	4.837348	2.413868	0.647884
56	6	0	3.883350	4.707063	0.793805
57	1	0	4.036313	4.468255	1.861291
58	1	0	4.454436	5.623162	0.535352
59	6	0	1.509286	4.651951	1.570239
60	6	0	-0.781726	5.452859	2.122541
61	1	0	-1.040476	6.532800	2.119632
62	1	0	-0.408913	5.166969	3.122145
63	6	0	-2.364586	3.624187	2.711861
64	6	0	-4.430775	2.276625	3.067989
65	1	0	-5.446612	2.709515	3.176402
66	1	0	-3.957291	2.198328	4.062702
67	6	0	-3.850662	-0.154706	3.075570
68	6	0	-3.984278	-2.632700	2.913956
69	1	0	-3.459130	-2.504252	3.877127
70	1	0	-4.933227	-3.186563	3.079101
71	6	0	-2.925545	-3.698230	-1.278104
72	6	0	-1.144829	-5.394816	-1.658932
73	1	0	-1.395844	-5.112053	-2.696764
74	1	0	-1.321449	-6.482435	-1.520092
75	6	0	1.003212	-4.380509	-2.392557
76	6	0	3.416999	-4.078675	-2.924379
77	1	0	2.966151	-3.901786	-3.917072
78	1	0	4.149738	-4.909071	-2.995181
79	6	0	3.940476	-1.655837	-3.221602
80	6	0	5.179209	0.493953	-3.376039
81	1	0	4.635234	0.482638	-4.337192
82	1	0	6.272292	0.527895	-3.569082
83	6	0	3.720908	2.496309	-3.100170
84	6	0	2.914138	4.814685	-2.663597
85	1	0	2.485761	4.640770	-3.666696
86	1	0	3.542583	5.729897	-2.684243
87	6	0	0.469555	4.896512	-2.172074
88	6	0	-1.774204	5.612537	-1.326777
89	1	0	-2.062262	6.656935	-1.085206
90	1	0	-2.017263	5.400234	-2.383135
91	6	0	-3.306400	3.661043	-1.072082
92	6	0	-5.262593	2.263017	-0.412290
93	1	0	-5.303968	2.158687	-1.511194
94	1	0	-6.233835	2.653746	-0.041502
95	6	0	-4.861472	-0.170796	-0.706671
96	6	0	-5.062110	-2.652242	-0.516013
97	1	0	-5.942657	-3.200632	-0.122621
98	1	0	-5.163731	-2.527296	-1.608726
99	6	0	-3.622489	-4.210338	0.933369
100	1	0	-4.527917	-4.777509	1.233466
101	6	0	-2.400621	-5.122634	0.555127
102	1	0	-2.639709	-6.205971	0.535535
103	6	0	1.091130	-5.739911	-0.439252
104	1	0	0.954604	-6.840994	-0.444684
105	6	0	2.546540	-5.279066	-0.823914
106	1	0	3.240276	-6.119557	-1.032198
107	6	0	5.153754	-2.806904	-1.534812
108	1	0	5.898579	-3.614671	-1.690650
109	6	0	5.744914	-1.361676	-1.700649
110	1	0	6.793726	-1.346614	-2.062855
111	6	0	5.568547	2.317010	-1.612671
112	1	0	6.627607	2.430747	-1.923844
113	6	0	4.831363	3.685546	-1.365873
114	1	0	5.479986	4.574083	-1.510036
115	6	0	1.922143	5.750166	-0.494089
116	1	0	2.505666	6.682727	-0.638925
117	6	0	0.430538	5.996777	-0.066467
118	1	0	0.189405	7.065017	0.113320
119	6	0	-2.973789	4.997711	0.864660
120	1	0	-3.297100	6.054927	0.957780
121	6	0	-4.121788	3.957646	1.144672
122	1	0	-5.093665	4.425076	1.405381
123	6	0	-5.462965	0.543636	1.480040
124	1	0	-6.486084	0.919935	1.687763
125	6	0	-5.359609	-1.024993	1.454946
126	1	0	-6.294834	-1.539533	1.758549
127	6	0	-0.543658	0.873322	1.364875
128	1	0	-1.345317	0.410946	1.975292
129	6	0	0.708641	-0.036681	1.362899
130	6	0	-1.023022	1.096194	-0.091676
131	6	0	1.837861	0.640371	0.548665
132	6	0	0.352809	-1.395734	0.714516
133	1	0	-1.916418	1.746034	-0.094157
134	6	0	0.110827	1.769968	-0.900329
135	6	0	-1.376871	-0.264852	-0.739916
136	1	0	2.745935	0.006216	0.576416

137	1	0	2.107847	1.607082	1.017944
138	6	0	1.362228	0.859452	-0.909301
139	1	0	-0.431307	-1.893672	1.316289
140	1	0	1.241673	-2.055489	0.729015
141	6	0	-0.128830	-1.179723	-0.741830
142	1	0	0.365375	2.741145	-0.435451
143	1	0	-0.225215	1.987269	-1.934050
144	1	0	-2.197558	-0.749421	-0.179832
145	1	0	-1.750316	-0.112856	-1.772847
146	1	0	2.161713	1.340505	-1.500074
147	6	0	1.005372	-0.504210	-1.549960
148	1	0	-0.385104	-2.150471	-1.208936
149	1	0	0.702929	-0.366090	-2.608305
150	1	0	1.894950	-1.160924	-1.560279
151	1	0	-0.301620	1.843134	1.843441
152	1	0	1.051454	-0.205861	2.405241

Frequencies -- 35.5465 36.5849 37.8462
Frequencies -- 45.3634 48.9708 54.9752
Frequencies -- 64.0389 68.4300 75.3659
Frequencies -- 83.5858 86.0357 86.4370
Frequencies -- 90.9687 92.2717 94.6592
Frequencies -- 95.7959 97.9063 104.7299
Frequencies -- 106.9298 111.4325 114.1958
Frequencies -- 115.6604 119.6804 122.0279
Frequencies -- 122.2971 125.2730 127.1799
Frequencies -- 130.0784 131.0300 132.4171
Frequencies -- 135.7509 145.7250 147.2810
Frequencies -- 153.5148 156.3850 157.7068
Frequencies -- 163.0724 168.9070 171.9519
Frequencies -- 178.0789 180.0353 181.9683
Frequencies -- 191.6402 192.6608 195.0562
Frequencies -- 195.5622 196.3340 200.8243
Frequencies -- 208.1386 216.1921 227.9023
Frequencies -- 228.1489 240.5224 241.5771
Frequencies -- 250.1283 261.2157 261.9080
Frequencies -- 269.3460 270.0927 282.2898
Frequencies -- 283.1560 287.8676 289.4059
Frequencies -- 324.5881 328.4742 330.1794
Frequencies -- 333.6832 342.6518 345.5335
Frequencies -- 347.8483 349.7066 350.0300
Frequencies -- 351.6541 354.4803 355.2260
Frequencies -- 355.7129 359.3693 361.8323
Frequencies -- 361.8723 362.5412 364.9361
Frequencies -- 365.6714 366.2957 369.9443
Frequencies -- 373.3754 410.7123 411.6265
Frequencies -- 412.3371 413.4140 415.8899
Frequencies -- 429.9280 437.2332 438.4751
Frequencies -- 441.7815 442.9588 450.3667
Frequencies -- 451.1193 453.2433 454.1684
Frequencies -- 458.5114 467.2212 474.9535
Frequencies -- 507.8671 509.2771 578.3825
Frequencies -- 579.5516 604.6884 605.8294
Frequencies -- 609.7555 610.9821 614.8382
Frequencies -- 615.1353 619.0537 622.6973
Frequencies -- 624.9957 627.4328 638.5112
Frequencies -- 639.1115 641.5239 642.6747
Frequencies -- 644.8534 645.9324 647.0772
Frequencies -- 649.3544 661.8080 662.7985
Frequencies -- 663.4212 666.1827 666.7640
Frequencies -- 671.2603 673.1555 681.7817
Frequencies -- 683.1631 694.5234 695.1614
Frequencies -- 699.3968 700.5666 706.1341
Frequencies -- 708.1524 709.4576 712.7310
Frequencies -- 714.0029 715.5511 717.0029
Frequencies -- 718.0265 719.3968 721.7286
Frequencies -- 725.4205 726.0234 732.0621
Frequencies -- 733.4825 750.5426 768.2863
Frequencies -- 769.0733 776.1907 777.7066
Frequencies -- 779.6023 780.9150 789.2616
Frequencies -- 790.5131 790.8686 793.2320
Frequencies -- 793.4727 795.4883 796.8135
Frequencies -- 805.8658 812.6482 812.8570
Frequencies -- 813.7706 814.3940 815.2007
Frequencies -- 815.7762 816.5668 817.4956
Frequencies -- 818.2563 819.3131 870.6590
Frequencies -- 880.4448 881.1370 883.1022
Frequencies -- 884.2533 885.7765 894.5210
Frequencies -- 895.3576 901.5408 904.4506
Frequencies -- 909.7866 910.9445 939.1366
Frequencies -- 942.4906 943.2180 945.2000
Frequencies -- 946.1074 951.2984 951.7990
Frequencies -- 955.1946 955.8992 956.9829
Frequencies -- 959.1631 959.8715 961.4164
Frequencies -- 961.9001 969.5931 970.9193
Frequencies -- 979.2885 979.6120 983.2803
Frequencies -- 994.4555 1001.5281 1004.4770
Frequencies -- 1010.7403 1011.2688 1019.7014
Frequencies -- 1025.0245 1026.8390 1027.6663
Frequencies -- 1030.2203 1031.0984 1033.1149
Frequencies -- 1033.5467 1034.2236 1035.0554
Frequencies -- 1035.9071 1091.0070 1094.4409
Frequencies -- 1096.7836 1098.3502 1102.5401
Frequencies -- 1104.1921 1105.2608 1106.1974
Frequencies -- 1107.7338 1108.5183 1109.9884

Frequencies -- 1111.6739 1112.4406 1113.3412
Frequencies -- 1115.5911 1116.5733 1122.0409
Frequencies -- 1137.5006 1138.0055 1141.4953
Frequencies -- 1151.8780 1165.5182 1166.1978
Frequencies -- 1167.8142 1181.2889 1182.3879
Frequencies -- 1183.1345 1188.3775 1196.7911
Frequencies -- 1197.8206 1198.0280 1198.8463
Frequencies -- 1200.3501 1201.4534 1209.5512
Frequencies -- 1210.6502 1211.2041 1212.0242
Frequencies -- 1213.1528 1213.6652 1215.3478
Frequencies -- 1215.7506 1216.0602 1217.4386
Frequencies -- 1226.0812 1227.1614 1227.6801
Frequencies -- 1227.9877 1228.5660 1237.7970
Frequencies -- 1238.6056 1252.6610 1252.9466
Frequencies -- 1258.0461 1258.6668 1264.7887
Frequencies -- 1265.0136 1268.3217 1269.4888
Frequencies -- 1271.5146 1272.3890 1272.7719
Frequencies -- 1273.7406 1274.7810 1275.6118
Frequencies -- 1277.6919 1282.4867 1285.4670
Frequencies -- 1291.0769 1296.7556 1297.8032
Frequencies -- 1298.2499 1301.0741 1302.5246
Frequencies -- 1302.9602 1303.1612 1303.6142
Frequencies -- 1306.1178 1308.7302 1311.5000
Frequencies -- 1314.3646 1315.0962 1316.1920
Frequencies -- 1317.2595 1317.6880 1318.6864
Frequencies -- 1319.5089 1328.9767 1350.4544
Frequencies -- 1351.2507 1360.7637 1362.5208
Frequencies -- 1363.2545 1364.6260 1366.3392
Frequencies -- 1367.1134 1368.0182 1368.4941
Frequencies -- 1370.2330 1370.8485 1371.1642
Frequencies -- 1372.5024 1373.4700 1373.5803
Frequencies -- 1374.6106 1375.6595 1376.0418
Frequencies -- 1377.0633 1377.8453 1377.8972
Frequencies -- 1378.6739 1379.3998 1380.8683
Frequencies -- 1381.5492 1382.0071 1382.9828
Frequencies -- 1383.4827 1384.7872 1385.4940
Frequencies -- 1385.6865 1386.9808 1388.6512
Frequencies -- 1389.6898 1390.1211 1390.3656
Frequencies -- 1392.5618 1394.5636 1394.9773
Frequencies -- 1396.0978 1398.2854 1401.9459
Frequencies -- 1403.7676 1406.5551 1407.2417
Frequencies -- 1408.8543 1419.7382 1426.0694
Frequencies -- 1432.5467 1433.5632 1436.0530
Frequencies -- 1436.9990 1437.4099 1437.6629
Frequencies -- 1440.3134 1441.0827 1442.7362
Frequencies -- 1444.2549 1444.9154 1445.3983
Frequencies -- 1445.9600 1446.5178 1450.5293
Frequencies -- 1452.8960 1453.5248 1459.9199
Frequencies -- 1707.7494 1709.2559 1713.4732
Frequencies -- 1713.9539 1716.2001 1717.9884
Frequencies -- 1720.4341 1720.7372 1724.7561
Frequencies -- 1726.1974 1726.9503 1737.8632
Frequencies -- 1738.3312 1744.2036 2951.9058
Frequencies -- 2958.0748 2963.1436 2965.1602
Frequencies -- 2965.6636 2966.1327 2967.4248
Frequencies -- 2967.6323 2968.4122 2972.7588
Frequencies -- 2973.1770 2973.7461 2974.6853
Frequencies -- 2975.0188 2975.3271 2975.7999
Frequencies -- 2976.5583 2976.8434 2976.8816
Frequencies -- 2977.2190 2977.9408 2978.3272
Frequencies -- 2978.5020 2978.6407 2979.0268
Frequencies -- 2980.4845 2980.8096 2982.1462
Frequencies -- 2982.4707 2982.6017 2982.9361
Frequencies -- 2984.1369 2984.3668 2985.1092
Frequencies -- 3000.7060 3009.9078 3018.0262
Frequencies -- 3019.4966 3021.2183 3023.4405
Frequencies -- 3032.0553 3034.3723 3045.0627
Frequencies -- 3046.9142 3066.2612 3066.7459
Frequencies -- 3066.8748 3067.3629 3067.9247
Frequencies -- 3068.1588 3068.4244 3068.6719
Frequencies -- 3068.7814 3069.6404 3071.2062
Frequencies -- 3071.6376 3071.7410 3072.1562

E(RB-LYP) = -4598.90439462 (BLYP-D3BJ/def2SVP/SMD (H_2O))
Sum of electronic and zero-point Energies= -4597.715303
Sum of electronic and thermal Energies= -4597.646828
Sum of electronic and thermal Free Energies= -4597.809161

E(RB-LYP) = -4603.98401102 (BLYP-D3BJ/def2TZVPP/SMD (H_2O))

G11

Center Number	Atomic Number	Atomic Type	Coordinates (Angstroms) X	Y	Z
1	6	0	-0.543563	0.872147	1.366228
2	1	0	-1.354224	0.405551	1.964927
3	6	0	0.709246	-0.040236	1.369246
4	6	0	-1.023371	1.100899	-0.089949
5	6	0	1.839256	0.636412	0.551912
6	6	0	0.352712	-1.402806	0.720985
7	1	0	-1.920109	1.755201	-0.088654
8	6	0	0.111003	1.775233	-0.903115
9	6	0	-1.375337	-0.264550	-0.734369
10	1	0	2.749027	-0.000458	0.562197
11	1	0	2.117399	1.604923	1.018654

12	6	0	1.365989	0.865299	-0.906198
13	1	0	-0.443295	-1.906232	1.309420
14	1	0	1.238065	-2.073140	0.733533
15	6	0	-0.124560	-1.179753	-0.736882
16	1	0	0.358878	2.763713	-0.461779
17	1	0	-0.226188	1.960595	-1.944828
18	1	0	-2.200867	-0.749658	-0.171751
19	1	0	-1.737296	-0.112170	-1.773264
20	1	0	2.175867	1.350786	-1.489761
21	6	0	1.006364	-0.498785	-1.549425
22	1	0	-0.378700	-2.156120	-1.199564
23	1	0	0.681575	-0.349303	-2.600793
24	1	0	1.902271	-1.154629	-1.577949
25	1	0	-0.305668	1.845123	1.845831
26	1	0	1.049904	-0.202388	2.412997

Frequencies -- 315.0152 317.1653 319.7293
Frequencies -- 401.5210 402.1223 442.0886
Frequencies -- 445.6256 446.9420 635.1561
Frequencies -- 637.9619 638.3504 739.2150
Frequencies -- 782.5678 784.1783 786.3218
Frequencies -- 872.7847 874.4056 874.7604
Frequencies -- 884.9726 886.8149 947.5142
Frequencies -- 948.3272 949.3138 1016.0685
Frequencies -- 1017.3303 1018.5749 1029.3217
Frequencies -- 1082.5230 1082.8203 1083.6499
Frequencies -- 1091.8881 1094.1343 1095.2140
Frequencies -- 1097.6487 1189.7595 1190.6668
Frequencies -- 1268.9018 1269.9199 1270.7228
Frequencies -- 1286.5293 1287.7008 1288.6869
Frequencies -- 1302.3203 1303.0352 1304.1768
Frequencies -- 1339.3346 1340.5609 1340.9139
Frequencies -- 1352.1880 1353.9405 1412.6966
Frequencies -- 1414.3591 1424.4800 1424.7532
Frequencies -- 1425.6371 1442.6556 2941.8164
Frequencies -- 2942.1921 2942.4830 2942.8636
Frequencies -- 2943.1645 2943.5900 2962.1898
Frequencies -- 2962.3806 2963.0808 2975.4251
Frequencies -- 2982.9562 2983.2968 2983.8826
Frequencies -- 2985.3048 2985.3461 2985.8548

E(RB-LYP) = -390.250746935 (BLYP-D3BJ/def2SVP/SMD (H_2O))
Sum of electronic and zero-point Energies= -390.014497
Sum of electronic and thermal Energies= -390.007305
Sum of electronic and thermal Free Energies= -390.045396

E(RB-LYP) = -390.678956997 (BLYP-D3BJ/def2TZVPP/SMD (H_2O))

HG12

Center Number	Atomic Number	Atomic Type	Coordinates (Angstroms) X	Y	Z
1	8	0	-2.459173	-3.615942	2.518308
2	8	0	0.960680	-4.257152	2.465372
3	8	0	3.771100	-1.619936	2.498960
4	8	0	3.956940	2.152087	2.729637
5	8	0	0.802495	4.151723	2.659496
6	8	0	-2.965416	3.431026	2.815161
7	8	0	-4.105548	-0.086760	2.559352
8	8	0	-2.584956	-3.266056	-3.635374
9	8	0	1.011913	-3.927053	-3.687614
10	8	0	3.932267	-1.576000	-3.714008
11	8	0	3.616791	2.164248	-3.478772
12	8	0	0.792358	4.597957	-3.535610
13	8	0	-2.672901	3.317280	-3.394568
14	8	0	-4.401274	-0.072075	-3.623154
15	7	0	-3.879430	-3.438695	0.663303
16	7	0	-2.234117	-4.975542	0.620923
17	7	0	0.191956	-5.410836	0.573184
18	7	0	2.303310	-4.631359	0.584362
19	7	0	4.113142	-2.969335	0.614269
20	7	0	5.099433	-0.942986	0.689278
21	7	0	5.081803	1.521080	0.772079
22	7	0	4.115925	3.554426	0.859516
23	7	0	2.062454	4.926505	0.841035
24	7	0	-0.159925	5.329675	0.874755
25	7	0	-2.554631	4.735780	0.910651
26	7	0	-4.307581	3.322473	0.898028
27	7	0	-5.150529	1.009379	0.769348
28	7	0	-4.975302	-1.240348	0.715064
29	7	0	-4.036084	-3.417963	-1.800527
30	7	0	-2.218696	-4.746034	-1.853697
31	7	0	0.195986	-5.204916	-1.900429
32	7	0	2.357915	-4.577382	-1.881410
33	7	0	4.231991	-2.978453	-1.861695
34	7	0	5.074679	-0.893251	-1.783101
35	7	0	5.022190	1.564761	-1.704287
36	7	0	3.958584	3.551583	-1.617918
37	7	0	2.054695	5.114754	-1.631468
38	7	0	-0.158127	5.512427	-1.598770
39	7	0	-2.506487	4.774087	-1.565549
40	7	0	-4.148003	3.227093	-1.576038
41	7	0	-5.199600	1.006461	-1.700291
42	7	0	-5.196061	-1.242120	-1.754995
43	6	0	-2.804308	-3.958099	1.388041
44	6	0	-1.116360	-5.776984	1.089314
45	1	0	-1.073979	-5.663692	2.187145
46	1	0	-1.312118	-6.838807	0.836188
47	6	0	1.124763	-4.698339	1.328184
48	6	0	3.554409	-4.192029	1.172809
49	1	0	3.355422	-3.998874	2.242241
50	1	0	4.305890	-5.005391	1.075791
51	6	0	4.258233	-1.812409	1.384502
52	6	0	5.634916	0.275432	1.277708
53	1	0	5.412459	0.242641	2.359213
54	1	0	6.734963	0.281320	1.125609
55	6	0	4.320870	2.373425	1.575861
56	6	0	3.385252	4.682691	1.407923
57	1	0	3.249900	4.480075	2.485350
58	1	0	3.990678	5.603609	1.277497
59	6	0	0.887935	4.721238	1.571278
60	6	0	-1.476165	5.536492	1.465463
61	1	0	-1.735013	6.612346	1.368422
62	1	0	-1.402533	5.273156	2.535772
63	6	0	-3.229645	3.772264	1.663373
64	6	0	-5.246689	2.328166	1.381695
65	1	0	-6.279964	2.706392	1.235529
66	1	0	-5.049358	2.206110	2.461641
67	6	0	-4.663610	-0.101318	1.461554
68	6	0	-4.870874	-2.575149	1.282533
69	1	0	-4.580258	-2.457907	2.341866
70	1	0	-5.866794	-3.065267	1.222282
71	6	0	-2.900671	-3.741168	-2.544412
72	6	0	-1.118068	-5.480715	-2.454551
73	1	0	-1.086085	-5.202688	-3.523269
74	1	0	-1.322540	-6.567904	-2.362737
75	6	0	1.166194	-4.488245	-2.602813
76	6	0	3.638724	-4.173657	-2.437075
77	1	0	3.478503	-3.964507	-3.509841
78	1	0	4.352942	-5.016433	-2.326040
79	6	0	4.347575	-1.785406	-2.574623
80	6	0	5.580032	0.364618	-2.305942
81	1	0	5.329787	0.389191	-3.381533
82	1	0	6.683283	0.390531	-2.181199
83	6	0	4.125183	2.392585	-2.380580
84	6	0	3.353181	4.757098	-2.168717
85	1	0	3.213093	4.590897	-3.251798
86	1	0	4.054642	5.603327	-2.011679
87	6	0	0.881564	5.001576	-2.377086
88	6	0	-1.503753	5.672464	-2.116901
89	1	0	-1.838671	6.715887	-1.940555
90	1	0	-1.450577	5.479935	-3.203278
91	6	0	-3.051585	3.715650	-2.292728
92	6	0	-5.139427	2.364443	-2.205306

93	1	0	-4.885013	2.295020	-3.277999
94	1	0	-6.137724	2.839243	-2.092774
95	6	0	-4.859138	-0.098315	-2.481298
96	6	0	-5.104559	-2.577516	-2.317927
97	1	0	-6.069847	-3.101015	-2.156068
98	1	0	-4.929413	-2.456065	-3.401517
99	6	0	-4.135018	-4.184146	-0.567821
100	1	0	-5.121389	-4.689650	-0.510074
101	6	0	-2.921895	-5.179879	-0.647516
102	1	0	-3.223645	-6.243012	-0.747100
103	6	0	0.726607	-5.858990	-0.707201
104	1	0	0.616847	-6.959403	-0.798892
105	6	0	2.221484	-5.373311	-0.669721
106	1	0	2.959677	-6.202126	-0.672876
107	6	0	4.939810	-2.946382	-0.588965
108	1	0	5.687035	-3.766749	-0.550970
109	6	0	5.580103	-1.511300	-0.562047
110	1	0	6.689867	-1.521781	-0.571363
111	6	0	5.513686	2.158051	-0.467603
112	1	0	6.621608	2.224861	-0.493247
113	6	0	4.802105	3.560728	-0.426415
114	1	0	5.508347	4.415798	-0.472814
115	6	0	1.846239	5.757195	-0.339423
116	1	0	2.462170	6.677918	-0.268333
117	6	0	0.298582	6.036413	-0.317587
118	1	0	0.045099	7.113973	-0.236299
119	6	0	-3.240696	5.049953	-0.339618
120	1	0	-3.576471	6.108069	-0.332212
121	6	0	-4.424548	4.015564	-0.376779
122	1	0	-5.424366	4.490632	-0.462660
123	6	0	-5.853461	0.637795	-0.451796
124	1	0	-6.889026	1.036860	-0.429121
125	6	0	-5.788209	-0.933418	-0.460481
126	1	0	-6.781587	-1.420752	-0.370676
127	6	0	-1.045559	1.297569	1.433454
128	1	0	-2.040613	1.019012	1.826424
129	6	0	0.021668	0.311035	1.952881
130	6	0	-1.056835	1.291862	-0.109743
131	6	0	1.400598	0.756553	1.422564
132	6	0	-0.297084	-1.113628	1.447942
133	1	0	-1.829544	1.992329	-0.480939
134	6	0	0.324513	1.719162	-0.678096
135	6	0	-1.379731	-0.133107	-0.640152
136	1	0	2.192289	0.090510	1.812926
137	1	0	1.619418	1.773335	1.795433
138	6	0	1.398201	0.743544	-0.121070
139	1	0	-1.283151	-1.446067	1.830993
140	1	0	0.454046	-1.835631	1.827990
141	6	0	-0.302586	-1.115400	-0.094726
142	1	0	0.557900	2.742221	-0.327080
143	1	0	-2.367649	-0.438810	-0.246748
144	1	0	2.391284	1.054494	-0.497844
145	6	0	1.084357	-0.683740	-0.652290
146	1	0	-0.533255	-2.129899	-0.469514
147	1	0	1.859797	-1.380913	-0.275616
148	1	0	-0.817906	2.310036	1.813154
149	6	0	1.071040	-0.700205	-2.195137
150	1	0	2.057909	-0.394551	-2.590816
151	1	0	0.880782	-1.725608	-2.568632
152	6	0	0.306788	1.695137	-2.221670
153	1	0	-0.452737	2.399728	-2.607081
154	1	0	1.283675	2.021202	-2.623946
155	6	0	-1.397444	-0.152218	-2.182688
156	1	0	-1.664694	-1.161571	-2.554210
157	1	0	-2.165555	0.544797	-2.567351
158	6	0	-0.011620	0.267860	-2.718303
159	1	0	-0.019772	0.252332	-3.829278
160	1	0	0.028543	0.322640	3.064030

Frequencies -- 26.0262 40.0725 47.6411
Frequencies -- 51.2247 52.4960 57.5047
Frequencies -- 63.8316 64.5812 69.5938
Frequencies -- 76.4831 81.9792 88.1168
Frequencies -- 90.4526 96.2143 100.5057
Frequencies -- 101.7702 106.1706 108.9196
Frequencies -- 112.3488 116.1970 118.0486
Frequencies -- 119.9076 121.2171 127.7877
Frequencies -- 127.9854 131.0651 133.0671
Frequencies -- 133.7813 137.5324 143.7899
Frequencies -- 146.9967 147.3334 152.7397
Frequencies -- 157.3272 160.2568 161.6653
Frequencies -- 164.5394 167.7110 170.2143
Frequencies -- 179.9661 180.9468 185.7950
Frequencies -- 190.2820 193.6994 193.9859
Frequencies -- 199.2601 200.4307 207.4319
Frequencies -- 209.2101 223.1592 227.3218
Frequencies -- 231.0277 234.8374 236.1400
Frequencies -- 245.3277 256.9557 262.2714
Frequencies -- 265.1460 267.3534 282.3558
Frequencies -- 284.7980 285.8235 287.2376
Frequencies -- 296.1460 317.6866 323.0821
Frequencies -- 326.4835 328.0160 330.3602
Frequencies -- 334.1742 338.5930 348.4517
Frequencies -- 349.3978 350.9881 352.5553
Frequencies -- 352.9861 354.0339 356.6635
Frequencies -- 359.6710 360.4522 361.6926
Frequencies -- 362.9402 364.8620 370.7868
Frequencies -- 371.2254 371.6114 409.3075
Frequencies -- 410.8882 412.3815 413.7596
Frequencies -- 415.1244 416.7327 424.2148
Frequencies -- 424.6501 431.0692 434.3236
Frequencies -- 441.4447 442.0505 445.1680
Frequencies -- 446.5605 448.0855 451.8365
Frequencies -- 454.0176 455.6059 459.6988
Frequencies -- 509.7417 510.6452 578.1000
Frequencies -- 579.6463 602.6118 605.1696
Frequencies -- 608.3639 609.1164 613.7817
Frequencies -- 614.0890 614.2004 616.2755
Frequencies -- 617.3028 617.8724 624.9824
Frequencies -- 626.8135 636.8439 639.3358
Frequencies -- 640.4726 641.8994 642.3620
Frequencies -- 642.7070 644.1537 658.3490
Frequencies -- 663.3656 664.2791 665.0204
Frequencies -- 666.7122 670.0087 671.0198
Frequencies -- 682.6514 683.5090 686.8098
Frequencies -- 692.7300 696.5313 698.1044
Frequencies -- 700.6319 702.5253 703.4557
Frequencies -- 705.9451 710.6191 713.1846
Frequencies -- 715.8583 717.1627 719.7399
Frequencies -- 720.8730 721.2341 722.6238
Frequencies -- 724.4051 725.7468 728.6545

Frequencies -- 731.6268 765.9166 766.4340
Frequencies -- 774.0063 775.6469 777.5287
Frequencies -- 777.7178 786.4824 787.0977
Frequencies -- 790.0126 794.6622 795.1804
Frequencies -- 795.7421 805.4943 809.0469
Frequencies -- 810.9356 812.6036 813.6994
Frequencies -- 815.2582 816.4659 818.5622
Frequencies -- 819.0118 819.6774 820.3105
Frequencies -- 821.3832 822.4393 857.0989
Frequencies -- 882.3127 882.4751 883.1425
Frequencies -- 885.3668 887.2795 894.1203
Frequencies -- 895.4866 898.4659 909.0104
Frequencies -- 909.5209 928.1409 933.3545
Frequencies -- 933.7292 937.0162 941.6243
Frequencies -- 943.9624 945.8720 947.8401
Frequencies -- 949.2828 952.8147 954.7407
Frequencies -- 957.2997 958.4912 962.5687
Frequencies -- 963.7400 969.8607 970.1906
Frequencies -- 970.7577 978.1815 979.6520
Frequencies -- 980.5434 985.6245 990.9053
Frequencies -- 1000.5575 1003.5587 1008.8089
Frequencies -- 1010.1571 1022.4121 1025.8978
Frequencies -- 1027.2175 1027.7163 1029.7132
Frequencies -- 1031.2708 1034.4410 1035.5927
Frequencies -- 1039.2055 1044.8566 1045.7399
Frequencies -- 1052.8939 1060.2090 1068.0956
Frequencies -- 1072.3137 1077.7743 1084.4557
Frequencies -- 1089.9718 1091.8896 1095.6258
Frequencies -- 1102.1310 1102.9758 1107.4895
Frequencies -- 1108.5034 1109.2219 1111.0403
Frequencies -- 1113.6087 1114.2984 1115.1793
Frequencies -- 1135.2803 1137.8168 1140.5671
Frequencies -- 1147.2812 1150.5311 1158.0500
Frequencies -- 1161.9150 1164.7724 1166.0753
Frequencies -- 1166.2455 1180.7897 1181.2537
Frequencies -- 1181.7246 1183.3392 1188.0361
Frequencies -- 1196.2486 1196.6520 1197.9193
Frequencies -- 1198.3901 1199.1198 1200.6323
Frequencies -- 1202.1447 1210.5751 1210.7381
Frequencies -- 1212.2689 1213.6978 1214.1330
Frequencies -- 1214.9740 1215.6013 1216.4036
Frequencies -- 1225.5579 1226.3848 1226.6461
Frequencies -- 1227.6611 1228.6596 1233.6299
Frequencies -- 1236.9885 1237.4997 1239.0793
Frequencies -- 1249.7002 1250.7583 1252.9685
Frequencies -- 1255.6576 1255.7960 1261.6792
Frequencies -- 1263.1402 1266.2859 1269.8503
Frequencies -- 1271.6846 1272.5521 1272.8254
Frequencies -- 1275.4236 1276.0187 1276.6705
Frequencies -- 1279.0398 1289.8972 1290.7275
Frequencies -- 1291.4092 1294.3315 1294.7011
Frequencies -- 1296.9907 1298.5911 1299.2521
Frequencies -- 1300.2217 1301.5027 1306.8540
Frequencies -- 1308.5684 1310.8781 1311.3103
Frequencies -- 1315.9590 1316.6998 1317.4065
Frequencies -- 1320.2730 1323.4227 1328.3217
Frequencies -- 1329.7936 1333.3389 1337.8568
Frequencies -- 1339.7322 1344.4006 1347.4129
Frequencies -- 1354.9674 1360.0080 1360.4266
Frequencies -- 1361.9723 1362.7385 1365.5163
Frequencies -- 1365.7999 1367.6153 1368.5113
Frequencies -- 1369.0737 1370.0746 1371.1532
Frequencies -- 1371.8961 1372.1515 1373.4449
Frequencies -- 1374.0465 1374.0882 1374.9928
Frequencies -- 1375.8522 1376.5014 1376.8445
Frequencies -- 1377.7363 1378.6073 1378.9182
Frequencies -- 1380.2757 1380.9095 1381.1408
Frequencies -- 1382.3837 1383.2420 1384.1378
Frequencies -- 1384.4968 1385.0522 1385.7859
Frequencies -- 1387.4344 1387.6880 1388.4750
Frequencies -- 1388.8468 1389.7704 1392.4955
Frequencies -- 1394.0117 1395.1134 1395.3603
Frequencies -- 1395.7962 1396.9660 1400.1264
Frequencies -- 1403.3966 1405.0149 1411.5926
Frequencies -- 1426.4079 1431.9904 1432.1955
Frequencies -- 1433.2506 1434.9896 1436.4737
Frequencies -- 1437.7693 1438.6046 1440.9378
Frequencies -- 1441.2793 1442.9686 1443.3923
Frequencies -- 1444.1779 1447.6074 1448.2713
Frequencies -- 1449.9408 1450.7034 1452.0027
Frequencies -- 1452.9033 1454.1437 1706.2250
Frequencies -- 1707.2828 1710.7745 1711.5823
Frequencies -- 1713.1841 1713.6420 1718.0299
Frequencies -- 1718.7059 1724.2306 1725.3688
Frequencies -- 1726.1921 1735.6831 1736.8058
Frequencies -- 1742.3148 2936.1253 2938.5459

Frequencies -- 2954.0538 2954.9322 2958.2369
Frequencies -- 2960.2497 2961.5619 2964.0863
Frequencies -- 2965.5414 2966.3769 2967.5906
Frequencies -- 2969.2338 2970.1837 2970.6263
Frequencies -- 2970.6656 2970.8331 2971.5408
Frequencies -- 2971.6451 2972.0380 2972.3698
Frequencies -- 2973.1962 2973.5041 2974.3268
Frequencies -- 2975.3026 2976.2969 2976.9162
Frequencies -- 2977.3207 2977.9326 2979.1637
Frequencies -- 2980.1261 2981.5788 2982.4529
Frequencies -- 2985.5567 2991.3588 2992.7186
Frequencies -- 2995.0441 2996.5002 2997.6022
Frequencies -- 3002.8462 3005.5711 3008.1149
Frequencies -- 3009.0261 3014.9843 3031.8186
Frequencies -- 3038.9946 3047.6269 3048.0323
Frequencies -- 3052.3154 3061.5041 3065.1200
Frequencies -- 3065.1213 3065.9693 3066.2871
Frequencies -- 3066.6624 3066.8397 3067.3668
Frequencies -- 3068.1912 3068.5381 3069.8603
Frequencies -- 3071.4909 3071.7541 3074.9303

E(RB-LYP) = -4753.60139135 (BLYP-D3BJ/def2SVP/SMD (H_2O))
Sum of electronic and zero-point Energies= -4752.340239
Sum of electronic and thermal Energies= -4752.270167
Sum of electronic and thermal Free Energies= -4752.434302

E(RB-LYP) = -4758.83046595 (BLYP-D3BJ/def2TZVPP/SMD (H_2O))

G12

Center Number	Atomic Number	Atomic Type	Coordinates (Angstroms) X	Y	Z
1	6	0	-1.052453	1.300712	1.432884
2	1	0	-2.051728	1.012207	1.822001
3	6	0	0.024613	0.321375	1.958068
4	6	0	-1.064594	1.288502	-0.111912
5	6	0	1.409739	0.754530	1.421112
6	6	0	-0.294236	-1.105570	1.450625
7	1	0	-1.838830	1.992173	-0.485193
8	6	0	0.322304	1.721077	-0.672091
9	6	0	-1.385333	-0.140821	-0.642496
10	1	0	2.197157	0.070240	1.801630
11	1	0	1.658378	1.772208	1.789304
12	6	0	1.400965	0.740594	-0.123740
13	1	0	-1.279255	-1.438247	1.840769
14	1	0	0.463641	-1.823171	1.830073
15	6	0	-0.306604	-1.121387	-0.094066
16	1	0	0.551152	2.746337	-0.310874
17	1	0	-2.380978	-0.451789	-0.260522
18	1	0	2.396627	1.051545	-0.505703
19	6	0	1.080347	-0.688771	-0.654277
20	1	0	-0.535503	-2.146624	-0.455213
21	1	0	1.854543	-1.392439	-0.280963
22	1	0	-0.845255	2.327520	1.801657
23	6	0	1.068104	-0.701058	-2.199067
24	1	0	2.067407	-0.412735	-2.588240
25	1	0	0.860897	-1.727925	-2.567719
26	6	0	0.310004	1.705302	-2.216796
27	1	0	-0.447871	2.422821	-2.596386
28	1	0	1.295086	2.037771	-2.606961
29	6	0	-1.393996	-0.154878	-2.187280
30	1	0	-1.642520	-1.172653	-2.555302
31	1	0	-2.181484	0.529196	-2.568044
32	6	0	-0.008919	0.278134	-2.724243
33	1	0	-0.016318	0.267358	-3.833641
34	1	0	0.031984	0.332472	3.067467

Frequencies -- 271.4814 295.2267 300.9271
Frequencies -- 340.2967 393.8402 402.1342
Frequencies -- 403.6052 403.9171 428.5025
Frequencies -- 436.6739 451.0378 607.6609
Frequencies -- 609.6600 629.7389 632.4408
Frequencies -- 680.7052 691.6672 784.9043
Frequencies -- 789.5401 789.7992 792.1227
Frequencies -- 850.0327 870.8978 876.6231
Frequencies -- 887.4913 910.4710 911.9928
Frequencies -- 918.4270 921.9399 962.0508
Frequencies -- 966.9598 1012.6693 1015.7398
Frequencies -- 1023.6522 1032.5145 1035.1081
Frequencies -- 1043.6455 1046.1317 1055.6025
Frequencies -- 1067.4808 1067.9296 1069.2592
Frequencies -- 1100.2339 1117.8557 1125.8688
Frequencies -- 1128.1305 1156.5618 1159.6203
Frequencies -- 1211.7623 1214.8803 1232.7455
Frequencies -- 1245.5776 1264.0895 1267.8406
Frequencies -- 1281.1212 1283.5520 1299.0443
Frequencies -- 1300.0607 1301.2061 1306.3336
Frequencies -- 1307.4754 1319.1484 1322.3805
Frequencies -- 1323.8682 1333.4926 1334.6645
Frequencies -- 1336.3422 1358.4615 1362.1257
Frequencies -- 1365.1551 1416.6742 1417.5542
Frequencies -- 1420.4657 1421.3694 1434.5873
Frequencies -- 1436.1014 2937.2728 2938.1751
Frequencies -- 2938.2710 2938.5325 2938.7602
Frequencies -- 2939.8892 2944.8789 2945.4108
Frequencies -- 2945.4621 2951.1170 2951.4462
Frequencies -- 2958.4522 2968.0272 2974.2024
Frequencies -- 2981.7902 2982.2033 2983.4190
Frequencies -- 2983.7844 2983.9196 2984.3156

E(RB-LYP) = -544.935403435 (BLYP-D3BJ/def2SVP/SMD (H_2O))
Sum of electronic and zero-point Energies= -544.628402
Sum of electronic and thermal Energies= -544.619381
Sum of electronic and thermal Free Energies= -544.661434

E(RB-LYP) = -545.524276046 (BLYP-D3BJ/def2TZVPP/SMD (H_2O))

HG13

Center	Atomic	Atomic	Coordinates (Angstroms)

Number	Number	Type	X	Y	Z
1	8	0	-2.447489	-2.745473	2.765051
2	8	0	1.367092	-3.612973	2.764514
3	8	0	4.282180	-1.841132	2.880742
4	8	0	3.647133	1.386541	2.776603
5	8	0	0.401219	3.637731	2.816243
6	8	0	-3.167675	3.246073	2.798740
7	8	0	-4.499482	0.245909	2.758312
8	8	0	-2.501596	-3.366119	-3.238426
9	8	0	1.013883	-4.034374	-3.205805
10	8	0	3.748262	-1.641521	-3.238922
11	8	0	3.714621	2.178782	-3.177272
12	8	0	0.908507	4.392296	-3.147756
13	8	0	-2.553007	3.346467	-3.240313
14	8	0	-4.070557	-0.087197	-3.311307
15	7	0	-4.003014	-3.185039	1.071312
16	7	0	-2.078808	-4.347505	1.089879
17	7	0	0.324815	-4.883210	1.089982
18	7	0	2.564734	-4.719363	1.080503
19	7	0	4.460705	-3.153217	0.948951
20	7	0	5.501713	-1.163659	0.999069
21	7	0	5.259136	1.288980	1.077221
22	7	0	3.888094	3.064435	1.160341
23	7	0	1.862388	4.454522	1.169639
24	7	0	-0.250574	5.229362	1.226341
25	7	0	-2.624327	4.637520	0.990254
26	7	0	-4.552768	3.475931	0.922795
27	7	0	-5.507766	1.196110	0.864918
28	7	0	-5.158986	-1.026269	0.904624
29	7	0	-3.949042	-3.308487	-1.394363
30	7	0	-2.189421	-4.710645	-1.344866
31	7	0	0.224246	-5.237369	-1.354193
32	7	0	2.379738	-4.586424	-1.380343
33	7	0	4.351427	-3.120059	-1.524997
34	7	0	5.113311	-1.002909	-1.442161
35	7	0	5.023328	1.446106	-1.374669
36	7	0	4.081817	3.486223	-1.265491
37	7	0	2.113542	4.986276	-1.226885
38	7	0	-0.117951	5.302455	-1.243501
39	7	0	-2.539948	4.883666	-1.469636
40	7	0	-4.142039	3.303949	-1.516550
41	7	0	-5.150709	1.068491	-1.580214
42	7	0	-5.185514	-1.179525	-1.561110
43	6	0	-2.795946	-3.343105	1.745768
44	6	0	-0.971100	-5.025061	1.737533
45	1	0	-0.874978	-4.596393	2.751165
46	1	0	-1.208075	-6.108610	1.816774
47	6	0	1.411523	-4.314548	1.745695
48	6	0	3.900260	-4.365813	1.522486
49	1	0	3.858095	-4.212887	2.615131
50	1	0	4.571121	-5.218945	1.296278
51	6	0	4.687810	-2.023000	1.730979
52	6	0	5.964608	0.102229	1.532390
53	1	0	5.848458	0.045746	2.628856
54	1	0	7.036215	0.229306	1.282685
55	6	0	4.192576	1.852977	1.768100
56	6	0	3.098181	4.077685	1.836619
57	1	0	2.827712	3.669361	2.826594
58	1	0	3.724995	4.986349	1.971305
59	6	0	0.635952	4.346048	1.836633
60	6	0	-1.612049	5.416043	1.686113
61	1	0	-1.858032	6.494933	1.604098
62	1	0	-1.645892	5.111633	2.747023
63	6	0	-3.411629	3.714336	1.689117
64	6	0	-5.600041	2.562796	1.348960
65	1	0	-6.575557	2.979020	1.029508
66	1	0	-5.560572	2.520667	2.451425
67	6	0	-4.981976	0.155879	1.631048
68	6	0	-5.061844	-2.321122	1.554778
69	1	0	-4.867352	-2.129276	2.624884
70	1	0	-6.026548	-2.859099	1.442915
71	6	0	-2.829474	-3.734967	-2.111992
72	6	0	-1.106264	-5.528271	-1.860759
73	1	0	-1.077076	-5.373349	-2.953833
74	1	0	-1.333622	-6.592439	-1.644677
75	6	0	1.180002	-4.544253	-2.099531
76	6	0	3.654078	-4.288487	-2.024147
77	1	0	3.440812	-4.110029	-3.092954
78	1	0	4.322652	-5.167910	-1.922600
79	6	0	4.323605	-1.889482	-2.181034
80	6	0	5.561781	0.257635	-2.012430
81	1	0	5.227962	0.280132	-3.065334
82	1	0	6.671424	0.294394	-1.976438
83	6	0	4.202227	2.344182	-2.060119
84	6	0	3.447999	4.707979	-1.731940
85	1	0	3.362900	4.630907	-2.830039
86	1	0	4.106886	5.561227	-1.471180
87	6	0	0.959941	4.822414	-1.997128
88	6	0	-1.381416	5.649691	-1.882853
89	1	0	-1.591849	6.724356	-1.701444
90	1	0	-1.246885	5.477979	-2.965612
91	6	0	-3.009808	3.780669	-2.183990
92	6	0	-5.069935	2.393263	-2.166886
93	1	0	-4.724692	2.267280	-3.208964
94	1	0	-6.083326	2.849339	-2.164345
95	6	0	-4.707879	-0.069627	-2.258770
96	6	0	-5.012251	-2.542338	-2.027193
97	1	0	-5.972575	-3.081737	-1.887997
98	1	0	-4.773525	-2.492178	-3.104383
99	6	0	-4.101672	-4.011434	-0.121399
100	1	0	-5.049020	-4.588828	-0.111437
101	6	0	-2.811077	-4.906801	-0.046843
102	1	0	-3.021811	-5.982567	0.124278
103	6	0	0.731834	-5.687220	-0.070253
104	1	0	0.479627	-6.754309	0.096867
105	6	0	2.271247	-5.403540	-0.169784
106	1	0	2.892170	-6.317254	-0.262236
107	6	0	5.176123	-3.106258	-0.327363
108	1	0	5.928569	-3.920259	-0.367449
109	6	0	5.802674	-1.665437	-0.334299
110	1	0	6.898324	-1.657134	-0.506573
111	6	0	5.569732	2.016607	-0.142479
112	1	0	6.665128	2.163434	-0.231624
113	6	0	4.757614	3.349610	0.012283
114	1	0	5.385420	4.240350	0.218353
115	6	0	1.826852	5.469879	0.111600
116	1	0	2.495483	6.316497	0.370679
117	6	0	0.308753	5.860467	0.041775
118	1	0	0.125629	6.954386	0.065467
119	6	0	-3.276121	5.103225	-0.236442
120	1	0	-3.554798	6.172671	-0.140365
121	6	0	-4.506572	4.139574	-0.369995
122	1	0	-5.465119	4.662489	-0.566289
123	6	0	-5.995027	0.749418	-0.431233
124	1	0	-7.026744	1.121828	-0.598847
125	6	0	-5.890698	-0.814462	-0.343372
126	1	0	-6.874157	-1.326972	-0.303599
127	6	0	-1.210107	0.661399	0.915244
128	1	0	-1.993334	0.085347	1.449504
129	6	0	0.179297	-0.000475	1.163184
130	6	0	-1.514346	0.708326	-0.600477
131	6	0	1.268133	0.817687	0.417548
132	6	0	0.166607	-1.432459	0.568509
133	1	0	-2.499151	1.180513	-0.765921
134	6	0	-0.419097	1.533055	-1.318989
135	6	0	-1.532713	-0.733621	-1.160170
136	1	0	2.255414	0.340721	0.574567
137	1	0	1.323755	1.837064	0.838685
138	6	0	0.960260	0.870218	-1.099869
139	1	0	-0.568883	-2.048000	1.114863
140	1	0	1.159244	-1.899297	0.710592
141	6	0	-0.152551	-1.390419	-0.943332
142	1	0	-0.405027	2.565573	-0.922516
143	1	0	-0.646938	1.613304	-2.399904
144	1	0	-2.314111	-1.326846	-0.648017
145	1	0	-1.794320	-0.727277	-2.235122
146	1	0	1.738343	1.459154	-1.621926
147	6	0	0.940475	-0.570016	-1.663286
148	1	0	-0.167463	-2.417576	-1.350827
149	1	0	0.755527	-0.557318	-2.756861
150	1	0	1.926949	-1.046990	-1.515108
151	1	0	-1.212309	1.681376	1.348959
152	1	0	2.529417	-0.160794	2.835597
153	1	0	1.705106	-0.678897	4.194336
154	1	0	1.751184	-1.684872	2.840239
155	7	0	1.676036	-0.685403	3.132510
156	6	0	0.403570	-0.021373	2.685887
157	1	0	-0.421145	-0.566257	3.183404
158	1	0	0.432028	1.011037	3.081712
159	53	0	1.483137	-0.290846	6.573894

Frequencies --	8.5483	17.2968	36.4803
Frequencies --	40.9360	42.8143	45.8719
Frequencies --	52.3683	55.1146	63.1454
Frequencies --	69.0012	69.9337	75.7098
Frequencies --	79.3387	82.5918	85.9532
Frequencies --	88.1760	89.8628	93.9877

Frequencies -- 99.0443 103.1747 105.4758
Frequencies -- 106.5740 110.5007 113.8872
Frequencies -- 119.5840 123.0012 123.4407
Frequencies -- 125.4758 127.8115 131.0160
Frequencies -- 134.0062 138.3815 143.0961
Frequencies -- 144.4288 147.2587 154.7867
Frequencies -- 157.4428 159.8796 163.3926
Frequencies -- 165.3784 168.1027 171.4280
Frequencies -- 172.4145 177.1480 184.6374
Frequencies -- 190.1558 191.6386 192.6741
Frequencies -- 198.1524 199.5363 206.1146
Frequencies -- 207.4635 208.5459 218.1396
Frequencies -- 222.6760 235.0542 243.1278
Frequencies -- 243.8302 246.9549 247.6250
Frequencies -- 259.6548 263.7036 268.3828
Frequencies -- 269.2875 269.8868 281.7101
Frequencies -- 284.3213 290.3201 292.5514
Frequencies -- 326.2416 330.4578 331.3501
Frequencies -- 333.1963 343.6480 346.6199
Frequencies -- 346.8600 349.0166 352.3962
Frequencies -- 353.4787 356.8489 358.7011
Frequencies -- 359.9470 361.3017 363.5499
Frequencies -- 365.8220 367.5106 369.2487
Frequencies -- 370.1085 372.8474 377.9001
Frequencies -- 384.6057 390.8224 412.1554
Frequencies -- 413.2066 414.6987 417.1871
Frequencies -- 421.0518 433.3807 436.3407
Frequencies -- 437.8626 443.6734 445.2479
Frequencies -- 451.2044 455.1777 458.6174
Frequencies -- 460.7179 462.2962 462.4668
Frequencies -- 478.9344 481.1390 507.4489
Frequencies -- 508.7941 573.6411 577.8688
Frequencies -- 578.8319 600.9689 601.5902
Frequencies -- 609.7944 610.9033 612.1062
Frequencies -- 614.3763 617.5954 620.6278
Frequencies -- 623.5132 626.8858 638.7442
Frequencies -- 639.8033 645.5752 648.8286
Frequencies -- 650.5974 650.9070 653.1292
Frequencies -- 657.2771 660.7379 663.1283
Frequencies -- 665.5600 669.2325 670.3215
Frequencies -- 674.4140 684.5021 689.0422
Frequencies -- 694.5499 696.0472 701.2343
Frequencies -- 703.5243 708.1083 711.4130
Frequencies -- 712.2655 714.0526 715.2605
Frequencies -- 717.5653 718.1448 720.2830
Frequencies -- 721.1524 723.6400 727.1359
Frequencies -- 729.2936 730.2945 732.4286
Frequencies -- 734.2339 767.3913 769.0659
Frequencies -- 775.4240 777.8705 778.2709
Frequencies -- 778.7964 780.2009 787.5712
Frequencies -- 788.2784 790.6265 795.7939
Frequencies -- 798.1692 801.5299 809.9047
Frequencies -- 812.4067 814.4525 814.9773
Frequencies -- 816.8870 817.0961 817.9935
Frequencies -- 818.6811 819.5957 821.3006
Frequencies -- 822.9641 847.7494 872.7811
Frequencies -- 877.0983 878.3689 883.5730
Frequencies -- 886.1398 889.2230 892.8945
Frequencies -- 894.9686 896.6055 910.3373
Frequencies -- 911.8331 930.5302 936.5931
Frequencies -- 937.1565 939.9254 940.3972
Frequencies -- 944.4409 946.9007 951.6104
Frequencies -- 952.4478 953.9261 957.8174
Frequencies -- 961.6346 964.8988 965.9770
Frequencies -- 969.4317 970.5980 972.1668
Frequencies -- 976.6287 981.6888 981.8493
Frequencies -- 983.9467 986.8493 992.5090
Frequencies -- 1003.8666 1006.8428 1008.9794
Frequencies -- 1010.3645 1025.4892 1026.7319
Frequencies -- 1028.8942 1029.9236 1030.5498
Frequencies -- 1034.0177 1035.2449 1036.3208
Frequencies -- 1036.8111 1037.8851 1077.6395
Frequencies -- 1078.5690 1086.7404 1089.8713
Frequencies -- 1094.6982 1096.3667 1099.2439
Frequencies -- 1104.6030 1105.2017 1107.7573
Frequencies -- 1109.9587 1111.2652 1111.9890
Frequencies -- 1116.0052 1116.3090 1121.6796
Frequencies -- 1133.5710 1137.2664 1139.6352
Frequencies -- 1140.7054 1144.5236 1150.9945
Frequencies -- 1165.3908 1165.8437 1167.1059
Frequencies -- 1178.3611 1180.1279 1180.8172
Frequencies -- 1190.8366 1192.9392 1193.3579
Frequencies -- 1195.1252 1197.3744 1199.0983
Frequencies -- 1200.9775 1203.5999 1204.6276
Frequencies -- 1207.9554 1208.7570 1209.9889
Frequencies -- 1211.5402 1212.6433 1213.8879

Frequencies -- 1216.8251 1217.5708 1223.8667
Frequencies -- 1225.9605 1226.9874 1228.3622
Frequencies -- 1231.1737 1235.9603 1236.9632
Frequencies -- 1249.3931 1250.2204 1256.0298
Frequencies -- 1259.5534 1265.3353 1265.6221
Frequencies -- 1268.0687 1268.6610 1269.4331
Frequencies -- 1271.2231 1272.0806 1272.6679
Frequencies -- 1275.3383 1276.3175 1277.3138
Frequencies -- 1279.0701 1288.6241 1290.2196
Frequencies -- 1294.2174 1295.0156 1295.8504
Frequencies -- 1296.7009 1298.6311 1303.0143
Frequencies -- 1304.2916 1305.3593 1310.5092
Frequencies -- 1311.8629 1312.4493 1313.6568
Frequencies -- 1316.5834 1317.8265 1318.2366
Frequencies -- 1320.6072 1321.9418 1323.2048
Frequencies -- 1327.3475 1332.2745 1343.5617
Frequencies -- 1357.9302 1361.8823 1362.2154
Frequencies -- 1363.5469 1364.6356 1366.8133
Frequencies -- 1367.7707 1368.5037 1370.0515
Frequencies -- 1370.4227 1371.4959 1371.8839
Frequencies -- 1372.7344 1372.9390 1373.5114
Frequencies -- 1374.7097 1375.5007 1377.1843
Frequencies -- 1377.9016 1378.4244 1379.1784
Frequencies -- 1379.7330 1380.1667 1380.7350
Frequencies -- 1381.4860 1382.3818 1384.0339
Frequencies -- 1384.1436 1384.8711 1385.0150
Frequencies -- 1385.5111 1386.2582 1387.8554
Frequencies -- 1389.1320 1389.1671 1391.7380
Frequencies -- 1392.1342 1392.7191 1393.6292
Frequencies -- 1396.1731 1396.4455 1397.7703
Frequencies -- 1399.7921 1401.7938 1404.4421
Frequencies -- 1406.2584 1408.2703 1412.4610
Frequencies -- 1422.0641 1425.7006 1431.7406
Frequencies -- 1432.4903 1435.4773 1437.1380
Frequencies -- 1437.8532 1438.2759 1438.8516
Frequencies -- 1442.0626 1443.5404 1443.9652
Frequencies -- 1445.3845 1445.9042 1446.3295
Frequencies -- 1447.9245 1448.3070 1450.9675
Frequencies -- 1455.5269 1458.8639 1461.4879
Frequencies -- 1541.7991 1569.7861 1693.2607
Frequencies -- 1697.2726 1710.3426 1714.0578
Frequencies -- 1717.4313 1717.8550 1720.0012
Frequencies -- 1722.0056 1724.6582 1726.8903
Frequencies -- 1729.8765 1738.2302 1739.6524
Frequencies -- 1746.1861 2876.4341 2945.8458
Frequencies -- 2950.1692 2956.4421 2958.5997
Frequencies -- 2969.2040 2969.5992 2972.4597
Frequencies -- 2972.7780 2972.8498 2977.2833
Frequencies -- 2978.5892 2979.1008 2980.0800
Frequencies -- 2980.9577 2982.0591 2982.2358
Frequencies -- 2982.6682 2983.9329 2984.4134
Frequencies -- 2984.5917 2986.8974 2987.3528
Frequencies -- 2987.7004 2988.2526 2988.4613
Frequencies -- 2988.7538 2990.4254 2992.0017
Frequencies -- 2994.9154 2997.4195 2997.4608
Frequencies -- 2998.3007 3000.3403 3002.6751
Frequencies -- 3012.9369 3014.9802 3017.6868
Frequencies -- 3020.8918 3029.4668 3030.8345
Frequencies -- 3034.8052 3041.6233 3058.4651
Frequencies -- 3060.9241 3062.1102 3065.3280
Frequencies -- 3066.2382 3066.8054 3066.8711
Frequencies -- 3066.9327 3068.1528 3071.3671
Frequencies -- 3072.1929 3072.2429 3074.4888
Frequencies -- 3074.8471 3076.6213 3078.2195
Frequencies -- 3078.6572 3170.6901 3220.2354

E(RB-LYP) = -4991.79467511 (BLYP-D3BJ/def2SVP/SMD (H_2O))
Sum of electronic and zero-point Energies= -4990.546220
Sum of electronic and thermal Energies= -4990.473128
Sum of electronic and thermal Free Energies= -4990.647764

E(RB-LYP) = -4991.79467511 (BLYP-D3BJ/def2TZVPP/SMD (H_2O))

G13

Center Number	Atomic Number	Atomic Type	Coordinates (Angstroms) X	Y	Z
1	6	0	-1.173326	0.705487	0.937711
2	1	0	-1.942025	0.153138	1.517177
3	6	0	0.222532	0.058632	1.179309
4	6	0	-1.525064	0.686183	-0.568976
5	6	0	1.284531	0.856589	0.368660
6	6	0	0.184323	-1.406258	0.655765
7	1	0	-2.521289	1.151140	-0.714089
8	6	0	-0.455322	1.483283	-1.355359
9	6	0	-1.552159	-0.778972	-1.070615
10	1	0	2.295194	0.417190	0.511206
11	1	0	1.327621	1.901134	0.741338
12	6	0	0.935130	0.836825	-1.140147
13	1	0	-0.566781	-1.986787	1.231019
14	1	0	1.166697	-1.903349	0.806270
15	6	0	-0.162672	-1.426042	-0.854138
16	1	0	-0.440691	2.539752	-1.015570
17	1	0	-0.705604	1.492184	-2.436268
18	1	0	-2.329796	-1.354375	-0.526501
19	1	0	-1.819578	-0.807181	-2.147107
20	1	0	1.705304	1.408656	-1.696389
21	6	0	0.908440	-0.629144	-1.639538
22	1	0	-0.180131	-2.477302	-1.206252
23	1	0	0.679799	-0.655995	-2.724896
24	1	0	1.906293	-1.096897	-1.506330
25	1	0	-1.166803	1.748968	1.315540

26	1	0	2.618777	0.000470	2.674115
27	1	0	1.916258	-0.438295	4.170519
28	1	0	1.879380	-1.487844	2.818829
29	7	0	1.814284	-0.493332	3.098573
30	6	0	0.496875	0.116336	2.690107
31	1	0	-0.280267	-0.427963	3.257938
32	1	0	0.516143	1.160283	3.053698
33	53	0	1.796909	-0.120475	6.491311

Frequencies -- 5.0452 36.7485 77.2177
Frequencies -- 90.6869 208.9520 244.5148
Frequencies -- 299.4020 309.9362 321.7378
Frequencies -- 378.3537 381.2943 404.8901
Frequencies -- 406.1015 444.4294 454.0228
Frequencies -- 467.2371 564.4755 646.1829
Frequencies -- 648.2570 695.3091 762.5167
Frequencies -- 788.7018 802.5681 825.0117
Frequencies -- 874.3809 874.9507 878.2953
Frequencies -- 883.0373 917.6278 920.8685
Frequencies -- 948.9894 951.9425 957.6203
Frequencies -- 972.9983 1012.1037 1016.7178
Frequencies -- 1023.5162 1050.0858 1061.0829
Frequencies -- 1084.9387 1095.3250 1098.1452
Frequencies -- 1100.1631 1109.4017 1137.2779
Frequencies -- 1175.7356 1178.3600 1244.7521
Frequencies -- 1250.9137 1273.1903 1277.0751
Frequencies -- 1278.7108 1296.3135 1301.0556
Frequencies -- 1303.0440 1305.2723 1321.5474
Frequencies -- 1331.6124 1339.7586 1349.8516
Frequencies -- 1351.1429 1357.5156 1370.1948
Frequencies -- 1403.5972 1414.0861 1416.1067
Frequencies -- 1426.0658 1426.5975 1428.2674
Frequencies -- 1431.8429 1448.2033 1498.1385
Frequencies -- 1525.9694 2609.3434 2936.3142
Frequencies -- 2941.8192 2952.1446 2952.7044
Frequencies -- 2953.2945 2954.9616 2976.2211
Frequencies -- 2976.4787 2983.3457 2986.0197
Frequencies -- 2988.5481 2995.0633 2995.6791
Frequencies -- 2996.9335 2997.2188 3012.1588
Frequencies -- 3069.5761 3339.8282 3398.7198

E(RB-LYP) = -783.107099316 (BLYP-D3BJ/def2SVP/SMD (H_2O))
Sum of electronic and zero-point Energies= -782.813274
Sum of electronic and thermal Energies= -782.800824
Sum of electronic and thermal Free Energies= -782.856127

E(RB-LYP) = -783.660023222 (BLYP-D3BJ/def2TZVPP/SMD (H_2O))

HG14

G14

HG15

G15

HG16

Center Number	Atomic Number	Atomic Type	Coordinates (Angstroms) X	Y	Z
1	8	0	-2.582012	-3.531831	2.751371
2	8	0	0.937295	-4.170119	2.828043
3	8	0	3.478114	-1.633006	2.901775
4	8	0	3.380276	2.121758	2.959789
5	8	0	0.703723	4.399597	2.988651
6	8	0	-2.621230	3.173549	2.859214
7	8	0	-3.976535	-0.343046	2.693877
8	8	0	-2.426517	-3.002309	-3.193244
9	8	0	1.099344	-3.666215	-3.228585
10	8	0	4.047838	-1.379090	-3.088118
11	8	0	3.904290	2.002932	-3.036451
12	8	0	0.828972	3.849983	-3.025064
13	8	0	-2.852053	3.011070	-3.156413
14	8	0	-4.470782	-0.036831	-3.322682
15	7	0	-4.056524	-3.578851	0.926438
16	7	0	-2.275463	-4.944428	0.908014
17	7	0	0.170890	-5.216510	0.874184
18	7	0	2.346759	-4.660405	1.022278
19	7	0	4.200819	-3.034598	1.166002
20	7	0	4.986723	-0.930882	1.250720
21	7	0	4.871811	1.524145	1.251471
22	7	0	4.044495	3.615968	1.277887
23	7	0	1.989416	4.967989	1.111538
24	7	0	-0.205141	5.462419	1.110292
25	7	0	-2.546181	4.687527	1.067527
26	7	0	-4.174190	3.139561	1.105794
27	7	0	-5.045165	0.848679	0.980020
28	7	0	-5.208834	-1.398017	1.001738
29	7	0	-4.027471	-3.426583	-1.537573
30	7	0	-2.131895	-4.636512	-1.535820
31	7	0	0.280579	-5.136328	-1.594926
32	7	0	2.403799	-4.421346	-1.432777
33	7	0	4.296230	-2.867038	-1.297203
34	7	0	5.337259	-0.879193	-1.194384
35	7	0	5.282312	1.590102	-1.185917
36	7	0	4.004564	3.444124	-1.188745
37	7	0	2.061953	4.951178	-1.363112
38	7	0	-0.181345	5.121487	-1.334036
39	7	0	-2.567796	4.525900	-1.393148
40	7	0	-4.352173	3.159610	-1.358107
41	7	0	-5.476656	0.961573	-1.452708
42	7	0	-5.197482	-1.268384	-1.465772
43	6	0	-2.919368	-3.950842	1.644832
44	6	0	-1.113245	-5.653181	1.402106
45	1	0	-1.083050	-5.501808	2.495737
46	1	0	-1.240271	-6.733659	1.182377
47	6	0	1.127780	-4.614279	1.696319
48	6	0	3.598749	-4.267347	1.644236
49	1	0	3.389946	-4.135459	2.720732
50	1	0	4.334680	-5.087066	1.510895
51	6	0	4.128739	-1.834076	1.876028
52	6	0	5.381254	0.315352	1.877636
53	1	0	4.989402	0.296331	2.910510
54	1	0	6.491362	0.365574	1.903183
55	6	0	4.006732	2.383982	1.933432
56	6	0	3.290956	4.768876	1.731463
57	1	0	3.112885	4.635470	2.813207
58	1	0	3.909814	5.674677	1.566706
59	6	0	0.810493	4.868150	1.856648
60	6	0	-1.558847	5.603612	1.611140
61	1	0	-1.902592	6.639817	1.415142
62	1	0	-1.513343	5.430833	2.700740
63	6	0	-3.051671	3.604607	1.789166
64	6	0	-5.059080	2.137121	1.658483
65	1	0	-6.098346	2.530096	1.652015
66	1	0	-4.736963	1.964934	2.700963
67	6	0	-4.650600	-0.307186	1.665107
68	6	0	-5.104227	-2.757726	1.502862

69	1	0	-4.899303	-2.693142	2.586059
70	1	0	-6.081321	-3.258475	1.343767
71	6	0	-2.808129	-3.603507	-2.189749
72	6	0	-1.033646	-5.349964	-2.167871
73	1	0	-0.983656	-5.014258	-3.218936
74	1	0	-1.258142	-6.436652	-2.139761
75	6	0	1.236553	-4.315729	-2.191549
76	6	0	3.697197	-4.015169	-1.949064
77	1	0	3.556835	-3.742687	-3.010315
78	1	0	4.396062	-4.875863	-1.876662
79	6	0	4.488839	-1.663191	-1.975419
80	6	0	5.902392	0.369659	-1.670593
81	1	0	5.802697	0.371430	-2.770396
82	1	0	6.976960	0.394326	-1.399199
83	6	0	4.332919	2.297991	-1.921913
84	6	0	3.383344	4.592530	-1.834864
85	1	0	3.291889	4.348659	-2.908023
86	1	0	4.045308	5.474606	-1.712187
87	6	0	0.895038	4.542928	-2.009340
88	6	0	-1.476978	5.278476	-1.976646
89	1	0	-1.742741	6.357663	-1.973413
90	1	0	-1.371296	4.927977	-3.018997
91	6	0	-3.202666	3.492286	-2.079867
92	6	0	-5.415587	2.337091	-1.910914
93	1	0	-5.268934	2.300518	-3.004780
94	1	0	-6.384144	2.827620	-1.685937
95	6	0	-4.974429	-0.103060	-2.202024
96	6	0	-5.079262	-2.582510	-2.070005
97	1	0	-6.043679	-3.121831	-1.962238
98	1	0	-4.865076	-2.421213	-3.141372
99	6	0	-4.169151	-4.266330	-0.357105
100	1	0	-5.118022	-4.838527	-0.406060
101	6	0	-2.879717	-5.166449	-0.397170
102	1	0	-3.091352	-6.244991	-0.546912
103	6	0	0.746421	-5.748798	-0.359185
104	1	0	0.607279	-6.848764	-0.399254
105	6	0	2.250525	-5.303363	-0.281597
106	1	0	2.970136	-6.145158	-0.349770
107	6	0	5.022513	-2.931113	-0.030698
108	1	0	5.768068	-3.752509	-0.055260
109	6	0	5.658658	-1.497008	0.083458
110	1	0	6.757276	-1.504797	0.239554
111	6	0	5.531939	2.178042	0.119169
112	1	0	6.623110	2.258284	0.303568
113	6	0	4.798248	3.562544	0.037809
114	1	0	5.485605	4.430296	-0.031348
115	6	0	1.798001	5.696902	-0.142587
116	1	0	2.389111	6.635694	-0.131284
117	6	0	0.244071	5.928331	-0.191808
118	1	0	-0.044962	6.988606	-0.343775
119	6	0	-3.268364	4.920010	-0.174629
120	1	0	-3.587849	5.980669	-0.236999
121	6	0	-4.461223	3.898731	-0.108898
122	1	0	-5.458779	4.378731	-0.036072
123	6	0	-5.941484	0.549815	-0.138340
124	1	0	-6.950372	0.965825	0.061142
125	6	0	-5.908422	-1.016925	-0.213617
126	1	0	-6.913140	-1.486701	-0.239636
127	6	0	0.219221	1.583413	0.616860
128	1	0	-0.370764	1.927263	1.490070
129	6	0	0.925802	0.243481	0.941865
130	6	0	-0.696315	1.407846	-0.641415
131	6	0	1.829984	-0.157161	-0.252331
132	6	0	-0.138875	-0.862186	1.149714
133	1	0	-0.464999	2.163554	-1.415439
134	1	0	2.288265	-1.140045	-0.039282
135	1	0	2.665964	0.560187	-0.350923
136	6	0	0.988666	-0.220785	-1.569387
137	1	0	-0.824143	-0.579454	1.975578
138	1	0	0.355754	-1.803893	1.462565
139	6	0	-0.949338	-1.054691	-0.174942
140	1	0	1.129701	-1.192996	-2.082498
141	1	0	-0.810910	-2.073038	-0.584797
142	1	0	0.987916	2.358185	0.437043
143	6	0	-0.507952	-0.010780	-1.230291
144	1	0	-2.027801	-0.923680	0.023856
145	1	0	-1.758699	1.550717	-0.367118
146	1	0	1.324766	0.564432	-2.277690
147	1	0	1.546981	0.356085	1.851920
148	1	0	-1.129856	-0.126598	-2.141989

Frequencies -- 11.4409 27.3854 34.8769
Frequencies -- 40.8630 48.2128 50.9754
Frequencies -- 57.8178 62.8660 63.4297
Frequencies -- 76.9278 78.5583 82.4187
Frequencies -- 82.6109 85.7495 86.8232
Frequencies -- 91.6255 93.6276 94.7380
Frequencies -- 96.7866 105.0620 107.4999
Frequencies -- 109.3126 110.9207 111.6495
Frequencies -- 113.8193 118.2277 123.2897
Frequencies -- 124.4813 128.5751 131.4436
Frequencies -- 133.7229 144.1132 147.0469
Frequencies -- 150.4515 154.9958 158.9965
Frequencies -- 161.0902 164.8696 166.2185
Frequencies -- 170.2714 179.1001 183.4263
Frequencies -- 188.4467 191.0103 193.6298
Frequencies -- 199.0465 200.9660 202.6228
Frequencies -- 208.4943 212.0988 220.8184
Frequencies -- 226.1911 231.4928 241.4849
Frequencies -- 242.2681 248.2073 261.6093
Frequencies -- 262.3106 263.6385 269.7957
Frequencies -- 283.7597 286.1435 291.0535
Frequencies -- 291.9244 314.3154 326.3088
Frequencies -- 329.7751 332.3147 333.7669
Frequencies -- 346.7414 349.4840 350.4137
Frequencies -- 352.6902 353.0206 354.5846
Frequencies -- 356.0371 358.9997 361.8731
Frequencies -- 362.9944 365.5288 366.4848
Frequencies -- 368.4773 370.0693 371.6342
Frequencies -- 375.5347 390.0859 405.8532
Frequencies -- 412.1937 412.4983 417.2233
Frequencies -- 433.4174 437.8591 438.0733
Frequencies -- 441.8470 444.8438 454.2863
Frequencies -- 456.2448 458.0765 459.8421
Frequencies -- 507.4292 508.2781 519.9011
Frequencies -- 521.8951 578.3620 578.9548
Frequencies -- 602.4303 604.6043 607.8461
Frequencies -- 610.7254 613.8753 614.1622
Frequencies -- 618.5327 620.6824 624.3164
Frequencies -- 627.3656 627.6980 637.6883
Frequencies -- 638.6932 645.5410 646.9854
Frequencies -- 647.9982 655.5506 661.5762
Frequencies -- 664.4874 666.3276 668.0514
Frequencies -- 670.0072 674.1434 684.5591
Frequencies -- 686.3867 692.2989 694.6425
Frequencies -- 698.7491 702.8782 707.1038
Frequencies -- 708.1390 708.8826 712.4154

Frequencies -- 713.7377 715.8289 716.5822
Frequencies -- 719.6612 720.5379 722.2165
Frequencies -- 723.1027 724.8767 726.6261
Frequencies -- 727.9248 769.0059 770.1539
Frequencies -- 776.7104 778.4324 778.7520
Frequencies -- 780.0080 780.7895 788.0710
Frequencies -- 788.6730 790.6350 793.2264
Frequencies -- 795.4866 797.7468 798.3589
Frequencies -- 810.3433 811.8224 812.4058
Frequencies -- 813.8810 814.8944 815.9631
Frequencies -- 816.6978 817.1365 818.3183
Frequencies -- 819.7058 820.2636 830.7377
Frequencies -- 852.9803 867.5731 879.5529
Frequencies -- 881.4722 884.7033 894.3362
Frequencies -- 896.1287 909.2183 911.9391
Frequencies -- 927.4990 936.8986 939.9375
Frequencies -- 941.0100 943.9394 945.6027
Frequencies -- 949.2229 950.2790 952.3175
Frequencies -- 953.7413 954.4760 955.6129
Frequencies -- 961.5099 964.0030 969.0176
Frequencies -- 969.8088 971.3052 980.7965
Frequencies -- 982.0707 983.5764 994.2665
Frequencies -- 1003.9706 1005.6589 1010.7166
Frequencies -- 1011.5498 1013.2544 1025.3370
Frequencies -- 1028.2381 1029.1750 1032.6501
Frequencies -- 1034.5720 1036.4212 1039.1192
Frequencies -- 1040.5990 1041.9325 1090.6339
Frequencies -- 1093.5783 1094.8229 1097.9455
Frequencies -- 1100.7443 1103.1352 1103.5275
Frequencies -- 1105.6800 1109.0525 1110.4019
Frequencies -- 1111.4635 1116.3263 1118.3832
Frequencies -- 1124.1702 1136.0217 1137.2731
Frequencies -- 1140.7521 1141.5863 1153.1984
Frequencies -- 1166.6355 1167.1487 1169.9908
Frequencies -- 1180.5641 1182.3381 1184.1244
Frequencies -- 1189.8059 1195.7076 1198.3925
Frequencies -- 1198.5751 1200.0182 1201.1087
Frequencies -- 1201.8120 1210.0082 1211.6569
Frequencies -- 1211.8349 1213.6086 1214.3054
Frequencies -- 1215.1047 1216.3259 1217.8015
Frequencies -- 1223.8224 1226.1085 1226.6159
Frequencies -- 1227.2693 1228.7601 1229.2982
Frequencies -- 1230.1065 1237.4419 1237.7637
Frequencies -- 1240.4557 1252.0630 1253.4600
Frequencies -- 1257.3330 1258.5685 1260.0821
Frequencies -- 1265.2631 1265.8783 1266.7043
Frequencies -- 1269.3451 1273.1096 1273.5170
Frequencies -- 1276.0876 1276.5424 1277.2134
Frequencies -- 1277.6529 1279.8841 1291.8147
Frequencies -- 1297.4266 1298.8042 1302.4918
Frequencies -- 1303.4045 1304.7545 1305.1925
Frequencies -- 1306.2321 1306.3507 1311.5871
Frequencies -- 1311.6233 1314.2995 1315.3190
Frequencies -- 1318.6173 1319.5887 1320.3062
Frequencies -- 1320.5954 1323.3303 1326.5995
Frequencies -- 1339.6643 1344.6719 1350.6089
Frequencies -- 1361.5866 1363.7910 1364.6127
Frequencies -- 1365.7078 1367.9812 1368.4964
Frequencies -- 1369.4661 1369.8252 1370.4562
Frequencies -- 1371.9285 1373.1714 1374.7427
Frequencies -- 1375.2736 1375.9828 1376.2616
Frequencies -- 1376.5735 1377.2405 1379.1181
Frequencies -- 1379.6364 1381.1948 1381.5590
Frequencies -- 1382.2405 1383.2588 1383.5851
Frequencies -- 1384.4720 1384.9160 1385.6252
Frequencies -- 1386.4728 1387.9480 1388.7156
Frequencies -- 1390.6545 1391.7189 1393.0354
Frequencies -- 1394.0376 1397.0782 1397.5847
Frequencies -- 1398.6750 1400.6553 1404.0740
Frequencies -- 1405.5661 1406.7928 1410.3972
Frequencies -- 1429.5148 1434.3966 1435.1189
Frequencies -- 1436.8078 1437.2923 1438.3238
Frequencies -- 1439.9949 1441.6964 1442.0911
Frequencies -- 1443.8819 1444.4248 1444.6233
Frequencies -- 1446.6225 1447.0542 1448.1963
Frequencies -- 1450.4804 1453.9555 1454.5353
Frequencies -- 1458.3317 1469.6939 1707.6429
Frequencies -- 1708.0324 1712.6159 1713.1302
Frequencies -- 1716.3866 1716.9054 1720.9089
Frequencies -- 1720.9466 1723.1883 1725.8754
Frequencies -- 1728.8191 1738.4362 1739.4698
Frequencies -- 1744.9468 2953.3325 2954.0855
Frequencies -- 2957.3589 2958.5639 2961.0142
Frequencies -- 2961.1910 2967.5390 2971.3437
Frequencies -- 2972.5015 2973.1091 2974.1757
Frequencies -- 2975.5492 2976.6681 2978.0885

Frequencies -- 2978.4008 2979.2465 2979.6923
Frequencies -- 2979.7156 2980.3078 2980.9964
Frequencies -- 2982.5598 2982.8970 2983.1961
Frequencies -- 2984.2935 2984.9633 2985.9811
Frequencies -- 2987.6007 2988.0269 2988.5363
Frequencies -- 2989.3381 2989.7604 2990.7184
Frequencies -- 2993.0145 3001.6596 3005.7176
Frequencies -- 3006.1664 3011.2379 3020.5204
Frequencies -- 3028.7635 3046.1323 3054.5952
Frequencies -- 3062.2188 3064.9408 3065.0850
Frequencies -- 3065.4812 3068.4738 3070.0489
Frequencies -- 3071.5816 3071.7703 3071.9111
Frequencies -- 3072.6322 3073.6200 3073.7853
Frequencies -- 3075.9976 3076.9623 3077.1347

E(RB-LYP) = -4521.54232617 (BLYP-D3BJ/def2SVP/SMD (H_2O))
Sum of electronic and zero-point Energies= -4520.389801
Sum of electronic and thermal Energies= -4520.321456
Sum of electronic and thermal Free Energies= -4520.486432

E(RB-LYP) = -4526.54173562 (BLYP-D3BJ/def2TZVPP/SMD (H_2O))

G16

Center Number	Atomic Number	Atomic Type	Coordinates (Angstroms) X	Y	Z
1	6	0	0.200659	1.574997	0.636591
2	1	0	-0.429249	1.857025	1.504580
3	6	0	0.927901	0.241400	0.938007
4	6	0	-0.671011	1.422080	-0.655180
5	6	0	1.841283	-0.123481	-0.258049
6	6	0	-0.123047	-0.878220	1.135002
7	1	0	-0.370455	2.163822	-1.422813
8	1	0	2.374604	-1.071026	-0.039466
9	1	0	2.621113	0.655459	-0.381531
10	6	0	0.980625	-0.258878	-1.558704
11	1	0	-0.768973	-0.629357	2.001492
12	1	0	0.390160	-1.828540	1.386601
13	6	0	-0.977956	-1.035517	-0.167106
14	1	0	1.096084	-1.268257	-2.003305
15	1	0	-0.882174	-2.060744	-0.579035
16	1	0	0.948805	2.384326	0.512955
17	6	0	-0.511124	-0.007656	-1.227228
18	1	0	-2.054675	-0.880828	0.048722
19	1	0	-1.740580	1.613318	-0.432422
20	1	0	1.314859	0.465921	-2.328654
21	1	0	1.539015	0.347488	1.857268
22	1	0	-1.122496	-0.113475	-2.146356

Frequencies -- 46.8554 282.5506 285.1330
Frequencies -- 372.2132 372.8565 505.1152
Frequencies -- 506.9160 624.5482 770.7188
Frequencies -- 774.7399 784.7945 804.5057
Frequencies -- 807.3010 850.3151 853.2446
Frequencies -- 908.6617 942.2993 943.1794
Frequencies -- 966.0262 1003.6975 1034.2273
Frequencies -- 1034.3740 1083.8249 1085.5404
Frequencies -- 1102.6820 1120.2268 1122.9871
Frequencies -- 1208.6556 1209.8728 1217.9898
Frequencies -- 1249.9014 1251.4892 1292.9264
Frequencies -- 1294.4339 1305.8269 1307.6626
Frequencies -- 1308.4978 1331.9725 1332.8533
Frequencies -- 1334.3725 1413.6208 1415.8973
Frequencies -- 1427.3144 1427.9906 1430.9878
Frequencies -- 1446.8043 2952.6903 2953.6551
Frequencies -- 2953.7925 2962.2224 2965.0248
Frequencies -- 2965.2380 2976.1842 2986.5325
Frequencies -- 2989.2384 2989.6374 2990.0323
Frequencies -- 3006.9429 3009.4859 3010.0451

E(RB-LYP) = -312.897251272 (BLYP-D3BJ/def2SVP/SMD (H_2O))
Sum of electronic and zero-point Energies= -312.696979
Sum of electronic and thermal Energies= -312.690014
Sum of electronic and thermal Free Energies= -312.728211

E(RB-LYP) = -313.246128246 (BLYP-D3BJ/def2TZVPP/SMD (H_2O))

Table 1

Structures	H (B1)	T.qh-S (B1)	qh-G(T) (B1)	□H (B1)	T□S (B1)	□G (B1)
G1	-465.16537	0.03843	-465.20380			
CB[7]	-4207.57697	0.14113	-4207.71810			
HG1	-4672.81474	0.15642	-4672.97116	**-45.4**	**-14.5**	**-30.9**
G2	-743.57268	0.04620	-743.61888			
CB[7]	-4207.57697	0.14113	-4207.71810			
HG2	-4951.23790	0.16072	-4951.39863	**-55.4**	**-16.7**	**-38.7**
G3	-445.29094	0.03885	-445.32979			
CB[7]	-4207.57697	0.14113	-4207.71810			
HG3	-4652.94002	0.15534	-4653.09535	**-45.2**	**-15.5**	**-29.8**
G4	-1175.59827	0.06049	-1175.65875			
CB[7]	-4207.57697	0.14113	-4207.71810			
HG4	-5383.27285	0.17452	-5383.44737	**-61.3**	**-17.0**	**-44.3**
G5	-579.02705	0.04779	-579.07484			
CB[7]	-4207.57697	0.14113	-4207.71810			
HG5	-4786.68629	0.16171	-4786.84800	**-51.6**	**-17.1**	**-34.5**
G6	-861.23371	0.05349	-861.28721			
CB[7]	-4207.57697	0.14113	-4207.71810			
HG6	-5068.90582	0.16813	-5069.07395	**-59.7**	**-16.6**	**-43.1**
G7	-1251.74871	0.05864	-1251.80735			
CB[7]	-4207.57697	0.14113	-4207.71810			
HG7	-5459.44219	0.17107	-5459.61326	**-73.1**	**-18.0**	**-55.1**
G8	-655.18674	0.04492	-655.23165			
CB[7]	-4207.57697	0.14113	-4207.71810			
HG8	-4862.84832	0.16061	-4863.00894	**-53.1**	**-16.0**	**-37.1**
G9	-1015.84586	0.05766	-1015.90352			
CB[7]	-4207.57697	0.14113	-4207.71810			
HG9	-5223.52866	0.17003	-5223.69869	**-66.4**	**-18.0**	**-48.4**
G10	-1487.07059	0.07390	-1487.14449			
CB[7]	-4207.57697	0.14113	-4207.71810			
HG10	-5694.77999	0.18685	-5694.96683	**-83.1**	**-17.7**	**-65.4**
G11	-390.00636	0.03603	-390.04239			
CB[7]	-4207.57697	0.14113	-4207.71810			
HG11	-4597.64588	0.15269	-4597.79858	**-39.3**	**-15.3**	**-23.9**
G12	-544.61844	0.03999	-544.65843			
CB[7]	-4207.57697	0.14113	-4207.71810			

HG12	-4752.26922	0.15480	-4752.42403	**-46.3**	**-16.5**	**-29.8**
G13	-782.79988	0.05033	-782.85021			
CB[7]	-4207.57697	0.14113	-4207.71810			
HG13	-4990.47218	0.16233	-4990.63452	**-59.8**	**-18.3**	**-41.5**
G14	-541.46104	0.04669	-541.50773			
CB[7]	-4207.57697	0.14113	-4207.71810			
HG14	-4749.12611	0.16153	-4749.28764	**-55.3**	**-16.5**	**-38.8**
G15	-1098.27364	0.06178	-1098.33542			
CB[7]	-4207.57697	0.14113	-4207.71810			
HG15	-5305.97306	0.17319	-5306.14625	**-76.8**	**-18.6**	**-58.2**
G16	-312.68907	0.03553	-312.72459			
CB[7]	-4207.57697	0.14113	-4207.71810			
HG16	-4520.32051	0.15361	-4520.47412	**-34.2**	**-14.5**	**-19.7**

Table 2

Structures	**H (B2)**	**T.qh-S (B2)**	**qh-G(T) (B2)**	**□H (B2)**	**T□S (B2)**	**□G (B2)**
G1	-465.68869	0.03843	-465.72712			
CB[7]	-4212.25115	0.14113	-4212.39228			
HG1	-4677.98505	0.15642	-4678.14147	**-28.4**	**-14.5**	**-13.9**
G2	-744.08062	0.04620	-744.12682			
CB[7]	-4212.25115	0.14113	-4212.39228			
HG2	-4956.38866	0.16072	-4956.54939	**-35.7**	**-16.7**	**-19.0**
G3	-445.78766	0.03885	-445.82651			
CB[7]	-4212.25115	0.14113	-4212.39228			
HG3	-4658.08230	0.15534	-4658.23764	**-27.3**	**-15.5**	**-11.8**
G4	-1176.23621	0.06049	-1176.29669			
CB[7]	-4212.25115	0.14113	-4212.39228			
HG4	-5388.58064	0.17452	-5388.75516	**-58.5**	**-17.0**	**-41.5**
G5	-579.67894	0.04779	-579.72673			
CB[7]	-4212.25115	0.14113	-4212.39228			
HG5	-4791.97599	0.16171	-4792.13770	**-28.8**	**-17.1**	**-11.7**
G6	-861.87636	0.05349	-861.92985			
CB[7]	-4212.25115	0.14113	-4212.39228			
HG6	-5074.18398	0.16813	-5074.35211	**-35.4**	**-16.6**	**-18.8**
G7	-1252.49683	0.05864	-1252.55547			
CB[7]	-4212.25115	0.14113	-4212.39228			
HG7	-5464.81892	0.17107	-5464.98998	**-44.5**	**-18.0**	**-26.5**

G8	-655.91271	0.04492	-655.95763			
CB[7]	-4212.25115	0.14113	-4212.39228			
HG8	-4868.21029	0.16061	-4868.37091	**-29.1**	**-16.0**	**-13.2**
G9	-1016.64920	0.05766	-1016.70686			
CB[7]	-4212.25115	0.14113	-4212.39228			
HG9	-5228.95857	0.17003	-5229.12860	**-36.5**	**-18.0**	**-18.5**
G10	-1488.08838	0.07390	-1488.16228			
CB[7]	-4212.25115	0.14113	-4212.39228			
HG10	-5700.41404	0.18685	-5700.60088	**-46.8**	**-17.7**	**-29.1**
G11	-390.43457	0.03603	-390.47060			
CB[7]	-4212.25115	0.14113	-4212.39228			
HG11	-4602.72550	0.15269	-4602.87819	**-25.0**	**-15.3**	**-9.6**
G12	-545.20731	0.03999	-545.24730			
CB[7]	-4212.25115	0.14113	-4212.39228			
HG12	-4757.49830	0.15480	-4757.65310	**-25.0**	**-16.5**	**-8.5**
G13	-783.35280	0.05033	-783.40313			
CB[7]	-4212.25115	0.14113	-4212.39228			
HG13	-4995.66314	0.16233	-4995.82547	**-37.1**	**-18.3**	**-18.9**
G14	-542.08744	0.04669	-542.13413			
CB[7]	-4212.25115	0.14113	-4212.39228			
HG14	-4754.39278	0.16153	-4754.55430	**-34.0**	**-16.5**	**-17.5**
G15	-1098.87129	0.06178	-1098.93307			
CB[7]	-4212.25115	0.14113	-4212.39228			
HG15	-5311.20369	0.17319	-5311.37688	**-51.0**	**-18.6**	**-32.3**
G16	-313.03795	0.03553	-313.07347			
CB[7]	-4212.25115	0.14113	-4212.39228			
HG16	-4525.31992	0.15361	-4525.47353	**-19.3**	**-14.5**	**-4.9**

Table 3. Thermodynamics for the reaction $(H_2O)_x$ (aq., 1M, SMD) + CB[7] (g, 1 atm) ⇢ CB[7]. x H_2O (aq., 1M, SMD) at 298.15 K at BLYP-D3/DEF2-SVP level.

Structures	H (B1)	T.qh-S (B1)	qh-G(T) (B1)	□H (B1)	T□S (B1)	□G (B1)
$(H_2O)_8$	-610.73000	0.05400	-610.78400			
CB[7]	-4207.46543	0.14410	-4207.60952			
CB[7] . 8 H_2O complex	-4818.39526	0.16498	-4818.56024	**-125.4**	**-20.8**	**-104.6**
$(H_2O)_{12}$	-916.11575	0.07063	-916.18638			

CB[7]	-4207.46543	0.14410	-4207.60952			
CB[7] . 12 H_2O complex	-5123.79322	0.18113	-5123.9744	**-133.1**	**-21.1**	**-112.0**
$(H_2O)_{16}$	-1221.49449	0.08773	-1221.58223			
CB[7]	-4207.46543	0.14410	-4207.60952			
CB[7] . 16 H_2Ocomplex	-5429.19101	0.19783	-5429.38883	**-145.0**	**-21.3**	**-123.7**
$(H_2O)_{18}$	-1374.19439	0.09411	-1374.28851			
CB[7]	-4207.46543	0.14410	-4207.60952			
CB[7] . 18 H_2O complex	-5581.87770	0.20304	-5582.08073	**-136.7**	**-22.1**	**-114.6**

Table 4. Thermodynamics for the reaction $(H_2O)_x$ (aq., 1M, SMD) + CB[7] (g, 1 atm) ⇢ CB[7]. x H_2O (aq., 1M, SMD) at 298.15 K at BLYP-D3/DEF2-TZVPP correction.

Structures	H (B2)	T.qh-S (B2)	qh-G(T) (B2)	□H (B2)	T□S (B2)	□G (B2)
$(H_2O)_8$	-611.53194	0.05400	-611.58594			
CB[7]	-4212.11866	0.14410	-4212.26276			
CB[7] . 8 H_2O complex	-4823.82813	0.16498	-4823.99311	**-111.4**	**-20.8**	**-90.6**
$(H_2O)_{12}$	-917.30552	0.07063	-917.37615			
CB[7]	-4212.11866	0.14410	-4212.26276			
CB[7] . 12 H_2O complex	-5129.60968	0.18113	-5129.79081	**-116.4**	**-21.1**	**-95.3**
$(H_2O)_{16}$	-1223.08576	0.08773	-1223.17349			
CB[7]	-4212.11866	0.14410	-4212.26276			
CB[7] . 16 H_2O complex	-5435.38984	0.19783	-5435.58766	**-116.3**	**-21.3**	**-95.0**
$(H_2O)_{18}$	-1375.97095	0.09411	-1376.06507			
CB[7]	-4212.11866	0.14410	-4212.26276			
CB[7] . 18 H_2O complex	-5588.26615	0.20304	-5588.46918	**-110.8**	**-22.1**	**-88.7**

Table 5. Thermodynamics for the reaction $(H_2O)_x$ (aq., 1M, SMD) + CB[7] (aq., SMD) ⇢ CB[7]. x H_2O (aq., 1M, SMD) at 298.15 K at BLYP-D3/DEF2-SVP level.

Structures	H (B1)	T.qh-S (B1)	qh-G(T) (B1)	□H (B1)	T□S (B1)	□G (B1)
$(H_2O)_8$	-610.73000	0.05400	-610.78400			
CB[7]	-4207.57697	0.14113	-4207.71810			
CB[7] . 8 H_2O complex	-4818.39526	0.16498	-4818.56024	**-55.4**	**-18.9**	**-36.5**
$(H_2O)_{12}$	-916.11575	0.07063	-916.18638			
CB[7]	-4207.57697	0.14113	-4207.71810			
CB[7] . 12 H_2O complex	-5123.79322	0.18113	-5123.97435	**-63.1**	**-19.2**	**-43.8**
$(H_2O)_{16}$	-1221.49449	0.08773	-1221.58223			
CB[7]	-4207.57697	0.14113	-4207.71810			
CB[7] . 16 H_2O complex	-5429.19101	0.19783	-5429.38883	**-75.0**	**-19.5**	**-55.5**
$(H_2O)_{18}$	-1374.19439	0.09411	-1374.28851			
CB[7]	-4207.57697	0.14113	-4207.71810			
CB[7] . 18 H_2O complex	-5581.87770	0.20304	-5582.08073	**-66.7**	**-20.2**	**-46.5**

Table 6. Thermodynamics for the reaction $(H_2O)_x$ (aq., 1M, SMD) + CB[7] (aq., SMD) ⇢ CB[7]. x H_2O (aq., 1M, SMD) at 298.15 K at BLYP-D3/DEF2-TZVPP correction.

Structures	H (B2)	T.qh-S (B2)	qh-G(T) (B2)	□H (B2)	T□S (B2)	□G (B2)
$(H_2O)_8$	-611.53194	0.05400	-611.58594			
CB[7]	-4212.25115	0.14113	-4212.39228			
CB[7] . 8 H_2O complex	-4823.82813	0.16498	-4823.99311	**-28.3**	**-18.9**	**-9.3**
$(H_2O)_{12}$	-917.30552	0.07063	-917.37615			
CB[7]	-4212.25115	0.14113	-4212.39228			
CB[7] . 12 H_2O complex	-5129.60968	0.18113	-5129.79081	**-33.3**	**-19.2**	**-14.0**
$(H_2O)_{16}$	-1223.08576	0.08773	-1223.17349			
CB[7]	-4212.25115	0.14113	-4212.39228			
CB[7] . 16 H_2O complex	-5435.38984	0.19783	-5435.58766	**-33.2**	**-19.5**	**-13.7**
$(H_2O)_{18}$	-1375.97095	0.09411	-1376.06507			
CB[7]	-4212.25115	0.14113	-4212.39228			

CB[7] . 18 H_2O complex	-5588.26615	0.20304	-5588.46918	**-27.6**	**-20.2**	**-7.4**

VI.2. Educational YouTube channel: Named reactions in organic chemistry.

With over a thousand unique viewers (at the time of writing), this YouTube channel was created with the aim to provide an easy to follow explanation of common named chemical reactions to facilitate their study and review. Additionally, you will find challenging videos to prove your knowledge in organic chemistry.

A sample of some name reactions:

Suzuki cross coupling: https://youtu.be/5zr4_BkrBNc

Baeyer-Villiger oxidation: https://youtu.be/0PbETmYKm5E

Corey-Kim oxidation: https://youtu.be/9f8uA_F_0g4

Barton-McCombie reaction: https://youtu.be/2Rzt5l5l4bk

Cope elimination: https://youtu.be/LEdzaZOWS28

Heck coupling reaction: https://youtu.be/3IIAyG-b8_U

Mitsunobu reaction: https://youtu.be/5XIaLDv1RSs

Swern oxidation: https://youtu.be/GIM_nQkoDAM

Parikh-Doering oxidation: https://youtu.be/8-BwyQw9aWo

Ley Griffith oxidation: https://youtu.be/gtN11ddTc0A

Doering Laflamme reaction: https://youtu.be/JCMXc0fml4A

Sonogashira Cross Coupling: https://youtu.be/XtYOki4gY0c

Stille Cross Coupling: https://youtu.be/devRGaWbKI0

Ley-Griffith reaction: https://youtu.be/gtN11ddTc0A